eman ta zabal zazu

Universidad del País Vasco | **Euskal Herriko Unibertsitatea**

Irida-β-diketones and Iridapyrazoles: Reactivity and catalytic activity in amine-borane solvolysis for hydrogen release

PhD Student: ITXASO BUSTOS ROSAS

Supervisors: MARÍA ÁNGELES GARRALDA HUALDE

CLAUDIO MENDICUTE FIERRO

Euskal Herriko Unibertsitatea UPV-EHU

Donostia (Gipuzkoa), 2021

Contents

Glossary of Abbreviations

Abbreviations

AB	Ammonia-borane
ACN	Acetonitrile
Bar^F_4	Sodium tetrakis[3,5-bis(trifluoromethyl)phenyl]borate
COD	*Cis,cis*-1,5-cyclooctadiene
COE	*Cis*-cyclooctene
DCM	Dichloromethane
DMAB	Dimethylamine-borane
DMF	Dimethylformamide
EDA	Ethyldiazoacetate
EtOH	Ethanol
^{i}PrOH	Isopropanol
IR	Infrared
m/z	Mass-to-charge ratio
MeOH	Methanol
Py	Pyridine
Pyr	Pyrazole
TBAB	Tert-butylamine-borane
TEAB	Triethylamine-borane
THF	Tetrahydrofuran
TOF	Turnover frequency

Chapter 1

Introduction

1.1 Irida-β-diketones

Metalla-β-diketones are acylhydroxycarbene type organometallic complexes which are stabilised by an intramolecular hydrogen bond between the acyl and the hydroxycarbene groups. They are similar to the organic β-diketones which contain an intramolecular hydrogen bond between the keto and the enol groups (Figure 1.1).
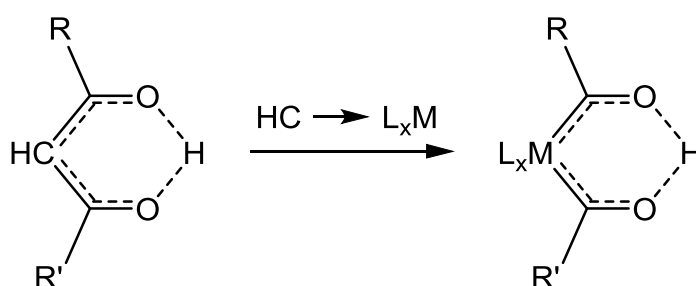
Figure 1.1 Organic-β-diketones and metalla-β-diketones.

The first metalla-β-diketone complexes were reported by Lukehart in 1981 and they were synthesised through the protonation of anionic diacylmetallated complexes $[L_xM(COR)(COR')]^-$ where M = Mo, W, Mn, Re, Fe and Os.[1,2] These complexes present an electronically saturated coordination sphere and are kinetically inert.

Irida-β-diketone type complexes have been synthesised from the diolefin dimer $[IrCl(COD)]_2$ and the o-(diphenylphosphino)benzaldehyde ligand, $PPh_2(o$-$C_6H_4CHO)$. When the reaction is carried out in benzene the olefinic hydridoacyl complex $[IrHCl(COD)(PPh_2(o$-$C_6H_4CO))]$ (**I**) is obtained.[3] In this process there has been a cleavage of the chloride bridge in the starting dimer with phosphorus coordination and the aldehyde in the ligand gives an oxidative addition to the iridium(I) affording an acylhydride iridium(III) species.

On the other hand, when the reaction takes place in methanol with an Ir:P = 1:2 ratio, or when the $[IrHCl(COD)(PPh_2(o$-$C_6H_4CO))]$ complex is dissolved in

methanol and another equivalent of PPh$_2$(o-C$_6$H$_4$CHO) is added, the diolefin is completely displaced upon coordination of phosphine and, most likely, occurrence of a second oxidative addition of another aldehyde affording a dihydride-diacyl iridium(V) intermediate. Finally, an iridium-to-oxygen proton transfer is proposed to give the hydridoirida-β-diketone complex[4] [IrHCl{(PPh$_2$(o-C$_6$H$_4$CO))$_2$H}] (**1**) (Scheme 1.1).
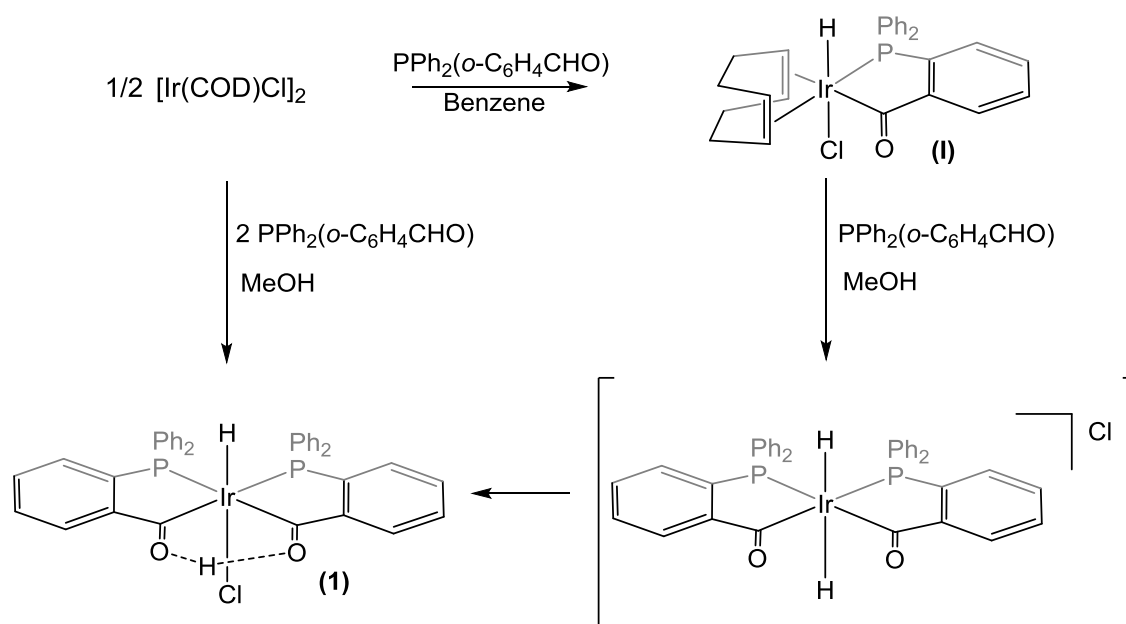
Scheme 1.1 Synthesis of [IrHCl{(PPh$_2$(o-C$_6$H$_4$CO))$_2$H}], complex 1.

1.1.1 Reactivity of chlorohydridoirida-β-diketone (1).

The hydridoirida-β-diketone [IrHCl{(PPh$_2$(o-C$_6$H$_4$CO))$_2$H}] complex is very stable and fails to react with σ-donor ligands such as pyridine or triphenylphosphine.

Nonetheless, complex **1** reacts with SnCl$_2$ which inserts in the Ir-Cl bond affording the trichlorostannate complex [IrH{(PPh$_2$(o-C$_6$H$_4$CO))$_2$H}(SnCl$_3$)] (**II**).[4] Added to that, complex **1** also reacts with halogen scavengers such as the

silver salts AgClO$_4$, AgOTs and AgOTf. As a result of these reactions, the chloride atom is eliminated as AgCl salt and the iridium bonds the anion of the added silver salt affording new neutral complexes [IrHX{(PPh$_2$(o-C$_6$H$_4$CO))$_2$H}] (**III**) where X = ClO$_4^-$, OTs$^-$ or OTf$^-$.[4,5] The obtained neutral complexes contain labile ligands that can be substituted by σ-donor ligands such as pyridine, triphenylphosphine and carbon monoxide[6] affording cationic species [IrHL{(PPh$_2$(o-C$_6$H$_4$CO))$_2$H}]X (**IV**) (Scheme 1.2).
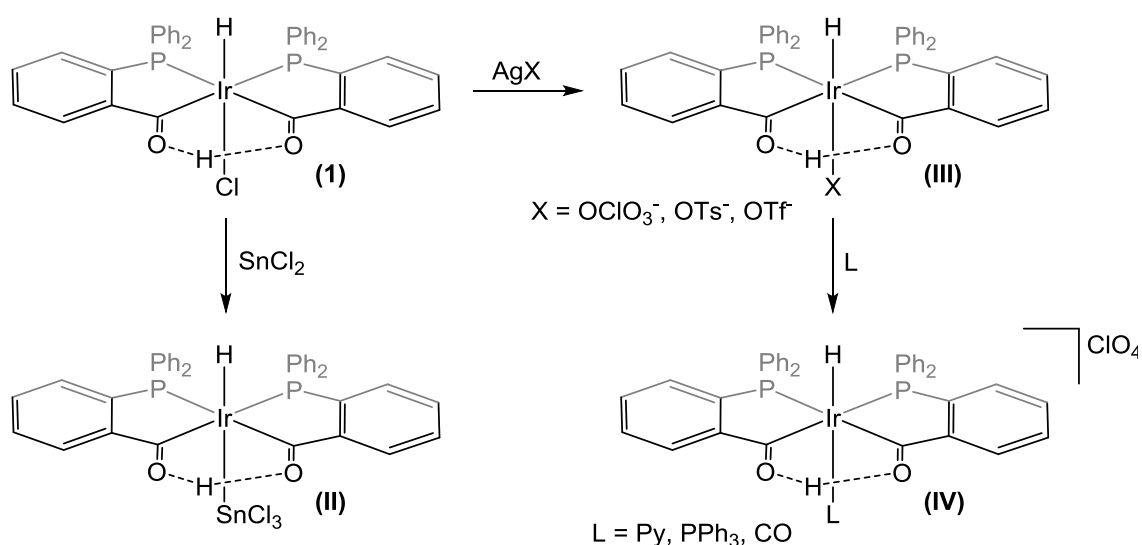
Scheme 1.2 Reactivity of complex 1 involving Ir-Cl bond cleavage

Complex **IV** (where L = CO) shows a deprotonation/protonation equilibrium which is displaced to the protonated form at low temperatures. Complex **V**, the deprotonated form of complex **IV**, can be isolated after dissolving complex **IV** (L = CO) in dimethylsulfoxide or by reacting it with triethylamine. After the deprotonation reaction a ligand rearrangement happens affording complex **VI**. In complex **VI** the hydride and one of the phosphorus atoms are in *trans* position. If both complex **V** and complex **VI** are dissolved in an acidic media the initial complex **IV** is obtained (Scheme 1.3). These results revealed that the PCCP coplanarity observed in the irida-β-diketone complexes is stabilised by the hydrogen bond between the hydroxyl and the acyl groups.[6]
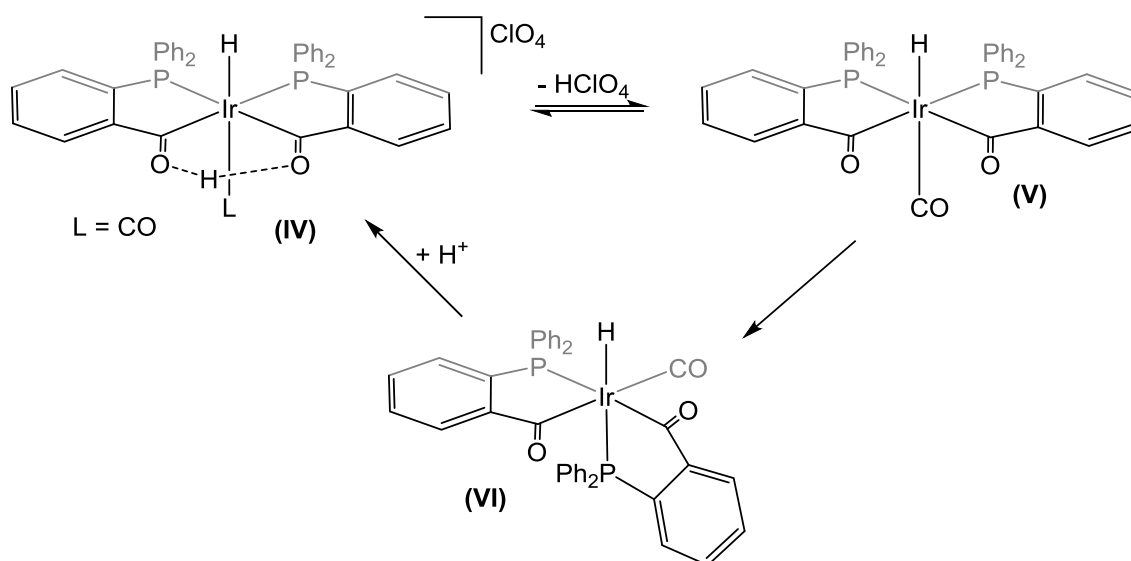
Scheme 1.3 Deprotonation / protonation equilibrium of complex V and isometisation

A complex containing an ethylene group (**VII**) could also be synthesised from complex **1** and ethylene in the presence of AgBF$_4$. When this complex is dissolved in dimethylsulfoxide the ethylene group is substituted by one molecule of solvent affording complex **IX**, confirming that an ethylene group in a *trans* position to a hydride is easily displaced by other more coordinating molecules.[7] Complex **VII** as well as complex **IX** react with triethylamine and therefore loose the bridging hydroxy-acyl protons affording neutral diacyl complexes **VIII** and **X** with hydride *trans* to ethylene or dimethylsulfoxide, respectively[6] (Scheme 1.4).
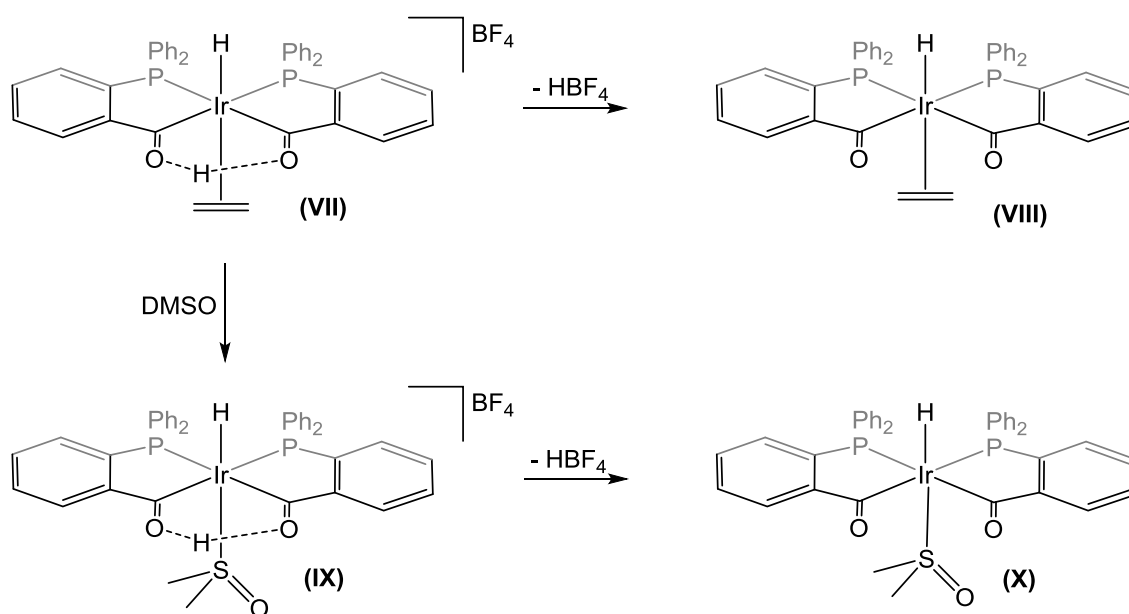
Scheme 1.4 Deprotonation of cationic hydridoirida-β-diketones maintaining a PCCP planar fragment.

When [IrHCl{(PPh$_2$(*o*-C$_6$H$_4$CO))$_2$H}] (**1**) is reacted with halide scavengers containing noncoordinating anions such as AgBF$_4$, Et$_3$OBF$_4$ or Et$_3$OPF$_6$ and a Ir/scavenger ratio of 2:1 is used, only half of the chlorine atoms are lost and the compound [{IrH[{PPh$_2$(*o*-C$_6$H$_4$CO)}$_2$H]}$_2$(µ-Cl)]X (X = BF$_4$ or PF$_6$) (**XI**) is formed.[5] Complex **XI** is a cationic dimer which contains two hydridoirida-β-diketone fragments bonded by a chlorine atom bridge.
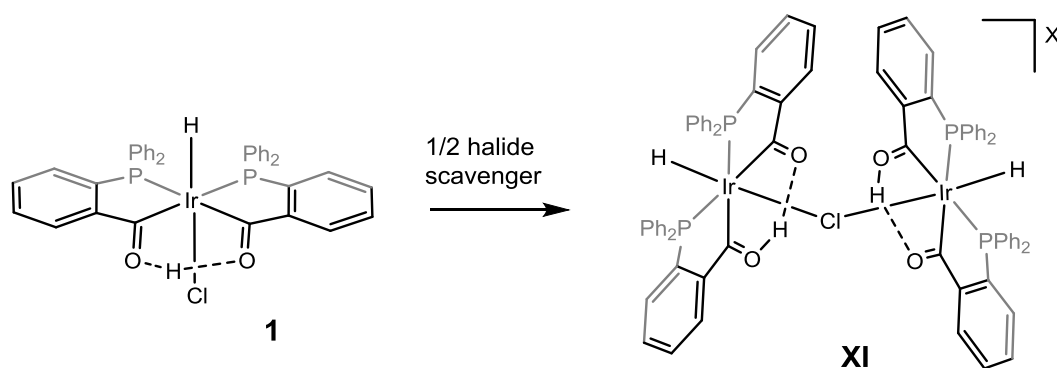
Scheme 1.5 Formation of a dinuclear hydridoirida-β-diketone, complex XI.

The reactions of complex **1** towards bases in methanol solution have been studied. When the used base is sodium hydroxide or sodium bicarbonate and the reaction is carried out under reflux conditions a dihydridoirida-β-diketone complex [IrH$_2${(PPh$_2$(*o*-C$_6$H$_4$CO))$_2$H}], complex **2**, is obtained.[8]
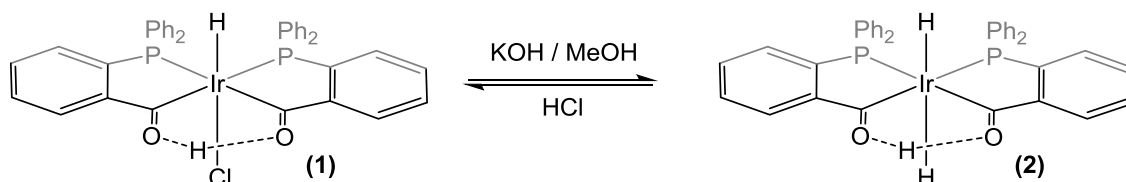
Scheme 1.6 Formation of complex 2.

This chloride / hydride exchange reaction has been proposed to occur with the solvent, methanol, being the source of the hydride, *via* methoxide coordination followed by β-H transfer.

1.1.1.1 Reactivity of irida-β-diketones towards amines or hydrazine

Hydridoirida-β-diketones have demonstrated a rich chemistry on their reactions with amines. They react with simple primary or secondary aliphatic and aromatic amines and with ammonia affording different complexes. The reaction of complex **1** with primary aliphatic amines or ammonia in dry solvents affords hydridoirida-β-ketoimines (**XII**), which are stabilised by an intramolecular N–H⋯O hydrogen bond. These hydridoirida-β-ketoimines type complexes can be hydrolysed and give hydridoamino complexes (**XIII**); which can also be obtained by reacting complex **1** with ammonia or aliphatic amines in a tetrahydrofuran and water mixture.[9,10]

On the other hand, secondary amines are not able to perform the condensation reaction in order to afford hydridoirida-β-ketoiminiums complexes (**XII**) and only hydridoamino complexes (**XIII**) are obtained (Scheme 1.7).
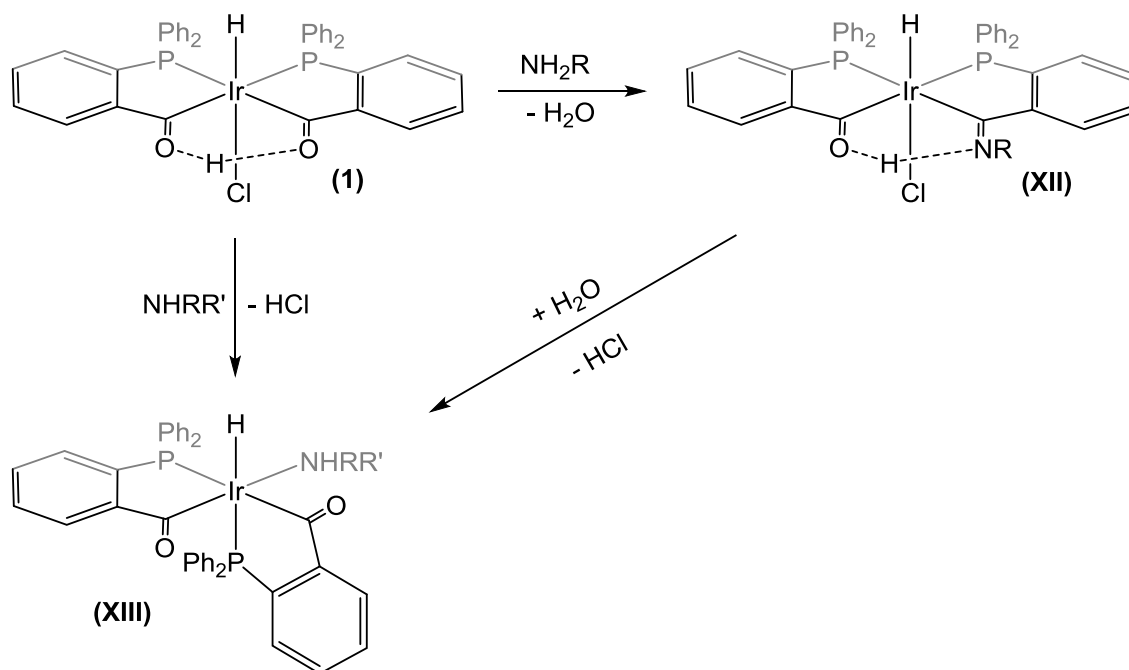
Scheme 1.7 Reactivity of complex 1 towards aliphatic amines and ammonia.

Furthermore, the reactivity of the irida-β-diketone [IrH(OClO$_3$){(PPh$_2$(*o*-C$_6$H$_4$CO))$_2$H}] (**III**) with amines and ammonia was also reported.[9] The reaction with aliphatic amines or with ammonia led to the hydridoamino complex (**XIII**). Contrarily, the reaction of complex **III** with the aromatic amine aniline, less nucleophilic, led to displacement of the coordinated perchlorate and formation of a new cationic hydridoirida-β-diketone with coordinated amine (**XIV**) (Scheme 1.8).
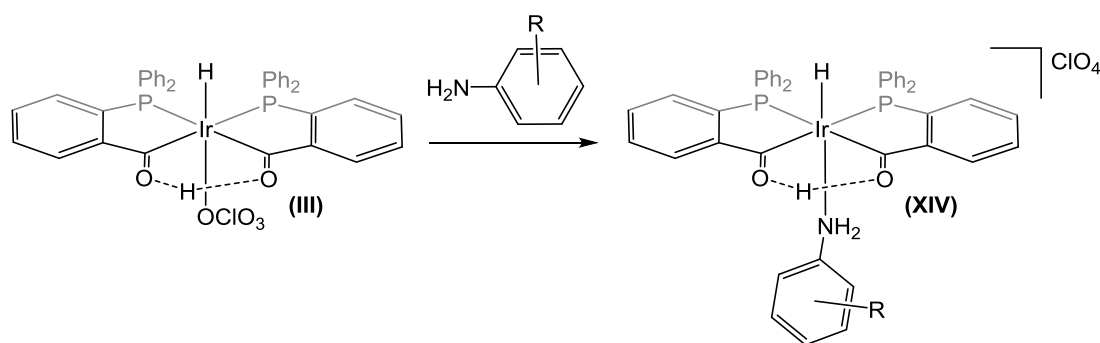
Scheme 1.8 Reactivity of complex III towards aromatic amines.

More complex 2-aminopyridines contain an amine group and a pyridine group and both groups could potentially react with organometallic compounds. Indeed, when 2-aminopyridines were reacted with complex **1** chloride complexes with a PCN terdentate ligand (**XV**) are obtained. The PCN terdentate ligand is formed by a condensation reaction of the amine group with the hydroxycarbene fragment leading to a transient aminocarbene with dangling pyridine whose coordination promotes a hydrogen transfer from the iridium to the carbon atom. Complexes **XV** are kinetic reaction products. If the reaction is carried out at higher temperature, or complex **XV** is dissolved in methanol and heated, the thermodinamically stable complex **XVI** is obtained, which has two phosphorus atoms in *trans* position (Scheme 1.9).[10]
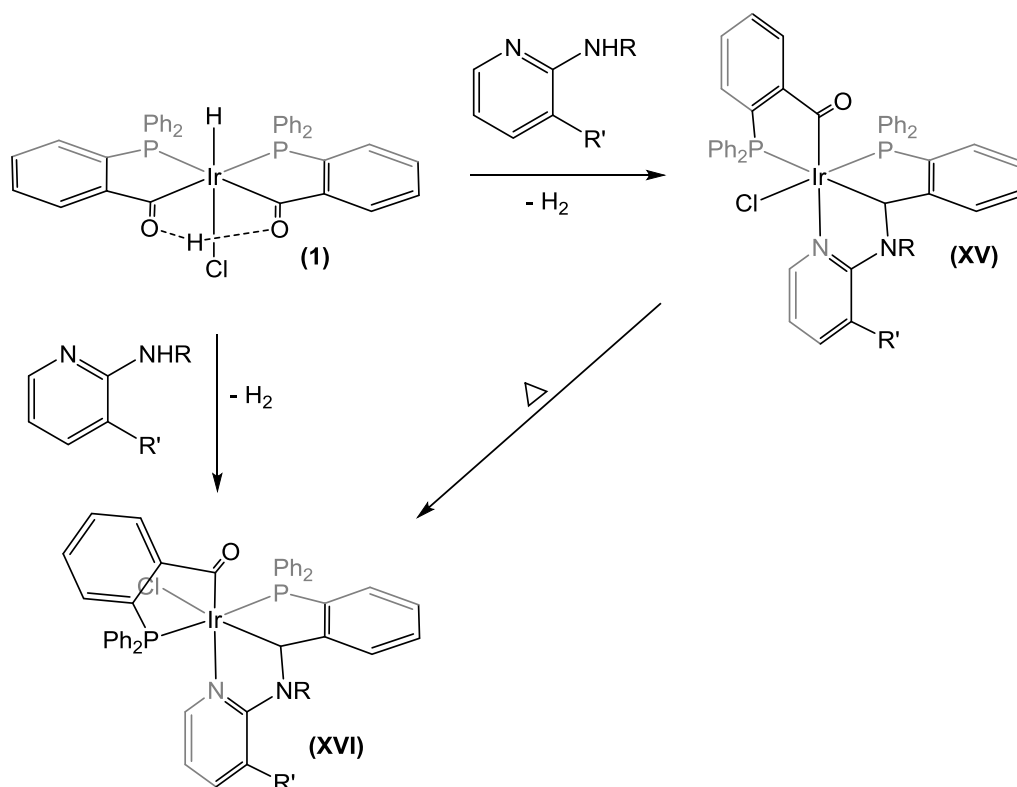
Scheme 1.9 Reactivity of complex 1 towards 2-aminepyridines.

When irida-β-diketone complex **1** reacts with potentially chelating 2-aminoalkylpyridines hydridoirida-β-ketoimines with a dangling pyridine (**XVII**) are obtained, which in protic media transform into complexes containing terdentate PCN ligands (**XVIII**) via dehydrochlorination of an intermediate iminium-acyl species. On the other hand complex **2** in protic media undergoes hydrogen evolution and affords hydrido derivatives with amino-coordinated ligand and a dangling pyridine (**XIX**) (Scheme 1.10).[11]
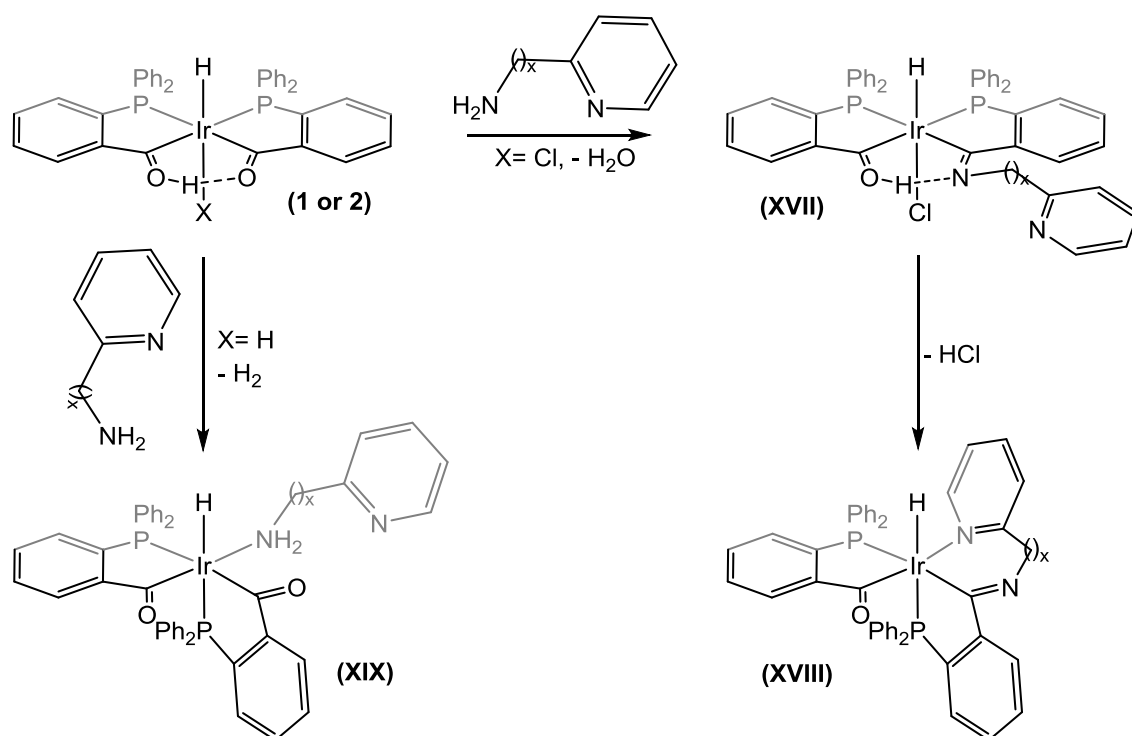
Scheme 1.10 Reactivity of complexes 1 and 2 towards 2-aminoalkylpyridines.

Finally, hydrazine has two nucleophilic nitrogen atoms that could potentially interact with the irida-β-diketone complex **1** in different ways. When complex **1** and hydrazine are mixed in tetrahydrofuran a hydridoirida-β-ketoimine (**XX**) is obtained, as it happened with aliphatic amines and ammonia,[9,10] but in this case the condensation of the second amine occurred under reflux yielding the formation of a new metallacycle (complex **3**)[12] (Scheme 1.11).
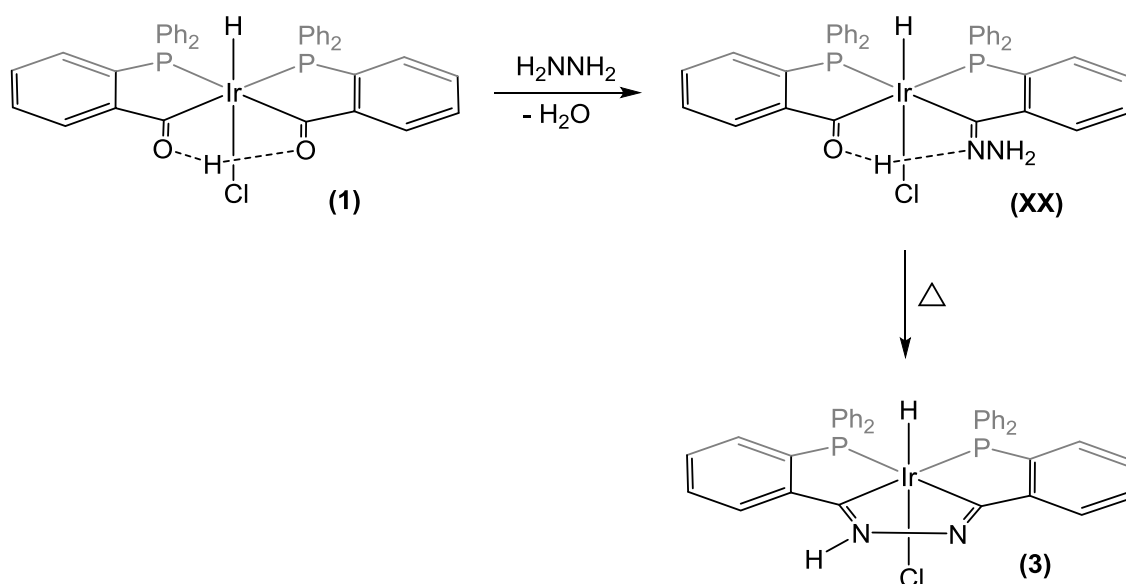
Scheme 1.11 Formation of hydridoiridapyrazole complex 3.

Complex **3**, [IrHCl{Ph$_2$P(o-C$_6$H$_4$)CNNHC(o-C$_6$H$_4$)PPh$_2$}] and the dihydrido derivative [IrH$_2${Ph$_2$P(o-C$_6$H$_4$)CNNHC(o-C$_6$H$_4$)PPh$_2$}] have been the first reported metallapyrazole compounds.[12] Similar compounds have been reported from the reaction of [Ir(F$_2$ppy)$_2$(CNAr)$_2$]PF$_6$ with hydrazine in dichloromethane[13] where the cycle is formed by the same type of atoms. However the latter are best described as Chugaev biscarbene compounds (Scheme 1.12).
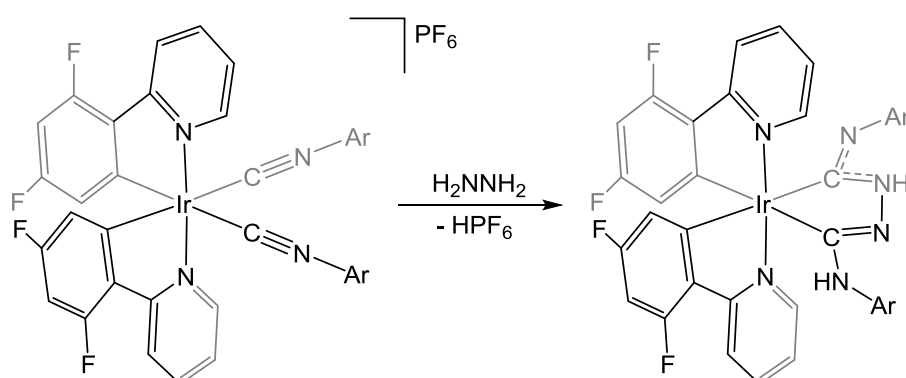
Scheme 1.12 Formation of Chugaev – type iridium carbene complexes.

Chugaev type metallacarbene complexes are bidentate acyclic diaminocarbene chelate complexes in which the carbenes are stabilised by amino groups.[14] The aforementioned iridapyrazole complexes show similar C=N bond lengths and angles to those in the organic pyrazoles whereas in the metallacycle formed by the Chugaev – type biscarbenes these structural features differ.

Several attempts to obtain similar iridapyrazole complexes were made with phenylhydrazine but unfortunately only the ketoimine type complex was achieved, the second condensation reaction did not result in the formation of the desired metallacycle.[12]

1.2 Solvolysis of ammonia-borane to release H$_2$

Hydrogen is considered one of the best candidates to replace fossil fuels for energy supply. This is the reason why the deliverance of hydrogen from chemical hydrides upon demand has been recently the subject of intensive research.[15] Its combustion reaction is not as environmentally taxing as fossil fuels are, inasmuch as there is only one by-product, water, and represents a greener energy source.[16]

Hydrogen can be produced catalytically from different sources; such as, formic acid,[17] methanol[18] and ammonia-borane (H_3N-BH_3, AB). In fact, AB presents one of the highest hydrogen contents, 19.6 wt%,[19–21] which makes this substance attractive as solid hydrogen storage material.

Ammonia- and amine-boranes can undergo hydrogen release via a dehydrocoupling reaction as shown in Scheme 1.13.

$$H_3NBH_3 \xrightarrow{\text{cat.}} H_2NBH_2 \quad + \quad H_2$$

Scheme 1.13 Catalytic dehydrogenation of AB.

This process can be homogeneously catalysed by, for example, iridium,[22,23] ruthenium,[24,25] rhodium,[26,27] iron[28] and cobalt[29] complexes (Figure 1.2), which can liberate up to 2 equivalents of H_2 per equivalent of AB. Dehydrocoupling has also been achieved using nanoparticles, obtaining more than 2 equivalents of H_2.[30–32]
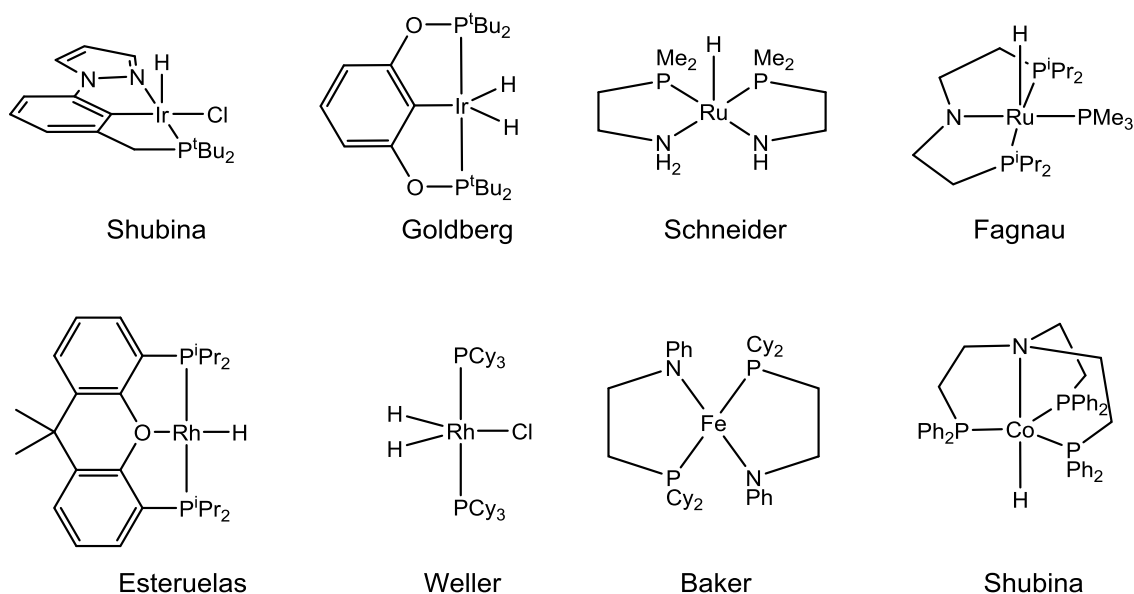
Figure 1.2 Examples of homogeneous catalysts for AB dehydrocoupling.

Another method to obtain hydrogen from AB is the metal-assisted hydrolysis[33] (Scheme 1.14). In this process the hydridic hydrogen comes from the borane moiety and the protons are obtained from water to form molecular hydrogen. Up to three equivalents of H_2 can be released with this reaction.[20]

$$H_3NBH_3 \ + \ 2\,H_2O \ \xrightarrow{\text{cat.}} \ 3\,H_2 \ + \ BO_2^- \ + \ NH_4^+$$
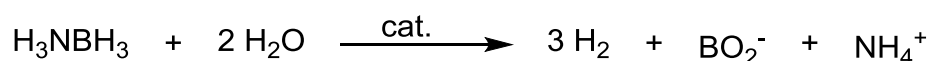
Scheme 1.14 Catalytic hydrolysis of AB.

Noble metals can catalyse this reaction heterogeneously obtaining a fast hydrogen evolution.[34,35] Non-noble metal nanoparticles are also able to carry out this catalysis, as well as combined noble- and non-noble metal containing nanoparticles.[36–42]

The first homogeneous catalyst able to perform the hydrolysis of ammonia- or amine-borane adducts was reported by our group.[9,43] The precatalysts are the described above stable hydridoirida-β-diketones complexes **1** and **2**.

The catalysis of the hydrolysis reaction of ammonia- and amine-boranes was studied and a dormant species was proposed, [IrH(PPh$_2$(o-C$_6$H$_4$CO))$_2$(NHRR')].[9,43] In this species the hydride is maintained and it has two phosphorus atoms in *cis* position and an amine group in a *trans* position.

Later on, other late transition catalysts such as iridium PNP, carbene, or hydroxy-bipyridine complexes,[44–46] acylhydrido-rhodium derivatives,[47,48] and dicarbonylruthenacyclic compounds or ruthenium-bipyridine-p-cymene complexes[49–51] proved to be efficient homogeneous catalysts for this hydrolysis reaction.

An alternative method to obtain up to three hydrogen equivalents from ammonia- and amine-borane adducts is the catalysed methanolysis (Scheme 1.15), in this procedure the hydridic hydrogens come from the borane moiety and the protons from the methanol.

$$H_3NBH_3 \quad + \quad 4\ MeOH \quad \xrightarrow{\text{cat.}} \quad 3\ H_2 \quad + \quad [NH_4][B(OCH_3)_4]$$
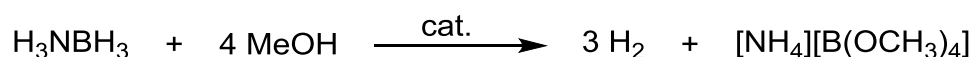
Scheme 1.15 Catalytic methanolysis of AB.

The methanolysis of ammonia- and amine-borane adducts has not been studied as deeply as the hydrolysis. Catalytic heterogeneous methanolysis

reactions usually allow slower hydrogen evolution than hydrolysis reactions and methanolysis is weight wise less desirable than the hydrolysis, however, the methanolysis has its advantages, which include higher stability of AB in methanol solution and possibility of hydrogen release below 0 ºC.[52] Also, an easy regeneration method of AB from the methanolysis product, ammonium tetramethoxyborate $[NH_4][B(OCH_3)_4]$, by a room temperature reaction has been reported.[53]

As in the hydrolysis reactions, noble metal nanoparticles are among the most active catalysts for the methanolysis of AB,[54–56] and recently homogenized heterogeneous metal nanoparticle catalysts have proved useful to achieve enhanced catalytic performance on the methanolysis of AB.[57]

The first homogeneous methanolysis of ammonia-borane was recently reported using a half sandwich ruthenium complex containing 6,6'-dihydroxy-2,2´-bipyridine ligand. This ruthenium complex showed an excellent activity represented by an initial $TOF_{10\%}$ of 448 $mol_{H_2} \cdot mol_{Ir}^{-1} \cdot min^{-1}$ or $TOF_{50\%}$ of 120 $mol_{H_2} \cdot mol_{Ir}^{-1} \cdot min^{-1}$ at 60 ºC, showing an initial activity that surpassed that of any other system known for the alcoholysis of AB, though the system suffered from deactivation at extended conversions.[58]

1.3 Objectives

Given this background, we thought that it was interesting to study the reactivity of irida-β-diketone complexes towards new ligands and the catalytic activity of the new complexes.

In this report the reactivity of $[IrHCl\{(PPh_2(o\text{-}C_6H_4CO))_2H\}]$, complex **1**, towards the furfurylamine ligand ($NH_2\text{-}CH_2\text{-}C_4H_3O$) in different conditions is studied. Furfurylamine was selected because the aminoether ligands could behave as bidentate hemilabile ligands affording suitable complexes for catalytic purposes. One of the objectives was to test whether the obtained

complexes, containing furfurylamine, improve the catalytic hydrolysis of AB for hydrogen generation.

Then, we consider that it was appropriate to study the catalytic activity of the irida-β-diketone complexes [IrHCl{(PPh$_2$(o-C$_6$H$_4$CO))$_2$H}] **1** and [(IrH{(PPh$_2$(o-C$_6$H$_4$CO))$_2$H})$_2$(μ-Cl)]BF$_4$ **7** for the homogeneous methanolysis of AB for hydrogen release. In fact, this reaction has been widely studied for heterogeneous processes but not for homogeneous ones. Besides, *in situ* NMR experiments and deuteration studies were carried out in order to understand the catalytic process.

We also found interesting the reactivity of irida-β-diketone complexes **1** and **2** towards alkyldiamines because of their potential to coordinate the metal centre in different ways and afford a wide variety of complexes that could include complexes containing bidentate N-donor ligands and complexes containing PCN terdentate ligands among others. Added to that, the catalytic activity of the new complexes for the methanolysis of AB was studied.

Finally, with the aim to study the iridapyrazole complex **3** in depth, a new synthetic route for the obtaining of the mentioned complex was proposed. After that, the reactivity of complex **3** was studied on the metal centre and on the iridapyrazole ring. Some typical organic pyrazole reactions were carried out in order to study the similarities of the metallacycle and the organic cycle.

Chapter 2

Reactivity of irida-β-diketone with furfurylamine. Characterisation and catalytic activity

2.1 Introduction

Unsaturated pincer complexes are of considerable current interest as they may lead to a variety of bond activation and catalytic processes.[59–62] Coordinatively unsaturated Ir-pincer complexes are efficient catalysts for the dehydrocoupling of amine-boranes under anhydrous conditions.[22,23] The complexes previously described in the introduction containing PCN ligands derived from aminopyridines are coordinatively saturated and inactive in the hydrolysis of AB.

With all this in mind we reasoned that aminoether ligands could behave as hemilabile ligands and afford new complexes that could be active for the catalytic hydrolysis of the borane adducts.

2.2 Synthesis of complexes

From the reaction of complex **1** with furfurylamine three different complexes were obtained depending on the reaction conditions (Figure 2.1).

The reaction of the hydridoirida-β-diketone **1** with furfurylamine in THF/H_2O leads to dehydrodechlorination and amine coordination to give complex **4**. This means that the intramolecular hydrogen bond that stabilized the structure of complex **1** is lost and the coplanarity of the phosphorus atoms and both acyl groups in the starting material disappears.[6]
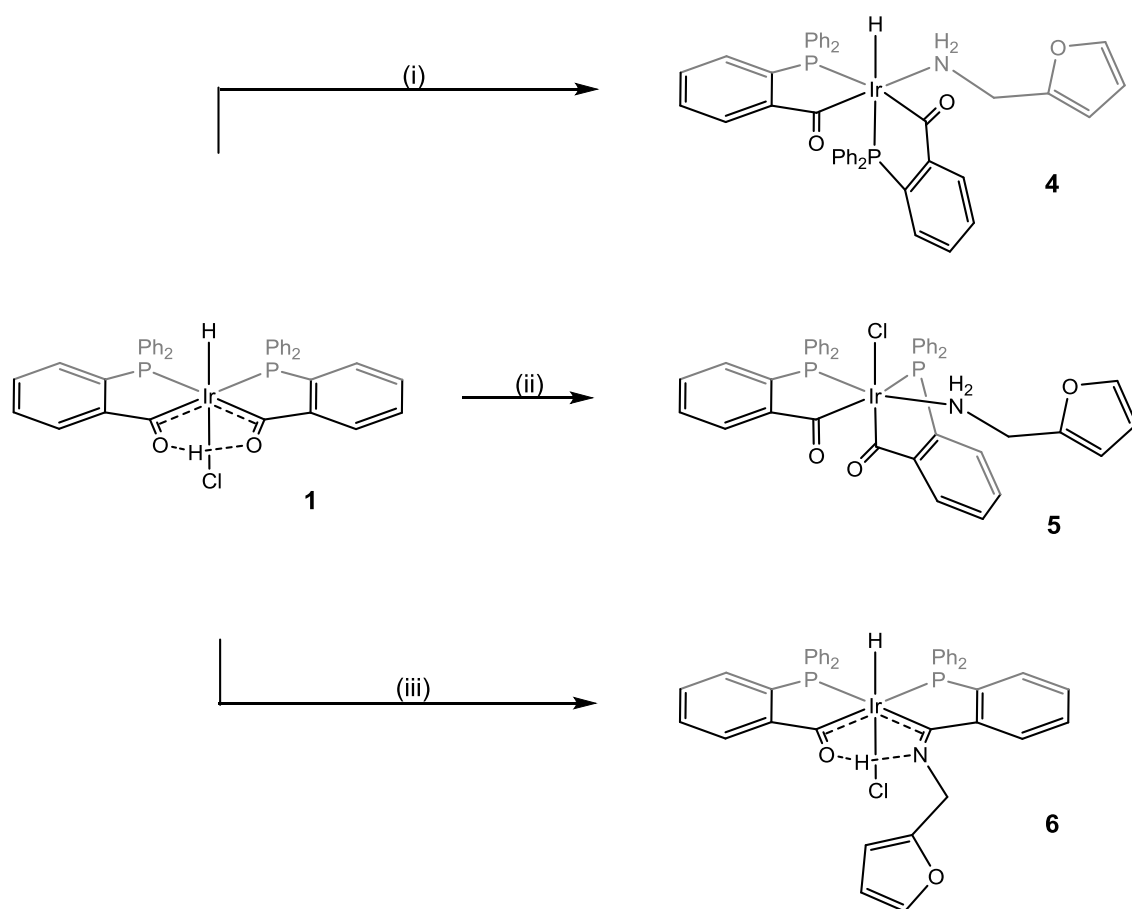
Figure 2.1 Reactivity of complex 1 with furfurylamine.

(i) THF/H$_2$O 50/50, 25 °C, 24 h; (ii) MeOH, 65 °C, 5 h; (iii) THF, 25 °C, 120 h

In addition, there is a rearrangement of the ligands around the iridium atom, and this makes the metal a stereogenic centre. While an acylphosphine ligand, the second acyl fragment and the hydride remain in their initial location, the second phosphorus atom is now in *trans* position to the hydride. This leaves the furfurylamine coordinated by the amino group in a *trans* position to an acyl group.
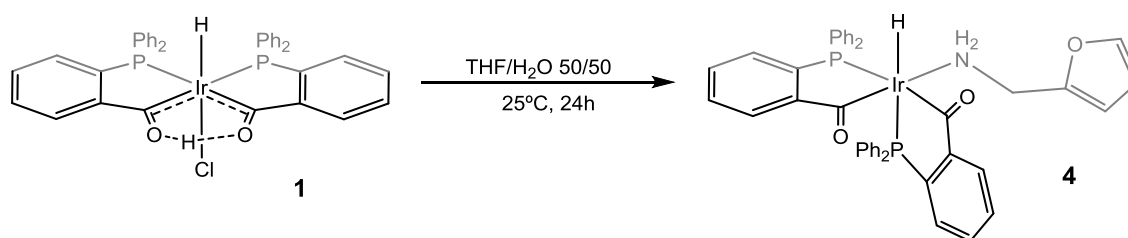
Figure 2.2 Formation of complex 4

In the ^{1}H NMR spectrum of complex **4** the signal of the hydride can be found at high field, a doublet of doublets is seen at −7.9 ppm ($^2J_{(P,H)}$ = 19 Hz and $^2J_{(P,H)}$ = 131 Hz) indicating that the hydride is located *trans* to one phosphorus atom and *cis* to another (Figure B. 1).

In accordance with this, in the ^{31}P NMR spectrum two signals can be seen, one doublet at 31.9 ppm ($^2J_{(H,P)}$ = 130 Hz), which is assigned to the phosphorus in a *trans* position to the hydride, and one singlet at 23.8 ppm that is assigned to the other phosphorus atom in *cis* (Figure B. 2).

In the ^{13}C{^{1}H} NMR spectrum the signals of both acyl groups can be found; a doublet at 233.3 ppm ($^2J_{(P,C)}$ = 105 Hz) whose coupling constant indicates a *trans* disposition of a phosphorus atom and a doublet at 212.5 ppm ($^2J_{(P,C)}$ = 5 Hz) that corresponds to the acyl positioned *cis* to both phosphorus atoms(Figure B. 3).

The IR spectrum shows the expected strong bands due to hydride and acyl groups at 2028 and 1597 cm^{-1} respectively; weaker bands due to the coordinated amine appears at 3306 and 3271 cm^{-1} (Figure A. 1).
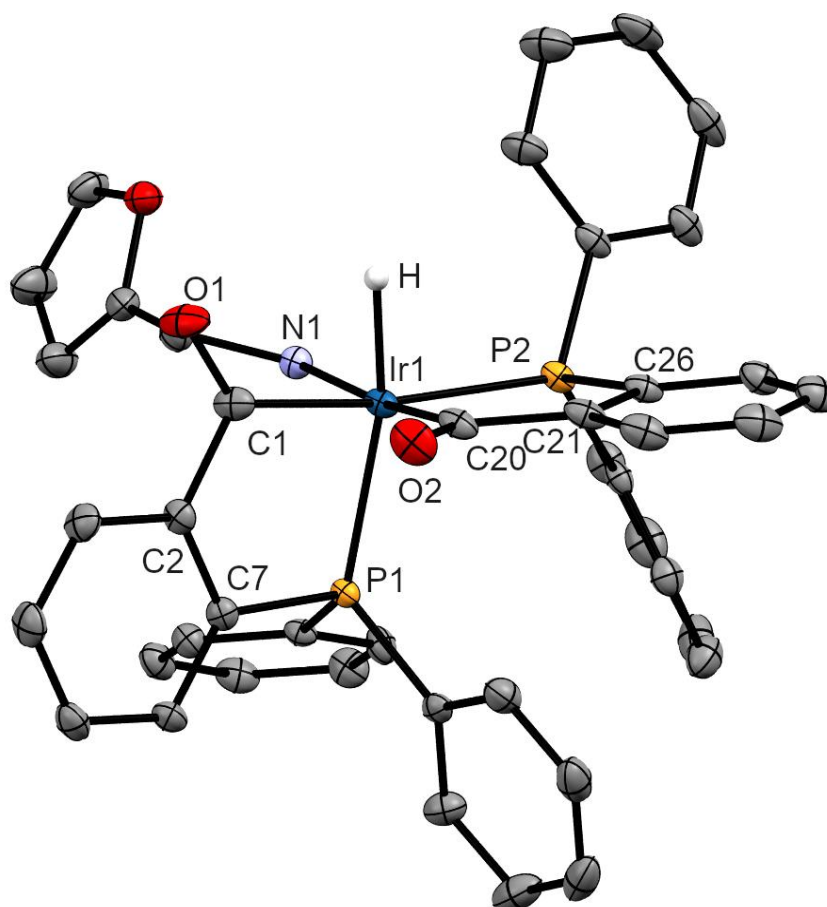
Figure 2.3 Molecular structure of complex 4 (50% probability ellipsoids)

Yellow single crystals were obtained from a DMF solution. The single crystal X-ray study of complex **4** revealed a mixture of enantiomers (Figure B. 5) and confirmed the structure proposed by NMR (Figure 2.2).

The iridium shows a distorted octahedral coordinative environment (P1-Ir-H 166.4(9)° and P1-Ir-C1 84.09(6)°). Four positions are occupied by two acylphosphine ligands and the other two by the hydride and the N-bonded furfurylamine. The bond lengths in this complex are in the expected ranges reported for similar complexes[11,63](Figure 2.3). The different *trans* influence of the phosphine and amine groups is reflected in the iridium-acyl bond lengths, being Ir-C1 significantly longer than Ir-C20 (Ir-C1 2.059(2) Å, Ir-C20 2.013(2) Å) (Table C. 1).

In a protic solvent such as methanol, and in the presence of furfurylamine, complex **1** undergoes dehydrogenation to afford complex **5** (Figure 2.4). This causes formal loss of the hydride and the keto-enolic proton to produce hydrogen and the coordination of the furfurylamine to the iridium by the amine group. Similarly to complex **4**, the loss of the enolic proton provokes the rearrangement of the atoms around the iridium centre, now placing an acyl group *trans* to the chloride ligand while the amine group binds to the coordination site left vacant.
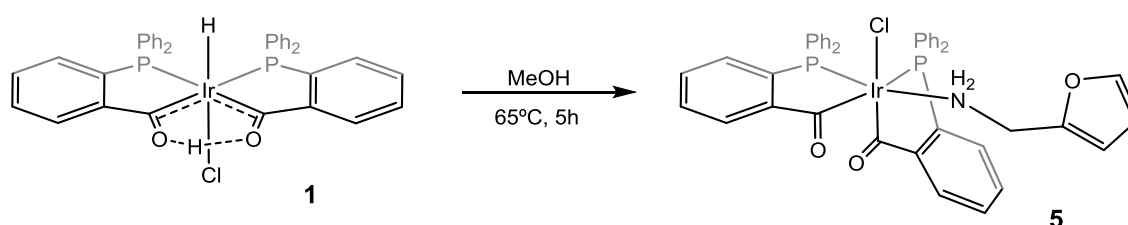

Figure 2.4 Formation of complex 5

This is revealed in the ^{1}H NMR spectrum because neither the signal of the hydride, nor the signal of the keto-enolic proton can be found, while the expected signals for the ligand are clearly observed (Figure B. 5).

The ^{31}P{^{1}H} spectrum shows two signals at 9.3 and 22.3 ppm as doublets ($^2J_{(P,P)}$ = 5.2 Hz) indicating two phosphorus atoms *cis* to each other (Figure B. 6).

In the ^{13}C{^{1}H} spectra two signals belonging to the acyl groups can be seen. One signal is a doublet of doublets at 208.3 ppm ($^2J_{(P,C)}$ = 8 Hz and $^2J_{(P,C)}$ = 2 Hz), thus this acyl group is *cis* to both phosphorus atoms. The other one is a doublet at 231.0 ppm ($^2J_{(P,C)}$=108 Hz) signalling a carbon atom *trans* to one of the phosphine groups (Figure B. 7).

In the IR spectrum a strong band due to acyl groups at 1625 cm^{-1} and a weak band due to the coordinated amine at 3297 cm^{-1} are observed (Figure A. 2).

We were able to detect complex **4** as an intermediate product during the synthesis of complex **5**. ^{31}P{^{1}H} NMR spectra of reaction mixtures during the course of the reaction showed the presence of mixtures of **4** and **5**, with increasing amounts of the latter at longer reaction times (Figure B. 11).
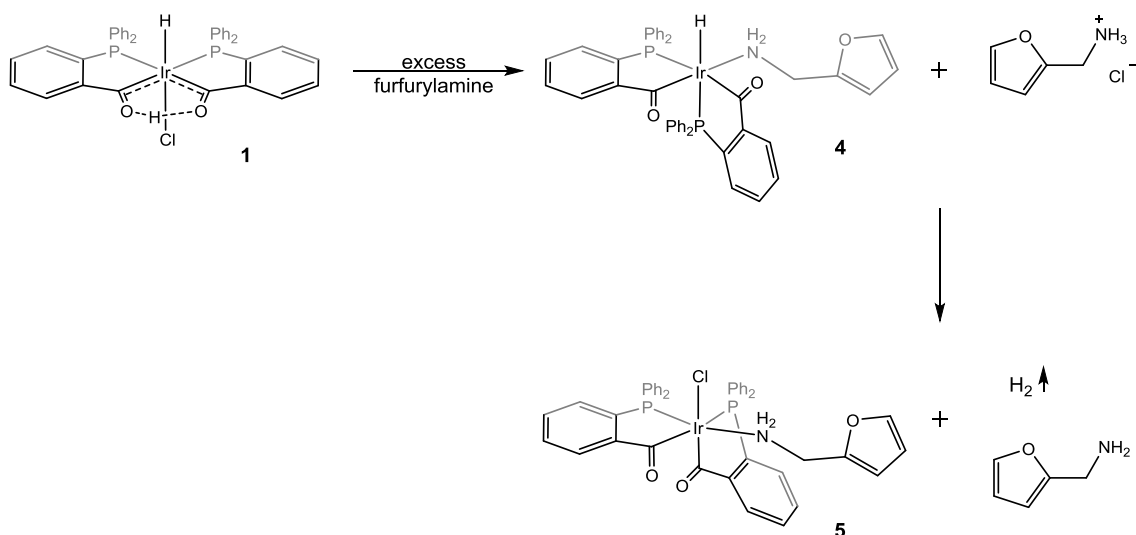
Figure 2.5 Proposed formation pathway of complex 5

This behaviour suggests a dehydrodehalogenation of **1** promoted by furfurylamine rendering the formation of hydride species **4**, from which abstraction of hydride by the methanolic proton allows coordination of the chloride ion present in the reaction environment (Figure 2.5). Iridium hydride complexes may release hydrogen upon establishment of a OH---HIr interaction.[64–66] Complex **4** presents a high tendency to exchange hydride by chloride. In chlorinated solvents, both chloroform and dichloromethane, **4** transforms readily into complex **5**.

Yellow crystals were obtained by slow evaporation of a solution of complex **5** in methanol. Single crystal X-ray diffraction studies reveal that **5** crystallises as an enantiomeric mixture (Figure C. 2) with one molecule of methanol which is hydrogen bonded to the chloride (Figure C. 3), and confirms the structure proposed (Figure 2.4).

The coordinative environment of the iridium is a distorted octahedron (P1-Ir-N1 164.93(5)° and P1-Ir-C1 83.20(5)°). Four positions are occupied by the phosphorus and carbon atoms of the bidentate ligand, the other two positions are occupied by a chlorine in a *trans* position to one acyl group and the nitrogen of the furfurylamine ligand (Figure 2.6), being all the distances in the range found for other similar compounds.[11,63]

Once again, we can relate the bond distances around iridium to the different *trans* influence of the different ligands. Similarly to complex **4**, the Ir-C bond lengths reflect the higher *trans* influence of a phosphorus atom compared to that of a chloride, Ir-C20 is 2.022(2) Å, while Ir-C1 is 2.066(2) Å. In **4**, the Ir-P distances also reflect the different *trans* influence of an acyl and an amine ligand, Ir-P1 is 2.2849(5) Å and Ir-P2 is 2.3642(6) Å (Table C. 1).
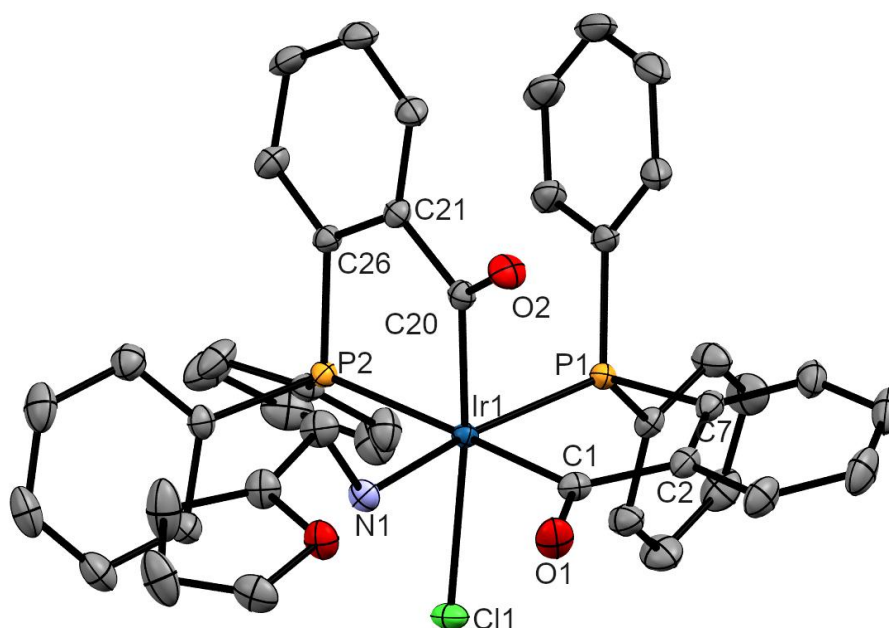

Figure 2.6 Molecular structure of complex 5 (50% probability ellipsoids)

In complex **4** these distances are much more alike, reflecting the similar *trans* influence of a hydride and an acyl. The hydrogen bond between the solvation molecule of methanol and the chloride ligand is of moderate strength,[67] with Cl···O distance 3.342 Å and the Cl···H–O angle 162.9°.
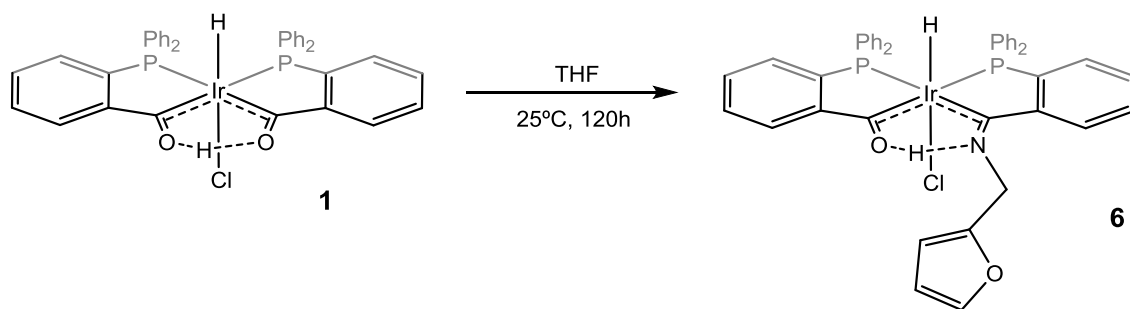

Figure 2.7 Formation of complex 6

In THF solution complex **1** reacts differently with furfurylamine, the hydroxycarbene moiety undergoes a condensation reaction to give an irida-β-ketoimine complex containing a O···H–N hydrogen bond, complex **6** (Figure 2.7). One molecule of water is released and the coordination environment around the iridium remains unmodified.

Furthermore, complex **6** is very stable and it is not easily hydrolysed to give the amino complex **4**, as observed in the case of aminoalkylpyridine derivatives.[11]

Two relevant signals can be seen in the ^{1}H NMR spectrum, the hydride and the keto-imine proton. The hydride appears as a triplet at −20.5 ppm ($^{2}J_{(P,H)}$ = 14 Hz), due to coupling to two phosphorus atoms in relative *cis* position to the hydride; the latter is a broad singlet which appears at 13.4 ppm (Figure B. 12).

In the ^{31}P{^{1}H} NMR spectrum two doublets are found at 14.8 ppm and 29.8 ppm ($^{2}J_{(P,P)}$ = 7 Hz), showing that the two phosphine groups are in *cis* position to each other (Figure B. 13).

In the $^{13}C\{^1H\}$ spectra two doublets can be seen at low field, due to the acyl and the imine groups *trans* to phosphorus atoms. One appears at 243.0 ppm ($^2J_{(P,C)}$ = 105 Hz) and the other at 223.0 ppm ($^2J_{(P,C)}$ = 102 Hz) (Figure B. 14).

In the IR spectrum the band due to the hydride, *trans* to a more electronegative atom than in the previous complexes, appears at higher frequency (2184 cm^{-1}) (Figure A. 3). The weak signal assigned to C=O and C=N groups can be seen at 1550 cm^{-1}.

Yellow crystals were obtained by slow diffusion of diethyl ether into a dichloromethane solution of **5** at −20 °C. Single-crystal X-ray analysis reveals that the complex crystallises as mixture of two enantiomers, which in the unit cell are not symmetry related (Figure C. 4).

The geometry around the iridium atom is a distorted octahedron, four positions are occupied by the P–C bonds of two bidentate ligands bonded together by an O---H---N hydrogen bond, (Figure 2.8). The other two positions are occupied by the hydride and the chlorine, in *trans* position one to the other. Both, Ir-C1 and Ir- C20 bond lengths are very similar,(Table C. 1) and together with the newly formed C20-N1 (1.300(5) Å and 1.314(5) Å) bond length are all in the expected range for this type of iridium ketoimine compound.[11]
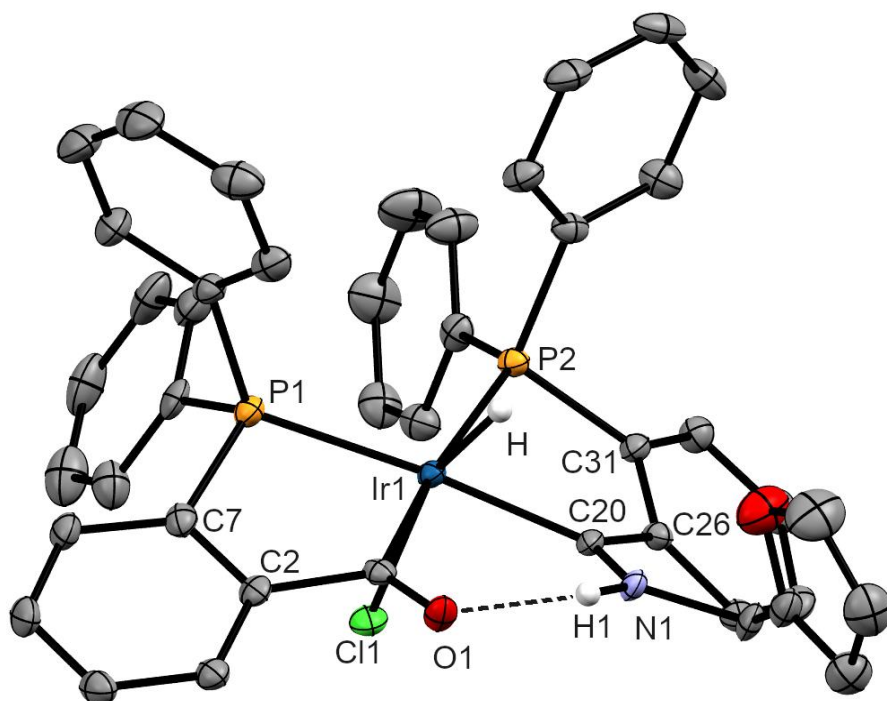
Figure 2.8 Molecular structure of one of symmetrically unrelated complexes of 6 (50% probability ellipsoids)

However, Ir-P1 and Ir-P2 are slightly dissimilar, probably due to a somewhat higher *trans* influence of the iminoacyl group compared to the acyl (Ir-P1 2.307(1) Å and 2.3106(9) Å; Ir-P2 2.3440(8) Å and 2.34406(9) Å). There is a hydrogen bond between the acyl and the imine group. The distance O1-N1 (2.683(4) Å and 2.692(3) Å) is similar to the ones found in similar compounds.[11] The angle O1-H1-N1 is 150.7° indicates that the bond is of a moderate strength.[67]

2.3 Catalytic activity

Complexes **4**, **5** and **6** are able to catalyse the hydrolysis of ammonia- and amine-boranes for hydrogen generation. This process was carried out in THF-H_2O mixtures, under mild temperatures and in the presence of air.

All the complexes were tested as catalysts for AB hydrolysis. Due to their low solubility in water, initial reaction conditions were a THF/ H_2O mixture of 80/20 and 30 °C. Complex **6** led to the slowest reaction, releasing 2.7 equivalents of hydrogen in 140 min, complex **5** needed 120 min to release 2.78 equivalents and complex **4** showed best results, by releasing 3.00 equivalents of hydrogen in 80 min (Figure 2.9).
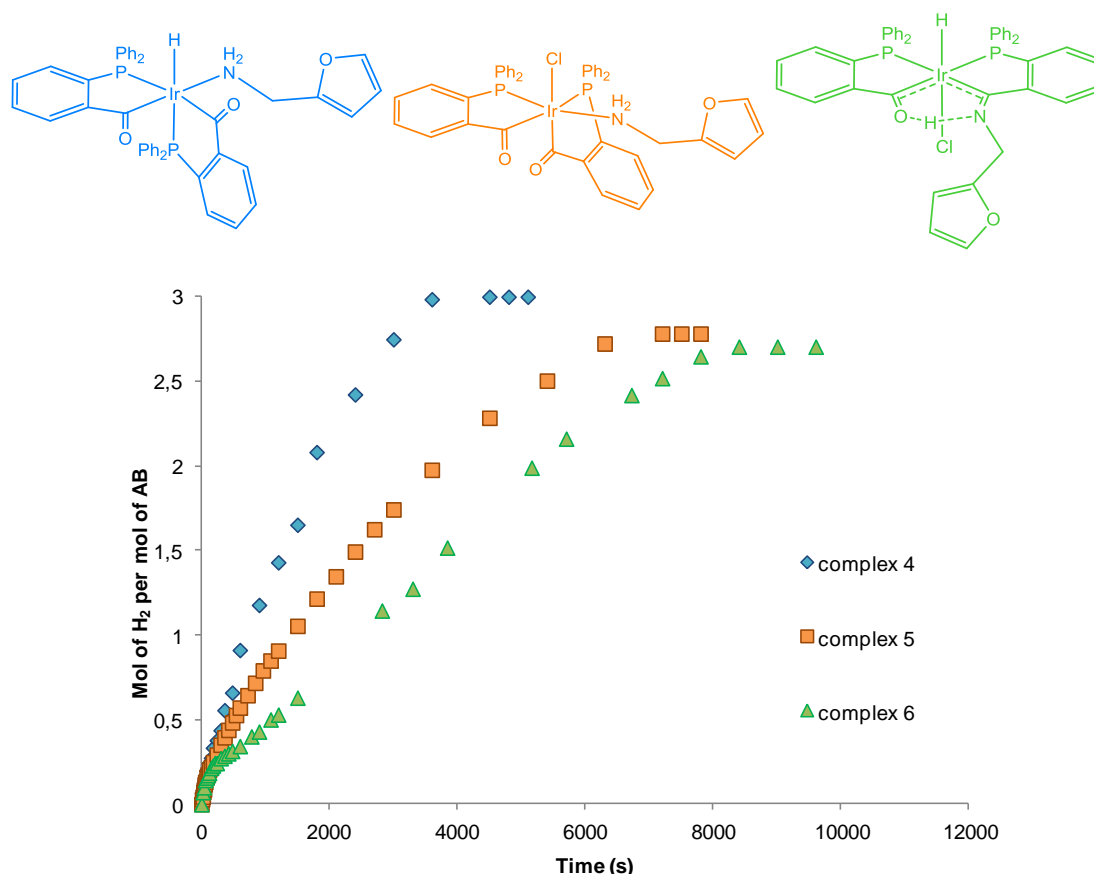

Figure 2.9 Hydrolysis of AB in THF/H$_2$O 80/20, 30 ºC and 0.6% of complexes 5 - 7.

Even though these complexes are not completely soluble in the used 80/20 THF/H$_2$O mixture, and the lack of solubility was deemed as responsible for the negligible activity of analogous aminoakylpyridine complexes, as the reaction evolves **4**, **5** and **6** are transformed into soluble species that, presumably, carry out the catalysis. Due to best results being achieved by **4** further studies were done using this complex.

Dependence of activity on the THF/H$_2$O ratio was studied and the optimal mixture was found to be 60% of THF and 40% of water. Using this ratio and performing the reaction at room temperature (24 °C), AB was hydrolysed in 70 min, while the other mixture ratios assayed rendered slower catalysis (Figure 2.10).
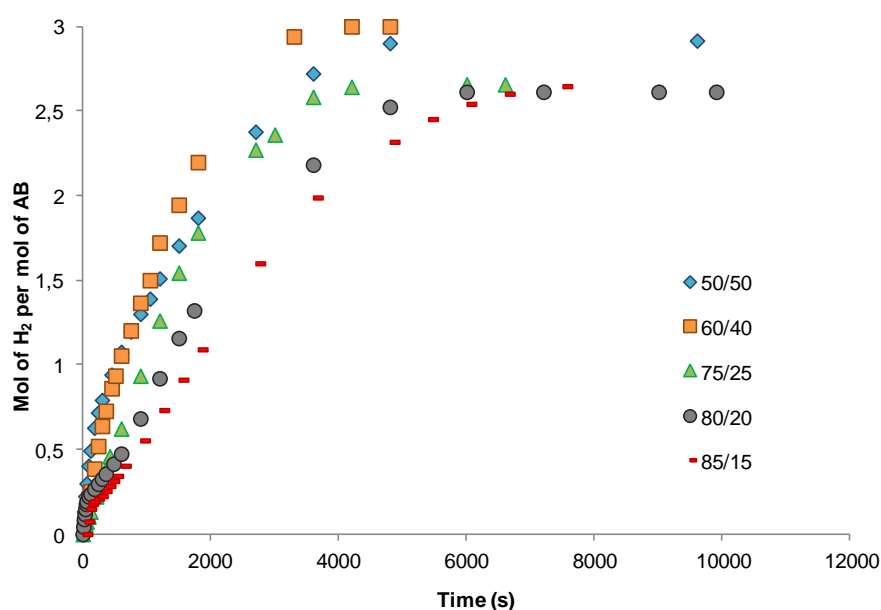
Figure 2.10 Hydrogen release in different THF/H$_2$O mixtures in the hydrolysis of AB by 0.5 % of complex 4 at 24 ⁰C

Substrate dependence was also studied at room temperature for complex **4** using a 60/40 THF/H$_2$O mixture optimised for AB. In these conditions **4** is able to completely hydrolyse dimethylamine borane (DMAB) in only 40 min, therefore faster than AB as it was the case for complex **1** (Figure 2.11).

The more hindered substrate, tert-butylamine borane (TBAB) can only release 2.8 equivalents in 120 min (Figure 2.11). Compound **4** can barely release any hydrogen from triethylamine borane (TEAB), as its parent compound **1** and related compounds.[9,43]
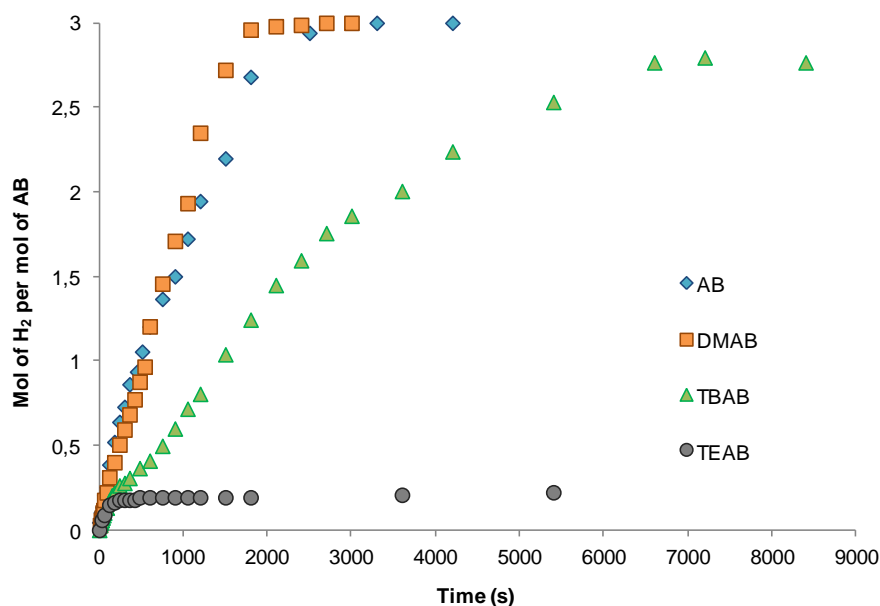
Figure 2.11 Hydrolysis of different substrates with a 0.5% mol of complex 4 in THF/H$_2$O 60/40, 24 ºC.

The catalysis of DMAB and complex **4** was studied in the presence of Hg. The same results were obtained, which supports the homogeneous nature of the catalysis (Figure 2.12).
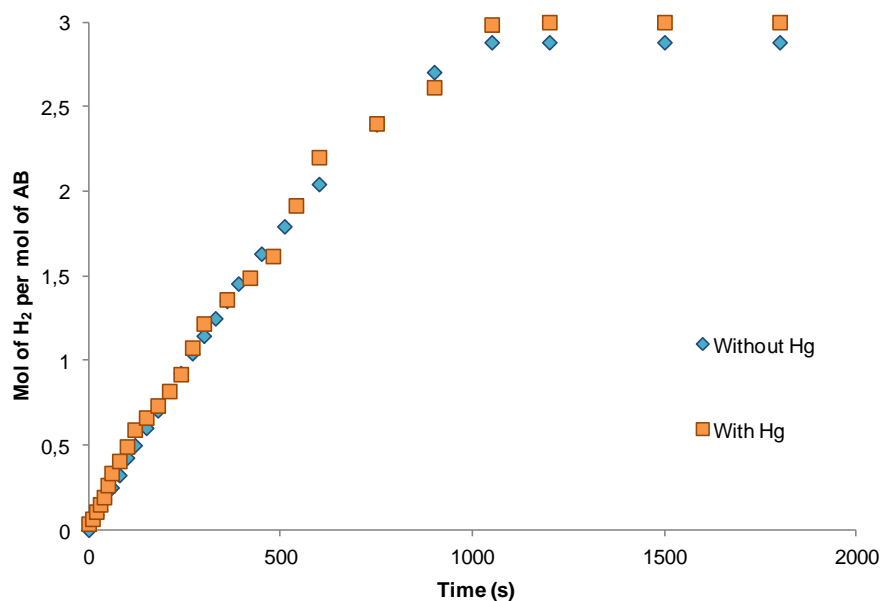
Figure 2.12 Hydrolysis of DMAB by complex 4 in presence and absence of Hg in a THF/H$_2$O 60/40 mixture at 24 ºC.

The recyclability of the catalyst in the hydrolysis reaction of DMAB was analysed (Figure 2.13). DMAB was added successively several times until 4200 equivalents of hydrogen per mole of catalyst were released. Although the reaction rate shows a slight decay, the catalyst remained active for at least 7 cycles.
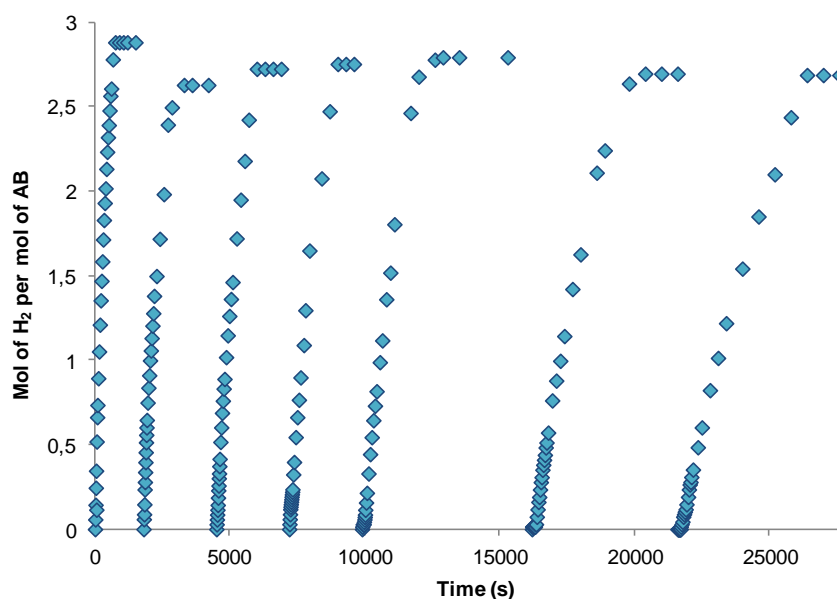
Figure 2.13 8 successive cycles of the DMAB hydrolysis reaction. 35 °C, 0.5% mol of complex 4, THF/H$_2$O 60/40

2.3.1 Study of intermediate species via *in situ* multinuclear NMR

In order to identify intermediate species involved in the catalytic reaction, *in situ* multinuclear NMR studies were carried out in a THF-d$_8$ and D$_2$O mixture, in a Young NMR tube.

The substrate first chosen was the more readily hydrolysed DMAB and catalyst **4**. Substrate disappearance can be followed by ^{11}B NMR (Figure 2.14) and even though only one type of borate can be identified at the beginning of the reaction, signals due to different borates can be seen in the latter stages (Figure B. 17). Equilibrium and rapid exchange between different borate species is frequently observed.[68–70]
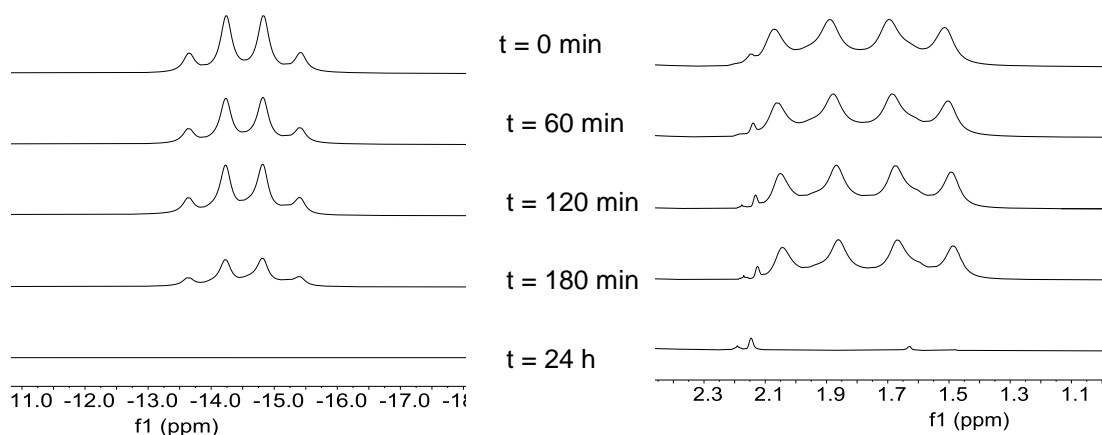
Figure 2.14 ^{11}B (left) and BH$_3$ region of ^{1}H spectra (right) of the disappearance of DMAB in the hydrolysis of DMAB by **4** in a THF-d^8/D$_2$O 60/40 mixture

The same occurs when the catalysis is followed by ^{1}H NMR, no other borane species can be detected and only the disappearance of DMAB can be observed (Figure 2.14), as plentiful release of hydrogen occurs.

Regarding the catalyst, this is only soluble in the presence of substrate, the ^{1}H NMR shows a doublet of doublet at −7.9 ppm attributed to a soluble hydride derived from **4**, which disappears readily while two new species A and B appear (Figure 2.15).

Species **A**, showing a triplet at −9.15 ppm $^2J_{(P,H)}$ = 10 Hz along with two singlets in the ^{31}P{^{1}H} NMR at 6.1 ppm and 7.2 ppm, appears as a major product. These resonances are the same as those proposed for the resting state in the related [IrH$_2${(PPh$_2$(o-C$_6$H$_4$CO))$_2$H}] and [IrHCl{(PPh$_2$(o-C$_6$H$_4$CO))$_2$H}] catalytic cycles: a solvent containing species with a hydride *trans* to an acyl group and *cis* to two phosphorus atoms.[9,43]
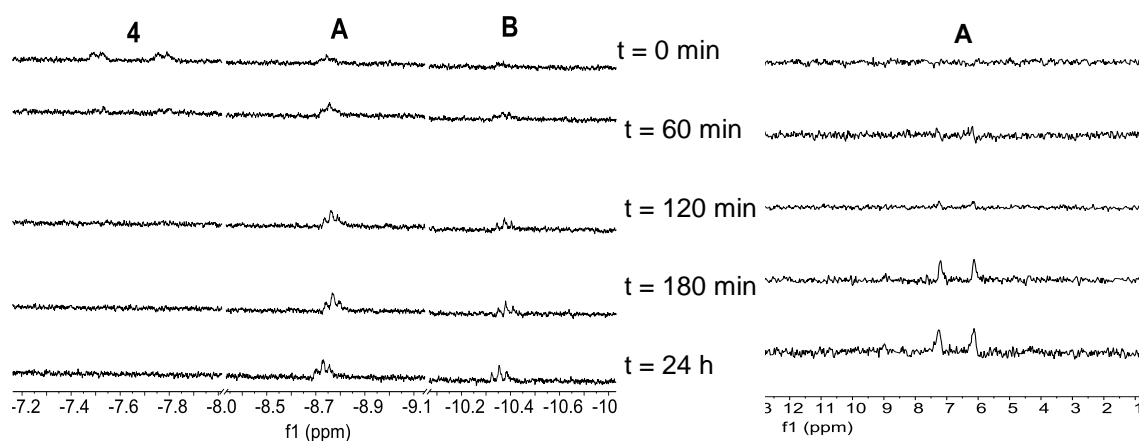
Figure 2.15 ^{1}H (left) and ^{31}P{^{1}H} (right) NMR spectra of the *in situ* DMAB hydrolysis showing the disappearance of the precursor 4 and the formation of new catalytic species

This observation suggests that the furfurylamine-iridium bond could be broken during the catalytic cycle, however the aforementioned [IrH$_2${(PPh$_2$(*o*-C$_6$H$_4$CO))$_2$H] is capable of hydrolysing DMAB in 8 min. The lower catalytic activity in the present case can be partly due to the formation of B, most likely a furfurylamine species, which shows a hydride as a triplet due to coupling with two *cis* phosphorus atoms at −10.75 ppm $^2J_{(P,H)}$ = 15 Hz. In this case no signals can be detected in the ^{31}P{^{1}H} NMR for this minor compound.

By performing the catalytic reaction in the presence of **4** and furfurylamine, a slower hydrolysis of DMAB was observed (Figure 2.16).
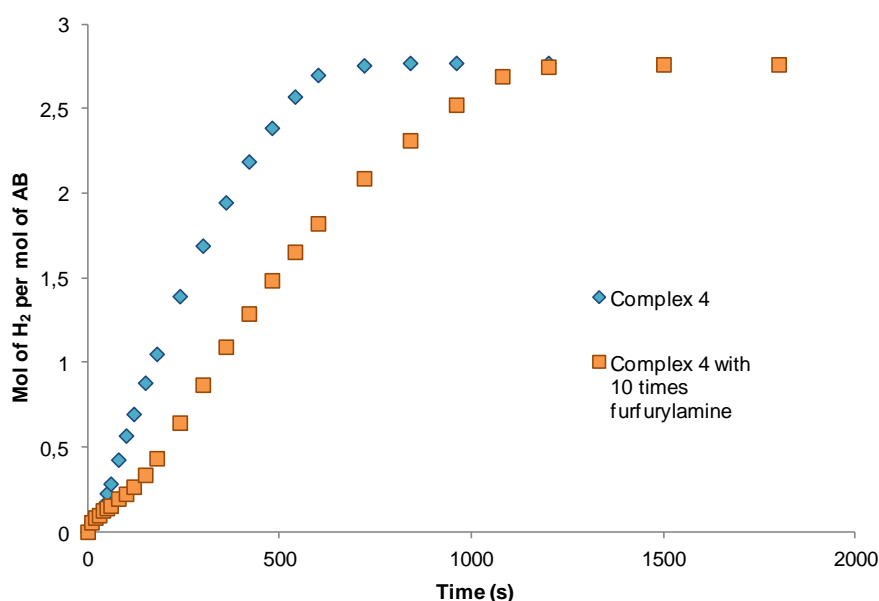
Figure 2.16 Hydrolysis in the presence and the absence of excess of furfurylamine in the hydrolysis of DMAB by 4 in a THF/H_2O 60/40 mixture at 35⁰C

When using complex **5** as catalyst, only intermediate B was observed. The hydride resonance (−10.75 ppm) along with signals due to coordinated furfurylamine and two singlets in the $^{31}P\{^1H\}$ NMR at 35.1 ppm and 30.7 ppm suggest a furfurylamine containing species with a hydride *trans* to an acyl group and *cis* to phosphorus atoms.
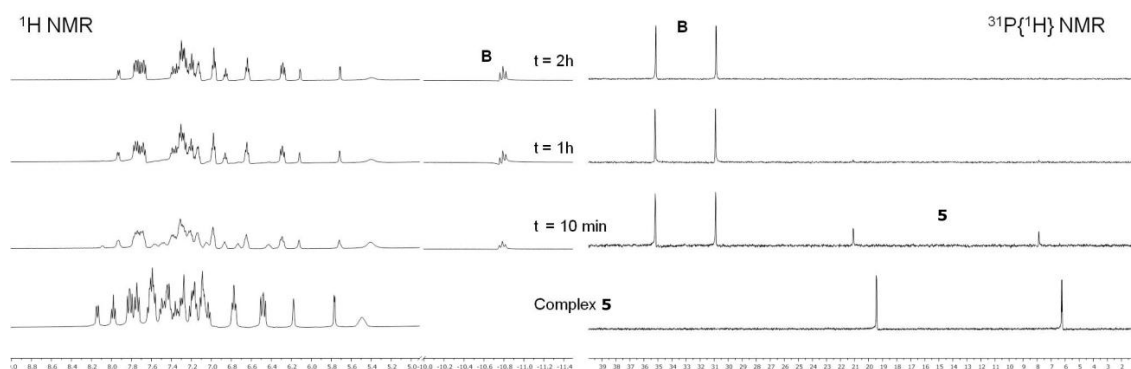
Figure 2.17 ^{1}H (left) and $^{31}P\{^1H\}$ (right) NMR spectra of the *in situ* DMAB hydrolysis showing the disappearance of the precursor 5 and the formation of species B in a THF-d$_8$/D$_2$O 60/40 mixture

Compound **6** afforded a complex mixture of species that were not able to be identified.

When using AB as substrate, the ^{1}H NMR spectrum of the hydrolytic reaction catalysed by **4** contains the same species as in DMAB hydrolysis but in this case an increasing amount of species **B** was observed. This may be responsible for the lower activity.

The hydrolysis of AB in the presence of furfurylamine with precatalyst **5** resulted in a lower reaction rate, very similar to what happened with DMAB (Figure 2.18).
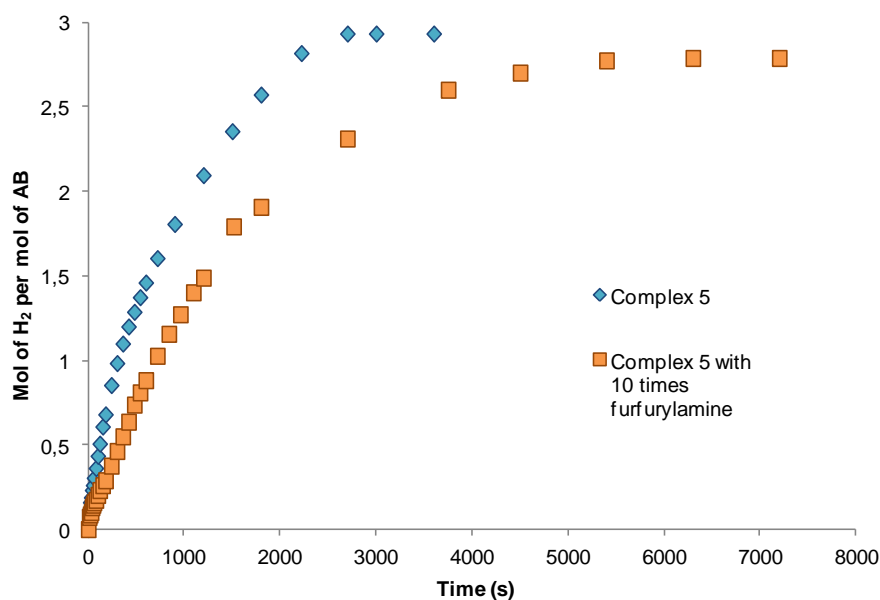

Figure 2.18 Hydrolysis in the presence and the absence of excess of furfurylamine in the hydrolysis of DMAB by 5 in a THF/H$_2$O 60/40 mixture at 35 ºC

Chapter 3

# Homogeneous Methanolysis of Ammonia-borane catalysed by Hydridoirida-β-diketones

3.1 Introduction

Irida-β-diketone complexes have proved to be efficient catalysts in the hydrolysis of AB for hydrogen release in the presence of air.[9,43] With that in mind, the methanolysis of AB catalysed by an irida-β-diketone is analysed here below. In this reaction, hydrides of the borane in the adduct combine with protons of methanol to release hydrogen with formation of $[NH_4][B(OMe)_4]$ as shown in Reaction 3.1.

$$H_3BNH_3 \;+\; 4\,MeOH \xrightarrow{\;\;cat.\;\;} 3H_2 \;+\; [NH_4][B(OCH_3)_4]$$
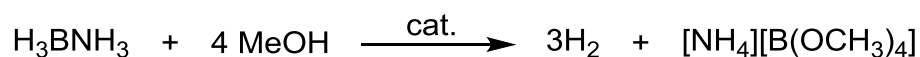
Reaction 3.1 Methanolysis reaction of AB

3.2 Catalytic activity of Chlorohydridoirida-β-diketone [IrHCl{PPh₂(*o*-C₆H₄CO))₂)H}] (1)

Complex **1** is an effective catalyst for the release of hydrogen by the methanolysis reaction of AB. With an initial AB concentration of 0.46 M and a 0.4% of catalyst loading ($1.86\cdot10^{-3}$ M), 2.7 equivalents of hydrogen are obtained after 14 min at 30 °C (Figure 3.1). At this temperature, an induction period of 120 s can be seen before the hydrogen release starts. This induction period could be as a result of the low solubility of complex **1** in methanol. When the reaction is performed at 60 °C the induction period can barely be seen, in fact it is only of 10 s, and 3 equivalents of hydrogen are released within only 2 min. The TOF values were calculated at 50% of conversion, computing time as that elapsed post-induction, resulting in values of 104 $mol_{H_2}\cdot mol_{Ir}^{-1}\cdot min^{-1}$ (30 °C) and 865 $mol_{H_2}\cdot mol_{Ir}^{-1}\cdot min^{-1}$ (60 °C), respectively.
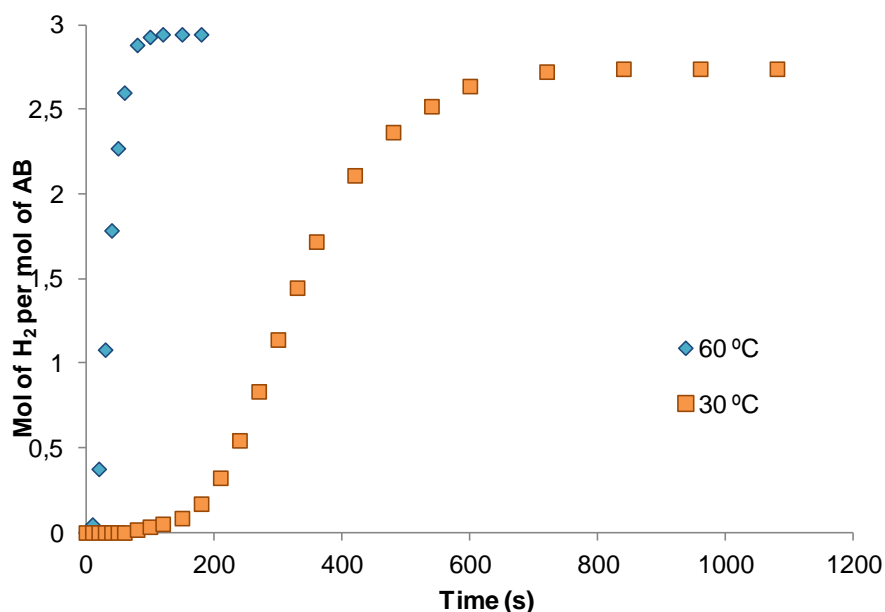
Figure 3.1 Hydrogen release from the methanolysis of AB with complex 1 as catalyst at 30 ºC (□, orange) and 60 ºC (◊, blue) in MeOH.

In order to avoid the induction period and taking into account that complex **1** is moderately soluble in the more coordinating tetrahydrofuran, an 80/20 mixture of methanol/tetrahydrofuran was used. As seen in Figure E. 1, at 60 ºC no induction period is observed in the MeOH/THF mixture and the hydrogen evolution is very similar for both solvents (only methanol and methanol/tetrahydrofuran mixture). Consequently, the use of methanol as the only solvent for these catalytic processes was decided.

The homogeneity of the catalytic reaction was proved by adding excess Hg 20 seconds after beginning of productive turnover. The results were very similar with and without the presence of Hg (Figure 3.2) and the clear yellow solution suffered no darkening proving the homogeneity of the catalysis.
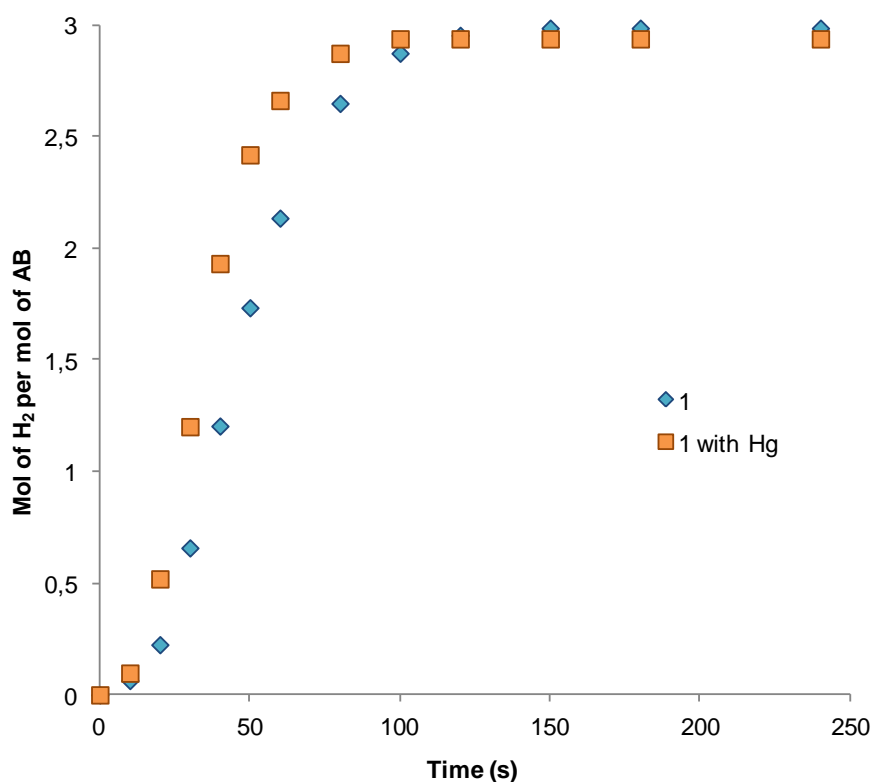
Figure 3.2 Hydrogen release from the methanolysis of AB with complex 1 without Hg (◊, blue) and with Hg (□, orange) in MeOH. T, 60 ºC.

A method frequently used to prove the involvement of nanoparticles in catalysed reactions is the addition of CS_2, which deactivates the catalyst and collapses the reaction.[54] CS_2 was added 20 seconds after the start of the catalysis to our methanolic solution that resulted in a slight slowdown (Figure E. 2). In the present case we believe that this slowdown can be due to coordination of the CS_2 molecule to the metal centre of the catalyst,[71] which can compete with the substrate in the homogeneous reaction.

Six successive runs of the methanolysis of AB catalysed by complex **1** were recorded in order to determine the recyclability of the catalyst (Figure 3.3). Even if the reaction rate shows a slight decay, the catalyst is able to release at least 4100 equivalents of hydrogen per mole of catalyst.
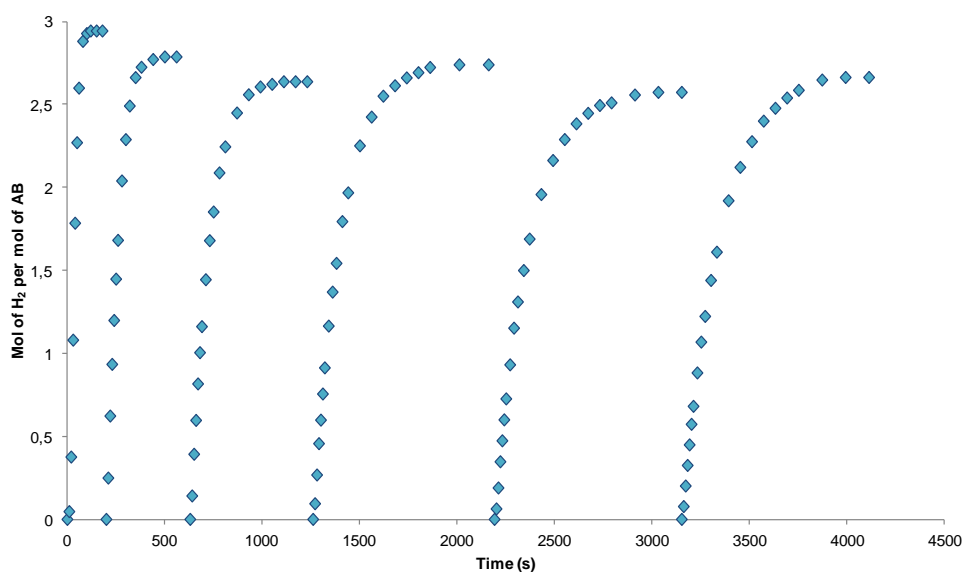
Figure 3.3 Six consecutive runs of hydrogen release from the methanolysis of AB with complex 1 as catalyst in MeOH. Solutions of AB in 0.6 mL of MeOH are used for the consecutive runs. T, 60 ºC.

The dependence of the catalytic activity on the concentration of the catalyst was the next subject under discussion. For this purpose the methanolysis of 0.46 M solutions of AB was performed with different concentrations of catalyst between $0.46 \cdot 10^{-3}$ M (0.1 %) and $1.86 \cdot 10^{-3}$ M (0.4 %) see Figure 3.4. When the lowest concentration of complex **1** is used ($0.46 \cdot 10^{-3}$ M) 3 equivalents of hydrogen are released in 360 s (6 min); while using a concentration of $1.86 \cdot 10^{-3}$ M, the highest, 150 s (2.5 min) are only needed to release the 3 hydrogen equivalents.
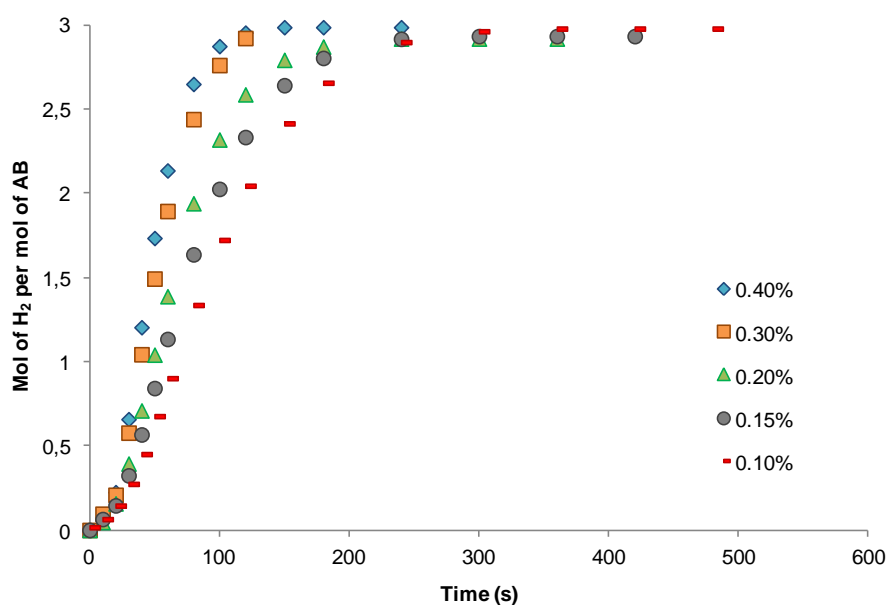
Figure 3.4 Hydrogen release from the methanolysis of AB with different loadings of complex 1: 0.40 % (◊, blue), 0.30 % (□, orange), 0.20 % (△, green), 0.15 % (○ ,gray) and 0.10 % (-, red) in MeOH. T, 60 ⁰C.

The kinetic profile obtained for these catalytic reactions can be considered to follow a pseudo-first-order reaction rate model with respect to the substrate concentration. This was applied to determine the rate constants, k_{obs}, see Figure 3.5.
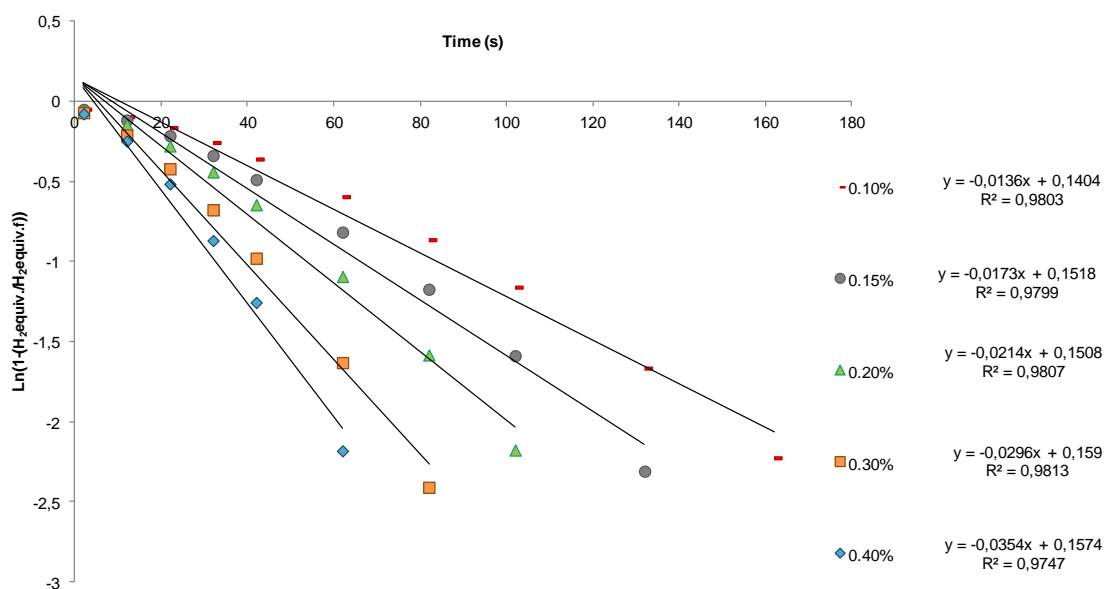
Figure 3.5 First order plots for the hydrogen release from 0.46 M AB with various [catalyst]$_0$ of 1 in MeOH: 0.40 % ($\Diamond$, blue), 0.30 % ($\square$, orange), 0.20 % (Δ, green), 0.15 % ($\circ$,gray) and 0.10 % (-, red). T, 60 ºC.

As shown by the plots above, the rate of the hydrogen release depends on the initial catalyst concentration. If a first order dependence of the rate on the [catalyst]$_0$ is assumed the rate law can be represented as:

$v_{exp} = k_{cat}$[catalyst]$_0$[substrate], where $k_{obs} = k_{cat}$[catalyst]$_0$. In Figure 3.6 the pseudo-first-order rate constants, k_{obs}, have been plotted versus the different initial catalyst concentrations; which confirms the first-order dependence on [catalyst]$_0$ and allows to determine the value of k_{cat} = 16.0 ± 0.6 M^{-1}s^{-1}. For detailed experimental data see Table 3.1
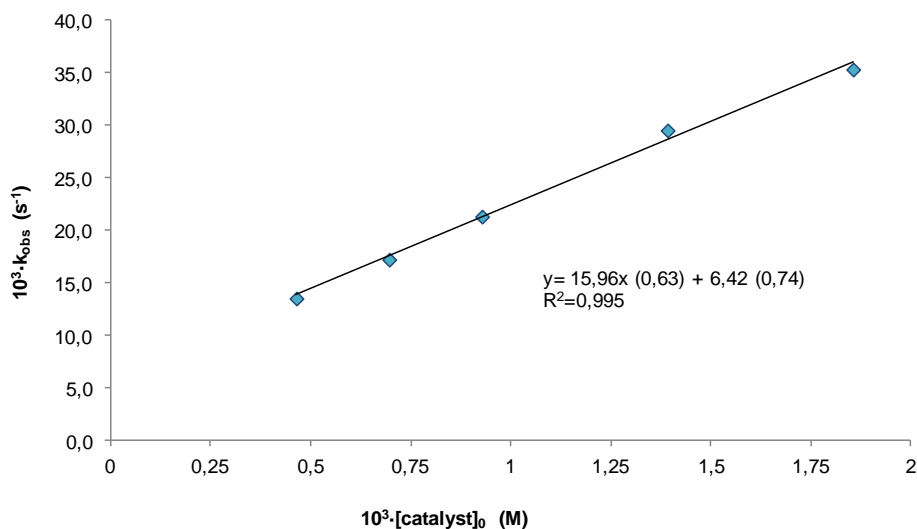
Figure 3.6 Influence of [catalyst]$_0$ on k$_{obs}$ for the hydrogen release from AB with 1 as catalyst in MeOH. Standard deviations are given in parentheses. T, 60 ºC.

Table 3.1 % Conversion, Time Required, and Rate Constants for the methanolysis of 0.46 M AB with different loadings of complex 1 as catalyst at 60 ºC.

% Catalyst	% Conversion	Time (s)	$10^3 \cdot k_{obs}$ (s^{-1})
0.10	99	360	13.6 ± 0.7
0.15	98	300	17.3 ± 0.9
0.20	97	240	21.4 ± 1.2
0.30	100	180	29.6 ± 1.8
0.40	100	150	35.4 ± 2.8

Other amineboranes such us dimethylamineborane (DMAB), tert-butylamineborane (TBAB) and triethylamineborane (TEAB) were tested for the methanolysis reaction catalysed by complex **1** in methanol and at 60 ºC (Figure

3.7). Under these reaction conditions complex **1** allows release of 2.8 hydrogen equivalents from DMAB in 100 s, showing an almost identical profile to the one observed for AB. When TBAB is used, only 2.6 equivalents are released after 180 s; this could be due to TBAB containing a bulkier substituent than the two previous substrates. TEAB behaves differently most likely due to the lack of protons in the amine group. As previously reported in the hydrolysis of TEAB with complex **1**,[43] failure of hydrogen release occurs.
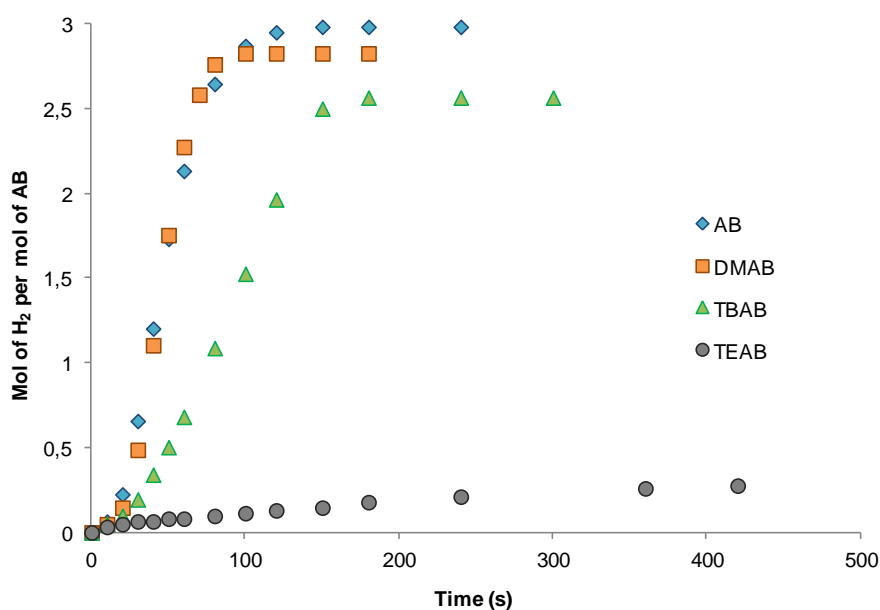
Figure 3.7 Hydrogen release from the methanolysis of different substrates: AB (◊, blue), DMAB (□, orange), TBAB (△, green), TEAB (○, gray) with complex 1 as catalyst in MeOH. Substrate concentration 0.46 M; T, 60 ºC.

Finally, the last thing to test was the viability of this catalytic hydrogen release to be carried out in other alcohols. In Figure 3.8 a comparison of the activity of complex **1** to afford hydrogen from AB in methanol, ethanol and isopropanol is represented. When using ethanol or isopropanol as solvents for hydrogen production poorer results were obtained if compared with those when using methanol; but, still 3 hydrogen equivalents are released in ethanol and 2.6 equivalents in isopropanol after 10 minutes. These results prove that is possible to perform the alcoholysis of AB in various alcohols and not only in methanol.
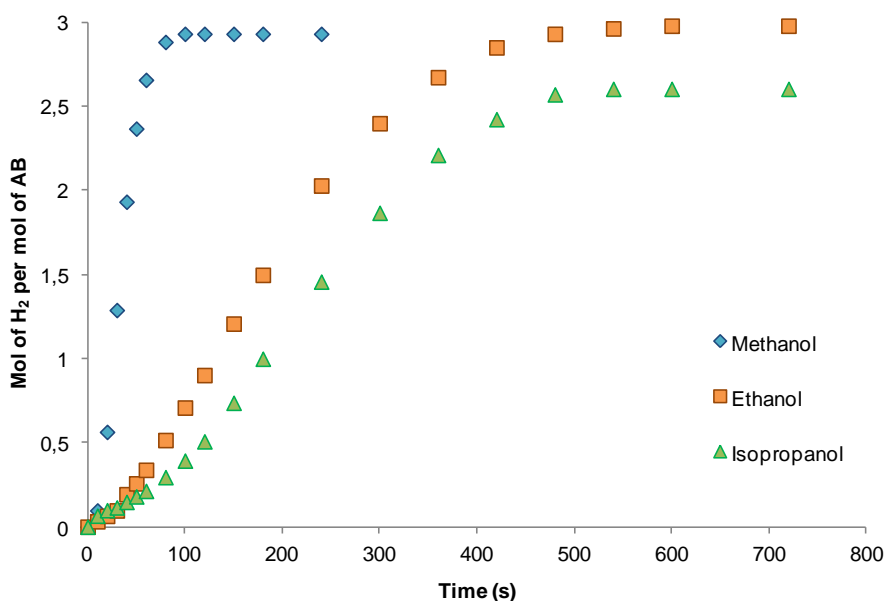
Figure 3.8 Hydrogen release from the methanolysis of AB with complex 1 as catalyst in different solvents: MeOH (◊, blue), EtOH (□, orange) and ^{i}PrOH (△, green). T, 60 ºC.

3.3 Catalytic activity of the ionic dimer [(IrH{(PPh$_2$(o-C$_6$H$_4$CO))$_2$H})$_2$(µ-Cl)]BF$_4$ (7)

As it has been mentioned in subchapter 3.1, the low solubility of complex **1** may have been the reason of the appearance of an induction period that could be seen prior to productive turnover. In order to find a methanol more soluble hydridoirida-β-diketone, the ionic dimer [(IrH{(PPh$_2$(o-C$_6$H$_4$CO))$_2$H})$_2$(µ-Cl)]BF$_4$ **(7)** was selected (Figure 3.9). Complex **7** contains two hydridoirida-β-diketone fragments which are bonded by a chloride bridge and is more soluble in methanol than complex **1**.
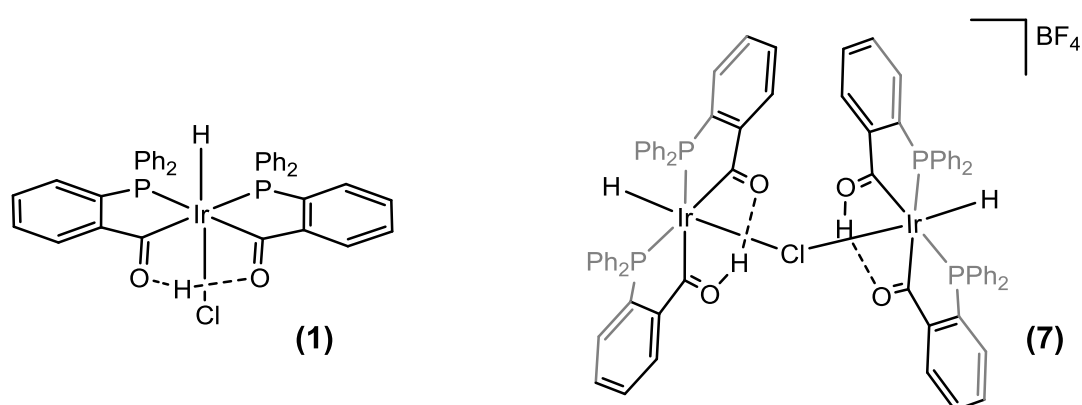
Figure 3.9 Complexes 1 and 7

Complex **7** allows fast hydrogen release from the catalysed methanolysis of AB. When an initial 0.46 M of AB in methanol and 0.2 % loading of complex **7** (0.4 % loading of iridium) are used, up to 2.8 hydrogen equivalents are released after 6 min at 30 ºC, with a TOF of 321 $mol_{H_2} \cdot mol_{Ir}^{-1} \cdot min^{-1}$ at 50 % conversion, computing time as that elapsed post-induction. An induction period of 40 s can still be observed under these reaction conditions but, much shorter than the one that appeared for complex **1** (Figure 3.10). When the reaction is carried out at 60 ºC, and under the same abovementioned conditions, 3 hydrogen equivalents are released within 80 s with an excellent TOF of 1991 $mol_{H_2} \cdot mol_{Ir}^{-1} \cdot min^{-1}$ at 50 % conversion. No induction period can be seen when the catalysis is carried out at 60 ºC with complex **7** (Figure 3.11).
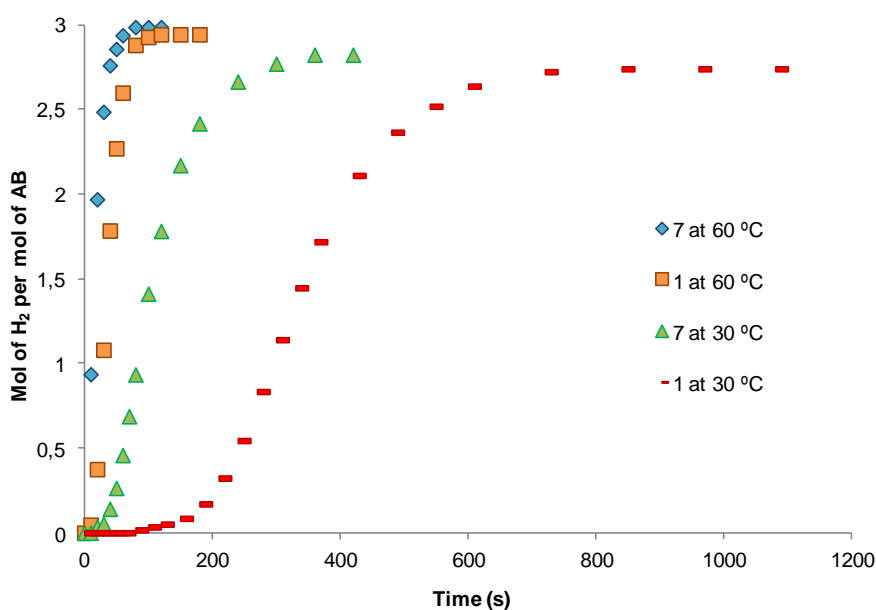
Figure 3.10 Hydrogen release from the methanolysis of AB with complexes 7 and 1 as catalyst at different temperatures: 7 at 60 ºC (◊, blue); 1 at 60 ºC (□, orange); 7 at 30 ºC (△, green) and 1 at 30 ºC (△, green) in MeOH.

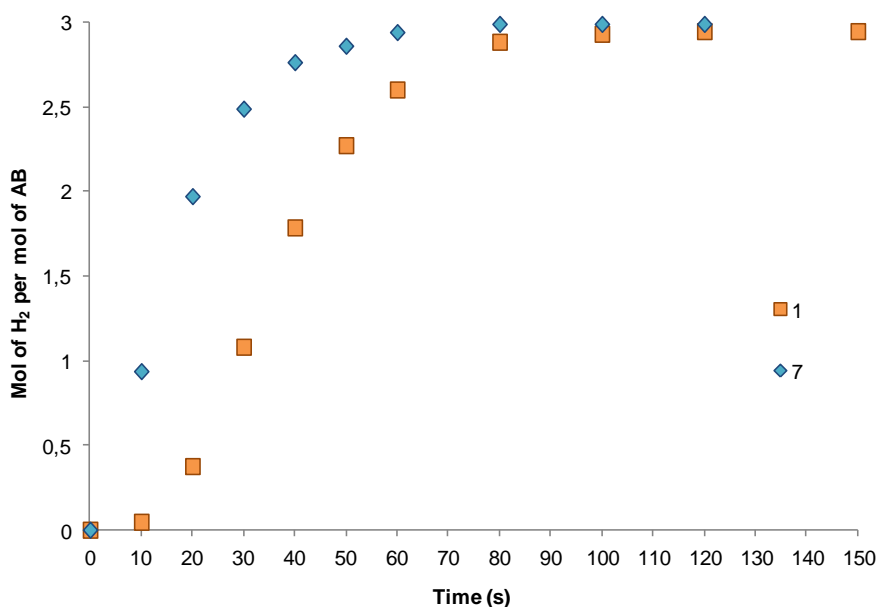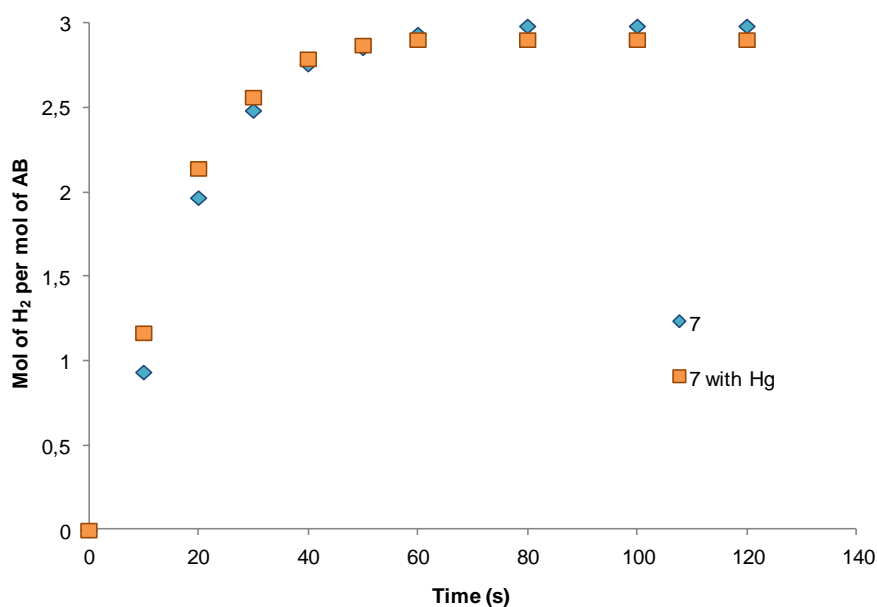**Figure 3.11 Hydrogen release from the methanolysis of AB with complex 7 (◊, blue) and complex 1 (□, orange) as catalysts in MeOH. T, 60 ºC.**

Excess Hg was added in order to prove the homogeneity of the catalytic reaction. The representations of **7** with and without the presence of Hg (Figure 3.12) are almost equal and the clear yellow solution suffered no darkening, nor appearance of any insoluble material proving the homogeneity of the catalysis.

The CS_2 method was also applied for complex **7**. The CS_2 solution was added 20 seconds after the reaction had begun, the same process that has been done with Hg, and a slowdown can be seen (Figure E. 3) probably because of the coordination of the CS_2 to the metal centre during the catalysis.

Figure 3.12 Hydrogen release from the methanolysis of AB with complex 7 as catalyst without Hg (◊, blue) and with Hg (□, orange) in MeOH. T, 60 ºC.

The activity of complex **7** was tested running six successive catalytic reactions (Figure 3.13) by adding more AB in 0.5 mL of methanol each time. Complex **7** remains active and can release at least 8300 H_2 equivalents per mole of complex **7** or 4150 H_2 equivalents per mole of Ir. Complex **7** only needs 1600 s to perform six successive catalytic reactions of the methanolysis of AB while complex **1** needs almost 4000 s to achieve the same goal.
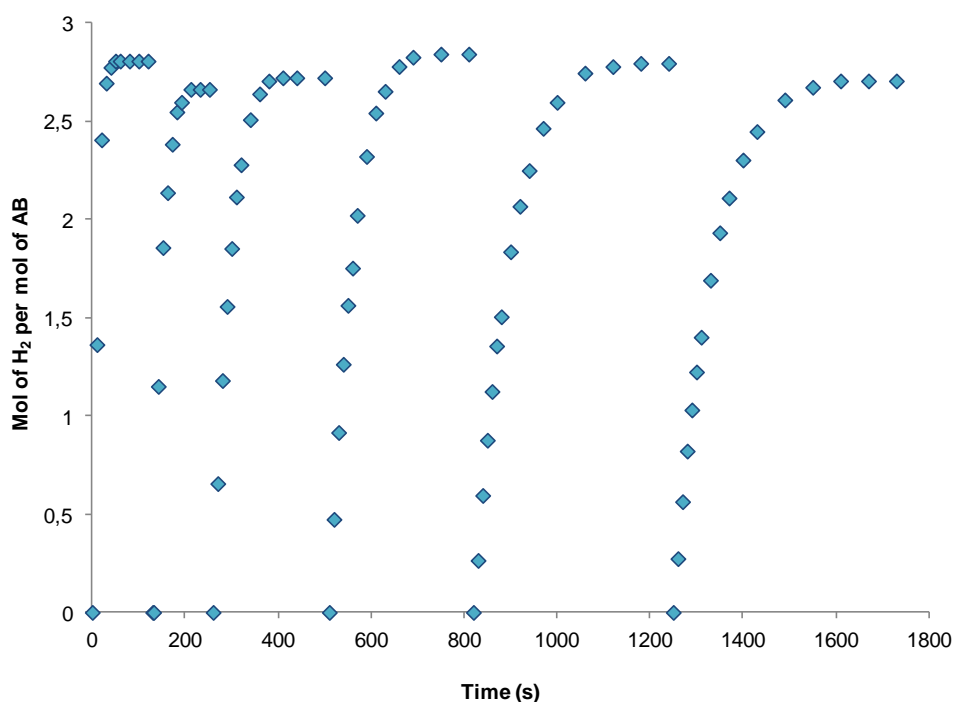
Figure 3.13 Six consecutive runs of hydrogen release from the methanolysis of AB with complex 7 as catalyst in MeOH. Solutions of AB in 0.6 mL of MeOH are used for the consecutive runs. T, 60 ºC.

For the purpose of conducting a kinetic study for complex **7**, the methanolysis of AB was performed at different concentrations of $[Ir]_0$ between $0.46 \cdot 10^{-3}$ M (0.1 % loading) and $1.86 \cdot 10^{-3}$ M (0.4 % loading) see Figure 3.14. As a dimer has been used this time, and aiming to compare these results with those of complex **1**, only half of the moles have to be used now in order to have the same $[Ir]_0$ than with complex **1**.

When the lowest concentration of $[Ir]_0$ is used ($0.46 \cdot 10^{-3}$ M) 2.9 equivalents of hydrogen are released in 240 s (4 min); while using a concentration of $1.86 \cdot 10^{-3}$ M, the highest, only 80 s are needed to release all 3 hydrogen equivalents.
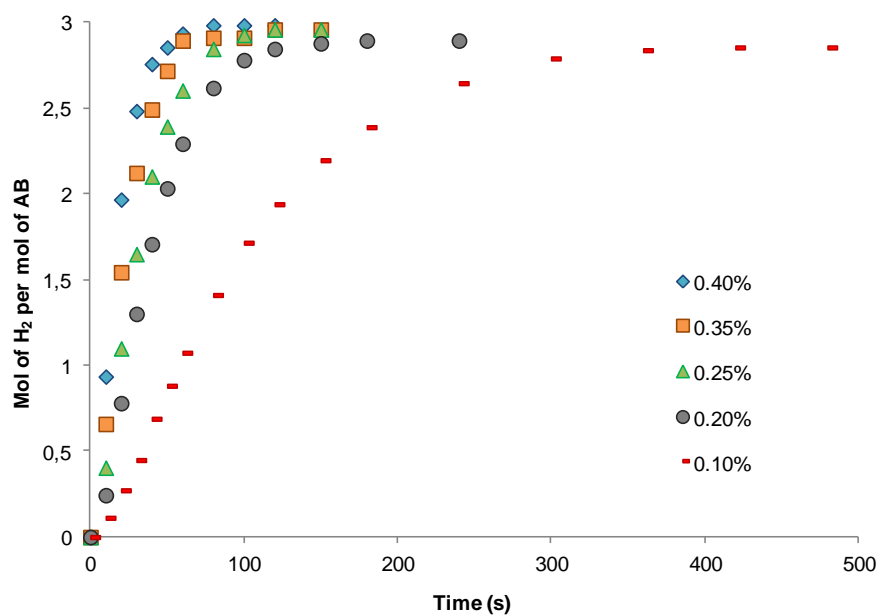
Figure 3.14 Hydrogen release from the methanolysis of AB with various [Ir]$_0$ of 7 as catalyst in MeOH: 0.40 % (◊, blue), 0.35 % (□, orange), 0.25 % (△, green), 0.20 % (○ ,gray) and 0.10 % (-, red). T, 60 ºC.

The kinetic profile seen in all the methanolysis of AB catalysed by **7** in different concentrations can be considered to represent a pseudo-first-order reaction model with respect to [substrate]. This model has been applied to determine the rate constants, k_{obs}, by plotting time versus Ln(1-(H$_2$ equiv./H$_2$ equiv.final)) Figure 3.15.
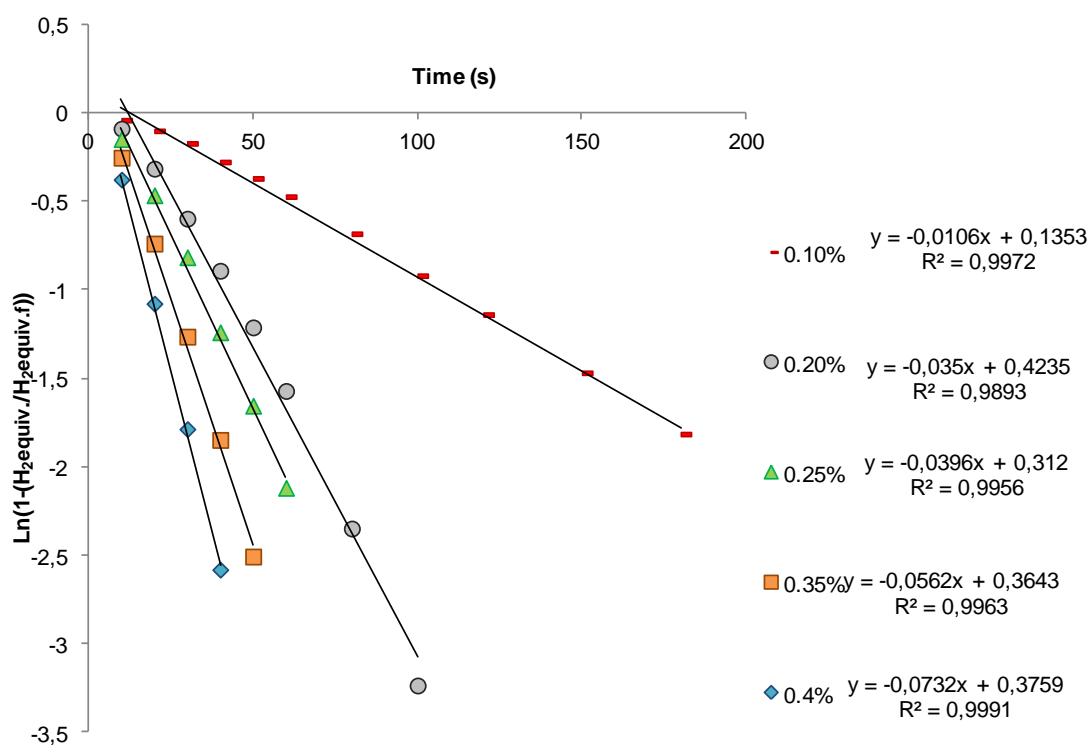
Figure 3.15 First order plots for the hydrogen release from AB with various [Ir]$_0$ of 7 as catalyst in MeOH: 0.40 % (◊, blue), 0.35 % (□, orange), 0.25 % (∆, green), 0.20 % (○ ,gray) and 0.10 % (-, red). T, 60 ºC.

Assuming, as in the previous reaction catalysed by **1**, a first order dependence of the reaction rate with respect to [catalyst]$_0$, we can apply $k_{cat}\cdot$[catalyst]$_0 = k_{obs}$. Taking this into account, a graph of the obtained values for the k_{obs} (for detailed values see Table 3.2) versus the concentrations of catalyst was plotted (Figure 3.16). This plot confirms our assumption and a value of k_{cat} = 42.0 ± 0.6 M^{-1}s^{-1} was obtained.
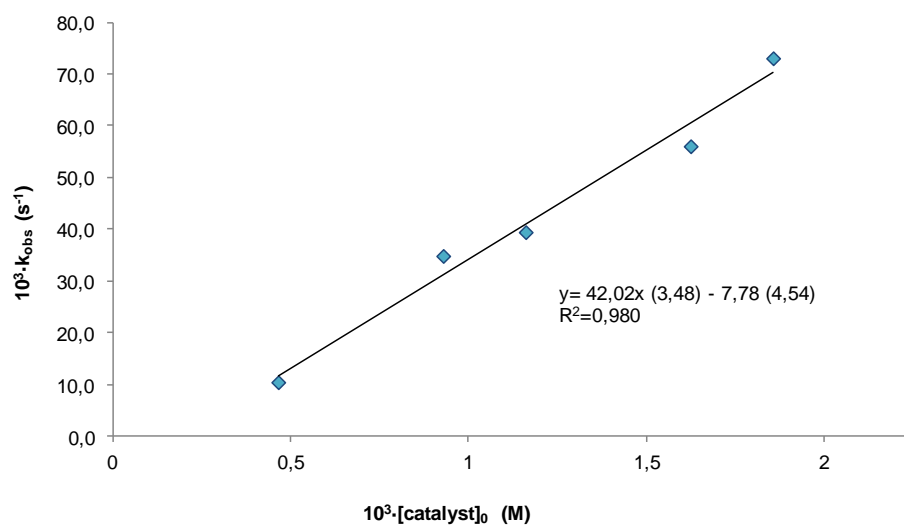
Figure 3.16 Influence of [catalyst]$_0$ on k$_{obs}$ for the hydrogen release from AB with 7 as catalyst in MeOH. Standard deviations are given in parentheses. T, 60 ⁰C

Table 3.2 % Conversion, Time Required, and Rate Constants for the methanolysis of 0.46 M AB with different loadings of complex 7 as catalyst at 60 ⁰C.

Iridium %	Conversion %	Time (s)	$10^3 \cdot k_{obs}$ (s^{-1})
0.10	95	420	10.6 ± 0.2
0.20	97	180	35.0 ± 1.5
0.25	99	120	39.6 ± 1.3
0.35	99	120	56.2 ± 2.0
0.40	100	80	73.2 ± 1.6

Along with AB, dimethylamineborane (DMAB), tert-butylamineborane (TBAB) and triethylamineborane (TEAB) have been used for the methanolysis reaction catalysed by complex **7** at 60 ⁰C. DMAB is the fastest one after AB but shows a longer induction period; with DMAB as the substrate 2.9 H$_2$ equivalents

are released after 80 s. When the substrate is TBAB 2.6 H_2 equivalents are released after 240 s (4 minutes); and finally, when the substrate is TEAB the H_2 release fails to occur.
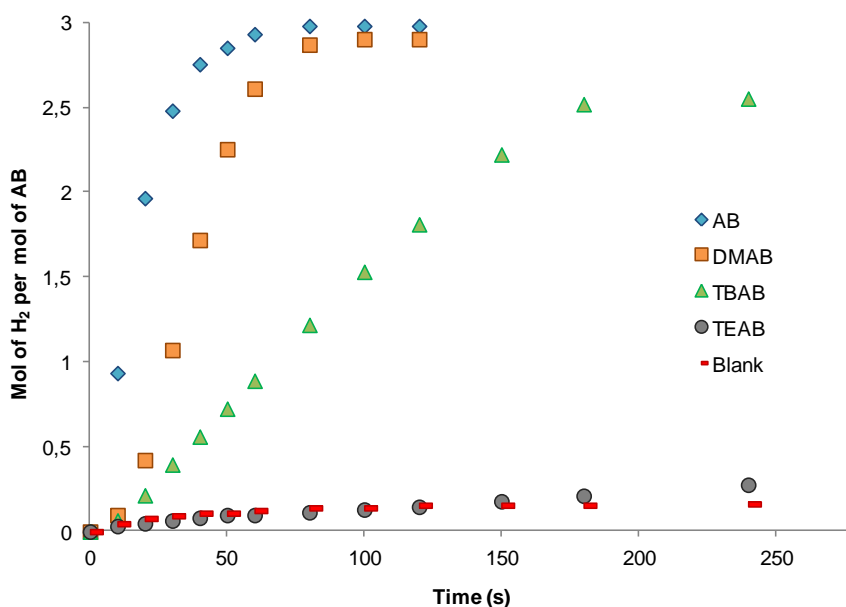

Figure 3.17 Hydrogen release from the methanolysis of different substrates: AB (◊, blue), DMAB (□, orange), TBAB (Δ, green), TEAB (○, gray), Blank test (-, red) with complex 7 as catalyst in MeOH. Substrate concentration 0.46 M; T, 60 ⁰C

Table 3.3 Substrate, % Conversion, Time Required, Induction period and TOF at 50 % for the methanolysis of 0.46 M different amineboranes with complex 7 as catalyst at 60 ⁰C.

Substrate	Conversion %	Time (s)	Induction period (s)	$TOF_{50\%}$ ($mol_{H_2} \cdot mol_{Ir}^{-1} \cdot min^{-1}$)
AB	100	80	-	1991
DMAB	97	100	10	848
TBAB	85	240	15	271

3.3.1 Deuteration studies

With the aim of obtaining more information on these catalysed AB methanolysis reactions, deuteration studies have been carried out. The performance of borane-deuterated ammonia-borane (H_3NBD_3) was compared with that of AB using complex **7** as catalyst, in methanol and at 60 ºC. The rate of hydrogen release obtained for H_3NBD_3 is almost identical to that obtained for H_3NBH_3 Figure 3.18 and a KIE of approximately 1 ($k_{H_3NBH_3/H_3NBD_3}$) was obtained, which means that cleavage of the B-H bond is not involved in the rate limiting step.
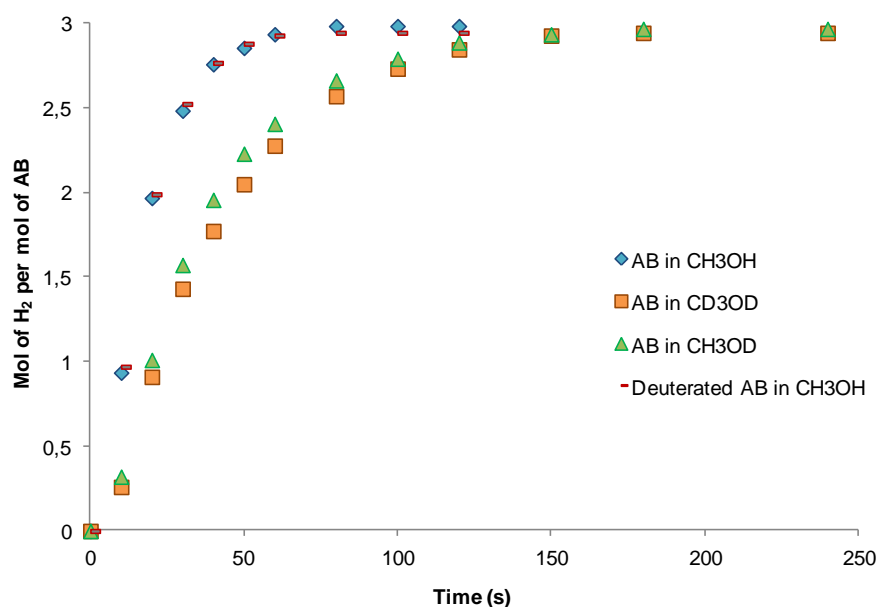
Figure 3.18 Hydrogen release from 0.46 M H_3NBH_3 solutions ($\Diamond$, blue) or H_3NBD_3 (-, red) using 0.4 mol% $[Ir]_0$ with 7 as catalyst in MeOH. Hydrogen release from 0.46 M AB solutions using 0.40 mol% $[Ir]_0$ with 7 as catalyst in CD_3OD ($\square$, orange) or CH_3OD ($\triangle$, green), at 60 ºC.

On the other hand, the methanolysis of AB catalysed by complex **7** was carried out in deuterated solvents, CD_3OD and CH_3OD. With both deuterated solvents the hydrogen release was slower than with CH_3OH, see Table 3.4 for k_{obs} values, giving KIEs of 2.60 ± 0.08 (k_{CH_3OH/CD_3OD}) and 2.44 ± 0.09

(k_{CH_3OH/CH_3OD}). Having these values in mind it can be proposed that cleavage of the O-H bond in methanol is included in the rate determining step of the catalysed reaction.

Table 3.4 % Conversion, Time Required and Rate constants for the methanolysis of AB and deuterated AB with different solvents catalysed by complex 7 at 60 ºC.

| Solvent	Substrate	Conversion %	Time (s)	$10^3 \cdot k_{obs}$ (s^{-1})
CH_3OH	H_3NBH_3	100	80	73.2 ± 1.6
CH_3OH	H_3NBD_3	98	80	80.4 ± 2.1
CD_3OD	H_3NBH_3	98	180	28.2 ± 0.2
CH_3OD	H_3NBH_3	99	180	30.0 ± 0.5

3.4 The search for intermediate species via *in situ* multinuclear NMR

Multinuclear NMR is a powerful tool to study the course of catalytic reactions and, in the present case, taking advantage of the reactions being slower in CD_3OD, afforded valuable information.

The multinuclear *in situ* ^1H, ^{11}B and $^{31}P\{^1H\}$ NMR study was first conducted on the methanolysis of AB in CD_3OD catalysed by complex **7**. The reaction was too fast; so, only the reaction products could be observed.

In the ^1H NMR, Figure 3.19, the presence of HD due to the hydrogen release, formed by combining boron hydride and CD_3OD, can be seen at 4.55 ppm (t, $J_{D,H}$ = 42.6 Hz). The singlet at 4.59 ppm corresponds to H_2 due to

unavoidable OH in the solvent. There is not a trace of the signal related to AB at 1.45 ppm (q, $J_{B,H}$ = 90.4 Hz), indicating its complete consumption.
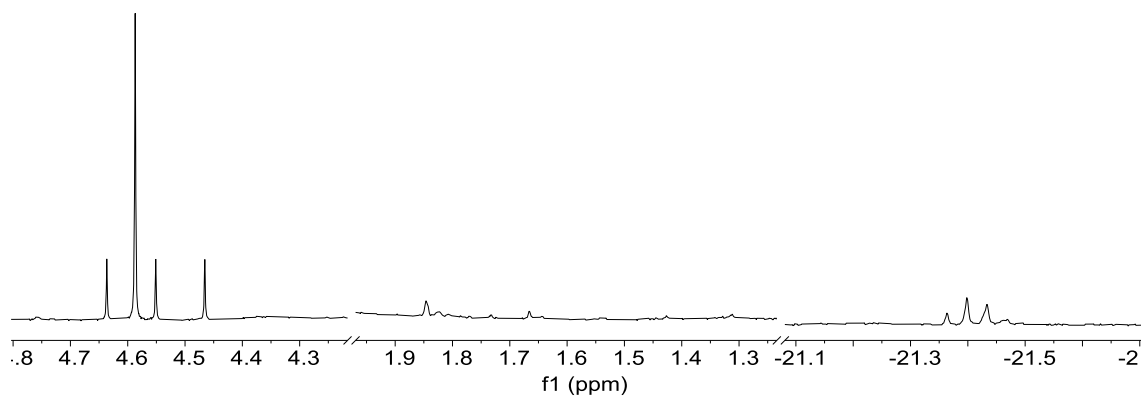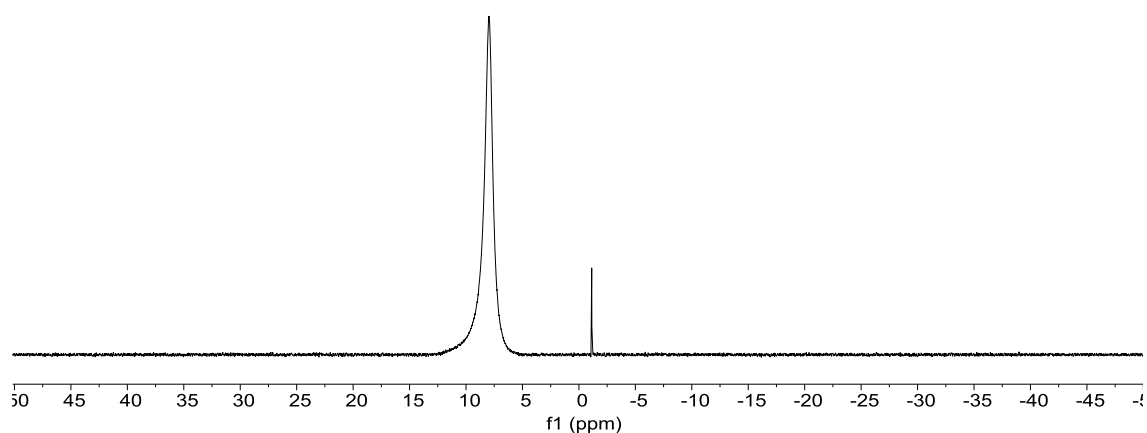

Figure 3.19 ^{1}H NMR spectrum in CD$_3$OD of the "*in situ*" methanolysis of AB catalysed by complex 7 at 25 ºC.

Two overlapped triplets appear at high field at -21.40 ppm (t, $J_{P,H}$ = 17.4 Hz) and -21.43 ppm (t, $J_{P,H}$ = 17.4 Hz) that along with the signal at 19.3 ppm in the ^{31}P{^{1}H} NMR in Figure 3.20 could belong to new iridium species. These species would contain a hydride in a *cis* position to two equivalents phosphorus atoms.
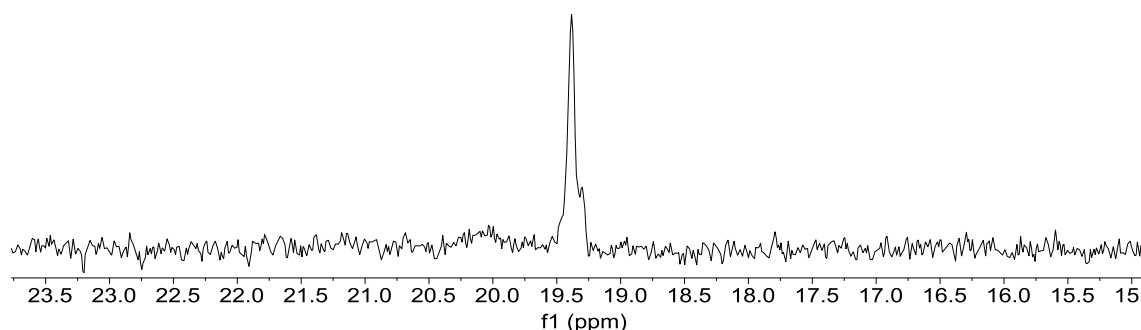
Figure 3.20 ^{31}P{^{1}H} NMR spectrum in CD$_3$OD of the "*in situ*" methanolysis of AB catalysed by complex 7 at 25 ºC

As the ^{1}H NMR, the ^{11}B NMR spectrum (Figure 3.21) contains no signal corresponding to AB (a quadruplet at -23.5 ppm). Instead, a singlet can be observed at 9.3 ppm which belongs to the product of the methanolysis of AB, the ammonium tetramethoxyborate $NH_4[B(OCH_3)_4]$.[53] This also means that all the AB has reacted. The small singlet that appears in the ^{11}B NMR, at -1.1 ppm belongs to the counterion of complex **7**, the $[BF_4]^-$ anion.

Figure 3.21 ^{11}B NMR spectrum in CD$_3$OD of the "*in situ*" methanolysis of AB catalysed by complex 7 at 25 ºC

In order to obtain more information about the mechanism, the multinuclear NMR of the *in situ* methanolysis of AB catalysed by complex **1** was carried out. As the reaction catalysed by complex **1** is slower than the one catalysed by complex **7**, intermediate species of the catalysis could be observed.

The first ^{11}B NMR spectrum (Figure 3.22) shows the signal of the substrate, AB, at -23.5 ppm (q, $J_{H,B}$ = 93 Hz), still unreacted. Another big signal in the spectrum is the singlet that appears at 9.3 ppm and belongs to the reaction product, the tetramethoxyborate $[B(OCH_3)_4]^-$. Two less intense signals can be seen, a triplet at -13.9 ppm ($J_{H,B}$ = 100 Hz) and a doublet at 5.9 ppm ($J_{H,B}$ = 120 Hz). These signals can be allocated to the intermediate adducts ammonia-methoxyborane, $H_3NBH_2(OCH_3)$, and ammonia-dimethoxyborane, $H_3NBH(OCH_3)_2$, respectively.[72]
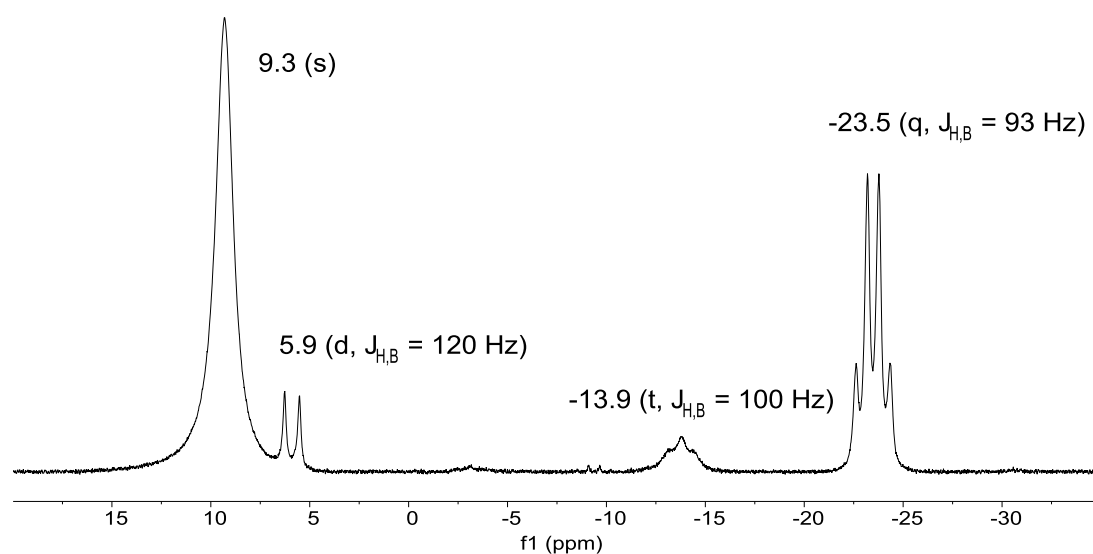
Figure 3.22 ^{11}B spectrum of AB (0.65 mmol) / complex 1 (0.006 mmol) in CD$_3$OD at t = 0.

The disappearance of AB and the increase of the tetramethoxyborate can be followed as time goes on by ^{11}B NMR (Figure 3.23). The signals belonging to the intermediate borane adducts remain in the course of the catalysis and disappear along with the substrate. These adducts can be observed again with a new addition of the substrate.
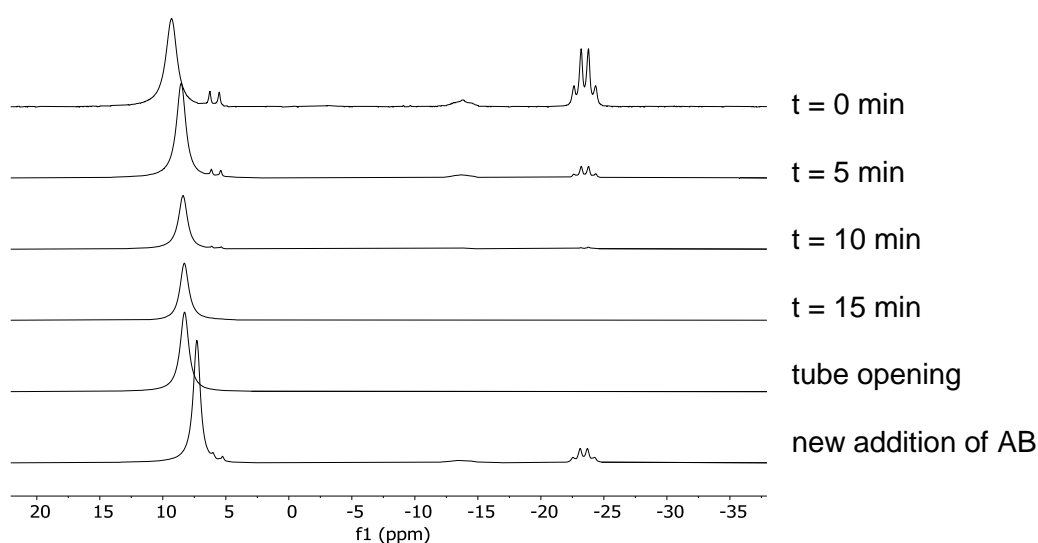
Figure 3.23 ^{11}B NMR spectra of the "*in situ*" methanolysis of AB catalyzed by 1 showing the gradual disappearance of borane adducts, with formation of methoxyborate and appearance of borane adducts upon new addition of AB.

The disappearance of the substrate can also be followed by ^{1}H NMR (Figure 3.24, left); a quadruplet at 1.45 ppm looses intensity to disappear and reappears with a new addition of substrate. The HD emergence can be observed at 4.55 ppm as a triplet with a coupling constant of $J_{D,H} = 43$ Hz.
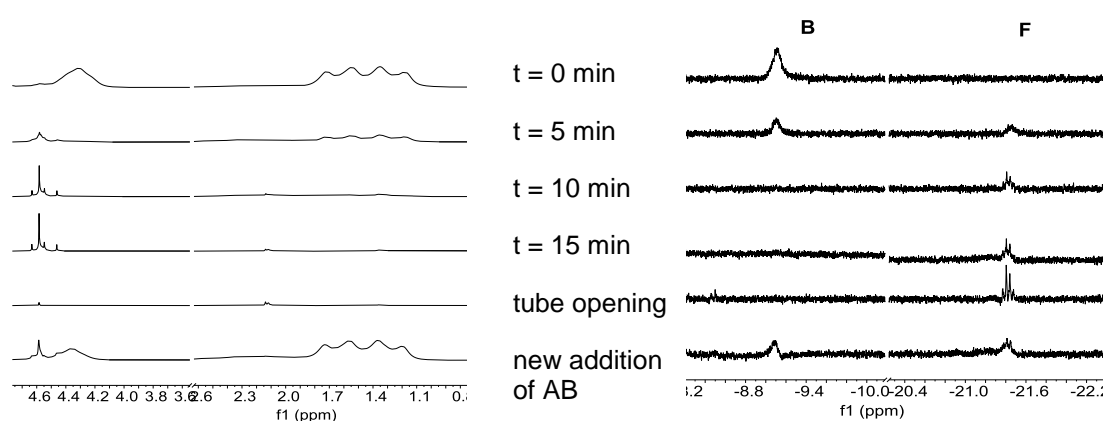
Figure 3.24 ^{1}H NMR spectra of the "*in situ*" AB methanolysis catalyzed by 1 showing release of H$_2$ and HD. Disappearance of AB (left); with formation of new iridium species (right).

The formation of new iridium species that contain a hydride is observed at high field in the ^{1}H NMR spectra (Figure 3.24, right) and in the ^{31}P{^{1}H} NMR spectra (Figure 3.25). In the early stages of the catalysis a new iridium species (**B**) can be detected as broad signals appearing at -9.15 ppm in the ^{1}H NMR and at 5.5 ppm in the ^{31}P{^{1}H} NMR. These signals are similar to the ones reported for the hydrolysis of AB catalysed by complex **1**,[43] and they belong to an iridium species which contains a hydride in a *trans* position to an acyl group and in a *cis* position to both phosphorus atoms.

The species observed at the beginning of the catalysis disappears and gives way to the emergence of the species that have been previously seen as final products in the methanolysis of AB catalysed by complex **7**. After adding more AB to the catalysis hydrogen evolution and **B** appear again.
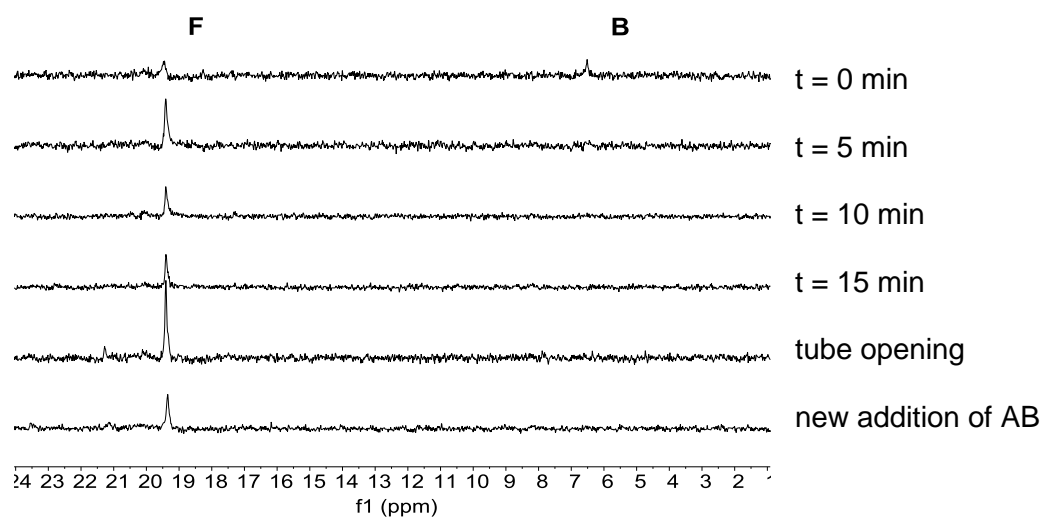
Figure 3.25 ^{31}P{^{1}H} NMR spectra of the "*in situ*" methanolysis of AB catalyzed by 1 showing the formation of new iridium species.

3.5 Reactivity studies. Synthesis of [IrH(H$_3$BNH$_3$){(PPh$_2$(o-C$_6$H$_4$CO))(PPh$_2$(o-C$_6$H$_4$CO))H}] (9)

Studies on the behaviour of complex **7** in methanol and in the presence of amine-boranes have been carried out with a view to understanding the catalytic process.

When complex **7** is dissolved in a 50/50 mixture of CDCl$_3$ and CD$_3$OD the chloride bridge that connects the two metallic centres is broken and a new cationic complex (**8**) along with complex **1** are obtained (Figure 3.26).
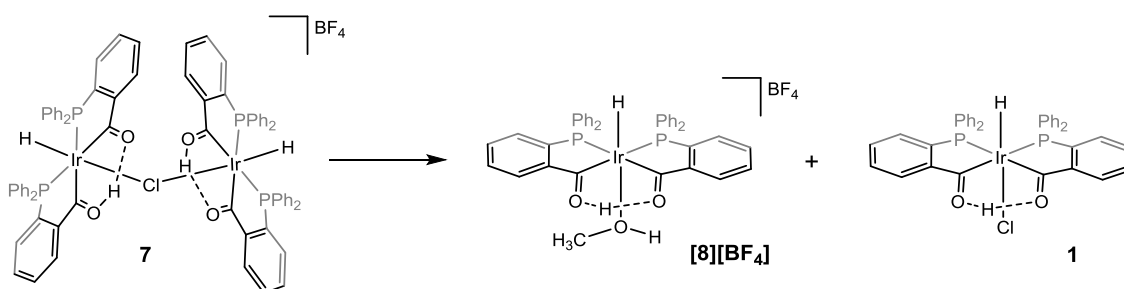

Figure 3.26 Cleavage of the chloride bridge of complex 7 in a CDCl$_3$/CD$_3$OD solution.

In both the ^{1}H NMR and ^{31}P NMR spectra (Figure 3.27), the mixture of the abovementioned three complexes can be observed. The iridium in complex **8** has the same coordinative environment that complex **1** has; but, a methanol molecule has replaced the chloride atom becoming an ionic complex which has the [BF$_4$]$^-$ ion as counterion. The attempts to isolate complex **8** were unsuccessful, although it was identified via NMR as a triplet at -25.20 ppm (J$_{P,H}$ = 14.3 Hz) due to the hydride in the ^{1}H NMR and a singlet at 29.4 ppm in the ^{31}P NMR. These spectroscopic data are very similar to the ones previously reported for complex ([IrH{PPh$_2$(o-C$_6$H$_4$CO))$_2$H}(acetone)]$^+$),[63] which is an analogous complex with an acetone molecule coordinated instead of methanol.
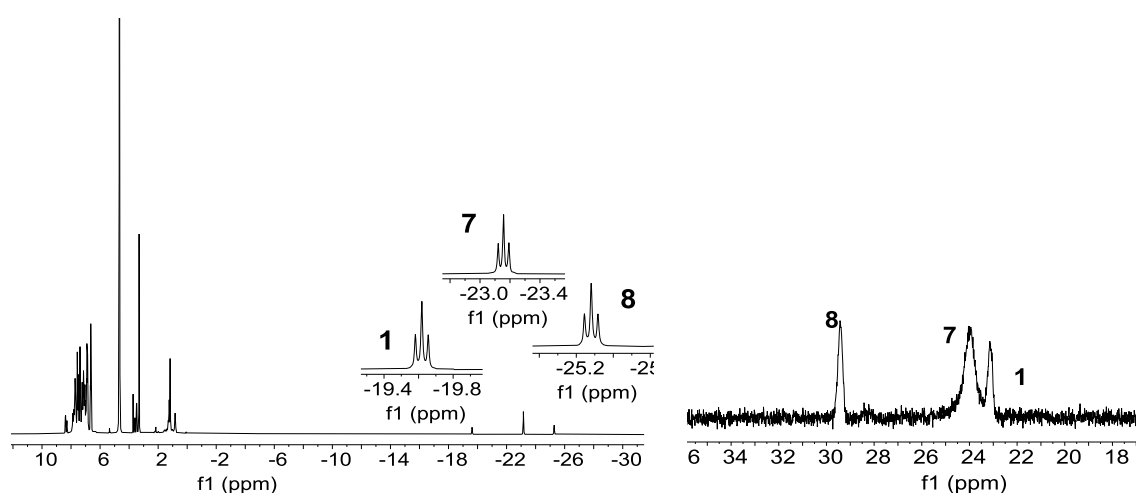
Figure 3.27 ^{1}H NMR (left) and ^{31}P NMR (right) spectra of a CDCl$_3$/CD$_3$OD solution of complex 7.

On the other hand, when complex **7** is dissolved in CD$_3$OD in the presence of the amineborane adduct trimethylamineborane, a new species is formed. Once the dimer, complex **7**, is dissolved in methanol and cleaved into two fragments, the amineborane adduct coordinates to the iridium through one of the hydrides of the borane moiety forming an ionic complex, complex **9** (Figure 3.28). The other fragment of the dimer is now complex **1** that precipitates in CD$_3$OD due to its low solubility in that solvent.
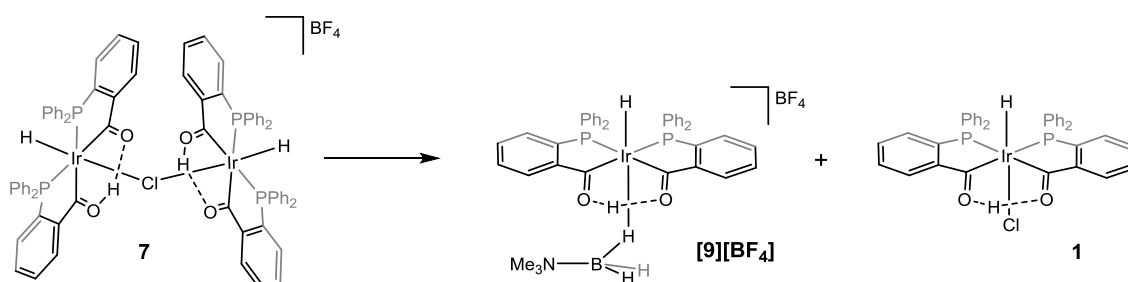
Figure 3.28 *In situ* reaction of complex 7 with Me$_3$N-BH$_3$ in CD$_3$OD.

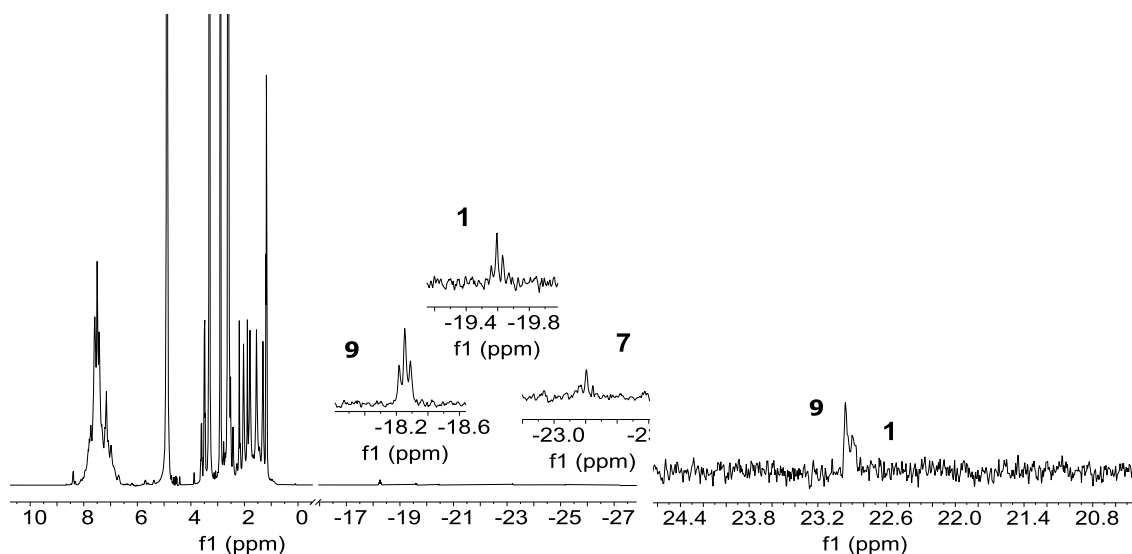In the NMR spectra (Figure 3.29) the three complexes can be identified, being the new complex **9** the main product.

Figure 3.29 ^{1}H NMR (left) and ^{31}P NMR (right) spectra of the *in situ* reaction of complex 7 with Me$_3$N-BH$_3$ in CD$_3$OD.

Complex **9** was isolated as [**9**][BAr$^F_4$] by reacting complex **1** with Me$_3$N-BH$_3$ in the presence of the halide scavenger Na[BAr$^F_4$] in dichloromethane (Figure 3.30). In this complex the iridium atom bonds the borane moiety in a M-H-B η^1-fashion *via* a three-centre two electron bond[73]. This new compound is stable and has been characterised by several techniques.

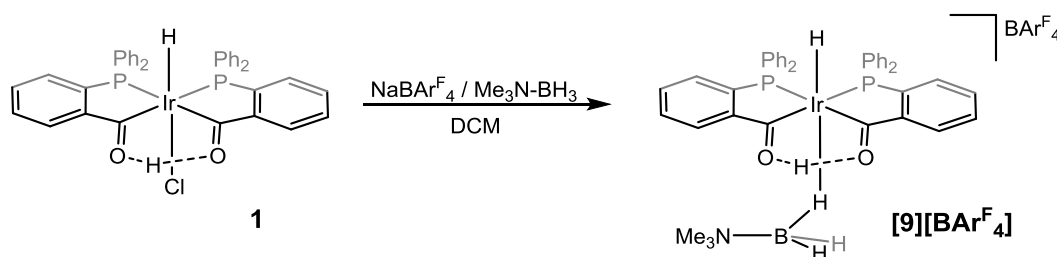**Figure 3.30 Reaction of complex 1 with Me$_3$N-BH$_3$ in the presence of NaBAr$^F_4$ in dichloromethane**

In the IR spectrum (Figure A. 4) the bands corresponding to the terminal boron hydrides can be observed at 2504 and 2444 cm^{-1}, the v(Ir-H) stretching can be seen at 1793 cm^{-1} as a broad signal that may include the bridging BH stretching; and finally, the bond due to v(C=O) is located at 1609 cm^{-1}.

An ESI-mass spectrum was carried out for this complex and the value obtained was ESI-MS (*m/z*): 846.2 [M]$^+$ (Figure D. 1 and Figure D. 2) confirms that the borane adduct is bonded to the metal centre.

Multinuclear NMR spectroscopy was performed for complex **9**. In the ^{31}P{^{1}H} NMR (Figure B. 19) a singlet can be observed at 23.1 ppm which means that the compound has two equivalent phosphorus atoms. Unfortunately, in the ^{11}B NMR only the signal of the counterion BAr$^F_4$ can be detected (Figure B. 20).

On the other hand, useful information can be obtained from the ^{1}H NMR spectrum (Figure 3.31). A hydride can be observed in the high field region, at -18.39 ppm, as a triplet because of the coupling with two phosphorus atoms in *cis* position (J$_{P,H}$ = 14.6 Hz). The position of the hydride fits with the one expected for iridium compounds with a B-H group in a *trans* position to the hydride[74]. In the low field region a singlet can be seen at 22.61 ppm which corresponds to the O -- H -- O hydrogen bond and confirms that the PCCP structure of complex **1** remains unaltered. The BH$_3$ fragment is detected as a broad signal at -2.40 ppm at room temperature.

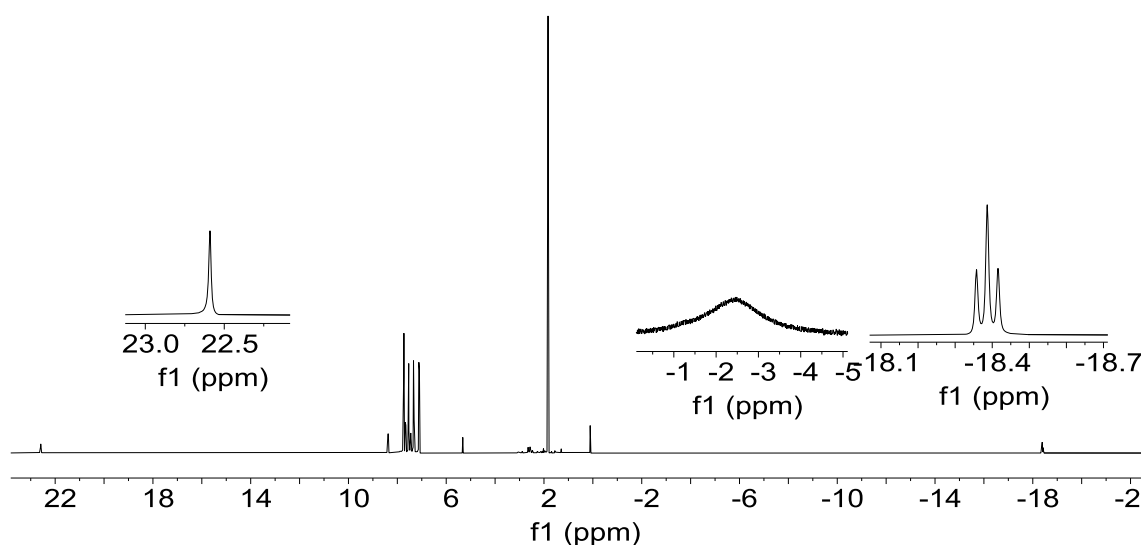**Figure 3.31 ^{1}H NMR of complex 9 in CDCl₃ at 298 K**

As other similar complexes containing a BH_3 fragment attached in the same fashion to the metal centre, complex **9** may undergo a dynamic behaviour in solution at room temperature (Figure 3.32).
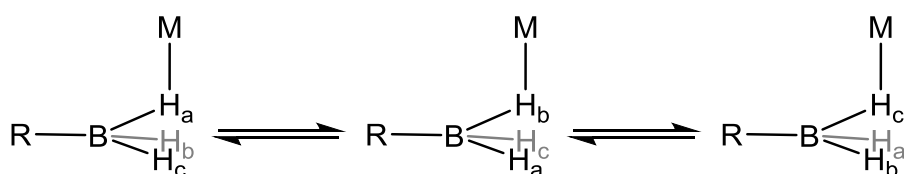

Figure 3.32 Dynamic behaviour of a coordinated BH₃ moiety

^{1}H NMR was carried out at different temperatures for the purpose of proving this dynamic behaviour. In Figure 3.33 it can be observed that the aforementioned hard to find signal at -2.40 ppm (a) undergoes coalescence as the temperature decreases to give way to the signals at -10.54 ppm (c) and 1.50 ppm (b), corresponding to 1H and 2H respectively. These two signals can be detected at around 233 K, and by 213 K the complex reaches nearly static

behaviour. The hydride and ketoenolic signals and the phosphorus resonance remain unaltered in all the temperature range.

Taking these data into account it can be said that iridium complexes with a borane adduct coordinated to the metal centre can be isolated.
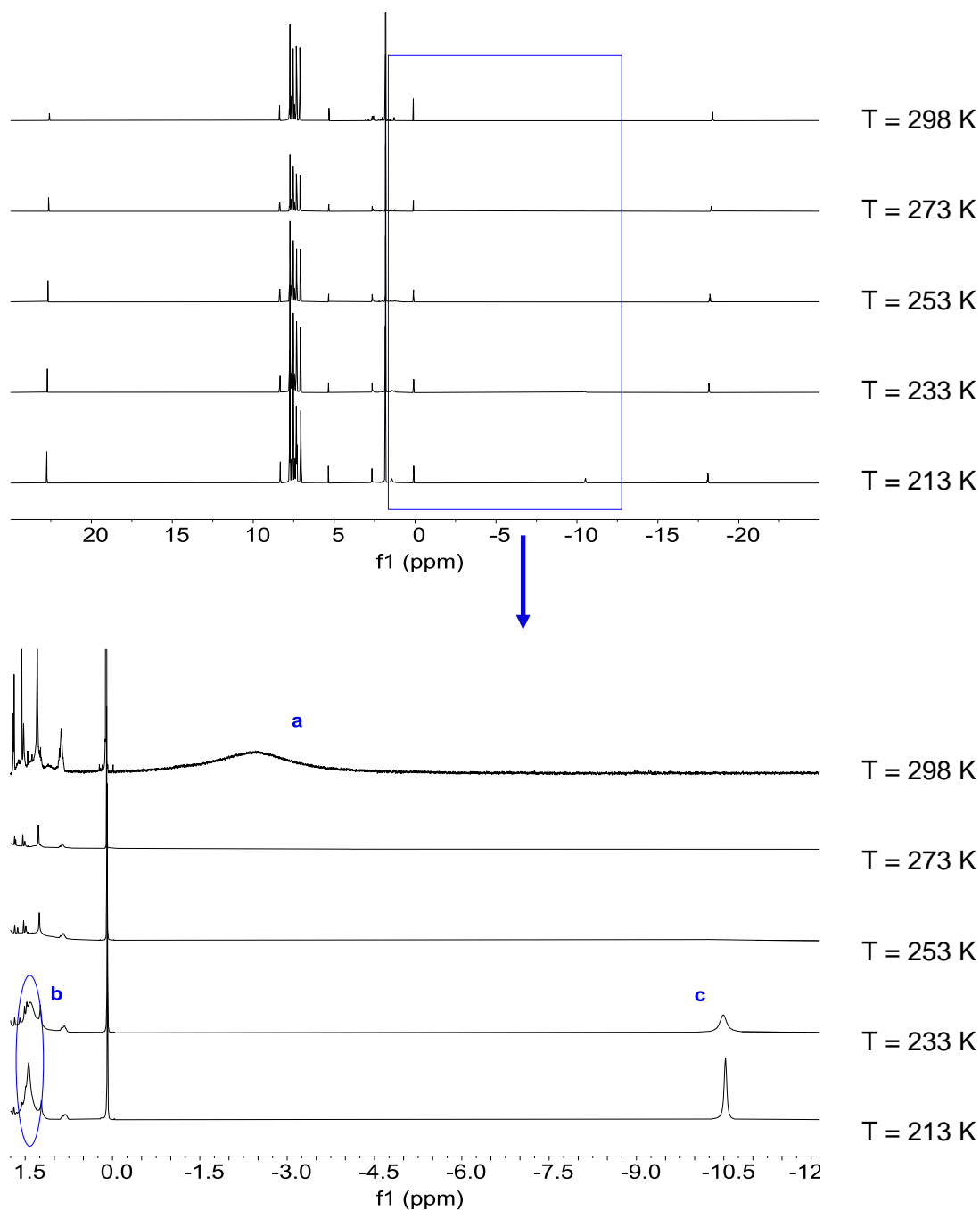

Figure 3.33 ^{1}H NMR spectrum of complex 9 at different temperatures in CDCl$_3$.

3.6 Proposed simplified catalytic cycle

In the view of these experimental results, the following simplified catalytic cycle has been proposed (Figure 3.34).
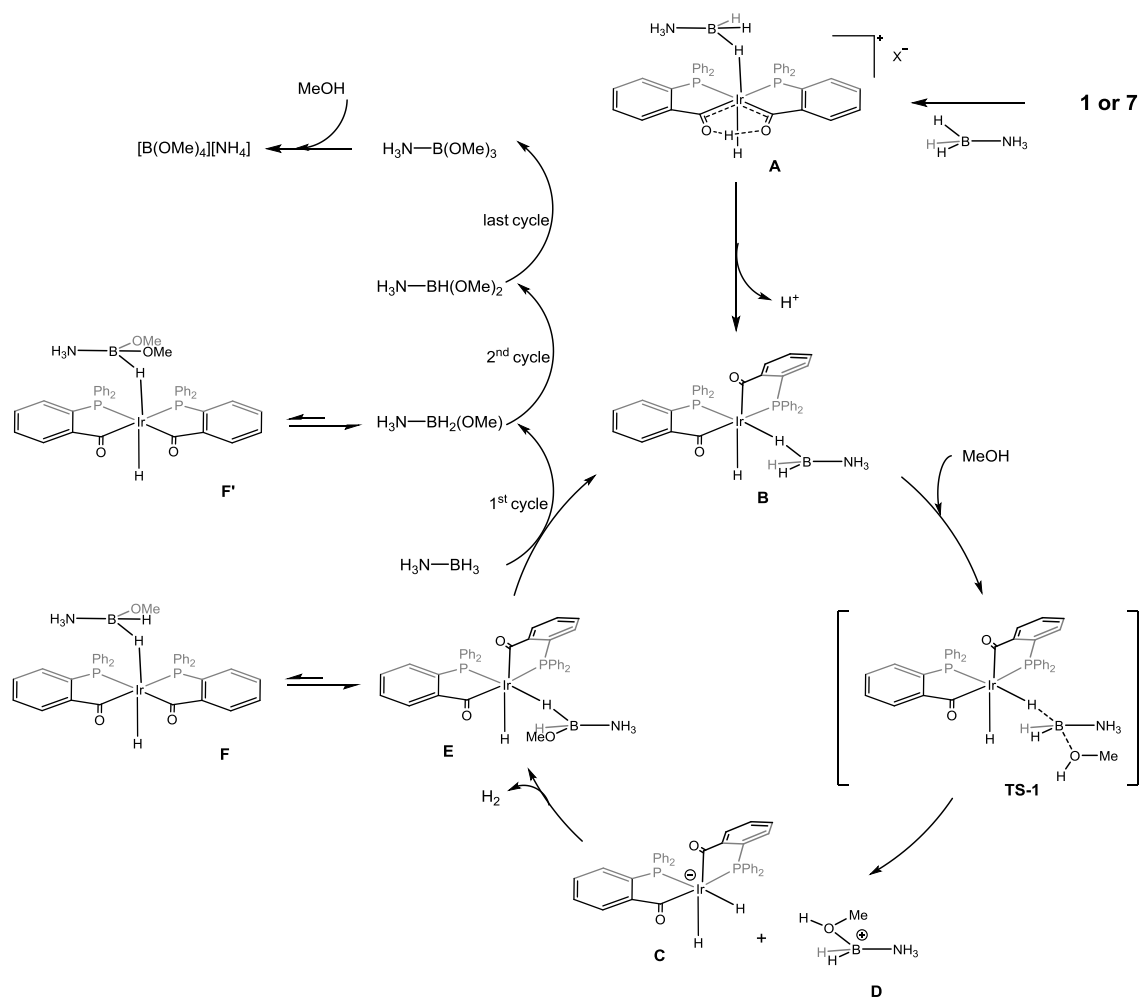

Figure 3.34 Simplified mechanism for the methanolysis of ammonia-borane with hydridoirida-β-diketones.

We propose the methanolysis of AB as a homogeneous metal-catalysed intermolecular process. The hydrogen release occurs in successive steps for each AB molecule, affording one molecule of hydrogen and H_3N-BH_2(OMe) in the first step, another molecule of hydrogen and H_3N-BH(OMe)$_2$ in the second

step and the third molecule of hydrogen and H_3N-$B(OMe)_3$ in the last step. One molecule of methanol assists the B-N bond cleavage of the H_3N-$B(OMe)_3$ borane adduct and leads to the ionic $[NH_4][B(OMe)_4]$ product seen in the *in situ* NMR. The appointed final product is related to that reported for the hydrolysis of AB[46,75,76] having replaced the hydroxyl group by a methoxy.

When complexes **1** or **7** are dissolved in a methanol solution of AB they release the chloride anion and coordinate a molecule of AB affording the irida-β-diketone complex (**A**) which is analogous to complex **9**.

Irida-β-diketone complexes have proven to be able to lose the ketoenolic proton when dissolved in methanol solutions and in the presence of a base, resulting in a rearrangement of the ligands[4]. In this case, the deprotonation of **A** and a rearrangement of the ligands is proposed; which would afford species **B**. This new species has a hydride *trans* to an acyl group and would be the species seen at the initial stages of the NMR followed methanolysis of AB.

In the next step, species **B** would undergo a nucleophilic attack to the boron atom from a MeOH molecule, via TS-1; which would afford the dihydridoiridate(III) species (**C**) and the methanol-stabilised boronium cation (**D**).

The hydrogen release may happen as a result of an O-to-Ir hydrogen transfer from the boronium cation **D** to the dihydridoiridate(III) species giving **E**, a neutral iridium species with a coordinated $H_3N-BH_2(OMe)$, as the next species. Hydrogen release from transient dihydridobis(acyldiphenylphosphine)iridate(III) species and formation of hydride derivatives by O-to-Ir hydrogen transfer from a hydroxyl fragment has been previously reported[4]. We propose an equilibrium between species **E** and **F** which are isomers; the difference is that while **E** has a hydride *cis* to the borane moiety **F** has a hydride *trans* to the H-B bond and may correspond to species **F** observed in the "*in situ*" AB methanolysis followed by NMR.

Competition between borane adducts yields the observed intermediate $H_3N-BH_2(OMe)$ and leads to species **B**, which restarts the hydrogen release from new H_3N-BH_3. Analogous catalytic cycles from **E**, containing $H_3N-BH_2(OMe)$, afford another equivalent of hydrogen, $H_3N-BH(OMe)_2$ and **F'**, analogous to **F**. Coordination of $H_3N-BH(OMe)_2$ to iridium allows the release of a third equivalent of hydrogen, and of $H_3N-B(OMe)_3$, which affords the tetramethoxyborate final product after reacting with one MeOH molecule.

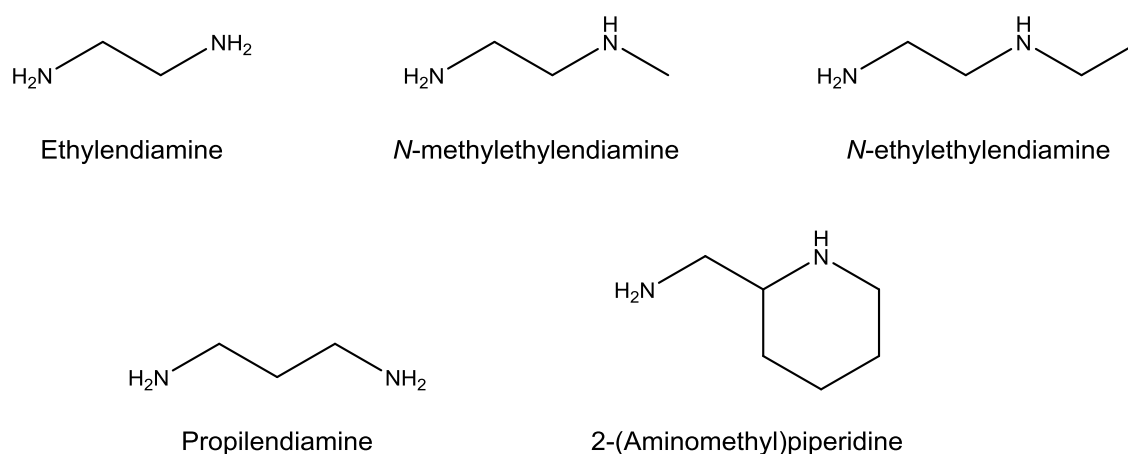**Chapter 4**

Reactivity of irida-β-diketones with alkyldiamines

4.1 Introduction

The reactivity of irida-β-diketones has been extensively studied towards ammonia,[9] simple primary and secondary aliphatic monoamines,[10,77] aromatic amines,[9] aminopyridines,[10,64] aminoalkylpyridines[11] and hydrazines.[10,12]

Taking all this background into account the study of the reactivity of irida-β-diketone complexes **1** and **2** towards alkyldiamines was carried out as the flexibility and nucleophilicity of these ligands is very different to that of the ligands studied before.

4.2 Reactivity of chloroirida-β-diketone.

Alkyldiamines shown in Figure 4.1 react with chloroirida-β-diketones to give many different compounds. From complex **1** we can synthesise ketoimine complexes that can go on to form cationic terdentate complexes containing PCN ligands and, after the reaction with a base, neutral ones (Figure 4.2).

Ethylendiamine   *N*-methylethylendiamine   *N*-ethylethylendiamine

Propilendiamine   2-(Aminomethyl)piperidine

Figure 4.1 Alkyldiamines used as reactants.

All the selected alkyldiamines have at least one primary amine group and some of them have two, like the ethylendiamine and the propilendiamine. In the case of the *N*-methylethylendiamine that secondary amine group is a prochiral

centre that could create diastereomers when it is bonded to the metal centre. The same thing happens with 2-(aminomethyl)piperidine, from which a racemic mixture is used, but, in this case, the ligand already has a chiral centre itself, thus if a chiral centre is also formed in the metal at least a pair of diastereomers will always appear.
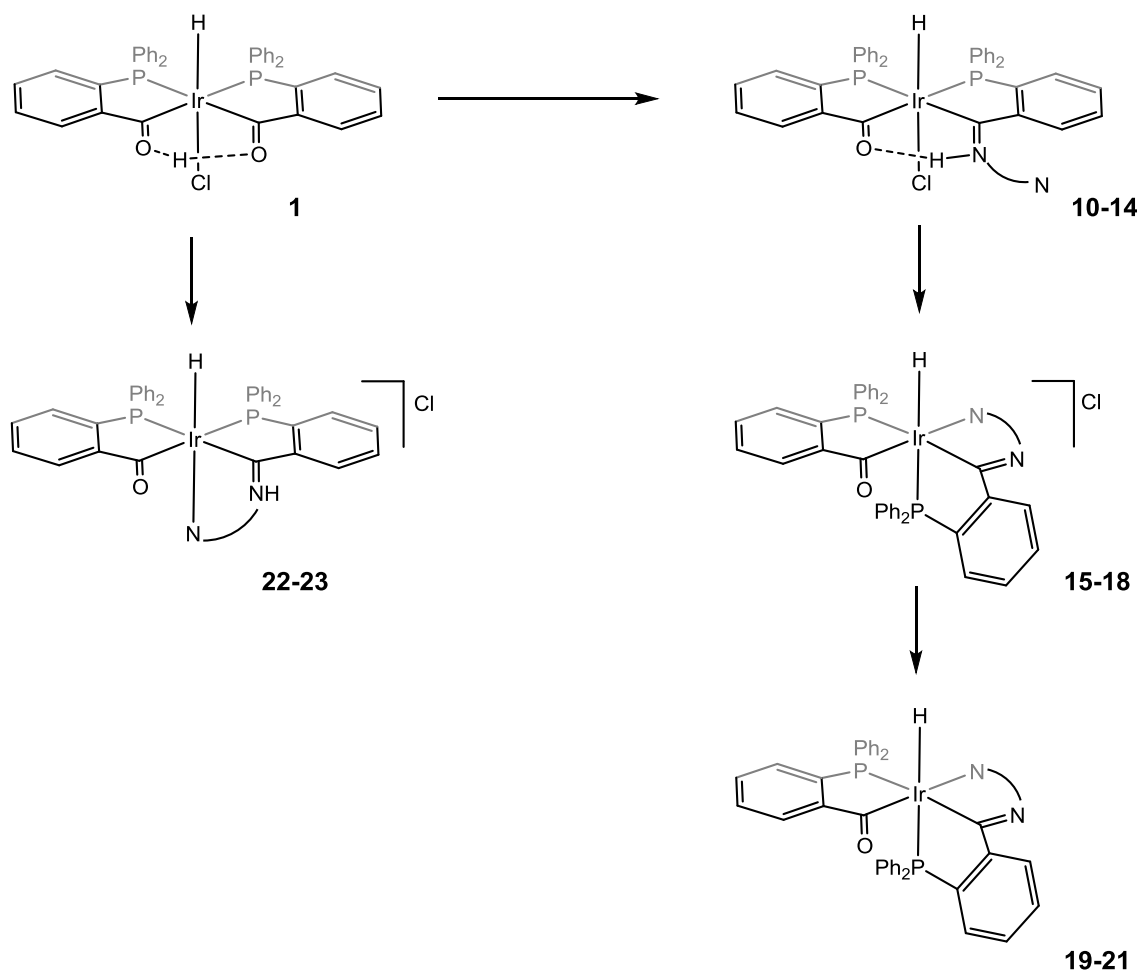

Figure 4.2 Reactivity of chlorohydridoirida-β-diketone with alkyldiamines. Used alkyl-amines: Ethylendiamine for complexes 10, 15, 19 and 22; *N*-methylethylendiamine for complexes 11, 16, 20 and 23; *N*-ethylethylendiamine for complex 12; propilendiamine for complexes 13, 17 and 21; and 2-(aminomethyl)piperidine for complexes 14 and 18.

4.2.1 Ketoimine type complex formation

The reaction of **1** with different alkyl diamines in THF leads to the formation of an array of ketoimine complexes derived from ethylendiamine **(10)**, *n*-methylethylendiamine **(11)**, *N*-ethylethylendiamine **(12)**, propilendiamine **(13)** and 2-(aminomethyl)piperidine **(14)**. In these complexes the condensation reaction of the amine leaves the coordination environment of **1** unchanged, and the initial ketoenolic proton is also located between two heteroatoms, in this case nitrogen and oxygen. However, this condensation reaction introduces another structural parameter, the variable dangling group from the nitrogen atom.
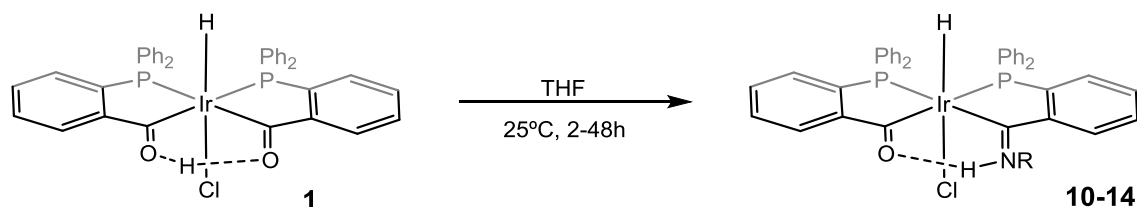
Figure 4.3 Ketoimine complex formation where: $R = CH_2CH_2NH_2$ **(10)**, $R = CH_2CH_2NHCH_3$ **(11)**, $R = CH_2CH_2NHCH_2CH_3$ **(12)**, $R = CH_2CH_2CH_2NH_2$ **(13)**, $R = CH_2(C_5H_9N)$ **(14)**.

In the infrared spectra signals of the vibration of υ(N-H) appear at 3372 cm^{-1} **(10)**, 3280 cm^{-1} **(11)**, 3268 cm^{-1} **(12)**, 3280 cm^{-1} **(13)** and at 3276 cm^{-1} **(14)**; the ones corresponding to the stretching vibration of Ir-H bond can be seen at 2177 cm^{-1} **(10)**, 2171 cm^{-1} **(11)**, 2179 cm^{-1} **(12)**, 2189 cm^{-1} **(13)** and at 2170 cm^{-1} for complex **(14)** and finally the signals of the vibration of the υ(C=O) and υ(C=N) groups are located at 1552 cm^{-1} **(10)**, 1564 cm^{-1} **(11)**, 1553 cm^{-1} **(12)**, 1553 cm^{-1} **(13)** and 1554 cm^{-1} **(14)**.

These five complexes have also been fully characterised via multinuclear NMR. For a summary of the most relevant NMR data see Table 4.1. For the ^{1}H NMR, ^{31}P{^{1}H} NMR, ^{13}C{^{1}H} NMR, COSY spectrum and ^{1}H-^{13}C HSQC spectrum of all complexes see Figure B. 21 to Figure B. 25 **(10)**; Figure B. 26 to Figure B. 30 **(11)**; Figure B. 31 to Figure B. 35 **(12)**; Figure B. 36 to Figure B. 40 **(13)** and Figure B. 41 to Figure B. 45 **(14)**.

Table 4.1 The most relevant NMR data of complexes 10-14. The spectra were recorded in CDCl$_3$ solution, the chemical shift is given in ppm and the coupling constants in Hz.

| Complex	^{1}H NMR	^{31}P{^{1}H} NMR	^{13}C{^{1}H} NMR
10	δ Ir-H = -20.5 (t) $^2J_{P,H}$= 14 δ O--*H*--N = 12.8 (br)	δ Ir-P = 15.6 (d) δ Ir-P = 29.9 (d) $^2J_{P,P}$= 7	δ C=O or C=N 224.0 (d) $^2J_{P,C}$= 102 243.0 (d) $^2J_{P,C}$= 106
11	δ Ir-H = -20.4 (t) $^2J_{P,H}$= 14 δ O--*H*--N = 12.6 (br)	δ Ir-P = 16.0 (d) δ Ir-P = 29.9 (d) $^2J_{P,P}$= 7.4	δ C=O or C=N 224.3 (d) $^2J_{P,C}$= 102 242.0 (d) $^2J_{P,C}$= 104
12	δ Ir-H = -20.4 (t) $^2J_{P,H}$= 14 δ O--*H*--N = 12.6 (br)	δ Ir-P = 16.0 (d) δ Ir-P = 30.4 (d) $^2J_{P,P}$= 7.4	δ C=O or C=N 224.2 (d) $^2J_{P,C}$= 102 242.0 (d) $^2J_{P,C}$= 104
13	δ Ir-H = -20.7 (t) $^2J_{P,H}$= 14 δ O--*H*--N = 13 (br)	δ Ir-P = 14.6 (d) δ Ir-P = 29.6 (d) $^2J_{P,P}$= 7	δ C=O or C=N 221.4 (d) $^2J_{P,C}$= 103 243.4 (d) $^2J_{P,C}$= 106
14	**B** δ Ir-H = -20.6 (dd) $^2J_{P,H}$= 15 $^2J_{P,H}$= 14 **A** δ Ir-H = -20.4 (dd) $^2J_{P,H}$= 16 $^2J_{P,H}$= 14 **A** δ O--*H*--N = 12.8 (br) **B** δ O--*H*--N = 13 (br)	**B** δ Ir-P = 15.1 (s) **A** δ Ir-P = 16.9 (s) **B** δ Ir-P = 29.1 (d) $^2J_{P,P}$= 7 **A** δ Ir-P = 29.9 (d) $^2J_{P,P}$= 7	δ C=O or C=N **A** and **B** 224.1 (d) $^2J_{P,C}$= 102 **A** 242.0 (d) $^2J_{P,C}$= 104 **B** 242.8 (d) $^2J_{P,C}$= 104

As previously mentioned, the reaction of complex **1** with an amine in THF to give the Schiff-base derivative leaves the coordination around the iridium unchanged, except that now the symmetry in **1** is lost. This means that in all cases one hydride is going to be in a *trans* position to one chloride atom and *cis* to both phosphorus atoms, the acyl and the imine group. In the same way, both phosphorus atoms are in *cis* position one to the other and each one *trans* to one acyl or imine group.

In the ^{1}H NMR the hydride signals can be seen between -20.3 and -20.7 ppm and in most of the cases appear as a triplet because even if the two phosphorus atoms have different environments the coupling constants are very similar. In the case of complex **14** they are different enough that we can see two doublet of doublets.

The formation of diastereomers for complex **14** can be explained by the chirality of the ligand and the metal centre. Having two chiral centres in the complex four enantiomers could be expected, giving us two signals from the two different diastereomers. The proportion of the diastereomers was calculated from the ^{1}H NMR giving us a value of 55/45.

Another important signal in the ^{1}H NMR is the ketoimine proton that appears as a broad signal around 13 ppm for all complexes (Figure 4.4). This signal in particular has suffered the major shift of all the signals as a result of the substitution of one oxygen atom for the nitrogen of the imine group.
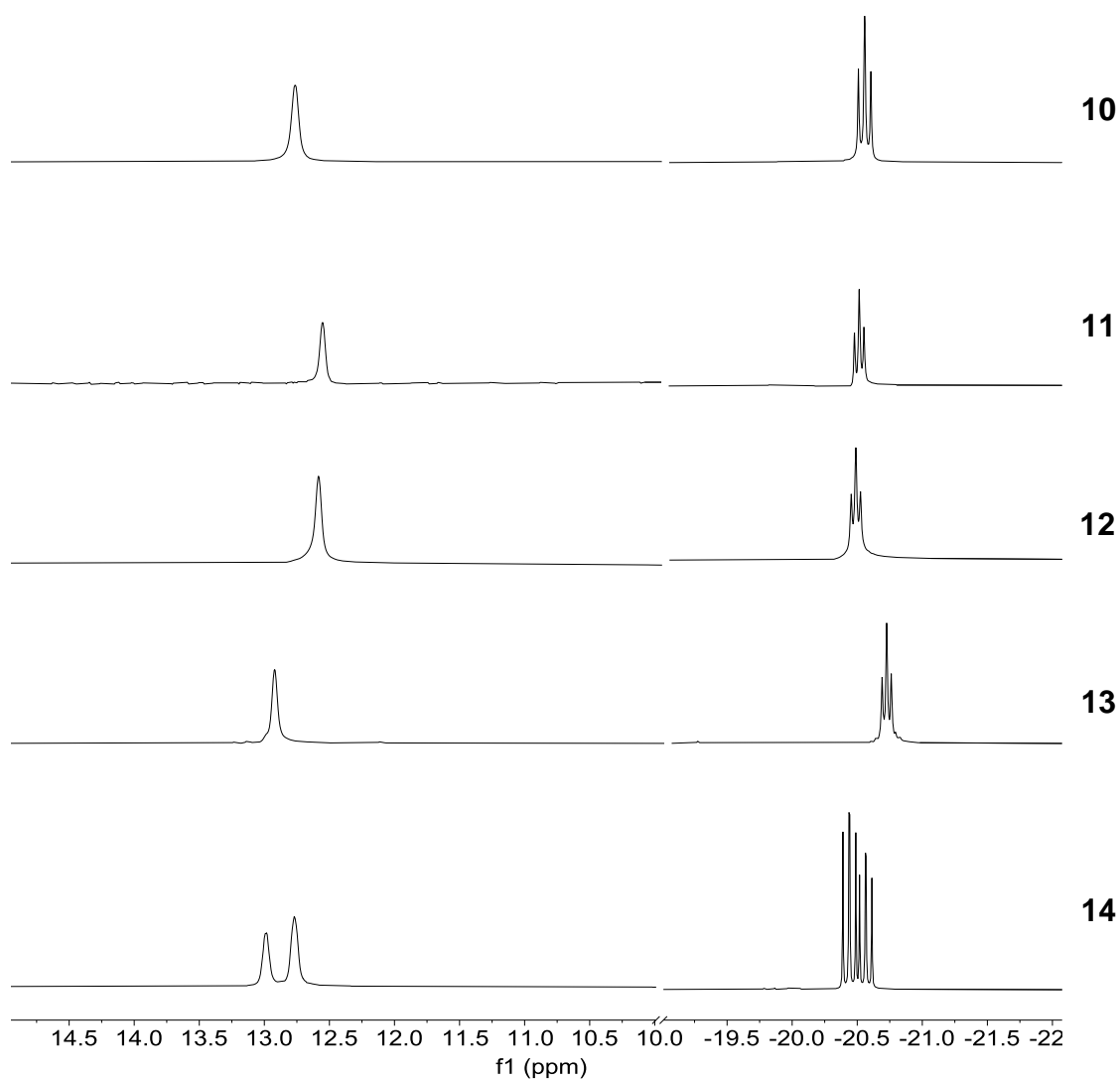
Figure 4.4 Most characteristic peaks of ^{1}H NMR for complexes (10-14)

In the ^{31}P{^{1}H} NMR spectra of all complexes two signals can be seen, except for complex **14** where 4 signals are seen due to the two diastereomers. The signals of the major product (A) appear at 16.9 and 29.9 ppm and the signals of the minor product (B) at 15.1 and 29.1 ppm. The ones at low field appear as doublets with a coupling constant around 7 Hz which indicates that the two phosphorus atoms are in a *cis* position one to the other.

In the $^{13}C\{^{1}H\}$ spectra the most important signals are the doublets that appear around 224 ppm and 242 ppm. These signals belong to the acyl and the imine groups which couple with the phosphorus with 102-106 Hz coupling constants.

Yellow monocrystals of complex **10** were obtained from a vapour diffusion of diethyl ether into a methanol solution at -20 ºC of complex **10** and an X-Ray diffraction study could be done. The results confirm the proposed structure. A selection of bond lengths and angles are given in Table C. 2.

The coordinative environment of the iridium atom is a slightly distorted octahedron where four positions are occupied by the phosphorus and carbon atoms of the bidentate ligands. The other two positions are occupied by a hydride and a chlorine atom which are mutually in *trans* position (Figure 4.5). All bond distances and angles are very similar to the analogous reported structures with methylamine[43], 2-(aminoethyl)pyridine[11] and furfurylamine[77].

It is worth mentioning the presence of the intramolecular hydrogen bond (O1 - - H1N = 1.8799(6)Å) of a moderate strength[67] between the hydrogen atom H1 and the oxygen O1 from the acyl group.
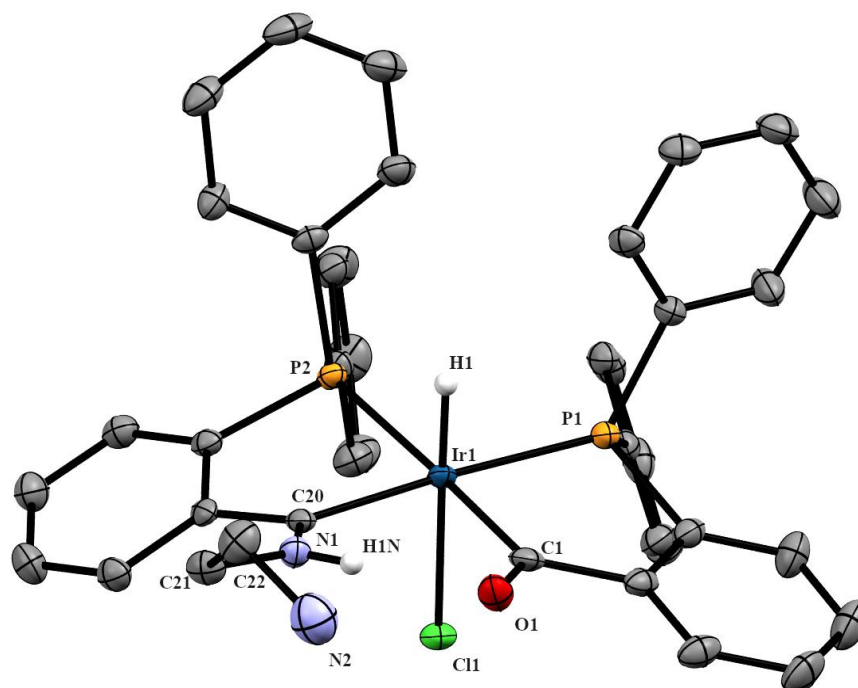
Figure 4.5 Molecular structure of complex 10 (50% probability ellipsoids)

4.2.2 Cationic PCN chelate formation

Ketoimine complexes synthesised from alkyldiamines have a free amine group. In protic solvents, such as methanol, the amine group coordinates to the metal centre forming a new six membered metallacycle and thus the condensed phosphine becomes a terdentate PCN chelate. The amine replaces the chloride in the coordination sphere and it becomes an anion. This leaves us with a cationic complex in which the proton has moved from the ketoimine bond to afford an iminium group.
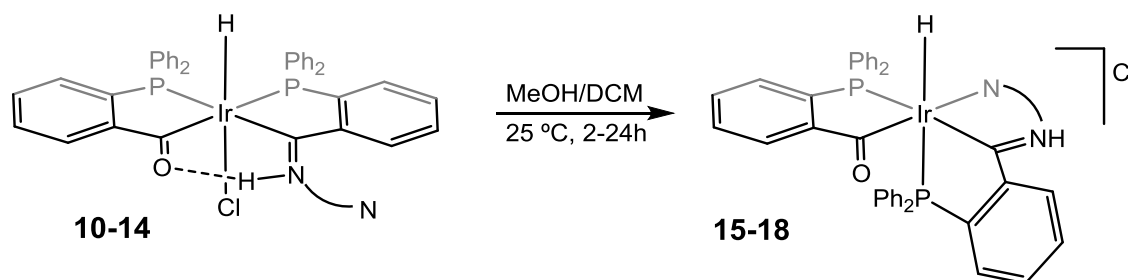
Figure 4.6 Cationic PCN chelate complex formation derived from: *Ethylendiamine (15); N-methylethylendiamine (16); propilendiamine (17); and 2-(aminomethyl)piperidine (18).*

In the infrared spectra signals of the vibration of υ(N-H) appear at 3316 cm^{-1} **(15)**, 3282 cm^{-1} **(16)**, 3311 cm^{-1} **(17)** and at 3320 and 3238 cm^{-1} **(18)**; the ones corresponding to the vibration of Ir-H bond stretching can be seen at 2015 cm^{-1} **(15)**, 2014 cm^{-1} **(16)**, 2036 cm^{-1} **(17)** and at 2086 cm^{-1} for complex **(18)** and finally the signals of the vibration of the υ(C=O) and υ(C=N) groups are located at 1575 cm^{-1} **(15)**, 1575 cm^{-1} **(16)**, 1575 cm^{-1} **(17)**, and 1560 cm^{-1} **(18)**.

The conductivity values obtained for these cationic complexes are lower than what could be expected, being 40 **(15)**; 30 **(16)**; 40 **(17)** and 50 ohm^{-1}·cm^2·mol^{-1} **(18)**. This happens because the chloride anion and the cationic complex make a strong ionic pair. When the anion is changed to perchlorate the values appear in the range of uni-univalent electrolytes: 130 **(14b)**, 120 **(15b)**, 120 **(16b)** and 140 ohm^{-1}·cm^2·mol^{-1} for complex **(18)**.

A mass spectroscopy study was carried out for these complexes and the values obtained were ESI-MS (*m/z*): 813.1 [M-H$_2$]$^+$ **(15)**; 829.2 [M]$^+$ **(16)**; 827.2 [M-H$_2$]$^+$ **(17)**; and 867.2 [M-H$_2$]$^+$ **(18)** (Figure D. 3 to Figure D. 10).

Table 4.2 The most relevant NMR data of complexes 15-18. The spectra were recorded in CD$_3$OD (14) or CDCl$_3$ (15), (16), (17) solutions, the chemical shift is given in ppm and the coupling constants in Hz.

| Complex	^{1}H NMR	^{31}P NMR (15) (16) ^{31}P{^{1}H} NMR (17) (18)	^{13}C{^{1}H} NMR
15	δ Ir-H = -8.7 (dd) $^2J_{P,H}$= 122 $^2J_{P,H}$= 18	δ Ir-P = 15.5 (d) $^2J_{P,H}$= 122 δ Ir-P = 25.8 (s)	δ C=O 217.8 (dd) $^2J_{P,C}$= 16 $^2J_{P,C}$= 6 δ C=N 232.2 (dd) $^2J_{P,C}$= 90
16	**A** δ Ir-H = -8.5 (dd) $^2J_{P,H}$= 123 $^2J_{P,H}$= 20 **B** δ Ir-H = -9.2 (dd) $^2J_{P,H}$= 124 $^2J_{P,H}$= 19	**A** δ Ir-P = 15.4 (d) $^2J_{P,H}$= 127 δ Ir-P = 25.7 (s)	**A** δ C=O 208.4 (s) δ C=N 228.8 (dd) $^2J_{P,C}$= 92
17	δ Ir-H = -8.4 (dd) $^2J_{P,H}$= 126 $^2J_{P,H}$= 19 δ C=NH 12.8 (br)	δ Ir-P = 18.2 (d) δ Ir-P = 27.0 (d) $^2J_{P,P}$= 12	δ C=O 211.2(d) $^2J_{P,C}$= 6 δ C=N 226.7(d) $^2J_{P,C}$= 93
18	**A** δ Ir-H = -9.1 (dd) $^2J_{P,H}$= 124 $^2J_{P,H}$= 20 **B** δ Ir-H = -8.6 (dd) $^2J_{P,H}$= 123 $^2J_{P,H}$= 20	**A** δ Ir-P = 23.0 (s) δ Ir-P = 30.0 (d) $^2J_{P,P}$= 15 **B** δ Ir-P = 21.0 (s) δ Ir-P = 27.0 (d) $^2J_{P,P}$= 13	**A** δ C=O 206.2(d) $^2J_{P,C}$= 6 δ C=N 227.6(d) $^2J_{P,C}$= 85 **B** δ C=O 211.2(d) $^2J_{P,C}$= 6 δ C=N 231.0(d) $^2J_{P,C}$= 95

The four complexes have been fully characterised via multinuclear NMR. For a summary of the most relevant NMR data see Table 4.2. For the ^{1}H NMR, ^{31}P{^{1}H} NMR or ^{31}P NMR, ^{13}C{^{1}H} NMR, COSY spectrum and ^{1}H-^{13}C HSQC spectrum of all complexes see Figure B. 46 to Figure B. 50 **(15)**; Figure B. 51 to Figure B. 55 **(16)**; Figure B. 56 to Figure B. 60 **(17)** and Figure B. 61 to Figure B. 66 **(18).**

These NMR data suggest that the ketoimine compounds have undergone a rearrangement. In the ^{1}H NMR the signal of the hydride appears between -8.30 and -9.20 ppm and for all the compounds is a doublet of doublets with two very different coupling constants (one around 120 Hz and the other one around 20 Hz); see Figure 4.7. This implies that the hydride is in a *trans* position to one of the phosphorus atoms and *cis* to the other phosphorus. The iminium proton could only be assigned for complex **17** as a broad signal around 13 ppm.

The new arrangement is also confirmed by the phosphorus NMR; for complexes **15** and **16** a ^{31}P experiment was carried out and two different signals can be observed, a doublet and a singlet. The doublets have a coupling constant of 120-130 Hz which is related to the biggest coupling constants seen in the ^{1}H NMR spectra. For complexes **17** and **18** a ^{31}P{^{1}H} experiment was performed; in the spectrum of complex **17** two doublets with the same coupling constant were observed meaning that the two phosphorus atoms are found both in a *cis* position one to the other.

When the amine group that coordinates the metal centre is a secondary amine a chiral centre is formed and because the metal itself is a chiral centre diastereomers formed. This happens in complexes **16** and **18**, and diastereomers appear in a proportion, as calculated from NMR, of 80/20 for complex **16** and 65/35 for complex **18**. The diastereomers of complex **18** can also be seen in the ^{31}P{^{1}H} NMR where four signals appear instead of two.
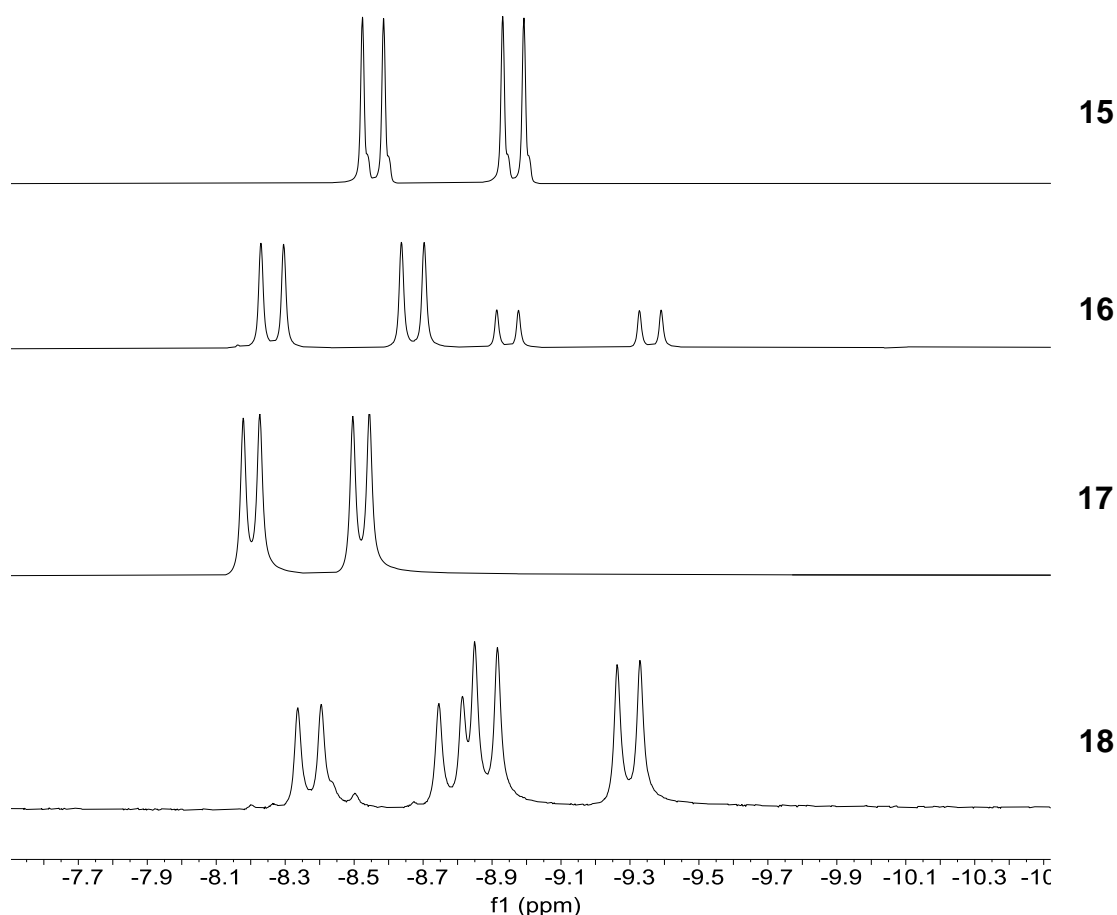
Figure 4.7 Hydride peaks from ¹H NMR for complexes 15-18

In the $^{13}C\{^{1}H\}$ spectra the most important signals are the doublets that appear around 210 ppm and 230 ppm. The first ones have low coupling constants values. The signals around 230 ppm have coupling constants around 85-95 Hz which means that they are in a *trans* position to a phosphorus atom.

Yellow monocrystals of complexes **15** (from a vapour diffusion of diethyl ether into a methanol solution of complex **15** at -20 °C) and **16** (from a vapour diffusion of hexane into a chloroform solution of complex **16** at -20 °C) were obtained. An X-Ray diffraction study could be done and the results confirm the proposed structure. A selection of bond lengths and angles are given in Table C. 3(for complex **15**) and in Table C. 4 (for complex **16**).

In both cases the space group of the unit cell is P$\bar{1}$ which indicates that both crystallise as a mixture of enantiomers.

Complex **15** (Figure 4.8) and complex **16** (Figure 4.9) show an iridium(III) pseudo-octahedral environment with a hydride, a bidentate ligand (linked by the phosphorus atom (P1) and the carbon (C1) of the acyl group) and a terdentate ligand (linked by the phosphorus atom (P2), a sp^2 carbon (C20) and the amine group of the ligand (N2)). The phosphorus of the bidentate ligand (P1) is in a *trans* position to the sp^2 carbon (C20).
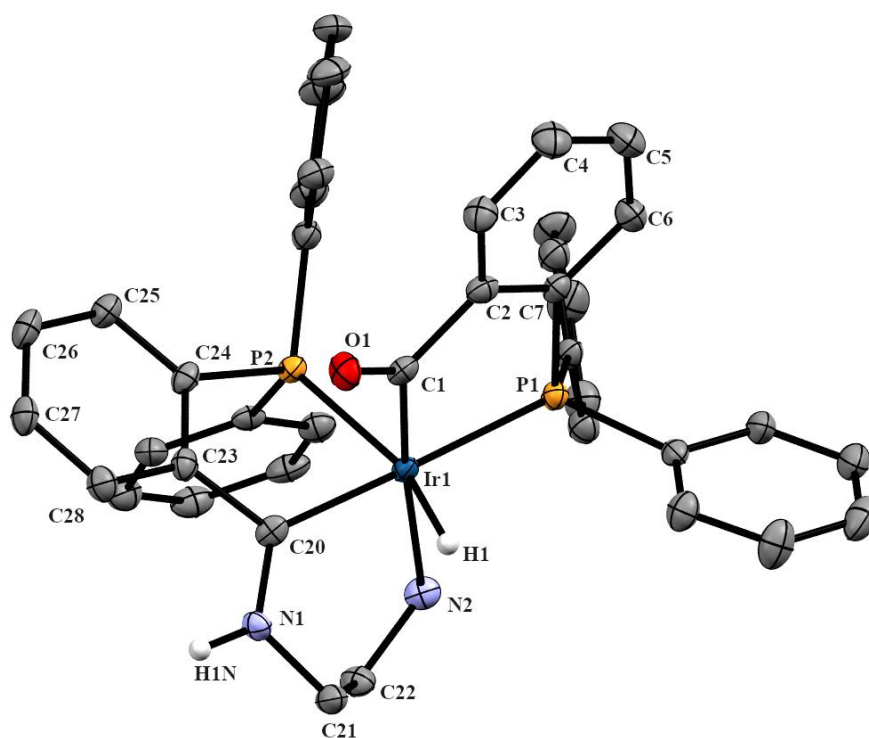
Figure 4.8 Molecular structure of complex 15 (50% probability ellipsoids)
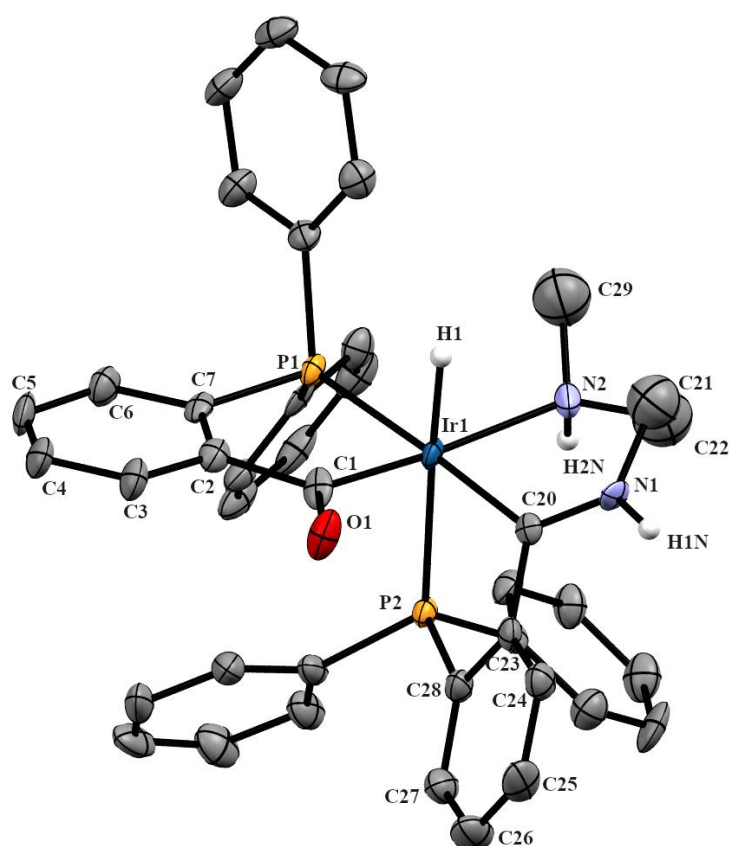
Figure 4.9 Molecular structure of complex 16 (50% probability ellipsoids)

4.2.3 Neutral PCN chelate formation

Cationic PCN complexes can react with bases and lose the protic proton of the iminium group; this deprotonation leads to neutral complexes with the same structure as the starting complexes.
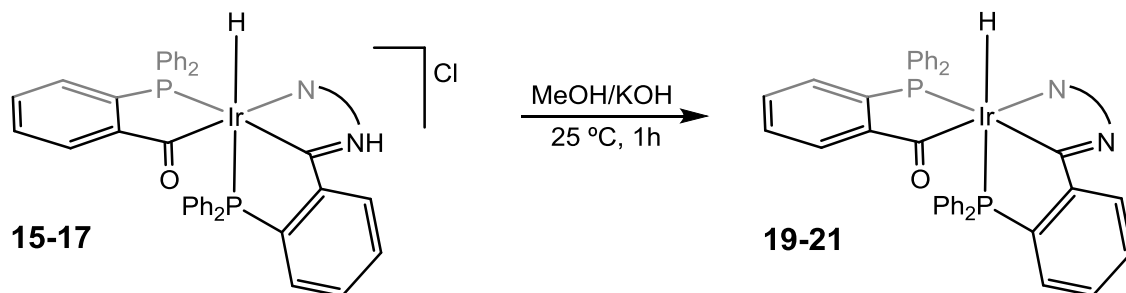
Figure 4.10 Neutral PCN chelate complex formation derived from: *Ethylendiamine (19); N-methylethylendiamine (20) ;and propilendiamine (21).*

The structure proposed for these complexes is the one we proposed for the cationic PCN complexes; the difference is that the proton has been removed by a base, as well as the counterion.

In the infrared spectra signals of the vibration of υ(N-H) appear at 3318 and 3356 cm^{-1} **(19)**, 3281 cm^{-1} **(20)** and at 3312 and 3244 cm^{-1} **(21)**; the ones corresponding to the vibration of Ir-H bond stretching can be seen at 2011 cm^{-1} **(19)**, 2009 cm^{-1} **(20)** and at 2027 cm^{-1} for complex **(21)** and finally the signals of the vibration of the υ(C=O) and υ(C=N) groups are located at 1601 cm^{-1} **(19)**, 1600 cm^{-1} **(20)** and 1559 cm^{-1} **(21)**.

Mass spectroscopy was carried out for complexes **19** and **21** and the values obtained were ESI-MS (*m/z*): 815.2 [M+H$^+$]$^+$ **(19)** and 829.2 [M+H$^+$]$^+$ **(21)** (Figure D. 11 to Figure D. 14).

The three complexes have been fully characterised via multinuclear NMR. For the most relevant NMR data see Table 4.3. For the ^{1}H NMR, ^{31}P{^{1}H} NMR or ^{31}P NMR, ^{13}C{^{1}H} NMR, COSY spectrum and ^{1}H-^{13}C HSQC spectrum of all complexes see Figure B. 67 to Figure B. 71 **(19)**; Figure B. 72 to Figure B. 76 **(20)**; and Figure B. 77 to Figure B. 81 **(21).**

Table 4.3 The most relevant NMR data of complexes 19-21. The spectra were recorded in CDCl$_3$ solution, the chemical shift is given in ppm and the coupling constants in Hz.

Complex	^{1}H NMR	^{31}P{^{1}H} NMR **(19)** **(21)** ^{31}P NMR **(20)**	^{13}C{^{1}H} NMR
19	δ Ir-H = -8.5 (dd) $^2J_{P,H}$= 122 $^2J_{P,H}$= 18	δ Ir-P = 25.6 (s) δ Ir-P = 27.3 (d) $^2J_{P,P}$= 7	δ C=N 208.3 (d) $^2J_{P,C}$= 80 δ C=O 214.8 (d) $^2J_{P,C}$= 67
20	**A** δ Ir-H = -8.4 (dd) $^2J_{P,H}$= 123 $^2J_{P,H}$= 20 **B** δ Ir-H = -9.0 (dd) $^2J_{P,H}$= 124 $^2J_{P,H}$= 18	**A** δ Ir-P = 24.8 (d) $^2J_{P,H}$= 123 δ Ir-P = 26.7 (s)	**A** δ C=O 213.5 (s)
21	δ Ir-H = -7.7 (dd) $^2J_{P,H}$= 125 $^2J_{P,H}$= 18	δ Ir-P = 25.9 (s) δ Ir-P = 27.5 (d) $^2J_{P,P}$= 6.4	δ C=O 213.1(s)

In the ^{1}H NMR spectra the hydride signals can be observed between -7.7 and -9.2 ppm as a doublet of doublets with two different coupling constants; the bigger being around 125 Hz and the smaller around 19 Hz Figure 4.11. Only complex **20** has a chiral nitrogen and a pair of diastereomers can be detected, one is much more abundant than the other with a calculated ratio of 90/10.
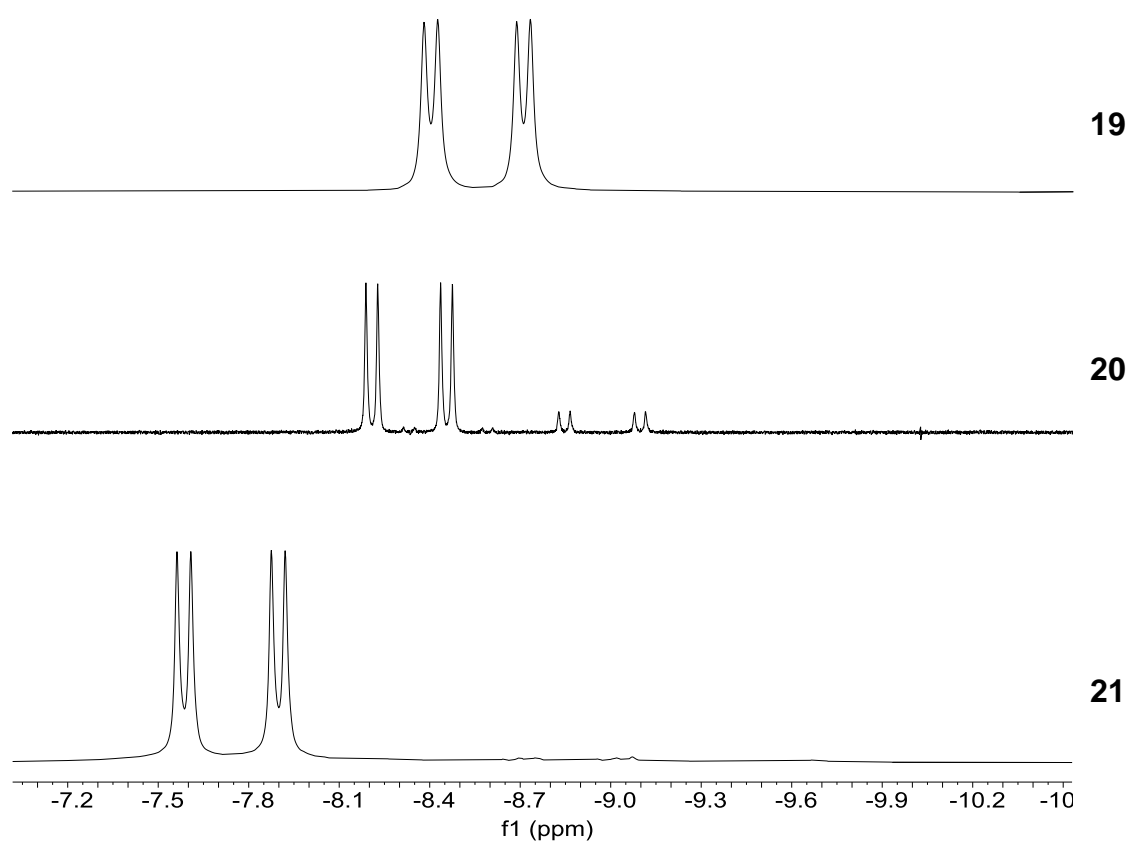
Figure 4.11 Hydride peaks from ^{1}H NMR for complexes 19-21

^{31}P{^{1}H} NMR spectra were done for complexes **19** and **21** in which two different signals can be observed, a doublet around 27 ppm and a singlet around 25 ppm, indicating that we have non equivalent phosphorous atoms in the complexes. The doublets have a coupling constant of 6-7 Hz which confirms the relative *cis* position of the phosphorus atoms.

^{31}P NMR spectrum was done for complex **20**; two signals can be differentiated, a singlet around 27 ppm and a doublet around 25 ppm. The doublet shows a coupling constant of 123 Hz, indicating that it is located *trans* to the hydride.

Regarding the [13]C{[1]H} spectra the most important signals are the ones that correspond to the acyl and the imine groups. Both groups can be differentiated for complex **19**, the signal of the imine appears at 208 ppm as a

doublet with a coupling constant of 80 Hz what supports that this group is in a *trans* position to a phosphorus atom. The signal of the acyl group appears at 215 ppm as a doublet with a coupling constant of 7 Hz, meaning that the acyl group is in a *cis* position to both phosphorus atoms. For complexes **20** and **21** only the signal of the acyl group was found as a singlet at 213 ppm.

Yellow monocrystals of complex **20** were obtained from a vapour diffusion of diethyl ether into a chloroform solution of complex **20** at -20 ºC and an X-Ray diffraction study could be done. The results confirm the proposed structure. A selection of bond lengths and angles are given in Table C. 5.

The coordinative environment of the iridium in complex **20** is a slightly distorted octahedron. The complex is composed of a hydride, a bidentate ligand (bonded by a phosphorus atom (P1) and a carbon (C1) of an acyl group), and a PCN terdentate ligand (bonded by a phosphorus atom (P2), a sp^2 carbon (C20) and a nitrogen (N2) from the secondary amine).
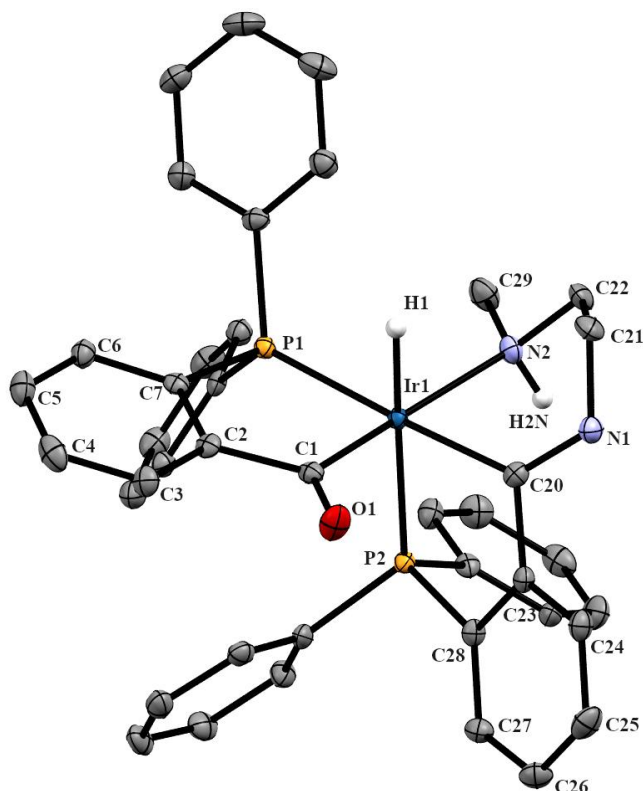
Figure 4.12 Molecular structure of complex 20 (50% probability ellipsoids)

4.2.4 Cationic PCN *N-trans* formation

Ketoimine complexes derived from ethylendiamine ligands can coordinate the free amine group to the metal centre in protic solvents to create a PCN six membered ring chelate. When the protic solvent is methanol the resultant cationic species is the one abovementioned in 4.2.2 for complexes **15** and **16**. On the other hand, when the solvent is a mixture of tetrahydrofuran and water, the result is a mixture of the already described complexes **15** and **16** and a new isomer; however, they could not be separated. These new isomers preserve the stereochemistry of the ketoimine complexes but the amine group replaces the chloride forming a chelate and the ketoimine proton has moved to the iminium group. The proportion of the mixture of isomers is different for ethylendiamine and *N*-methylethylendiamine being 20/80 for complexes **15/22** and 40/60 for complexes **16/23**. In both cases the more abundant complex is the isomer here described.
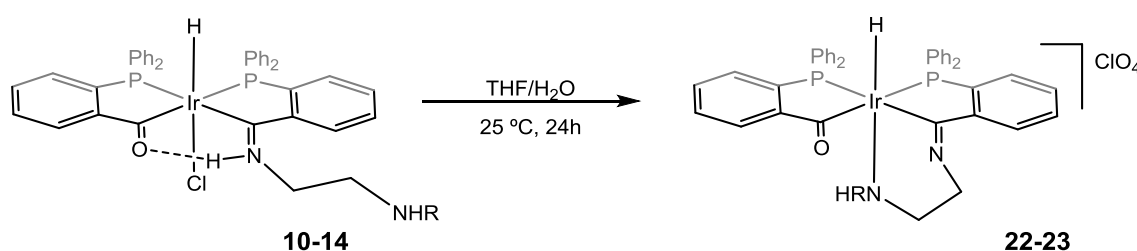
Figure 4.13 Cationic PCN *N-trans* chelate complex formation where: *R = H (22), R = CH$_3$ (23)*

Infrared study of complexes **22** and **23** was done and some characteristic signals could be seen; like the vibration of υ(N-H) at 3316 cm^{-1} **(22)** and 3224 cm^{-1} **(23)**. The signals corresponding to the vibration of Ir-H bond stretching can be seen at 2165 cm^{-1} **(22)** and at 2156 cm^{-1} for complex **(23)**; finally, the signals of the vibration of the υ(C=O) and υ(C=N) groups are located at 1575 cm^{-1} **(22)** and 1604 and 1573 cm^{-1} for complex **(23).** The presence of the perchlorate ion as a counterion was confirmed by the vibration signal υ(Cl-O) around 1099 cm^{-1}.

The two complexes have been fully characterised via multinuclear NMR. For the most relevant NMR data see Table 4.4 . For the ^{1}H NMR, ^{31}P{^{1}H} NMR , ^{13}C{^{1}H} NMR, COSY spectrum and ^{1}H-^{13}C HSQC spectrum of all complexes see Figure B. 82 to Figure B. 86 **(22)**; and Figure B. 87 to Figure B. 91 **(23).**

Table 4.4 The most relevant NMR data of complexes 22 and 23. The spectra were recorded CDCl$_3$ solution, the chemical shift is given in ppm and the coupling constants in Hz.

Complex	^{1}H NMR	^{31}P{^{1}H} NMR	^{13}C{^{1}H} NMR
22	δ Ir-H = -17.6 (t) ^{2}J$_{P,H}$= 16 δ O--*H*--N = 11.0 (br)	δ Ir-P = 10.8 (s) δ Ir-P = 32.4 (s)	δ C=O or C=N 228.1 (d) ^{2}J$_{P,C}$= 88 235.2 (d) ^{2}J$_{P,C}$= 93
23	**A** δ Ir-H = -19.6 (t) ^{2}J$_{P,H}$= 18 **B** δ Ir-H = -19.8 (t) ^{2}J$_{P,H}$= 18 **A** δ O--*H*--N = 11.1 (br) **B** δ O--*H*--N = 10.8 (br)	**A** δ Ir-P = 6.6 (d) δ Ir-P = 33.8 (d) ^{2}J$_{P,P}$= 12 **B** δ Ir-P = 11.5 (d) δ Ir-P = 28.9 (d) ^{2}J$_{P,P}$= 11	

According to NMR data, complexes **10** and **11** maintain their stereochemistry when they turn into complexes **22** and **23**. In the ^{1}H NMR a triplet can be seen at -17.6 ppm for complex **22** and two triplets at -19.6 and -19.8 ppm for complex **23** (Figure 4.14) , meaning that the hydride is placed *trans* to an electronegative atom and *cis* to two phosphori. The two diastereomers seen in complex **23** appear in an 80/20 ratio and are the result of a chiral metal centre and chiral nitrogen in the PCN chelate. The iminium proton could be detected for both complexes as it appeared as a broad signal around 11 ppm.
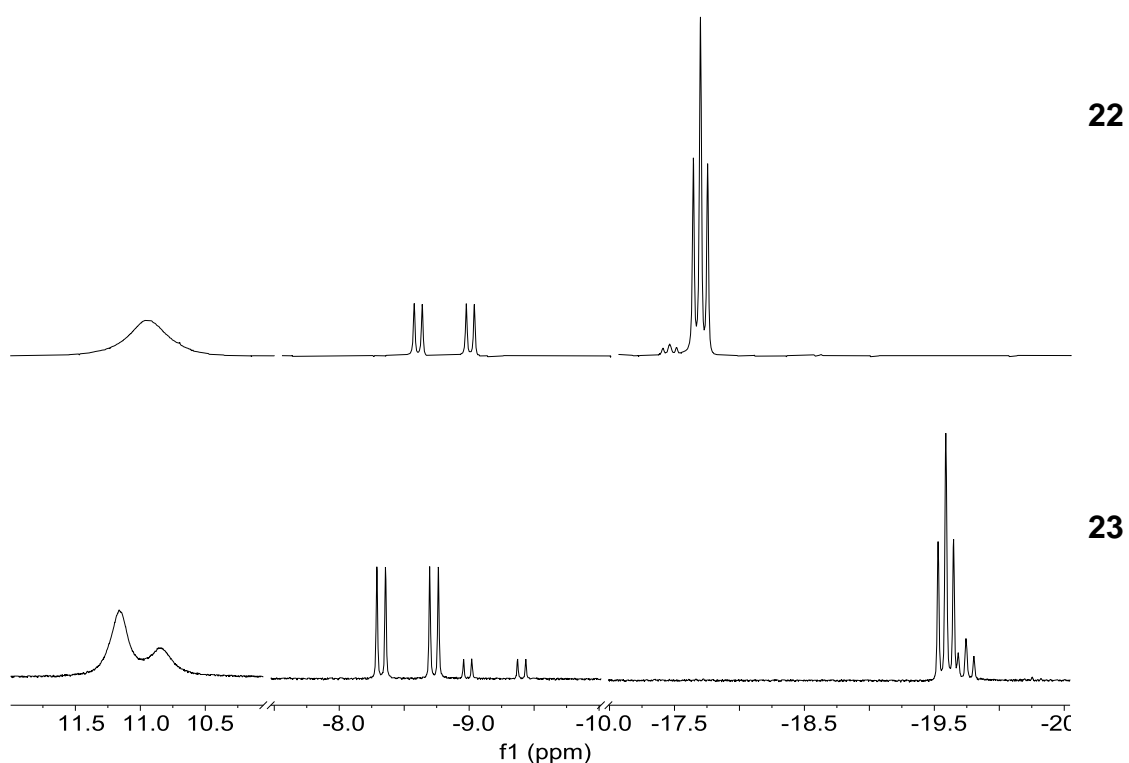
Figure 4.14 Most characteristic signals of complexes 22 and 23

In the $^{31}P\{^1H\}$ NMR spectra two signals that belong to two different phosphori appear for each complex with a coupling constant of 12 Hz that proves the *cis* position of the phosphori to each other. Furthermore, in the $^{13}C\{^1H\}$ spectrum of complex **22** two doublets appear at low field corresponding to the acyl and iminium groups. The coupling constant of these signals have a value around 90 Hz and it follows that these groups are in a *cis* position to phosphorus atoms.

Yellow monocrystals of complex **22** were obtained from a vapour diffusion of diethyl ether into a methanol solution at -20 ºC of the mixture of complexes **15** and **22** and a monocrystal of complex **22** could be obtained. The X-Ray diffraction study could be done and the results confirm the proposed structure. A selection of bond lengths and angles are given in Table C. 6.

Compound **22** crystallises as a mixture of enantiomers in the $P2_1/c$ spacegroup. This structure (Figure 4.15) shows a coordinative environment of the iridium of a slightly distorted octahedron. In addition, the structure reveals that there is a nitrogen atom from the PCN tridentate ligand *trans* to the hydride.
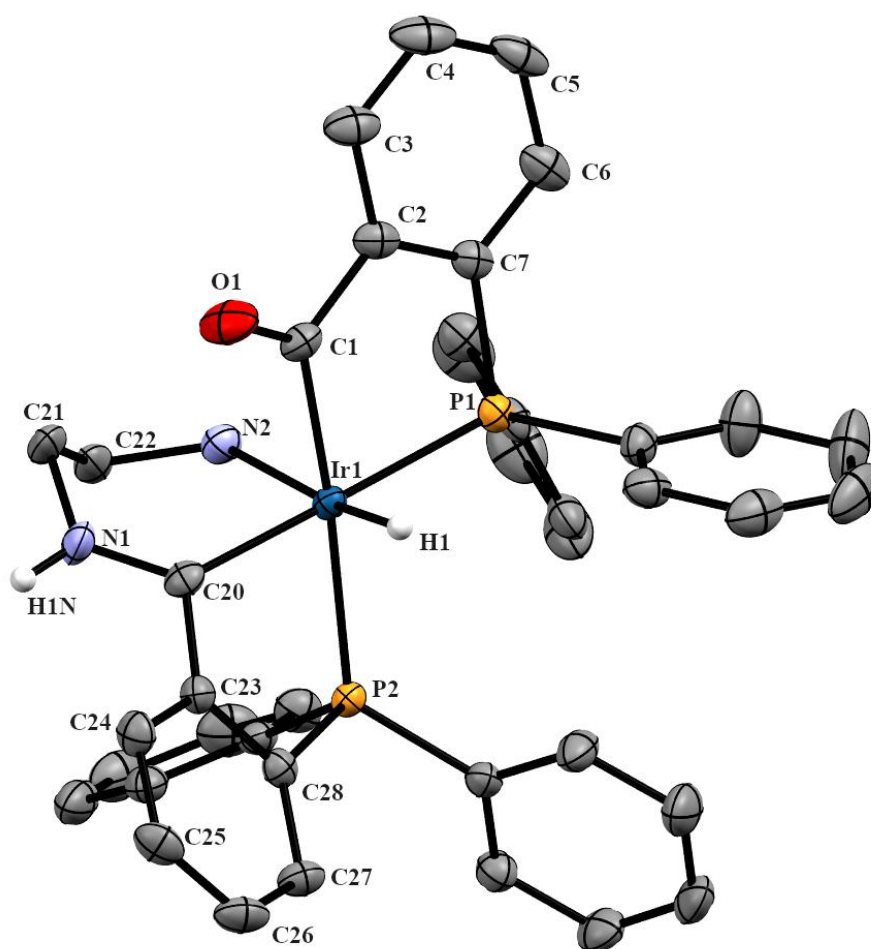
Figure 4.15 Molecular structure of complex 22 (50% probability ellipsoids)

4.2.5 Analysis of the X-Ray structures

The structure of compound **10** is very similar to the other ketoimine type of compounds reported, and to the parent compound **1**. When the Schiff base is formed, the proton that was delocalised between both oxygen atoms now is localised on the nitrogen. In order to maximise the strength of this hydrogen bond and accommodate the bulkiness of the organic group of the amine two main changes occur in the structure, firstly the C1-Ir-C20 angle widens slightly and secondly the P-C chelates twist.

In compound **1** the P, C coordinating atoms are coplanar with the aromatic ring they are supported on, this twist upon the Schiff base formation alters this and to a greater degree in the chelate bearing the imine carbon, 15.03° between the mean plane formed with P1, Ir and C1 and the mean plane formed with C2-C7 aryl ring and 25.07° between the mean plane formed with P2, Ir and C20 and the mean plane formed with C23-C28 aryl ring.

Except in **10** all the rest of complexes show PCN coordination, and two types can be seen, the ones where the imine is protonated and those lacking this proton.

When the ketoimine complexes **10 - 14** rearrange they give the isomeric acyl-iminium type compounds **15 - 18**. All the distances and angles in **15** and **16** are very similar to those found in the related neutral acyl-imine complex with 2-(aminomethyl)pyridine as the amine derivative and in complex **20**. The only effect that the methyl has upon **16** is the slight lengthening of the Ir-P1 bond, from 2.299(1) Å in **15** to 2.324(2) Å in **16**. This can be easily explained by steric reasons. The biggest changes come in the twist of both P,C chelate rings. The chelate ring containing the acyl group recovers the planarity of **1** with angles between the mean plane formed with P1, Ir and C1 and the mean plane formed with C2-C7 aryl ring of 8.16° for **15**, 9.27° for **16** and 4.87° for **20**.

The cationic complex **22**, has the same structure as **2** but the dangling amine has replaced the chloride atom in the apical positions *trans* to the hydride. This compound shows very similar bond lengths to those showed by

10, however, as consequence of the formation of the new bond the hydrogen bond between the acyl group and the acyliminium breaks. It was expected that the newly formed bond would twist the P,C chelate of the iminium group more than in **10**, and this is reflected in the angle between the mean plane formed with P2, Ir and C20 and the mean plane formed with C23-C28 aryl ring which it is now 38.69°. This may seem as a very big change, however this angle is comparable to the one showed in other ketoimine type of complexes such as when methylamine (35.02°), 2-(aminoethyl)pyridine[11] (34.27°) or furfurylamine[77] (37.88°) are used.

All of them also adopt a twisted boat conformation, interestingly the protonated compounds are more twisted than the neutral counterparts, thus the N2-C22-C21-N1 torsion angle for **20** is 44.2(5)°, while for **15**, **16** and **22** is 75.3(5)°, 82(1)° and 75.1(3)° respectively

Table 4.5 Selected bond lengths (Å) and angles (°) for 10, 15, 16, 20 and 22. Standard deviation appears in parentheses.

	10	15	16	20	22
Ir1-P1	2.3000(7)	2.2984(6)	2.3241(7)	2.3145(10)	2.3029(8)
Ir1-P2	2.3361(8)	2.3425(7)	2.3425(5)	2.3268(10)	2.3508(8)
Ir1-C1	2.0486(7)	2.0306(5)	2.0258(6)	2.014(4)	2.079(3)
Ir1-C20	2.0625(7)	2.0450(5)	2.0390(6)	2.077(4)	2.038(3)
Ir1-N2	-	2.2163(6)	2.2846(7)	2.249(4)	2.232(3)
Ir1-Cl1	2.4919(7)	-	-	-	-
Ir1-H1	1.4844(4)	1.4193(5)	1.4955(3)	1.59(6)	1.57(3)
C20-N1	1.2994(3)	1.2911(3)	1.2966(3)	1.288(5)	1.296(4)
P1-Ir1-C1	82.9(1)	84.5(1)	84.5(3)	84.82(12)	83.22(9)
P2-Ir1-C20	81.5(1)	78.4(1)	78.2(2)	80.22(12)	76.81(9)
P2-Ir1-C1	173.0(1)	89.8(1)	89.4(3)	90.60(12)	169.10(9)
P1-Ir1-C20	175.9(1)	177.1(1)	175.7(2)	175.10(11)	177.2(1)
C20-Ir1-N2	-	88.1(2)	86.5(3)	79.41(15)	88.5(1)

4.3 Reactivity of dihydridoirida-β-diketone

Dihydridoirida-β-diketone can react with alkyl diamines which contain one primary amine group to form new hydridoamino complexes. The selected amines were the *N*-methylethylendiamine and 2-(aminomethyl)piperidine. This process can happen in protic solvents such as methanol and in the presence of a base.
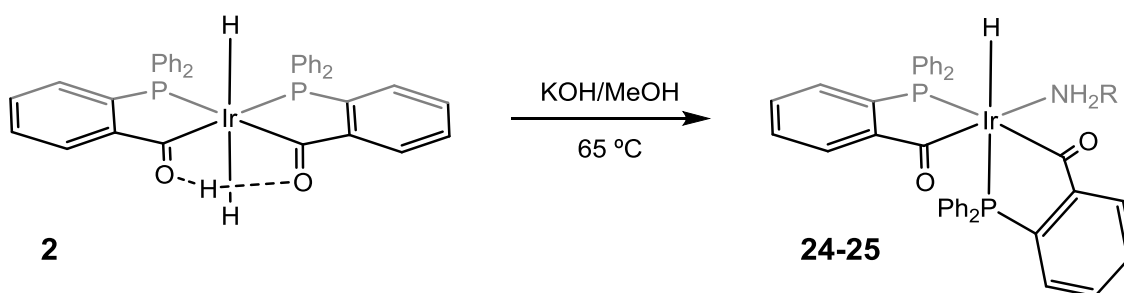
Figure 4.16 Reactivity of dihydridoirida-β-diketone with alkyl-amines where: *R = CH₂CH₂NHCH₃ (24), R = CH₂(C₅H₉N) (25).*

In the infrared spectra signals of the vibration of υ(N-H) appear at 3313 and 3266 cm^{-1} **(24)** and 3405 cm^{-1} **(25)**; the ones corresponding to the vibration of Ir-H bond stretching can be seen at 2021 cm^{-1} **(24)** and at 2036 cm^{-1} for complex **(25)** and finally the signals of the vibration of the υ(C=O) and υ(C=N) groups are located at 1574 cm^{-1} **(24)** and 1608 cm^{-1} **(25)**.

Complexes **24** and **25** have been fully characterised via multinuclear NMR. For the most relevant NMR data see Table 4.6. For the ^{1}H NMR, ^{31}P{^{1}H} NMR , ^{13}C{^{1}H} NMR, COSY spectrum and ^{1}H-^{13}C HSQC spectrum of both complexes see Figure B. 92 to Figure B. 96 **(24)**; and Figure B. 97 to Figure B. 101 **(25).**

Table 4.6 The most relevant NMR data of complexes 24 and 25. The spectra were recorded in $CDCl_3$ solution, the chemical shift is given in ppm and the coupling constants in Hz.

Complex	^{1}H NMR	^{31}P{^{1}H} NMR	^{13}C{^{1}H} NMR
24	δ Ir-H = -8.0 (dd) $^2J_{P,H}$= 130 $^2J_{P,H}$= 20 δ H_2N = 2.6(m) δ H_2N = 2.8(m)	δ Ir-P = 24.8 (s) δ Ir-P = 30.2 (s)	δ C=O 214.7 (s) δ C=O 238.8 (d) $^2J_{P,C}$= 103
25	δ Ir-H = -8.30 (dd) $^2J_{P,H}$= 137 $^2J_{P,H}$= 19 δ Ir-H = -8.29 (dd) $^2J_{P,H}$= 137 $^2J_{P,H}$= 19	δ Ir-P = 22.6 (s) δ Ir-P = 22.7 (s) δ Ir-P = 28.1 (s) δ Ir-P = 28.5 (s)	δ C=O 218.2 (d) $^2J_{P,C}$= 4 δ C=O 218.6 (d) $^2J_{P,C}$= 7 δ C=O 236.9 (d) $^2J_{P,C}$= 106 δ C=O 237.1 (d) $^2J_{P,C}$= 106

As it has been mentioned above, the primary amine bonds the metal centre and this triggers a rearrangement in the stereochemistry of the iridium. The ketoenolic proton and one of the hydrides are released as a dihydrogen molecule and the other hydride remains untouched.

With regard to the ^{1}H NMR the hydride appears as a doublet of doublets around -8.0 ppm for complex **24** and -8.3 ppm for complex **25.** This agrees the hydride being *trans* to one phosphorous atom and *cis* the other, being the coupling constants around 130 Hz for the phosphorus in *trans* and around 20 Hz for the phosphorus in *cis*. In the hydride signal of complex **25** the peaks corresponding to two diastereomers appear interwoven and with the same height, indicating that they appear in a 50/50 ratio see Figure 4.17.
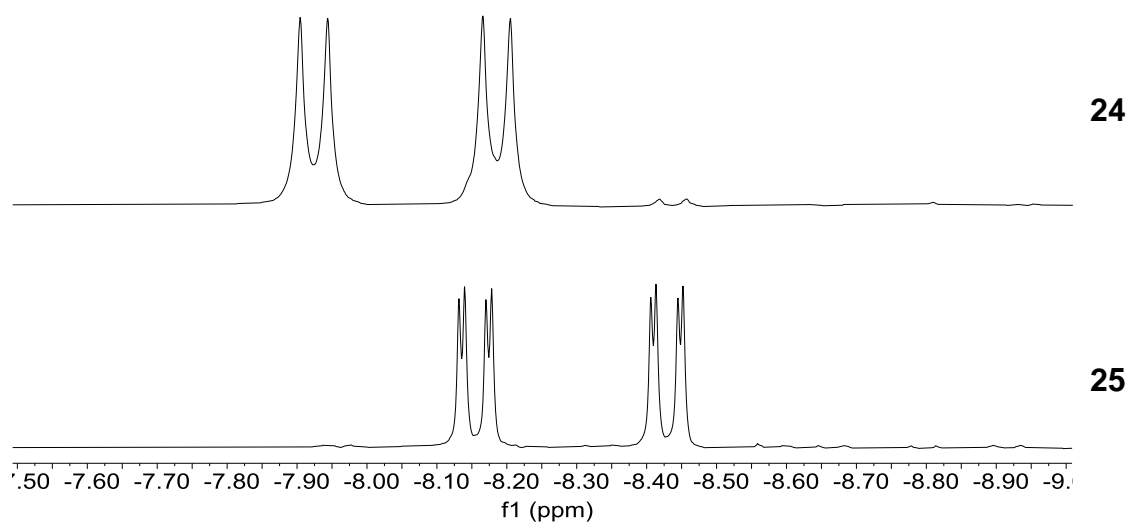
Figure 4.17 Hydride signals of complexes 24 and 25

As for the ^{31}P{^{1}H} NMR it can be said that two different phosphori appear for complex **24** and four different phosphori for complex **25**. In the ^{13}C{^{1}H} NMR the most important signals are the ones of the acyl groups. Because of the coupling constant values it can be known the positions of these carbons. The acyl groups that appear around 215 ppm with a coupling constant of 0-7 Hz are in a *cis* position to both phosphori; on the other hand, the ones that appear around 240 ppm with a coupling constant of 103-106 Hz are in a *trans* position to one phosphorus and *cis* to the other.

Yellow monocrystals of complex **25** were obtained from a vapour diffusion of hexane into a chloroform solution of complex **25** at -20 ºC. The X-Ray diffraction study was done; but, because of the disorder of the ligand all the atoms could not be placed. Nevertheless, the stereochemistry around the metal centre is confirmed by this study; see Figure C. 5.

4.4 Catalytic activity of the new complexes for the methanolysis of ammonia-borane

Homogeneous methanolysis of ammonia-borane (AB) has been demonstrated to be efficient by complexes **1** and **7** in the previous chapter. With that in mind, the aim of this subchapter is to study if the alkyl diamine derivatives can also carry out the abovementioned methanolysis reaction. Moreover, the performance of complex **13** is analysed at different temperatures and catalyst loading.

Ketoimine complexes **10**, **11**, **12**, **13** and **14** have been tested for the catalytic methanolysis of AB in 2.5 mL of methanol in which all complexes are completely soluble. Complex **10** can release 3.0 equivalents in 360 seconds (6 min), complex **11** and complex **14** need 240 seconds (4 min) to release 2.9 and 2.8 equivalents respectively, complex **12** releases 2.9 equivalents after 180 seconds (3 min) and finally, complex **13** needs only 150 (2.5 min) seconds to release 2.9 equivalents of H_2 (Figure 4.18). As can be seen, the nature of the dangling amine does not affect much the rate of hydrogen liberation.
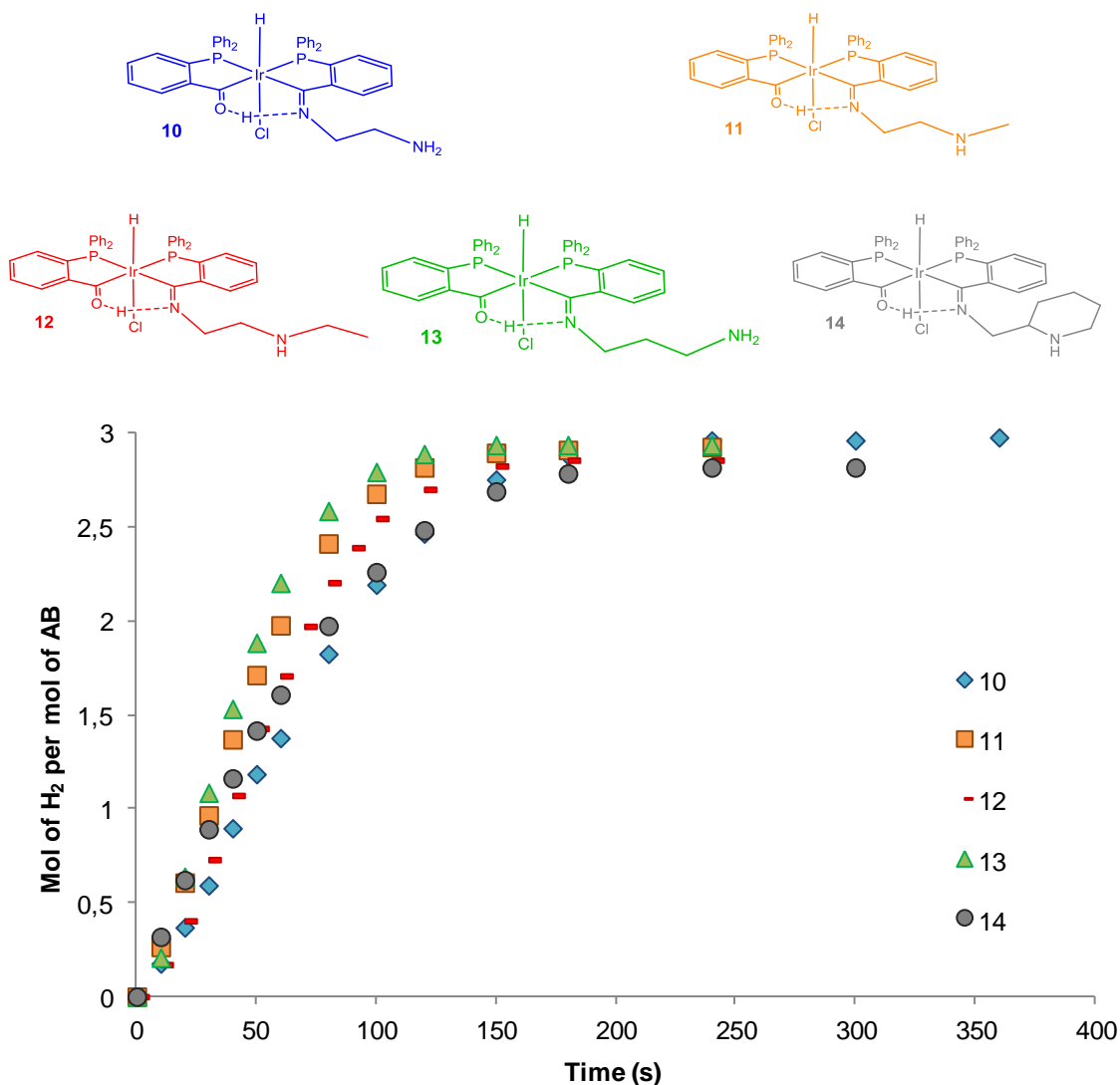
Figure 4.18 Hydrogen release in the methanolysis of AB by complexes 10-14. 2.5mL of methanol, 0.5% catalyst loading at 60 ºC

Cationic PCN complexes **15**, **16**, **17** and **18** have also been tested for this catalysis with slightly lower performance than the ketoimine ones. Complex **15** releases 2.9 equivalents after 1200 seconds (20 min), complex **16** and **18** need 960 seconds (16 min) to release 2.7 and 2.8 equivalents and it only takes 360 seconds (6 min) to complex **17** to release 2.8 equivalents (Figure 4.19).
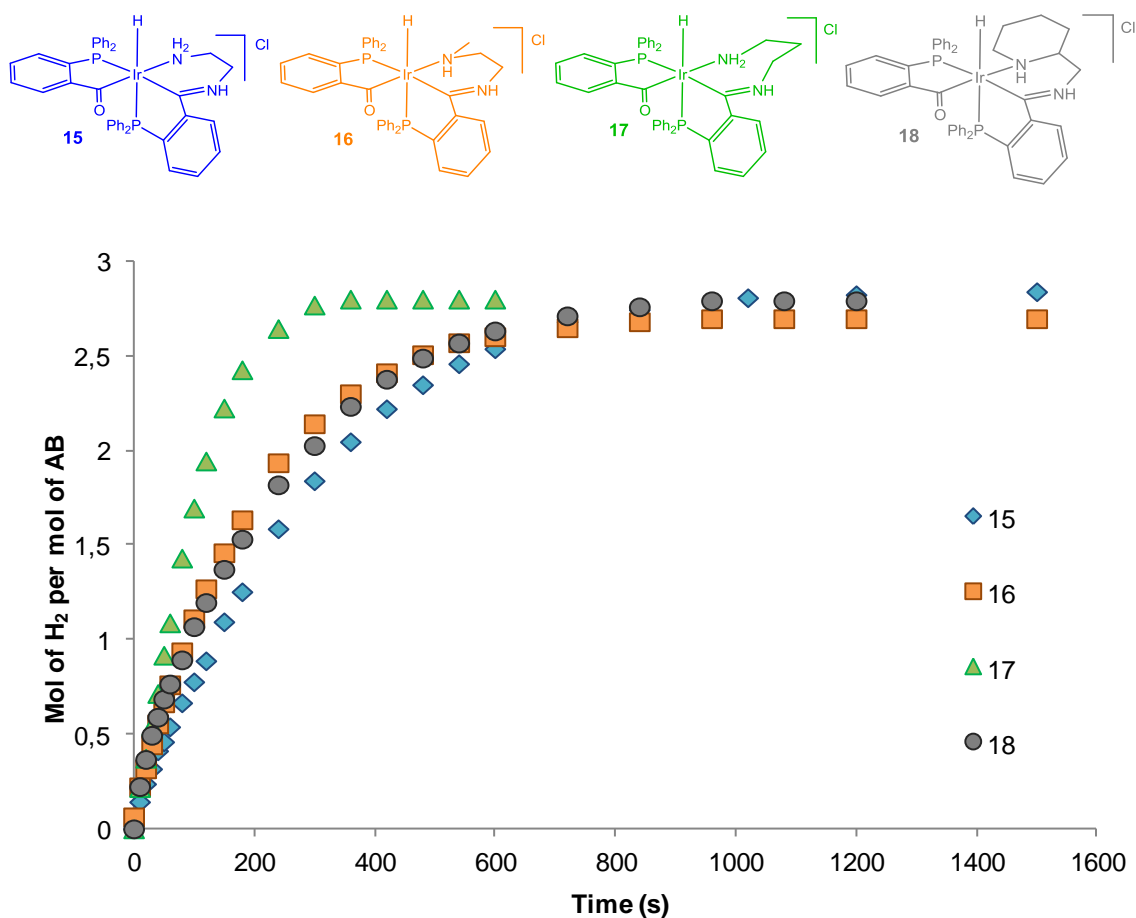
Figure 4.19 Hydrogen release in the methanolysis of AB by complexes 15-18. 2.5mL of methanol, 0.5% catalyst loading at 60 ⁰C

The best results obtained for complex **17** can be explained by the number of members that the PCN chelate has in this complex. Whereas in the other complexes the rings are six membered, the one in complex **17** is seven membered which makes it less stable. According to what was described in the previous chapter for the catalytic cycle of the methanolysis of AB, a coordinative vacant is needed in order to coordinate the AB and start the catalysis. Having a seven membered ring could make complex **17** more likely to open the chelate and perform better in the catalysis.

In order to have a comparison among the different type of complexes derived from the same alkyl diamine, complexes **10**, **15** and **19** were evaluated.

Complex **19** needs 3000 seconds (50 min) to release 2.7 H_2 equivalents (Figure 4.19).
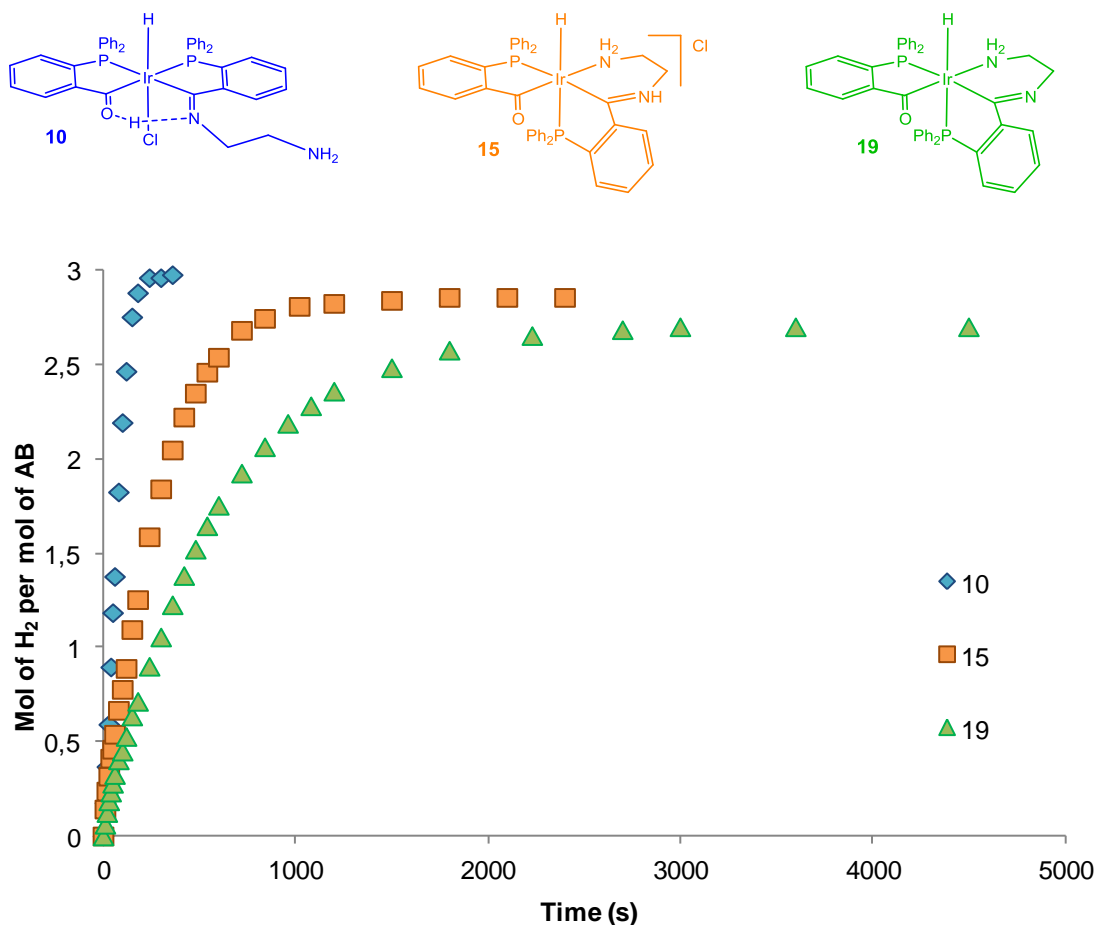
Figure 4.20 Hydrogen release in the methanolysis of AB by ethylendiamine derived complexes 10, 15 and 19. 2.5 mL of methanol, 0.5% catalyst loading at 60 ºC

In conclusion, alkyl diamines derived complexes have shown to be efficient catalyst for the H_2 release from the methanolysis reaction of AB. After a comparison among the different complexes ketoimines tend to perform better than the cationic PCN chelates and these cationic complexes show better results than the neutral ones. Moreover, the presence of a ketoiminium or iminium proton could improve the good results in the catalysis.

4.4.1 Kinetic study of AB methanolysis with complex 13

After testing the ability of the different alky diamines derived complexes for the catalytic hydrogen release from AB in methanol a kinetic study for the best performing complex, complex **13**, was carried out.

In order to study the dependence of the activity on the concentration of the catalyst, the catalysis of the methanolysis of AB was carried out with a 0.46 M of AB and different loadings of complex **13**. As it could be expected, the higher the catalyst loading the faster the hydrogen release is (Figure 4.21). When a concentration of $0.46 \cdot 10^{-3}$ M of $[catalyst]_0$ is used (0.1%) 2.9 equivalents of hydrogen are released in 480 seconds (8 min); while using a concentration of $1.86 \cdot 10^{-3}$ M (0.4%) it only needs 240 seconds (4 min) to release hydrogen, 2.9 equivalents.
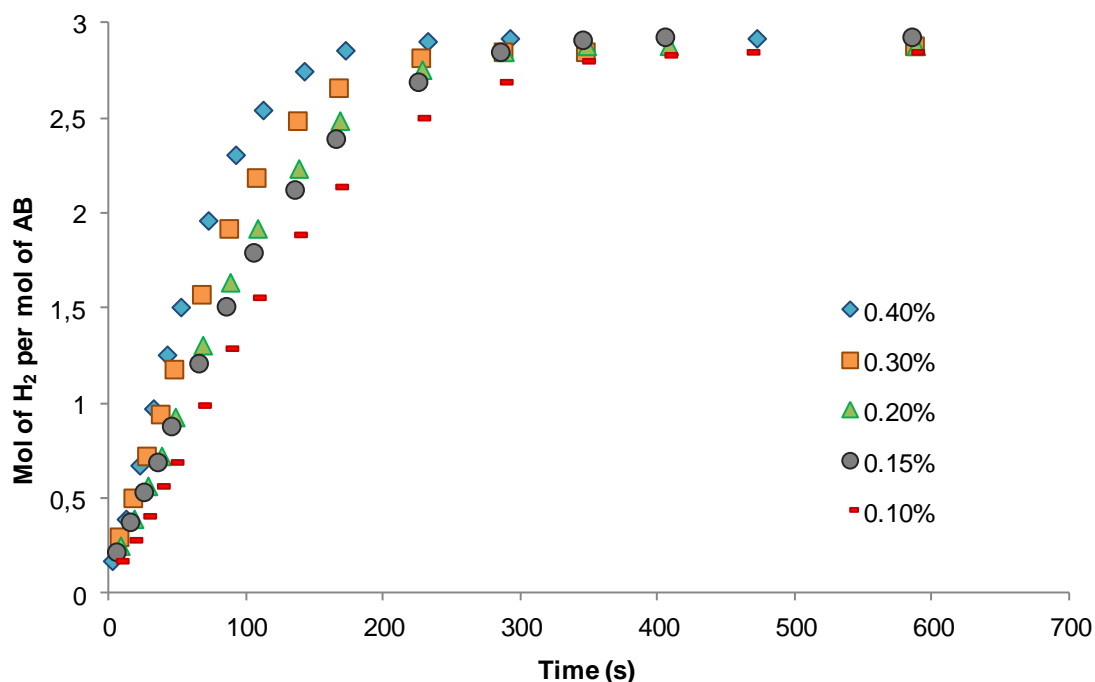
Figure 4.21 Hydrogen release from 0.46 M AB with various $[catalyst]_0$ of 13 in 2.5 mL of MeOH . T, 60 ºC

The kinetic profile seen in all the methanolysis of AB catalysed by **13** in different concentrations can be considered as a pseudo-first-order reaction model with respect to the [substrate]. This has been applied to determine the rate constants, the k_{obs}, by plotting time versus Ln(1-(H$_2$ equiv./H$_2$ equiv.final)) Figure 4.22.
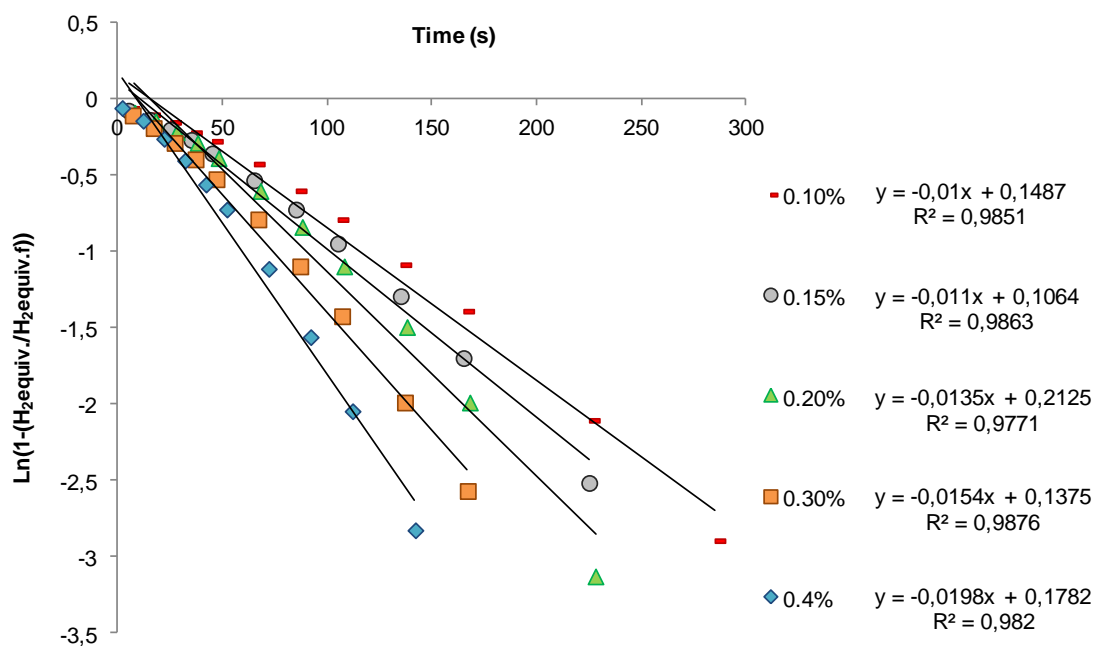
Figure 4.22 First order plots for the hydrogen release from 0.46 M AB with various [catalyst]$_0$ of 13 in 2.5 mL of MeOH. T, 60 ºC

As expected, when the concentration of the catalyst increases the value of the k_{obs} raises and the time needed to complete the catalysis decreases. The achieved conversions do not change much with the loading of the catalyst as we obtain values between 95 and 98 % for all the cases see Table 4.7.

Table 4.7 % Conversion, Time Required, and Rate Constants for the methanolysis of 0.46 M AB with different loadings of catalyst 13 at 60 ºC.

Catalyst %	Conversion %	Time (s)	$10^3 \cdot k_{obs}$ (s^{-1})
0.10	95	480	10±0.4
0.15	97.7	420	11±0.4
0.20	96	360	13.5±0.7
0.30	96	300	15.4±0.6
0.40	97.3	240	19.8±0.9

Once it has been assumed a first order dependence with respect to [catalyst]$_0$, it can be applied that $k_{cat} \cdot$[catalyst]$_0$ = k_{obs}. With that in mind, a graph of the obtained values for the k_{obs} versus the concentrations of catalyst was plotted (Figure 4.23) and a value of k_{cat} = 6.91±0.58 M^{-1}s^{-1} was obtained.
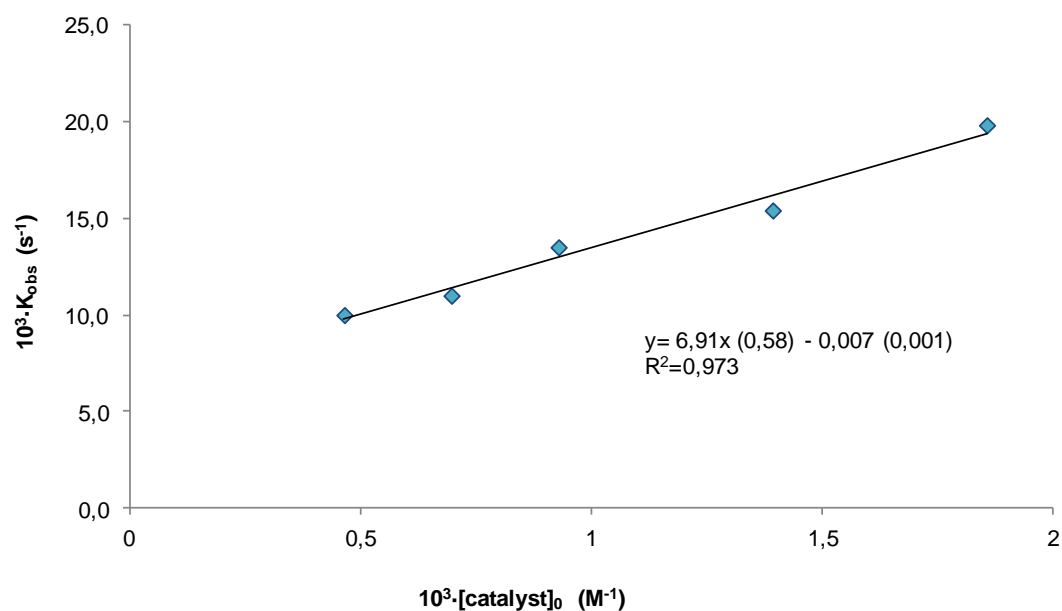
Figure 4.23 Influence of [catalyst]$_0$ on K_{obs} for the hydrogen release from AB with 13 as catalyst in MeOH, Standard deviations are given in parentheses. T, 60 ºC

The activity of the catalysis at different temperatures has been tested in a range from 45 to 60 ºC (Figure 4.24). The temperature has a definitive influence on the reaction rate; the higher the temperature the faster the hydrogen release is.
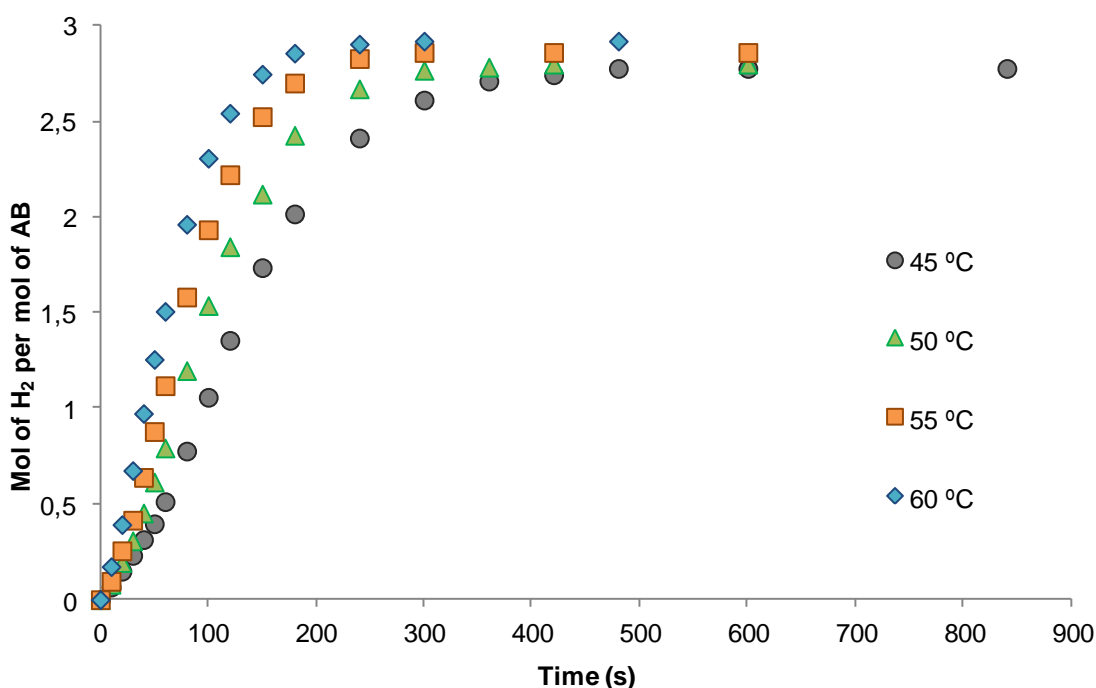
Figure 4.24 Hydrogen release from 0.46 M AB with complex 13 as catalyst in 2.5 mL of MeOH at different temperatures.

The k_{obs} values obtained at different temperatures were used to obtain the activation parameters for the methanolysis reaction of AB. By representing $\ln(k_{obs}/T)$ versus $1/T$ (Eyring's equation) the values for ΔH^+ and ΔS^+ can be determined (Figure 4.25). The enthalpy value, $\Delta H^+ = 8.41 \pm 1.01$ kcal·mol^{-1}, is the expected one for reactions carried out in solution; a negative value for ΔS^+ is obtained, $\Delta S^+ = -41.23 \pm 3.12$ cal·mol^{-1}·K^{-1}, which shows that the molecular disorder is lower in the intermediates.
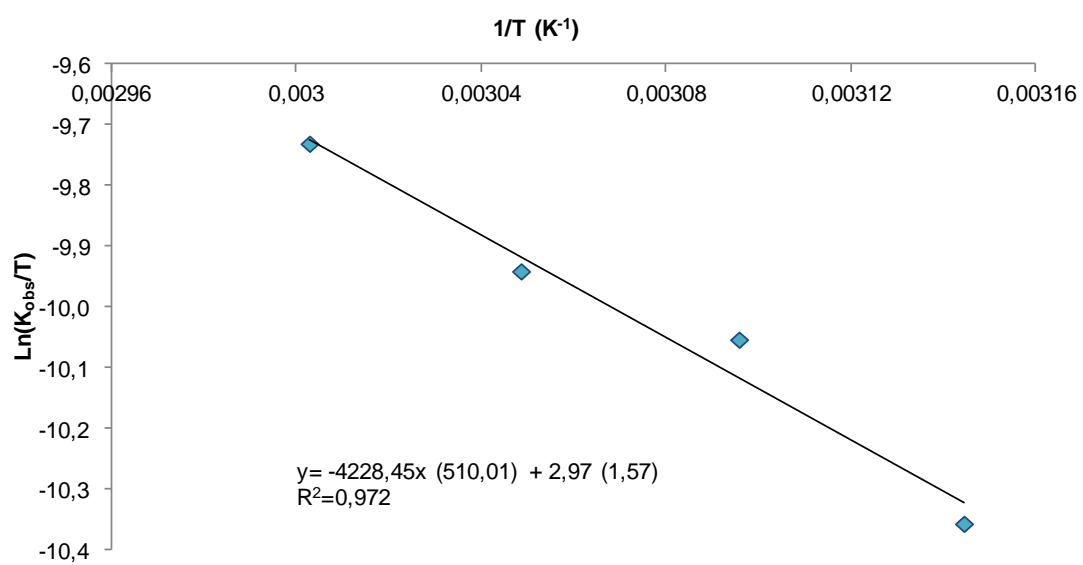
Figure 4.25 Eyring's plot of the hydrogen release from 0.46 M AB with 13 as catalyst in 2.5 mL of MeOH.

4.4.2 Study of intermediate species via *in situ* multinuclear NMR

In an attempt to obtain some insights on how the catalysis of the methanolysis of AB works with the new described complexes, the catalytic reaction was carried out in deuterated methanol and it was followed by multinuclear NMR techniques. The chosen complex for this purpose has been complex **10** because it is the easiest to be identified.
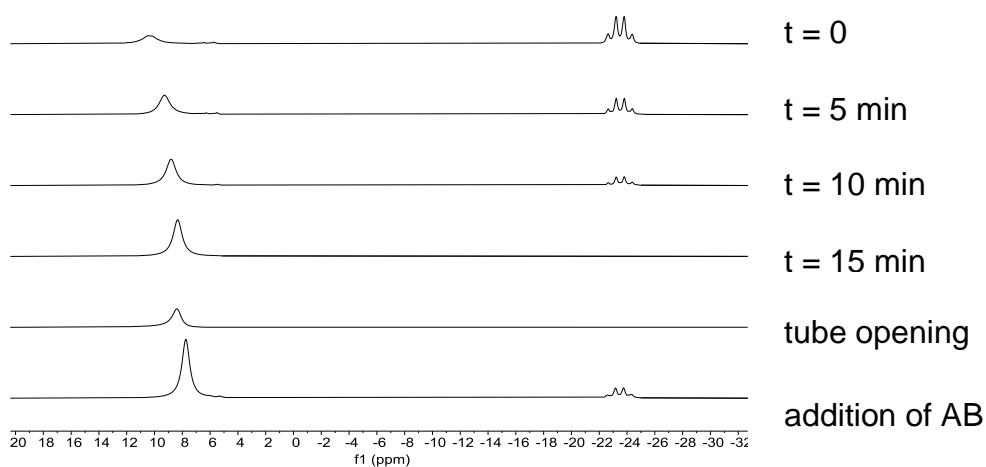
Figure 4.26 ^{11}B NMR of the *in situ* methanolysis of AB by complex 10

The substrate disappearance can be seen in the ^{11}B NMR (Figure 4.26); as time goes on, the signal corresponding to the substrate, the quadruplet at -23.5 ppm, disappears and a singlet at 9.3 ppm appears. If the first recorded spectrum of ^{11}B NMR is in depth analysed the intermediate species can be identified (Figure 4.27). These minor species are observed as a triplet at -13.8 ppm with a coupling constant of 109 Hz and as a doublet at 5.3 ppm with a coupling constant of 119 Hz; and could belong to two ammonia-methoxyborane adduct intermediates.

9.3 ppm (s)

-23.5 ppm (q, $J_{H,B}$ = 110 Hz)

5.3 ppm (d, $J_{H,B}$ = 119 Hz)

-13.8 ppm (t, $J_{H,B}$ = 109 Hz)

f1 (ppm)
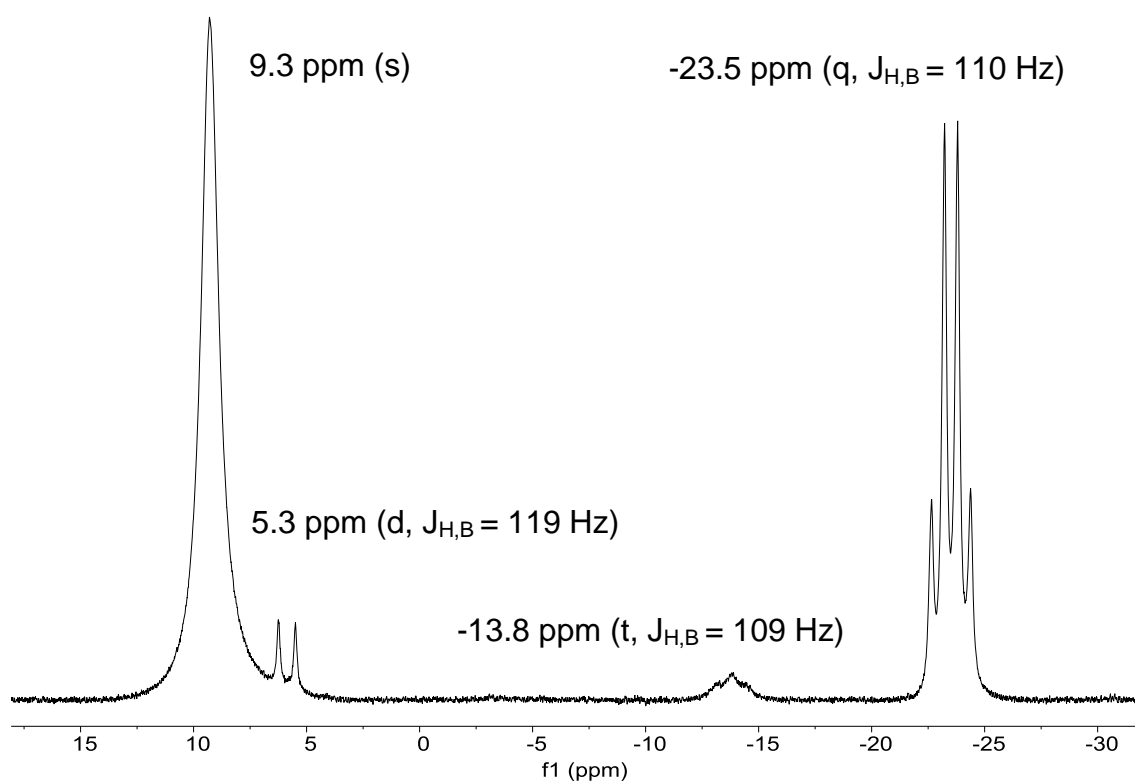
Figure 4.27 ^{11}B NMR of the *in situ* methanolysis of AB by complex 10 where different intermediates appear

When the catalysis is followed by ^{1}H NMR the disappearance of AB can be seen between 1.1 and 1.8 ppm. The emergence of hydrogen can be found at 4.6 ppm as a singlet for H_2 and as a triplet for HD ($J_{D,H}$ = 43 Hz) in Figure 4.28.

t = 0

t = 5 min

t = 10 min

t = 15 min

tube opening

addition of AB

f1 (ppm)
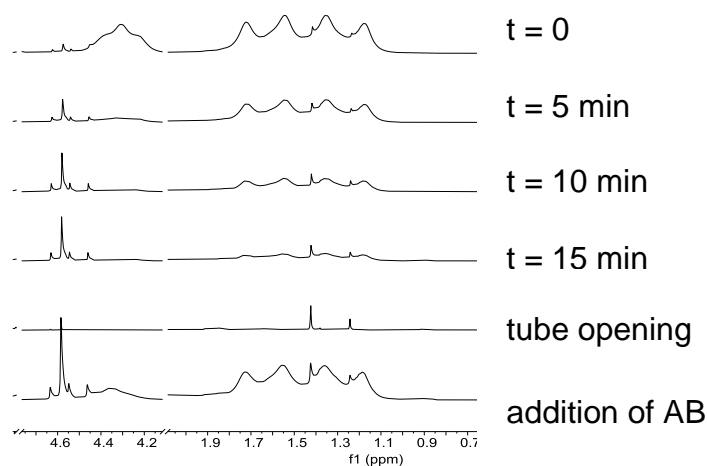
Figure 4.28 ^{1}H NMR of the *in situ* methanolysis of AB by complex 10

Unfortunately, many species can be detected in both ^{1}H NMR (Figure 4.29) and ^{31}P{^{1}H} NMR (Figure 4.30); making it impossible to know which species is involved in the catalytic reaction.
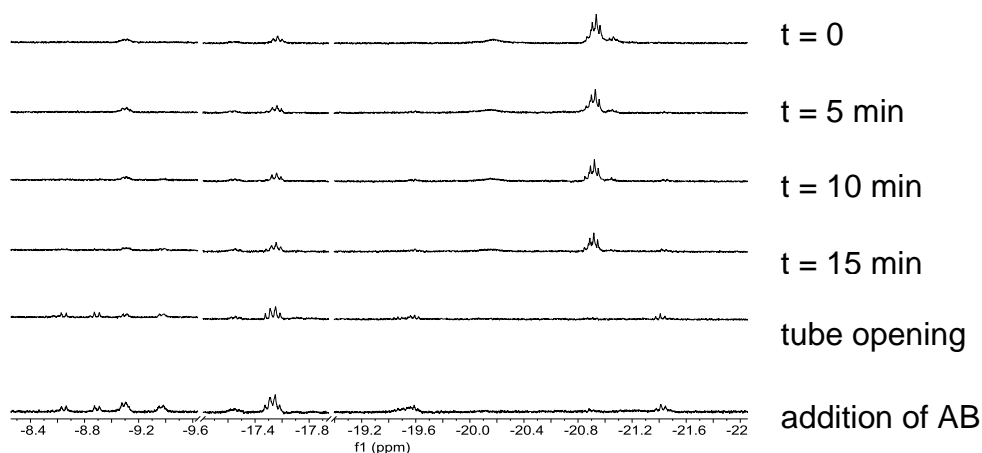
Figure 4.29 ^{1}H NMR of the *in situ* methanolysis of AB by complex 10
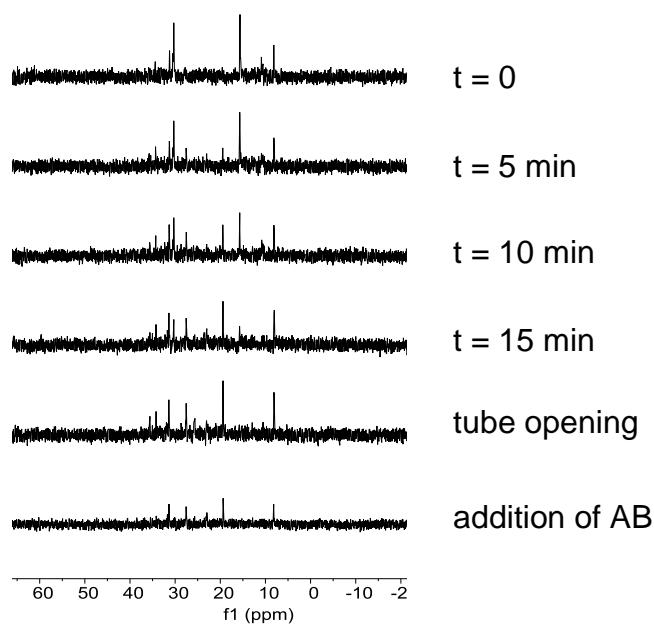
Figure 4.30 ^{31}P{^{1}H} NMR of the *in situ* methanolysis of AB by complex 10

Chapter 5

Iridapyrazole derived complexes, synthesis and catalytic activity

5.1 Introduction

In previous chapters we have reported on the reactivity of irida-β-diketones with amines have afforded new complexes, containing terdentate ligands among others, and on their catalytic activity towards hydrogen release from solid storage materials. Previous work from our laboratory revealed that the reaction of irida-β-diketones with hydrazine afforded a previously unknown type of metallacycle, the iridapyrazole complex **3**, which was obtained in very low yield.

The goal of this chapter is to improve the synthesis of complex **3** using a different reaction pathway. Once this is achieved, the reactivity of the above mentioned complex will be studied. On the one hand, the reactivity of the bond between the iridium and the chloride atoms to afford new iridapyrazole complexes will be tested. On the other hand, the behaviour of the iridapyrazole ring will be studied in order to establish a comparison with the behaviour of organic pyrazoles.

Finally, the catalytic activity of the new iridapyrazole derived complexes for the methanolysis reaction of ammonia-borane will be studied.

5.2 Synthesis of an iridapyrazole, complex 3

5.2.1 Synthesis of L_1

In the search for obtaining complex **3** with a better yield, we tried the imination reaction of *o*-(diphenylphosphino)benzaldehyde with hydrazine to afford a new ligand, which could react with the metal centre. After a reflux in ethanol the ligand 1,2-bis-2-((diphenylphosphaneyl)benzylidene)hydrazine (**L_1**) was indeed obtained (Figure 5.1).
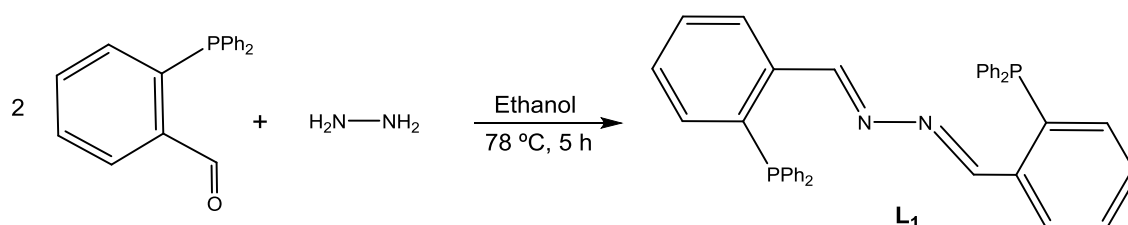
Figure 5.1 Formation of new ligand L_1.

L_1 has been characterised by multinuclear NMR, IR spectroscopy and monocrystal X-Ray diffraction.

In the ^{1}H NMR the signal of the imine protons appears at 9.23 ppm as a doublet with a coupling constant of $J_{P,H}$ = 4.5 Hz (Figure B. 102) while the proton of the aldehyde in the starting material appeared at 10.54 ppm. On the other hand, the aromatic protons maintain the shape and the position of the starting material. In the ^{31}P{^{1}H} NMR **L_1** appears as a singlet at -14.6 ppm (Figure B. 103). The ^{15}N NMR spectrum was measured and a singlet at 367.4 ppm could be observed.

The newly created imine groups have also been detected by the IR spectroscopy. The signal due to the C=N group is located at 1614 cm^{-1}.

Yellow monocrystals of **L₁** were obtained by vapour diffusion of pentane into a dichloromethane solution at -20 ºC and the X-Ray diffraction study was done, see Table 5.1.

Table 5.1 Selected bond lengths (Å) and angles (º) on L₁. Standard deviation appears in parentheses. Symmetry operation (i) –x, -y, -z.

Bond lengths			
N1-N1'(i)	1.406(3)	C1-C2	1.465(2)
N1-C1	1.276(2)		
Bond angles			
C1-N1-N1'(i)	111.88(18)	N1-C1-C2	120.37(16)

L₁ crystallises in the monoclinic $P2_1/c$ space group, being the asymmetric unit half of the molecule, the other half has been generated by a symmetry operation.

The N1-N1' bond length (1.406(3) Å) is shorter than that expected for a single bond between two nitrogen atoms; this feature along with the sp^2 hybridization of C1 (N1-C1-C2 angle is 120.37(16)º) confirms π-electron delocalization extended to the N1-N1' bond.
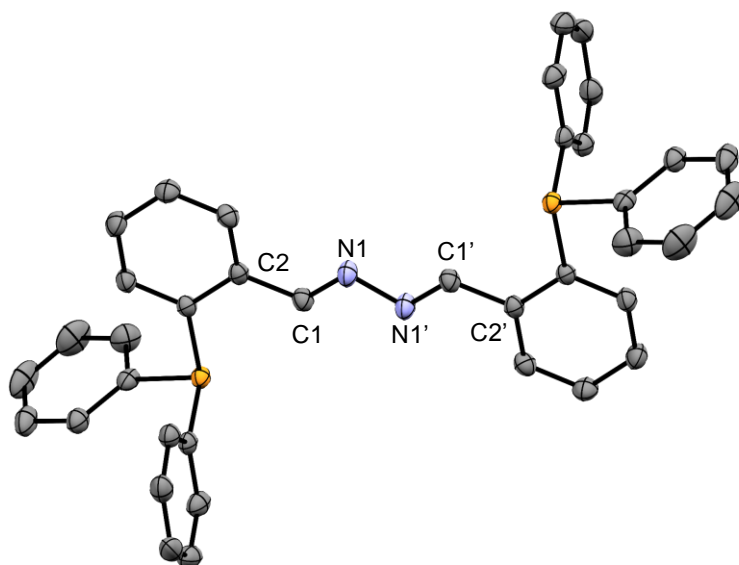
Figure 5.2. Molecular structure of L$_1$.

L$_1$ has also been synthesised by reaction of *o*-(diphenylphosphino)benzaldehyde and hydrazinium sulphate (N$_2$H$_6$SO$_4$) and ^{15}N marked hydrazinium sulphate as the source of hydrazine under the same conditions previously mentioned.

5.2.2 Formation of complex 3 from L$_1$

L$_1$ reacts with the iridium dimer [Ir(COD)Cl]$_2$ in chloroform to give complex **3**. We propose a pathway of two successive oxidative additions going through an iridium(V) (**A**) species followed by a hydrogen transfer to afford the iridium(III) complex **3** (Figure 5.3).
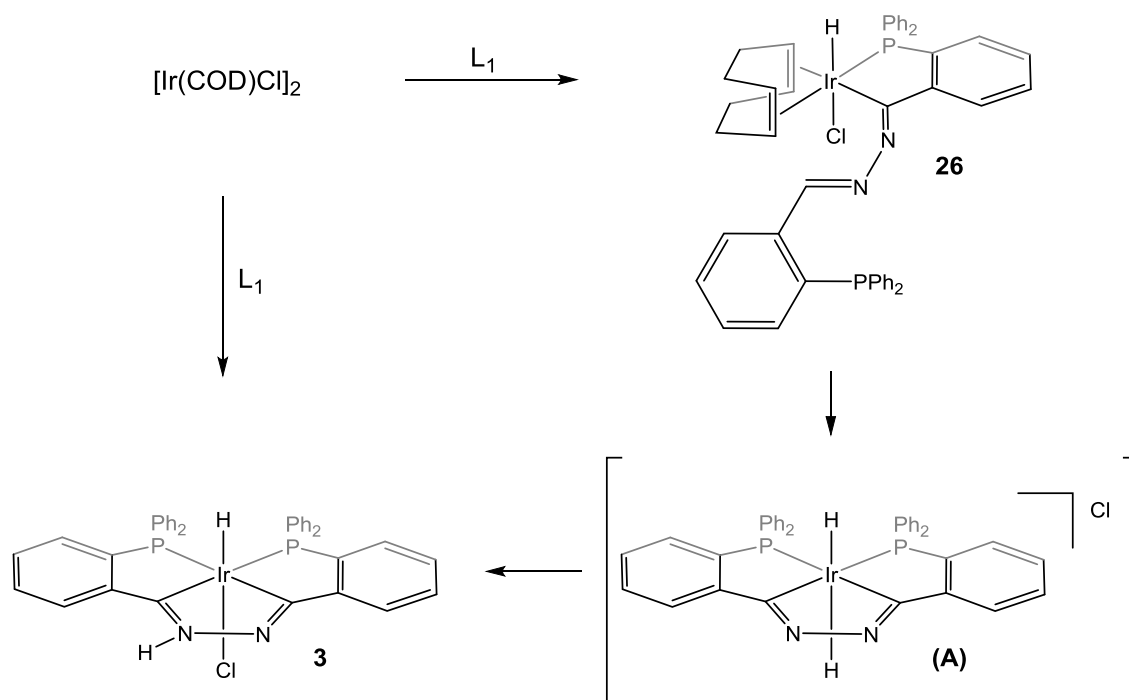
Figure 5.3 Proposed pathway for the formation of complex 3

The formation of complex **3** was followed by ^{1}H and ^{31}P{^{1}H} NMR (Figure 5.4). At early stages of the reaction, when unreacted **L$_1$** is still present, the ^{1}H NMR spectrum shows two resonances in the high field region due to hydrides, along with resonances due to free 1,5-cyclooctadiene. The multiplet at -19.69 ppm can be attributed to complex **3** and we propose that the doublet at -16.19 ppm ($J_{P,H}$ = 10.4 Hz) is due to a hydrido-iminoacyl-iridium(III) intermediate **26** formed by oxidative addition of an imine fragment of **L$_1$**. The ^{31}P{^{1}H} NMR spectrum shows a singlet at 31.4 ppm. These spectroscopic features are similar to those of [IrHCl(COD)(PPh$_2$(o-C$_6$H$_4$CO))], formed by oxidative addition of o-(diphenylphosphino)benzaldehyde to [Ir(COD)Cl]$_2$, that shows a doublet at -16.12 ($J_{P,H}$ = 15 Hz) in the ^{1}H NMR spectrum and a singlet at 38.1 ppm in the ^{31}P{^{1}H} NMR spectrum[3] and is an intermediate in the formation of hydridoirida-β-diketones. The intermediate species **26** could be detected but not isolated.

A second oxidative addition of the remaining imine fragment could afford the dihydride Ir(V) species (**A**) which may lead to the final product by an iridium-to-nitrogen proton transfer and a chloride coordination.

Nevertheless, a second pathway cannot be completely discarded in which elimination of hydrogen chloride could happen before the occurrence of a second oxidative addition.
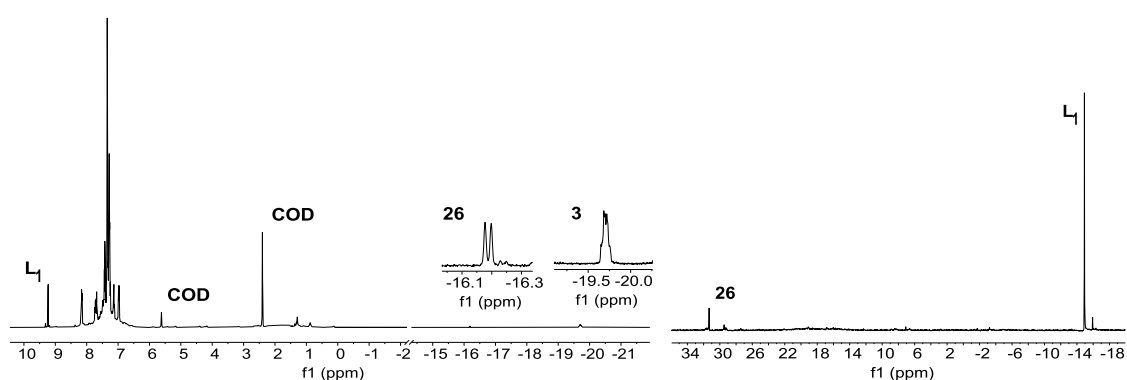
Figure 5.4 *In situ* [1]H (left) and ^{31}P{^{1}H} (right) NMR spectra of the formation of complex 3 in CDCl$_3$

Orange monocrystals were obtained from a dimethylsulfoxide solution of complex **3** at room temperature and the X-Ray diffraction study was done. The results were the same than those previously reported for complex **3** with the first synthetic pathway,[12] which confirms that the same complex can be obtained from **L$_1$** and the iridium dimer [Ir(COD)Cl]$_2$ gaining much higher yields.

5.3 Reactivity of complex 3

Complex **3** is an organometallic complex that contains a metallacycle, in this case an iridapyrazole. In order to fully analyse the reactivity of this complex two different approaches were taken into account; the reactivity of the metal centre itself, due to the labile position occupied by the chloride atom, and the reactivity of the iridapyrazole ring.

5.3.1 Reactivity on the iridium centre

5.3.1.1 Formation of cationic complexes

In order to replace the chloride ligand with neutral ligands complex **3** was reacted with the halide scavenger $NaBAr^F_4$ in the presence of the ligand (Figure 5.5).
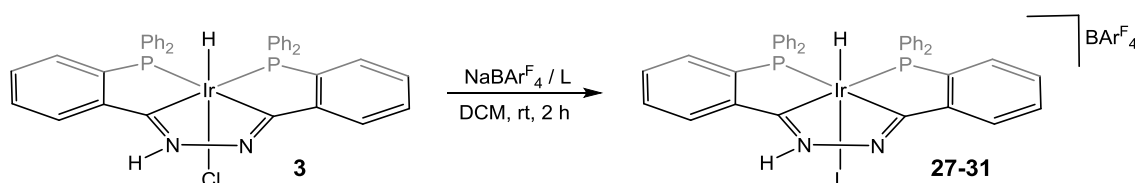
Figure 5.5 Formation of cationic complexes from complex 3, $NaBAr^F_4$ and L, where L is: pyrazole (27); pyridine (28); acetonitrile (29); triphenylphosphine (30) and *cis*-cyclooctene (31)

Five new cationic complexes have been synthesised using different ligands to occupy the vacant site left by abstraction of the chloride atom. Among the chosen ligands there are three nitrogen donors: pyrazole (**27**), pyridine (**28**) and acetonitrile (**29**); a phosphine, the triphenylphosphine (**30**); and an olefin, the *cis*-cyclooctene (**31**). All the complexes have been characterised by multinuclear NMR, IR spectroscopy and mass spectroscopy.

The success of these reactions is based on the high solubility of the newly created complexes comparing to complex **3** and the formation of the NaCl salt that precipitates in dichloromethane.
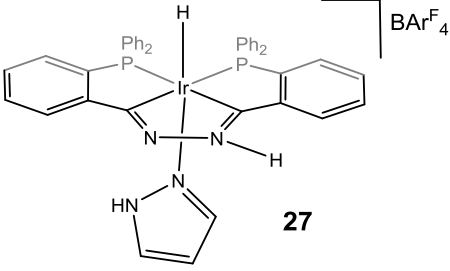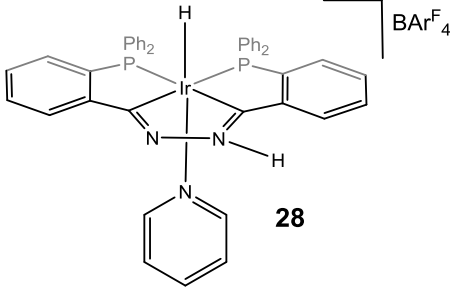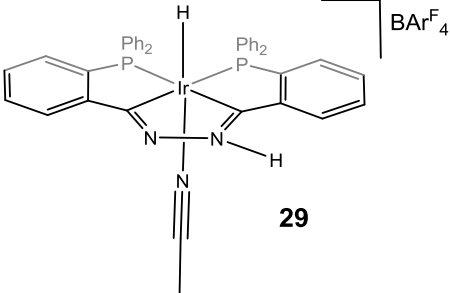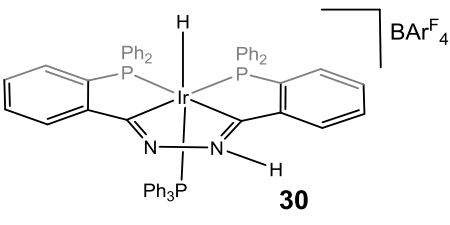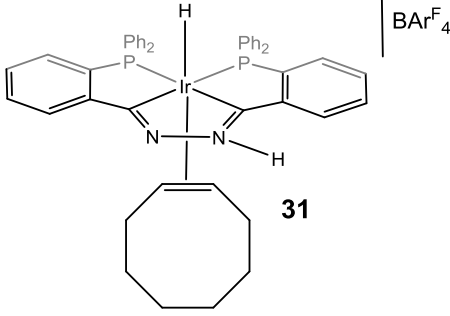
The NMR spectra for the five complexes have been measured at low temperature (213 K) and at room temperature (298 K) because of the fluxional behaviour due to the known NH prototropy of pyrazoles that exchanges the proton between both nitrogen atoms. This tautomerism makes the phosphorus atoms to become equivalent at room temperature. This dynamic behaviour not only depends on the temperature but also on the amount of water as was previously reported for a dihydride iridapyrazole analogous to complex **3**.[12] The most relevant peaks from the NMR spectra appear in Table 5.2, for the full spectra see Figure B. 105 and Figure B. 106 **(27)**; Figure B. 108 and Figure B. 109 **(28)**; Figure B. 110 and Figure B. 111 **(29)**; Figure B. 112 and Figure B. 113 **(30)** and Figure B. 114 and Figure B. 115 **(31)** and ligand assignments are collected in the experimental part.

The signal of the hydride for the complexes containing *trans* N-donor ligands (**27**, **28** and **29)** appear between -18.0 and -18.6 ppm as a triplet, due to the coupling with two *cis* phosphorus atoms. The signal belonging to complex **31**, which contains an olefin, appears at -12.26 ppm also as a triplet. On the other hand, complex **30** shows a resonance at -12.31 ppm as a doublet of triplets due to the coupling with three phosphorus atoms, two from the original complex and another one from the triphenylphosphine ligand *trans* to the hydride.

The $^{31}P\{^1H\}$ NMR spectra for all these complexes show sharp signals at low temperature (213 K) because the complexes have reached static behaviour. The peaks broaden as the temperature rises. In the case of complex **27** a single signal can be observed at room temperature as is well above coalescence.

Complex **27** was selected in order to carry out a ^{15}N NMR spectrum and it showed a singlet at 285.6 ppm, the value is very similar to the one for the organic pyrazole.[78]

Table 5.2 The most relevant NMR data of complexes 27-31. The spectra were recorded in CD_2Cl_2 or $CDCl_3$ solution, the chemical shift is given in ppm and the coupling constants in Hz.

Complex	^1H NMR (298 K)	$^{31}P\{^1H\}$ NMR (213 K)
27	δ Ir-H = -18.60 (t) $^2J_{P,H}$ = 15.8 δ N-H = 12.54 (br)	δ Ir-P = 19.4 (s) δ Ir-P = 25.0 (s)
28	δ Ir-H = -18.57 (t) $^2J_{P,H}$ = 15.9 δ N-H = 13.45 (br)	δ Ir-P = 22.7 (s) δ Ir-P = 26.9 (s)
29	δ Ir-H = -18.02 (t) $^2J_{P,H}$ = 14.6 δ N-H = 12.18 (br)	δ Ir-P = 18.8 (s) δ Ir-P = 23.7 (s)
30	δ Ir-H = -12.31 (dt) $^2J_{P,H}$ = 19.6 $^2J_{P,H}$ = 89.3 δ N-H = 12.50 (br)	δ Ir-P = -5.0 (s) δ Ir-P = 6.1 (s) δ Ir-P = 11.4 (s)
31	δ Ir-H = -12.26 (t) $^2J_{P,H}$ = 19.6 δ N-H = 11.96 (br)	δ Ir-P = 11.6 (s) δ Ir-P = 15.5 (s)

IR spectra were recorded for all these complexes. The v(Ir-H) stretching for all complexes is a very weak signal that only in some cases can be seen at 2192 **(27)**; 2191 **(28)**; 2190 **(29)** and 2113 **(30)** cm^{-1} as a broad signal; the stronger signal due to v(C=N) is located at 1610 **(27)**; 1608 **(28)**; 1631 **(29)**; 1610 **(30)** and 1610 **(31)** cm^{-1}.

Mass spectra were carried out for these complexes and the values obtained were ESI-MS (*m/z*): 837.2 [M]$^+$ **(27)**; 848.2 [M]$^+$ **(28)**; 810.2 [M]$^+$ **(29)**; 1031.2 [M]$^+$ **(30)** and 769.2 [M-COE]$^+$ **(31)** (Figure D. 15 to Figure D. 24). There was a good fit to both the principal molecular ion and the overall isotopic distribution.

After the success of the chloride substitution reactions, using the halide scavenger NaBAr$^F_4$ and the above mentioned neutral ligands, the same conditions were used to synthesise two complexes with ligands which contain a borane moiety, triethylamineborane and triphenylphosphineborane (Figure 5.6).
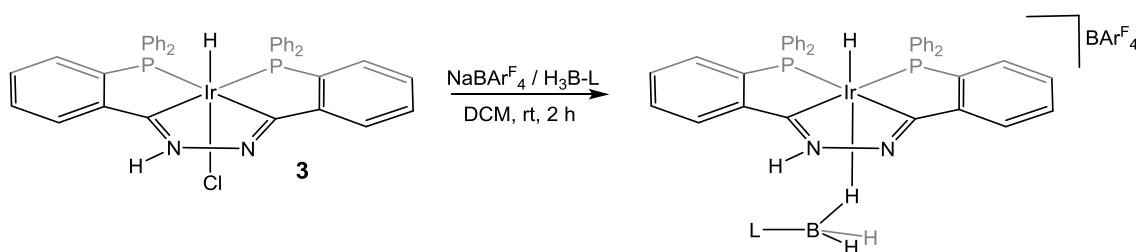
Figure 5.6 Formation of cationic complexes from complex 3, NaBAr$^F_4$ and different boranes; where L is: NEt$_3$ (32) and PPh$_3$ (33).

In complex **32** as well as in complex **33** the metal centre bonds the borane moiety in an M-H-B η^1-fashion *via* a three-centre two electron bond.[73] These two complexes have been characterised by several techniques.

ESI-mass spectra were carried out for these complexes and the obtained values were ESI-MS (m/z): 884.3 [M]$^+$ (Figure D. 25 and Figure D. 26) for complex **32** and 1045.3 [M]$^+$ (Figure D. 27 and Figure D. 28) for complex **33**.

Complexes **32** and **33** show the characteristic fluxional behaviour that other complexes with a BH_3 bonded in the same fashion have revealed. Besides, these complexes also show an exchange of the NH proton of the iridapyrazole ring. Both behaviours can be seen *via* NMR spectroscopy.

The first analysed complex was complex **32**, in which the metal centre is bonded to the triethylamineborane ligand.

The ^{1}H NMR (Figure 5.7) provides information about the dynamic behaviour of the BH_3 fragment. A hydride can be observed in the high field region, at -18.29 ppm, as a triplet with a coupling constant of $J_{P,H} = 16.1$ Hz, due to two phosphorus atoms in *cis* position. The hydride chemical shift in complex **32** and the position of the hydride in related irida-β-diketone complex **9** are almost the same. At room temperature the signal corresponding to the BH_3 group can be located at -3.00 ppm as a broad signal indicating exchange of the three B-H bonds. The signal belonging to the NH of the iridapyrazole ring appears at 12.11 ppm as a broad signal.
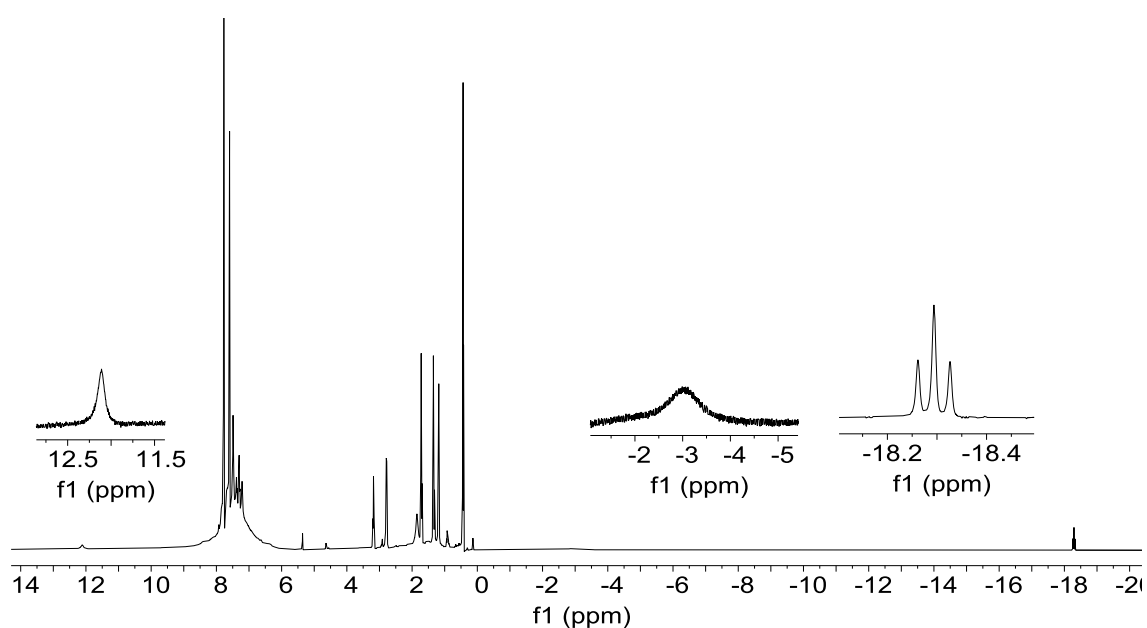
Figure 5.7 ^{1}H NMR of complex 32 in CDCl$_3$.

^{1}H NMR was also carried out at different temperatures in order to prove the exchange in the BH$_3$ fragment. The broad signal allocated to the BH$_3$ group that appears at -3.00 ppm coalesces when the temperature decreases; a signal at -12.24 ppm emerges at 233 K which corresponds to 1H (Figure 5.8). This observation suggests exchange between terminal and bridging B-H protons or dissociation of the ligand. At this low temperature a signal around 1.60 ppm could be expected corresponding to the other 2H from the BH$_3$ moiety; but, unfortunately, we were not able to detect it as it may be overlapped by the signal due to the ethyl groups. The signals from the hydride and the NH proton from the iridapyrazole ring do not suffer any variation in all the temperature range.

On the other hand, the ^{31}P{^{1}H} NMR shows the tautomerism of the NH proton of the iridapyrazole ring in this complex. At low temperatures two neat signals can be observed. As the temperature increases the signals broaden and approach coalescence until room temperature is reached, when they are at coalescence (Figure B. 116).
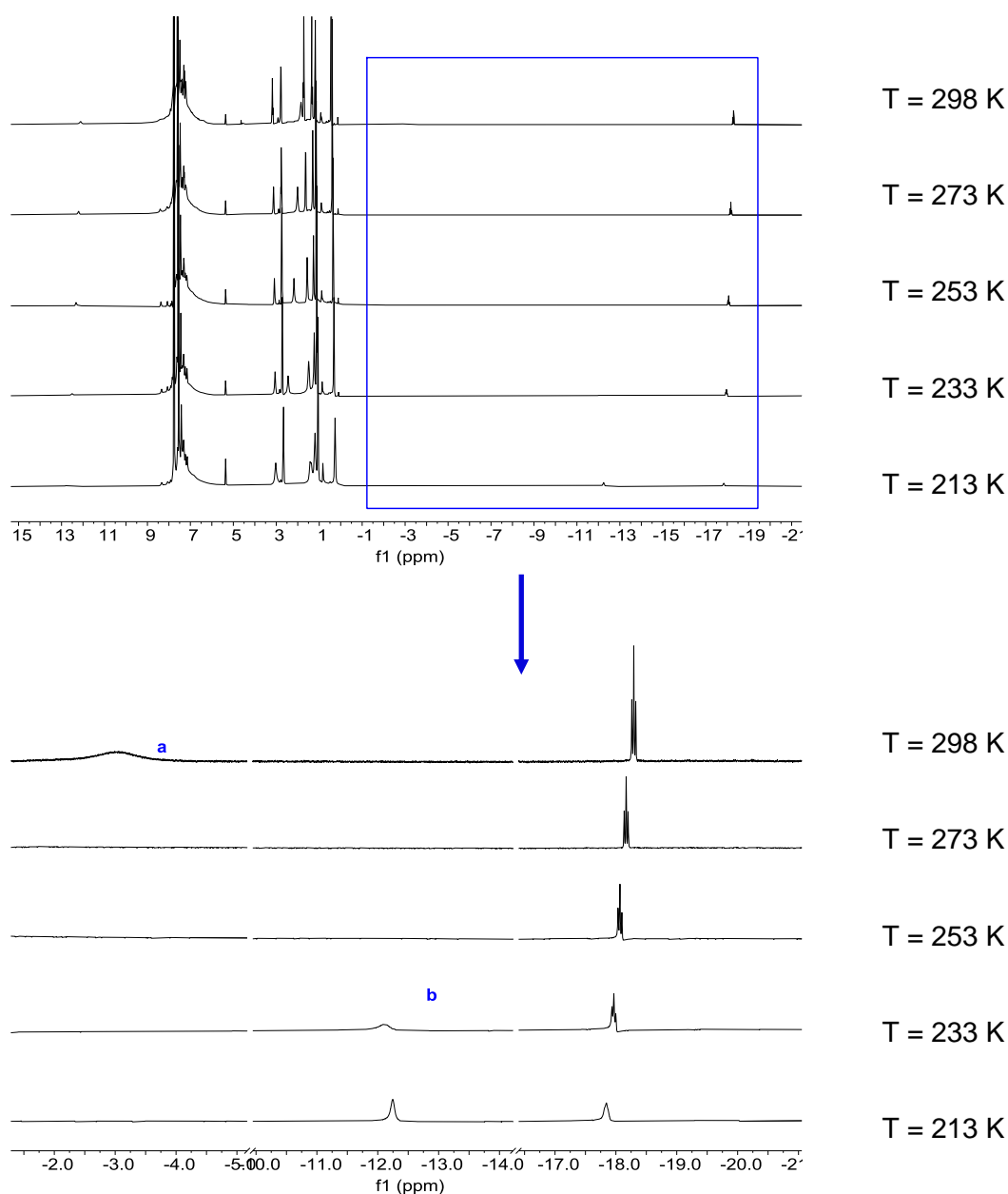
Figure 5.8 ^{1}H NMR spectrum of complex 32 at different temperatures in CDCl$_3$.

When the used borane is the triphenylphosphineborane, obtaining complex **33**, a similar ^{1}H NMR spectrum at room temperature can be observed (Figure 5.9). A doublet of triplets can be seen in the high field region at -18.02 ppm that belongs to the hydride which is coupled to two *cis* phosphorus atoms with a coupling constant of $J_{P,H} = 10.3$ Hz and to the bonded H$_3$B-PPh$_3$ *trans* to

the hydride (J = 16.3 Hz). The BH_3 group can be detected at -2.64 ppm as a broad signal. Finally, the signal belonging to the NH group from the iridapyrazole group appears at 11.92 ppm also as a broad signal.
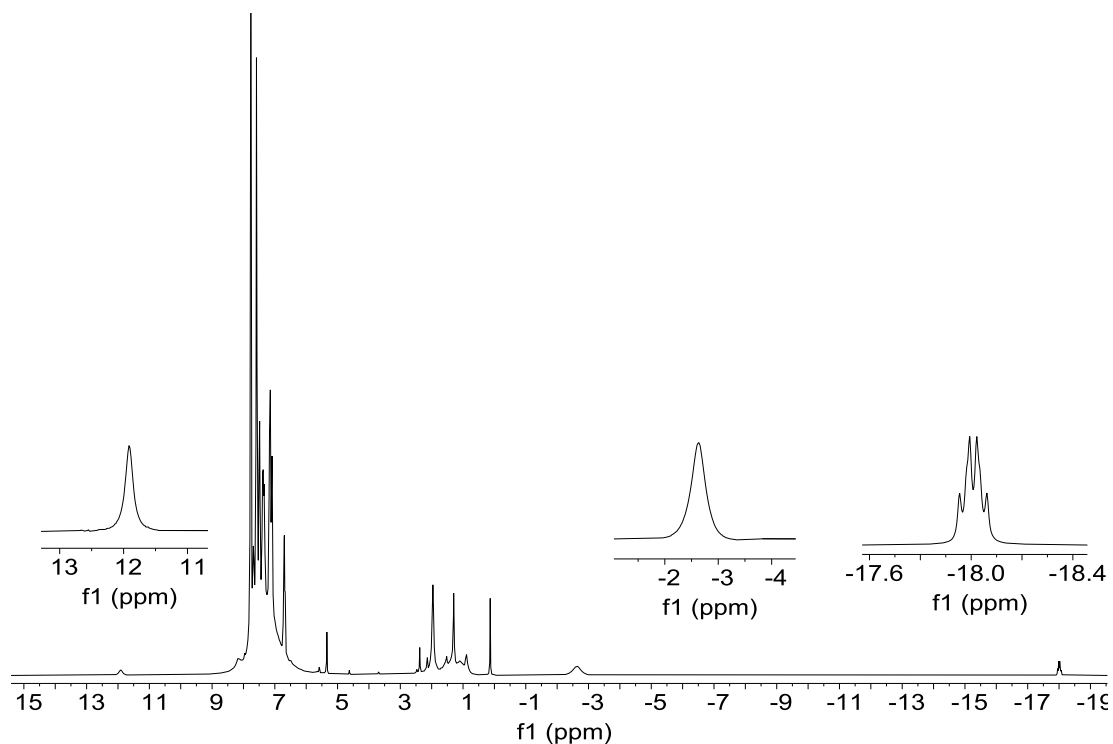
Figure 5.9 ^{1}H NMR of complex 33 in CD$_2$Cl$_2$.

The ^{31}P{^{1}H} NMR spectrum at room temperature shows broad resonances that can be due to the occurrence of several fluxional processes. On lowering the temperature down to 212 K four sharp resonances can be observed (see Figure B. 117). The singlets at 13.3 and 17.6 ppm can be attributed to the phosphorus atoms connected to the iridapyrazole ring and the singlet at -6.9 ppm to the phosphine connected to the bonded BH_3. The fourth signal at 18.9 ppm can be due to free H_3B-PPh_3. These observations lead us to propose that in the exchange of BH_3 protons in complex **33** dissociation of the ligand is involved.

5.3.1.2   Formation of a neutral complex

With the aim to obtain a neutral compound different attempts with halides and hydride sources were done but unfortunately all were unsuccessful. On the other hand, the reaction of complex **3** with excess of $SnCl_2$ was performed with similar results as for an irida-β-diketone related complex.[4] In this reaction the chloride atom bonded to the metal centre migrates to the tin atom and a trichlorostannate complex is formed (Figure 5.10).
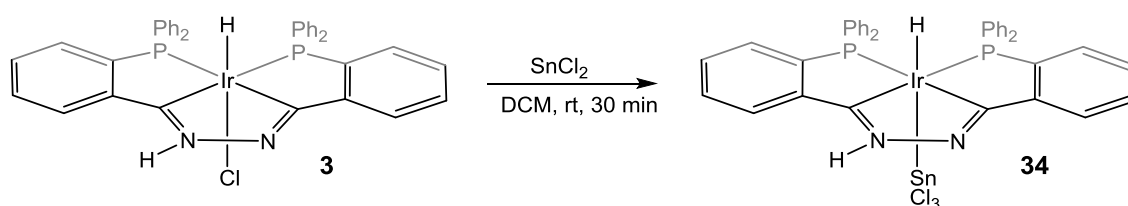
Figure 5.10 Reaction of complex 3 with tin dichloride to form complex 34

The v(Ir-H) stretching appears at 2090 cm^{-1} in the IR spectrum as a broad signal and the v(C=N) stretching can be located at 1730 cm^{-1}.

Multinuclear NMR spectra were carried out for complex **34**. In the ^{1}H NMR the most important signal is the one corresponding to the hydride that appears as a triplet at -12.85 ppm with a coupling constant of $J_{P,H}$ = 16.9 Hz due to two phosphorus atoms in a *cis* position to the hydride. The tin satellites can be seen with high values of $J_{119Sn,H}$ = 831.7 Hz and $J_{117Sn,H}$ = 865.9 Hz, which proves that the hydride is in a *trans* position to the tin atom (Figure B. 118).

The ^{31}P{^{1}H} NMR spectrum shows a sharp singlet at 10.2 ppm, in accordance with the absence of the NH resonance in the ^{1}H NMR spectrum and means that at room temperature complex **34** is well above the coalescence temperature. The tin satellites can also be observed as doublets with coupling constant of $J_{119Sn,P}$ = 233.0 Hz and $J_{117Sn,P}$ = 226.5 Hz. The values of these

coupling constants suggest that the tin atom is in a *cis* position to the phosphorus atoms (Figure B. 119).

The ^{119}Sn NMR was also carried out and the spectrum shows a doublet of triplets at -146.5 ppm ($J_{H,^{119}Sn}$ = 1044.4 Hz and $J_{P,^{119}Sn}$ = 228.8 Hz) that confirms the presence of a hydride *trans* to the tin atom and two phosphorus atoms in a *cis* position (Figure B. 120).

5.3.2 Reactivity of the iridapyrazole ring

5.3.2.1 Acid-Base reactions

The first selected reactions in order to see whether our iridapyrazole ring can undergo some reactions that organic pyrazoles do were the reactions towards acids and bases to obtain protonated and deprotonated pyrazole rings. For this purpose the selected acid was the tetrafluoroboric acid (HBF$_4$) and the selected base the tetrabutylammonium hydroxide (N(*n*-Bu)$_4$)(OH) (Figure 5.11).
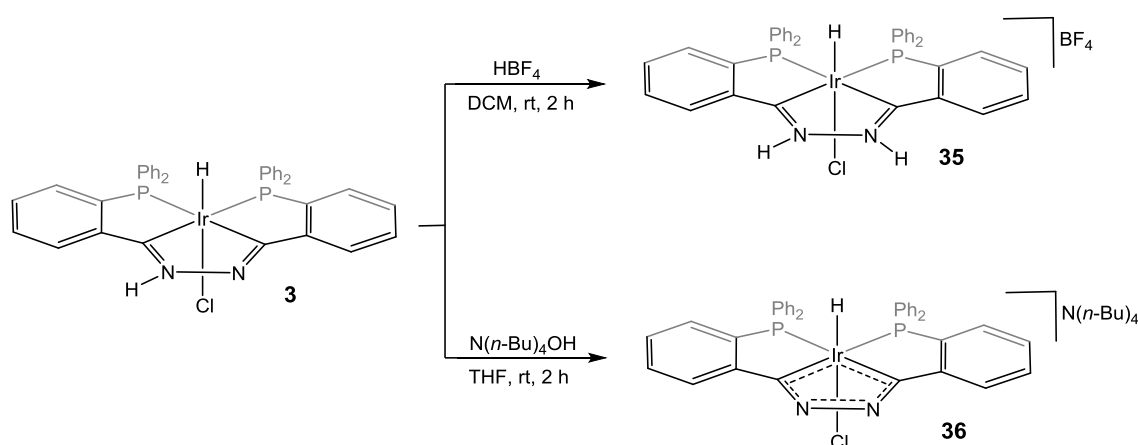
Figure 5.11 Reaction of complex 3 towards acid and bases.

After reacting complex **3** with the above mentioned tetrafluoroboric acid, the protonated complex **35** was obtained. This complex has both nitrogen atoms from the iridapyrazole ring protonated and therefore, has lost the fluxionality of the NH proton present in the starting material.

Complex **35** has been characterised *via* multinuclear NMR. In the ^{1}H NMR spectrum there are two characteristic peaks, one belonging to the hydride at high field and one belonging to the two protons in the iridapyrazole ring. The hydride appears as a triplet at -17.47 ppm with a coupling constant of $J_{P,H}$ = 16.6 Hz due to two equivalent phosphorus atoms in *cis* position. The signal corresponding to the two NH protons appears at 14.49 ppm as a singlet.

The ^{31}P{^{1}H} NMR shows a sharp singlet at room temperature at 15.25 ppm which agrees with a static behaviour because of the protonation of the iridapyrazole ring and the conversion of complex **35** in a symmetrical complex. In the ^{13}C{^{1}H} spectrum a doublet can be observed at 220.5 ppm, in the range expected for iminoacyliridium complexes,[4] with a large coupling constant ($J_{P,C}$ = 97.6 Hz) which confirms that the C=N groups are located *trans* to the phosphorus atoms. The ^{15}N NMR spectrum was carried out and a singlet a 206.7 ppm was observed, this value is similar to the ones obtained for protonated organic pyrazoles.[79]

Orange monocrystals of complex **35** were obtained from vapour diffusion of diethyl ether into a chloroform solution of **35** at -20 ºC and an X-Ray diffraction study could be done. A selection of bond lengths and angles are given in Table 5.3.

Table 5.3 Selected bond lengths (Å) and angles (º) on complex 35. Standard deviation appears in parentheses.

Bond lengths			
Ir1-P1	2.3321(11)	Ir1-Cl1	2.4835(11)
Ir1-P2	2.3333(11)	C1-N1	1.316(6)
Ir1-C1	1.973(4)	C2-N2	1.317(6)
Ir1-C2	1.983(4)	N1-N2	1.388(5)
Bond angles			
P1-Ir1-C2	83.67(14)	Ir1-C2-N2	115.0(3)
P2-Ir1-C1	83.11(13)	C1-N1-N2	115.9(4)
C1-Ir1-C2	79.18(18)	C2-N2-N1	115.0(4)
Ir1-C1-N1	114.9(3)	C1-Ir1-Cl1	89.48(12)

The coordinative environment of the iridium atom in complex **35** is a slightly distorted octahedron. The complex has a hydride and a chloride atom in axial positions and a PCCP tetradentate ligand occupying all the equatorial positions.

The N−N distance observed for complex **35** (1.388(5) Å) is slightly shorter than the one found for complex **3** (1.409(4) Å), and this can indicate that the aromaticity in the iridacycle may have increased with its protonation. This agrees with the case of the organic pyrazole, where the N-N distance also decreases upon protonation as it changes from 1.351(10) Å[80] to 1.343(6) Å[81].

The C1−Ir1−C2 angle in the iridapyrazole ring (79.18(18)°) is significantly smaller than the C−C−C angle in regular pyrazoliums (106.5(5))[81], this makes the rest of the angles in the iridapyrazole ring larger achieving a value of around 115º for all of them. In the case of the regular pyrazoliums the other angles have very similar values to the C-C-C one, being them between 107º and 110º.
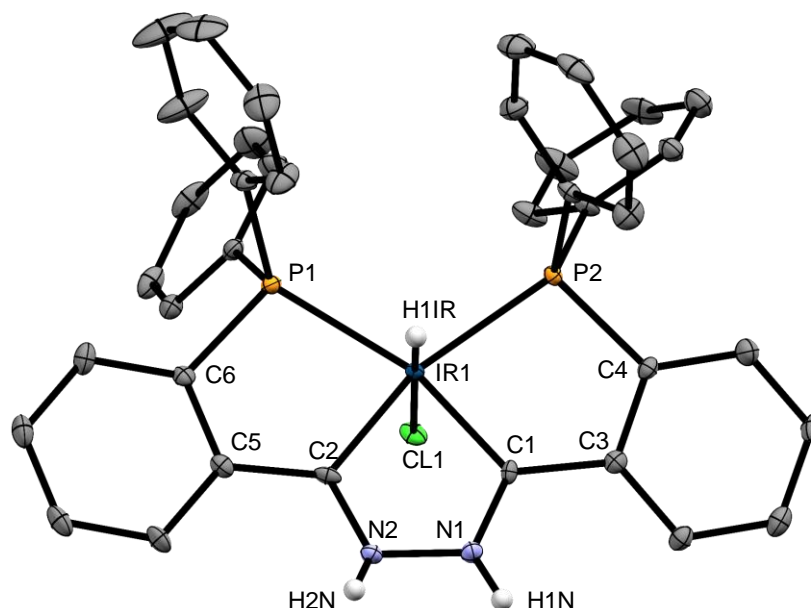
Figure 5.12 Molecular structure of complex 35 (50% probability ellipsoids)

On the other hand, when complex **3** reacts with the tetrabutylammonium hydroxide base the proton from the iridapyrazole ring disappears and an anionic complex is formed, complex **36**.

In the ^{1}H NMR the hydride can be observed at -21.01 ppm as a triplet with a coupling constant of $J_{P,H}$ = 15.9 Hz, due to two equivalent *cis* phosphorus atoms. As expected, the signal of the NH proton cannot be found for complex **36**. In the ^{31}P{^{1}H} NMR a sharp singlet is observed at 18.9 ppm which confirms the loss of the previous fluxionality.

ESI-mass spectrum was carried out for complex **36**, but in this case the negative anion mode was selected. The expected value of ESI-MS (m/z): 803.1 [M]⁻ was obtained (Figure D. 31) and (Figure D. 32).

Coordination of pyrazolates to metal centres is very well known, they are able to create different metallacycles such as copper(I) and silver(I) dimeric complexes[82] and trinuclear gold complexes[83] with metals of the group 11. Pyrazolates can also coordinate to metals of the group 4 in a η^2 fashion as in

η^2-pyrazolate zirconium and hafnium complexes[84]. With the aim to prove that our iridapyrazolate can behave in a similar way towards transition metals it was reacted with the zirconium salt $ZrCl_4$ (Figure 5.13).
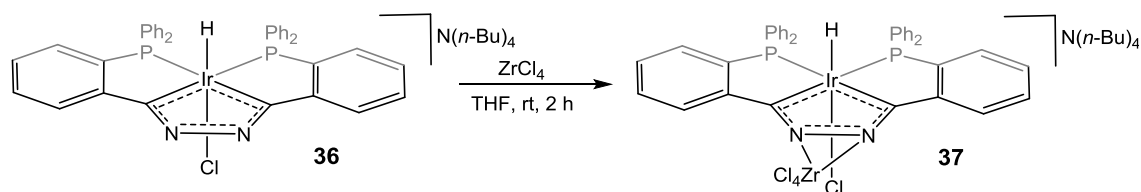
Figure 5.13 Formation of complex 37.

Complex **37** has been characterised *via* multinuclear NMR. In the ^{1}H NMR the signal corresponding to the hydride appears at -17.63 ppm with a coupling constant of $J_{P,H}$ = 17.5 Hz. In the ^{31}P{^{1}H} NMR a sharp singlet can be observed at 15.5 ppm. This spectroscopic data sustain that complex **37** maintains the symmetry.

In order to prove that complex **37** is a monomer DOSY experiments were carried out for complexes **36** (Figure B. 127) and **37** (Figure B. 130). From the DOSY spectra the diffusion coefficients of **36** and **37** are obtained and applying the Stokes-Einstein equation (1) on them the hydrodynamic radius of each complex is achieved. The values obtained were r_s = 6.35 Å for complex **36** and r_s = 7.24 Å for complex **37** which agrees with the premise that complex **37** is a monomer in which the iridapyrazolate ring is bonded to the zirconium metal in a η^2-fashion.

$$D = \frac{k \cdot T}{6\pi \cdot \eta \cdot r_S}$$

(1)

5.3.2.2   Alkylation reactions

Alkylation reactions are very common reactions for organic pyrazoles. The purpose of this subchapter is to test whether our iridapyrazole can undergo some alkylation reactions such as methylation. For this end, complex **3** was reacted with the sodium hydride base and methyl iodide (Figure 5.14) on account of previously reported conditions for methylation of indazoles[85].
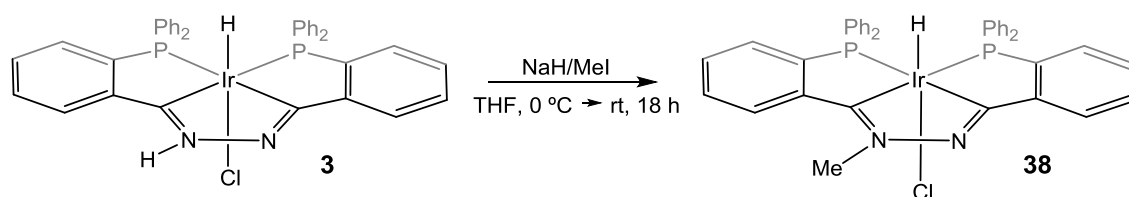
Figure 5.14 Formation of the metilated complex, complex 38.

Multinuclear NMR spectra were carried out for complex **38**. In the ^{1}H NMR there is no signal corresponding to an NH group and a singlet can be observed at 4.45 ppm, which belongs to the newly attached methyl group in the iridapyrazole group. Another important signal is that corresponding to the hydride that appears at -19.35 ppm with a coupling constant of $J_{P,H}$ = 16.9 Hz. The ^{31}P{^{1}H} NMR shows two signals, a broad singlet at 22.9 ppm and a doublet at 11.2 ppm with a coupling constant of $J_{P,P}$ = 5.6 Hz.

A ^{15}N NMR spectrum was also carried out and two signals could be detected for complex **38**, one singlet at 240.3 ppm and another singlet at 369.0 ppm. The signal at higher field, the one at 240.3 ppm, belongs to the nitrogen which contains the methyl group according to comparison with organic pyrazoles[78].

Complex **38** was characterised by ESI-mass spectroscopy as well. A value of ESI-MS (m/z): 841.1 [M+Na]$^+$ was obtained (Figure D. 33 and Figure D. 34).

When complex **38** is dissolved in a protic solvent, such as methanol, in the presence of an alkaline salt the chloride atom can be exchanged by another anion. This process was successfully achieved using sodium iodide and potassium thiocyanate salts (Figure 5.15).
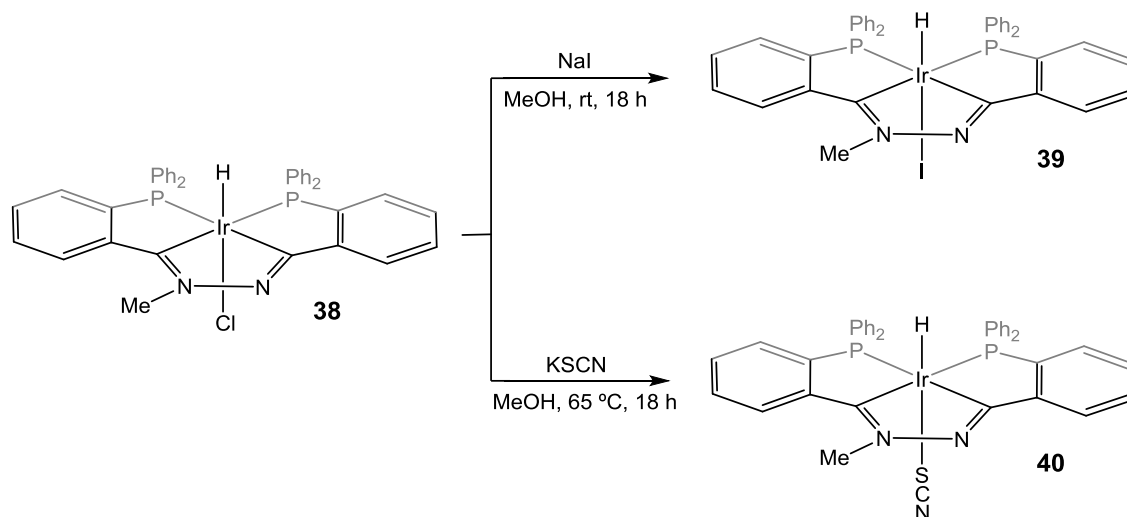
Figure 5.15 Formation of complexes 39 and 40.

Complex **39** contains an iodide atom in a *trans* position to the hydride, this chloride/iodide metathesis can be observed in the ^{1}H NMR spectrum (Figure B. 134) due to the shift of the hydride signal. The hydride now appears at -16.46 ppm as a doublet of doublets with coupling constants of $J_{P,H}$ = 16.7 Hz and $J_{P,H}$ = 17.7 due to the two phosphorus atoms being slightly inequivalent. The signal belonging to the three protons of the methyl group appears as a singlet at 4.48 ppm, almost the same chemical shift as in the chloride derivative **38**. In the [31]P{[1]H} bigger differences can be spotted; two sharp doublets can be observed at 15.0 and 5.7 ppm with a coupling constant of $J_{P,P}$ = 6.2 Hz (Figure B. 135).

On the other hand, when potassium thiocyanate is used two possible isomers can be synthesised the κ-S and the κ-N. When the reaction was carried out at room temperature a mixture of both isomers was obtained. This was supported by the ^{1}H NMR, as two different signals can be seen (Figure B. 136)

in the ranges expected for N-donor and S-donor in *trans* position to a hydride. With the aim to obtain a single complex the reaction was performed under reflux and the thermodynamic isomer was isolated, the κ-S complex **40**.

Complex **40** was characterised *via* ^{1}H (Figure B. 137) and ^{31}P{^{1}H} NMR (Figure B. 138) spectra. In the ^{1}H NMR the signal of the hydride can be observed at -15.58 ppm as a triplet with a coupling constant of $J_{P,H}$ = 16.9 Hz , the signal which belongs to the methyl group appears at 4.59 ppm as a singlet. In the ^{31}P{^{1}H} NMR two singlets can be observed, at 10.3 and 21.4 ppm.

ESI-mass spectroscopy was carried out for these two complexes and the values obtained were ESi-MS (m/z): 901.1 [M+H]$^+$ and 933.1 [M+Na]$^+$ for complex **39** (Figure D. 35 and Figure D. 36) and 783.2 [M-SCN]$^+$ for complex **40** (Figure D. 37 and Figure D. 38).

Orange monocrystals of complex **39** were obtained from a chloroform solution of **39** at -20 ºC and an X-Ray diffraction study could be undertaken. A selection of bond lengths and angles are given in Table 5.4.

The coordinative environment of the iridium atom in complex **38** is a slightly distorted octahedron. The complex has a hydride and a iodide atom in axial positions and a PCCP tetradentate ligand occupying all the equatorial positions.

The N−N distance observed for complex **39** (1.413(6) Å) is very similar to the one found for complex **3** (1.409(4) Å). The methylation does not affect the electronic system in the iridapyrazole ring. The C1−Ir1−C2 angle in the iridapyrazole ring (77.25(19)°) is even smaller in complex **39** than in complexes **3** and **35**, which makes the rest of the angles in the iridacycle larger.

Table 5.4 Selected bond lengths (Å) and angles (⁰) on complex 39. Standard deviation appears in parentheses.

Bond lengths			
Ir1-P1	2.3150(12)	Ir1-I1	2.7574(4)
Ir1-P2	2.3109(11)	C1-N1	1.321(6)
Ir1-C1	1.997(5)	C2-N2	1.305(6)
Ir1-C2	2.003(4)	N1-N2	1.413(6)
N1-C1B	1.474(6)		
Bond angles			
P1-Ir1-C1	83.98(13)	Ir1-C2-N2	119.4(3)
P2-Ir1-C2	84.15(14)	C1-N1-N2	118.6(4)
C1-Ir1-C2	77.25(19)	C2-N2-N1	110.3(4)
Ir1-C1-N1	114.3(3)	C1-Ir1-I1	90.77(14)
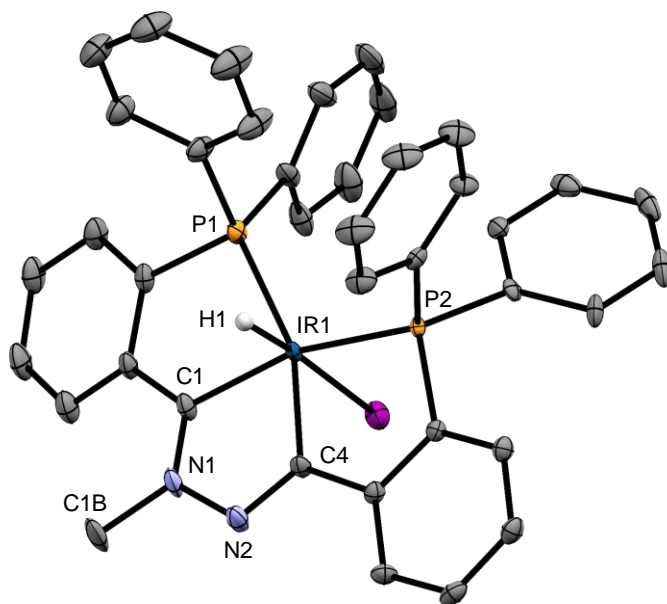
Figure 5.16 Molecular structure of complex 38 (50% probability ellipsoids)

A method to selectively N-alkylate pyrazoles is the use of diazo derivatives[86] such as the ethyldiazoacetate (EDA). In order to test whether complex **3** can be alkylated using EDA the two reactants were mixed in dichloromethane for 48 h. The reaction resulted in the formation of complex **41** (Figure 5.17).
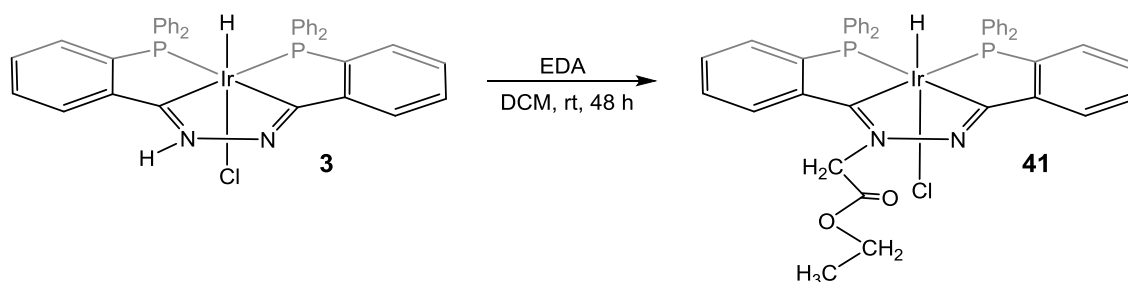
Figure 5.17 Formation of complex 41.

Complex **41** was characterised *via* multinuclear NMR and ESI-mass spectroscopy. In the ^{1}H NMR spectra the signal related to the hydride is observed at -19.01 ppm as a triplet with a coupling constant of $J_{P,H}$ = 16.8 Hz; the signal is very similar to one of the methylated complex **38**. Two doublets can be seen at 5.50 and 5.63 ppm with a coupling constant of $J_{H,H}$ = 17.6 Hz, they belong to geminal protons (Figure B. 139).

In the ^{31}P{^{1}H} NMR spectrum two sharp doublets can be observed at 12.1 and 20.4 ppm with a coupling constant of $J_{P,P}$ = 6.7 Hz (Figure B. 140). These values are very similar to the ones obtained for complex **38** as well.

ESI-mass spectroscopy was carried out for complex **41**. A value of ESI-MS (m/z): 913.15 [M+Na]$^+$ was obtained (Figure D. 39 and Figure D. 40).

5.4 Catalytic activity of the iridapyrazole derived complexes for the methanolysis of ammonia-borane

Complexes **1** and **7** in Chapter 3 and alkyl diamine derived complexes in Chapter 4 have proven to be effective catalysts for the homogeneous methanolysis of AB. In this section, the iridapyrazole derived complexes will be tested for this homogeneous catalysed reaction. Due to the inability of these iridapyrazole complexes to perform a rearrangement around the iridium, because of the robust PCCP ligand occupying the four positions of a plane, it is interesting to see whether it affects the activity for the methanolysis of AB.

Complexes **27 – 31** were the first ones to be tested as catalysts for the above mentioned catalytic reaction. These complexes have the same structure and the only difference is the ligand that is located in a *trans* position to the hydride. They were compared in order to see how the type of ligand could affect in the catalysis (Figure 5.18).
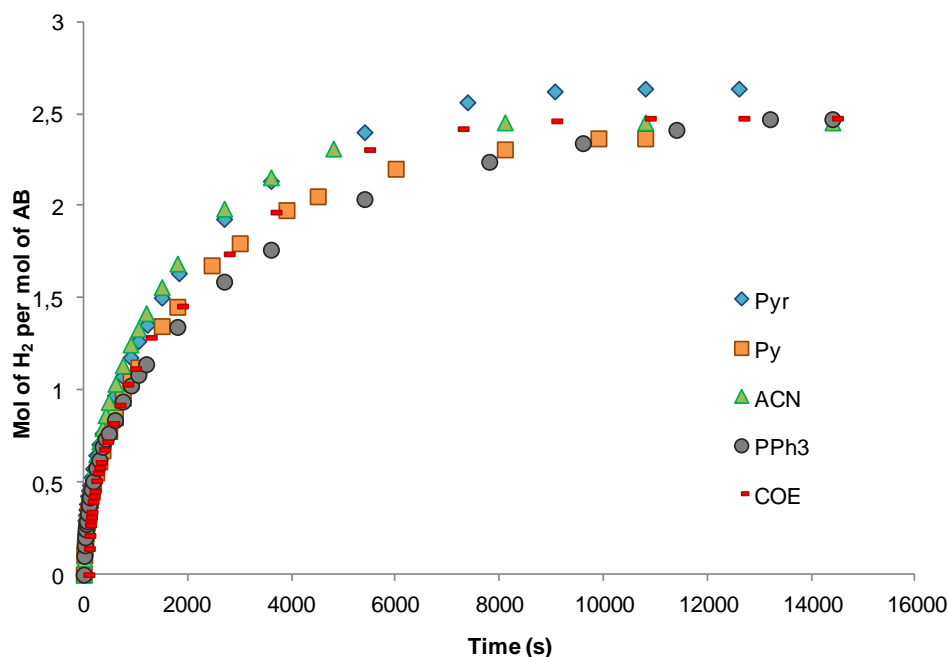
Figure 5.18 Hydrogen release from the methanolysis of AB with complexes 27-31 as catalysts in MeOH. T, 35 ºC.

All the tested complexes showed very similar activity for the catalytic hydrogen release from the methanolysis of AB. The five complexes released between 2.4 and 2.6 hydrogen equivalents in times ranging from 8100 to 13200 seconds.

The kinetic profiles seen in Figure 5.18 can be considered to follow a pseudo-first-order reaction rate with respect to [substrate]. This was applied to determine the rate constants, k_{obs}, plotting time versus Ln(1-(H$_2$ equiv./H$_2$ equiv.final)) (Figure 5.19).
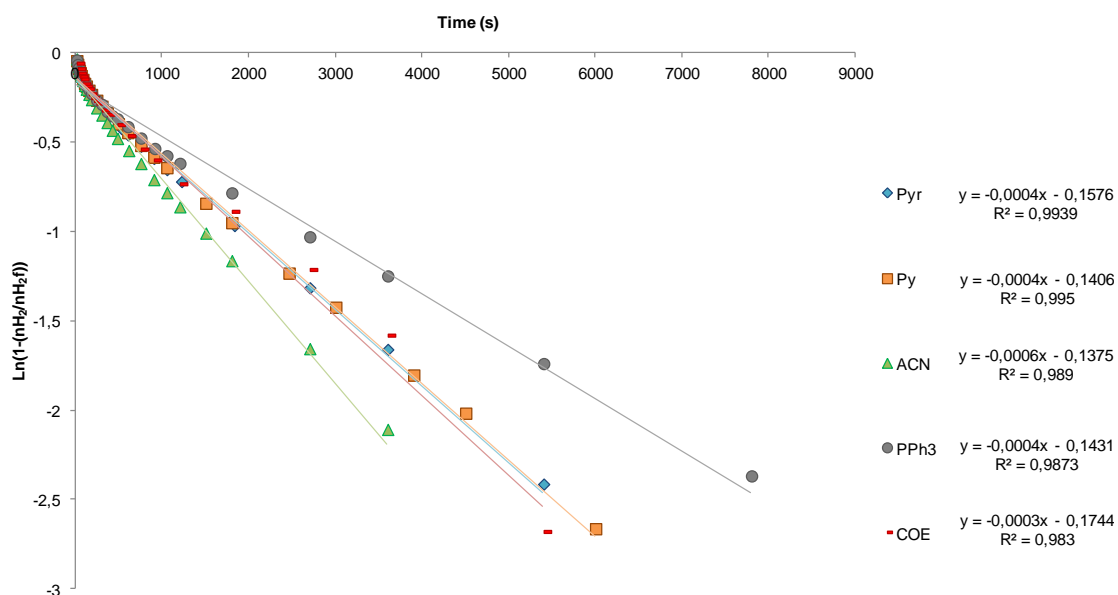
Figure 5.19 First order plots for the hydrogen release from AB with complexes 27-31 as catalysts in MeOH. T, 35 ºC.

The obtained k_{obs} values for the methanolysis of AB catalysed by complexes **27** – **31** are presented in Table 5.5, as well as the reached conversion and the time required for the process. The rate values obtained for these complexes as catalysts are much lower than the ones found in the previous chapters for irida-β-diketone derived complexes.

Table 5.5 % Conversion, Time Required, and Rate Constants for the methanolysis of AB with complexes 27-31 as catalyst at 35 ⁰C.

Ligand	Conversion %	Time (s)	$10^3 \cdot k_{obs}$ (s^{-1})
Pyrazole	88	10800	0.427 ± 0.007
Pyridine	79	9900	0.428 ± 0.006
Acetonitrile	82	8100	0.570 ± 0.012
Triphenylphosphine	82	13200	0.294 ± 0.008
Cis-cyclooctene	82	10800	0.444 ± 0.011

Complex **32**, a complex which is very similar to the ones that have been tested above and has a triethylaminoborane ligand coordinated in a *trans* position to the hydride, was also tested for this catalytic reaction. A k_{obs} value of 0.427 ± 0.004 s^{-1} was obtained and an 81 % of conversion was reached after 12600 s. These values are in the same range that the ones that appear in Table 5.5 for complexes **27** - **31**.

Taking this data into account, it can be said that the kind of ligand that these complexes have does not affect in the rate of the catalysis. Consequently, an outer-sphere mechanism could be proposed.

With the objective of collecting more information about the behaviour of the iridapyrazole derived complexes for the catalytic methanolysis of AB the complexes with little difference in the iridapyrazole ring were tested (Figure 5.20). For this purpose complexes **35** – **38** and **41** were selected.
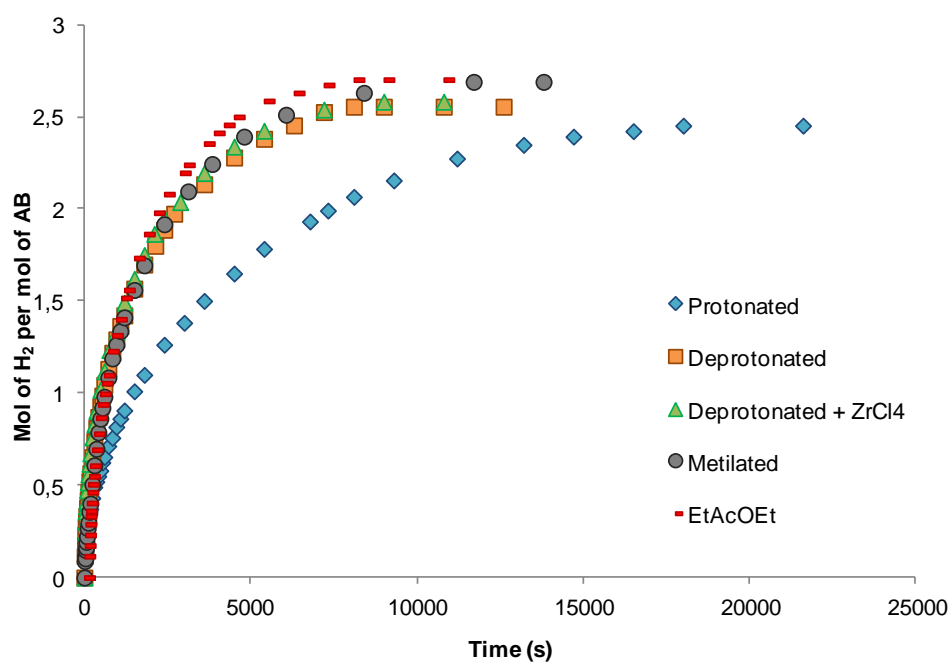
Figure 5.20 Hydrogen release from the methanolysis of AB with complexes 35-38 and 41 as catalysts in MeOH. T, 35 ºC

All the selected complexes showed similar catalytic activity except for complex **35**, the only protonated one, which shows lower rate. As all the kinetic profiles can be considered to follow a pseudo-first-order reaction rate with respect to [substrate], that approach was applied to determine the rate constants, the k_{obs} (Figure 5.21).
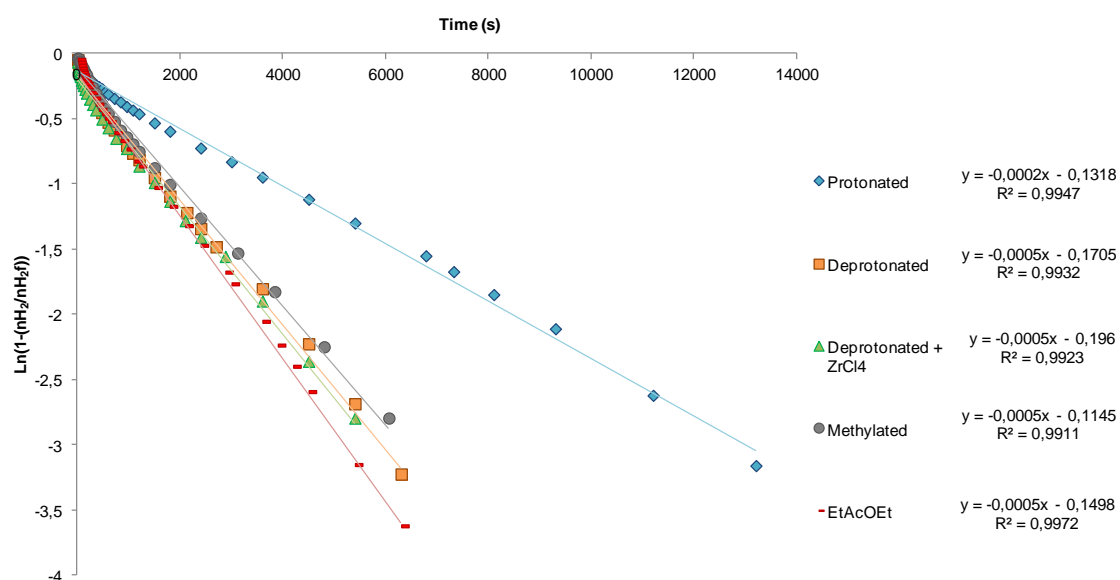
Figure 5.21 First order plots for the hydrogen release from AB with complexes 35-38 and 41 as catalysts in MeOH. T, 35 ºC.

The obtained k_{obs} values for these complexes are shown in Table 5.6, as well as the reached conversion and the time required for the catalysis.

Table 5.6 % Conversion, Time Required, and Rate Constants for the methanolysis of AB with complexes 27-31 as catalyst at 35ºC.

Complex	Conversion %	Time (s)	$10^3 \cdot k_{obs}$ (s^{-1})
35	82	16500	0.228 ± 0.003
36	85	8100	0.478 ± 0.007
37	86	9000	0.489 ± 0.009
38	90	11700	0.455 ± 0.008
41	90	8100	0.548 ± 0.005

Considering all the data, a coordination of the borane to the iridium is not very likely to happen during the catalysis, even if that type of complexes have been reported. However, when the iridapyrazole ring is modified the rate of the catalysis is affected indicating that a nitrogen with a free pair of electrons is needed.

Chapter 6

Conclusions

1. Three new complexes have been synthesised from the reaction of hydridochloroirida-β-diketone [IrHCl{(PPh$_2$(o-C$_2$H$_4$CO))$_2$H}], complex **1**, and furfurylamine. In the formation of complexes **4** and **5** complex **1** suffers an elimination of HCl and H$_2$ respectively and the coordination of furfurylamine through the amine group. This leads to the reorganisation of the coordination sphere. In the case of complex **6** a Schiff base reaction yields a ketoimine derivative complex which is stabilised by an intramolecular hydrogen bond and no reorganisation is observed.

2. Complexes **4**, **5** and **6** have been tested for the catalytic hydrolysis of AB. The most active complex among them is complex **4**, which can release up to three hydrogen equivalents in 70 min at room temperature under air. *In situ* NMR experiments suggest that the furfurylamine is released during the catalytic process because the same intermediate species identified in the catalytic hydrolysis of AB with **1** can be detected. The presence of furfurylamine allows the formation of a less active species than the one formed from **1** for the catalytic hydrolysis of AB.

3. [IrHCl{(PPh$_2$(o-C$_2$H$_4$CO))$_2$H}], **1** and [(IrH{(PPh$_2$(o-C$_6$H$_4$CO))$_2$H})$_2$(μ-Cl)][BF$_4$], **7** have proved to be efficient homogeneous precatalysts for the methanolysis of AB in air to release hydrogen. A simplified mechanism has been proposed in which the catalysed reaction occurs in successive and parallel steps for the whole substrate. A hydridodiacyl [IrH(H$_3$NBH$_{3-x}$(OCH$_3$)$_x$)(PPh$_2$(o-C$_6$H$_4$CO))$_2$] species with the different borane adducts coordinated to the iridium *via* the borane fragment may be involved in the catalytic process. The borane adduct coordination would be followed by a nucleophilic attack of a methanol molecule to the boron atom and a O-to-Ir hydrogen transfer would release the hydrogen. The deuteration studies indicate that the cleavage of the O-H bond in methanol is involved in the rate determinant step.

4. The reaction of complex **1** with trimethylamineborane leads to the formation of the fluxional borane-coordinated irida-β-diketone [IrH(Me$_3$NBH$_3$){(PPh$_2$(o-C$_6$H$_4$CO))$_2$H}]$^+$, complex **9**. This complex is an analogous complex to the species proposed to be involved in the catalytic methanolysis of AB.

5. The reaction of complex **1** with alkyldiamines in dry tetrahydrofuran allows the formation of ketoimine type complexes (complexes **10**, **11**, **12**, **13** and **14**) after a condensation reaction of the primary amine from the ligand and the β-diketone fragment of complex **1**. The coordination environment remains unchanged as there is a intramolecular hydrogen bond stabilising the structure.

6. Ketoimine type complexes suffer a rearrangement of the ligands in presence of a protic solvent to give acyl-iminium type compounds (complexes **15**, **16**, **17** and **18**). In this rearrangement the dangling amine group from the ketoimine type complex is coordinated to the metal centre affording a cationic complex. These cationic complexes react with a base, such as KOH, and suffer a deprotonation affording neutral acyl-imine type complexes (**19**, **20** and **21**).

7. The reaction of complex **2**, [IrH$_2${(PPh$_2$(o-C$_2$H$_4$CO))$_2$H}], with the alkyldiamines *N*-methylethylendiamine and the 2-(aminomethyl)piperidine in presence of KOH and methanol under reflux affords the hydridoamino complexes **22** and **23**. The failure to obtain these type of complexes with the other used alkyldiamines indicates that when the ligand has two primary amines the synthesis of other type of compounds predominate.

8. The obtained new complexes from the reaction of irida-β-diketones with alkyldiamines have been tested for the catalytic methanolysis of AB for hydrogen release. It was proven that the presence of the alkyldiamine ligands in the catalytic process lowers the reaction rate compared to the irida-β-diketone starting material.

9. A new synthetic pathway in order to obtain the iridapyrazole complex **3** with higher yields has been reported. For this purpose the ligand L_1 has been synthesised by reaction of $PPh_2(o\text{-}C_6H_4CHO)$ and hydrazine; the reaction of the iridium dimer $[Ir(COD)Cl]_2$ with L_1 affords complex **3** in a simple and fast way.

10. The reactivity of complex **3** has been studied in two different ways: the reactivity on the metal centre and the reactivity of the pyrazole ring. From the reactivity on the metal centre new cationic and neutral complexes have been obtained by replacing the chloride atom by N-donor ligands, olefins, triphenylphosphine, boranes and trichlorostannate. On the other hand, a cationic complex was obtained by iridapyrazole ring protonation, an anionic complex by deprotonation and some neutral complexes were also obtained *via* alkylation reactions.

11. The newly obtained iridapyrazole derived complexes have been tested as catalysts for the catalytic methanolysis of AB for hydrogen release. The activity of these complexes is lower than that showed by complexes **1** and **7** may be due to the inability of these complexes to rearrange the coordination sphere. Nevertheless, it is worth mentioning that complex **35** showed the lowest reaction rate for this catalysis which reveals that a nitrogen atom with a free electron pair is needed if higher reaction rates are to be achieved.

Chapter 7

Experimental section

7.1 Instrumental techniques

<u>General working conditions</u>

All manipulations, unless otherwise stated, were performed under an atmosphere of nitrogen, using standard Schlenk techniques. Solvents were previously distilled under nitrogen, degassed by successive freeze-pump-thaw cycles and stored over molecular sieves.

<u>Solvolysis of ammonia- and amine-boranes</u>

Hydrolysis

A typical hydrolysis experiment of amineboranes is described below. THF/H_2O = 60/40 mixtures, being the total volume 3 mL, and 0.5 mol% catalyst loading were used; a solution of 1.38 mmol of amine-borane in 1.2 mL of H_2O was prepared in a round bottom 40 mL flask fitted with a gas outlet and with a side arm sealed with a septum cap. The flask was connected via the gas outlet to a gas burette filled with water. A solution of 0.007 mmol of the selected precatalyst in 1.8 mL of dry THF was syringed through the septum while the magnetic stirring was on and the timing started. Gas evolution began and the released volume was measured by the volume of water displaced in the burette. Volumes were measured at atmospheric pressure in the 20 – 40 ºC range.

Methanolysis

A solution of 1.16 mmol of the desired amineborane adduct in 2 mL of methanol was prepared in a round bottom 40 mL flask fitted with a gas outlet and with a side arm sealed with a tight-fitting septum cap. The flask was connected via the gas outlet to a gas burette filled with water. The amine-borane adduct solution was immersed in a thermostated water bath to reach the desired temperature under atmospheric pressure (1 atm) and in the presence of air. A solution of the selected precatalyst (4.64×10^{-3} mmol for 0.4%) in 0.5 mL of methanol was syringed through the septum into the reaction flask, magnetic stirring connected and timing started. Gas evolution began immediately and the

released gas was measured by determining periodically the volume of water displaced in the burette.

The homogeneity test was performed by adding seventy times more Hg moles than that of the precatalyst; for this, the reaction was prepared as described above and the mercury was syringed through the septum at the beginning or during the catalysis.

Elemental analysis

Mass percentages of carbon, nitrogen, sulphur and hydrogen in the synthesised complexes were determined by elemental microanalysis. The analysis was carried out with a LECO Truspec Micro CHNS microanalyser.

Conductivity

Conductivity measures were performed at room temperature with a Metrohm-Herisau 712 electrical conductivity meter. The system was equipped with a 0.8 cm^{-1} constant Metrohm 00450920 conductivity cell. Measures were carried out in 2.5×10^{-4} M acetone solutions.

Infrared spectroscopy

IR spectra were obtained between a wave number range of 4000-500 cm^{-1} with a Nicolet FTIR 510 spectrometer. Measures were performed in a KBr disc.

Nuclear magnetic resonance spectroscopy

^1H, ^{11}B, $^{11}B\{^1H\}$, $^{13}C\{^1H\}$, ^{15}N, ^{31}P, $^{31}P\{^1H\}$ and ^{119}Sn RMN spectra were recorded on Bruker AVD 500, 400 or 300 MHz spectrometers at room temperature unless otherwise stated. ^1H and $^{13}C\{^1H\}$ NMR spectra were referenced to the solvent residual signal, or with TMS as internal standard. In ^{11}B and $^{11}B\{^1H\}$ NMR spectra $BF_3 \cdot OEt_2$ was used as a external standard. In $^{31}P\{^1H\}$ and ^{31}P NMR spectra H_3PO_4 (85%) was used as an external standard. In the case of ^{119}Sn spectra $SnMe_4$ was used as external standard.

Electrospray ionization mass spectrometry (ESI-MS)

ESI-MS were recorded on a Bruker MicrOTOF-Q instrument. Good fit to both the principal molecular ion and the overall isotopic distribution were obtained.

X-Ray diffraction

Obtained crystals were mounted on a glass fibre and used for data collection on a Bruker D8 Venture with Photon detector equipped with graphite monochromated MoKα radiation (λ=0.71073 Å). Lorentz-polarisation and empirical absorption corrections were applied. The structures were solved by direct methods and refined with full-matrix least-squares calculations on F2 using the program SHELXS-97 and SHELXS-2013. Crystallographic data are collected in Supporting Information.

7.2 Synthesis of starting materials

Synthesis of [Ir(COD)Cl]$_2$

[Ir(COD)Cl]$_2$ compound was synthesised as reported by Cushing and co-workers by reaction of IrCl$_3$·xH$_2$O with 1,5-cyclooctadiene in a 2-propanol and water mixture under reflux.[87]

Synthesis of PPh$_2$(o-C$_6$H$_4$CHO)

O-(diphenylphosphino)benzaldehyde was synthesised as reported by Liese and co-workers.[88]

Synthesis of [IrHCl{(PPh$_2$(o-C$_6$H$_4$CO))$_2$H}] **(1)**

Complex **1** was synthesised by the reaction of [Ir(COD)Cl]$_2$ with PPh$_2$(o-C$_6$H$_4$CHO) in methanol at room temperature.[4]

Synthesis of [IrH$_2${(PPh$_2$(o-C$_6$H$_4$CO))$_2$H}] **(2)**

Complex **2** was synthesised by the reaction of [IrHCl{(PPh$_2$(o-C$_6$H$_4$CO))$_2$H}] with KOH in methanol under reflux.[4]

Synthesis of [(IrH{(PPh$_2$(o-C$_6$H$_4$CO))$_2$H})$_2$(µ-Cl)]BF$_4$ **(7)**

Complex **7** was synthesised by the reaction of [IrHCl{(PPh$_2$(o-C$_6$H$_4$CO))$_2$H}] with Et$_3$OBF$_4$ in dichloromethane at room temperature.[5]

Synthesis of PPh$_2$(o-C$_6$H$_4$)CHNNCH(o-C$_6$H$_4$)PPh$_2$ **(L$_1$)**

L$_1$ was synthesised by the reaction of PPh$_2$(o-C$_6$H$_4$CHO) (2 mmol, 580.6 mg) and hydrazine (1 mmol, 48.5 µL) in ethanol. The suspension was heated and maintained under reflux for 5 hours. The yellow precipitate was centrifuged, washed twice with 5 mL of methanol and dried under vacuum. The solid was recrystallised from a dichloromethane/hexane.Yield 84%

IR (KBr, cm^{-1}): 1614 (m), ν(C=N)

Elemental Analysis for C$_{38}$H$_{30}$N$_2$P$_2$:

Calculated: C 79.15, H 5.24, N 4.86.

Found: C 79.61, H 5.25, N 4.95.

^{1}H NMR (CDCl$_3$): δ 6.8-8.2 (28 H, Aromatics); 9.23 (d, J$_{P,H}$=4.5 Hz, ^{2}J$_P$, 2H, *H*-C=N) ppm.

^{31}P{^{1}H} NMR (CDCl$_3$): δ -14.6 (s) ppm.

^{15}N NMR (CDCl$_3$): δ 367.4 (s) ppm

7.3 Synthesis and characterisation of complexes

Synthesis of [IrH(PPh$_2$(*o*-C$_6$H$_4$CO))$_2$(NH$_2$(CH$_2$)C$_4$H$_3$O)] **(4)**

Furfurylamine (0.096 mmol, 8.5 µL) was added to a tetrahydrofuran/water (1:1) yellow suspension of [IrHCl{(PPh$_2$(*o*-C$_6$H$_4$CO))$_2$H}] (0.037 mmol, 30 mg). The suspension was stirred for 24 hours obtaining a lighter yellow suspension. The yellowish solid was centrifuged and dried under vacuum. The solid was recrystallised from DMF. Yield 68 %.

IR (KBr, cm^{-1}): 3306 (m, N-H), 3271 (w, N-H), 2028 (s, Ir-H), 1597 (s, C=O).

Elemental Analysis for IrC$_{43}$H$_{36}$P$_2$O$_3$N·0.5H$_2$O:

Calculated: C 58.83, H 4.25, N 1.60.

Found: C 58.6, H 4.48, N 1.49.

^{1}H NMR (DMF-d^7): δ -7.90 (dd, $^2J_{P,H}$=19 Hz, $^2J_{P,H}$=131 Hz, 1H, *H*-Ir); 1.80 (s, 1H, *H*$_2$N); 3.85 (s, 1H, *H*$_2$N); 2.27 (br, 1H, *H*$_2$C); 3.65 (br, 1H, *H*$_2$C); 5.83 (s, 1H, *H*C-C); 6.21 (s, 1H, *H*C-CH); 7.41 (s, 1H, *H*C-O); 6.60-8.40 (28H, Aromatics) ppm.

^{31}P NMR (DMF-d^7): δ 23.8 (s); 31.9 (d, $^2J_{H,P}$= 130 Hz) ppm.

^{13}C{^{1}H} NMR (DMF-d^7): δ 40.7 (s, *C*H$_2$); 107.6 (s, *C*H-C); 110.6 (s, *C*H-CH); 133.0 (s, *C*H-O); 126.0-135.0 (Aromatics); 212.5 (d, $^2J_{P,C}$= 5 Hz, *C*=O); 233.3 (d, $^2J_{P,C}$= 105 Hz, *C*=O) ppm.

Conductivity (Λ$_M$): 5 ohm^{-1}·cm^2·mol^{-1}.

Synthesis of [IrCl(PPh$_2$(*o*-C$_6$H$_4$CO))$_2$(NH$_2$(CH$_2$)C$_4$H$_3$O)] **(5)**

Furfurylamine (0.078 mmol, 6.9 µL) was added to a suspension of [IrHCl{(PPh$_2$(*o*-C$_6$H$_4$CO))$_2$H}] (0.037 mmol, 30 mg) in methanol. The suspension

was heated to reflux for 5 hours and a yellow solution was obtained. It was left to cool down and a yellow solid appeared. The suspension was centrifuged and the yellow solid was dried under vacuum and recrystallised from methanol. Yield 54 %.

IR (KBr, cm^{-1}): 3297 (w, N-H); 1625 (s, C=O).

Elemental Analysis for IrC$_{43}$H$_{35}$P$_2$O$_3$NCl:

Calculated: C 57.17, H 3.90, N 1.55.

Found: C 57.18, H 3.89, N 1.62.

^{1}H NMR (CDCl$_3$): δ 3.23 (m, 1H, H_2N); 5.66 (m, 1H, H_2N); 2.44 (t, $^3J_{H,H}$=12.4 Hz, 1H, H_2C); 3.57 (t, $^3J_{H,H}$=13.2 Hz, 1H, H_2C); 5.73 (s, 1H, HC-C); 6.12 (s, 1H, HC-CH); 7.15 (s, 1H, HC-O); 6.40-8.30 (28H, Aromatics) ppm.

^{31}P{^{1}H} NMR (CDCl$_3$): δ 9.3(d, $^2J_{P,P}$= 5 Hz); 22.3 (d, $^2J_{P,P}$= 5 Hz) ppm.

^{13}C{^{1}H} NMR (CDCl$_3$): δ 41.4 (s, CH$_2$); 107.4 (s, CH-C); 110.1 (s, CH-CH); 142.1 (s, CH-O); 124.0-134.5 (Aromatics); 208.3 (d, $^2J_{P,C}$= 8 Hz, C=O); 231.0 (d, $^2J_{P,C}$= 108 Hz, C=O) ppm.

Conductivity (Λ$_M$): 10 ohm^{-1}·cm^2·mol^{-1}.

Synthesis of [IrH(PPh$_2$(*o*-C$_6$H$_4$CO)(PPh$_2$(*o*-C$_6$H$_4$C=N(CH$_2$)C$_4$H$_3$O))] **(6)**

Furfurylamine (0.096 mmol, 8.5 μL) was added to a tetrahydrofuran suspension of [IrHCl{(PPh$_2$(*o*-C$_6$H$_4$CO))$_2$H}] (0.037 mmol, 30 mg) and it was stirred for 120 hours (5 days). The volume was reduced and hexane was added until a yellow solid precipitated. The solid was centrifuged, dried under vacuum and recrystallised from dichloromethane/diethyl ether. Yield 46 %.

IR (KBr, cm^{-1}): 2184 (s, Ir-H); 1550 (s, C=O and C=N).

Elemental Analysis for IrC$_{43}$H$_{35}$P$_2$O$_2$NCl:

Calculated: C 58.20, H 3.98, N 1.58.

Found: C 57.83, H 4.28, N 1.57.

^{1}H NMR (CDCl$_3$): δ -20.50 (t, $^{2}J_{P,H}$= 14 Hz, 1H, *H*-Ir); 5.2 (d, $^{3}J_{H,H}$=8 Hz, 2H, *H$_2$*C); 6.50 (s, 1H, *H*C-C); 6.40 (s, 1H, *H*C-CH); 7.4 (s, 1H, *H*C-O); 6.8-8.3 (28H, Aromatics) 13.4 (br, 1H, O--*H*--N) ppm.

^{31}P{^{1}H} NMR (CDCl$_3$): δ 14.8(d, $^{2}J_{P,P}$= 7 Hz); 29.8 (d, $^{2}J_{P,P}$= 7 Hz) ppm.

^{13}C{^{1}H} NMR (CDCl$_3$): ^{13}C{^{1}H} NMR (CDCl$_3$): δ 47.7 (s, *C*H$_2$); 109.0 (s, *C*H-C); 110.0 (s, *C*H-CH); 142.8 (s, *C*H-O); 123.0-135.5 (Aromatics); 223.0 (d, $^{2}J_{P,C}$= 102 Hz, *C*=O or *C*=N); 243.0 (d, $^{2}J_{P,C}$= 105 Hz, *C*=O or *C*=N) ppm.

Conductivity ($Λ_M$): 5 ohm^{-1}·cm^2·mol^{-1}.

Synthesis of [IrH(H$_3$BNMe$_3$){(PPh$_2$(*o*-C$_6$H$_4$CO))(PPh$_2$(*o*-C$_6$H$_4$CO))H}] [BAr$^{F}_4$] **(9)**

Trimethylamine borane (0.037 mmol, 2.7 mg) was added to a Schlenk flask charged with a dichloromethane solution of [IrHCl{PPh$_2$(*o*-C$_6$H$_4$CO))$_2$)H}] (0.037mmol, 30 mg) and then, the sodium tetrakis[3,5-bis(trifluoromethyl)phenyl]borate salt (0.037 mmol, 32.8 mg) was added to the mixture affording instantly a yellow solution. It was left stirring for 30 minutes and then the salts were extracted with water, keeping the organic phase. The resulting dichloromethane solution was dried with magnesium sulphate and filtered. The solvent was removed under low pressure affording an off-yellow solid. Yield 72%.

IR (KBr, cm^{-1}): 2504 (w), ν(B-H$_t$); 2444 (w), ν(B-H$_t$); 1731 (br), ν(Ir-H); 1509 (m), ν(C=O)

Elemental Analysis for IrC$_{74}$H$_{57}$P$_2$O$_2$NB$_2$F$_{24}$·(CH$_2$Cl$_2$)$_{0.6}$:

Calculated: C 50.66, H 3.31, N 0.79.

Found: C 50.59, H 3.22, N 0.58.

^{1}H NMR (CDCl$_3$): δ -18.38 (t, $^2J_{P,H}$= 14.6 Hz, 1H, *H*-Ir); -2.50 (br, 3H, *H*-B); 1.80 (s, 9H, *H$_3$*C); 7-8.5 (28H, Aromatics); 22.58 (br, 1H, O--*H*--O) ppm.

^{1}H NMR (CDCl$_3$) (-60 ºC): δ -18.09 (t, $^2J_{P,H}$= 14.6 Hz, 1H, *H*-Ir); -10.50 (s, 1H, *H*-B); 1.42 (br, 2H, *H*-B); 1.80 (s, 9H, *H$_3$*C); 7-8.5 (28H, Aromatics); 22.75 (br, 1H, O--*H*--O) ppm.

^{31}P{^{1}H} NMR (CDCl$_3$): δ 23.1 (s) ppm.

ESI-MS (MeOH): Calculated for C$_{41}$H$_{42}$BIrNO$_2$P$_2$: 846.24; found: 846.24 [M]$^+$.

Conductivity (Λ$_M$): 130 ohm^{-1}·cm^2·mol^{-1}.

Synthesis of [IrHCl{(PPh$_2$(*o*-C$_6$H$_4$CO))(PPh$_2$(*o*-C$_6$H$_4$CN(CH$_2$)$_2$NH$_2$))H}] **(10)**

Etilendiamine (0.048 mmol, 3.2μL) was added to a Schlenk flask charged with a THF suspension of [IrHCl{PPh$_2$(*o*-C$_6$H$_4$CO))$_2$)H}] (0.037mmol, 30 mg). The suspension afforded a bright yellow solution that turned greenish after 2 hours. Then, the solvent was removed under vacuum allowing a yellow-green solid that was cleaned with diethyl ether and hexane and then dried. The compound was recrystallised from methanol/diethyl ether. Yield 86%.

IR (KBr, cm^{-1}): 3372 (w, N-H); 2177 (s, Ir-H); 1552 (s, C=O and C=N).

Elemental Analysis for IrC$_{40}$H$_{36}$P$_2$ON$_2$Cl:

Calculated: C 56.50, H 4.27, N 3.29.

Found: C 56.21, H 3.96, N 3.02.

^{1}H NMR (CDCl$_3$): δ -20.47 (t, $^2J_{P,H}$= 14.4 Hz, 1H, *H*-Ir); 3.10 (dt, $^2J_{H,H}$= 4.9 Hz, $^2J_{H,H}$= 13.4, 1H, *H$_2$*C-NH$_2$); 3.28 (m, 1H, *H$_2$*C-NH$_2$); 4.15 (p, $^2J_{H,H}$= 5.7 Hz, $^2J_{H,H}$= 6.3, 2H, *H$_2$*C-NC); 7-8.1 (28H, Aromatics); 12.82 (br, 1H, O--*H*--N) ppm.

^{31}P{^{1}H} NMR (CDCl$_3$): δ 15.6 (d, $^2J_{P,P}$= 7 Hz); 29.9 (d, $^2J_{P,P}$= 7 Hz) ppm.

^{13}C{^{1}H} NMR (CDCl$_3$): δ 42.1 (s, CH_2-NH$_2$); 54.7 (d, $^2J_{P,C}$= 5 Hz, H$_2$$C$-NC); 123.0-162.0 (Aromatics); 224.0 (d, $^2J_{P,C}$= 102 Hz, C=O or C=N); 243.0 (d, $^2J_{P,C}$= 106 Hz, C=O or C=N) ppm.

Conductivity (Λ$_M$): 10 ohm^{-1}·cm^2·mol^{-1}.

Synthesis of [IrHCl{(PPh$_2$(o-C$_6$H$_4$CO))(PPh$_2$(o-C$_6$H$_4$CN(CH$_2$)$_2$NHCH$_3$))H}] (11)

N-methyletilendiamine (0.056 mmol, 4.9μL) was added to a Schlenk flask charged with a THF suspension of [IrHCl{PPh$_2$(o-C$_6$H$_4$CO))$_2$)H}] (0.037mmol, 30 mg). After 5 minutes the solid dissolved and the yellow solution was left stirring for 2 hours at room temperature. Then, the solvent was removed under vacuum allowing a yellow solid. The obtained solid was cleaned with diethyl ether and hexane. Yield 66%.

IR (KBr, cm^{-1}): 3280 (w, N-H); 2171 (s, Ir-H); 1564 (s, C=O and C=N).

Elemental Analysis for IrC$_{41}$H$_{38}$P$_2$ON$_2$Cl·H$_2$O:

Calculated: C 55.81, H 4.57, N 3.17.

Found: C 55.82, H 4.68, N 3.34.

^{1}H NMR (CDCl$_3$): δ -20.44 (t, $^2J_{P,H}$= 14.5 Hz, 1H, *H*-Ir); 2.18 (s, 3H, H_3C-NH); 2.94 (m, 1H, H_2C-NH); 3.19 (m, 1H, H_2C-NH); 4.16 (m, 1H, H_2C-NC); 4.34 (m, 1H, H_2C-NC); 6.9-8.1 (28H, Aromatics); 12.62 (br, 1H, O--*H*--N) ppm.

^{31}P{^{1}H} NMR (CDCl3): δ 16.0 (d, $^2J_{P,P}$= 7.4 Hz); 29.9 (d, $^2J_{P,P}$= 7.4 Hz) ppm.

^{13}C{^{1}H} NMR (CDCl$_3$): δ 35.6 (s, CH_3-NH); δ 50.7 (s, CH_2-NH); 50.9 (d, $^2J_{P,C}$= 5 Hz, H$_2$$C$-NC); 122.0-162.0 (Aromatics); 224.3 (d, $^2J_{P,C}$= 102 Hz, C=O or C=N); 242.0 (d, $^2J_{P,C}$= 104 Hz, C=O or C=N) ppm.

Conductivity (Λ$_M$): 10 ohm^{-1}·cm^2·mol^{-1}.

Synthesis of [IrHCl{(PPh$_2$(*o*-C$_6$H$_4$CO))(PPh$_2$(*o*-C$_6$H$_4$CN(CH$_2$)$_2$NHCH$_2$CH$_3$))H}] **(12)**

N-Ethyletilendiamine (0.056 mmol, 5.9 µL) was added to a Schlenk flask charged with a THF suspension of [IrHCl{PPh$_2$(*o*-C$_6$H$_4$CO))$_2$)H}] (0.037mmol, 30 mg). The suspension afforded a yellow solution and was left stirring for 2 hours. Then, the solvent was removed under vacuum allowing a yellow solid that was cleaned with diethyl ether and hexane and then dried. Yield 72%.

IR (KBr, cm^{-1}): 3268 (w, N-H); 2179 (s, Ir-H); 1553 (s, C=O and C=N).

Elemental Analysis for IrC$_{42}$H$_{40}$P$_2$ON$_2$Cl:

Calculated: C 57.43, H 4.59, N 3.19.

Found: C 57.67, H 4.53, N 3.45.

^{1}H NMR (CDCl$_3$): δ -20.40 (t, ^{2}J$_{P,H}$= 14.5 Hz, 1H, *H*-Ir); 0.83 (m, 3H, *H$_3$*C-H$_2$C-NH); 2.46 (m, 2H, H$_3$C-*H$_2$*C-NH); 3.00 (m, 1H, *H$_2$*C-H$_2$C-NC); 3.22 (m, 1H, *H$_2$*C-H$_2$C-NC); 4.15 (m, 1H, *H$_2$*C-NC); 4.30 (m, 1H, *H$_2$*C-NC); 6.9-8.1 (28H, Aromatics); 12.64 (br, 1H, O--*H*--N) ppm.

^{31}P{^{1}H} NMR (CDCl3): δ 16.0 (d, ^{2}J$_{P,P}$= 7.4 Hz); 30.4 (d, ^{2}J$_{P,P}$= 7.4 Hz) ppm.

^{13}C{^{1}H} NMR (CDCl$_3$): δ 15.0 (s, *CH$_3$*-CH$_2$-NH); 43.6 (s, CH$_3$-*CH$_2$*-NH); 48.9 (s, *CH$_2$*-CH$_2$-NC); 50.9 (d, ^{2}J$_{P,C}$= 5.6 Hz, H$_2$*C*-NC); 122.0-162.0 (Aromatics); 224.2 (d, ^{2}J$_{P,C}$= 102 Hz, *C*=O or *C*=N); 242.0 (d, ^{2}J$_{P,C}$= 104 Hz, *C*=O or *C*=N) ppm.

Conductivity (Λ$_M$): 10 ohm^{-1}·cm^2·mol^{-1}.

Synthesis of [IrHCl{(PPh$_2$(*o*-C$_6$H$_4$CO))(PPh$_2$(*o*-C$_6$H$_4$CN(CH$_2$)$_3$NH$_2$))H}] **(13)**

Propilendiamine (0.056 mmol, 4.7 µL) was added to a Schlenk flask charged with a THF suspension of [IrHCl{PPh$_2$(*o*-C$_6$H$_4$CO))$_2$)H}] (0.037mmol,

30 mg). The suspension afforded a yellow solution and was left stirring for 2 hours. Then, the solvent was removed under vacuum allowing a yellow solid that was cleaned with diethyl ether and hexane and then dried. Yield 70%.

IR (KBr, cm^{-1}): 3280 (w, N-H); 2189 (s, Ir-H); 1553 (s, C=O and C=N).

Elemental Analysis for IrC$_{41}$H$_{38}$P$_2$ON$_2$Cl:

    Calculated: C 56.97, H 4.43, N 3.24.

    Found: C 56.89, H 4.50, N 3.16.

^{1}H NMR (CDCl$_3$): δ -20.66 (t, $^2J_{P,H}$= 14.0 Hz, 1H, *H*-Ir); 2.08 (m, 2H, H$_2$C-*H$_2$*C-CH$_2$); 2.88 (m, 2H, *H$_2$*C-NH$_2$); 4.11 (m, 2H, *H$_2$*C-NC); 6.9-8.1 (28H, Aromatics); 12.99 (br, 1H, O--*H*--N) ppm.

^{31}P{^{1}H} NMR (CDCl3): δ 14.6 (d, $^2J_{P,P}$= 7 Hz); 29.6 (d, $^2J_{P,P}$= 7 Hz) ppm.

^{13}C{^{1}H} NMR (CDCl$_3$): δ 33.3 (s, CH$_2$-*C*H$_2$-CH$_2$); δ 39.4 (s, *C*H$_2$-NH$_2$); 48.9 (d, $^2J_{P,C}$= 5.5 Hz, H$_2$*C*-NC); 122.0-162.0 (Aromatics); 221.4 (d, $^2J_{P,C}$= 103 Hz, *C*=O or *C*=N); 243.4 (d, $^2J_{P,C}$= 106 Hz, *C*=O or *C*=N) ppm.

Conductivity (Λ$_M$): 10 ohm^{-1}·cm^2·mol^{-1}.

<u>Synthesis of [IrHCl{(PPh$_2$(*o*-C$_6$H$_4$CO))(PPh$_2$(*o*-C$_6$H$_4$CNCH$_2$(C$_5$H$_9$N)))H}]</u> **(14)**

    2-(Aminomethyl)piperidine (0.0585 mmol, 7.1µL) was added to a Schlenk flask charged with a THF suspension of [IrHCl{PPh$_2$(*o*-C$_6$H$_4$CO))$_2$)H}] (0.037mmol, 30 mg). After 5 minutes the solid dissolved and the yellow solution was left stirring for 48 hours at room temperature. Then, the solvent was removed under vacuum allowing a yellow solid that was cleaned with diethyl ether and hexane and then dried. Yield 76%.

IR (KBr, cm^{-1}): 3276 (w, N-H); 2170 (s, Ir-H); 1554 (s, C=O and C=N).

Elemental Analysis for IrC$_{44}$H$_{42}$P$_2$ON$_2$Cl·(H$_2$O)$_{0.75}$:

Calculated: C 57.57, H 4.78, N 3.05.

Found: C 57.75, H 4.77, N 2.61.

^{1}H NMR (CDCl$_3$): δ -20.57 (dd, $^2J_{P,H}$= 14.8 Hz, $^2J_{P,H}$= 13.6 Hz, 1H, *H*-Ir); -20.44 (dd, $^2J_{P,H}$= 15.6 Hz, $^2J_{P,H}$= 14.1 Hz, 1H, *H*-Ir); 1.17 (m, 1H, *H*$_2$C-NH); 1.33 (m, 1H, *H*$_2$C-CH$_2$-CH) and (m, 1H, *H*$_2$C-CH$_2$-NH); 1.39 (m, 1H, *H*$_2$C-CH$_2$-CH) and (m, 1H, *H*$_2$C-CH$_2$-NH); 1.46 (m, 1H, *H*$_2$C-NH); 1.51 (m, 2H, *H*$_2$C-CH$_2$-CH); 1.72 (m, 1H, *H*$_2$C-NH); 1.77 (m, 1H, *H*$_2$C-CH$_2$-NH); 1.84 (m, 1H, *H*$_2$C-CH$_2$-NH); 1.86 (m, 1H, *H*$_2$C-NH); 2.55 (m, 1H, *H*$_2$C-CH); 2.57 (m, 1H, *H*$_2$C-CH); 2.76 (m, 1H, *H*$_2$C-CH); 2.88 (m, 1H, *H*$_2$C-CH); 3.07 (m, 1H, *H*C); 3.24 (m, 1H, *H*C); 4.00 (m, 1H, *H*$_2$C-NC); 4.01 (m, 1H, *H*$_2$C-NC); 4.10 (m, 1H, *H*$_2$C-NC); 4.16 (m, 1H, *H*$_2$C-NC); 6.8-8.0 (56 H, Aromatics); 12.77 (br, 1H, O--*H*--N) ; 12.98 (br, 1H, O--*H*--N) ppm.

^{31}P{^{1}H} NMR (CDCl3): δ 15.07 (s); 16.91 (s); 29.13 (d, $^2J_{P,P}$= 7.3 Hz); 29.89 (d, $^2J_{P,P}$= 7.0 Hz) ppm.

^{13}C{^{1}H} NMR (CDCl$_3$): 24.4 (s, *C*H$_2$-NH); 24.5 (s, *C*H$_2$-NH); 25.6 (s, *C*H$_2$-CH$_2$-NH); 25.7 (s, *C*H$_2$-CH$_2$-NH); 29.6 (s, *C*H$_2$-CH$_2$-CH); 30.1 (s, *C*H$_2$-CH$_2$-CH); 46.2 (s, *C*H$_2$-CH); 46.6 (s, *C*H$_2$-CH); 56.2 (s, *C*H); 56.6 (s, *C*H); 56.8 (s, *C*H$_2$-NC); 57.6 (s, *C*H$_2$-NC); 122.0-162.0 (Aromatics); 224.1 (d, $^2J_{P,C}$= 102 Hz, *C*=O or *C*=N); 242.0 (d, $^2J_{P,C}$= 104 Hz, *C*=O or *C*=N); 242.8 (d, $^2J_{P,C}$= 104 Hz, *C*=O or *C*=N) ppm.

Conductivity (Λ$_M$): 10 ohm^{-1}·cm^2·mol^{-1}.

Synthesis of [IrH(PPh$_2$(*o*-C$_6$H$_4$CO))(PPh$_2$(*o*-C$_6$H$_4$C=N(H)CH$_2$CH$_2$NH$_2$))]Cl **(15)**

Etilendiamine (0.0375 mmol, 2.5 µL) was added to a methanol suspension of [IrHCl{PPh$_2$(*o*-C$_6$H$_4$CO))$_2$)H}] (0.037mmol, 30 mg). The suspension was heated under reflux for 2 hours affording a yellow solution. Then, the solvent was removed under vacuum allowing a yellow solid. The compound was recrystallised from dichloromethane/diethyl ether at -20ºC. Yield 77%.

IR (KBr, cm^{-1}): 3316 (w, N-H); 2015 (s, Ir-H); 1575 (s, C=O and C=N).

Elemental Analysis for IrC$_{40}$H$_{36}$P$_2$ON$_2$Cl·(CH$_2$Cl$_2$)$_{0.25}$:

Calculated: C 55.47, H 4.22, N 3.21.

Found: C 55.16, H 4.37, N 3.02.

^{1}H NMR (CD$_3$OD): δ -8.74 (dd, $^2J_{P,H}$= 122.0 Hz, $^2J_{P,H}$= 18.4 Hz, 1H, *H*-Ir); 1.46 (m, 1H, *H*$_2$C-NH$_2$); 1.89 (m, 1H, N*H*$_2$); 2.80 (m, 1H, *H*$_2$C-NH$_2$); 3.88 (m, 1H, *H*$_2$C-NC); 3.96 (m, 1H, *H*$_2$C-NC); 4.71 (m, 1H, N*H*$_2$); 7-8.1 (28H, Aromatics) ppm.

^{31}P NMR (CD$_3$OD): δ 15.5 (d, $^2J_{H,P}$= 122 Hz); 25.8 (s) ppm.

^{13}C{^{1}H} NMR (CDCl$_3$): δ 39.7 (s, *C*H$_2$-NH$_2$); 55.8 (s, H$_2$*C*-NC); 123.0-162.0 (Aromatics); 217.8 (dd, $^2J_{P,C}$= 16 Hz, $^2J_{P,C}$= 6.2 Hz, *C*=O); 232.2 (d, $^2J_{P,C}$= 90 Hz, *C*=N) ppm.

ESI-MS (MeOH): Calculated for IrC$_{40}$H$_{34}$P$_2$ON$_2$: 813.2; found: 813.1 [M-H$_2$]$^+$.

Conductivity (Λ$_M$):

[15][Cl]: 40 ohm^{-1}·cm^2·mol^{-1}.

[15][ClO$_4$]: 130 ohm^{-1}·cm^2·mol^{-1}.

Synthesis of [IrH(PPh$_2$(*o*-C$_6$H$_4$CO))(PPh$_2$(*o*-C$_6$H$_4$C=N(H)CH$_2$CH$_2$NHCH$_3$))]Cl (16)

Complex **(11)** (0.037 mmol, 32 mg) was stirred in a 1:1 solution of methanol:dichoromethane for three hours at room temperature. Solvents were removed at reduced pressure affording a pale yellow solid. The solid was cleaned with diethyl ether and dried. Yield 70%.

IR (KBr, cm^{-1}): 3282 and 3198 (w, N-H); 2014 (s, Ir-H); 1575 (s, C=O and C=N).

Elemental Analysis for IrC$_{41}$H$_{38}$P$_2$ON$_2$Cl·(CH$_2$Cl$_2$):

Calculated: C 53.14, H 4.25, N 2.95.

Found: C 52.78, H 4.02, N 2.46.

^{1}H NMR (CDCl$_3$): δ -9.15 (dd, $^2J_{P,H}$= 124.5 Hz, $^2J_{P,H}$= 18.9 Hz, 1H, *H*-Ir); -8.46 (dd, $^2J_{P,H}$= 122.6 Hz, $^2J_{P,H}$= 19.8 Hz, 1H, *H*-Ir); 2.36 (d, $^3J_{H,H}$= 6 Hz, 3H, C*H$_3$*); 2.36 (m, 1H, C*H$_2$*-NC); 2.60 (m, 1H, C*H$_2$*-NC); 4.00 (m, 1H, C*H$_2$*-NIr); 4.47 (m, 1H, C*H$_2$*-NH); 6.3-8.7 (56H, Aromatics) ppm.

^{31}P NMR (CDCl$_3$): δ 15.4 (d, $^2J_{H,P}$= 127 Hz); 25.7 (s) ppm.

^{13}C{^{1}H} NMR (CDCl$_3$): δ 45.6 (s, *C*H$_3$); 52.5 (s, *C*H$_2$-NC); 54.5 (s, *C*H$_2$-NIr); 120-160 (Aromatics); 208.4 (s, *C*=O); 228.8 (d, $^2J_{P,C}$= 92 Hz, *C*=N).

ESI-MS (MeOH): Calculated for IrC$_{41}$H$_{38}$P$_2$ON$_2$: 829.2; found: 829.2 [M]$^+$.

Conductivity (Λ$_M$):

[16][Cl]: 30 ohm^{-1}·cm^2·mol^{-1}.

[16][ClO$_4$]: 120 ohm^{-1}·cm^2·mol^{-1}.

Synthesis of [IrH(PPh$_2$(*o*-C$_6$H$_4$CO))(PPh$_2$(*o*-C$_6$H$_4$C=N(H)CH$_2$CH$_2$CH$_2$NH$_2$))]Cl (**17**)

Complex **(13)** (0.037 mmol, 32 mg) was stirred in a 1:1 solution of methanol:dichoromethane for three hours at room temperature. Solvents were removed at reduced pressure affording a pale yellow solid. The solid was cleaned with diethyl ether and dried. Yield 70%.

IR (KBr, cm^{-1}): 3311 (w, N-H); 2036 (s, Ir-H); 1575 (s, C=O and C=N).

Elemental Analysis for IrC$_{41}$H$_{38}$P$_2$ON$_2$Cl·(H$_2$O)$_{0.6}$:

Calculated: C 56.38, H 4.50, N 3.21.

Found: C 56.21, H 4.66, N 2.40.

^{1}H NMR (CDCl$_3$): δ -8.36 (dd, $^2J_{P,H}$= 126.3 Hz, $^2J_{P,H}$= 19.1 Hz, 1H, *H*-Ir); 1.55 (m, 1H, N*H$_2$*); 1.94 (m, 2H, CH$_2$-*H$_2$C*-CH$_2$); 2.56 (m, 2H, *H$_2$*C-NH$_2$); 2.93 (m, 1H, N*H$_2$*); 4.56 (m, 1H, *H$_2$*C-NC); 4.85 (m, 1H, *H$_2$*C-NC); 6.2-8.9 (28H, Aromatics) 12.79 (br, 1H, *H*N=C) ppm.

^{31}P{^{1}H} NMR (CDCl$_3$): δ 18.2 (d, $^2J_{P,P}$= 12 Hz); 27.0 (d, $^2J_{P,P}$= 12 Hz) ppm.

^{13}C{^{1}H} NMR (CDCl$_3$): δ 28.9 (s, CH$_2$-*CH$_2$*-CH$_2$); 44.1 (s, H$_2$*C*-NH$_2$); 51.2 (s, H$_2$*C*-NC); 122.0-162.0 (Aromatics); 211.2 (d, $^2J_{P,C}$= 5.7 Hz, *C*=O); 226.7 (d, $^2J_{P,C}$= 93 Hz, *C*=N) ppm.

ESI-MS (MeOH): Calculated for IrC$_{41}$H$_{36}$P$_2$ON$_2$: 827.2; found: 827.2 [M-H$_2$]$^+$.

Conductivity (Λ$_M$):

[17][Cl]: 40 ohm^{-1}·cm^2·mol^{-1}.

[17][ClO$_4$]: 120 ohm^{-1}·cm^2·mol^{-1}.

Synthesis of [IrH(PPh$_2$(*o*-C$_6$H$_4$CO))(PPh$_2$(*o*-C$_6$H$_4$C=N(H)CH$_2$(C$_5$H$_9$N)))]Cl **(18)**

Complex **(14)** (0.037 mmol, 33.5 mg) was stirred in a 1:1 solution of methanol:dichoromethane for 24 hours at room temperature. Solvents were removed at reduced pressure affording a pale yellow solid. The solid was cleaned with diethyl ether and dried. Yield 73.5%.

IR (KBr, cm^{-1}): 3320 and 3238 (w, N-H); 2086 (s, Ir-H); 1560 (s, C=O and C=N).

Elemental Analysis for IrC$_{44}$H$_{42}$P$_2$ON$_2$Cl·(CH$_2$Cl$_2$)$_{0.75}$:

Calculated: C 55.52, H 4.53, N 2.89.

Found: C 55.63, H 4.35, N 2.73.

^{1}H NMR (CDCl$_3$): δ -9.08 (dd, ^{2}J$_{P,H}$= 124.2 Hz, ^{2}J$_{P,H}$= 19.8 Hz, 1H, *H*-Ir); -8.56 (dd, ^{2}J$_{P,H}$= 122.9 Hz, ^{2}J$_{P,H}$= 20.3 Hz, 1H, *H*-Ir); -0.3–4.4 (26H, Aliphatics from the piperidine ligand); 6.3-8.7 (56H, Aromatics) ppm.

^{31}P{^{1}H} NMR (CDCl$_3$): δ 21.05 (s); 22.96 (s); 26.97 (d, ^{2}J$_{P,P}$= 12.6 Hz); 29.99 (d, ^{2}J$_{P,P}$= 14.9 Hz) ppm.

^{13}C{^{1}H} NMR (CDCl$_3$): δ 20.0-80.0 (Aliphatics from the piperidine ligand); 122.0-162.0 (Aromatics); 206.2 (d, ^{2}J$_{P,C}$= 6 Hz, *C*=O); 211.2 (d, ^{2}J$_{P,C}$= 6 Hz, *C*=O); 227.6 (d, ^{2}J$_{P,C}$= 85 Hz, *C*=N); 231.0 (d, ^{2}J$_{P,C}$= 95 Hz, *C*=N) ppm.

ESI-MS (MeOH): Calculated for IrC$_{44}$H$_{40}$P$_2$ON$_2$: 867.2; found: 867.2 [M-H$_2$]$^{+}$.

Conductivity (Λ$_M$):

[18][Cl]: 50 ohm^{-1}·cm^2·mol^{-1}.

[18][ClO$_4$]: 140 ohm^{-1}·cm^2·mol^{-1}.

Synthesis of [IrH(PPh$_2$(*o*-C$_6$H$_4$CO))(PPh$_2$(*o*-C$_6$H$_4$C=NCH$_2$CH$_2$NH$_2$))] **(19)**

K(OH) (0.075mmol, 4.2 mg) was added to a solution of complex **(15)** (0.037 mmol, 31.5 mg) in methanol. The solution was stirred for an hour and then the solvent was evaporated under low pressure. The resulted solid was dissolved in dichloromethane and the salts were extracted with water. Then the solvent was removed affording a yellow solid which was cleaned with diethyl ether and hexane. Yield 71%.

IR (KBr, cm^{-1}): 3318 and 3356 (w, N-H); 2011 (s, Ir-H); 1601 (s, C=O and C=N).

Elemental Analysis for IrC$_{40}$H$_{35}$P$_2$ON$_2$·(CH$_2$Cl$_2$):

Calculated: C 54.79, H 4.15, N 3.12.

Found: C 54.81, H 4.18, N 2.70.

^{1}H NMR (CDCl$_3$): δ -8.53 (dd, ^{2}J$_{P,H}$= 122.0 Hz, ^{2}J$_{P,H}$ 18.2 Hz, 1H, *H*-Ir); 1.25 (m, 1H, *H*$_2$C-NH$_2$); 2.35 (m, 1H, *H*$_2$C-NH$_2$); 3.07 (m, 2H, N*H*$_2$); 3.54 (m, 1H, *H*$_2$C-NC); 4.23 (m, 1H, *H*$_2$C-NC); 6.5-8.3 (28H, Aromatics) ppm.

^{31}P{^{1}H} NMR (CDCl$_3$): δ 25.6 (s); 27.3 (d, ^{2}J$_{P,P}$= 7.1 Hz) ppm.

^{13}C{^{1}H} NMR (CDCl$_3$): δ 38.1 (s, *C*H$_2$-NH$_2$); 64.54 (s, H$_2$*C*-NC); 122.0-164 (Aromatics); 208.3 (d, ^{2}J$_{P,C}$= 80.3 Hz, *C*=N); 214.8 (d, ^{2}J$_{P,C}$= 6.8 Hz *C*=O) ppm.

ESI-MS (MeOH): Calculated for IrC$_{40}$H$_{36}$P$_2$ON$_2$: 815.2; found: 815.2 [M+H$^+$]$^+$.

Conductivity (Λ$_M$): 10 ohm^{-1}·cm^2·mol^{-1}.

Synthesis of [IrH(PPh$_2$(*o*-C$_6$H$_4$CO))(PPh$_2$(*o*-C$_6$H$_4$C=NCH$_2$CH$_2$NHCH$_3$))] **(20)**

K(OH) (0.075mmol, 4.2 mg) was added to a solution of complex **(16)** (0.037 mmol, 31.75 mg) in methanol. The solution was stirred for an hour and then the solvent was evaporated under low pressure. The resulted solid was dissolved in dichloromethane and the salts were extracted with water. Then the solvent was removed affording a yellow solid which was cleaned with diethyl ether and hexane. Yield 65%.

IR (KBr, cm^{-1}): 3281 (w, N-H); 2009 (s, Ir-H); 1600 (s, C=O and C=N).

Elemental Analysis for IrC$_{41}$H$_{37}$P$_2$ON$_2$·(CH$_2$Cl$_2$)$_{0.75}$:

Calculated: C 56.24, H 4.35, N 3.14.

Found: C 56.01, H 4.04, N 2.97.

^{1}**H NMR (CDCl$_3$):** δ -9.02 (dd, ^{2}J$_{P,H}$= 124.4 Hz, ^{2}J$_{P,H}$= 18.5 Hz, 1H, *H*-Ir); -8.35 (dd, ^{2}J$_{P,H}$= 123.2 Hz, ^{2}J$_{P,H}$= 19.7 Hz, 1H, *H*-Ir); 1.15 (m, 1H, N*H*); 2.19 (m, 1H, *H*$_2$C-NH); 2.27 (d, ^{3}J$_{H,H}$= 6.3 Hz, 3H, *H*$_3$C); 2.33 (m, 1H, *H*$_2$C-NH); 3.83 (td, ^{2}J$_{H,H}$= 11.2 Hz , ^{3}J$_{H,H}$= 6.6 Hz, 1H, *H*$_2$C-NC); 4.32 (dd, ^{2}J$_{H,H}$= 11.7 Hz , ^{3}J$_{H,H}$= 4.9 Hz, 1H, *H*$_2$C-NC); 6.4-8.4 (28H, Aromatics) ppm.

^{31}**P NMR (CDCl$_3$):** δ 24.8 (d, ^{2}J$_{H,P}$= 123 Hz); 26.7 (s) ppm.

^{13}**C{^{1}H} NMR (CDCl$_3$):** δ 46.8 (d, ^{2}J$_{P,C}$= 5.3 Hz, *C*H$_3$); 51.9 (d, ^{2}J$_{P,C}$= 5.1 Hz, *C*H$_2$-NH$_2$); 62.3 (s, H$_2$*C*-NC); 122.0-163.0 (Aromatics); 213.5 (s, *C*=O) ppm.

Conductivity (Λ$_M$): 10 ohm^{-1}·cm^2·mol^{-1}.

Synthesis of [IrH(PPh$_2$(*o*-C$_6$H$_4$CO))(PPh$_2$(*o*-C$_6$H$_4$C=NCH$_2$CH$_2$CH$_2$NH$_2$))] (21)

K(OH) (0.075mmol, 4.2 mg) was added to a solution of complex **(17)** (0.037 mmol, 31.75 mg) in methanol. The solution was stirred for an hour and then the solvent was evaporated under low pressure. The resulted solid was dissolved in dichloromethane and the salts were extracted with water. Then the solvent was removed affording a yellow solid which was cleaned with diethyl ether and hexane. Yield 68%.

IR (KBr, cm^{-1}): 3312 and 3244 (w, N-H); 2027 (s, Ir-H); 1559 (s, C=O and C=N).

Elemental Analysis for IrC$_{41}$H$_{37}$P$_2$ON$_2$·(CH$_2$Cl$_2$)$_{0.7}$:

Calculated: C 56.85, H 4.38, N 3.19.

Found: C 56.70, H 4.82, N 3.00.

^{1}**H NMR (CDCl$_3$):** δ -7.74 (dd, ^{2}J$_{P,H}$= 125.2 Hz, ^{2}J$_{P,H}$= 18.3 Hz, 1H, *H*-Ir); 1.66 (m, 1H, *H*$_2$C-NH$_2$); 1.69 (m, 1H, CH$_2$-*H*$_2$C-CH$_2$); 1.88 (m, 1H, CH$_2$-*H*$_2$C-CH$_2$); 2.20 (m, 1H, *H*$_2$C-NH$_2$); 4.32 (m, 1H, *H*$_2$C-NC); 4.48 (m, 1H, *H*$_2$C-NC); 6.2-8.5 (28H, Aromatics) ppm.

^{31}P{^{1}H} NMR (CDCl$_3$): δ 25.9 (s); 27.5 (d, ^{2}J$_{P,P}$= 6.4 Hz) ppm.

^{13}C{^{1}H} NMR (CDCl$_3$): δ 28.5 (s, CH$_2$-CH$_2$-CH$_2$); 42.3 (s, H$_2$C-NH$_2$); 58.1 (s, H$_2$C-NC); 122.0-163 (Aromatics); 213.1 (s, C=O) ppm.

ESI-MS (MeOH): Calculated for IrC$_{41}$H$_{38}$P$_2$ON$_2$: 829.2; found: 829.2 [M+H$^+$]$^+$.

Conductivity (Λ$_M$): 10 ohm^{-1}·cm^2·mol^{-1}.

<u>Synthesis of [IrH(PPh$_2$(o-C$_6$H$_4$CO))(PPh$_2$(o-C$_6$H$_4$C=N(H)CH$_2$CH$_2$NH$_2$))]ClO$_4$</u> **(22)**

3.6 mL of distilled water was added to a solution of **(10)** (0.029 mmol, 25 mg) in 5 mL of tetrahydrofuran and it was stirred for 24 hours. After that, the tetrahydrofuran was removed at reduced pressure and extractions were done with dichloromethane, keeping the organic phase. A solution of 0.03 mmol (4.3 mg) NaClO$_4$·H$_2$O in 2 mL of methanol was added to the organic phase. The solvents were removed under reduced pressure, the resulting solid was redissolved in anhydrous dichloromethane and the salts were filtered. The final product was precipitated with diethyl ether and dried obtaining a yellow solid. Yield 63%.

IR (KBr, cm^{-1}): 3316 (w, N-H); 2165 (s, Ir-H); 1575 (s, C=O and C=N).

Elemental Analysis for IrC$_{40}$H$_{36}$P$_2$O$_5$N$_2$Cl·(CH$_2$Cl$_2$):

Calculated: C 49.28, H 3.83, N 2.80.

Found: C 49.56, H 3.62, N 2.76.

^{1}H NMR (CDCl$_3$): δ -17.62 (t, ^{2}J$_{P,H}$= 16.5 Hz, 1H, H-Ir); 0.89 (m, 1H, H$_2$C-NH$_2$); 1.60 (m, 1H, NH$_2$); 2.74 (m, 1H, H$_2$C-NH$_2$); 3.07 (m, 1H, NH$_2$); 3.58 (m, 1H, H$_2$C-NC); 3.76 (m, 1H, H$_2$C-NC); 6.25-8.15 (28H, Aromatics) ppm.

^{31}P{^{1}H} NMR (CDCl$_3$): δ 10.8 (s); 32.4 (s) ppm.

^{13}C{^{1}H} NMR (CDCl$_3$): δ 41.5 (s, CH_2-NH$_2$); 51.6 (s, H$_2C$-NC); 121.0-162.0 (Aromatics); 228.1 (d, ^{2}J$_{P,C}$= 88 Hz, C=O or C=N); 235.2 (d, ^{2}J$_{P,C}$= 93 Hz, C=O or C=N) ppm.

Conductivity (Λ$_M$): 100 ohm^{-1}·cm^2·mol^{-1}.

Synthesis of [IrH(PPh$_2$(o-C$_6$H$_4$CO))(PPh$_2$(o-C$_6$H$_4$C=N(H)CH$_2$CH$_2$NHCH$_3$))]ClO$_4$ **(23)**

Complex **(11)** (0.029 mmol, 25 mg) was dissolved in 1.5 mL of tetrahydrofuran and 1.5 mL of water and was left stirring at room temperature for 24 hours. Solvents were removed under reduced pressure and the resulting solid was dissolved in a solution of 0.03 mmol (4.3 mg) NaClO$_4$·H$_2$O in 2 mL of methanol. A light yellow solid precipitated and was filtered and dried. Yield 45%.

IR (KBr, cm^{-1}): 3224 (w, N-H); 2156 (s, Ir-H); 1604 and 1573 (s, C=O and C=N) and 1099 (s, Cl-O).

Elemental Analysis for IrC$_{41}$H$_{38}$P$_2$O$_5$N$_2$Cl:

Calculated: C 53.04, H 4.13, N 3.02.

Found: C 52.66, H 4.40, N 2.67.

^{1}H NMR (CDCl$_3$): δ b-19.84 (t, ^{2}J$_{P,H}$= 18.3 Hz, 1H, H-Ir); a -19.63 (t, ^{2}J$_{P,H}$= 17.8 Hz, 1H, H-Ir); 1.31 (m, 1H, H_2C-NIr); 2.01 (m, 3H, H_3C); 2.08 (m, 1H, H_2C-NIr); 2.38 (m, 1H, HN-Ir), 3.90 (m, 1H, H_2C-NC); 4.17 (m, 1H, H_2C-NC); b 10.81 (s, 1H, HN-C); a 11.14 (s, 1H, HN-C); 6.25-8.15 (28H, Aromatics) ppm

^{31}P{^{1}H} NMR (CDCl$_3$): δ a 6.6 (d, ^{2}J$_{P,P}$= 11.7 Hz); b 11.5 (d, ^{2}J$_{P,P}$= 11.5 Hz); b 28.9 (d, ^{2}J$_{P,P}$= 11.5 Hz); a 33.8 (d, ^{2}J$_{P,P}$= 12 Hz) ppm.

^{13}C{^{1}H} NMR (CDCl$_3$): δ 45.6 (s, CH_3); 48.3 (s, H$_2C$-NC); 55.1 (s, H$_2C$-NIr); 121.0-162.0 (Aromatics) ppm.

Conductivity (Λ_M): 130 ohm^{-1}·cm^2·mol^{-1}.

<u>Synthesis of [IrH(PPh$_2$(*o*-C$_6$H$_4$CO))$_2$(NH$_2$CH$_2$CH$_2$NHCH$_3$)]</u> **(24)**

K(OH) (0.0429 mmol, 2.4 mg) and *N*-methylethylendiamine (0.058 mmol, 5.1 µL) were added to a suspension of complex **(2)** (0.039 mmol, 30 mg) in methanol. The solution was stirred under reflux overnight and then the solvent was evaporated under low pressure. The resulted solid was dissolved in dichloromethane and the salts were extracted with water. Then the solvent was removed affording a yellow solid which was cleaned with diethyl ether and hexane. Yield 49%.

IR (KBr, cm^{-1}): 3313 and 3266 (w, N-H); 2021 (s, Ir-H); 1574 (s, C=O and C=N).

Elemental Analysis for IrC$_{41}$H$_{39}$P$_2$O$_2$N$_2$(CH$_2$Cl$_2$)$_{0.7}$:

Calculated: C 55.71, H 4.52, N 3.12.

Found: C 55.60, H 4.09, N 2.80.

^{1}H NMR (CDCl$_3$): δ -8.05 (dd, $^2J_{P,H}$= 130.1 Hz, $^2J_{P,H}$= 19.6 Hz, 1H, *H*-Ir); 2.00 (m, 1H, C*H$_2$*); 2.05 (s, 3H, C*H$_3$*); 2.12 (m, 1H, C*H$_2$*); 2.34 (m, 1H, C*H$_2$*); 2.43 (m, 1H, C*H$_2$*); 2.64 (m, 1H, N*H$_2$*); 2.81 (m, 1H, N*H$_2$*); 6.3-8.3 (28H, Aromatics) ppm.

^{31}P{^{1}H} NMR (CDCl$_3$): δ 24.8 (s); 30.23 (s) ppm.

^{13}C{^{1}H} NMR (CDCl$_3$): δ 35.8 (s, *C*H$_3$); 49.6 (s, *C*H$_2$); 53.4 (s, *C*H$_2$); 122.0-165.0 (Aromatics); 214.7 (s, *C*=O); 238.8 (d, $^2J_{P,C}$= 103.2 Hz, *C*=O); ppm.

Conductivity (Λ_M): 10 ohm^{-1}·cm^2·mol^{-1}.

Synthesis of [IrH(PPh$_2$(o-C$_6$H$_4$CO))$_2$(NH$_2$CH$_2$(C$_5$H$_{10}$N))] **(25)**

K(OH) (0.0429 mmol, 2.4 mg) and 2-(Aminomethyl)piperidine (0.058 mmol, 7.1 μL) were added to a suspension of complex **(2)** (0.039 mmol, 30 mg) in methanol. The solution was stirred under reflux overnight and then the solvent was evaporated under low pressure. The resulted solid was dissolved in dichloromethane and the salts were extracted with water. Then the solvent was removed affording a yellow solid which was cleaned with diethyl ether and hexane. Yield 54%.

IR (KBr, cm^{-1}): 3405 (w, N-H); 2036 (s, Ir-H); 1608 (s, C=O and C=N).

Elemental Analysis for IrC$_{44}$H$_{43}$P$_2$O$_2$N$_2$(CH$_2$Cl$_2$)$_{0.6}$:

Calculated: C 57.57, H 4.78, N 3.02.

Found: C 57.27, H 4.34, N 2.62.

^{1}H NMR (CDCl$_3$): δ -8.30 (dd, ^{2}J$_{P,H}$= 136.9 Hz, ^{2}J$_{P,H}$= 19.3 Hz, 1H, *H*-Ir); -8.29 (dd, ^{2}J$_{P,H}$= 137.3 Hz, ^{2}J$_{P,H}$= 19.4 Hz, 1H, *H*-Ir); 0.54 (m, 1H, *H*$_2$C-CH); 0.62 (m, 1H, *H*$_2$C-CH); 0.80 (m, 1H, *H*$_2$C-CH$_2$-NH); 1.07 (m, 1H, *H*$_2$C-CH$_2$-NH); 1.09 (m, 2H, *H*$_2$C-CH$_2$-CH); 1.15 (m, 1H, *H*$_2$C-CH); 1.2 (m, 1H, *H*$_2$C-CH); 1.31 (m, 1H, *H*$_2$C-CH$_2$-NH); 1.4 (m, 1H, *H*$_2$C-CH$_2$-NH); 1.58 (m, 2H, *H*$_2$C-CH$_2$-CH); 2.57 (m, 1H, *H*$_2$C-NH); 2.64 (m, 1H, *H*$_2$C-NH); 2.75 (m, 1H, *H*C); 2.75 (m, 2H, *H*$_2$C-NH$_2$); 2.92 (m, 1H, *H*C); 3.02 (m, 1H, *H*$_2$C-NH); 3.14 (m, 1H, *H*$_2$C-NH); 3.35 (m, 2H, *H*$_2$C-NH$_2$); 6.2-8.6 (28H, Aromatics) ppm.

^{31}P{^{1}H} NMR (CDCl$_3$): δ 22.6 (d, ^{2}J$_{P,P}$= 2.7 Hz); 22.7 (d, ^{2}J$_{P,P}$= 3.2 Hz); 28.1 (d, ^{2}J$_{P,P}$= 7 Hz); 28.5 (d, ^{2}J$_{P,P}$= 4.9 Hz) ppm.

^{13}C{^{1}H} NMR (CDCl$_3$): δ 23.4 (s, *C*H$_2$-NH); 23.5 (s, *C*H$_2$-NH); 26.2 (s, 2C, *C*H$_2$-CH$_2$-NH); 30.8 (s, 2C, *C*H$_2$-CH$_2$-CH); 44.3 (s, *C*H$_2$-CH); 44.4 (s, *C*H$_2$-CH); 58.0 (s, *C*H); 58.4 (s, *C*H); 65.2 (s, *C*H$_2$-NC); 66.0 (s, *C*H$_2$-NC); 122.0-165.0 (Aromatics); 218.2 (d, ^{2}J$_{P,C}$= 4 Hz, *C*=O); 218.6 (d, ^{2}J$_{P,C}$= 7 Hz, *C*=O); 236.9 (d, ^{2}J$_{P,C}$= 106 Hz, *C*=O); 237.1 (d, ^{2}J$_{P,C}$= 106 Hz, *C*=O) ppm.

Conductivity (Λ_M): 10 ohm^{-1}·cm^2·mol^{-1}.

Synthesis of [IrH(C$_3$H$_4$N$_2$){PPh$_2$(o-C$_6$H$_4$)CNNHC(o-C$_6$H$_4$)PPh$_2$}] [BAr$^F_4$] **(27)**

Pyrazole (0.037 mmol, 2.5 mg) was added to a Schlenk flask charged with a suspension of [IrHCl{PPh$_2$(o-C$_6$H$_4$CN(H)NC-o-C$_6$H$_4$)PPh$_2$}] **(3)** (0.037mmol, 30 mg) in dichloromethane and then, the sodium tetrakis[3,5-bis(trifluoromethyl)phenyl]borate salt (0.037 mmol, 32.8 mg) was added to the mixture affording instantly a solution. It was left stirring for 2 hours and then the salts were extracted with water, keeping the organic phase. The resulting dichloromethane solution was dried with magnesium sulphate and filtered. The solvent was removed under low pressure affording an orange solid. Yield 72%

IR (KBr, cm^{-1}): 2192 (br), v(Ir-H); 1610 (m), v(C=N)

Elemental Analysis for IrC$_{73}$H$_{46}$BF$_{24}$N$_4$P$_2$:

Calculated: C 51.57, H 2.73, N 3.30.

Found: C 51.31, H 2.80, N 3.29.

^{1}H NMR (CDCl$_3$, 298 K): δ -18.30 (t, ^{2}J$_{P,H}$= 16 Hz, 1H, *H*-Ir); 5.53 (t, ^{3}J$_{H,H}$= 2.5 Hz, 1H, *H*C (pyr)); 6.06 (m, 1H, *H*C (pyr)); 6.30 (d, ^{3}J$_{H,H}$= 2.5 Hz, 1H, *H*C (pyr)); 7-8.4 (40H, Aromatics); 12.54 (br, 1H, *H*-N) ppm.

^{31}P{^{1}H} NMR (CDCl$_3$, 213 K): δ 19.4 (s); 25.0 (s) ppm.

^{15}N NMR (CDCl$_3$, 298 K): δ 285.6 (s) ppm.

ESI-MS (MeOH): Calculated for IrC$_{41}$H$_{34}$N$_4$P$_2$: 837.2; found: 837.2 [M]$^+$.

Conductivity (Λ_M): 70 ohm^{-1}·cm^2·mol^{-1}.

Synthesis of [IrH(C$_5$H$_5$N){PPh$_2$(*o*-C$_6$H$_4$)CNNHC(*o*-C$_6$H$_4$)PPh$_2$}] [BAr$^F_4$] (28)

Pyridine (0.037 mmol, 3 μL) was added to a Schlenk flask charged with a suspension of [IrHCl{PPh$_2$(*o*-C$_6$H$_4$CN(H)NC-*o*-C$_6$H$_4$)PPh$_2$}] (3) (0.037mmol, 30 mg) in dichloromethane and then, the sodium tetrakis[3,5-bis(trifluoromethyl)phenyl]borate salt (0.037 mmol, 32.8 mg) was added to the mixture affording instantly a solution. It was left stirring for 2 hours and then the salts were extracted with water, keeping the organic phase. The resulting dichloromethane solution was dried with magnesium sulphate and filtered. The solvent was removed under low pressure affording an orange solid. Yield 68%.

IR (KBr, cm^{-1}): 2191 (br), ν(Ir-H); 1608 (m), ν(C=N)

Elemental Analysis for IrC$_{75}$H$_{48}$BF$_{24}$N$_3$P$_2$·(CH$_2$Cl$_2$):

Calculated: C 52.14, H 2.82, N 2.42.

Found: C 51.96, H 2.82, N 2.05.

^{1}H NMR (CDCl$_3$, 298 K): δ -18.57 (t, $^2J_{P,H}$= 15.9 Hz, 1H, *H*-Ir); 6.9-8.3 (46H, Aromatics); 13.45 (br, 1H, *H*-N) ppm.

^{31}P{^{1}H} NMR (CDCl$_3$, 213 K): δ 22.7 (s); 26.9 (s) ppm.

ESI-MS (MeOH): Calculated for IrC$_{43}$H$_{36}$N$_3$P$_2$: 848.2; found: 848.2 [M]$^+$.

Conductivity (Λ$_M$): 80 ohm^{-1}·cm^2·mol^{-1}.

Synthesis of [IrH(C$_2$H$_3$N){PPh$_2$(*o*-C$_6$H$_4$)CNNHC(*o*-C$_6$H$_4$)PPh$_2$}] [BAr$^F_4$] (29)

Acetonitrile (1.9 mmol, 100 μL) was added to a Schlenk flask charged with a suspension of [IrHCl{PPh$_2$(*o*-C$_6$H$_4$CN(H)NC-*o*-C$_6$H$_4$)PPh$_2$}] (3) (0.037mmol, 30 mg) in dichloromethane and then, the sodium tetrakis[3,5-bis(trifluoromethyl)phenyl]borate salt (0.037 mmol, 32.8 mg) was added to the mixture affording instantly a solution. It was left stirring for 2 hours and then the

salts were extracted with water, keeping the organic phase. The resulting dichloromethane solution was dried with magnesium sulphate and filtered. The solvent was removed under low pressure affording an orange solid. Yield 64%.

IR (KBr, cm^{-1}): 2190 (br), v(Ir-H); 1631 (m), v(C=N)

Elemental Analysis for IrC$_{72}$H$_{45}$BF$_{24}$IrN$_3$P$_2$:

Calculated: C 51.69, H 2.71, N 2.51.

Found: C 51.39, H 2.67, N 2.36.

^{1}H NMR (CDCl$_3$): δ -18.02 (t, $^2J_{P,H}$= 14.6 Hz, 1H, H-Ir); 2.29 (s, 3H, H_3C); 7.1-8.4 (40H, Aromatics); 12.18 (br, 1H, H-N) ppm.

^{31}P{^{1}H} NMR (CDCl$_3$): δ 18.8 (s); 23.7 (s) ppm.

ESI-MS (MeOH): Calculated for IrC$_{40}$H$_{33}$N$_3$P$_2$: 810.2; found: 810.2 [M]$^+$.

Conductivity (Λ$_M$): 80 ohm^{-1}·cm^2·mol^{-1}.

Synthesis of [IrH(PPh$_3$){PPh$_2$(o-C$_6$H$_4$)CNNHC(o-C$_6$H$_4$)PPh$_2$}] [BAr$^F_4$] **(30)**

Triphenylphosphine (0.037 mmol, 9.7 mg) was added to a Schlenk flask charged with a suspension of [IrHCl{PPh$_2$(o-C$_6$H$_4$CN(H)NC-o-C$_6$H$_4$)PPh$_2$}] **(3)** (0.037mmol, 30 mg) in dichloromethane and then, the sodium tetrakis[3,5-bis(trifluoromethyl)phenyl]borate salt (0.037 mmol, 32.8 mg) was added to the mixture affording instantly a solution. It was left stirring for 2 hours and then the salts were extracted with water, keeping the organic phase. The resulting dichloromethane solution was dried with magnesium sulphate and filtered. The solvent was removed under low pressure affording an orange solid. Yield 70%.

IR (KBr, cm^{-1}): 2113 (br), v(Ir-H); 1610 (m), v(C=N)

Elemental Analysis for IrC$_{88}$H$_{57}$BF$_{24}$IrN$_2$P$_3$:

Calculated: C 55.80, H 3.03, N 1.48.

Found: C 56.10, H 3.17, N 1.59.

^{1}H NMR (CDCl$_3$): δ -12.31 (dt, ^{2}J$_{P,H}$= 19.6 Hz, ^{2}J$_{P,H}$= 89.3 Hz, 1H, *H*-Ir); 6.4-8.6 (55H, Aromatics); 12.50 (br, 1H, *H*-N) ppm.

^{31}P{^{1}H} NMR (CDCl$_3$): δ -5.0 (s); 6.1 (s); 11.4 (s) ppm.

ESI-MS (MeOH): Calculated for IrC$_{56}$H$_{45}$N$_2$P$_3$: 1031.2; found: 1031.2 [M]$^+$.

Conductivity ($Λ_M$): 80 ohm^{-1}·cm^2·mol^{-1}.

Synthesis of [IrH(C$_8$H$_{12}$){PPh$_2$(*o*-C$_6$H$_4$)CNNHC(*o*-C$_6$H$_4$)PPh$_2$}] [BAr$^F_4$] **(31)**

Cis,cis-1,5-cyclooctadiene (0.037 mmol, 4.5 µL) was added to a Schlenk flask charged with a suspension of [IrHCl{PPh$_2$(*o*-C$_6$H$_4$)CN(H)NC-*o*-C$_6$H$_4$)PPh$_2$}] **(3)** (0.037mmol, 30 mg) in dichloromethane and then, the sodium tetrakis[3,5-bis(trifluoromethyl)phenyl]borate salt (0.037 mmol, 32.8 mg) was added to the mixture affording instantly a solution. It was left stirring for 2 hours and then the salts were extracted with water, keeping the organic phase. The resulting dichloromethane solution was dried with magnesium sulphate and filtered. The solvent was removed under low pressure affording an orange solid. Yield 65%.

IR (KBr, cm^{-1}): 1610 (m), ν(C=N)

Elemental Analysis for IrC$_{78}$H$_{56}$BF$_{24}$IrN$_2$P$_2$:

Calculated: C 53.77, H 3.24, N 1.61.

Found: C 53.51, H 3.12, N 1.48.

^{1}H NMR (CDCl$_3$): δ -12.26 (t, ^{2}J$_{P,H}$= 19.6 Hz, 1H, *H*-Ir); 6.5-8.4 (40H, Aromatics); 11.96 (br, 1H, *H*-N) ppm.

$^{31}P\{^1H\}$ NMR (CDCl$_3$): δ 11.6 (s); 15.5 (s) ppm.

ESI-MS (MeOH): Calculated for IrC$_{38}$H$_{30}$N$_2$P$_2$: 769.2; found: 769.2 [M-COE]$^+$.

Conductivity (Λ_M): 80 ohm^{-1}·cm^2·mol^{-1}.

Synthesis of [IrH(C$_6$H$_{18}$NB){PPh$_2$(o-C$_6$H$_4$)CNNHC(o-C$_6$H$_4$)PPh$_2$}] [BAr$^F_4$] **(32)**

Trimethylamineborane (0.037 mmol, 5.5 μL) was added to a Schlenk flask charged with a suspension of [IrHCl{PPh$_2$(o-C$_6$H$_4$CN(H)NC-o-C$_6$H$_4$)PPh$_2$}] **(3)** (0.037mmol, 30 mg) in dichloromethane and then, the sodium tetrakis[3,5-bis(trifluoromethyl)phenyl]borate salt (0.037 mmol, 32.8 mg) was added to the mixture affording instantly a solution. It was left stirring for 2 hours and then the salts were extracted with water, keeping the organic phase. The resulting dichloromethane solution was dried with magnesium sulphate and filtered. The solvent was removed under low pressure affording an orange solid. Yield 64%.

IR (KBr, cm^{-1}): 2090 (br), ν(Ir-H); 1730 (m), ν(C=N)

Elemental Analysis for IrC$_{76}$H$_{60}$BF$_{24}$IrN$_3$P$_2$:

Calculated: C 52.25, H 3.46, N 2.41.

Found: C 51.96, H 3.22, N 2.04.

^1H NMR (CDCl$_3$, 298K): δ -18.29 (t, $^2J_{P,H}$ = 16.1 Hz, 1H, H-Ir); -3.00 (br, 3H, H-B); 1.11 (t, $^4J_{P,H}$= 7.3 Hz, 3H, H$_3$C); 2.72 (q, $^4J_{P,H}$= 7.3 Hz, 2H, H$_2$C); 6.8-8.4 (40H, Aromatics); 12.11 (br, 1H, H-N) ppm.

^1H NMR (CDCl$_3$, 213K): δ -17.84 (t, $^2J_{P,H}$ = 16.1 Hz, 1H, H-Ir); -12.24 (s, 1H, H-B); 1.11 (t, $^4J_{P,H}$= 7.3 Hz, 3H, H$_3$C); 2.72 (q, $^4J_{P,H}$= 7.3 Hz, 2H, H$_2$C); 7-8.5 (40H, Aromatics); 12.11 (br, 1H, H-N) ppm.

$^{31}P\{^1H\}$ NMR (CDCl$_3$): δ 13.6 (s); 17.6 (s) ppm.

ESI-MS (MeOH): Calculated for IrC$_{44}$H$_{48}$BN$_3$P$_2$: 884.3; found: 884.3 [M]$^+$.

Conductivity (Λ_M): 80 ohm^{-1}·cm^2·mol^{-1}.

Synthesis of [IrH(H$_3$BPPh$_3$){PPh$_2$(o-C$_6$H$_4$)CNNHC(o-C$_6$H$_4$)PPh$_2$}] [BAr$^F_4$] **(33)**

Triphenylphosphineborane (0.037 mmol, 10.2 mg) was added to a Schlenk flask charged with a suspension of [IrHCl{PPh$_2$(o-C$_6$H$_4$CN(H)NC-o-C$_6$H$_4$)PPh$_2$}] **(3)** (0.037mmol, 30 mg) in dichloromethane and then, the sodium tetrakis[3,5-bis(trifluoromethyl)phenyl]borate salt (0.037 mmol, 32.8 mg) was added to the mixture affording instantly a solution. It was left stirring for 2 hours and then the salts were extracted with water, keeping the organic phase. The resulting dichloromethane solution was dried with magnesium sulphate and filtered. The solvent was removed under low pressure affording an orange solid. Yield 68%.

^{1}H NMR (CDCl$_3$, 298K): δ -18.02 (dt, $^2J_{P,H}$= 10.3 Hz, $^4J_{P,H}$= 16.3 Hz, 1H, *H*-Ir); -2.64 (br, 3H, *H*-B); 6.4-8.4 (40H, Aromatics); -11.92 (br, 1H, *H*-N) ppm.

^{31}P{^{1}H} NMR (CDCl$_3$, 213K): δ -6.9 (s); 13.3 (s); 17.6 (s) ppm.

ESI-MS (MeOH): Calculated for IrC$_{56}$H$_{48}$BN$_2$P$_3$: 1045.3; found: 1045.3 [M]$^+$.

Conductivity (Λ_M): 80 ohm^{-1}·cm^2·mol^{-1}.

Synthesis of [IrH(SnCl$_3$){PPh$_2$(o-C$_6$H$_4$)CNNHC(o-C$_6$H$_4$)PPh$_2$}] **(34)**

SnCl$_2$ (0.074mmol, 14.0 mg) was added to a Schlenk flask charged with a suspension of [IrHCl{PPh$_2$(o-C$_6$H$_4$CN(H)NC-o-C$_6$H$_4$)PPh$_2$}] **(3)** (0.037mmol, 30 mg) in dichloromethane. After stirring for 30 min the unreacted SnCl$_2$ was filtered and the dichloromethane was evaporated from the solution to give a pale orange solid that was collected. Yield 58 %.

IR (KBr, cm^{-1}): 2090 (br), ν(Ir-H); 1730 (m), ν(C=N)

Elemental Analysis for IrC$_{38}$H$_{30}$N$_2$P$_2$SnCl$_3$·(CHCl$_3$)$_{0.5}$:

Calculated: C 43.89, H 2.92, N 2.66.

Found: C 43.96, H 2.55, N 2.50.

^{1}H NMR (CDCl$_3$): δ -12.85 (t, with tin satellites, $^2J_{P,H}$= 16.9 Hz, $^2J_{^{119}Sn,H}$= 831.7 Hz, $^2J_{^{117}Sn,H}$= 865.9 Hz, 1H, *H*-Ir); 6.8-8.5 (28H, Aromatics) ppm.

^{31}P{^{1}H} NMR (CDCl$_3$): δ 10.2 (s, with tin satellites, $^2J_{^{119}Sn,P}$= 233.0 Hz, $^2J_{^{117}Sn,P}$= 226.5 Hz) ppm.

^{119}Sn NMR (CDCl$_3$): δ -146.5 (dt, $^2J_{H,^{119}Sn}$= 1044.4 Hz, $^2J_{P,^{119}Sn}$= 228.8 Hz) ppm.

Conductivity (Λ$_M$): 20 ohm^{-1}·cm^2·mol^{-1}.

Synthesis of [IrHCl{PPh$_2$(*o*-C$_6$H$_4$)CNHNHC(*o*-C$_6$H$_4$)PPh$_2$}] [BF$_4$] **(35)**

HBF$_4$·O(CH$_2$CH$_3$)$_2$ (0.037 mmol, 5 µL) was added to a Schlenk flask charged with a suspension of [IrHCl{PPh$_2$(*o*-C$_6$H$_4$CN(H)NC-*o*-C$_6$H$_4$)PPh$_2$}] **(3)** (0.037mmol, 30 mg) in dichloromethane. It was left stirring for 2 hours and then the solvent was removed under low pressure affording an orange solid. Yield 85%.

IR (KBr, cm^{-1}): 2182 (br), ν(Ir-H); 1614 (m), ν(C=N)

Elemental Analysis for IrC$_{38}$H$_{31}$N$_2$P$_2$ClBF$_4$:

Calculated: C 51.16, H 3.50, N 3.14.

Found: C 50.60, H 3.12, N 3.51.

^{1}H NMR (CDCl$_3$): δ -17.47 (t, $^2J_{P,H}$= 16.6 Hz, 1H, *H*-Ir); 6.4-8.4 (40H, Aromatics); 14.49 (br, 2H, *H*-N) ppm.

31P{1H} NMR (CDCl3): δ 15.25 (s) ppm.

13C{1H} NMR (CDCl3): δ 220.5 (d, $^2J_{P,C}$= 97.6 Hz) ppm.

15N NMR (CDCl3): δ 206.7 (s), 120-150 (Aromatics) ppm.

ESI-MS (MeOH): Calculated for $IrC_{38}H_{30}N_2P_2$: 769.2; found: 769.2 [M-H-Cl]$^+$.

Conductivity (Λ$_M$): 60 ohm^{-1}·cm^2·mol^{-1}.

Synthesis of [IrHCl{PPh2(o-C6H4)CNNC(o-C6H4)PPh2}] [N(n-Bu)4] **(36)**

Tetrabutylammonium hydroxide 40% w/w in water (0.037 mmol, 24.2 μL) was added to a Schlenk flask charged with a suspension of [IrHCl{PPh2(o-C6H4CN(H)NC-o-C6H4)PPh2}] **(3)** (0.037mmol, 30 mg) in tetrahydrofuran. It was left stirring for 2 hours at room temperature. The solvent was then removed under low pressure and cleaned twice with diethyl ether affording a dark orange solid. Yield 78%.

IR (KBr, cm^{-1}): 2161 (br), ν(Ir-H); 1620 (m), ν(C=N)

Elemental Analysis for $IrC_{54}H_{65}N_3P_2Cl$:

Calculated: C 62.02, H 6.27, N 4.02.

Found: C 61.78, H 6.13, N 3.99.

1H NMR (CDCl3): δ -21.01 (t, $^2J_{P,H}$= 15.9 Hz, 1H, *H*-Ir); δ 3.34–3.16 (m, 2H, *H$_2$C*), 1.69–1.48 (m, 2H, *H$_2$C*), 1.33 (h, $^3J_{H,H}$ = 7.2 Hz, 1H,), 0.90 (t, J = 7.3 Hz, 3H, *H$_3$C*); 6.6-8.6 (28H, Aromatics) ppm.

31P{1H} NMR (CDCl3): δ 18.9 (s) ppm.

ESI-MS (MeOH): Calculated for $IrC_{38}H_{29}N_2P_2Cl$: 803.1; found: 803.1 [M]$^-$.

Conductivity (Λ$_M$): 120 ohm^{-1}·cm^2·mol^{-1}.

Synthesis of [IrHCl{PPh$_2$(*o*-C$_6$H$_4$)CNNC(*o*-C$_6$H$_4$)PPh$_2$}(ZrCl$_4$)] [N(n-Bu)$_4$] (37)

ZrCl$_4$ (0.037 mmol, 8.6 mg) was added to a Schlenk flask charged with a solution of [IrHCl{PPh$_2$(*o*-C$_6$H$_4$CNNC-*o*-C$_6$H$_4$)PPh$_2$}] **(36)** (0.037mmol, 38.7 mg) in tetrahydrofuran. It was left stirring for 2 hours at room temperature. Then the solvent was removed under low pressure affording an off orange solid which was washed with diethyl ether twice. Yield 74%.

^{1}H NMR (CDCl$_3$): δ -17.63 (t, ^{2}J$_{P,H}$= 17.5 Hz, 1H, *H*-Ir); 6.5-9.2 (28H, Aromatics) ppm.

^{31}P{^{1}H} NMR (CDCl$_3$): δ 15.5 (s) ppm.

Conductivity (Λ$_M$): 130 ohm^{-1}·cm^2·mol^{-1}.

Synthesis of [IrHCl{PPh$_2$(*o*-C$_6$H$_4$)CN(CH$_3$)NC(*o*-C$_6$H$_4$)PPh$_2$}] (38)

NaH (0.25 mmol, 8.9 mg) was added to a Schlenk flask charged with a suspension of [IrHCl{PPh$_2$(*o*-C$_6$H$_4$CN(H)NC-*o*-C$_6$H$_4$)PPh$_2$}] **(3)** (0.037mmol, 30 mg) tetrahydrofuran at 0°C and it was left stirring for 10 minutes. Then MeI (0.037 mmol, 2.3 µL) was added at 0°C and it was left stirring at room temperature for 18 hours. The solvent was removed under low pressure and the the remaining solid was dissolved in dichloromethane and filtered. The salts were extracted with water, keeping the organic phase. The resulting dichloromethane solution was dried with magnesium sulphate and filtered. The solvent was removed under low pressure affording a dark orange solid. Yield 62%.

IR (KBr, cm^{-1}): 2165 (br), ν(Ir-H); 1636 (m), ν(C=N)

Elemental Analysis for IrC$_{39}$H$_{32}$N$_2$P$_2$Cl:

Calculated: C 57.24, H 3.94, N 3.42.

Found: C 57.10, H 4.13, N 3.26.

^{1}H NMR (CDCl$_3$): δ -19.35 (t, $^2J_{P,H}$= 16.9 Hz, 1H, *H*-Ir); 4.45 (s, 3H, *H$_3$*C); 6.4-8.4 (28H, Aromatics) ppm.

^{31}P{^{1}H} NMR (CDCl$_3$): δ 11.2 (d, $^2J_{P,H}$= 5.6 Hz); 22.9 (br) ppm.

^{15}N NMR (CDCl$_3$): δ 243.0 (s); 369.0 (s) ppm.

ESI-MS (MeOH): Calculated for IrC$_{39}$H$_{32}$N$_2$P$_2$ClNa: 841.1; found: 841.1 [M+Na]$^+$.

Conductivity (Λ$_M$): 10 ohm^{-1}·cm^2·mol^{-1}.

Synthesis of [IrHI{PPh$_2$(*o*-C$_6$H$_4$)CN(CH$_3$)NC(*o*-C$_6$H$_4$)PPh$_2$}] **(39)**

Nal (0.185 mmol, 27.7 mg) was added to a Schlenk flask charged with a solution of [IrHCl{PPh$_2$(*o*-C$_6$H$_4$)CN(CH$_3$)NC-*o*-C$_6$H$_4$)PPh$_2$}] **(38)** (0.037mmol, 33.7 mg) in methanol. It was left stirring for 18 hours at room temperature and the solvent was removed under low pressure. Then the remaining solid was dissolved in dichloromethane and the salts were extracted with water, keeping the organic phase. The resulting dichloromethane solution was dried with magnesium sulphate and filtered. The solvent was removed under low pressure affording a dark orange solid. Yield 72%.

IR (KBr, cm^{-1}): 2016 (br), ν(Ir-H); 1620 (m), ν(C=N)

Elemental Analysis for IrC$_{39}$H$_{32}$N$_2$P$_2$I:

Calculated: C 51.49, H 3.55, N 3.08.

Found: C 51.18, H 3.23, N 2.92.

^{1}H NMR (CDCl$_3$): δ -16.46 (dd, $^2J_{P,H}$= 16.7 Hz, $^2J_{P,H}$= 17.7 Hz 1H, *H*-Ir); 4.48 (s, 3H, *H$_3$*C); 6.8-8.4 (28H, Aromatics) ppm.

^{31}P{^{1}H} NMR (CDCl$_3$): δ 5.7 (d, $^2J_{P,H}$= 6.2 Hz); 15.0 (d, $^2J_{P,H}$= 5.6 Hz) ppm.

ESI-MS (MeOH): Calculated for $IrC_{39}H_{33}N_2P_2I$: 901.1; found: 901.1 $[M+H]^+$ and calculated for $IrC_{39}H_{32}N_2P_2INa$: 933.1; found:933.1 $[M+Na]^+$.

Conductivity (Λ_M): 20 $ohm^{-1} \cdot cm^2 \cdot mol^{-1}$.

Synthesis of [IrH(SCN){PPh$_2$(*o*-C$_6$H$_4$)CN(CH$_3$)NC(*o*-C$_6$H$_4$)PPh$_2$}] **(40)**

KSCN (0.185 mmol, 18.0 mg) was added to a Schlenk flask charged with a solution of [IrHCl{PPh$_2$(*o*-C$_6$H$_4$CN(CH$_3$)NC-*o*-C$_6$H$_4$)PPh$_2$}] **(38)** (0.037mmol, 33.7 mg) in methanol. It was left stirring for 18 hours under reflux and the solvent was removed under low pressure. Then the remaining solid was dissolved in dichloromethane and the salts were extracted with water, keeping the organic phase. The resulting dichloromethane solution was dried with magnesium sulphate and filtered. The solvent was removed under low pressure affording an orange solid. Yield 58%.

IR (KBr, cm^{-1}): 2100 (s), ν(SC=N); 1718 (m), ν(C=N)

Elemental Analysis for $IrC_{40}H_{32}N_3P_2S$:

Calculated: C 57.13, H 3.84, N 5.00.

Found: C 56.94, H 3.72, N 5.13.

^{1}H NMR (CDCl$_3$): δ -15.58 (t, $^2J_{P,H}$= 16.9 Hz, 1H, *H*-Ir); 4.59 (s, 3H, *H*$_3$C); 6.8-8.5 (28H, Aromatics) ppm.

^{31}P{^{1}H} NMR (CDCl$_3$): δ 10.3 (s); 21.4 (s) ppm.

ESI-MS (MeOH): Calculated for $IrC_{39}H_{32}N_2P_2$: 783.2; found: 783.2 $[M-SCN]^+$.

Conductivity (Λ_M): 10 $ohm^{-1} \cdot cm^2 \cdot mol^{-1}$.

<u>Synthesis of [IrHCl{PPh$_2$(*o*-C$_6$H$_4$)CN(C$_4$H$_7$O$_2$)NC(*o*-C$_6$H$_4$)PPh$_2$}]</u> **(41)**

Ethyl diazoacetate (0.037 mmol, 4.5 µL) was added to a Schlenk flask charged with a suspension of [IrHCl{PPh$_2$(*o*-C$_6$H$_4$CN(H)NC-*o*-C$_6$H$_4$)PPh$_2$}] **(3)** (0.037mmol, 30 mg) in dichloromethane and it was left stirring for 48 hours. The solution was filtered and the solvent was removed under low pressure affording an orange solid. Yield 68%.

Elemental Analysis for IrC$_{42}$H$_{36}$O$_2$N$_2$P$_2$Cl:

Calculated: C 56.66, H 4.08, N 3.15.

Found: C 57.08, H 4.23, N 2.87.

^{1}H NMR (CDCl$_3$): δ -19.01 (t, $^2J_{P,H}$= 16.8 Hz, 1H, *H*-Ir); 1.31 (m, 3H, *H*$_3$C); 4.24 (m, 2H, *H*$_2$C-O); 5.50 (d, $^2J_{H,H}$= 17.6 Hz, 1H, *H*-CN); 5.63 (d, $^2J_{H,H}$= 17.6 Hz, 1H, *H*-CHN); 6.8-8.4 (H, Aromatics) ppm.

^{31}P{^{1}H} NMR (CDCl$_3$): δ 12.1 (d, $^2J_{P,P}$= 6.7 Hz); 20.4 (d, $^2J_{P,P}$= 6.7 Hz) ppm.

ESI-MS (MeOH): Calculated for IrC$_{42}$H$_{36}$N$_2$P$_2$ClNa: 913.2; found: 913.2 [M+Na]$^+$.

Conductivity (Λ$_M$): 10 ohm^{-1}·cm^2·mol^{-1}.

References

(1)   Lukehart, C. M. Metalla-β-Diketones and Their Derivatives. *Acc. Chem. Res.* **1981**, *14* (4), 109–116. https://doi.org/10.1021/ar00064a003.

(2)   Lukehart, C. M. Metalla-Derivatives of β-Diketones. *Adv. Organomet. Chem.* **1986**, *25*, 45–71. https://doi.org/10.1016/S0065-3055(08)60572-9.

(3)   Rauchfuss, T. B. Transition Metal Activation of Aldehydes: Platinum Metal Derivatives of *o*-Diphenylphosphinobenzaldehyde. *J. Am. Chem. Soc.* **1979**, *101* (4), 1045–1047. https://doi.org/10.1021/ja00498a049.

(4)   Garralda, M. A.; Hernández, R.; Ibarlucea, L.; Pinilla, E.; Torres, M. R. Synthesis and Characterization of Hydridoirida-β-Diketones Formed by the Reaction of [{Ir(Cod)Cl}₂] (Cod = 1,5-Cyclooctadiene) with o-(Diphenylphosphino)Benzaldehyde. *Organometallics* **2003**, No. 22, 3600–3603. https://doi.org/10.1021/om0301278.

(5)   Acha, F.; Garralda, M. A.; Hernández, R.; Ibarlucea, L.; Pinilla, E.; Torres, M. R.; Zarandona, M. Synthesis and Reactivity of New Mono- and Dinuclear Hydridoirida-β-Diketones - The Formation and Characterization of a Dinuclear Tris-μ-Acyliridium(III) Complex. *Eur. J. Inorg. Chem.* **2006**, *2* (19), 3893–3900. https://doi.org/10.1002/ejic.200600458.

(6)   Acha, F.; Garralda, A.; Ibarlucea, L.; Pinilla, E.; Torres, M. R. Novel Hydridoirida-β-Diketones Containing Small Molecules , CO, or Ethylene : Their Behavior in Coordinating Solvents Such as Dimethylsulfoxide or Acetonitrile. *Inorg. Chem.* **2005**, *44* (24), 9084–9091. https://doi.org/10.1021/ic051219n.

(7)   Sola, E.; Navarro, J.; López, J. A.; Lahoz, F. J.; Oro, L. A.; Werner, H. Labile Hydrido Complexes of Iridium(III): Synthesis, Dynamic Behaviour in Solution, and Reactivity Towar Alkenes. *Organometallics* **1999**, *18* (17), 3534–3546.

(8)   Acha, F.; Ciganda, R.; Garralda, M. A.; Hernández, R.; Ibarlucea, L.; Pinilla, E.; Torres, M. R. Reactivity of Hydridoirida-β-Diketones with Bases : The Selective Formation of New Di-μ-Acyl-μ-Hydridodiiridium(III) or Dihydridoirida- β-Diketone Complexes and Heterometallic Ir(III)– Rh(I) Derivatives. *Dalton Trans.* **2008**, 4602–4611. https://doi.org/10.1039/b803488e.

(9)   Garralda, M. A.; Mendicute-fierro, C.; Rodríguez-Diéguez, A.; Seco, J. M.; Ubide, C.; Zumeta, I. Efficient Hydridoirida-β-Diketone-Catalyzed Hydrolysis of Ammonia- or Amine-Boranes for Hydrogen Generation in Air. *Dalton Trans.* **2013**, *42*, 11652–11660. https://doi.org/10.1039/c3dt51261d.

(10)   Ciganda, R.; Garralda, M. A.; Ibarlucea, L.; Mendicute-fierro, C.; Torralba, M. C.; Torres, M. R. Reactions of Hydridoirida-β-Diketones with Amines or with 2-Aminopyridines: Formation of Hydridoirida-β-Ketoimines, PCN Terdentate Ligands, and Acyl Decarbonylation. *Inorg. Chem.* **2012**, *51*, 1760–1768. https://doi.org/10.1021/ic202065d.

(11)   Zumeta, I.; Mendicute-fierro, C.; Rodríguez-diéguez, A.; Seco, J. M.; Garralda, M. A. Acyliridium (III) Complexes with PCN Terdentate Ligands Including Imino- or Iminium-Acyl Moieties or Formation of Hydrido from Hydroxyl. *Eur. J. Inorg. Chem.* **2016**, 1790–1797. https://doi.org/10.1002/ejic.201600056.

(12)   Zumeta, I.; Mendicute-Fierro, C.; Bustos, I.; Huertos, M. A.; Rodríguez-Diéguez, A.; Seco, J. M.; San Sebastian, E.; Garralda, M. A. Irida-β-Ketoimines Derived from Hydrazines to Afford Metallapyrazoles or N-N Bond Cleavage: A Missing Metallacycle Disclosed by a Theoretical and

Experimental Study. *Inorg. Chem.* **2016**, *55* (20), 10284–10293. https://doi.org/10.1021/acs.inorgchem.6b01550.

(13) Na, H.; Maity, A.; Morshed, R.; Teets, T. S. Bis-Cyclometalated Iridium Complexes with Chelating Dicarbene Ancillary Ligands. *Organometallics* **2017**, *36* (15), 2965–2972. https://doi.org/10.1021/acs.organomet.7b00428.

(14) Cazin, C. S. J. *N-Heterocyclic Carbenes in Transition Metal Catalysis and Organocatalysis*; Springer Science & Business Media, 2010.

(15) Crabtree, G. W.; Dresselhaus, M. S.; Buchanan, M. V. The Hydrogen Economy. *Phys. Today* **2004**, *57* (12), 39–44. https://doi.org/10.1063/1.1878333.

(16) Service, R. F. The Hydrogen Backlash. *Science* **2004**, *305* (5686), 958–961. https://doi.org/10.1126/science.305.5686.958.

(17) Grasemann, M.; Laurenczy, G. Formic Acid as a Hydrogen Source - Recent Developments and Future Trends. *Energy Environ. Sci.* **2012**, *5* (8), 8171–8181. https://doi.org/10.1039/c2ee21928j.

(18) Nielsen, M.; Alberico, E.; Baumann, W.; Drexler, H. J.; Junge, H.; Gladiali, S.; Beller, M. Low-Temperature Aqueous-Phase Methanol Dehydrogenation to Hydrogen and Carbon Dioxide. *Nature* **2013**, *495* (7439), 85–89. https://doi.org/10.1038/nature11891.

(19) Stephens, F. H.; Pons, V.; Tom Baker, R. Ammonia–Borane: The Hydrogen Source Par Excellence? *Dalton Trans.* **2007**, *2* (25), 2613–2626. https://doi.org/10.1039/b703053c.

(20) Staubitz, A.; Robertson, A. P. M.; Manners, I. Ammonia-Borane and Related Compounds as Dihydrogen Sources. *Chem. Rev.* **2010**, *110* (7), 4079–4124. https://doi.org/10.1021/cr100088b.

(21) Bhunya, S.; Malakar, T.; Ganguly, G.; Paul, A. Combining Protons and

Hydrides by Homogeneous Catalysis for Controlling the Release of Hydrogen from Ammonia-Borane: Present Status and Challenges. *ACS Catal.* **2016**, *6* (11), 7907–7934. https://doi.org/10.1021/acscatal.6b01704.

(22) Denney, M. C.; Pons, V.; Hebden, T. J.; Heinekey, D. M.; Goldberg, K. I. Efficient Catalysis of Ammonia Borane Dehydrogenation. *J. Am. Chem. Soc.* **2006**, *128*, 12048–12049. https://doi.org/10.1021/ja062419g.

(23) Luconi, L.; Osipova, E. S.; Giambastiani, G.; Peruzzini, M.; Rossin, A.; Belkova, N. V; Filippov, O. A.; Titova, E. M.; Pavlov, A. A.; Shubina, E. S. Amine Boranes Dehydrogenation Mediated by an Unsymmetrical Iridium Pincer Hydride: (PCN) vs (PCP) Improved Catalytic Performance. *Organometallics* **2018**, *37*, 3142–3153. https://doi.org/10.1021/acs.organomet.8b00488.

(24) Blaquiere, N.; Diallo-garcia, S.; Gorelsky, S. I.; Black, D. A.; Fagnou, K. Ruthenium-Catalyzed Dehydrogenation of Ammonia Boranes. *J. Am. Chem. Soc.* **2008**, No. 130, 14034–14035.

(25) Marziale, A. N.; Friedrich, A.; Klopsch, I.; Drees, M.; Celinski, V. R.; Schmedt auf der Günne, J.; Schneider, S. The Mechanism of Borane − Amine Dehydrocoupling with Bifunctional Ruthenium Catalysts. *J. Am. Chem. Soc.* **2013**, *135*, 13342–13355. https://doi.org/10.1021/ja311092c.

(26) Sewell, L. J.; Huertos, M. A.; Dickinson, M. E.; Weller, A. S. Dehydrocoupling of Dimethylamine Borane Catalyzed by $Rh(PCy_3)_2H_2Cl$. *Inorg. Chem.* **2013**, *52*, 4509–4516. https://doi.org/10.1021/ic302804d.

(27) Esteruelas, M. A.; Nolis, P.; Oliván, M.; Oñate, E.; Vallribera, A.; Vélez, A. Ammonia Borane Dehydrogenation Promoted by a Pincer-Square- Planar Rhodium(I) Monohydride: A Stepwise Hydrogen Transfer from the Substrate to the Catalyst. *Inorg. Chem.* **2016**, *55,* 7176–7181. https://doi.org/10.1021/acs.inorgchem.6b01216.

(28) Baker, R. T.; Gordon, J. C.; Hamilton, C. W.; Henson, N. J.; Lin, P.;

Maguire, S.; Murugesu, M.; Scott, B. L.; Smythe, N. C. Iron Complex-Catalyzed Ammonia−Borane Dehydrogenation. A Potential Route toward B−N-Containing Polymer Motifs Using Earth-Abundant Metal Catalysts. *J. Am. Chem. Soc.* **2012**, *134,* 5598–5609. https://doi.org/10.1021/ja210542r.

(29) Todisco, S.; Luconi, L.; Giambastiani, G.; Rossin, A.; Peruzzini, M.; Golub, I. E.; Filippov, O. A.; Belkova, N. V; Shubina, E. S. Ammonia Borane Dehydrogenation Catalyzed by $(\kappa^4\text{-}EP_3)Co(H)$ [EP_3 = $E(CH_2CH_2PPh_2)_3$; E = N, P] and H_2 Evolution from Their Interaction with NH Acids. *Inorg. Chem.* **2017**, *56,* 4296–4307. https://doi.org/10.1021/acs.inorgchem.6b02673.

(30) Kim, S.; Kim, T.; Kim, T.; Lee, G.; Park, J. T.; Nam, S. W.; Kang, S. O. Tetraglyme-Mediated Synthesis of Pd Nanoparticles for Dehydrogenation of Ammonia Borane. *Chem. Commun.* **2012**, *48,* 2021–2023. https://doi.org/10.1039/c2cc15931g.

(31) Park, J. H.; Kim, S. K.; Kim, H. S.; Cho, Y. J.; Park, J.; Lee, K. E.; Yoon, C. W.; Nam, S. W.; Kang, S. O. Convenient Metal Embedment into Mesoporous Silica Channels for High Catalytic Performance in AB Dehydrogenation. *Chem. Commun.* **2013**, *49* (92), 10832–10834. https://doi.org/10.1039/c3cc46758a.

(32) Chen, G.; Desinan, S.; Rosei, R.; Rosei, F.; Ma, D. Synthesis of Ni – Ru Alloy Nanoparticles and Their High Catalytic Activity in Dehydrogenation of Ammonia Borane. *Chem. A Eur. J.* **2012**, *18,* 7925–7930. https://doi.org/10.1002/chem.201200292.

(33) Chandra, M.; Xu, Q. A High-Performance Hydrogen Generation System : Transition Metal-Catalyzed Dissociation and Hydrolysis of Ammonia – Borane. *J. Power Sources* **2006**, *156,* 190–194. https://doi.org/10.1016/j.jpowsour.2005.05.043.

(34) Fetz, M.; Gerber, R.; Blacque, O.; Frech, C. M. Hydrolysis of Ammonia

Borane Catalyzed by Aminophosphine-Stabilized Precursors of Rhodium Nanoparticles : Ligand Effects and Solvent-Controlled Product Formation. *Chem. A Eur. J.* **2011**, *17*, 4732–4736. https://doi.org/10.1002/chem.201003543.

(35) Clark, T. J.; Whittell, G. R.; Manners, I. Highly Efficient Colloidal Cobalt- and Rhodium-Catalyzed Hydrolysis of $H_3N \cdot BH_3$ in Air. *Inorg. Chem.* **2007**, *46* (18), 7522–7527. https://doi.org/10.1021/ic700806b.

(36) Yan, J.; Zhang, X.; Han, S.; Shioyama, H.; Xu, Q. Iron-Nanoparticle-Catalyzed Hydrolytic Dehydrogenation of Ammonia Borane for Chemical Hydrogen Storage. *Angew. Chemie Int. Ed.* **2008**, *47*, 2287–2289. https://doi.org/10.1002/anie.200704943.

(37) Peng, C.; Kang, L.; Cao, S.; Chen, Y.; Lin, Z.; Fu, W. Nanostructured Ni_2P as a Robust Catalyst for the Hydrolytic Dehydrogenation of Ammonia – Borane. *Angew. Chemie Int. Ed.* **2015**, *54*, 15725–15729. https://doi.org/10.1002/anie.201508113.

(38) Fu, Z.-C.; Xu, Y.; Chan, S. L.-F.; Wang, W.-W.; Li, F.; Liang, F.; Chen, Y.; Lin, Z.-S.; Fu, W.-F.; Che, C. Highly Efficient Hydrolysis of Ammonia Borane by Anion (^-OH, F^-,Cl^-)-Tuned Interactions between Reactant Molecules and CoP Nanoparticles. *Chem. Commun.* **2017**, *53*, 705–708. https://doi.org/10.1039/c6cc08120g.

(39) Metin, Ö.; Mazumder, V.; Özkar, S.; Sun, S. Monodisperse Nickel Nanoparticles and Their Catalysis in Hydrolytic Dehydrogenation of Ammonia Borane. *J. Am. Chem. Soc.* **2010**, *132*, 1468–1469. https://doi.org/10.1021/cm9013046.(14).

(40) Zacho, S. L.; Mielby, J.; Kegnæs, S. Hydrolytic Dehydrogenation of Ammonia Borane over ZIF-67 Derived Co Nanoparticle Catalysts. *Catal. Sci. Technol.* **2018**, No. 8, 4741. https://doi.org/10.1039/c8cy01500g.

(41) Baguc, I. B.; Ertas, I. E.; Yurderi, M.; Bulut, A.; Zahmakiran, M.; Kaya, M.

Nanocrystalline Metal Organic Framework (MIL-101) Stabilized Copper Nanoparticles : Highly Efficient Nanocatalyst for the Hydrolytic Dehydrogenation of Methylamine Borane. *Inorganica Chim. Acta* **2018**, *483*, 431–439. https://doi.org/10.1016/j.ica.2018.08.056.

(42) Fu, F.; Wang, C.; Wang, Q.; Martinez-Villacorta, A. M.; Escobar, A.; Chong, H.; Wang, X.; Moya, S.; Salmon, L.; Fouquet, E.; Ruiz, J.; Astruc, D. Highly Selective and Sharp Volcano-Type Synergistic Ni$_2$Pt@ZIF-8-Catalyzed Hydrogen Evolution from Ammonia Borane Hydrolysis. *J. Am. Chem. Soc.* **2018**, *140* (1), 10034–10042. https://doi.org/10.1021/jacs.8b06511.

(43) Ciganda, R.; Garralda, M. A.; Ibarlucea, L.; Pinilla, E.; Torres, M. R. A Hydridoirida-β-Diketone as an Efficient and Robust Homogeneous Catalyst for the Hydrolysis of Ammonia–Borane or Amine-Borane Adducts in Air to Produce Hydrogen. *Dalton Trans.* **2010**, *39*, 7226–7229. https://doi.org/10.1039/c0dt00091d.

(44) Graham, T. W.; Tsang, C.; Chen, X.; Guo, R.; Jia, W.; Lu, S.; Sui-seng, C.; Ewart, C. B.; Lough, A.; Amoroso, D.; Abdur-Rashid, K. Catalytic Solvolysis of Ammonia Borane. *Angew. Chemie Int. Ed.* **2010**, *49*, 8708–8711. https://doi.org/10.1002/anie.201003074.

(45) Nelson, D. J.; Truscott, B. J.; Egbert, J. D.; Nolan, S. P. Exploring the Limits of Catalytic Ammonia−Borane Dehydrogenation Using a Bis(N‐Heterocyclic Carbene) Iridium(III) Complex. *Organometallics* **2013**, *32*, 3769–3772. https://doi.org/10.1021/om400402r.

(46) Wang, W.; Tang, H.; Lu, W.; Li, Y.; Bao, M.; Himeda, Y. Mechanistic Insights into the Catalytic Hydrolysis of Ammonia Borane with Proton-Responsive Iridium Complexes : An Experimental and Theoretical Study. *ChemCatChem* **2017**, *9*, 3191–3196. https://doi.org/10.1002/cctc.201700325.

(47) San Nacianceno, V.; Ibarlucea, L.; Mendicute-fierro, C.; Rodríguez-

Diéguez, A.; Seco, J. M.; Zumeta, I.; Ubide, C.; Garralda, M. A. Hydrido{(Acylphosphine)(Diphenylphosphinous Acid)}rhodium(III) Complexes. Catalysts for the Homogeneous Hydrolysis of Ammonia- or Amine-Boranes under Air. *Organometallics* **2014**, *33*, 6044–6052. https://doi.org/10.1021/om500666w.

(48) San Nacianceno, V.; Azpeitia, S.; Ibarlucea, L.; Mendicute-fierro, C.; Rodríguez-diéguez, A.; Seco, J. M.; San Sebastian, E.; Garralda, M. A. Stereoselective Formation and Catalytic Activity of Hydrido(Acylphosphane)(Chlorido)(Pyrazole)Rhodium(III) Complexes. Experimental and DFT Studies. *Dalton Trans.* **2015**, *44*, 13141–13155. https://doi.org/10.1039/c5dt01705j.

(49) Boulho, C.; Djukic, J. The Dehydrogenation of Ammonia–Borane Catalysed by Dicarbonylruthenacyclic(II) Complexes. *Dalton Trans.* **2010**, *39*, 8893–8905. https://doi.org/10.1039/c0dt00241k.

(50) Muñoz-Olasagasti, M.; Telleria, A.; Pérez-Miqueo, J.; Garralda, M. A.; Freixa, Z. A Readily Accessible Ruthenium Catalyst for the Solvolytic Dehydrogenation of Amine–Borane Adducts. *Dalton Trans.* **2014**, *43*, 11404–11409. https://doi.org/10.1039/c4dt01216j.

(51) Telleria, A.; Vicent, C.; San Nacianceno, V.; Garralda, M. A.; Freixa, Z. Experimental Evidence Supporting Related Mechanisms for Ru(II)-Catalyzed Dehydrocoupling and Hydrolysis of Amine-Boranes. *ACS Catal.* **2017**, *7*, 8394–8405. https://doi.org/10.1021/acscatal.7b02958.

(52) Zhan, W.-W.; Zhu, Q.-L.; Xu, Q. Dehydrogenation of Ammonia Borane by Metal Nanoparticle Catalysts. *ACS Catal.* **2016**, *6* (10), 6892–6905. https://doi.org/10.1021/acscatal.6b02209.

(53) Ramachandran, P. V.; Gagare, P. D. Preparation of Ammonia Borane in High Yield and Purity, Methanolysis, and Regeneration. *Inorg. Chem.* **2007**, *46* (19), 7810–7817. https://doi.org/10.1021/ic700772a.

(54) Özhava, D.; Özkar, S. Rhodium(0) Nanoparticles Supported on Hydroxyapatite Nanospheres and Further Stabilized by Dihydrogen Phosphate Ion: A Highly Active Catalyst in Hydrogen Generation from the Methanolysis of Ammonia Borane. *Int. J. Hydrogen Energy* **2015**, *40*, 10491–10501. https://doi.org/10.1016/j.ijhydene.2015.06.144.

(55) Özkar, S. Transition Metal Nanoparticle Catalysts in Releasing Hydrogen from the Methanolysis of Ammonia Borane. *Int. J. Hydrogen Energy* **2020**, *45* (14), 7881–7891. https://doi.org/10.1016/j.ijhydene.2019.04.125.

(56) Lara, P.; Philippot, K.; Suárez, A. Phosphane-Decorated Platinum Nanoparticles as Efficient Catalysts for H_2 Generation from Ammonia Borane and Methanol. *ChemCatChem* **2019**, *11* (2), 766–771. https://doi.org/10.1002/cctc.201801702.

(57) Sun, J.-K.; Zhan, W.-W.; Akita, T.; Xu, Q. Toward Homogenization of Heterogeneous Metal Nanoparticle Catalysts with Enhanced Catalytic Performance: Soluble Porous Organic Cage as a Stabilizer and Homogenizer. *J. Am. Chem. Soc.* **2015**, *137* (22), 7063–7066.

(58) San Nacianceno, V.; García, M. Á.; Matxain, J. M.; Freixa, Z. Proton-Responsive Ruthenium(II) Catalysts for the Solvolysis of Ammonia-Borane. *Organometallics* **2020**, *39* (8), 1238–1248.

(59) Van Der Boom, M. E.; Milstein, D. Cyclometalated Phosphine-Based Pincer Complexes : Mechanistic Insight in Catalysis , Coordination , and Bond Activation. *Chem. Rev.* **2003**, *103*, 1759–1792. https://doi.org/10.1021/cr960118r.

(60) Poverenov, E.; Efremenko, I.; Frenkel, A. I.; Ben-david, Y.; Shimon, L. J. W.; Leitus, G.; Konstantinovski, L.; Martin, J. M. L.; Milstein, D. Evidence for a Terminal Pt(IV)-Oxo Complex Exhibiting Diverse Reactivity. *Nature* **2008**, *455* (October), 1093–1096. https://doi.org/10.1038/nature07356.

(61) Albrecht, M.; Lindner, M. M. Cleavage of Unreactive Bonds with Pincer

Metal Complexes. *Dalton Trans.* **2011**, *40*, 8733–8744. https://doi.org/10.1039/C1DT10339C.

(62) Poverenov, E.; Milstein, D. Noninnocent Behavior of PCP and PCN Pincer Ligands of Late Metal Complexes. *Oganometallic Pincer Chem.* **2013**, *40*, 21–48. https://doi.org/10.1007/978-3-642-31081-2.

(63) Ciganda, R.; Garralda, M. A.; Ibarlucea, L.; Mendicute, C.; Pinilla, E.; Torres, M. R. Dehydrogenation of Hydridoirida-β-Diketones in Methanol : The Selective Formation of Mono- and Dinuclear Acyl Complexes. *Eur. J. Inorg. Chem.* **2010**, 3167–3173. https://doi.org/10.1002/ejic.201000250.

(64) Zumeta, I.; Mendicute-fierro, C.; Rodríguez-Diéguez, A.; Seco, J. M.; Garralda, M. A. On the Reactivity of Dihydridoirida-β-Diketones with 2‐Aminopyridines. Formation of Acylhydrido Complexes with New PCN Terdentate Ligands. *Organometallics* **2015**, *34*, 349–354. https://doi.org/10.1021/om5011353.

(65) Lee, J. C.; Peris, E.; Rheingold, A. L.; Crabtree, R. H. An Unusual Type of H-H Interaction: Ir-H-H-O and Ir-H-H-N Hydrogen Bonding and Its Involvement in 0-Bond Metathesis. *J. Am. Chem. Soc.* **1994**, *116*, 11014–11019.

(66) Epstein, L. M.; Shubina, E. S. New Types of Hydrogen Bonding in Organometallic Chemistry. *Coord. Chem. Rev.* **2002**, *231*, 165–181.

(67) Steiner, T. The Hydrogen Bond in the Solid State. *Angew. Chemie Int. Ed.* **2002**, *41*, 48–76.

(68) Sambasivam, S.; Liu, L.; Yang, Y.; Han, G.; Bashir, B.; Yang, Z.; Pan, S. Syntheses, Crystal Structures and Characterization of Three Alkaline Metal Borates. *Cryst. Eng. Commun.* **2017**, *19*, 2561–2569. https://doi.org/10.1039/c7ce00450h.

(69) Salentine, C. G. High-Field ^{11}B NMR of Alkali Borates. Aqueous Polyborate Equilibria. *Inorg. Chem.* **1983**, *22* (26), 3920–3924.

(70) Cheng, F.; Ma, H.; Li, Y.; Chen, J. $Ni_{1-x}Pt_x$ (x = 0−0.12) Hollow Spheres as Catalysts for Hydrogen Generation from Ammonia Borane. *Inorg. Chem.* **2007**, *46* (3), 788–794. https://doi.org/10.1021/ic061712e.

(71) Yagupsky, M. P.; Wilkinson, G. Cationic π-Carbon Disulphide Complexes of Rhodium and Iridium; Thio-Carbonyl Complexes of Iridium. *J. Chem. Soc. A Inorg. Phys. Theor.* **1967**, 2813–2817.

(72) Kemmitt, T.; Gainsford, G. J. Regeneration of Sodium Borohydride from Sodium Metaborate , and Isolation of Intermediate Compounds. *Int. J. Hydrogen Energy* **2009**, *34* (14), 5726–5731. https://doi.org/10.1016/j.ijhydene.2009.05.108.

(73) Shimoi, M.; Nagai, S.; Ichikawa, M.; Kawano, Y.; Katoh, K.; Uruichi, M.; Ogino, H. Coordination Compounds of Monoborane-Lewis Base Adducts: Syntheses and Structures of $[M(CO)_5(\eta^1\text{-}BH_3 \cdot L)]$ (M = Cr, Mo, W; L = NMe_3, PMe_3, PPh_3). *J. Am. Chem. Soc.* **1999**, *121* (50), 11704–11712. https://doi.org/10.1021/ja990828p.

(74) Hebden, T. J.; Denney, M. C.; Pons, V.; Piccoli, P. M. B.; Koetzle, T. F.; Schultz, A. J.; Kaminsky, W.; Goldberg, K. I.; Heinekey, D. M. σ -Borane Complexes of Iridium : Synthesis and Structural Characterization. *J. Am. Chem. Soc.* **2008**, *130*, 10812–10820. https://doi.org/10.1021/ja801898m.

(75) Wang, Q.; Fu, F.; Yang, S.; Martinez Moro, M.; Ramirez, M. D. L. A.; Moya, S.; Salmon, L.; Ruiz, J.; Astruc, D. Dramatic Synergy in CoPt Nanocatalysts Stabilized by "Click" Dendrimers for Evolution of Hydrogen from Hydrolysis of Ammonia Borane. *ACS Catal.* **2019**, *9*, 1110–1119. https://doi.org/10.1021/acscatal.8b04498.

(76) Na, C.; Ma, H. Isokinetic Temperature and Size-Controlled Activation of Ruthenium-Catalyzed Ammonia Borane Hydrolysis. *ACS Catal.* **2015**, *5*, 1726–1735. https://doi.org/10.1021/cs5019524.

(77) Bustos, I.; Seco, J. M.; Rodríguez-Diéguez, A.; Garralda, M. A.;

Mendicute-Fierro, C. Acyl(Furfurylamine)Iridium(III) Complexes from Irida-β-Diketones. Characterisation and Catalytic Activity in Amine-Borane Hydrolysis. *Inorganica Chim. Acta* **2019**, *498*, 119165. https://doi.org/10.1016/j.ica.2019.119165.

(78) Bocian, W.; Jaźwiński, J.; Sadlej, A. ^{1}H, ^{13}C and ^{15}N NMR Studies on Adducts Formation of Rhodium(II) Tetraacylates with Some Azoles in $CDCl_3$ Solution. *Magn. Reson. Chem.* **2008**, *46* (2), 156–165. https://doi.org/10.1002/mrc.2149.

(79) Claramunt, R. M.; López, C.; García, M. Á.; Denisov, G. S.; Alkorta, I.; Elguero, J. Protonation and Phase Effects on the NMR Chemical Shifts of Imidazoles and Pyrazoles: Experimental Results and GIAO Calculations. *New J. Chem.* **2003**, *27* (4), 734–742. https://doi.org/10.1039/b210251j.

(80) Nygaard, L.; Christen, D.; Nielsen, J. T.; Pedersen, E. J.; Snerling, O.; Vestergaard, E.; Sørensen, G. O. Microwave Spectra of Isotopic Pyrazoles and Molecular Structure of Pyrazole. *J. Mol. Struct.* **1974**, *22* (3), 401–413. https://doi.org/10.1016/0022-2860(74)85010-6.

(81) Węcławik, M.; Szklarz, P.; Medycki, W.; Janicki, R.; Piecha-Bisiorek, A.; Zieliński, P.; Jakubas, R. Unprecedented Transformation of [I$^-$·I$_3^-$] to [I$_4^{2-}$] Polyiodides in the Solid State: Structures, Phase Transitions and Characterization of Dipyrazolium Iodide Triiodide. *Dalton Trans.* **2015**, *44* (42), 18447–18458. https://doi.org/10.1039/c5dt02265g.

(82) Titov, A. A.; Filippov, O. A.; Smol'yakov, A. F.; Baranova, K. F.; Titova, E. M.; Averin, A. A.; Shubina, E. S. Dinuclear Cu^I and Ag^I Pyrazolates Supported with Tertiary Phosphines: Synthesis, Structures, and Photophysical Properties. *Eur. J. Inorg. Chem.* **2019**, *2019* (6), 821–827. https://doi.org/10.1002/ejic.201801318.

(83) Kishimura, A.; Yamashita, T.; Aida, T. Phosphorescent Organogels via "Metallophilic" Interactions for Reversible RGB-Color Switching. *J. Am. Chem. Soc.* **2005**, *127* (1), 179–183. https://doi.org/10.1021/ja0441007.

(84) Sebe, E.; Guzei, I. A.; Heeg, M. J.; Liable-Sands, L. M.; Rheingold, A. L.; Winter, C. H. Synthesis, Structure, and Properties of Zirconium and Hafnium Complexes Containing η^2-Pyrazolato Ligands. *Eur. J. Inorg. Chem.* **2005**, No. 19, 3955–3961. https://doi.org/10.1002/ejic.200500378.

(85) Palit, S.; Bera, S.; Singh, M.; Mondal, D. Synthesis of Novel Indazole-Derived Ionic Liquids. *Synthesis* **2015**, *47* (21), 3371–3384. https://doi.org/10.1055/s-0034-1381135.

(86) Solovyev, I. V.; Zhukovsky, D. D.; Dar'in, D. V.; Krasavin, M. Y. N-Alkylation of Nitrogen Heterocycles with α-Diazocarbonyl Compounds. *Chem. Heterocycl. Compd.* **2020**, *56* (7), 809–813. https://doi.org/10.1007/s10593-020-02736-y.

(87) Herde, J. L.; Lambert, J. C.; Senoff, C. V.; Cushing, M. A. Cyclooctene and 1,5-Cyclooctadiene Complexes of Iridium(I). *Inorg. Synth.* **1974**, *15*, 18–20.

(88) Laue, S.; Greiner, L.; Wöltinger, J.; Liese, A. Continuous Application of Chemzymes in a Membrane Reactor: Asymmetric Transfer Hydrogenation of Acetophenone. *Adv. Synth. Catal.* **2001**, *343* (6–7), 711–720. https://doi.org/10.1002/1615-4169(200108)343:6/7<711::aid-adsc711>3.3.co;2-t.

Annex A

Infrared spectroscopy of complexes

Chapter 2
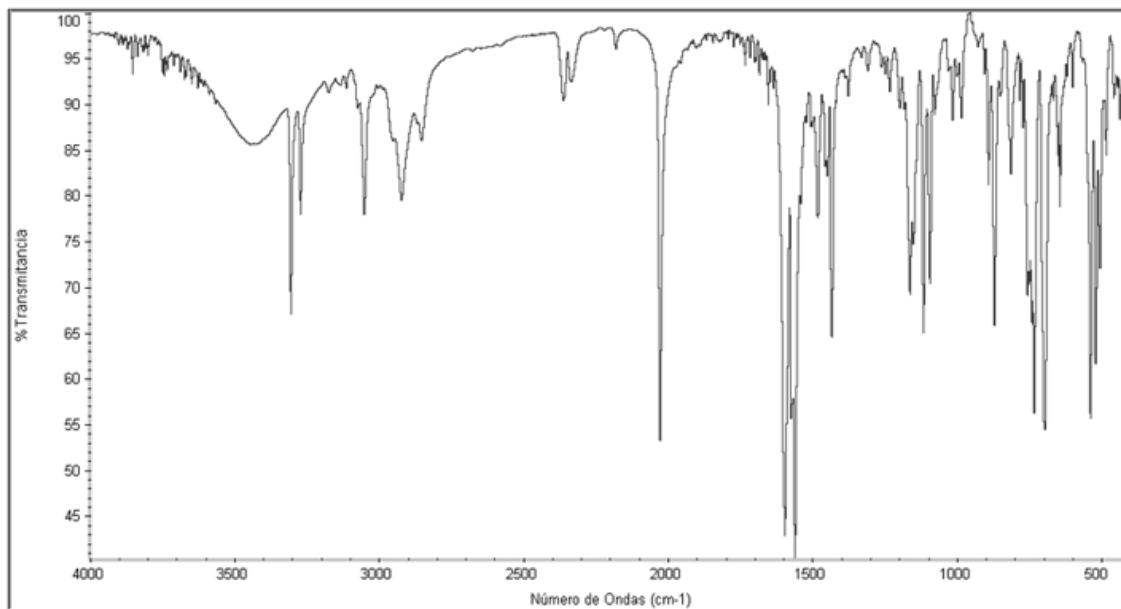
Figure A. 1 IR spectrum of complex 4
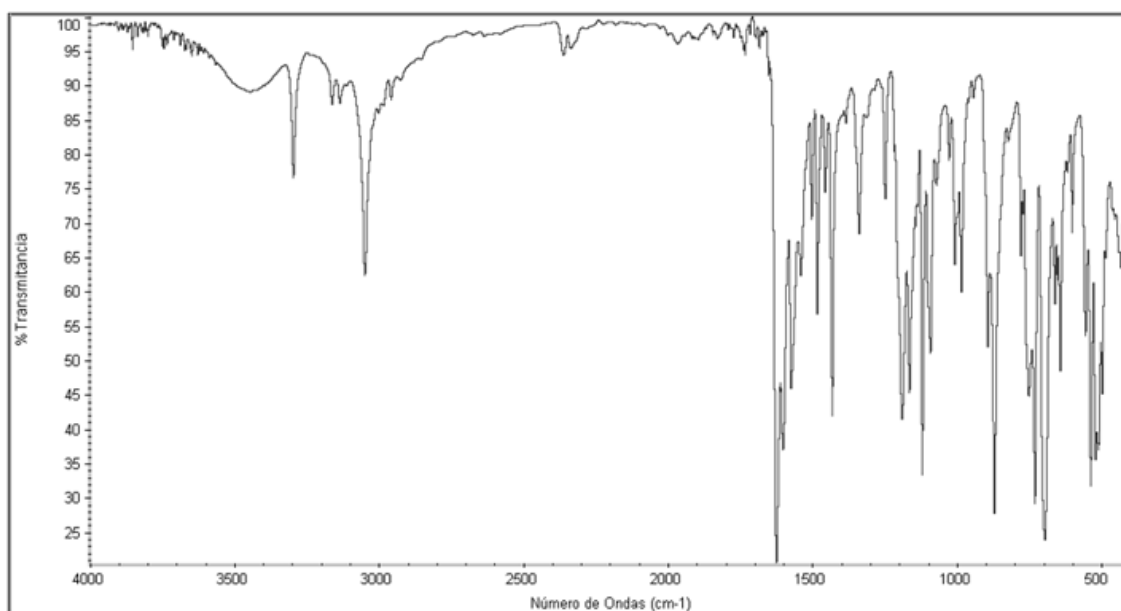
Figure A. 2 IR Spectrum of complex 5
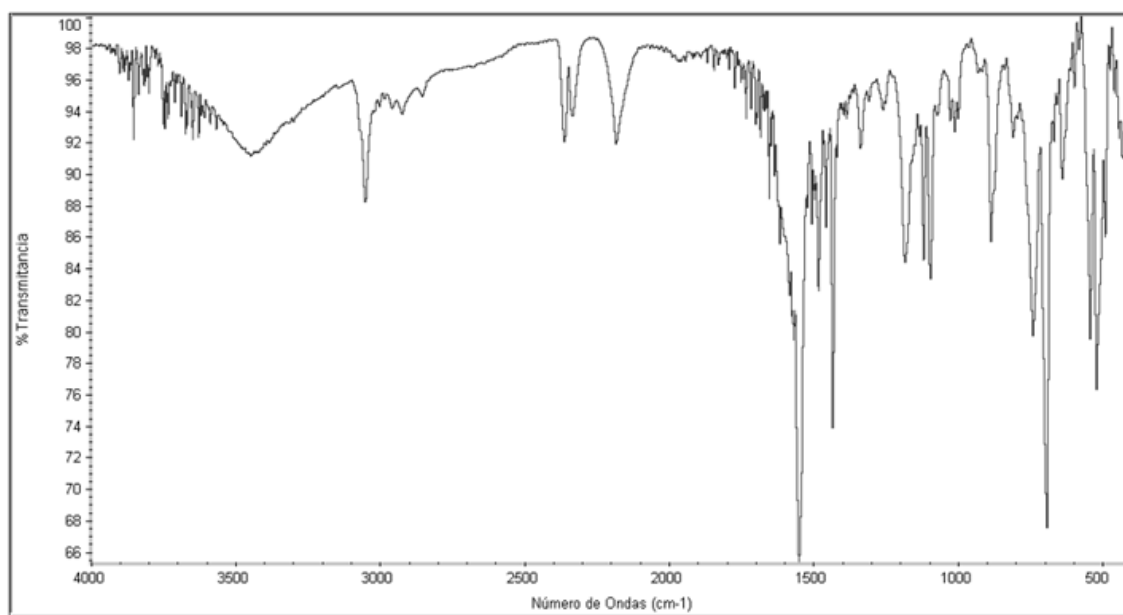
Figure A. 3 IR Spectrum of complex 6

Chapter 3
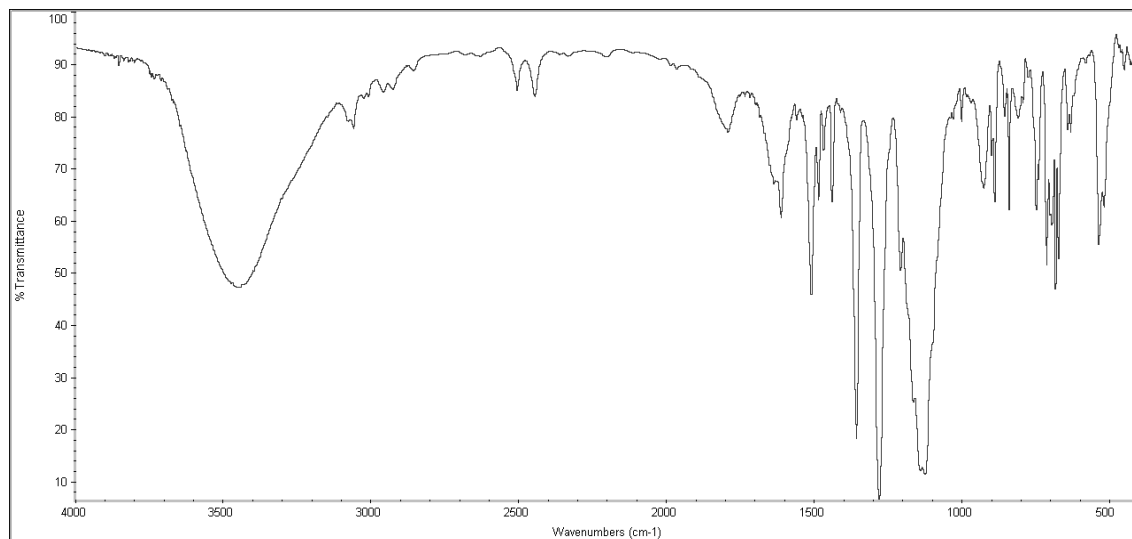
Figure A. 4 IR Spectrum of complex 9

Chapter 4
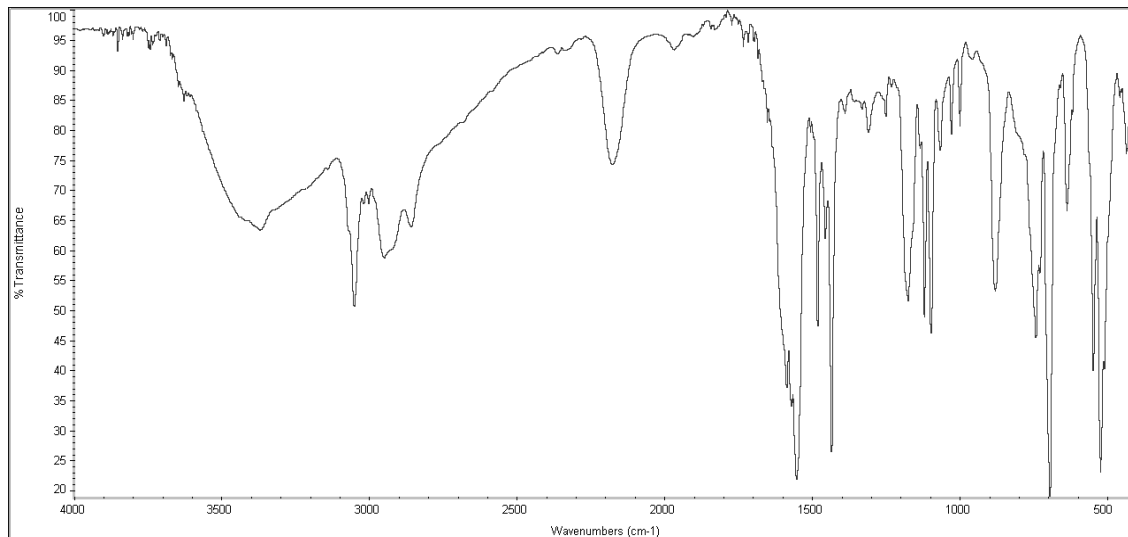
Figure A. 5 IR Spectrum of complex 10
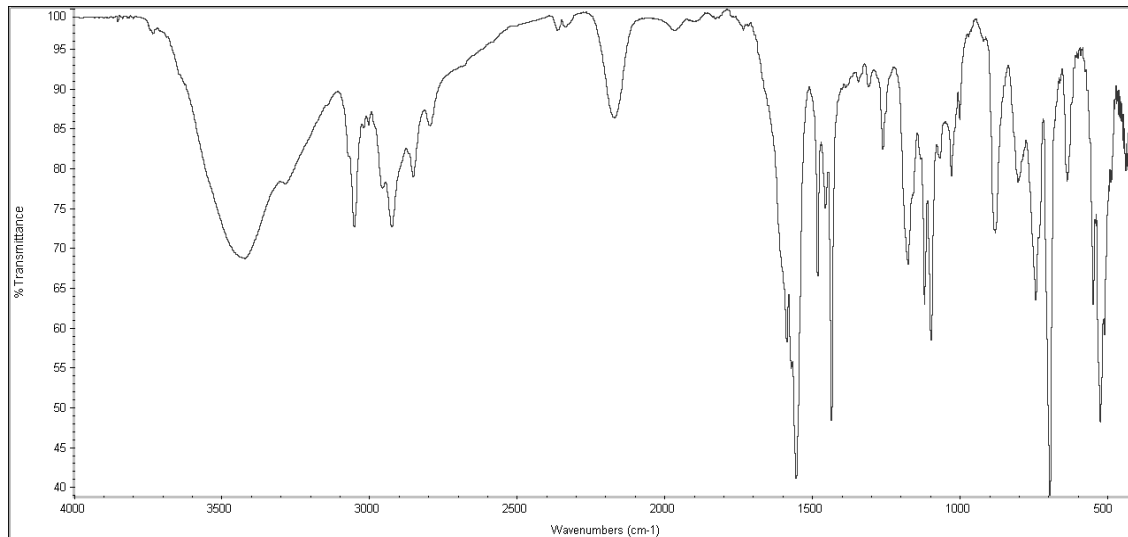
Figure A. 6 IR Spectrum of complex 11
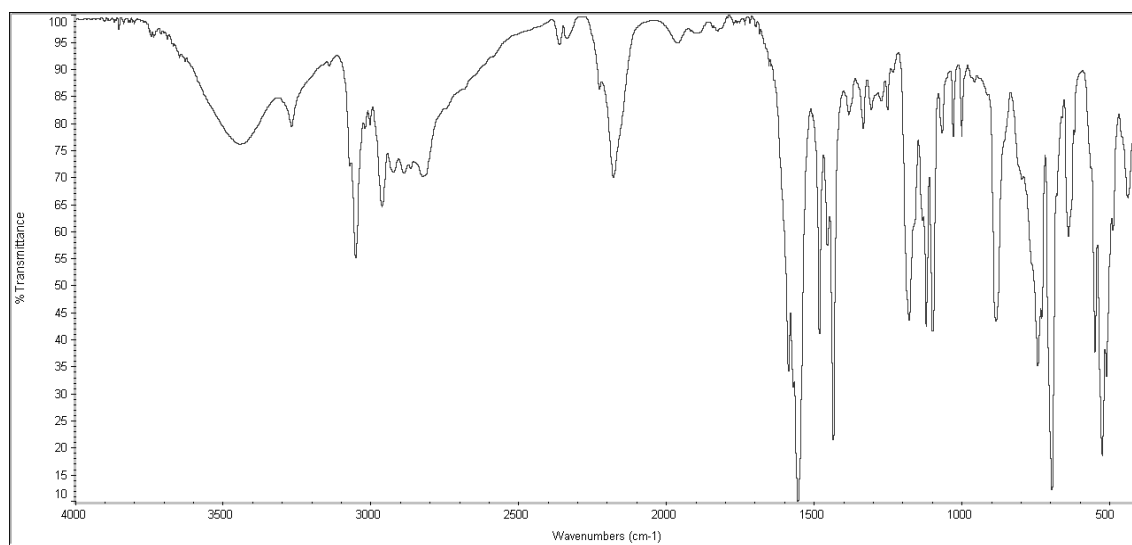
Figure A. 7 IR Spectrum of complex 12
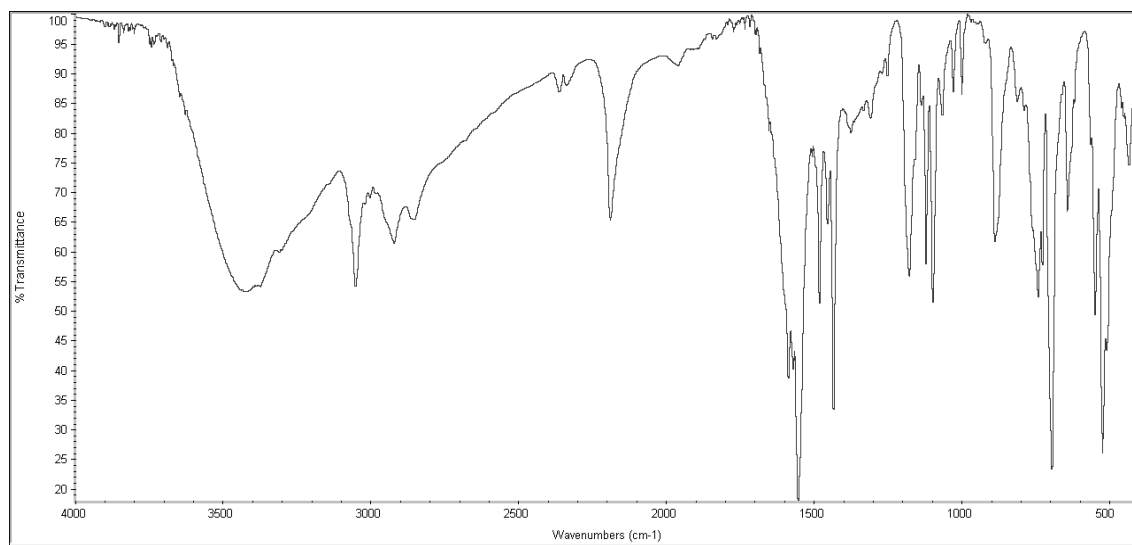
Figure A. 8 IR Spectrum of complex 13
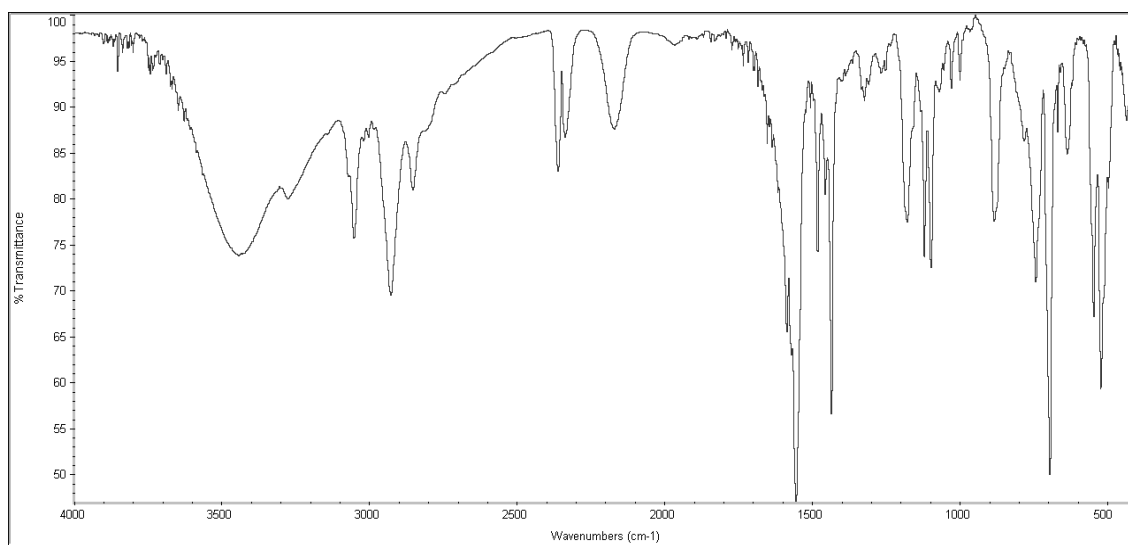
Figure A. 9 IR Spectrum of complex 14
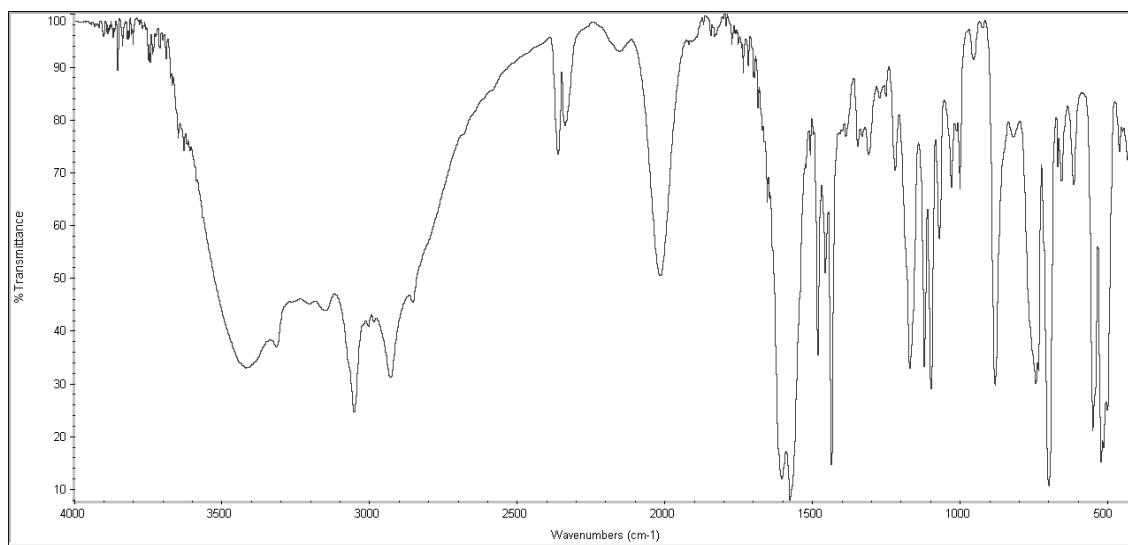
Figure A. 10 IR Spectrum of complex 15
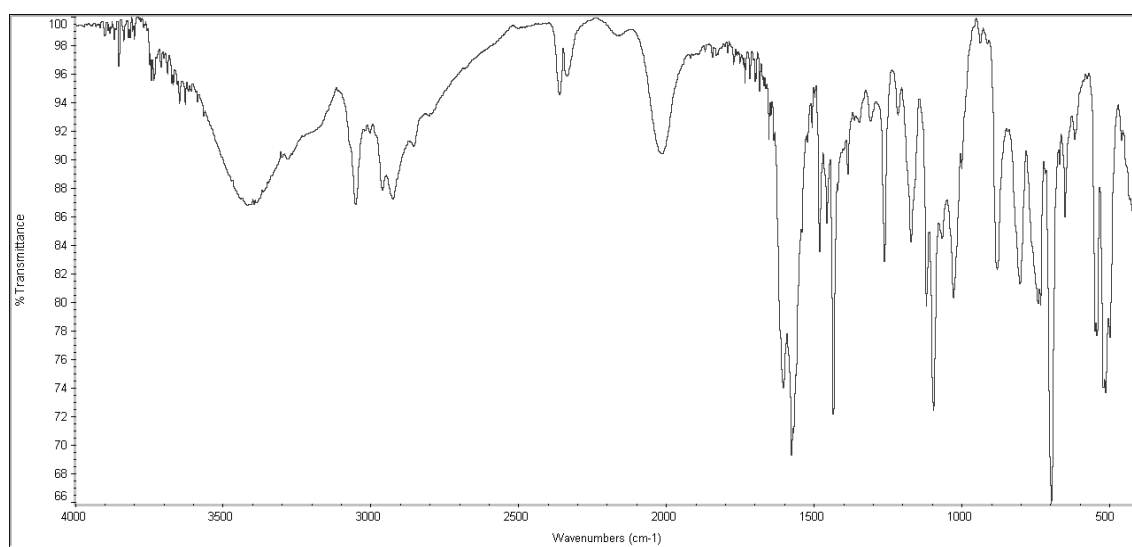
Figure A. 11 IR Spectrum of complex 16
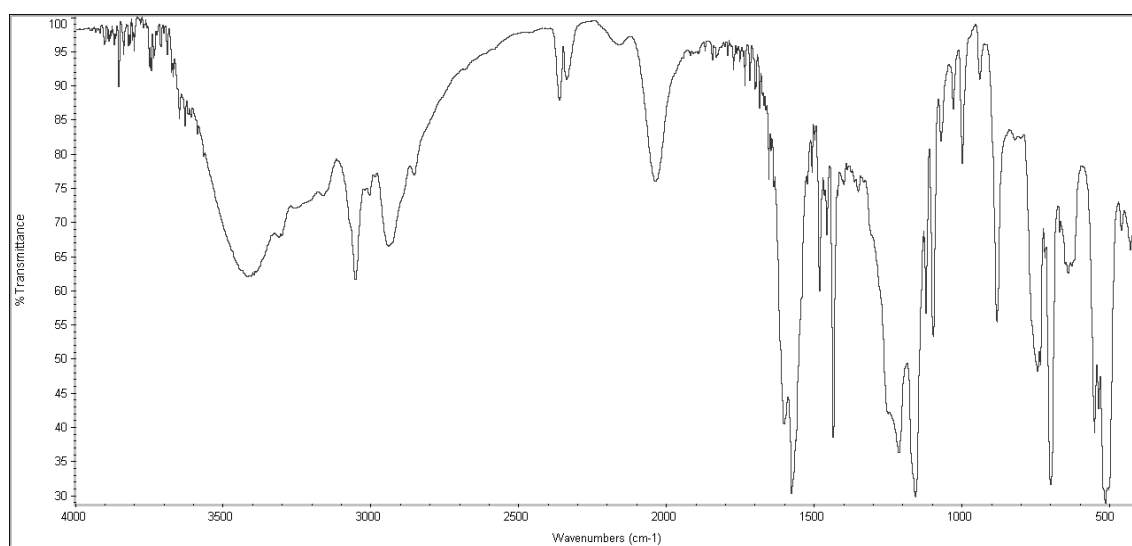
Figure A. 12 IR Spectrum of complex 17
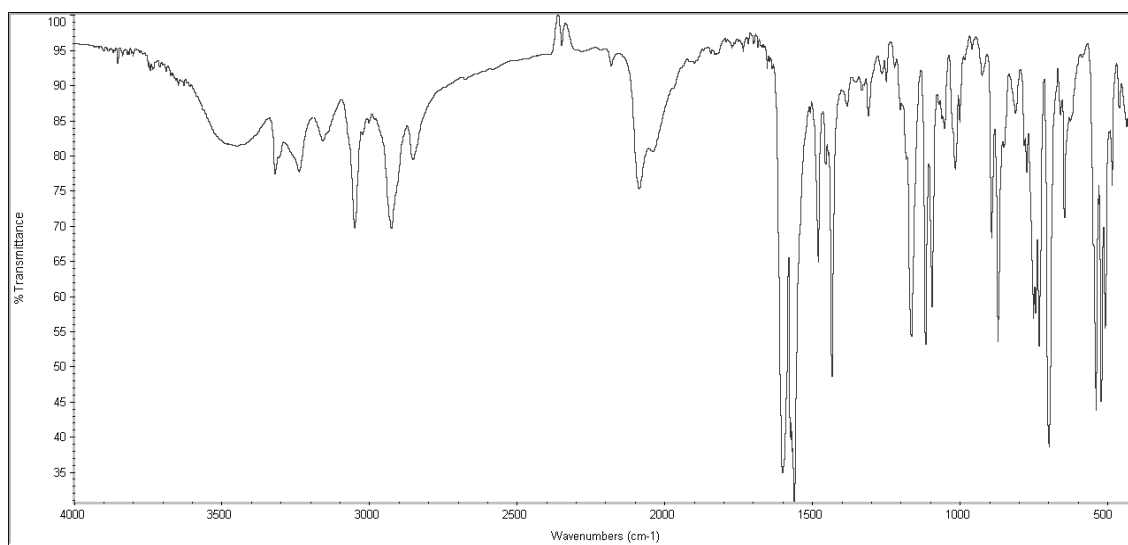
Figure A. 13 IR Spectrum of complex 18
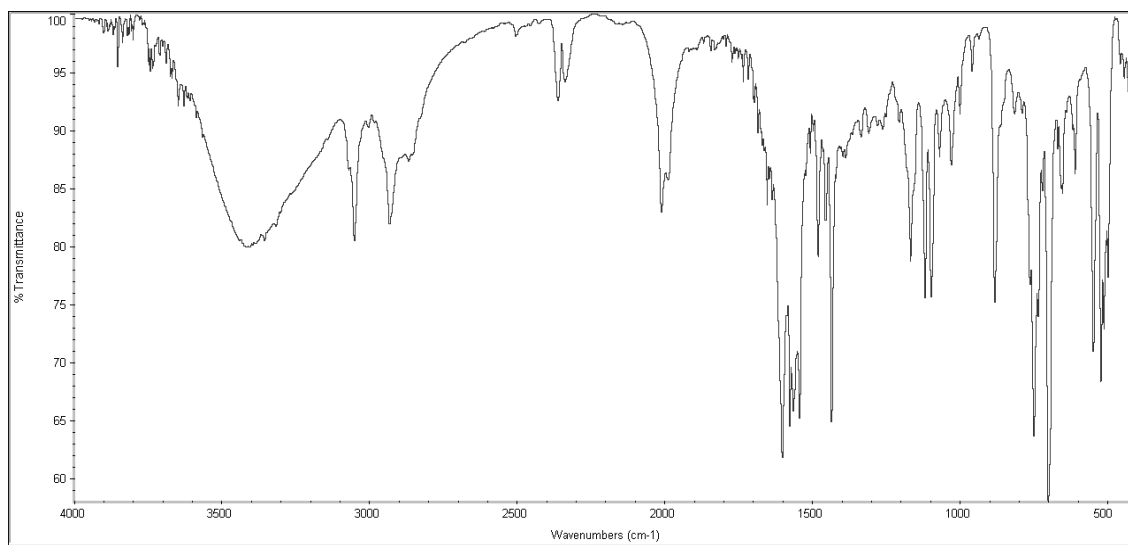
Figure A. 14 IR Spectrum of complex 19
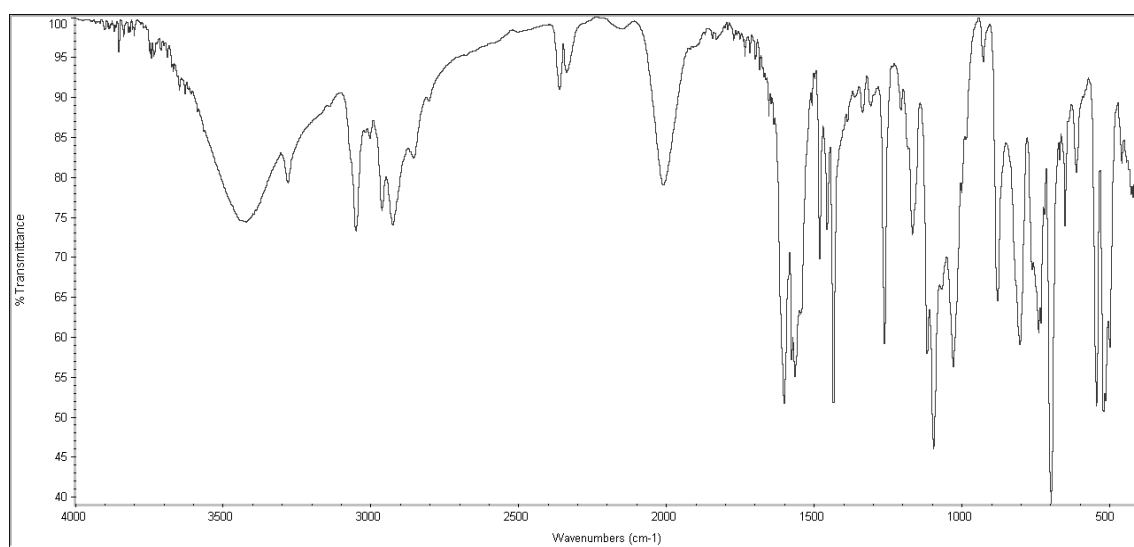
Figure A. 15 IR Spectrum of complex 20
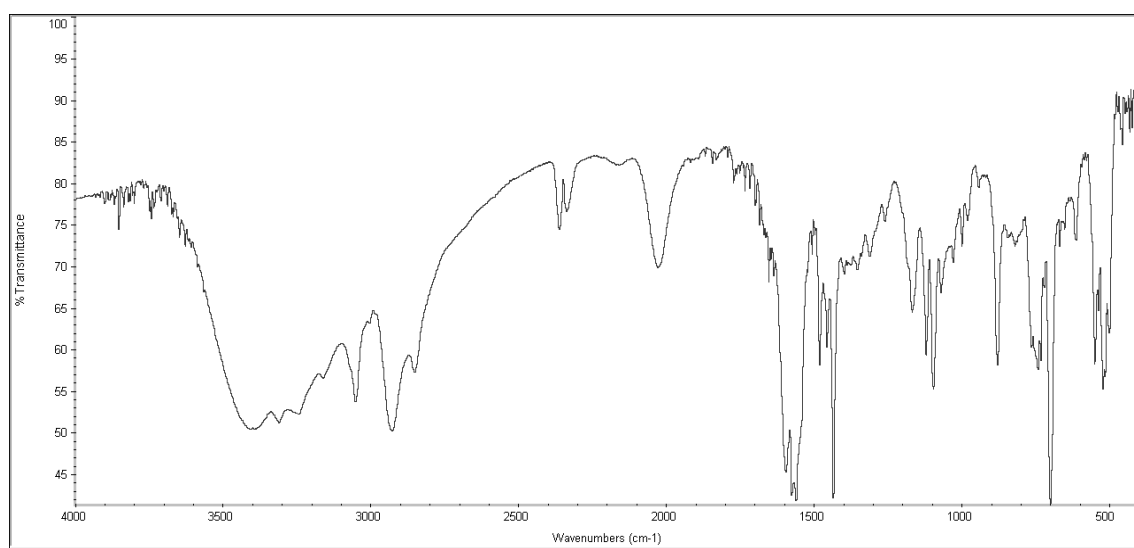
Figure A. 16 IR Spectrum of complex 21
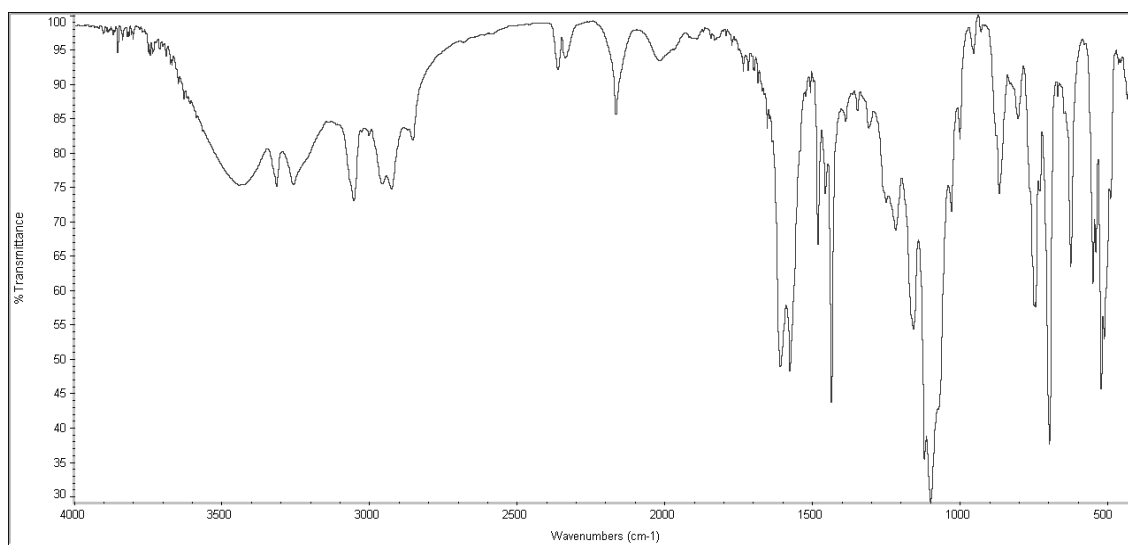
Figure A. 17 IR Spectrum of complex 22
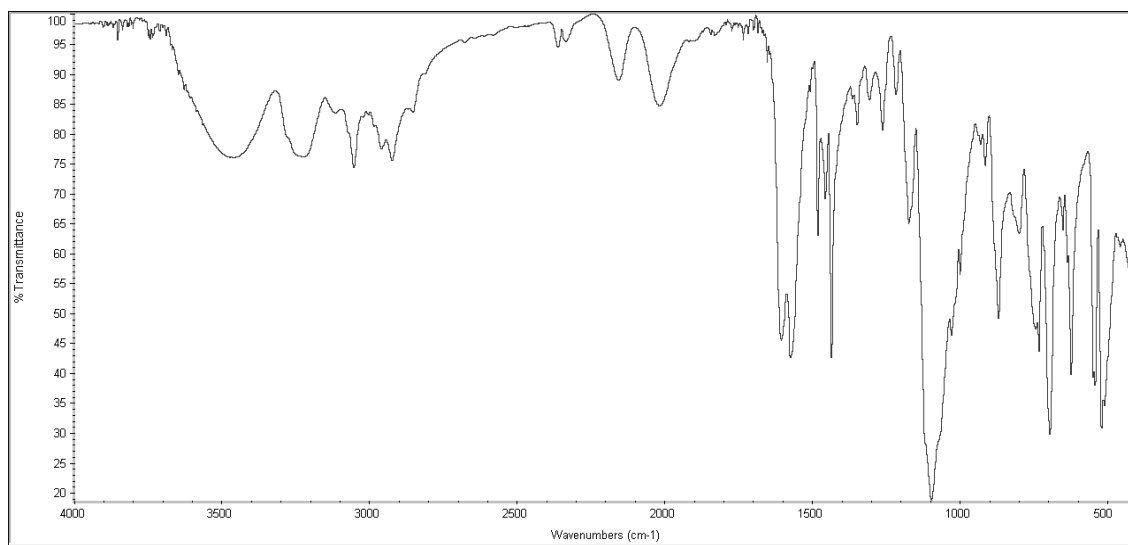
Figure A. 18 IR Spectrum of complex 23
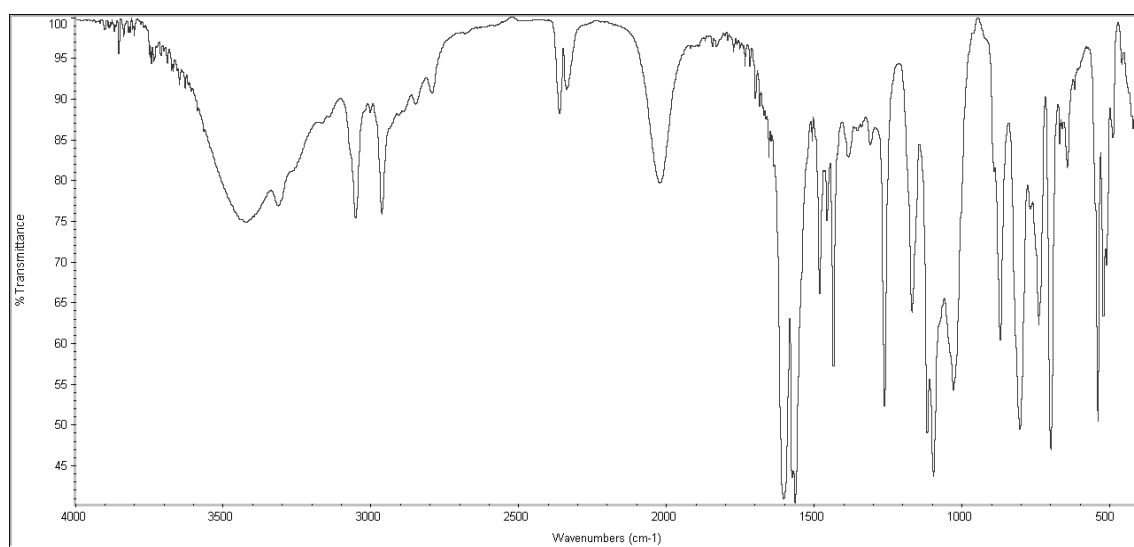
Figure A. 19 IR Spectrum of complex 24
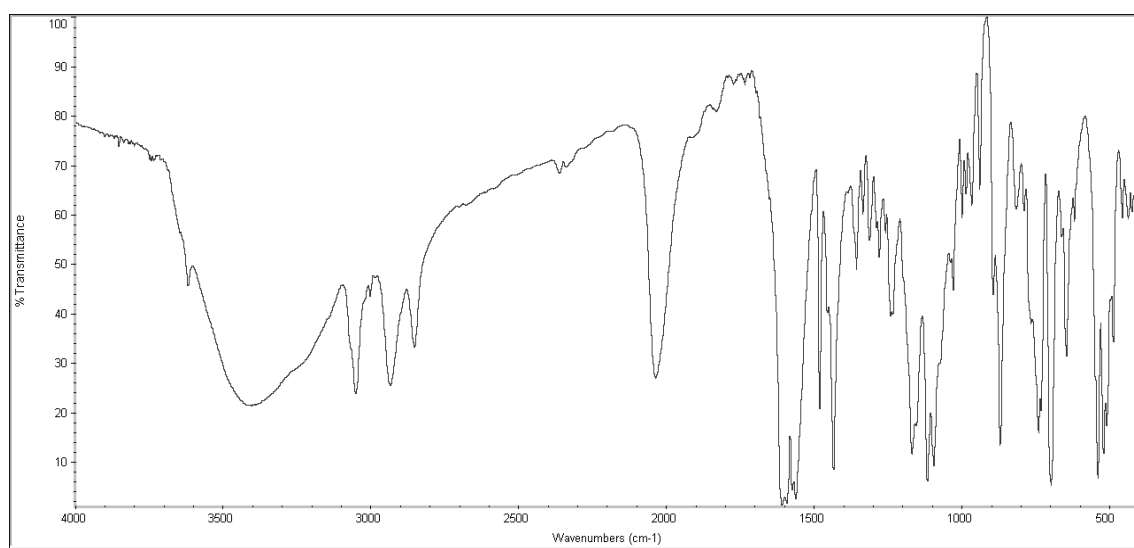
Figure A. 20 IR Spectrum of complex 25

Chapter 5
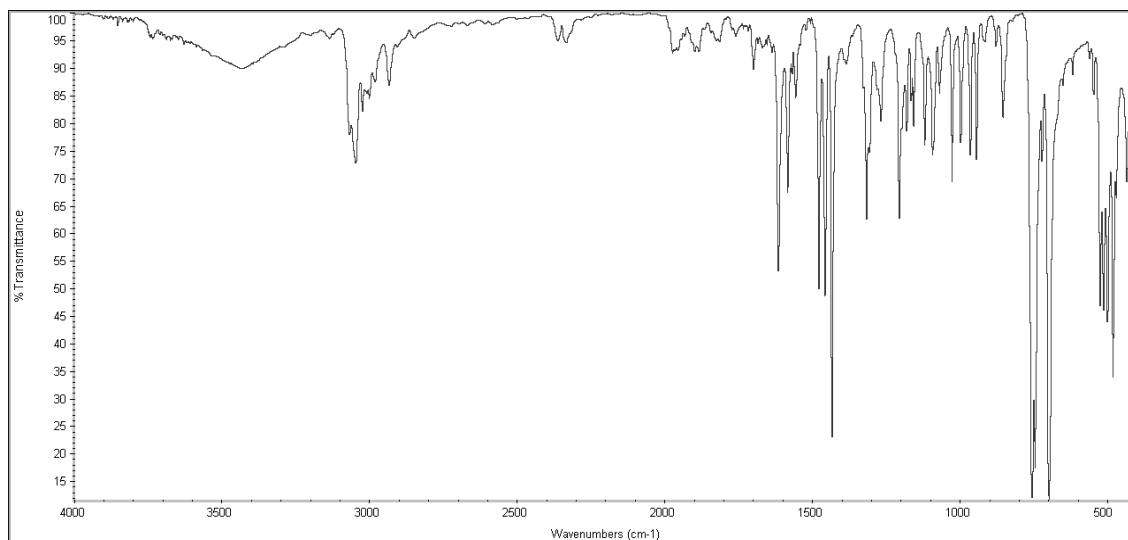
Figure A. 21 IR Spectrum of L1
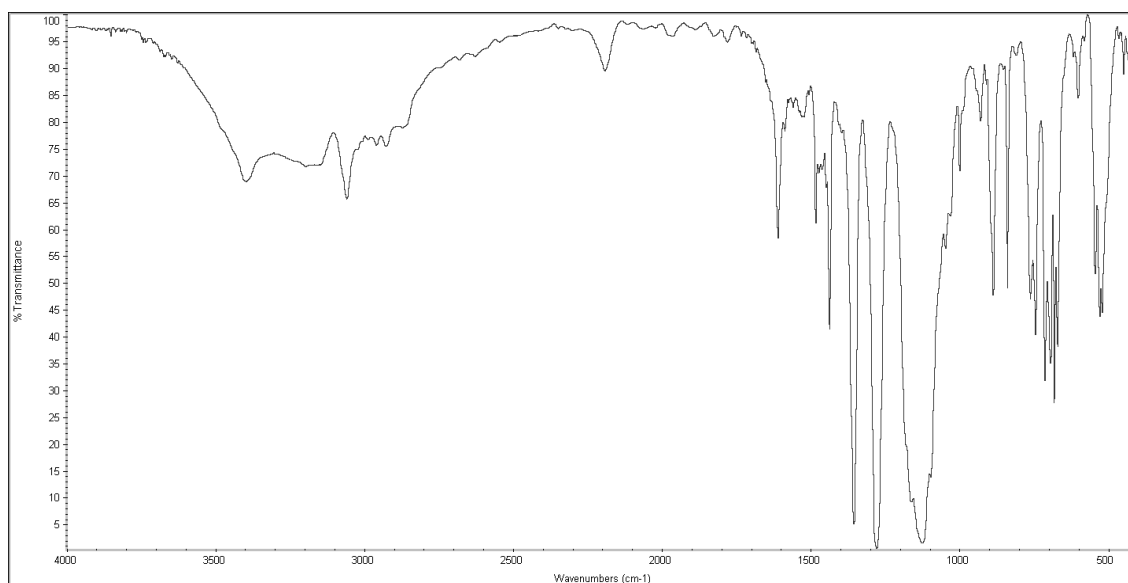
Figure A. 22 IR Spectrum of complex 27
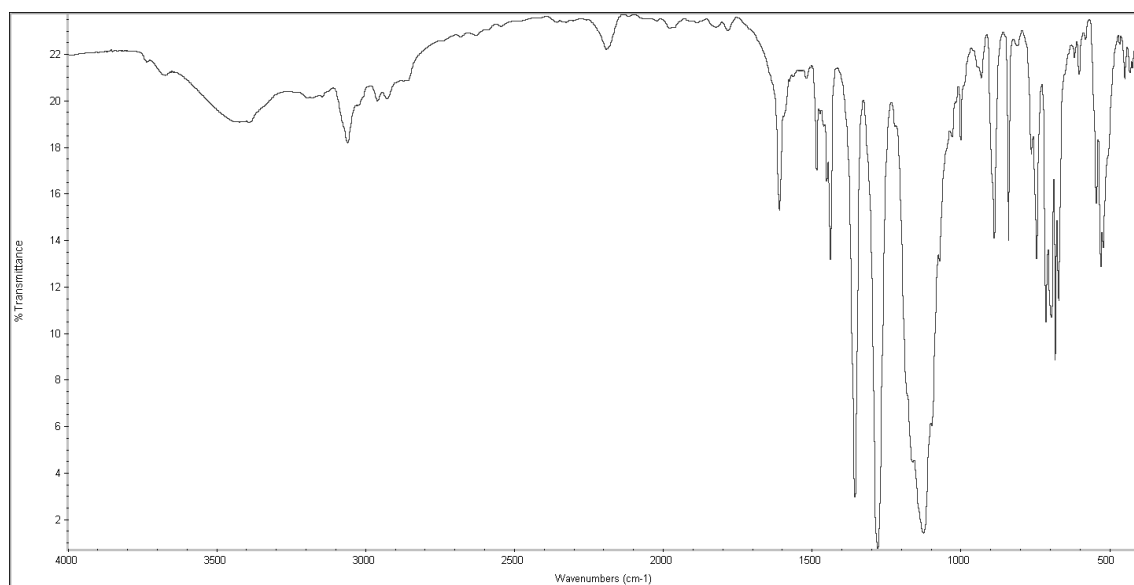
Figure A. 23 IR Spectrum of complex 28
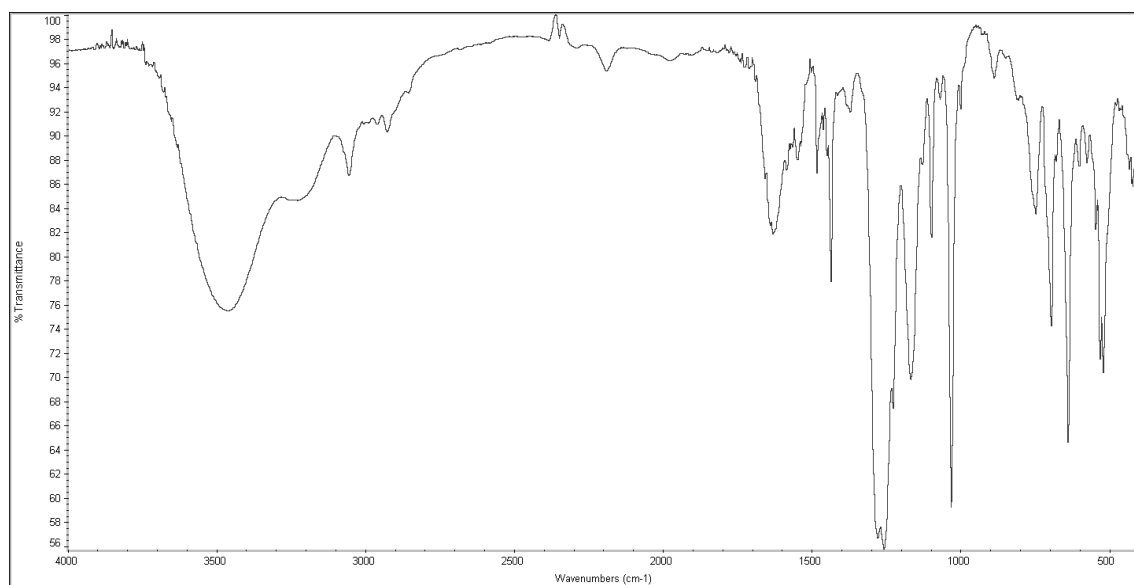
Figure A. 24 IR Spectrum of complex 29
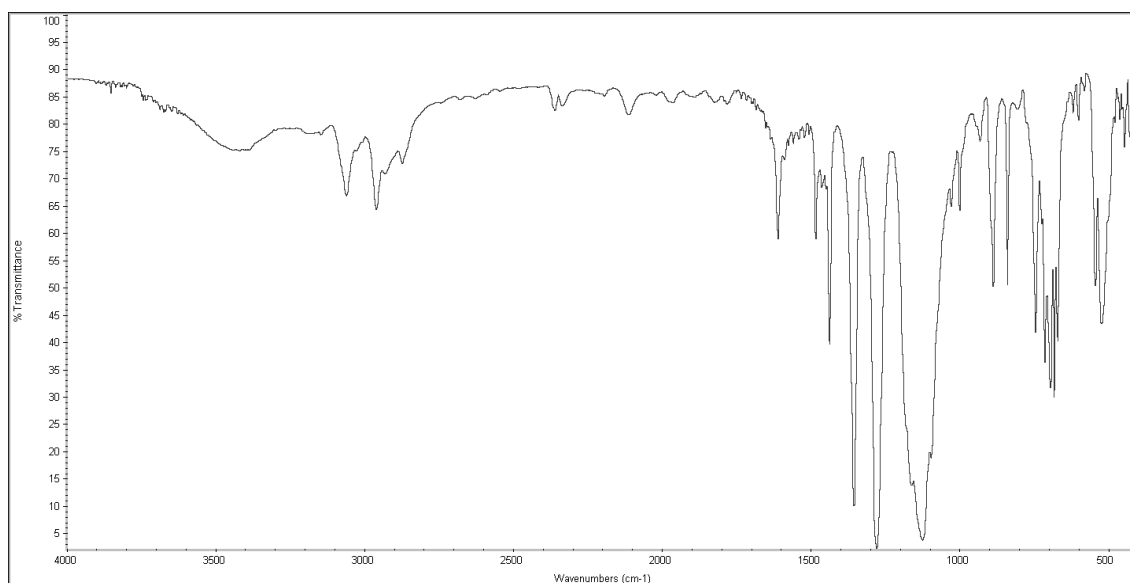
Figure A. 25 IR Spectrum of complex 30
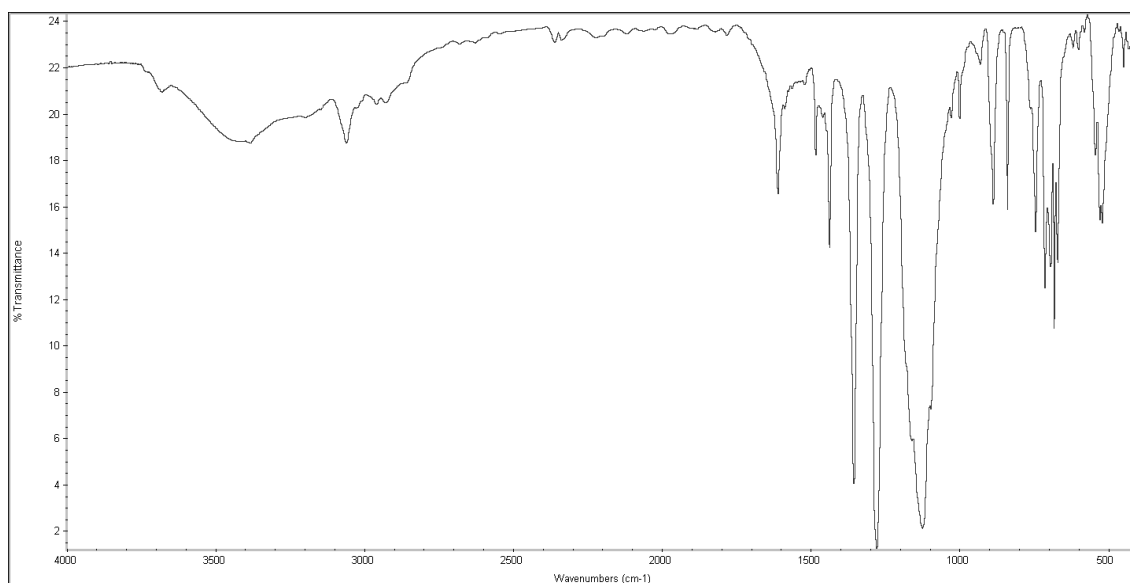
Figure A. 26 IR Spectrum of complex 31
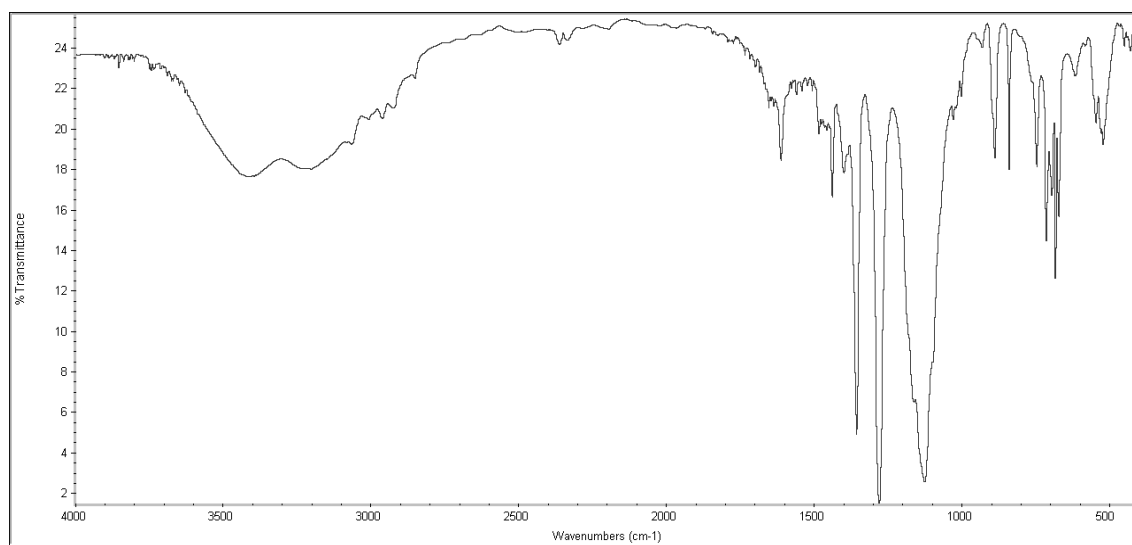
Figure A. 27 IR Spectrum of complex 32
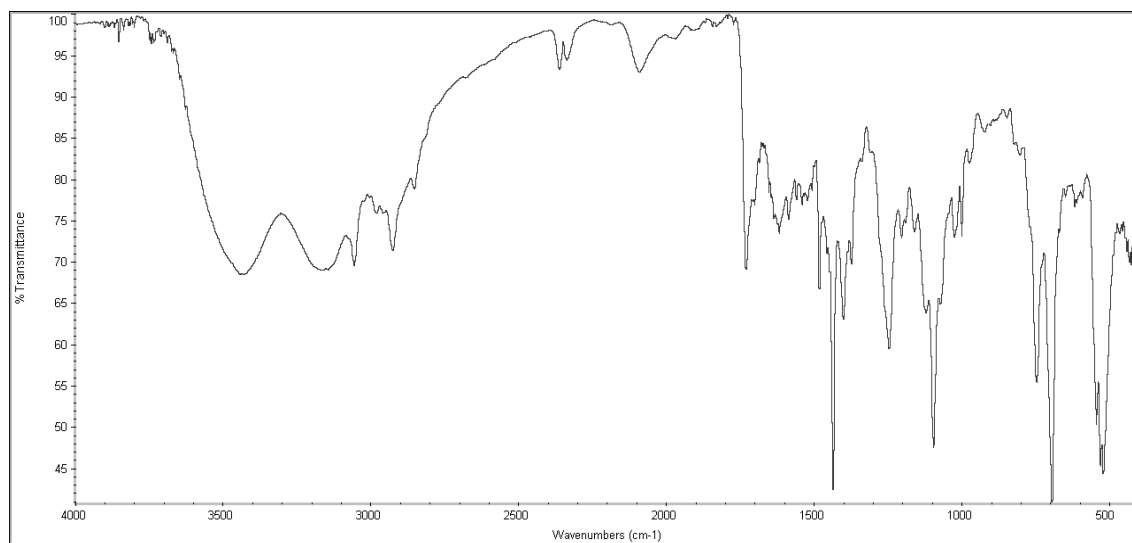
Figure A. 28 IR Spectrum of complex 34
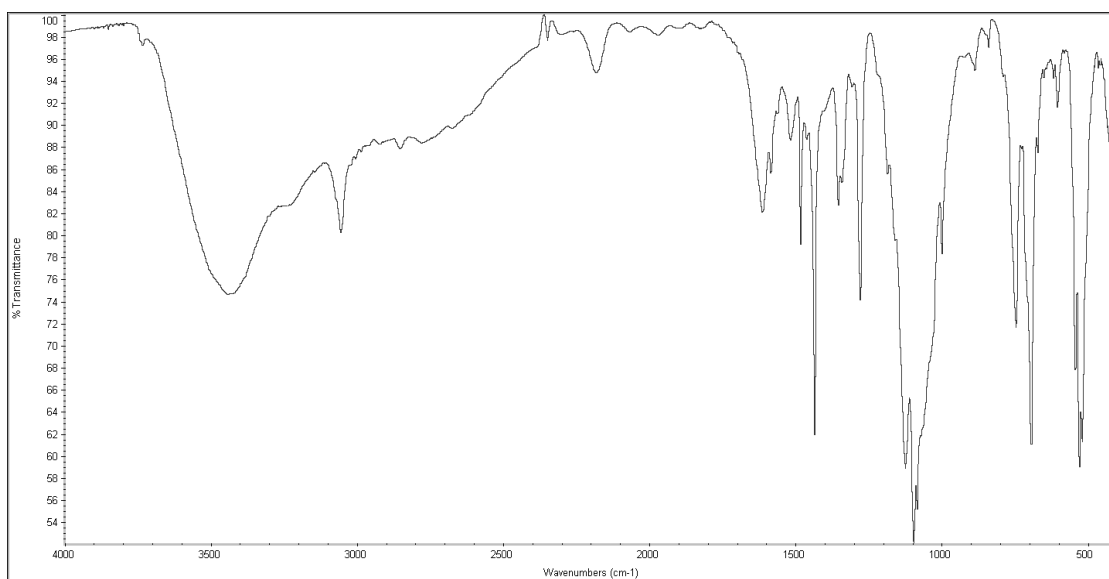
Figure A. 29 IR Spectrum of complex 35
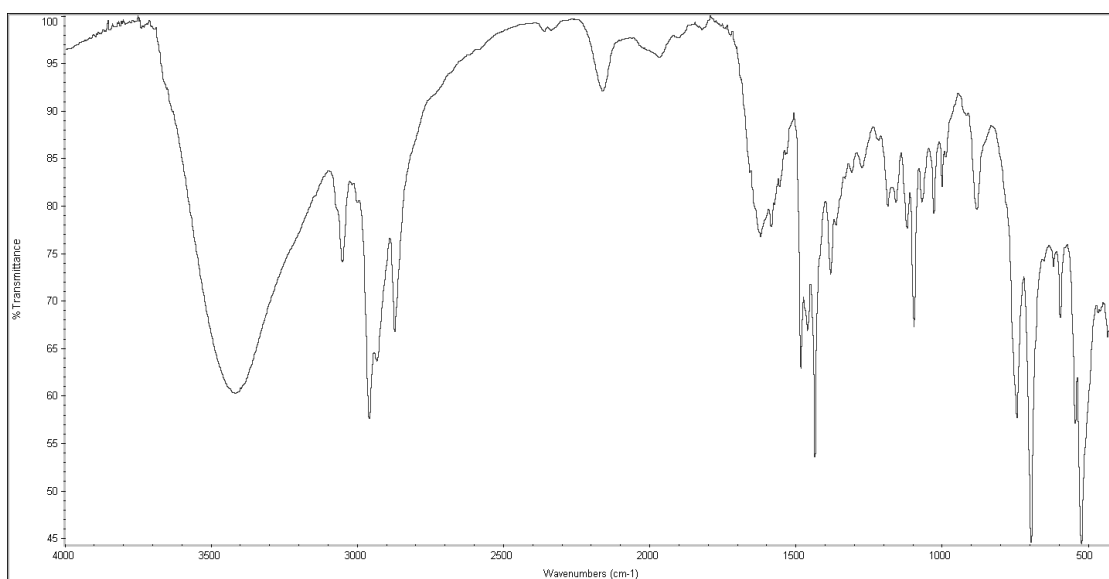
Figure A. 30 IR Spectrum of complex 36
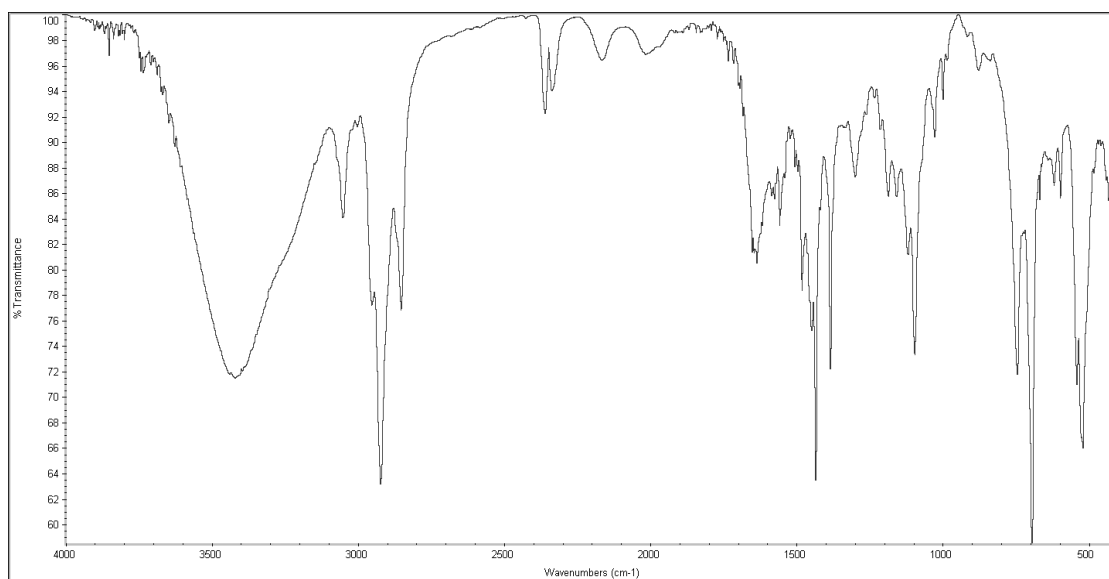
Figure A. 31 IR Spectrum of complex 38
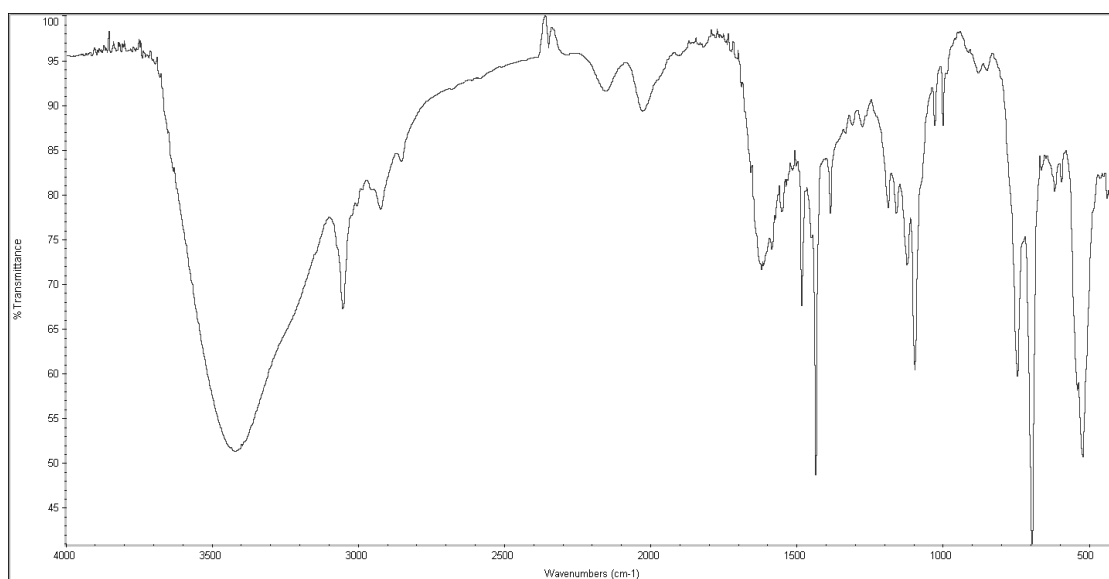
Figure A. 32 IR Spectrum of complex 39
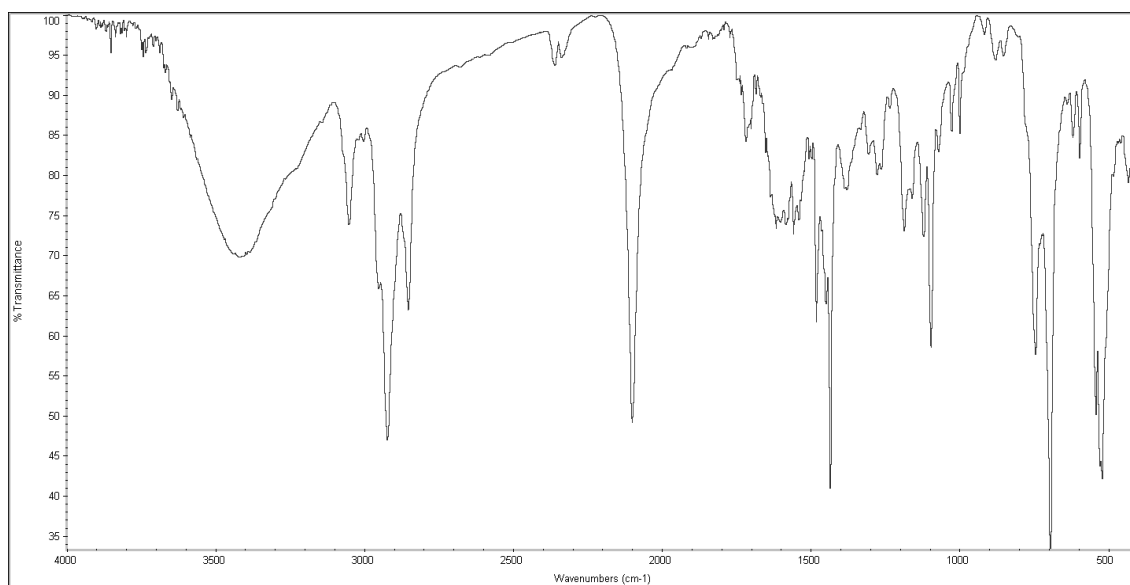
Figure A. 33 IR Spectrum of complex 40

Annex B

NMR spectroscopy

Chapter 2

Complex 4
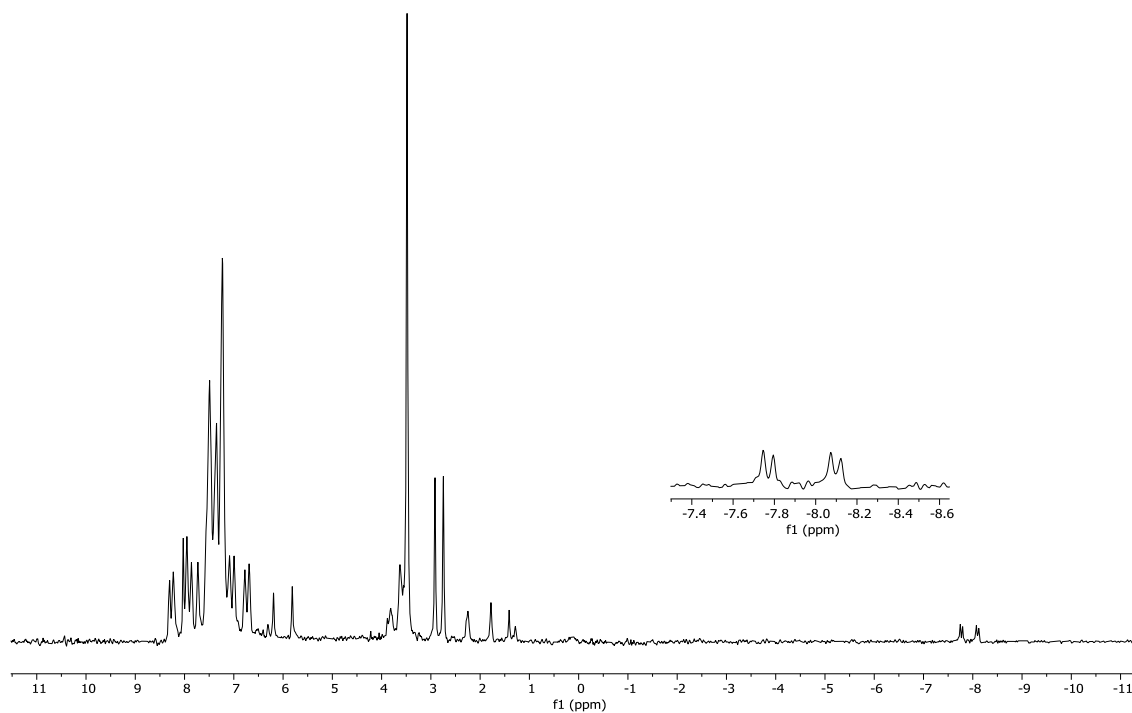
Figure B. 1 ^{1}H NMR of complex 4 in DMF-d^{7}
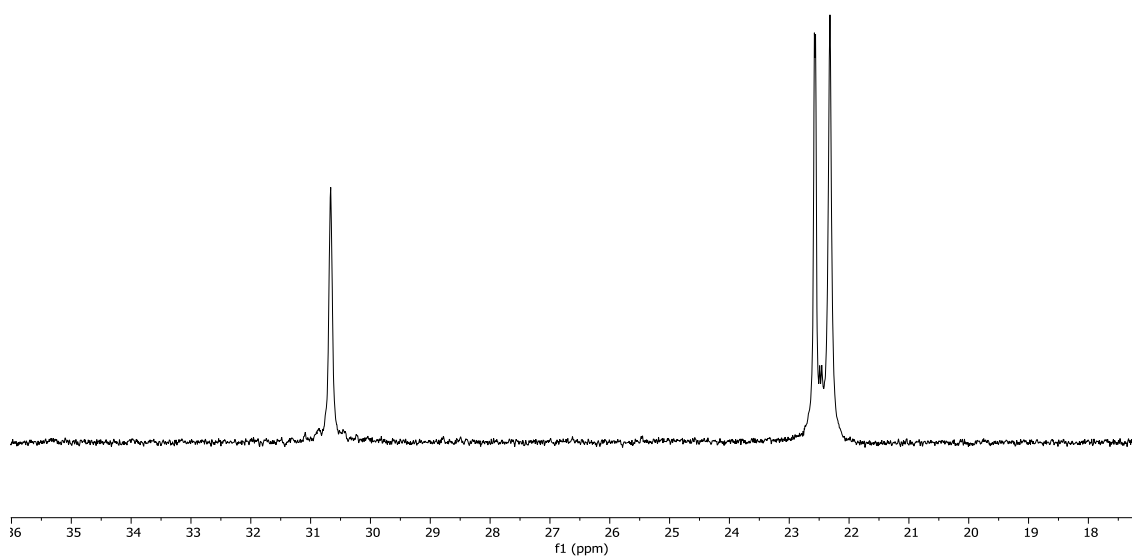
Figure B. 2 ^{31}P NMR of complex 4 in DMF-d^{7}
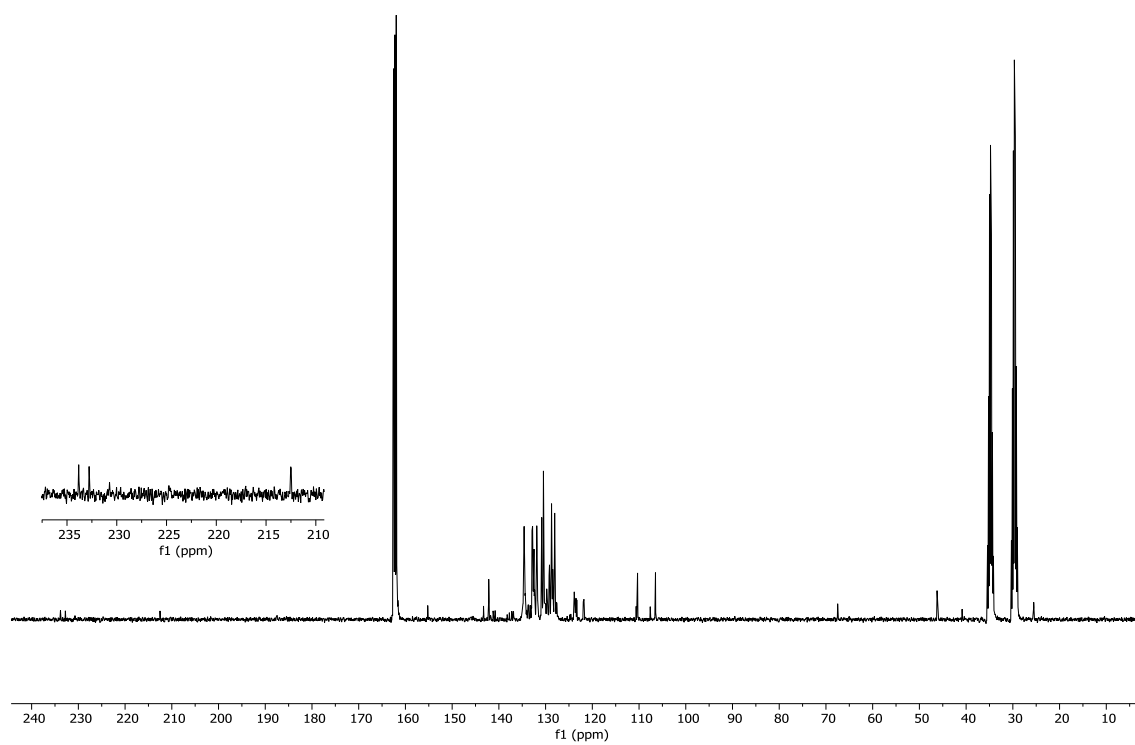
Figure B. 3 ^{13}C{^{1}H} NMR of complex 4 in DMF-d^7
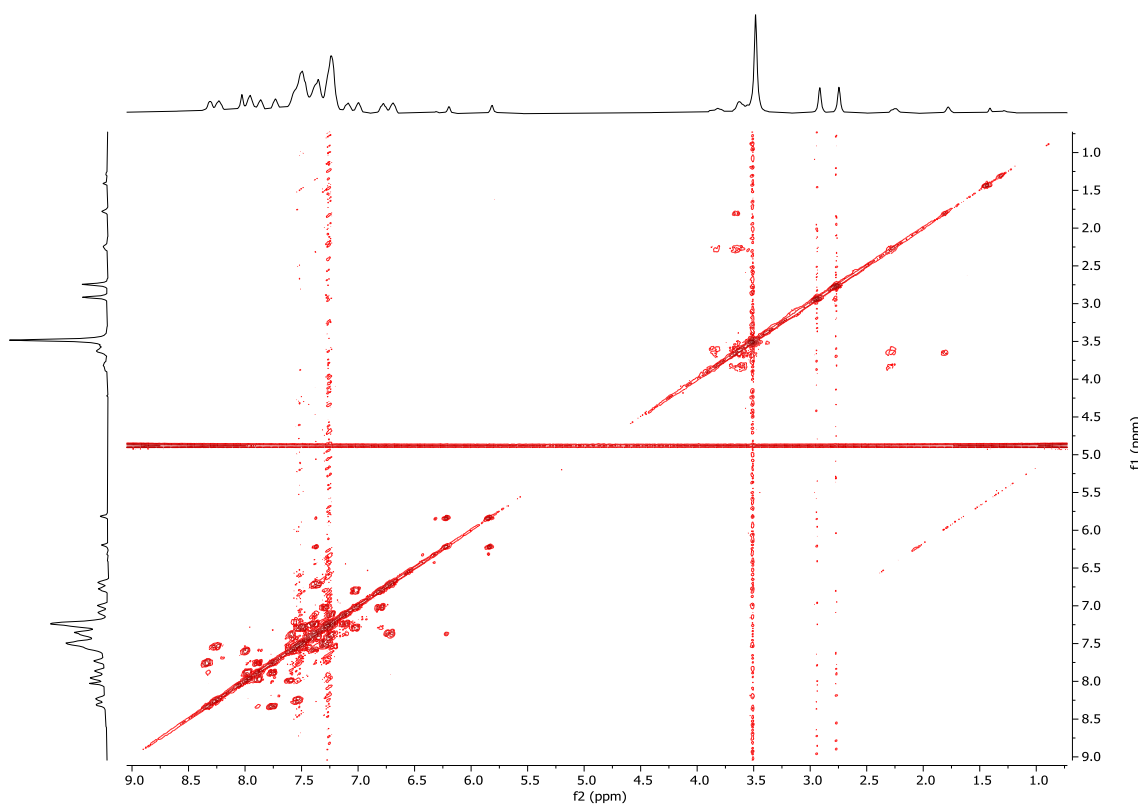
Figure B. 4 COSY spectrum of complex 4 in DMF-d^7

Complex 5
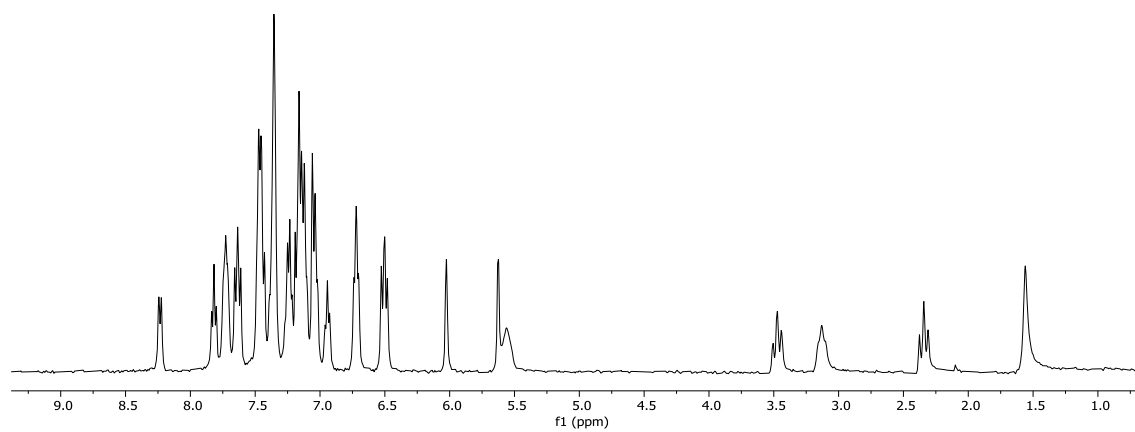
Figure B. 5 ^{1}H NMR of complex 5 in CDCl$_3$
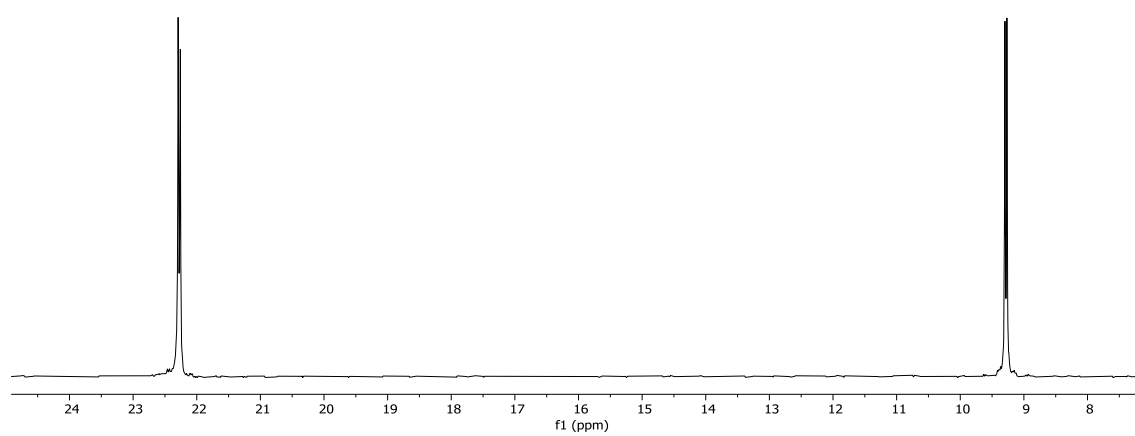
Figure B. 6 ^{31}P{^{1}H} NMR of complex 5 in CDCl$_3$
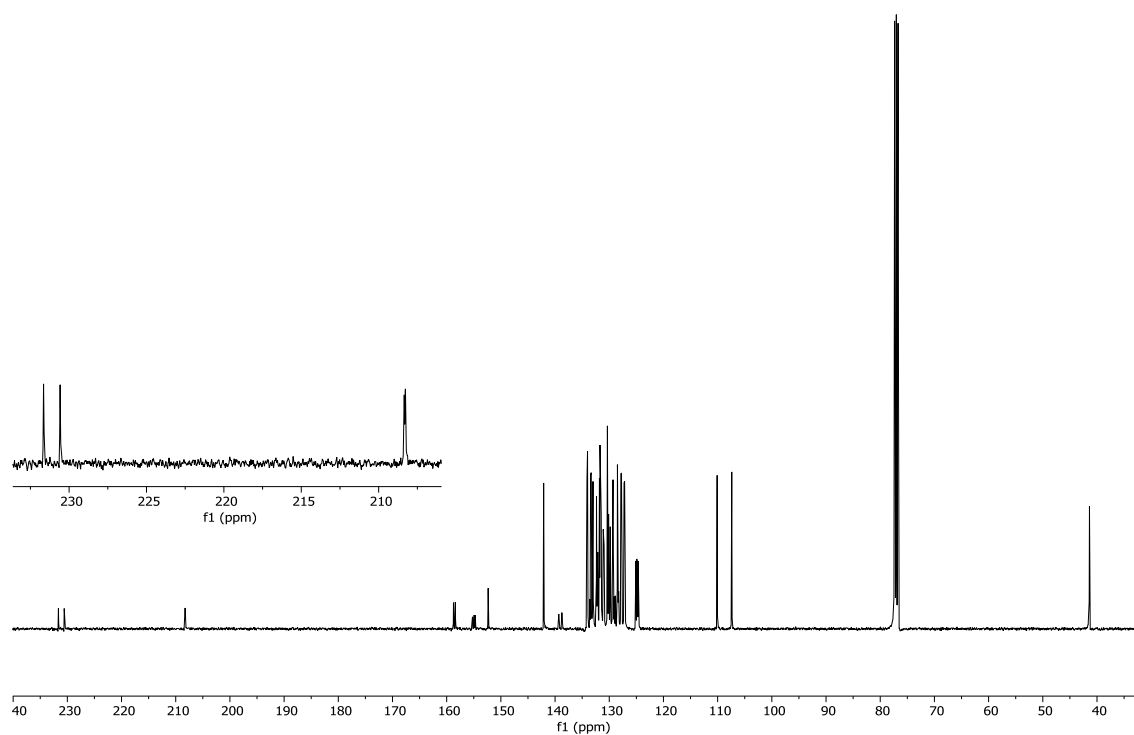
Figure B. 7 ^{13}C{^{1}H} NMR of complex 5 in CDCl$_3$
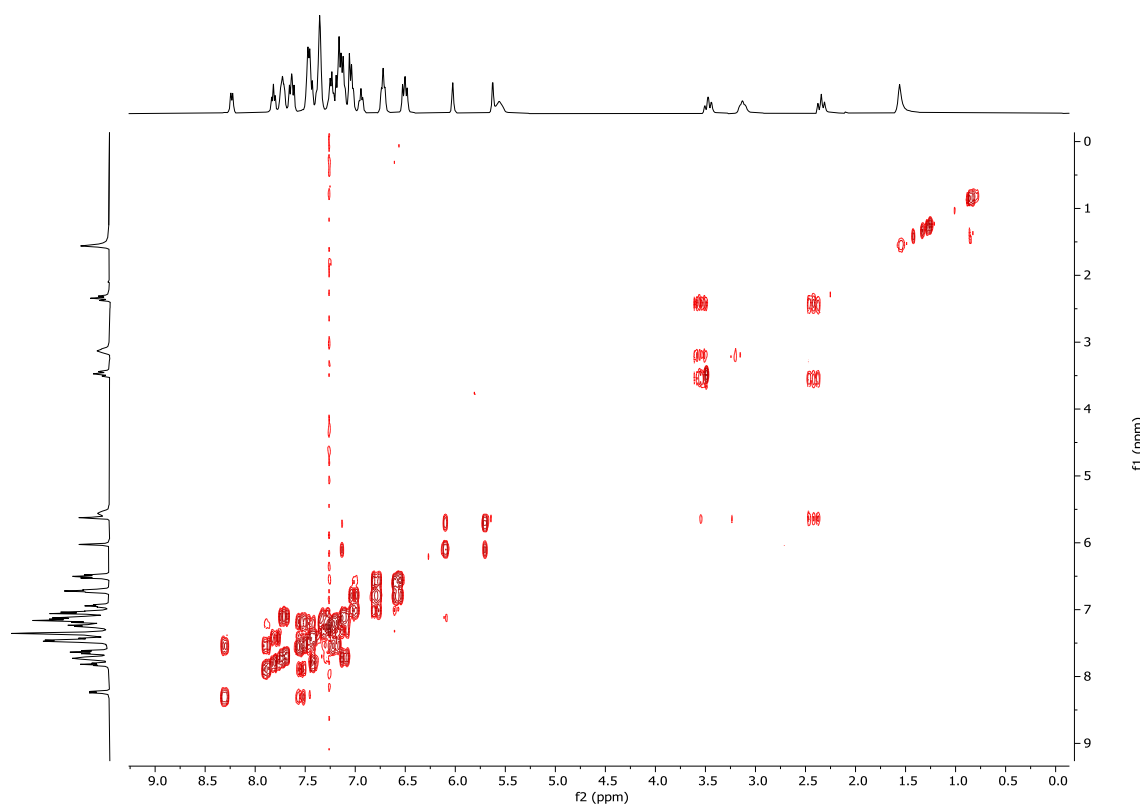
Figure B. 8 COSY spectrum of complex 5 in CDCl$_3$
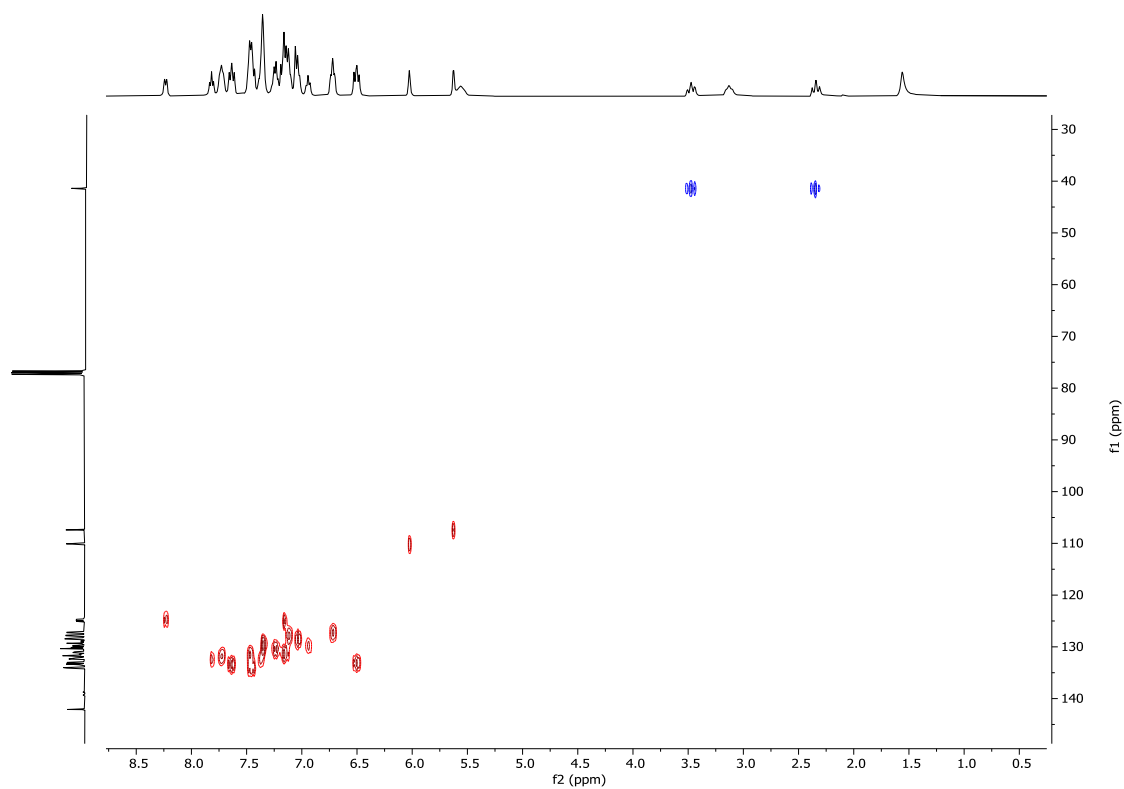
Figure B. 9 ^{1}H-^{13}C HSQC spectrum of complex 5 in CDCl$_3$
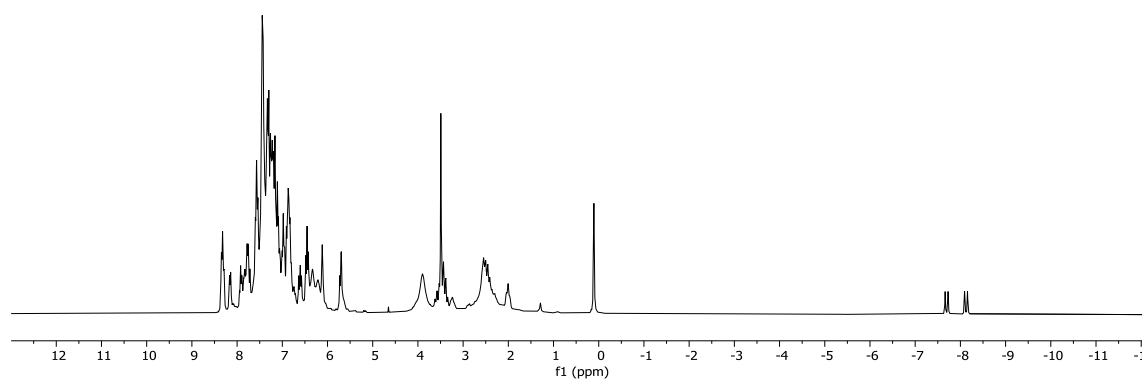
Figure B. 10 ^{1}H NMR of mixture of complexes 4 and 5 in CDCl$_3$
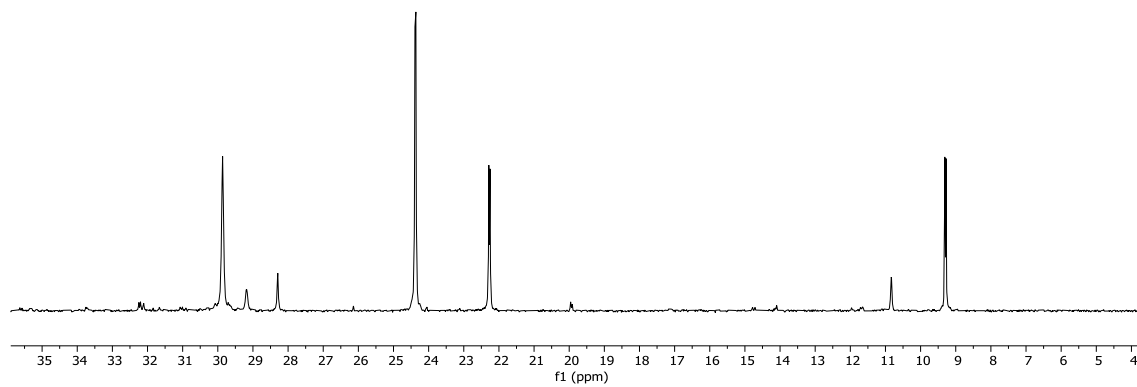
Figure B. 11 ^{31}P NMR of mixture of complexes 4 and 5 in CDCl$_3$

Complex 6
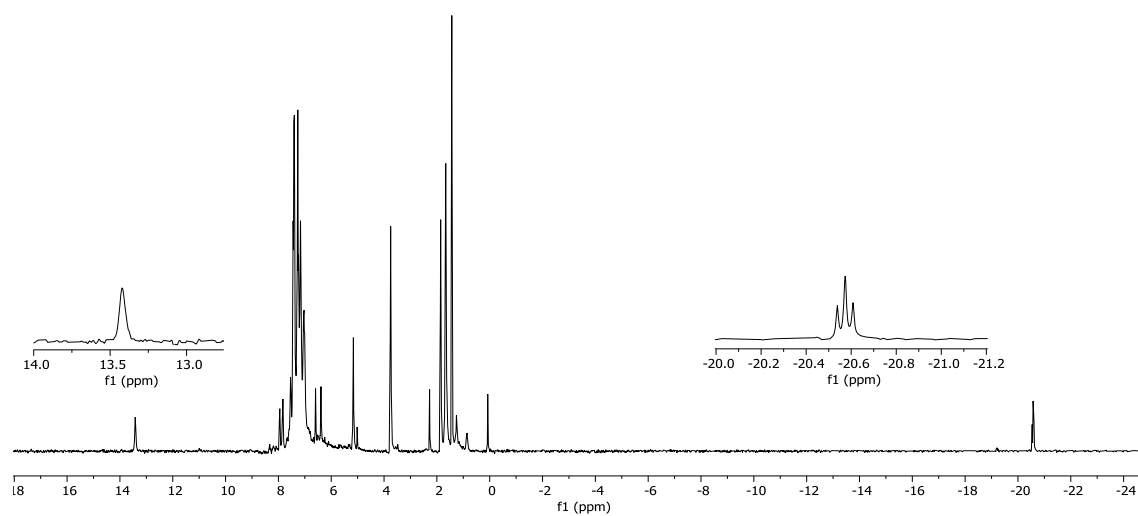
Figure B. 12 ^{1}H NMR of complex 6 in CDCl$_3$
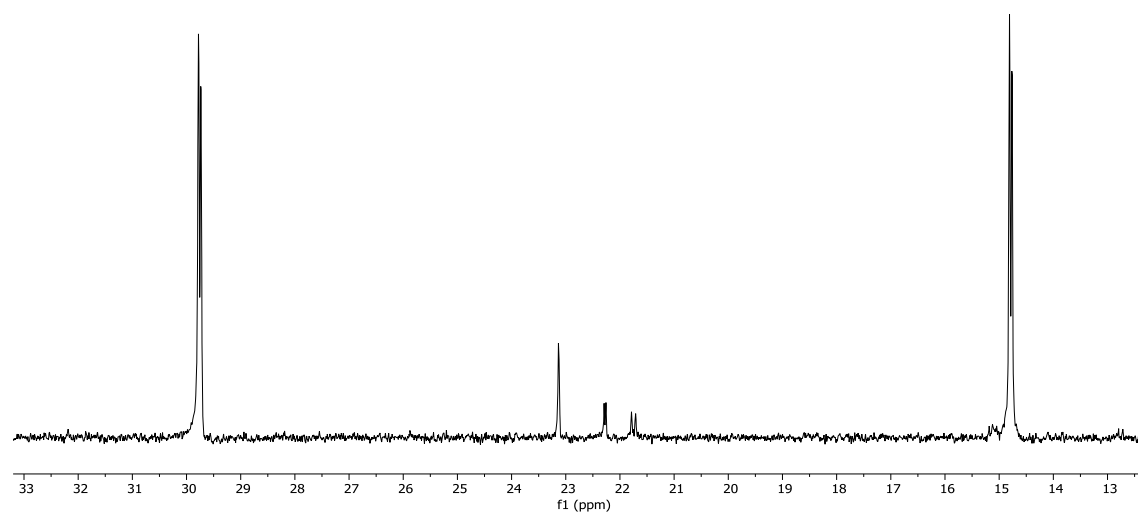
Figure B. 13 ^{31}P{^{1}H} NMR of complex 6 in CDCl$_3$
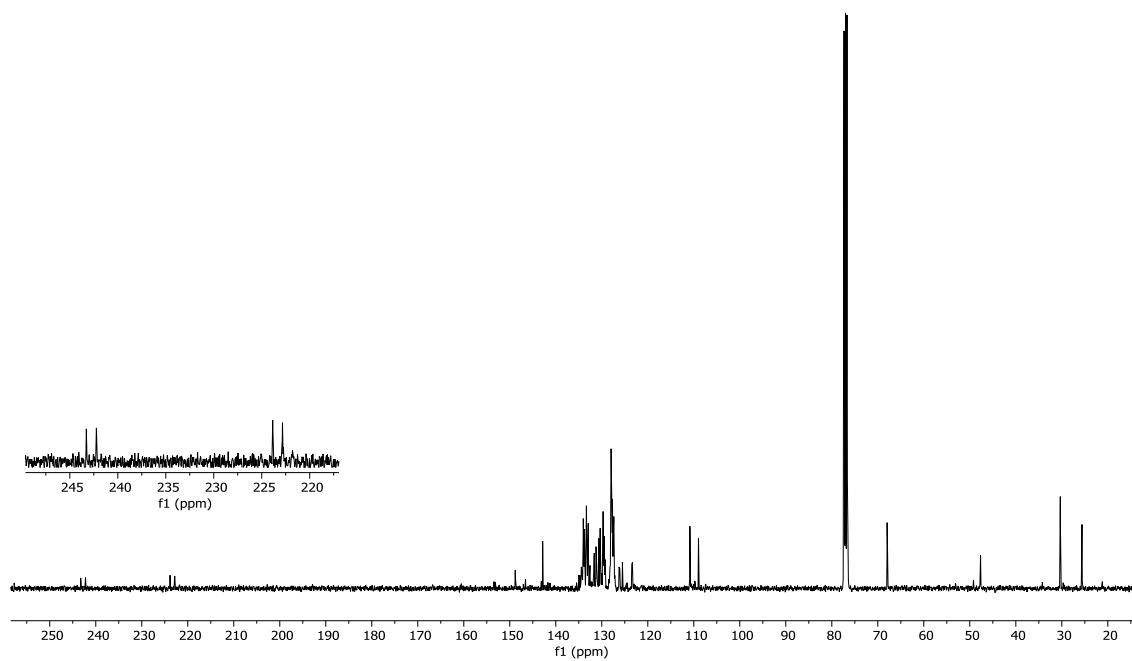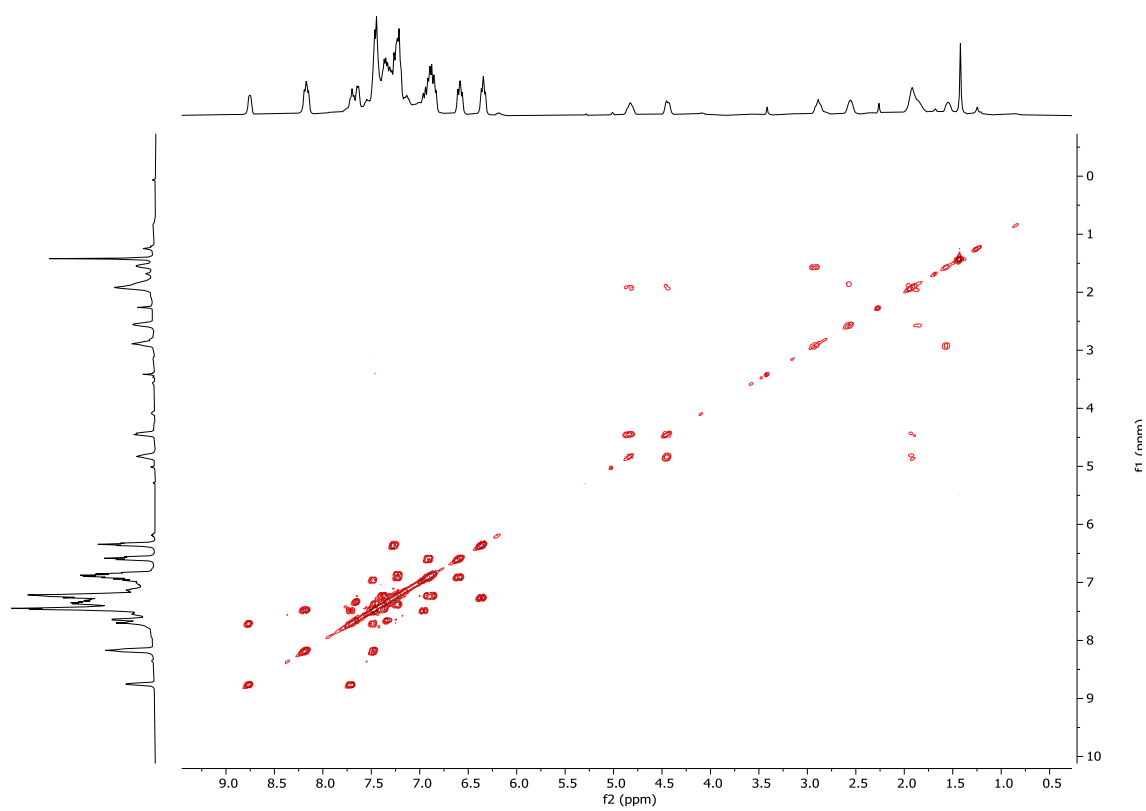
Figure B. 14 ^{13}C{^{1}H} NMR of complex 6 in CDCl$_3$
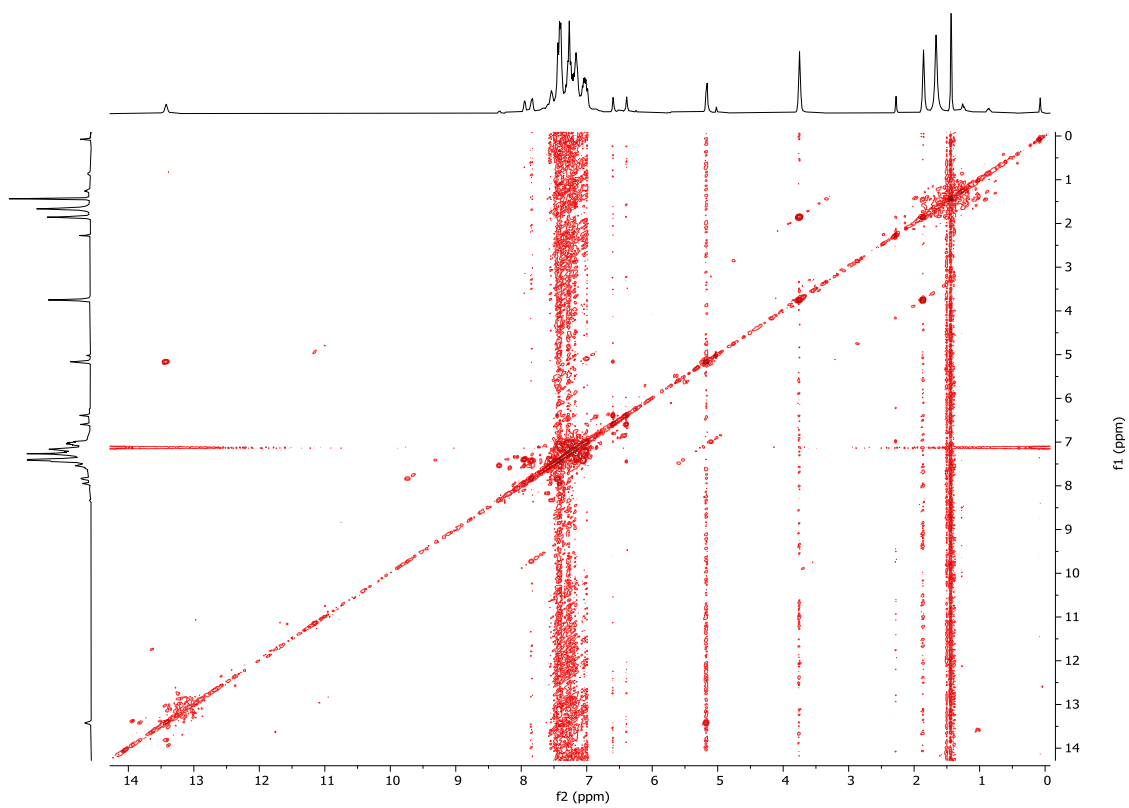
Figure B. 15 COSY spectrum of complex 6 in CDCl$_3$
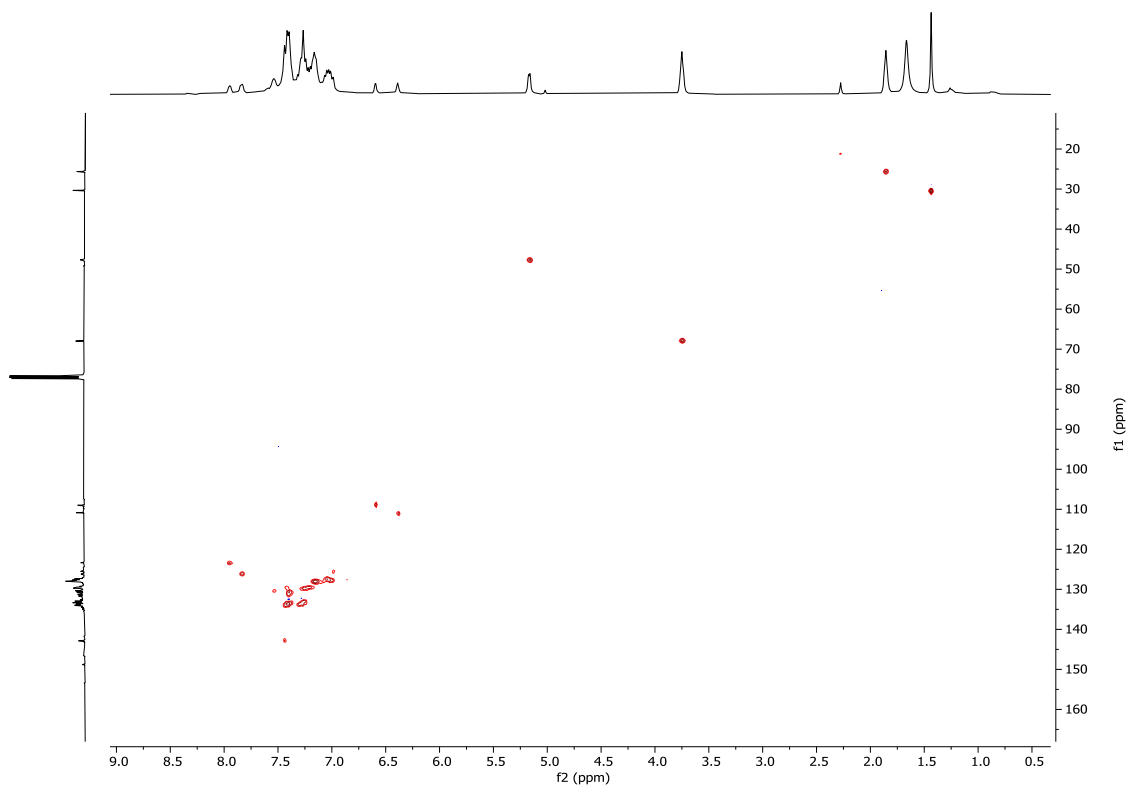
Figure B. 16 ^{1}H-^{13}C HSQC spectrum of complex 6 in CDCl$_3$

Catalysis
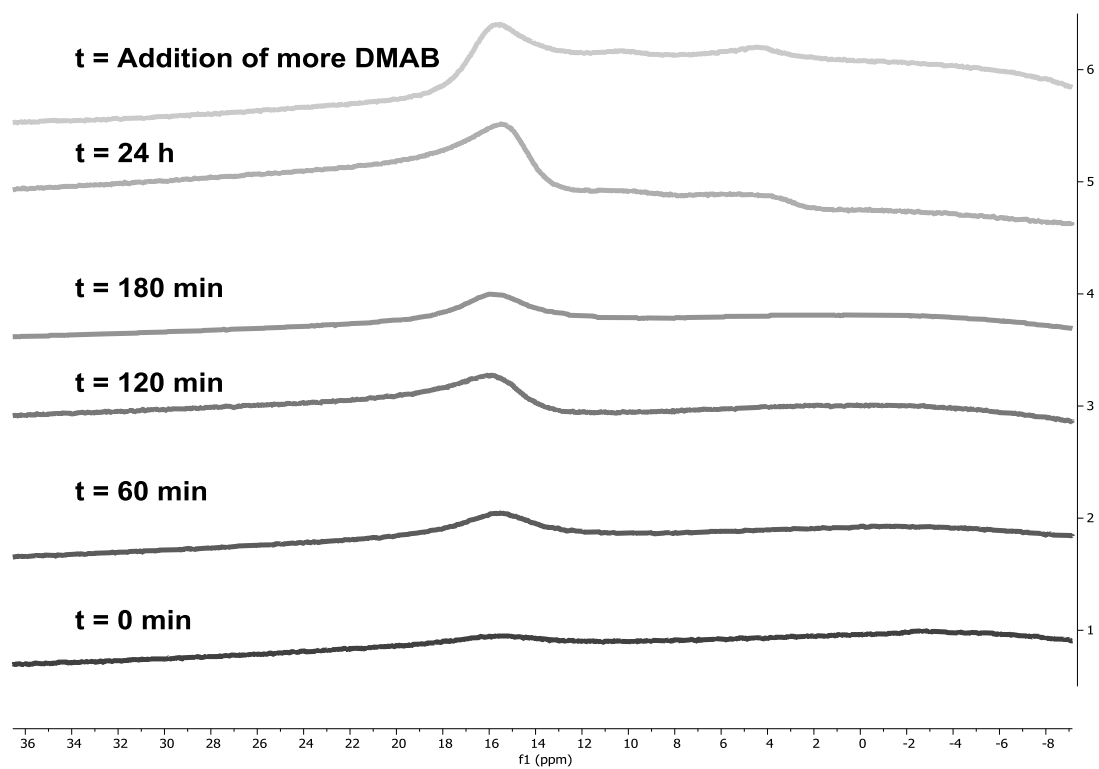
Figure B. 17 Appearance of borates in the [11]B spectra in the hydrolysis of DMAB by 4 in a THF-d[8]/D$_2$O 60/40 mixture

Chapter 3

Complex 9
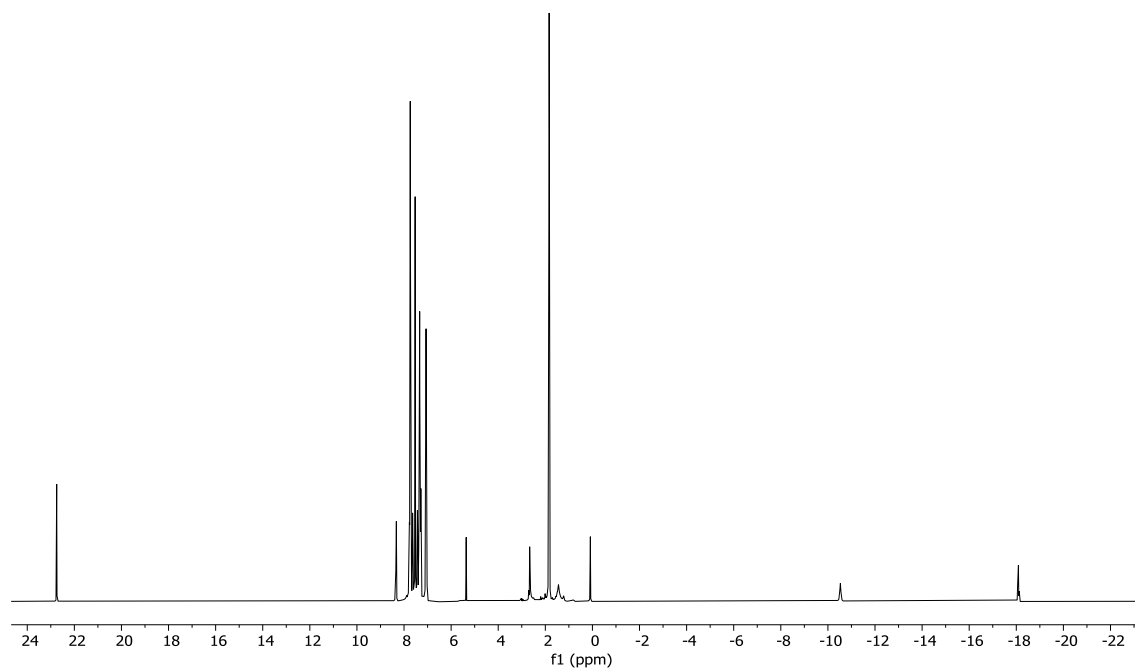
Figure B. 18 ^{1}H NMR of complex 9 in CDCl$_3$ at 213 K
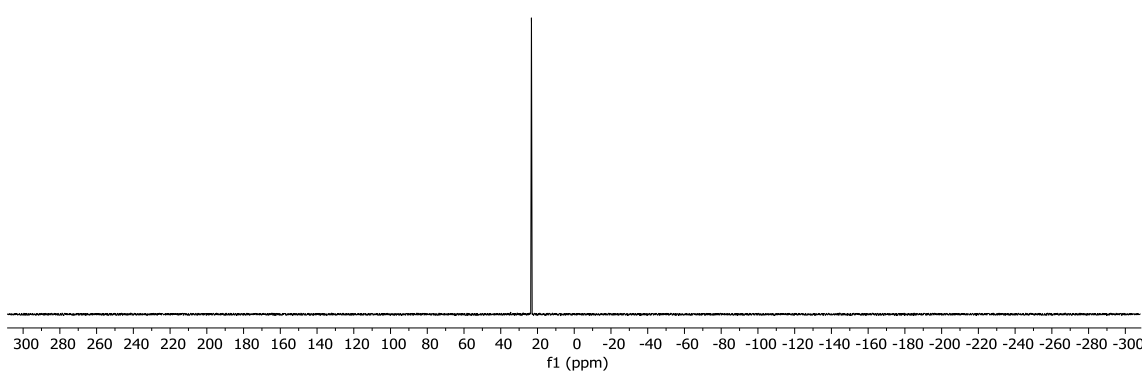
Figure B. 19 ^{31}P{^{1}H} NMR of complex 9 in CDCl$_3$
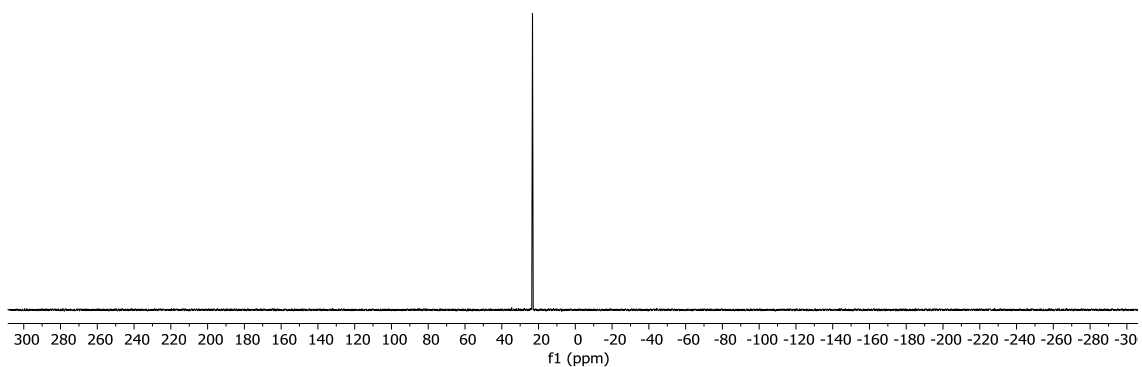
Figure B. 20 ^{11}B NMR of complex 9 in CDCl$_3$

Chapter 4

Complex 10
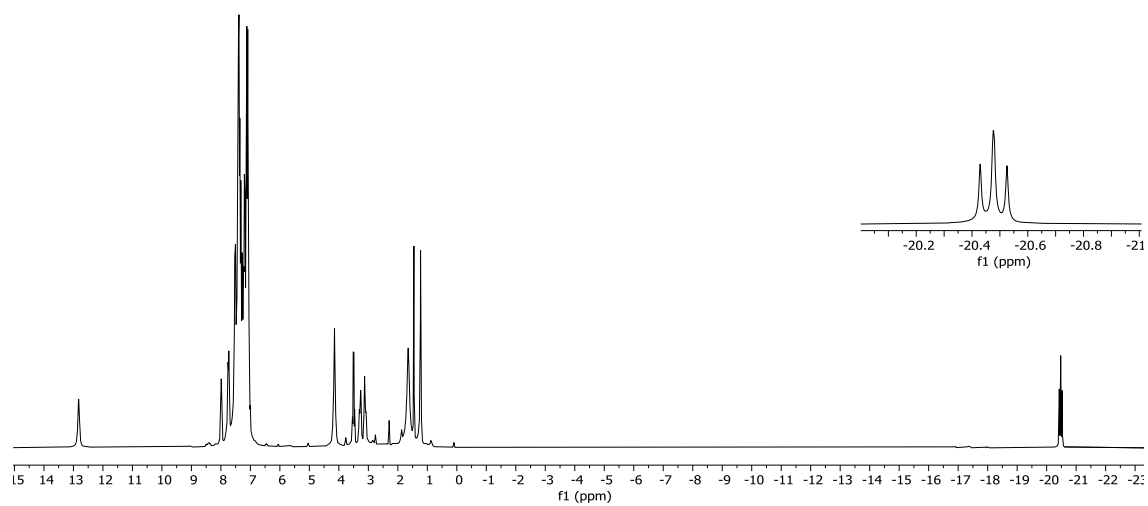
Figure B. 21 ¹H NMR of complex 10 in CDCl₃
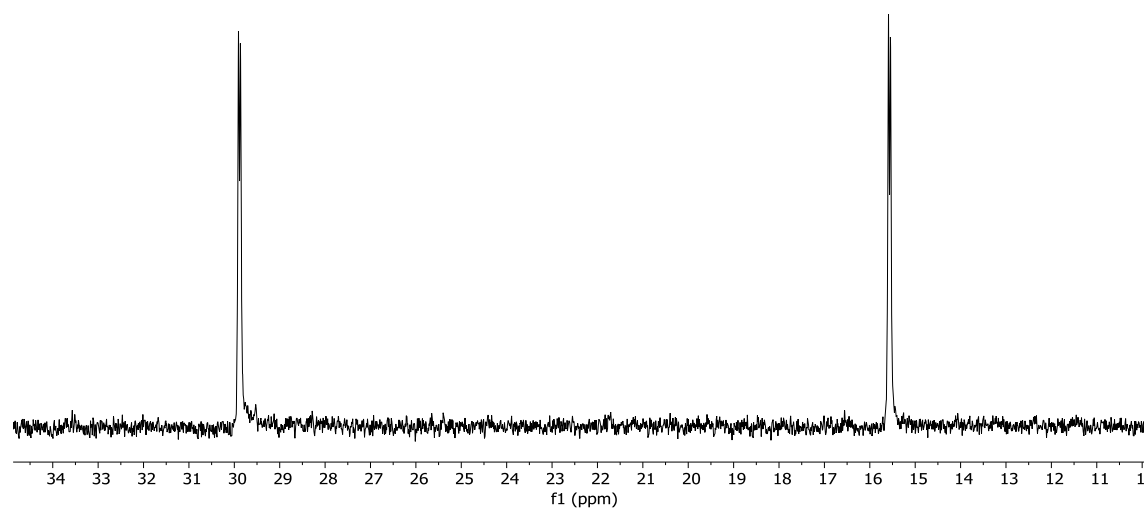
Figure B. 22 ³¹P{¹H} NMR of complex 10 in CDCl₃
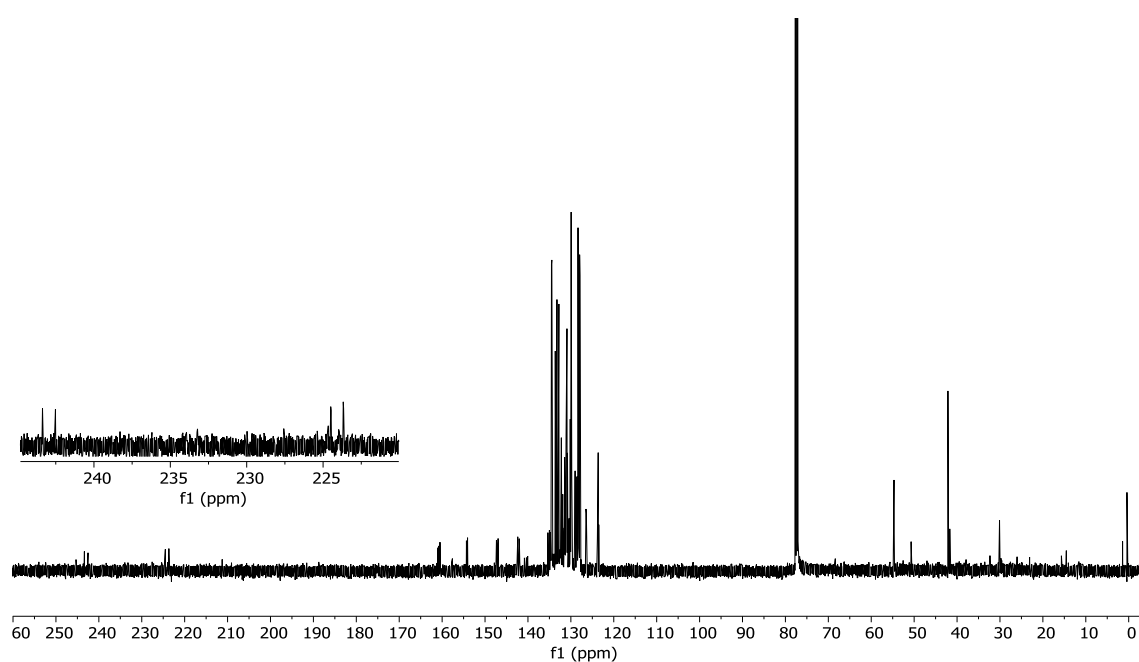
Figure B. 23 ^{13}C{^{1}H} NMR of complex 10 in CDCl$_3$
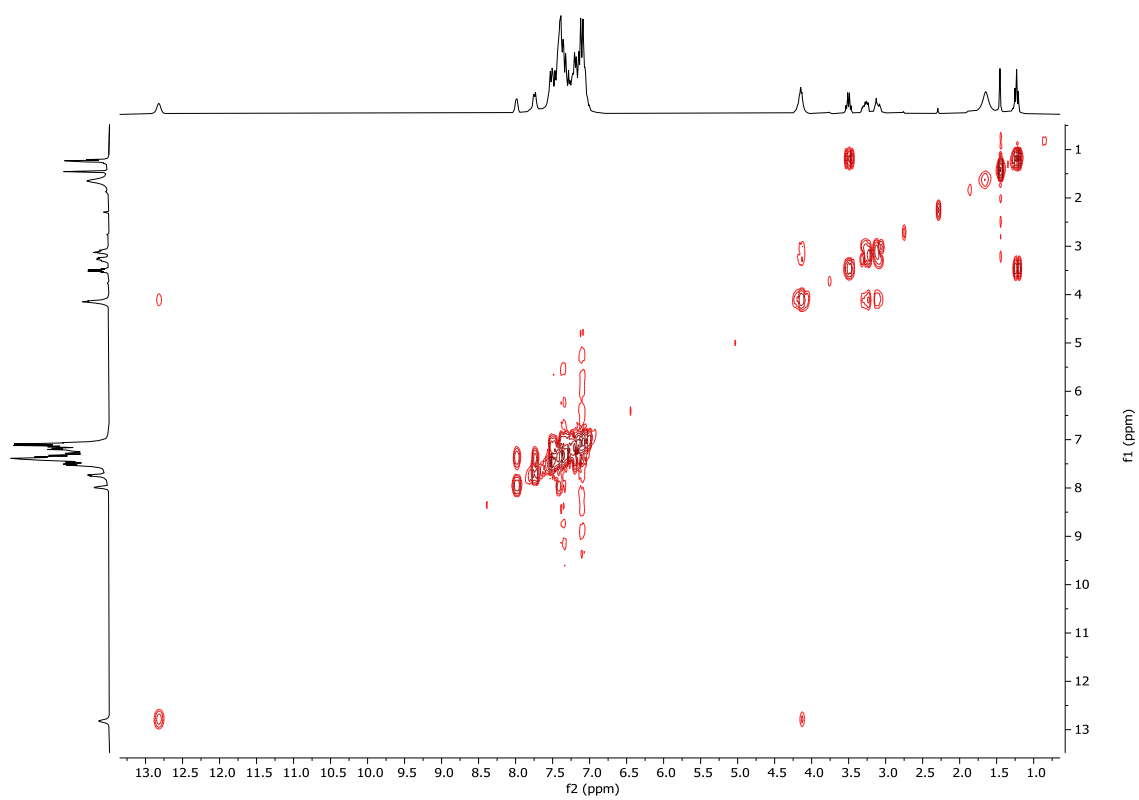
Figure B. 24 COSY spectrum of complex 10 in CDCl$_3$
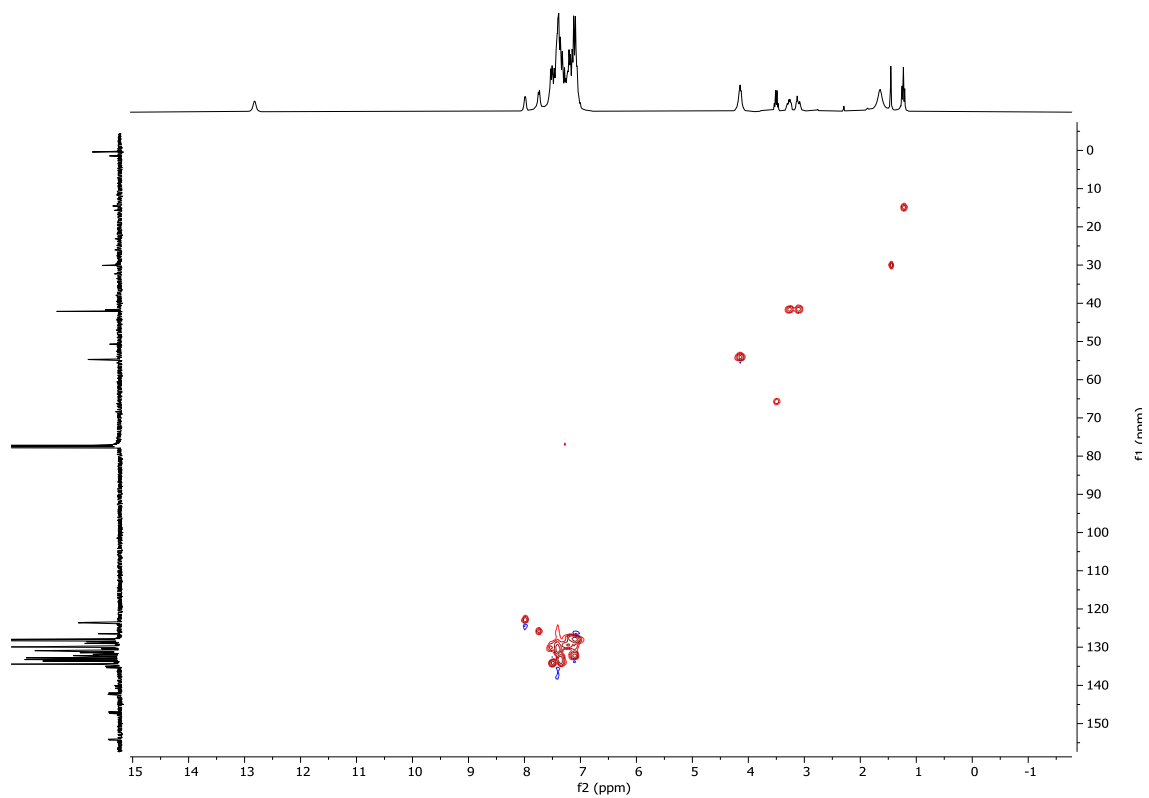
Figure B. 25 ^{1}H-^{13}C HSQC spectrum of complex 10 in CDCl$_3$

Complex 11
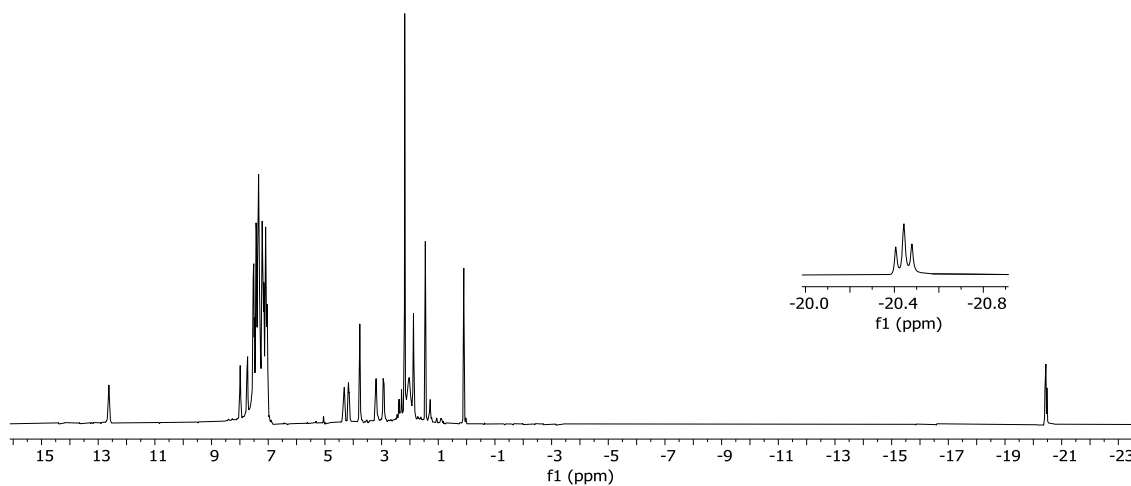
Figure B. 26 ^{1}**H NMR of complex 11 in CDCl$_3$**
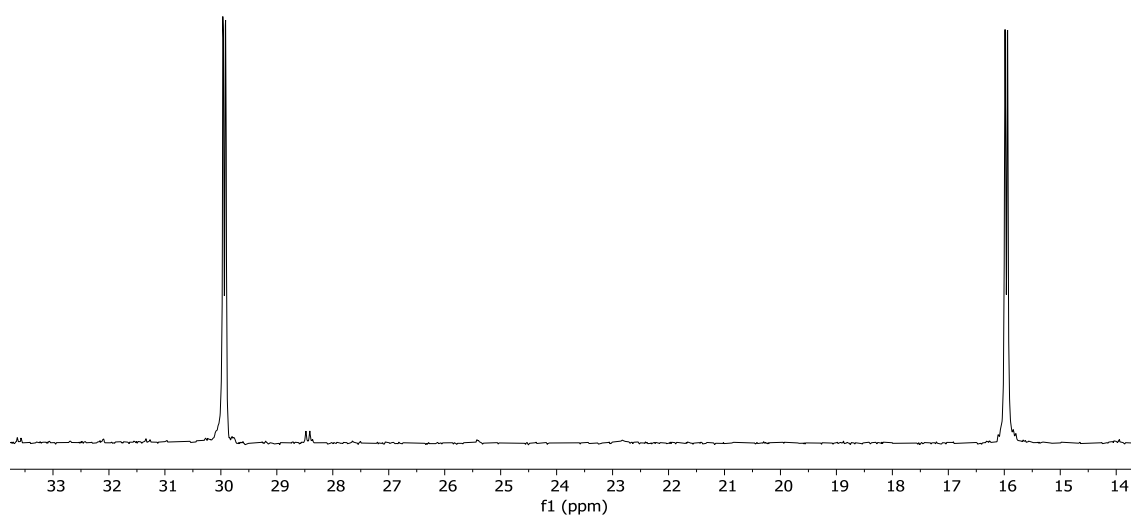
Figure B. 27 ^{31}**P{^{1}H} NMR of complex 11 in CDCl$_3$**
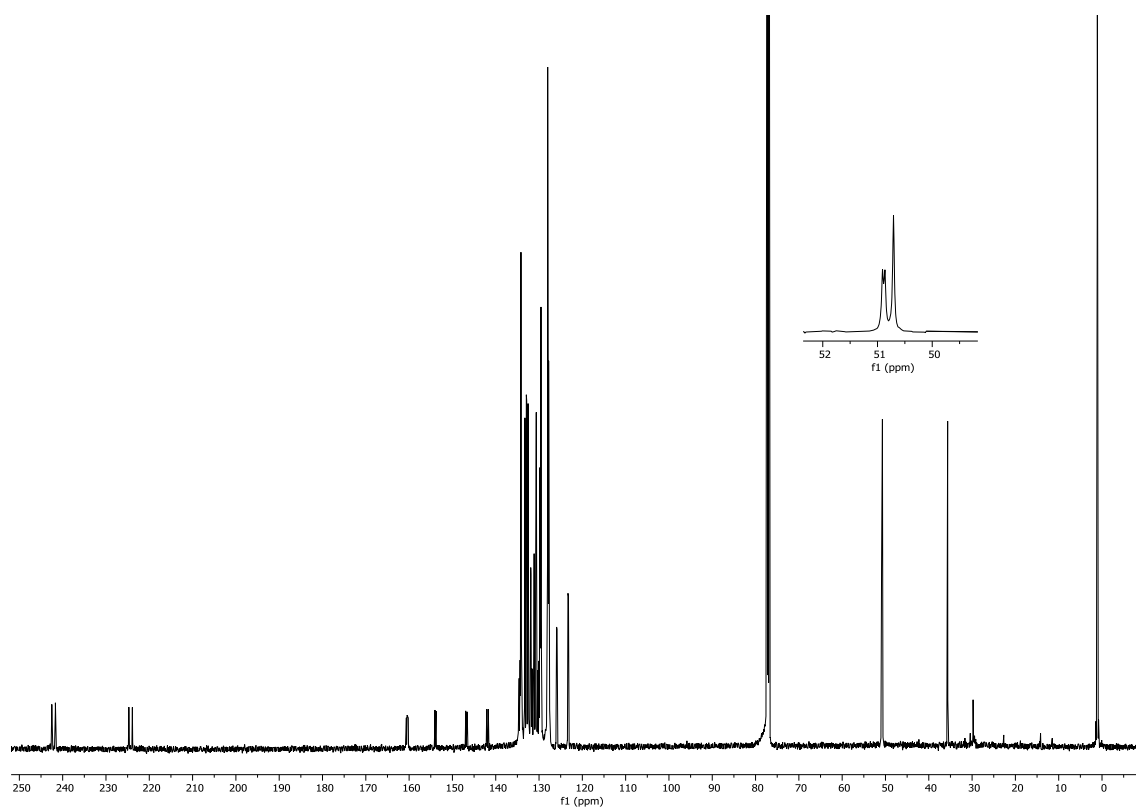
Figure B. 28 $^{13}C\{^1H\}$ NMR of complex 11 in CDCl$_3$
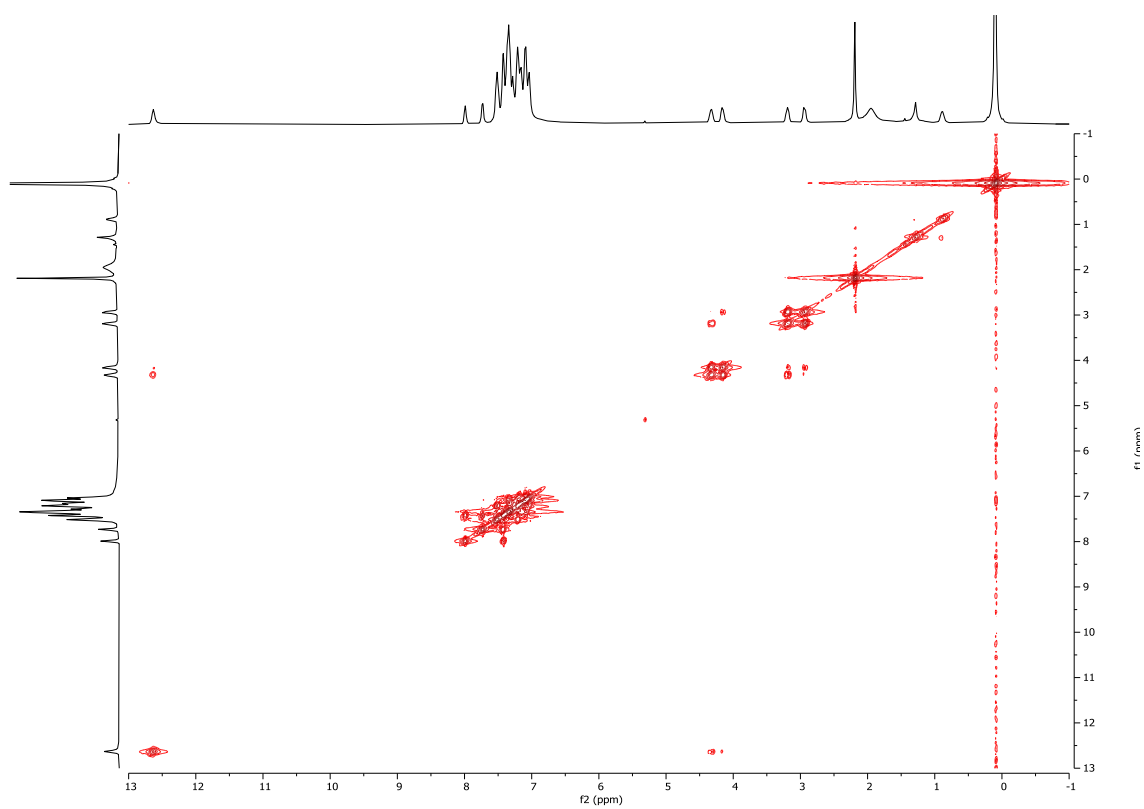
Figure B. 29 COSY spectrum of complex 11 in CDCl$_3$
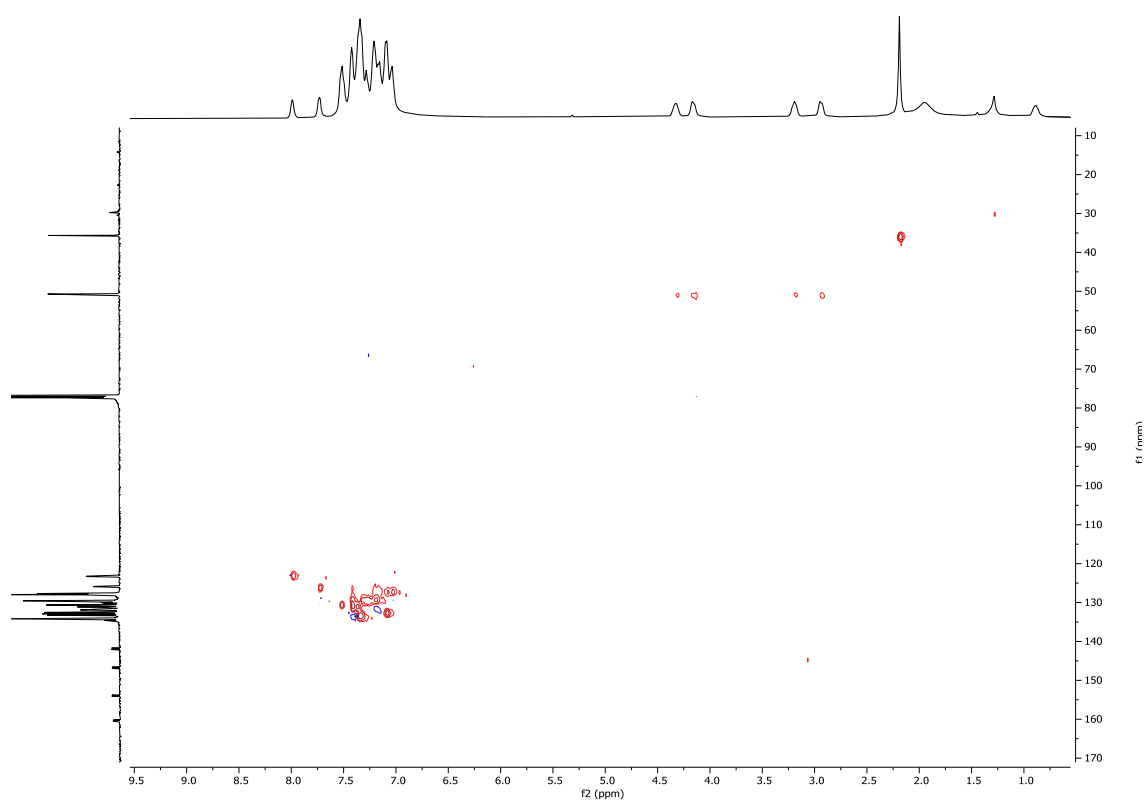
Figure B. 30 ^{1}H-^{13}C HSQC spectrum of complex 11 in CDCl$_3$

Complex 12
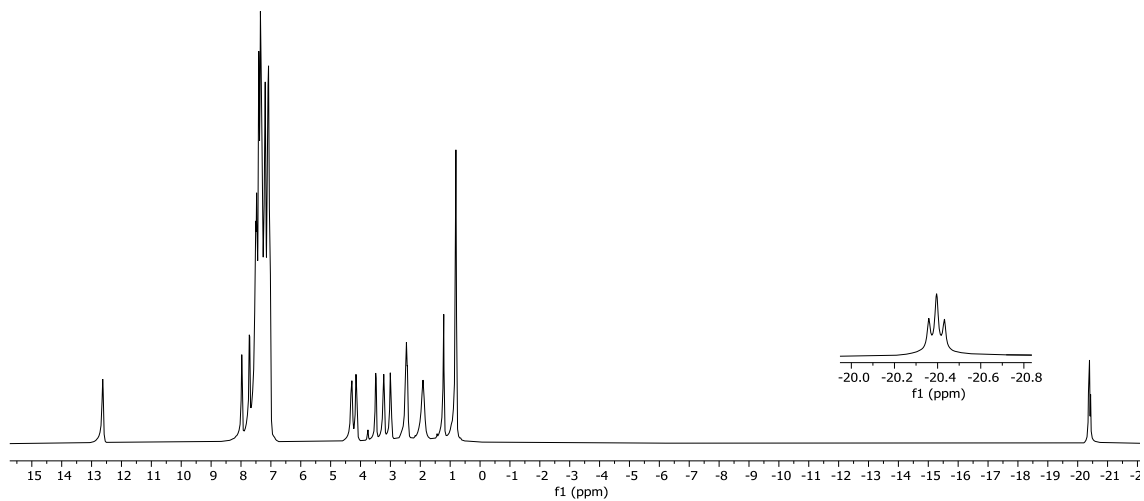
Figure B. 31 ¹H NMR of complex 12 in CDCl₃
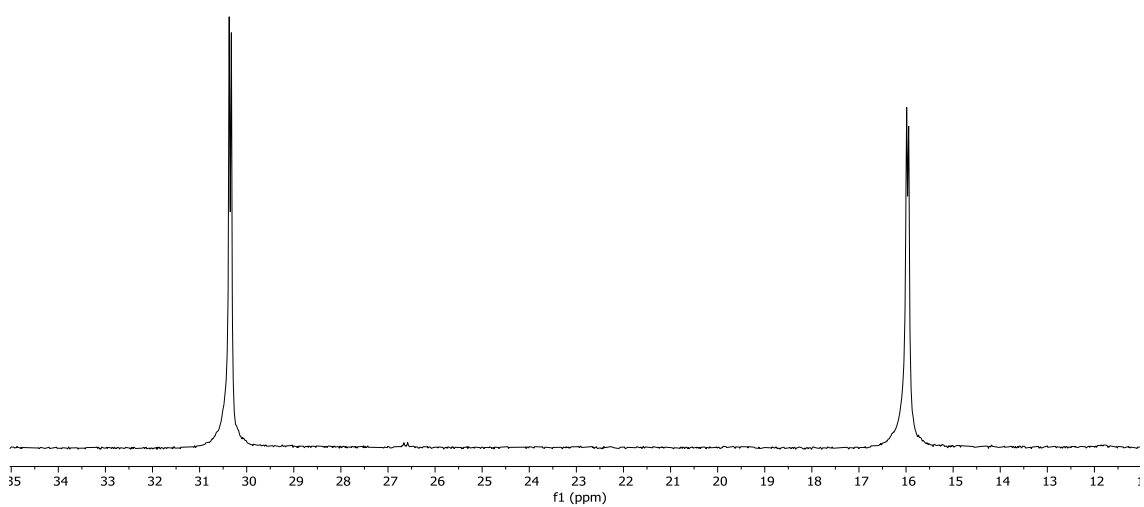
Figure B. 32 ³¹P{¹H} NMR of complex 12 in CDCl₃
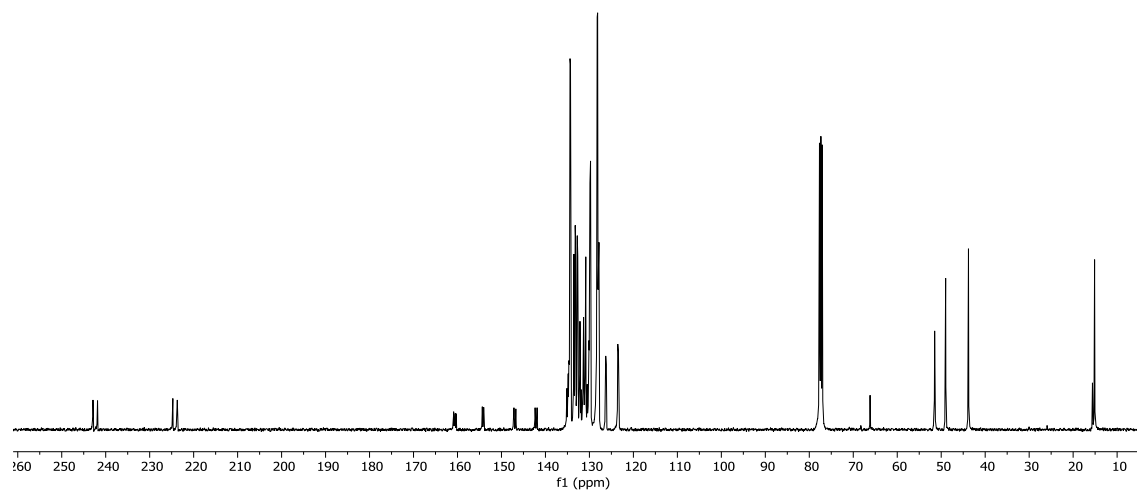
Figure B. 33 $^{13}C\{^{1}H\}$ NMR of complex 12 in CDCl$_3$
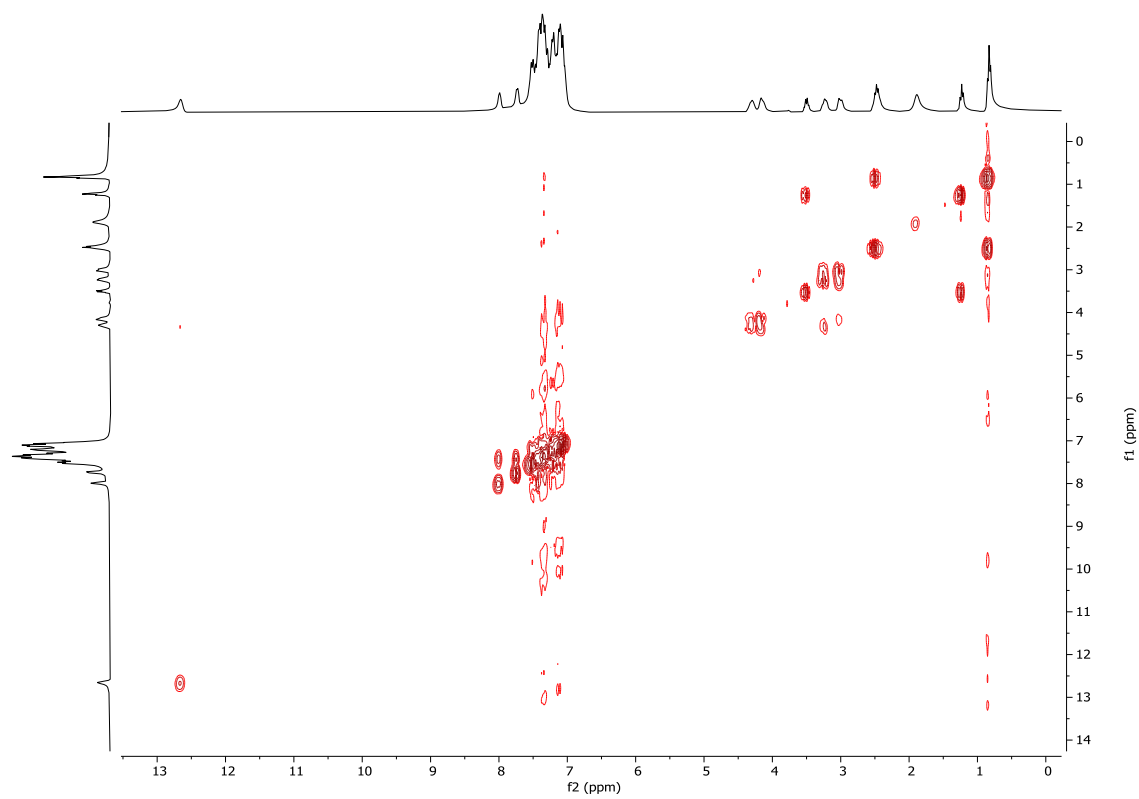
Figure B. 34 COSY spectrum of complex 12 in CDCl$_3$
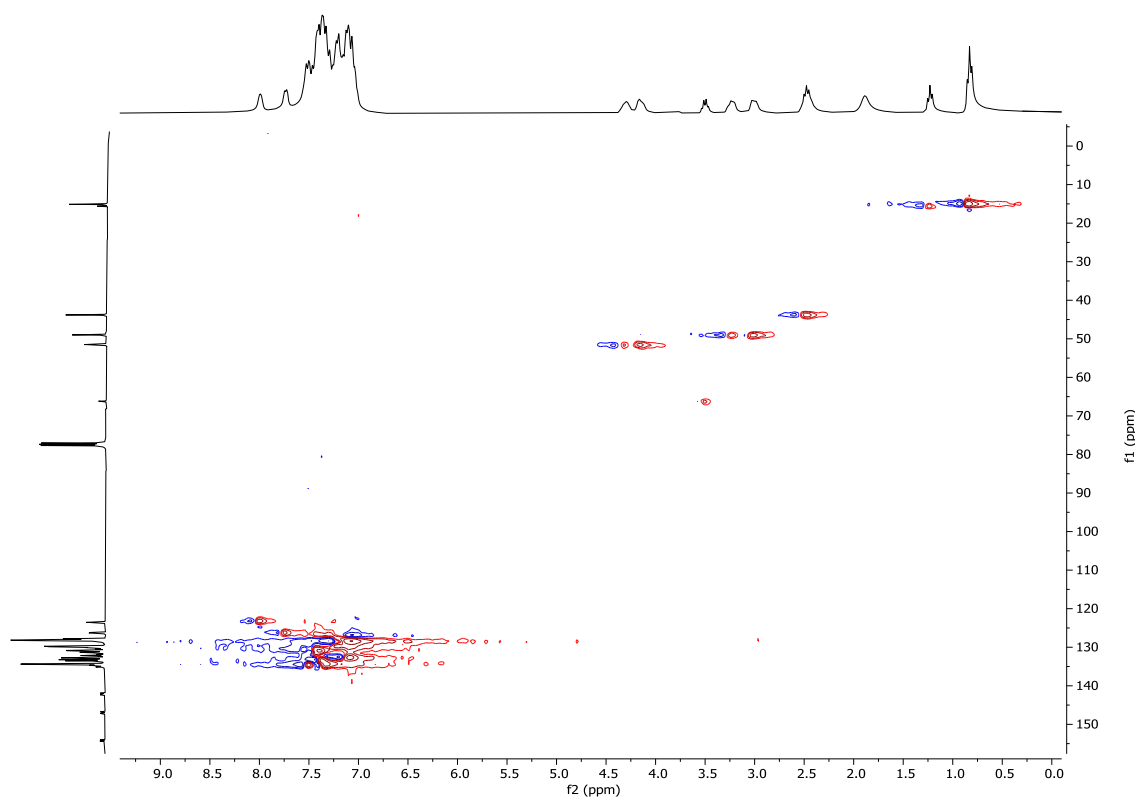
Figure B. 35 ^{1}H-^{13}C HSQC spectrum of complex 12 in CDCl$_3$

Complex 13
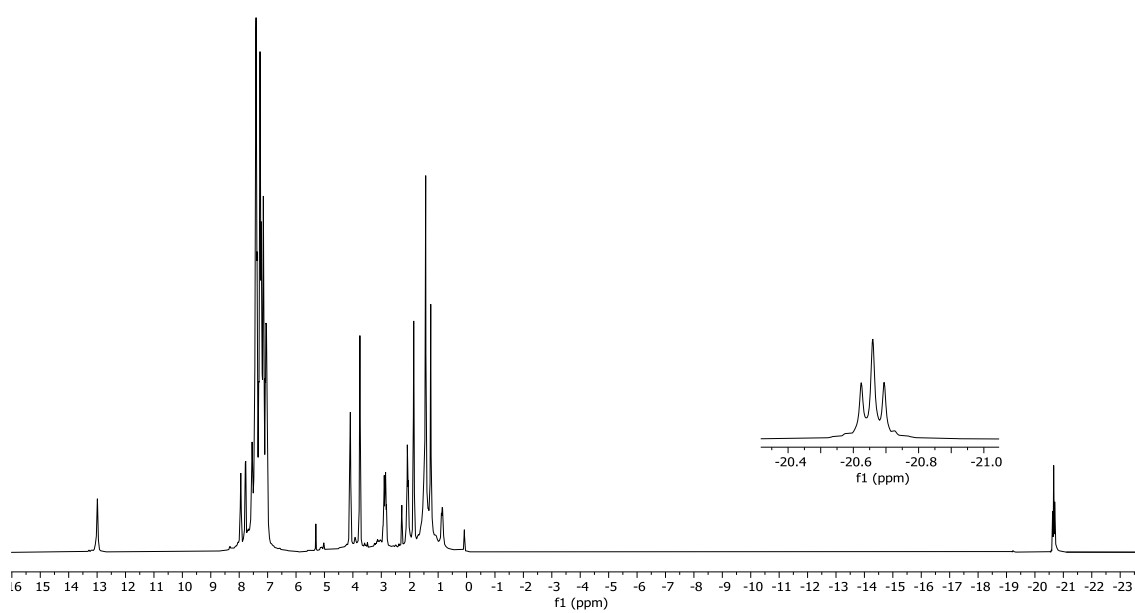
Figure B. 36 ^{1}H NMR of complex 13 in CDCl[3]
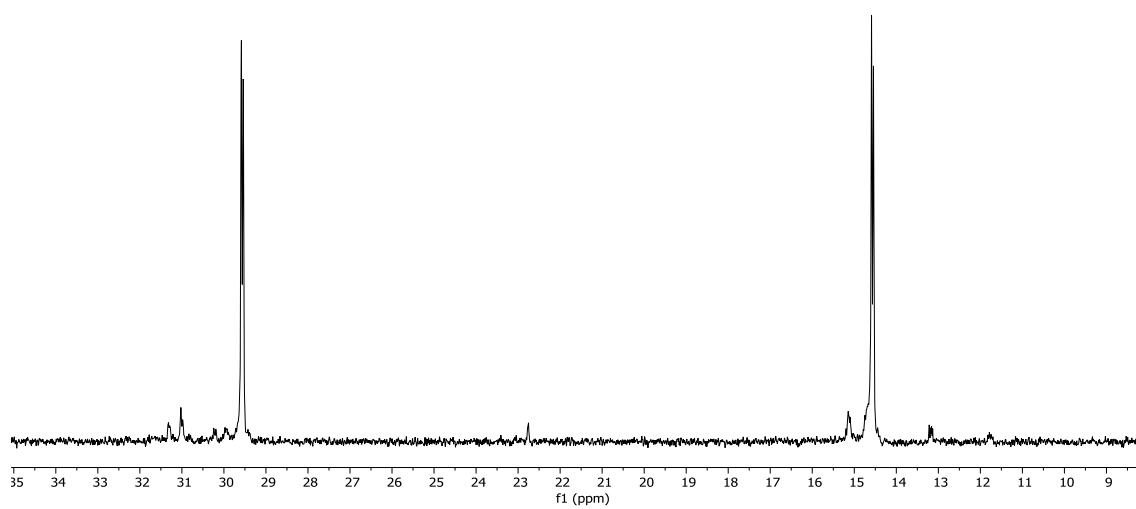
Figure B. 37 ^{31}P{^{1}H} NMR of complex 13 in CDCl[3]
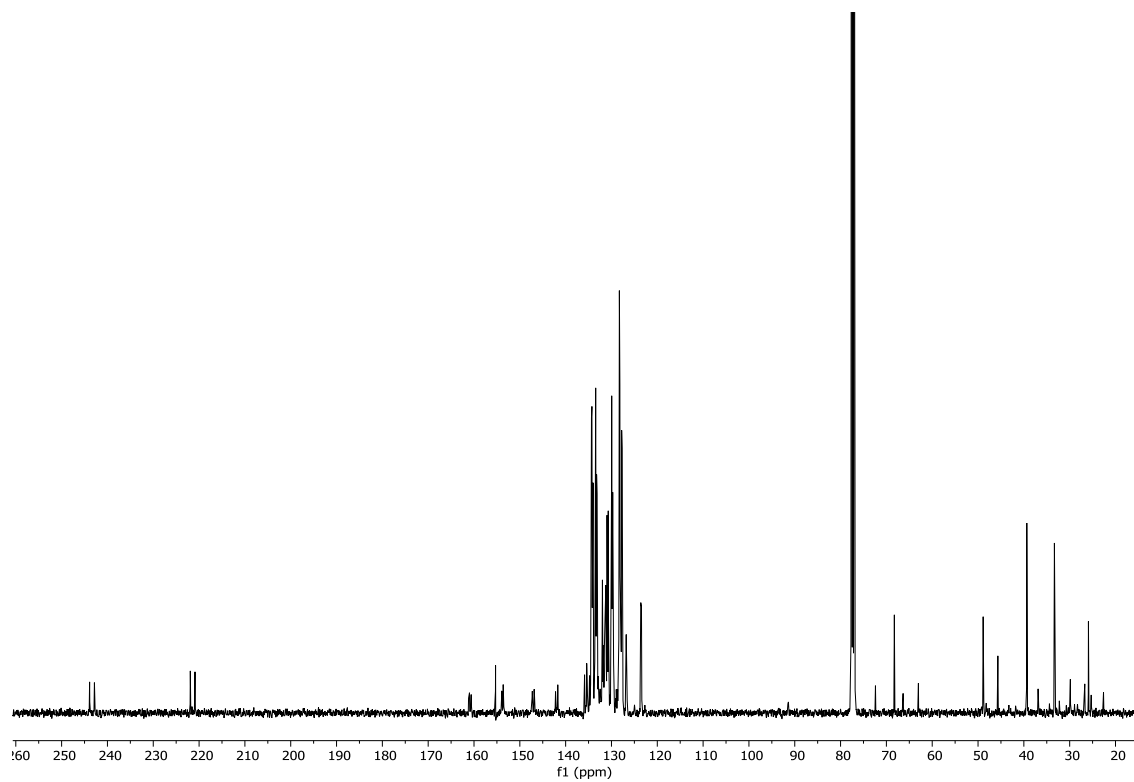
Figure B. 38 ^{13}C{^{1}H} NMR of complex 13 in CDCl$_3$
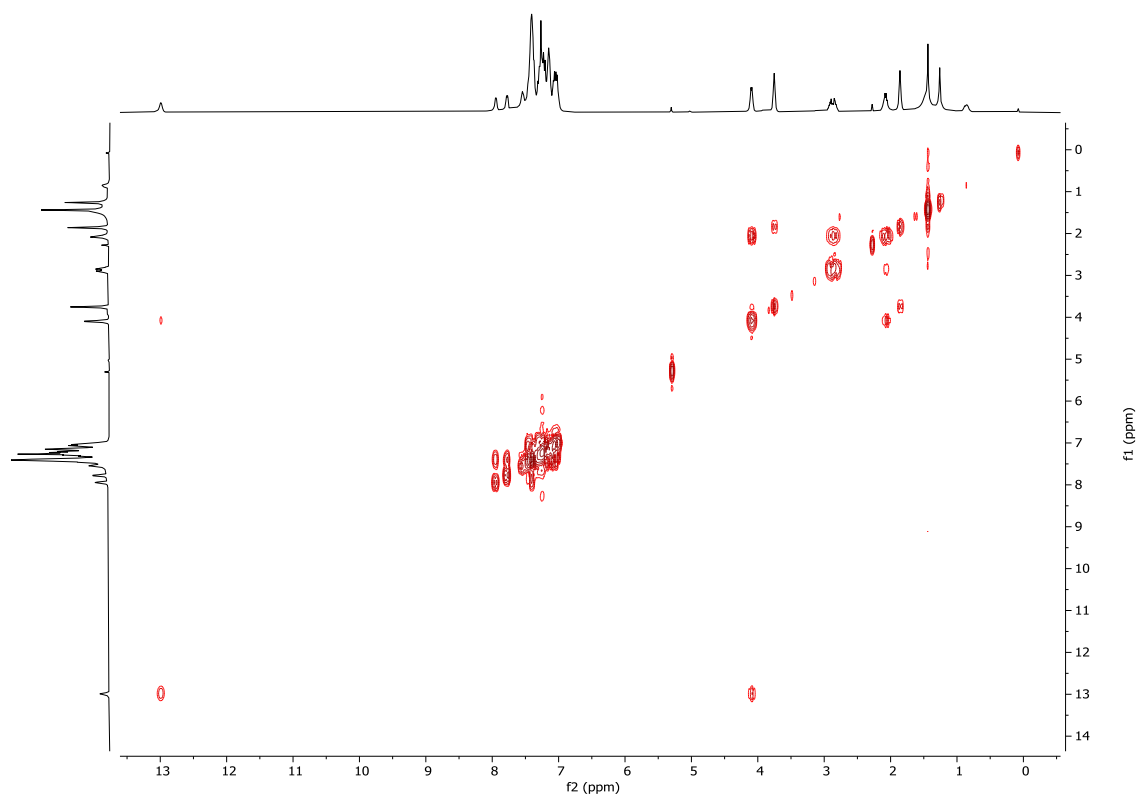
Figure B. 39 COSY spectrum of complex 13 in CDCl$_3$
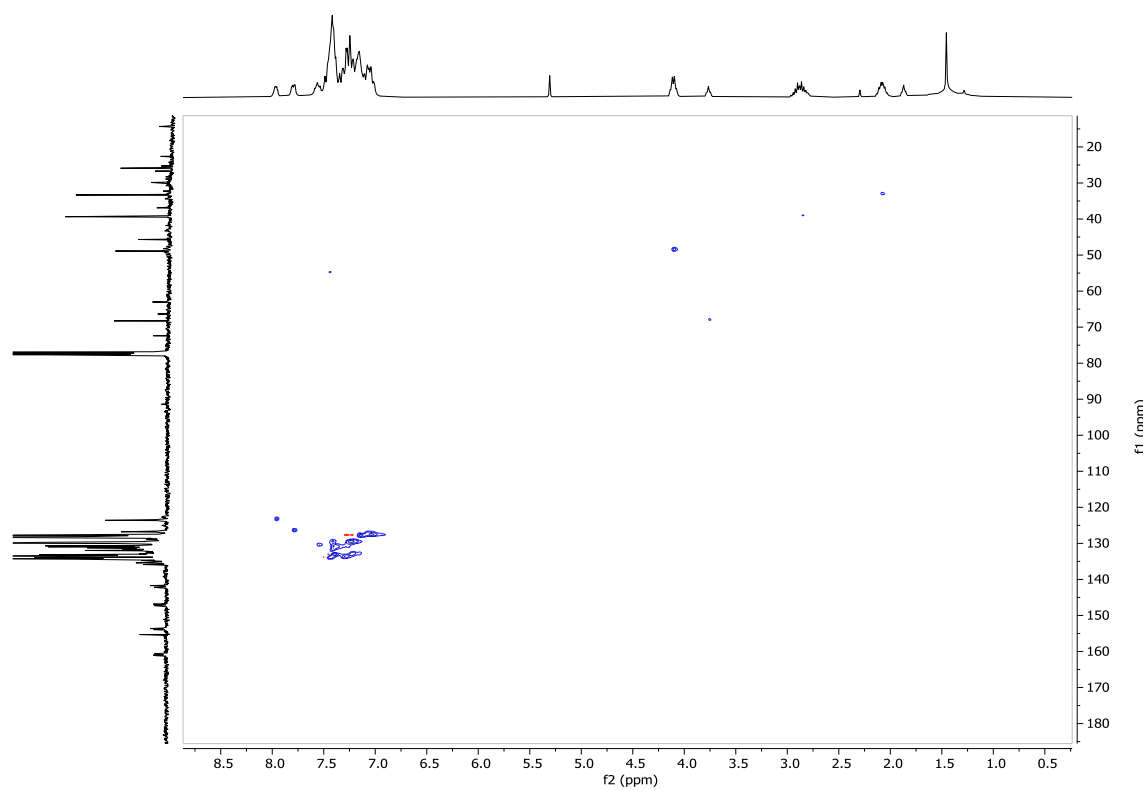
Figure B. 40 ^{1}H-^{13}C HSQC spectrum of complex 13 in CDCl$_3$

<u>Complex 14</u>
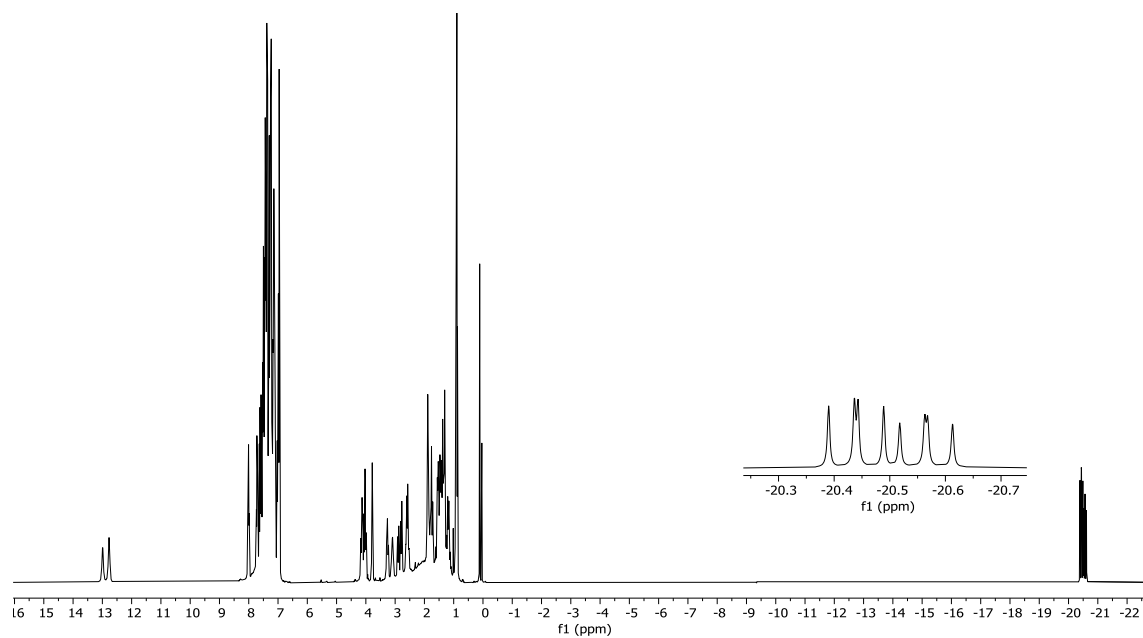
Figure B. 41 ^{1}H NMR of complex 14 in CDCl$_3$
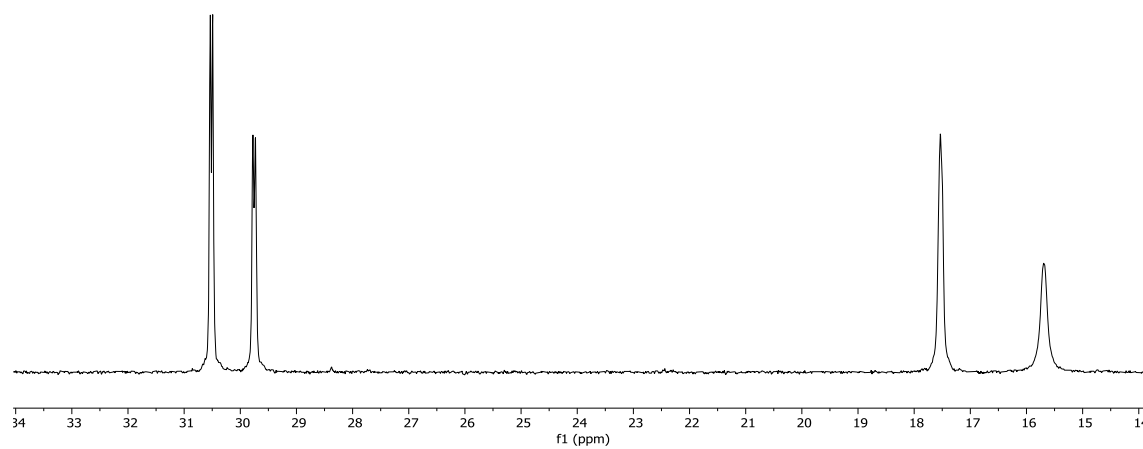
Figure B. 42 ^{31}P{^{1}H} NMR of complex 14 in CDCl$_3$
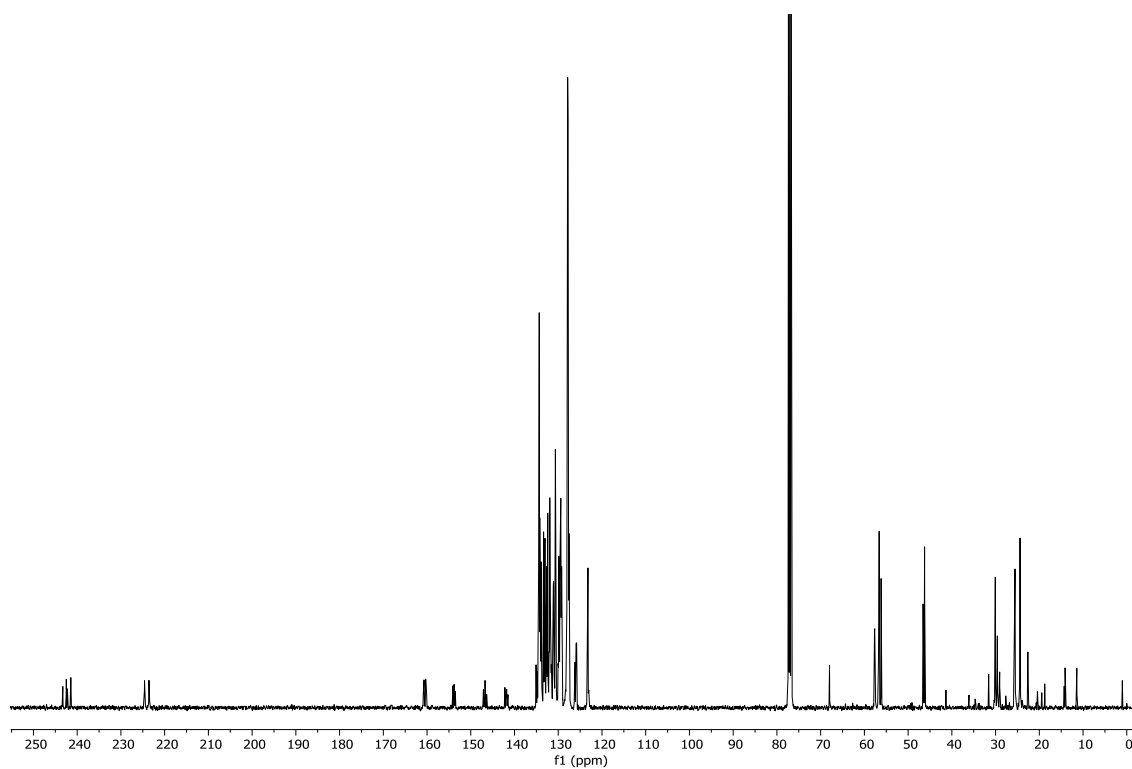
Figure B. 43 ^{13}C{^{1}H} NMR of complex 14 in CDCl$_3$
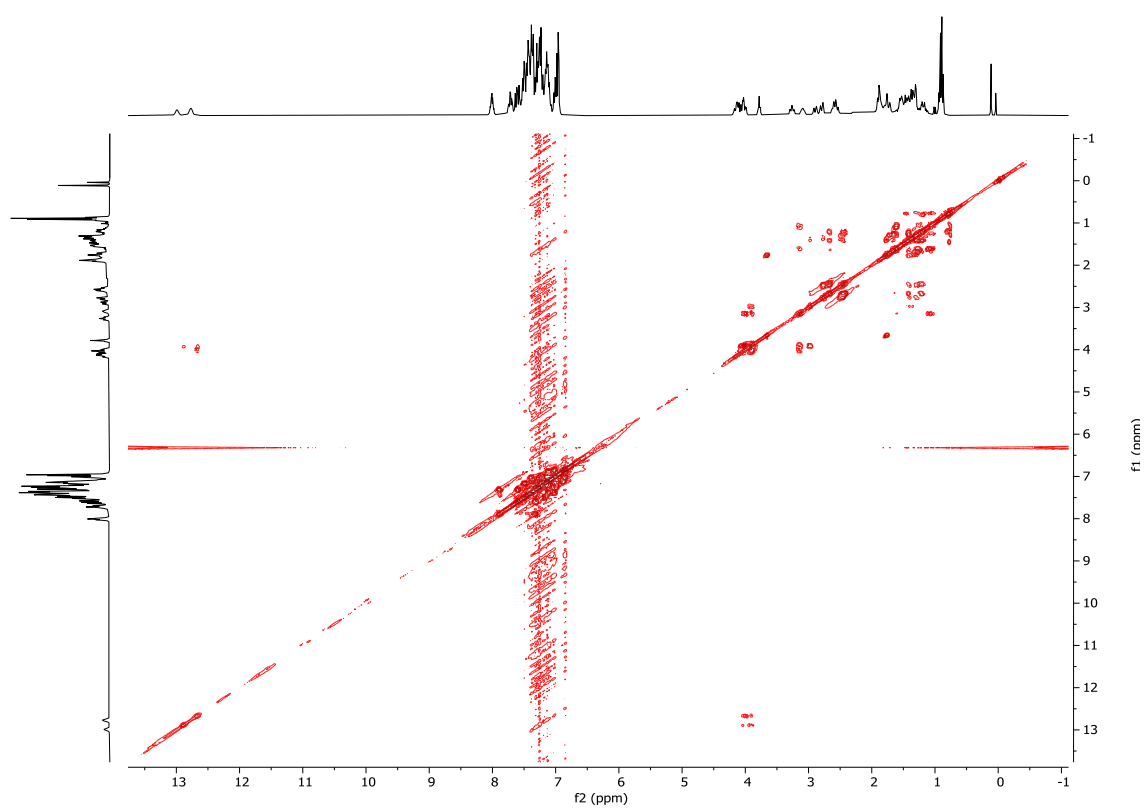
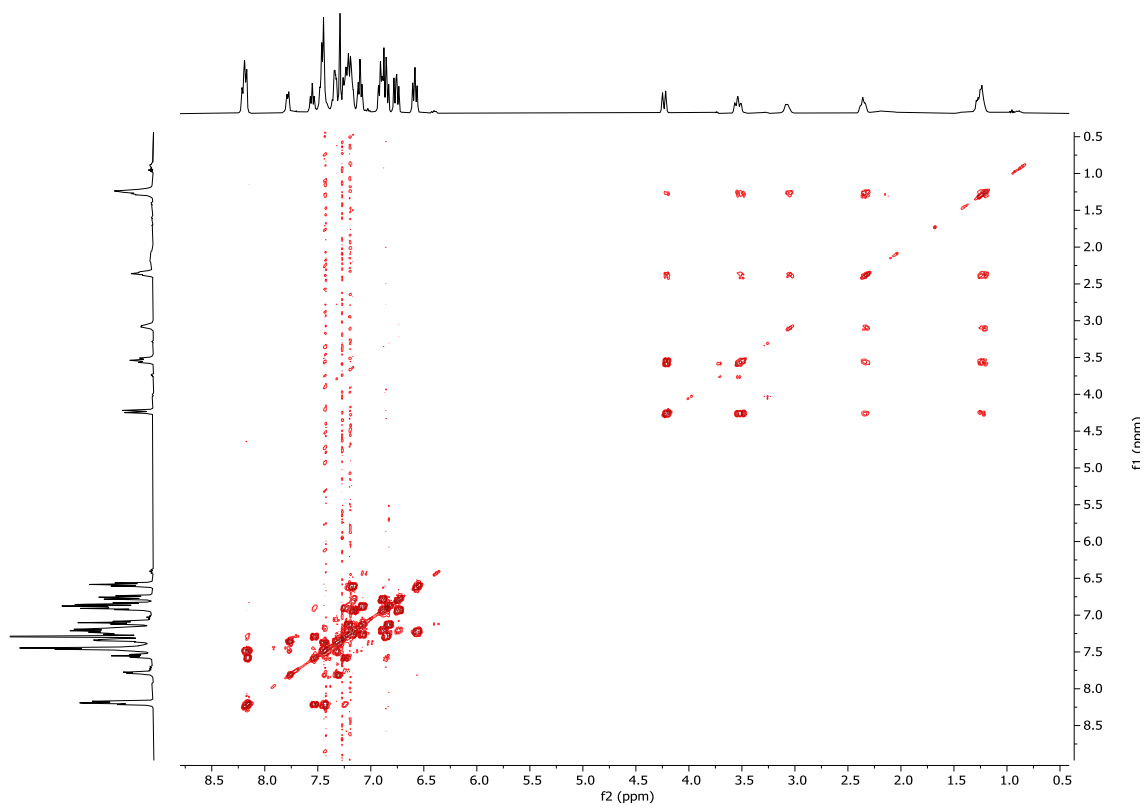**Figure B. 44 COSY spectrum of complex 14 in CDCl$_3$**
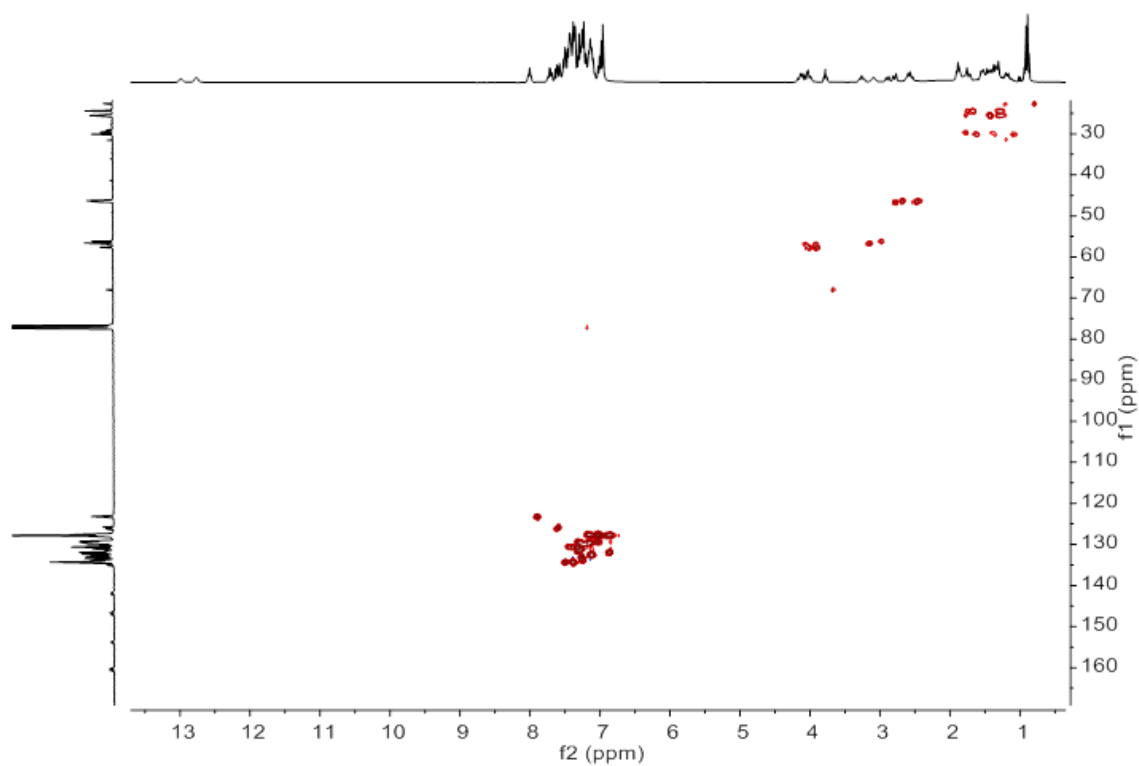
Figure B. 45 ^{1}H-^{13}C HSQC spectrum of complex 14 in CDCl$_3$

Complex 15
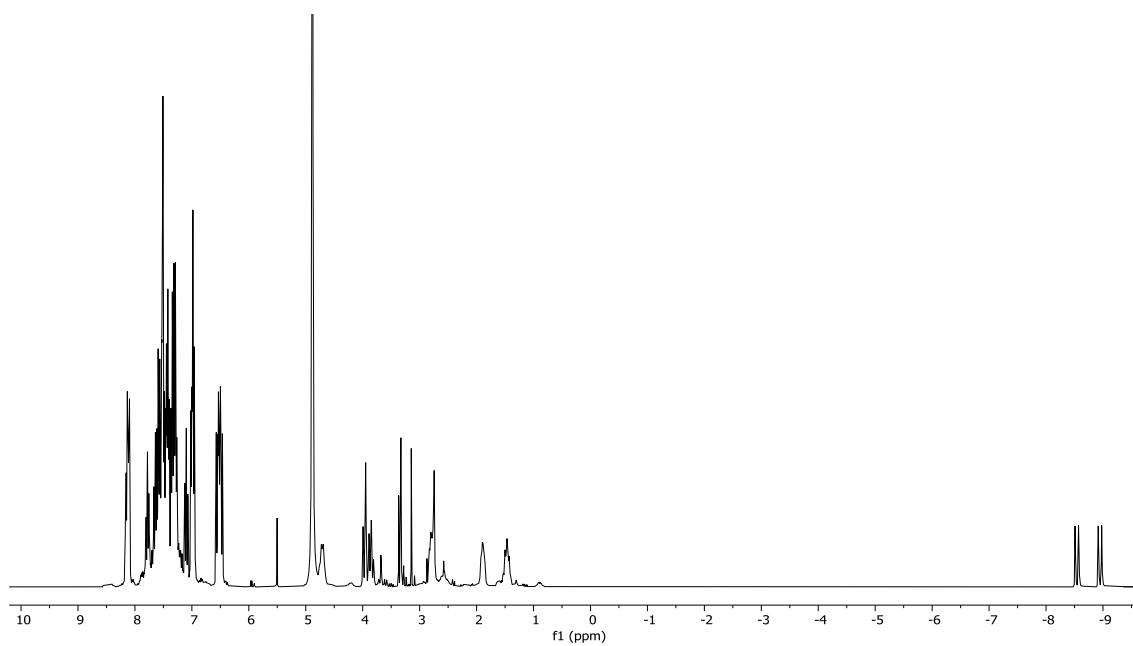
Figure B. 46 ^{1}H NMR of complex 15 in CD[3]OD
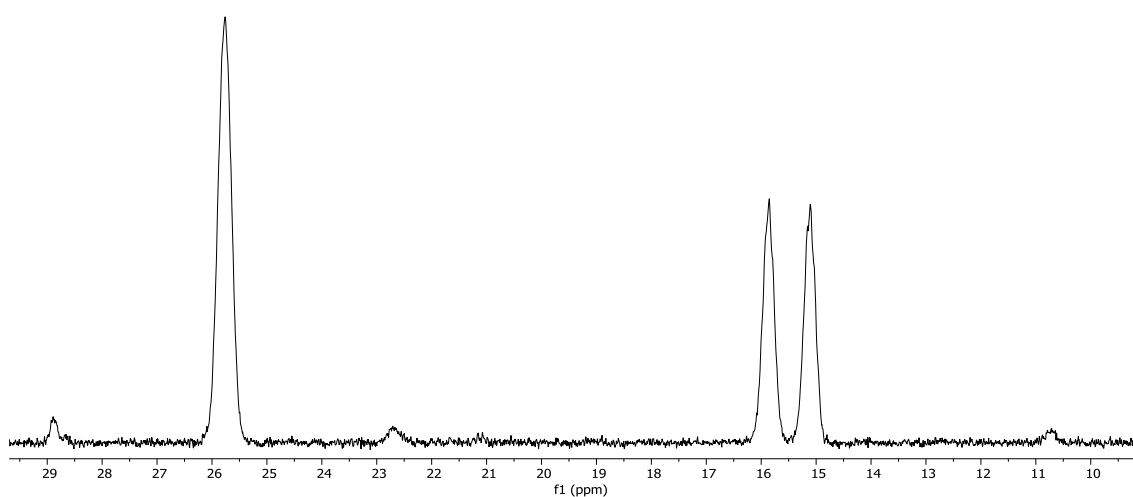
Figure B. 47 ^{31}P NMR of complex 15 in CD[3]OD
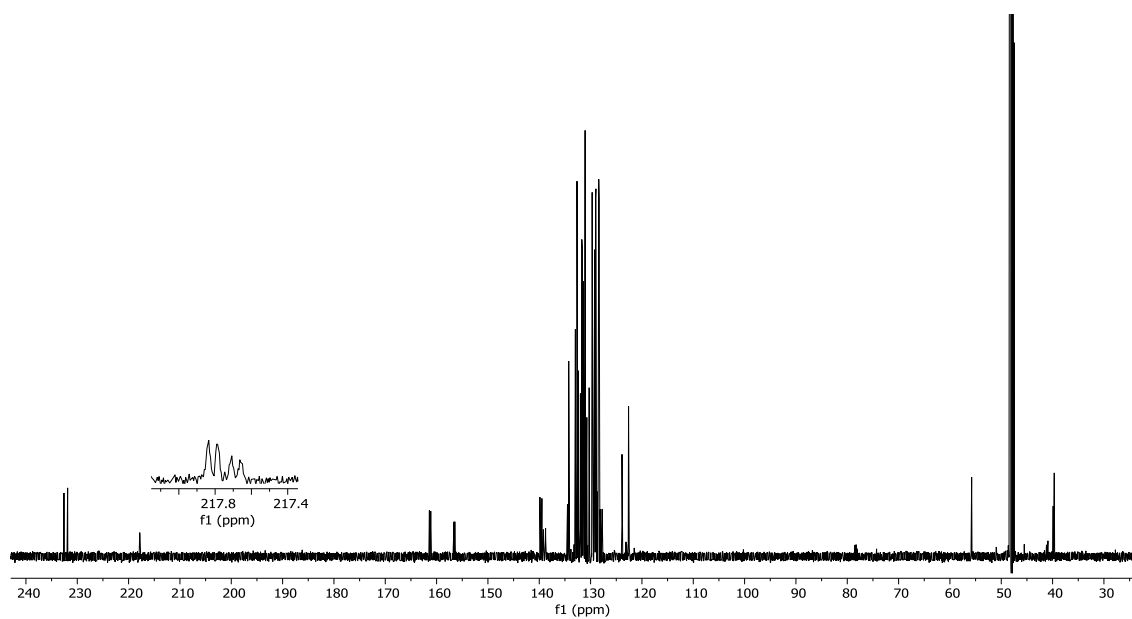
Figure B. 48 ^{13}C{^{1}H} NMR of complex 15 in CDCl$_3$
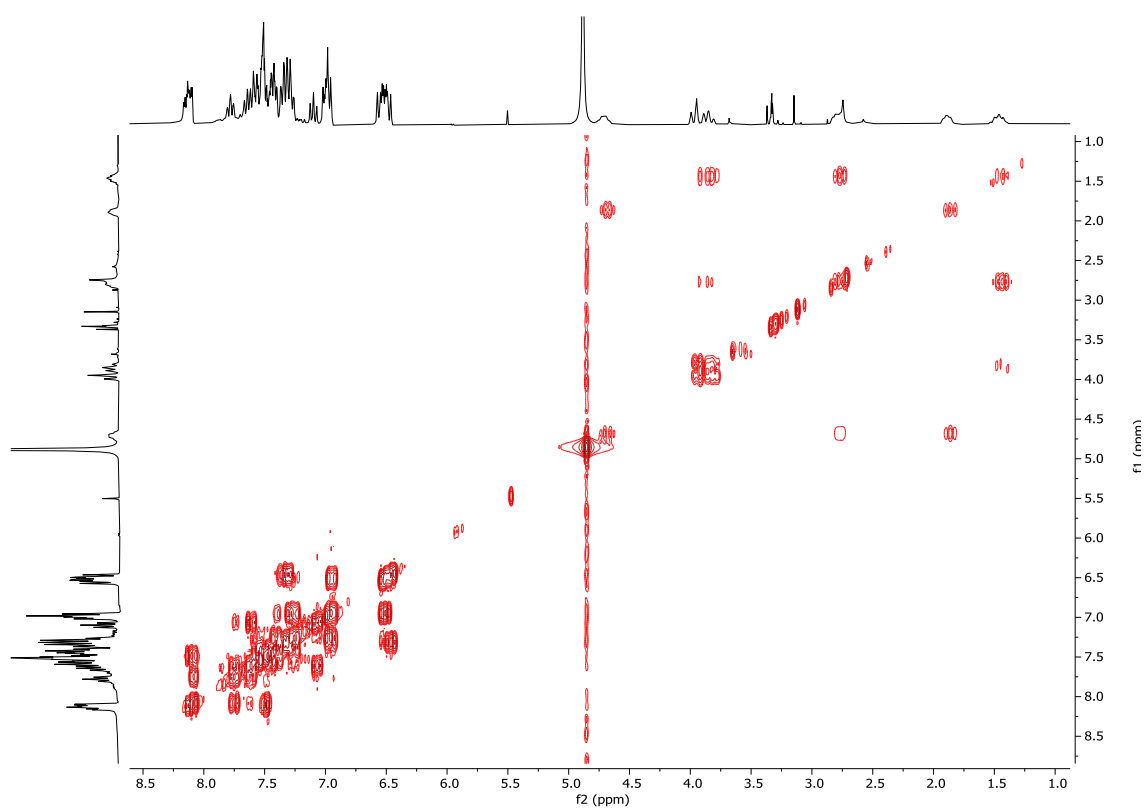
Figure B. 49 COSY spectrum of complex 15 in CD$_3$OD
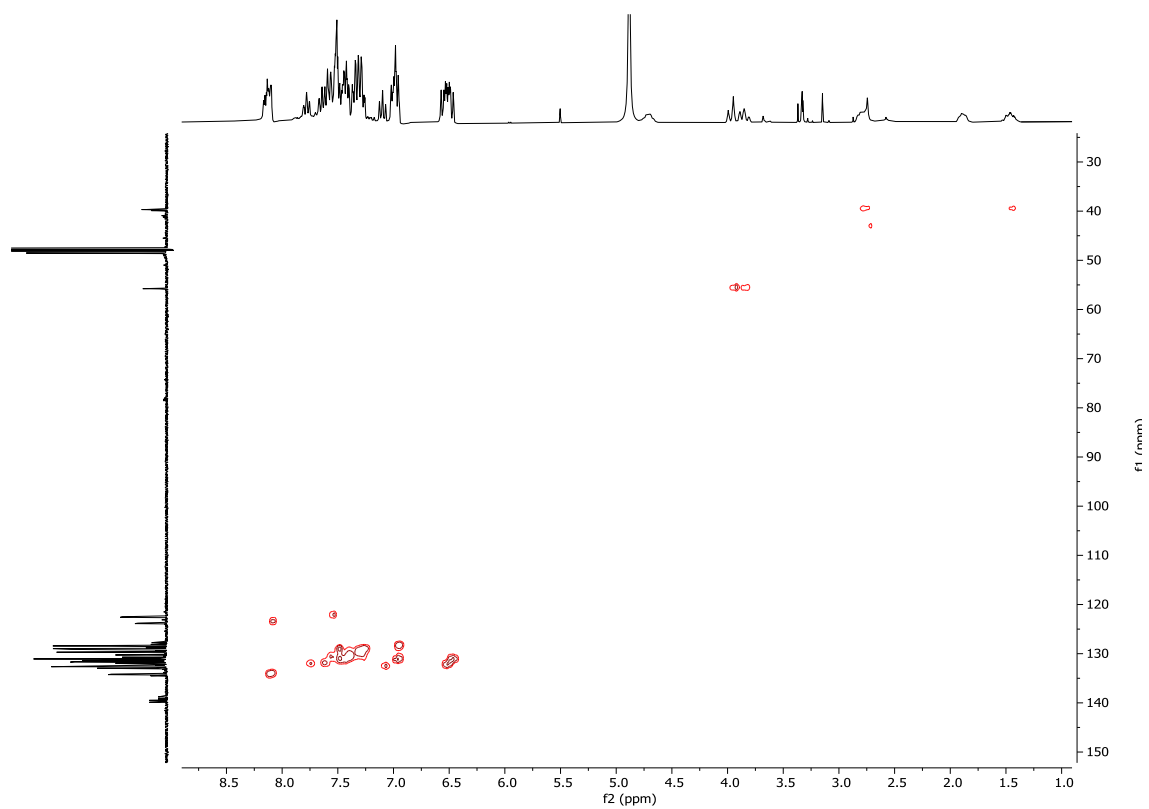
Figure B. 50 ^{1}H-^{13}C HSQC spectrum of complex 15 in CD$_3$OD

Complex 16
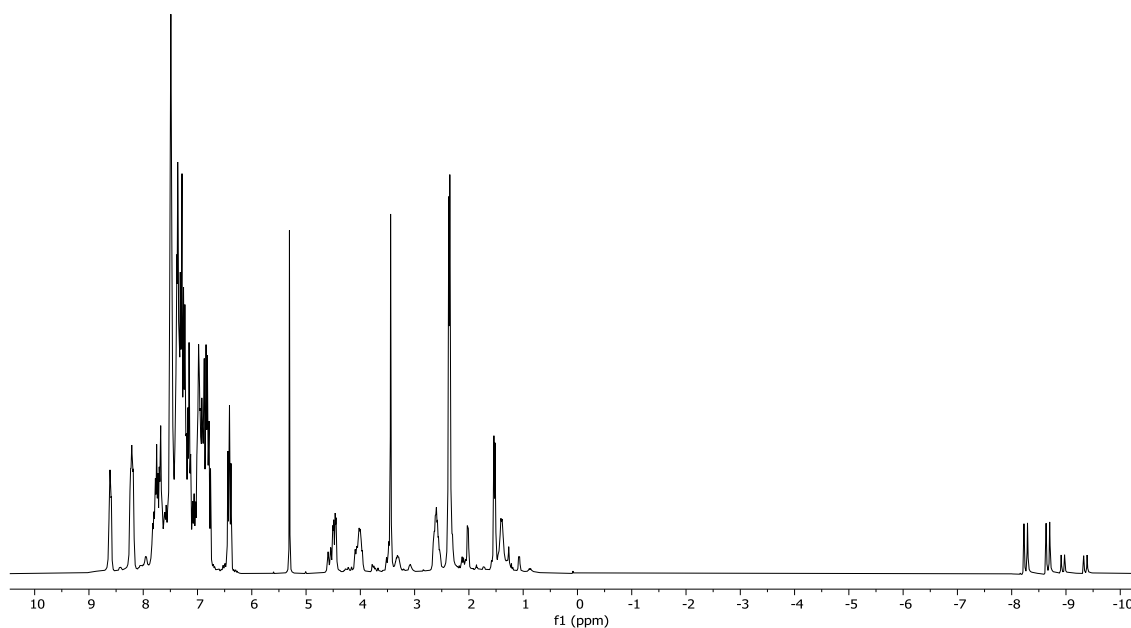
Figure B. 51 ^{1}H NMR of complex 16 in CDCl$_3$
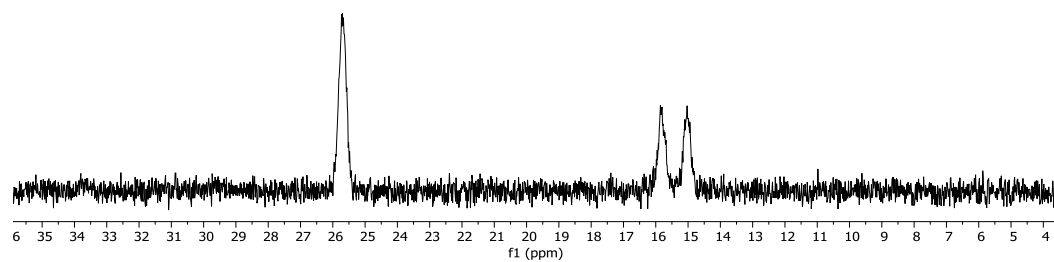
Figure B. 52 ^{31}P NMR of complex 16 in CDCl$_3$
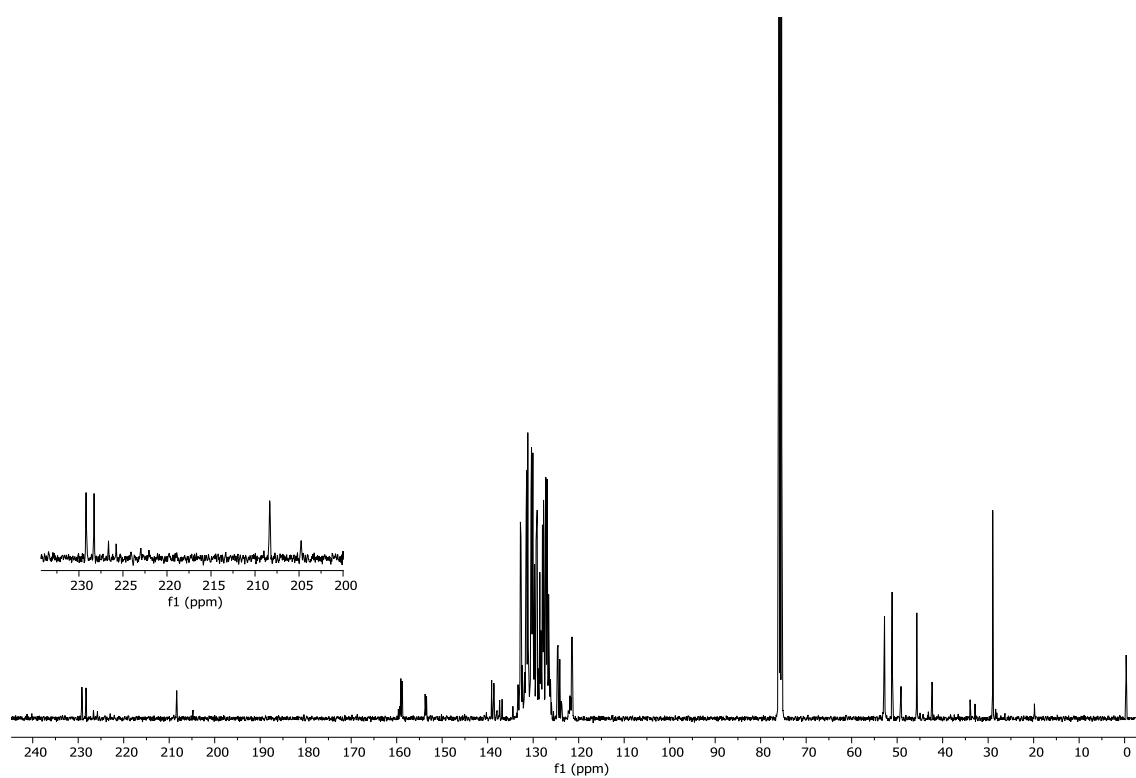
Figure B. 53 ^{13}C{^{1}H} NMR of complex 16 in CDCl$_3$
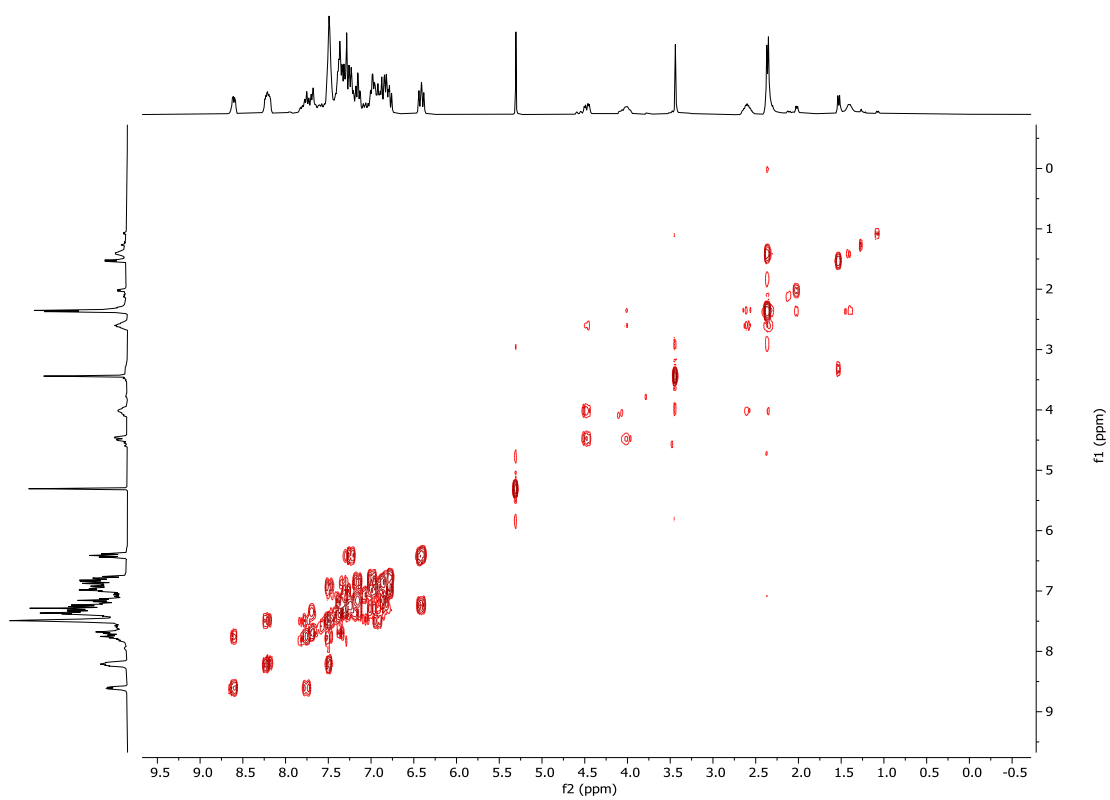
Figure B. 54 COSY spectrum of complex 16 in CDCl₃
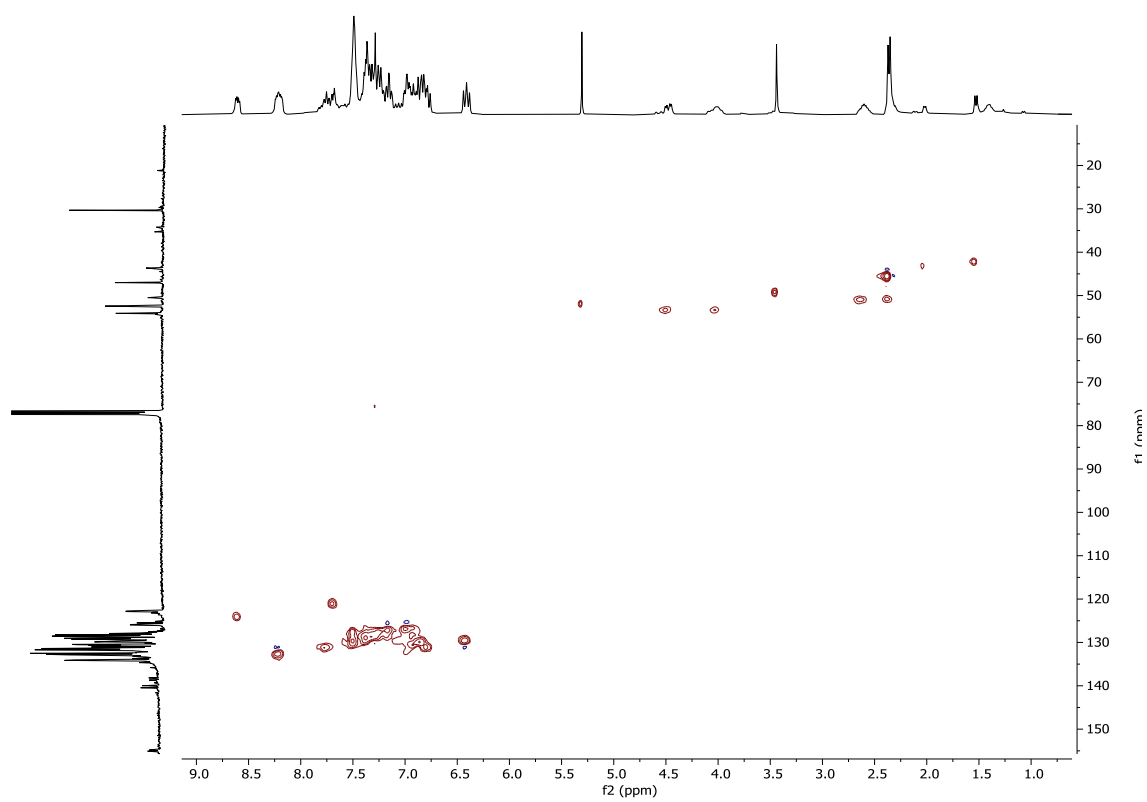
Figure B. 55 ^{1}H-^{13}C HSQC spectrum of complex 16 in CDCl$_3$

Complex 17
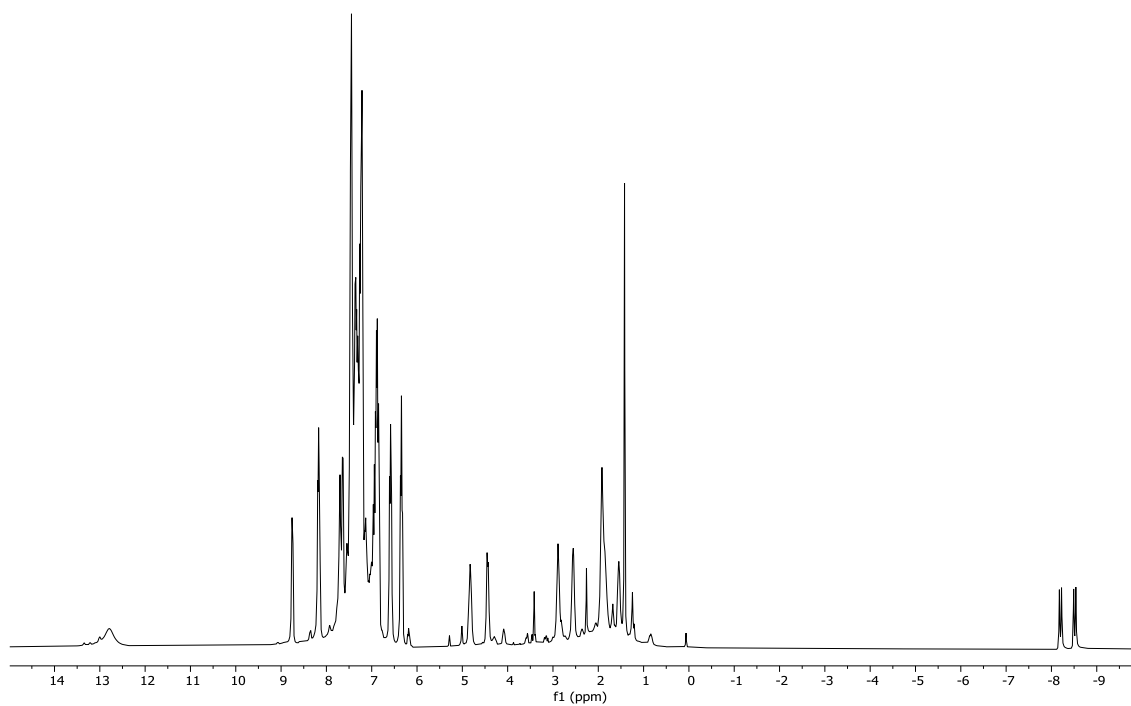
Figure B. 56 ^{1}H NMR of complex 17 in CDCl$_3$
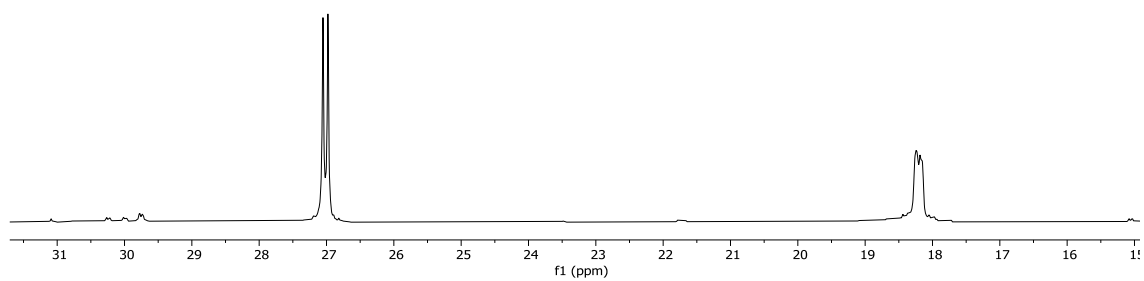
Figure B. 57 ^{31}P{^{1}H} NMR of complex 17 in CDCl$_3$
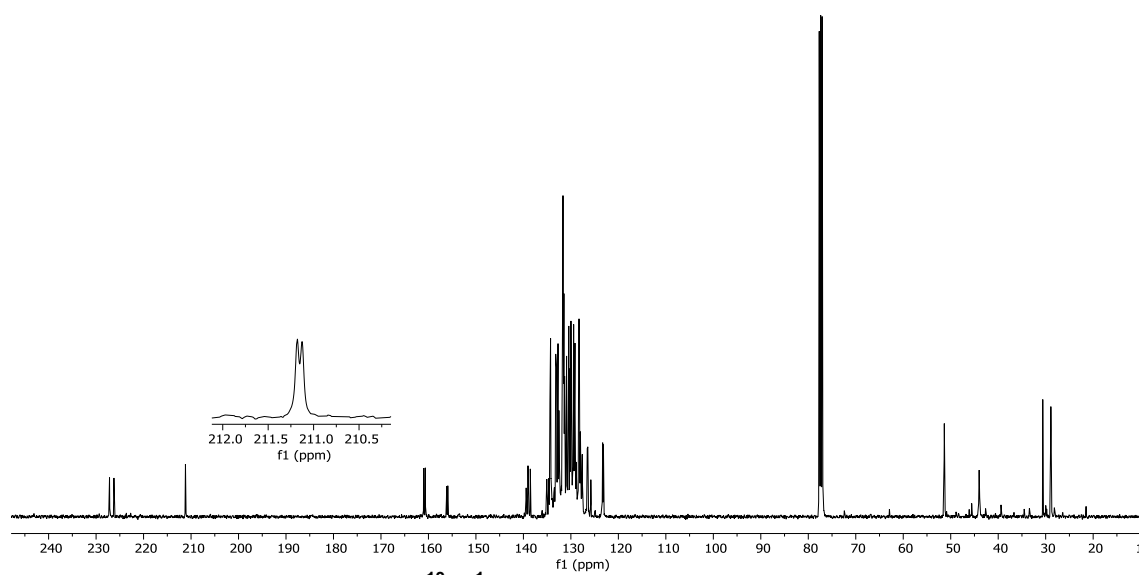
Figure B. 58 ^{13}C{^{1}H} NMR of complex 17 in CDCl$_3$

Figure B. 59 COSY spectrum of complex 17 in CDCl$_3$
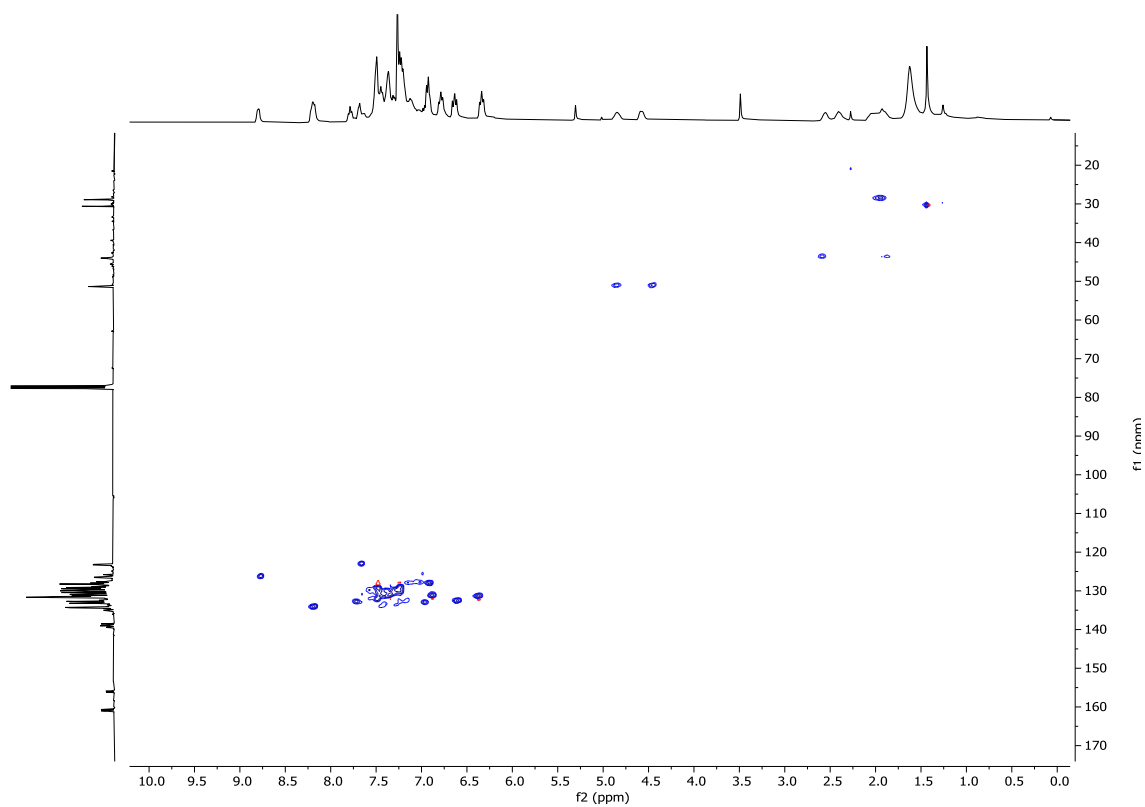
Figure B. 60 ^{1}H-^{13}C HSQC spectrum of complex 17 in CDCl$_3$

Complex 18
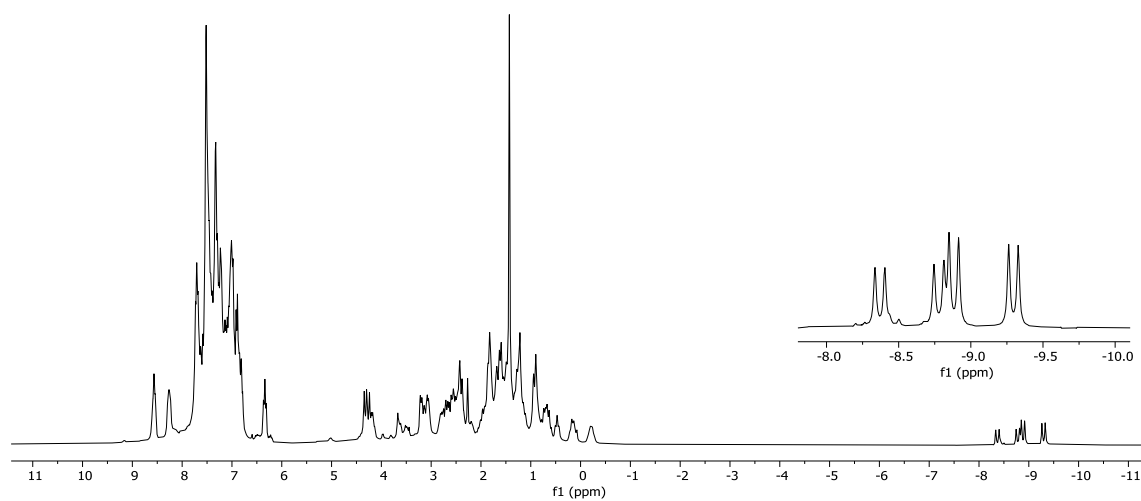
Figure B. 61 ^{1}H NMR of complex 18 in CDCl$_3$
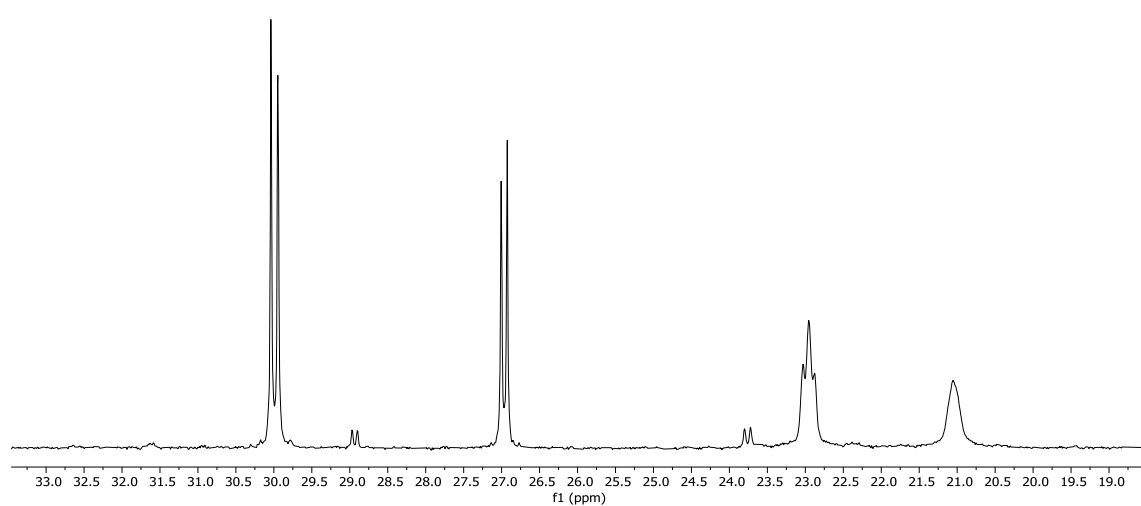
Figure B. 62 ^{31}P{^{1}H} NMR of complex 18 in CDCl$_3$
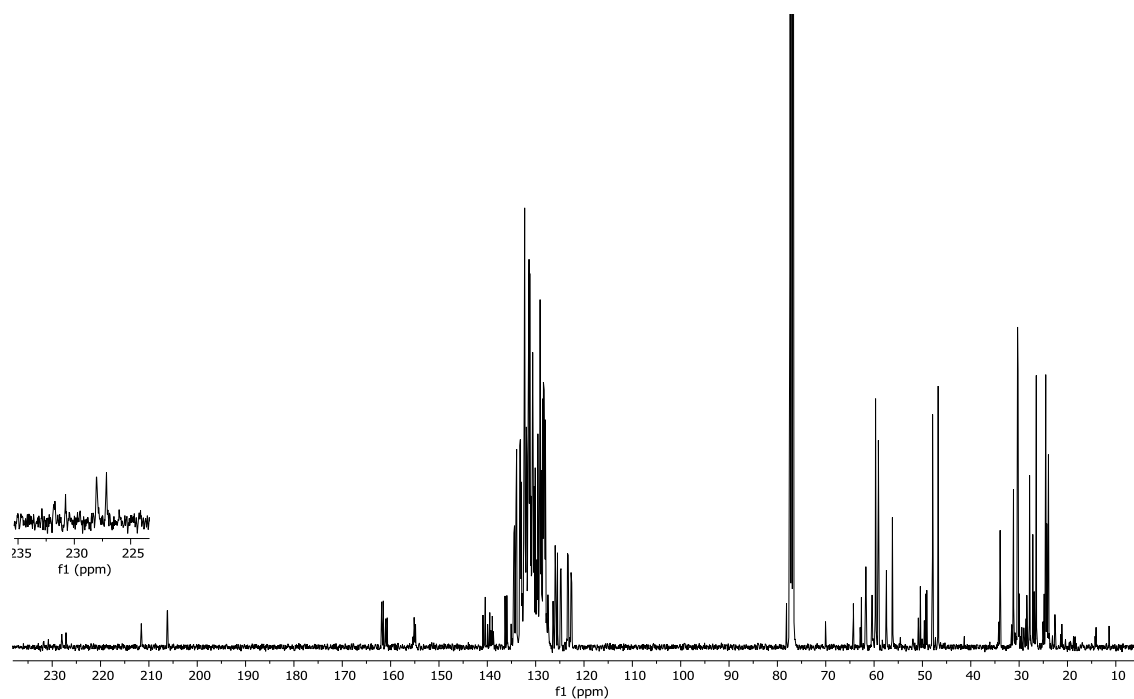
Figure B. 63 ^{13}C{^{1}H} NMR of complex 18 in CDCl$_3$
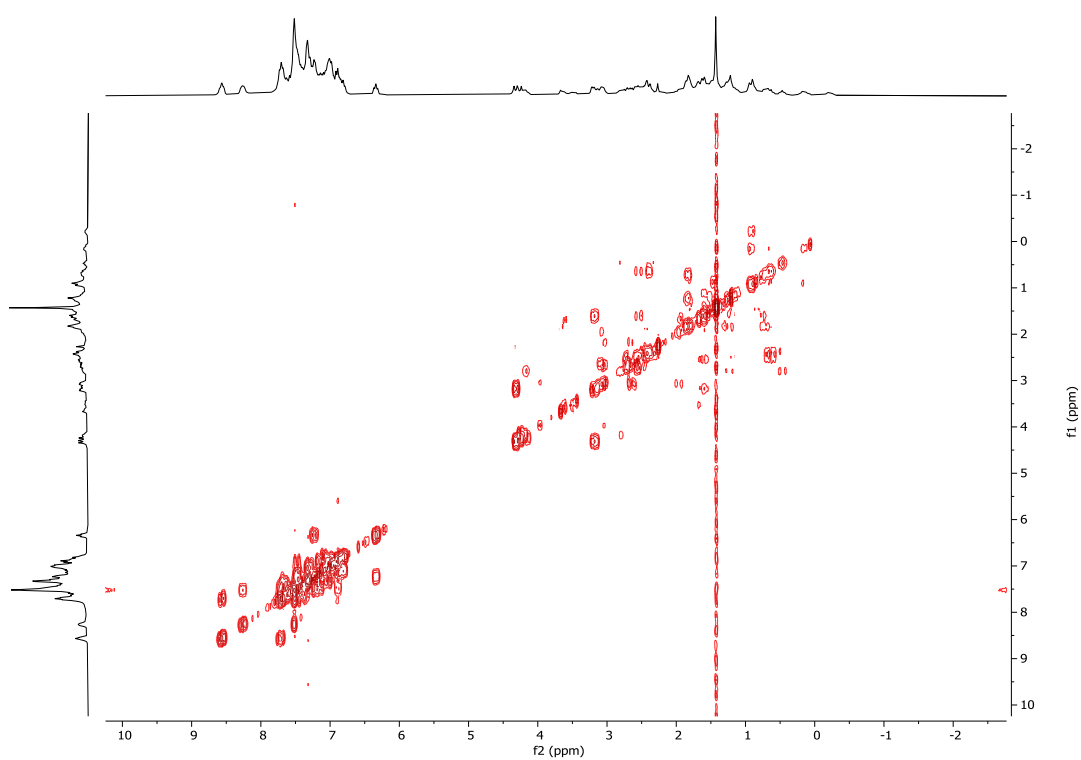
Figure B. 64 COSY spectrum of complex 18 in CDCl$_3$
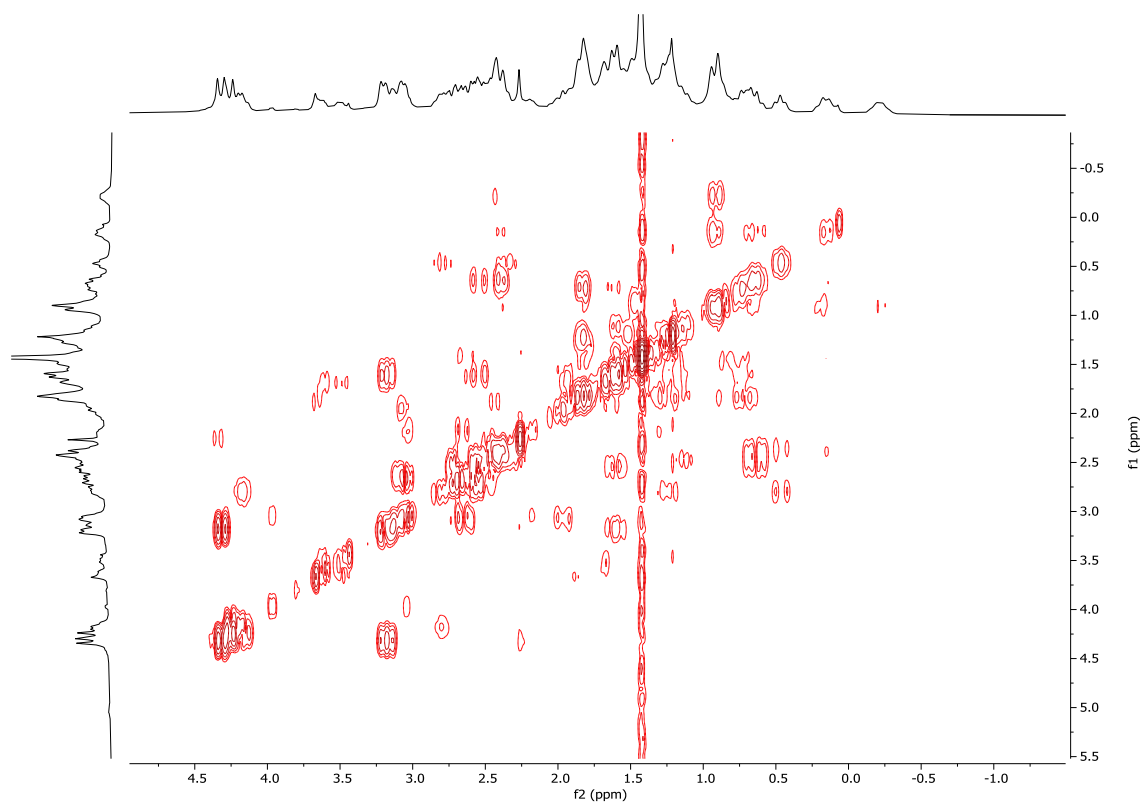
Figure B. 65 COSY spectrum of complex 18 in CDCl$_3$
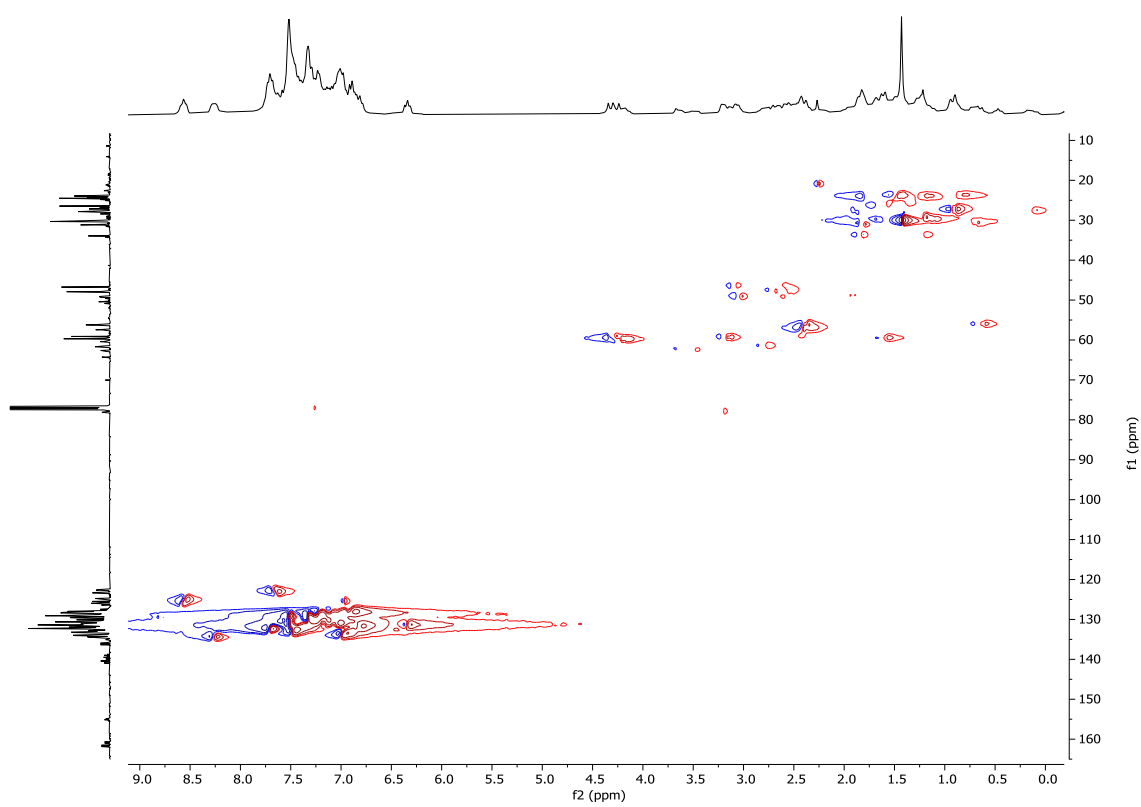
Figure B. 66 ^{1}H-^{13}C HSQC spectrum of complex 18 in CDCl$_3$

Complex 19
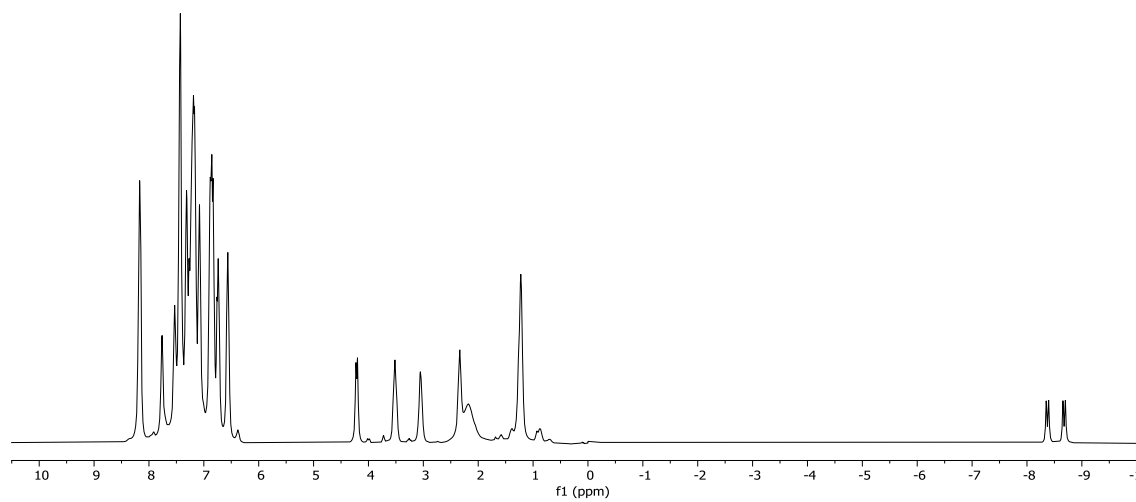
Figure B. 67 ^{1}H NMR of complex 19 in CDCl$_3$
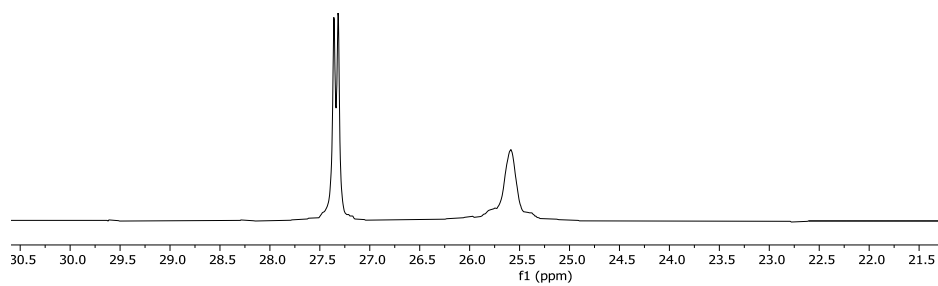
Figure B. 68 ^{31}P{^{1}H} NMR of complex 19 in CDCl$_3$
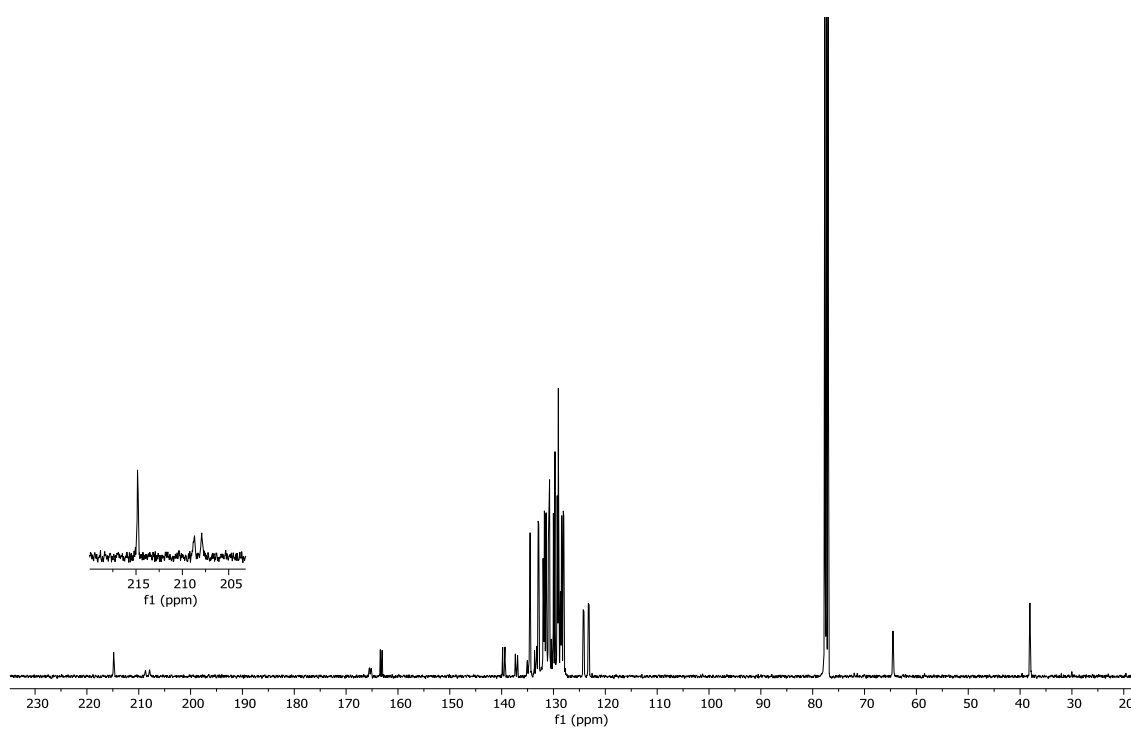
Figure B. 69 ^{13}C{^{1}H} NMR of complex 19 in CDCl$_3$

Figure B. 70 COSY spectrum of complex 19 in CDCl$_3$
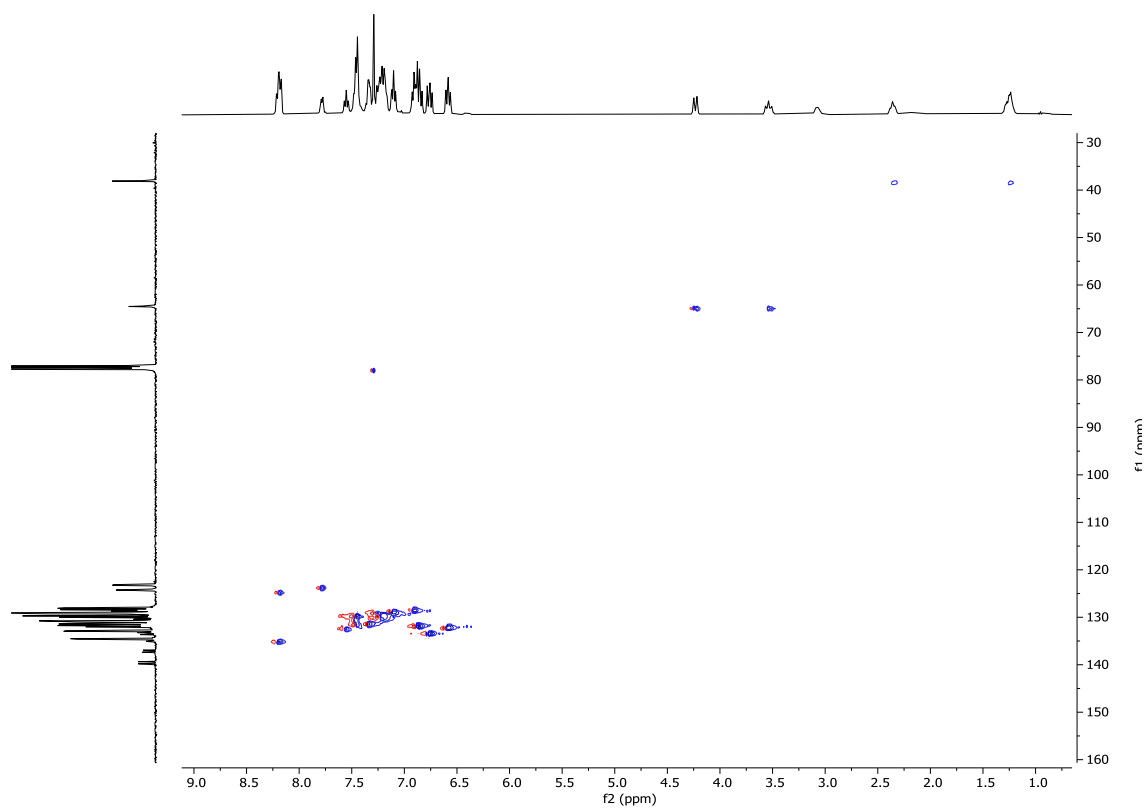
Figure B. 71 ^{1}H-^{13}C HSQC spectrum of complex 19 in CDCl$_3$

<u>Complex 20</u>
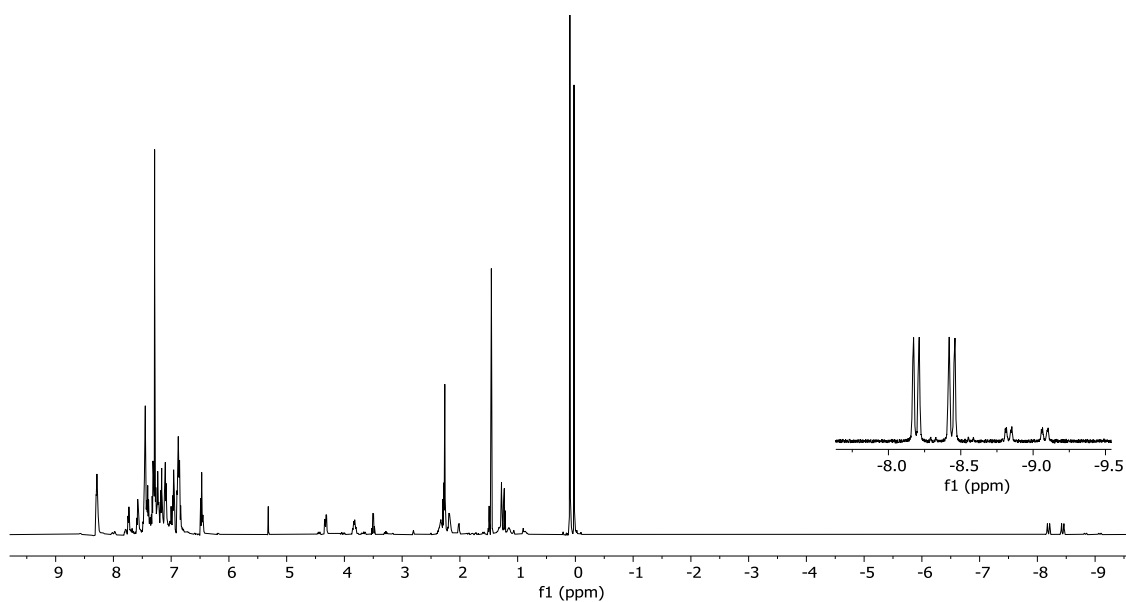
Figure B. 72 ¹H NMR of complex 20 in CDCl₃
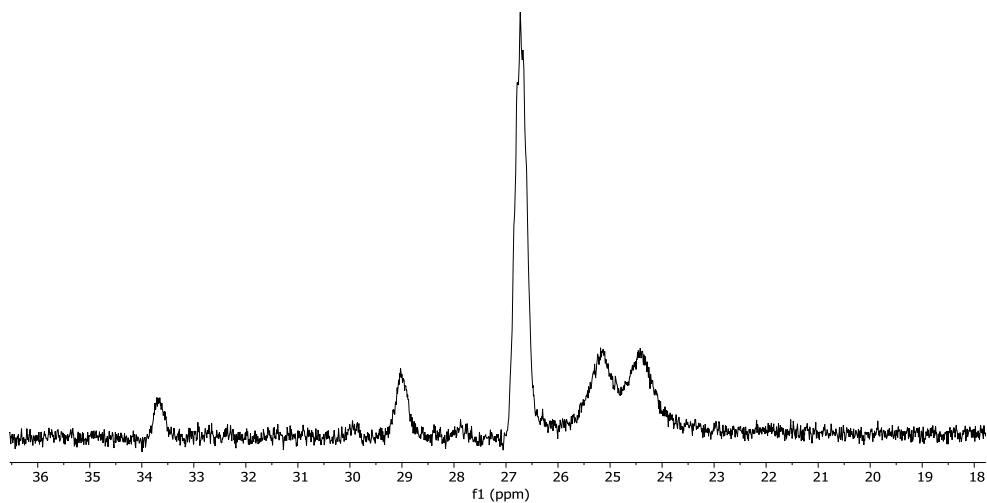
Figure B. 73 ³¹P NMR of complex 20 in CDCl₃
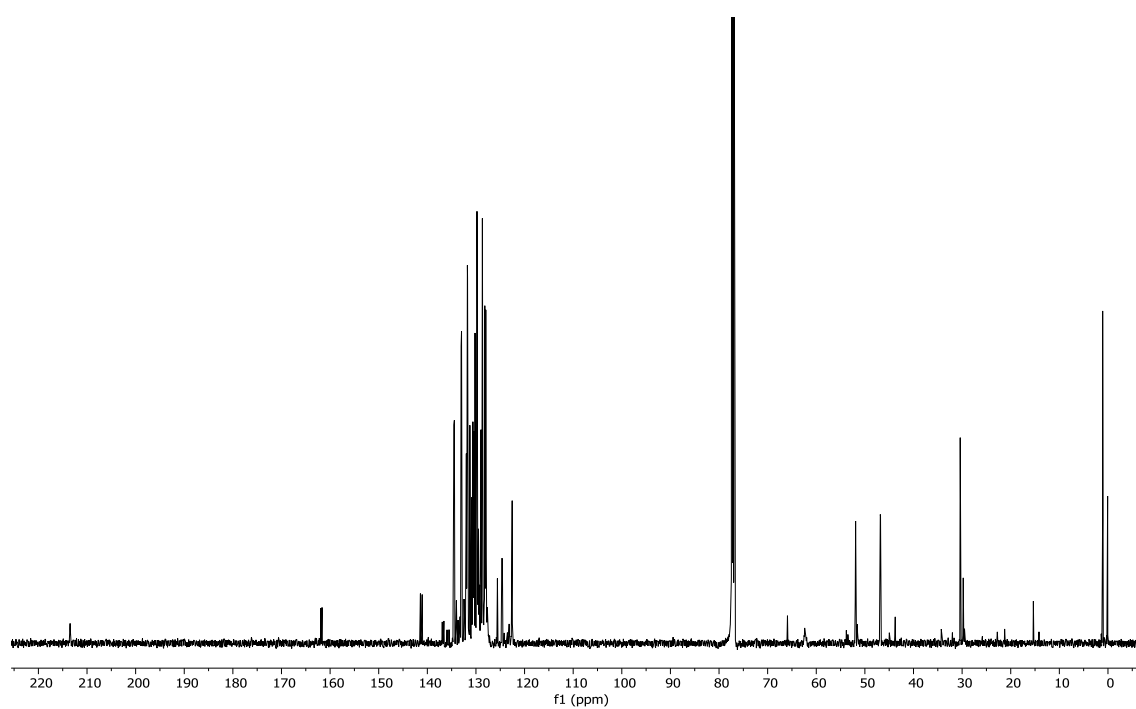
Figure B. 74 ^{13}C{^{1}H} NMR of complex 20 in CDCl$_3$
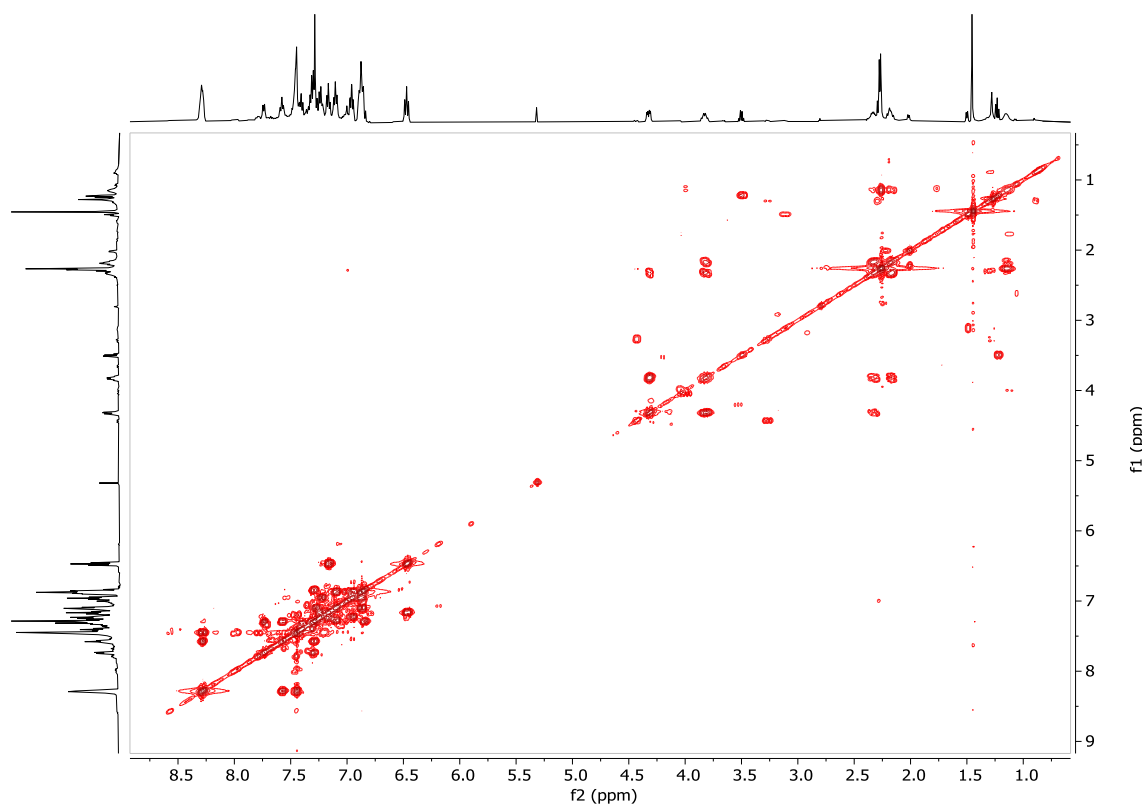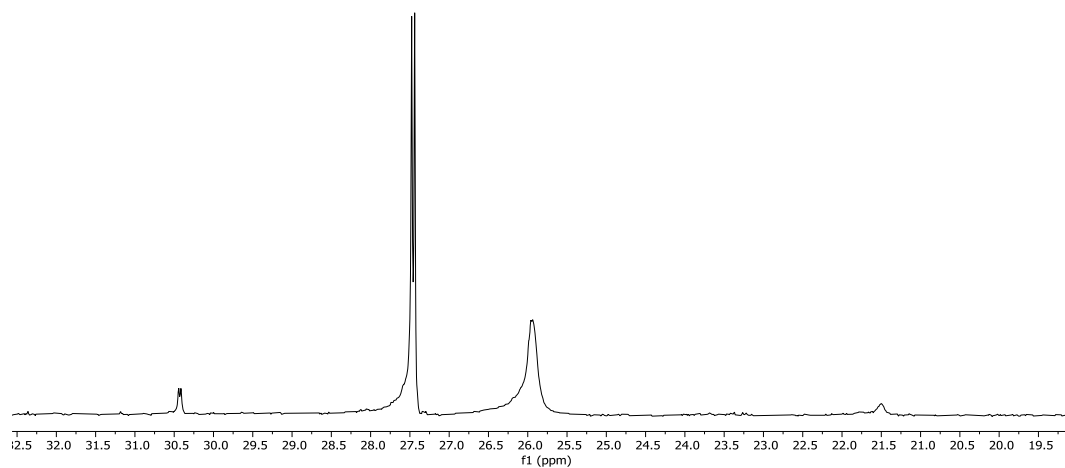

Figure B. 75 COSY spectrum of complex 20 in CDCl$_3$
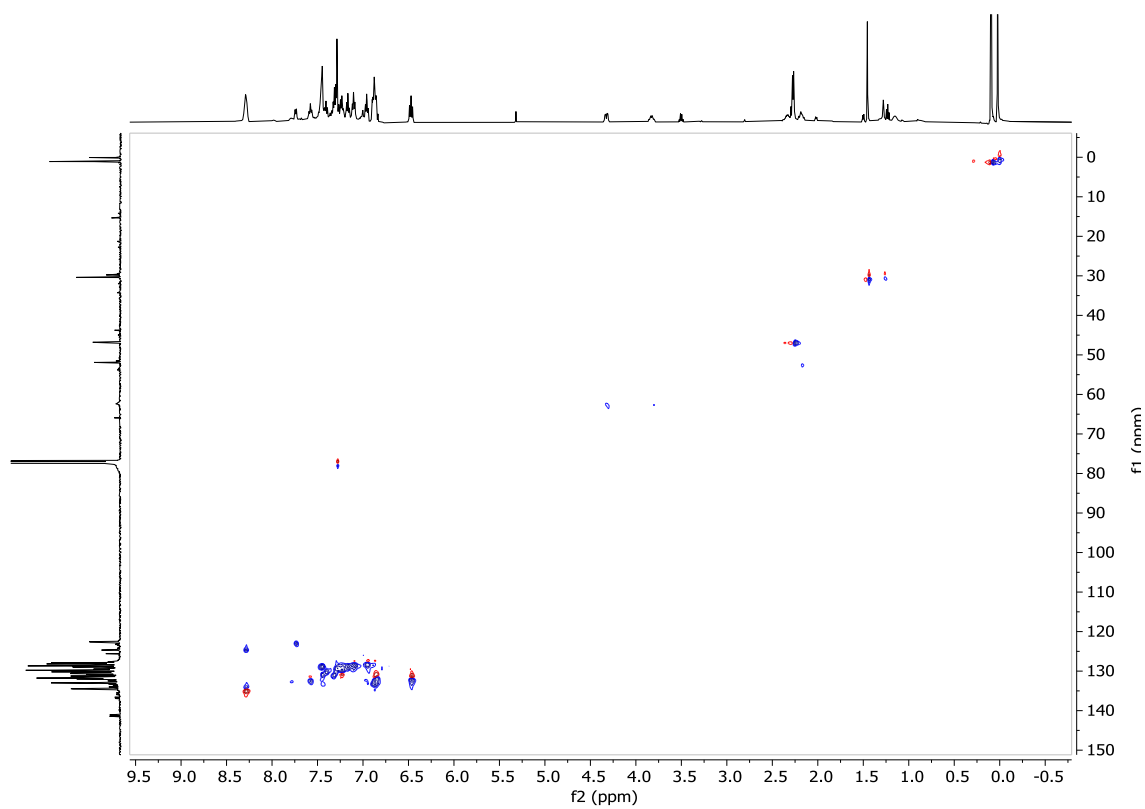
Figure B. 76 ^{1}H-^{13}C HSQC spectrum of complex 20 in CDCl$_3$

Complex 21
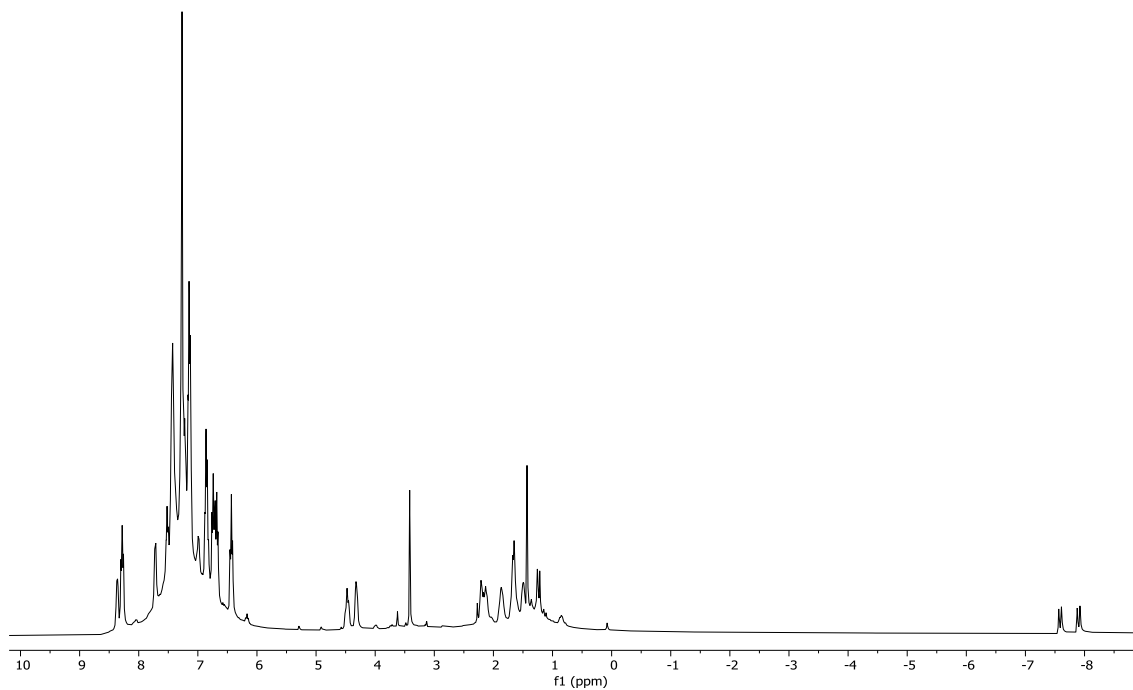
Figure B. 77 ^{1}H NMR of complex 21 in CDCl$_3$

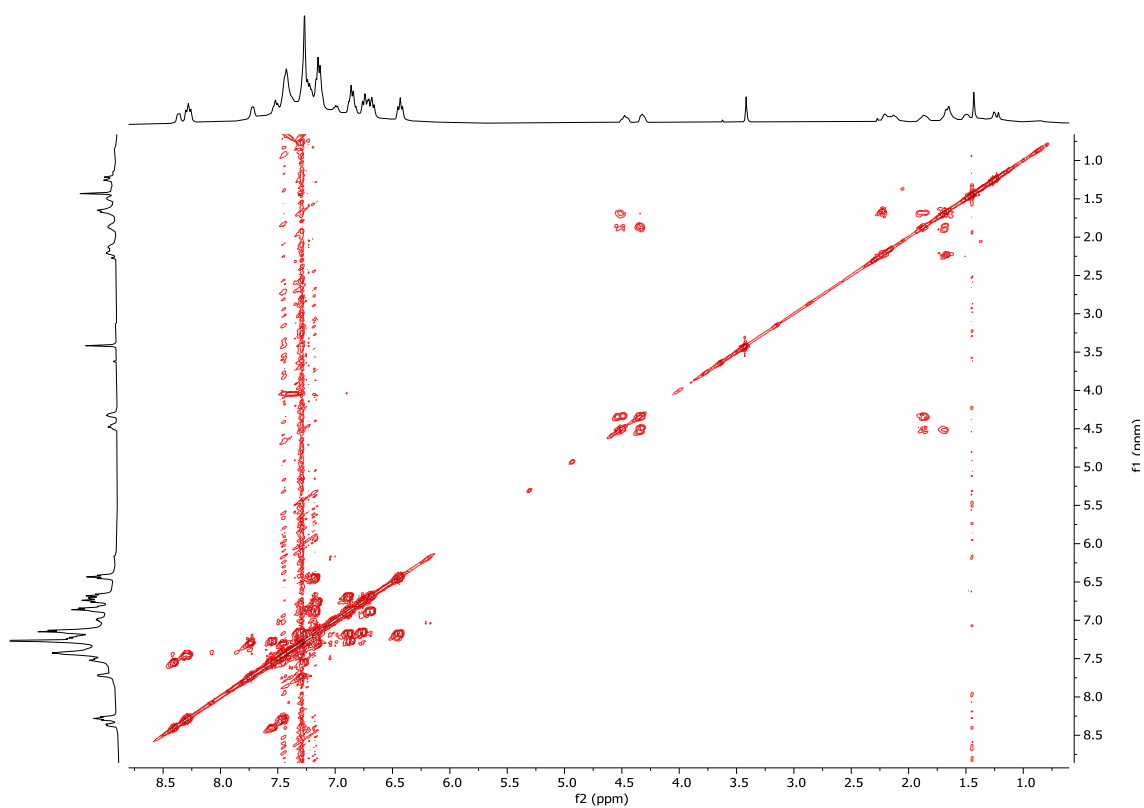**Figure B. 78 ^{31}P{^{1}H} NMR of complex 21 in CDCl$_3$**
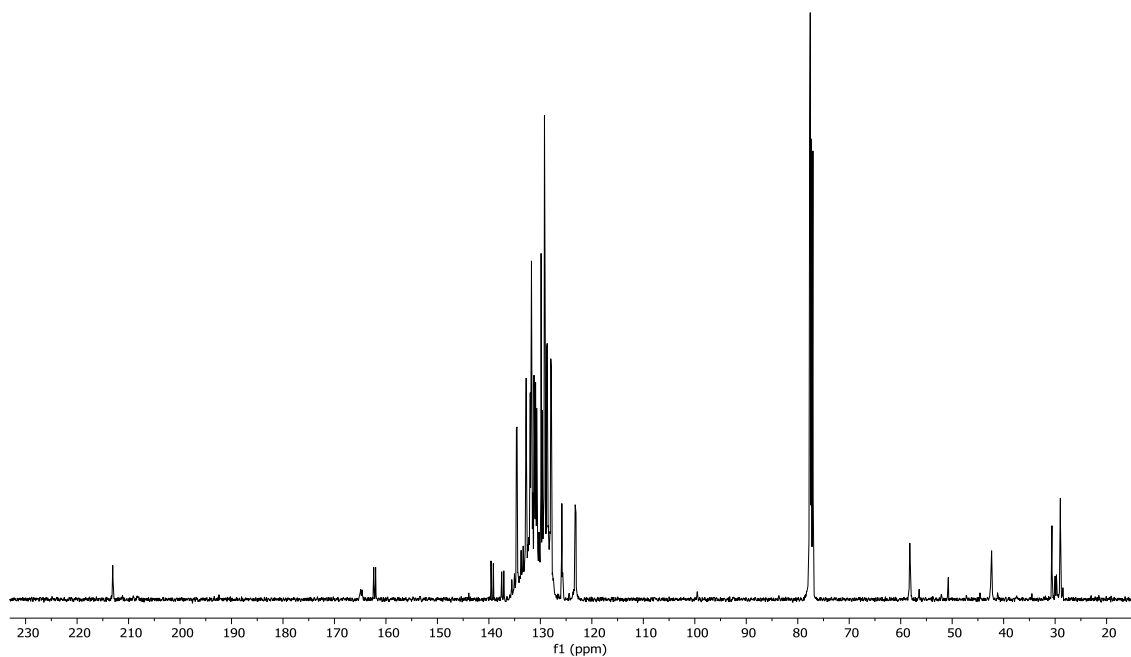
Figure B. 79 ^{13}C{^{1}H} NMR of complex 21 in CDCl$_3$

Figure B. 80 COSY spectrum of complex 21 in CDCl$_3$
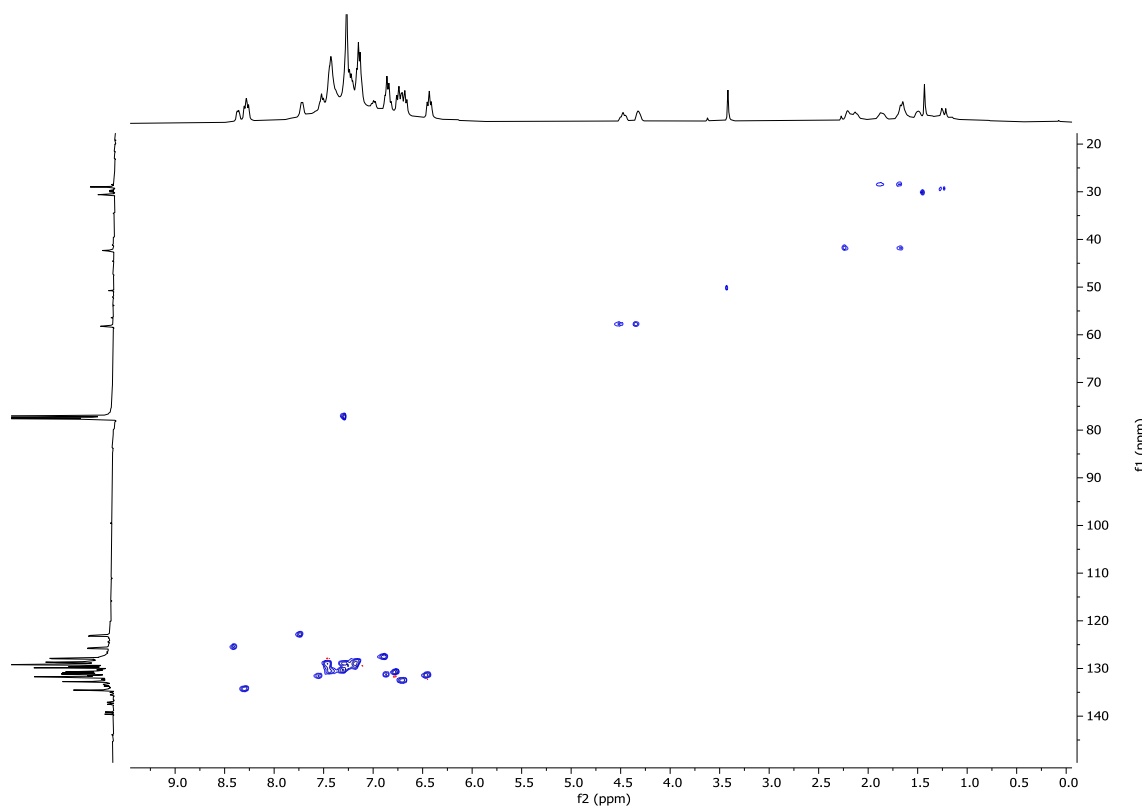
Figure B. 81 ¹H-¹³C HSQC spectrum of complex 21 in CDCl₃

Complex 22
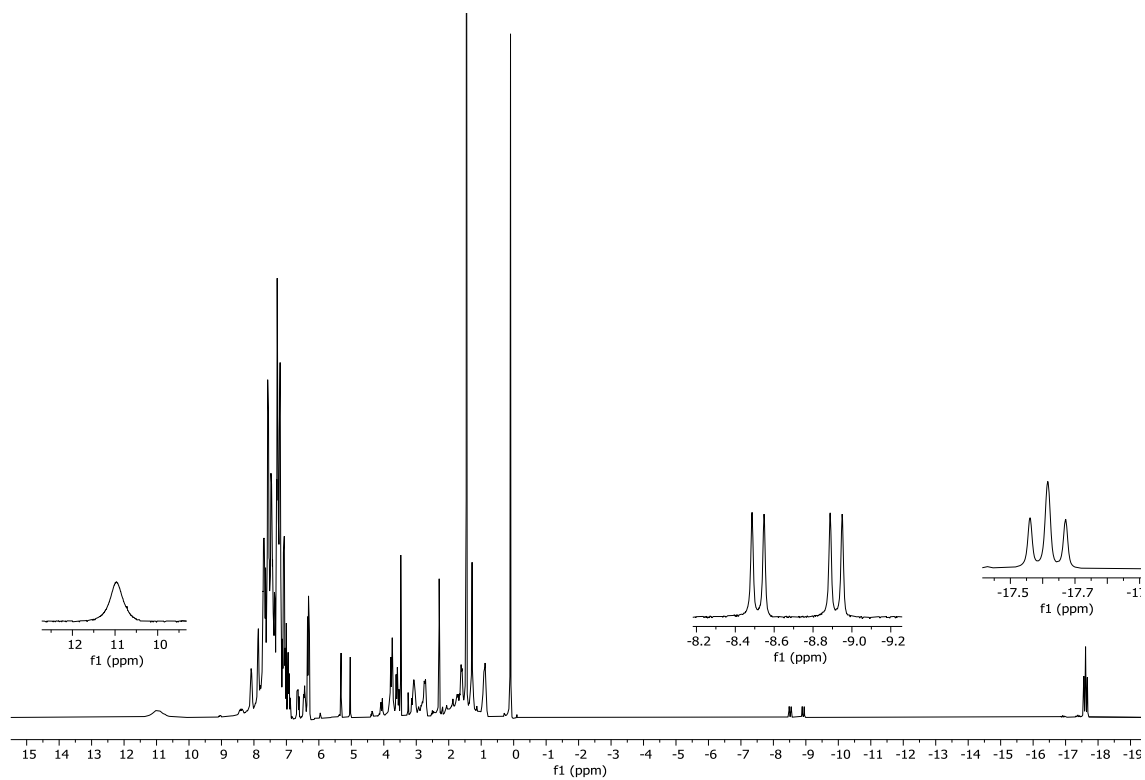
Figure B. 82 ¹H NMR of complex 22 in CDCl₃

Figure B. 83 ³¹P{¹H} NMR of complex 22 in CDCl₃
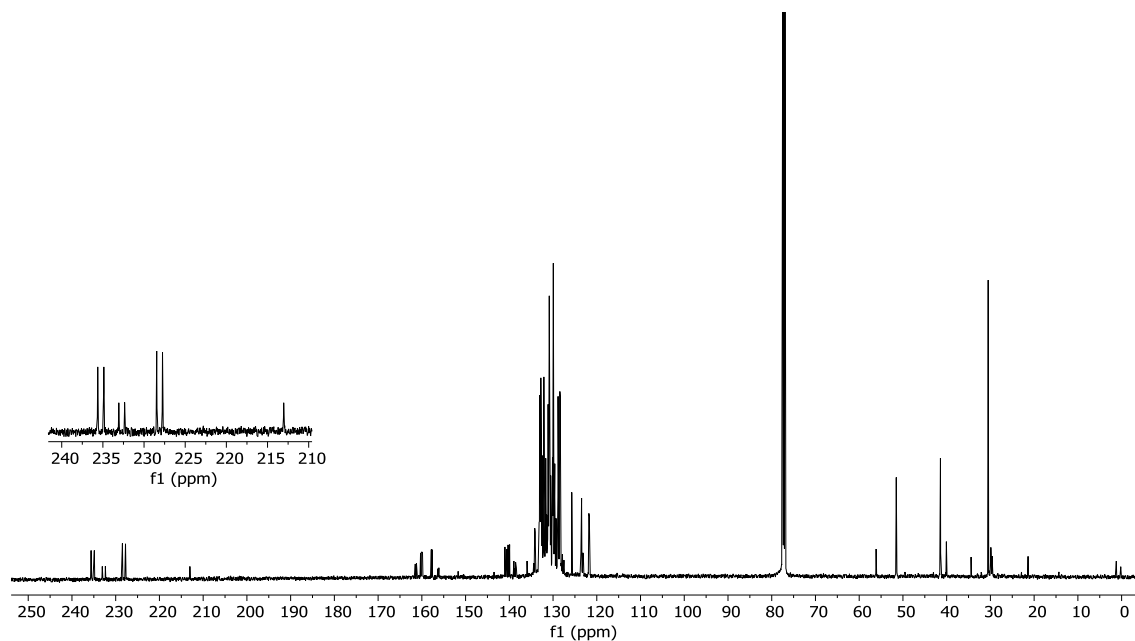
Figure B. 84 ^{13}C{^{1}H} NMR of complex 22 in CDCl$_3$
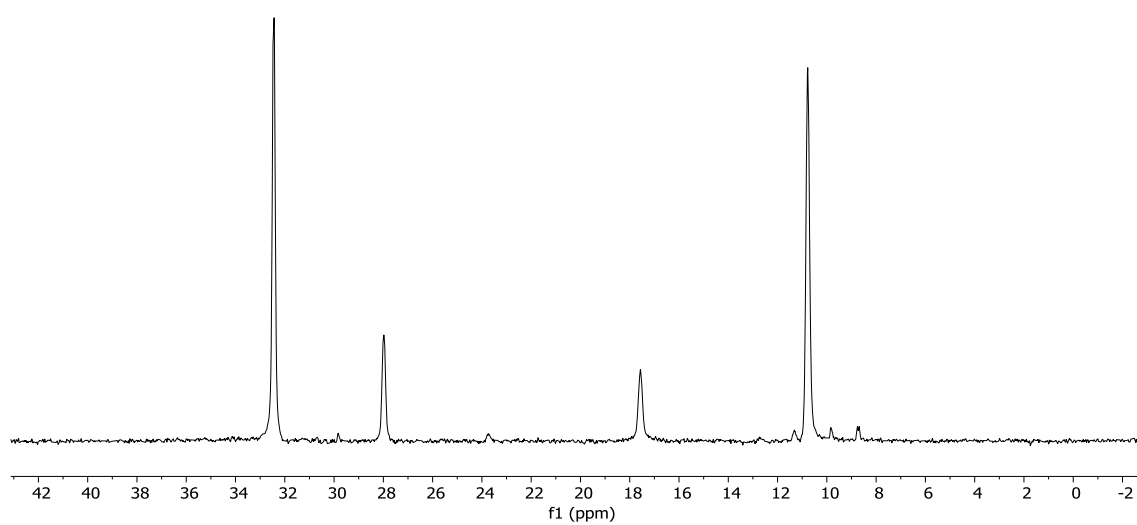

Figure B. 85 COSY spectrum of complex 22 in CDCl$_3$
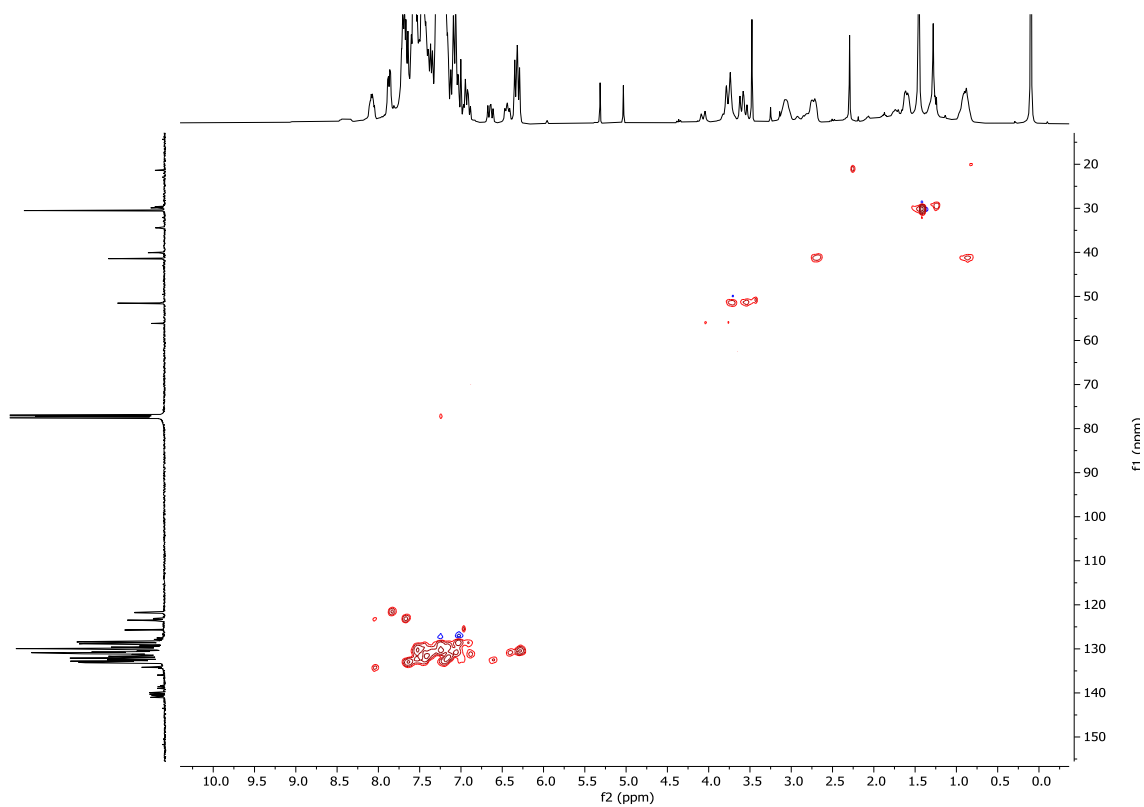
Figure B. 86 ^{1}H-^{13}C HSQC spectrum of complex 22 in CDCl$_3$

Complex 23
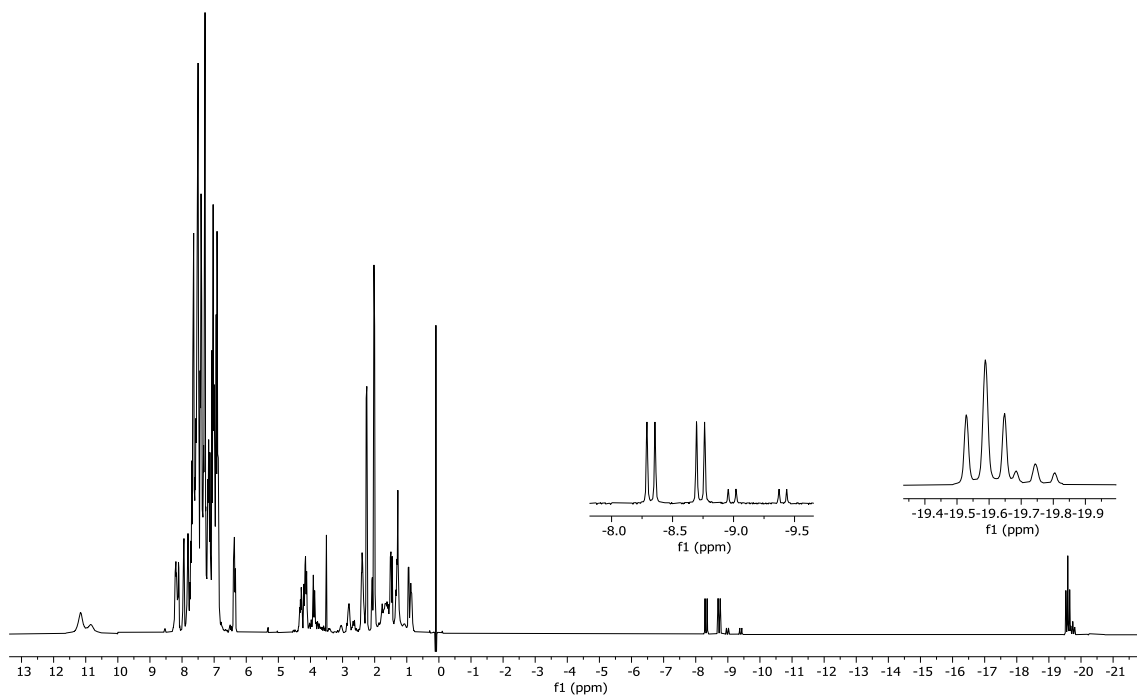
Figure B. 87 ^{1}H NMR of complex 23 in CDCl$_3$

Figure B. 88 ^{31}P{^{1}H} NMR of complex 23 in CDCl$_3$
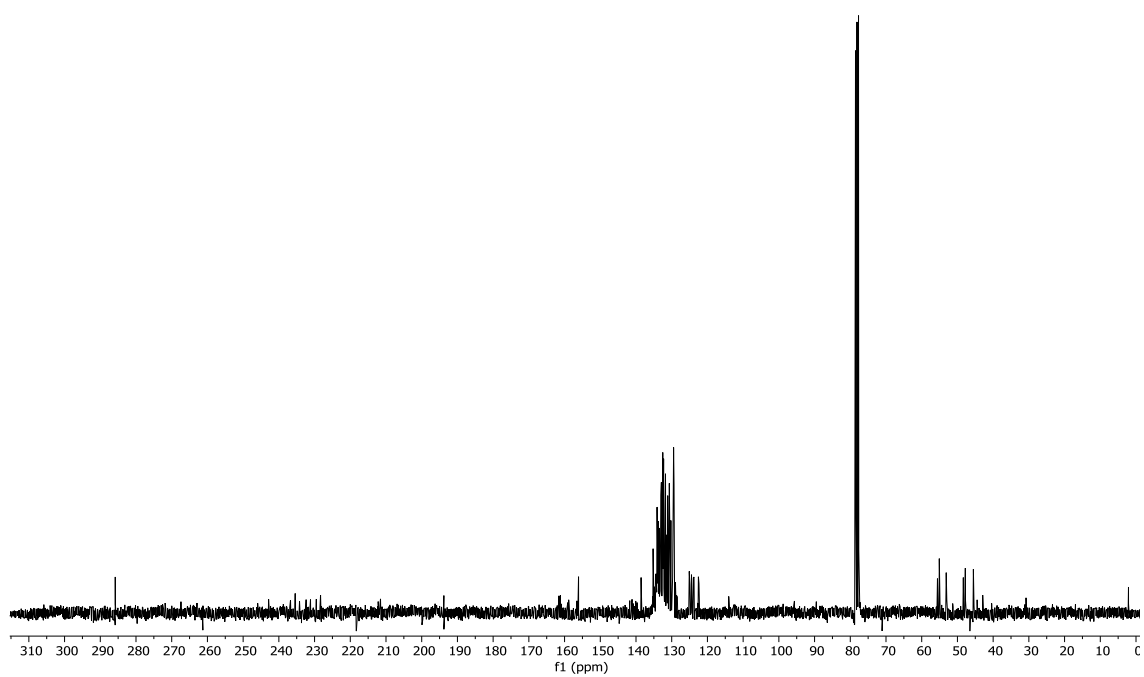
Figure B. 89 ^{13}C{^{1}H} NMR of complex 23 in CDCl$_3$
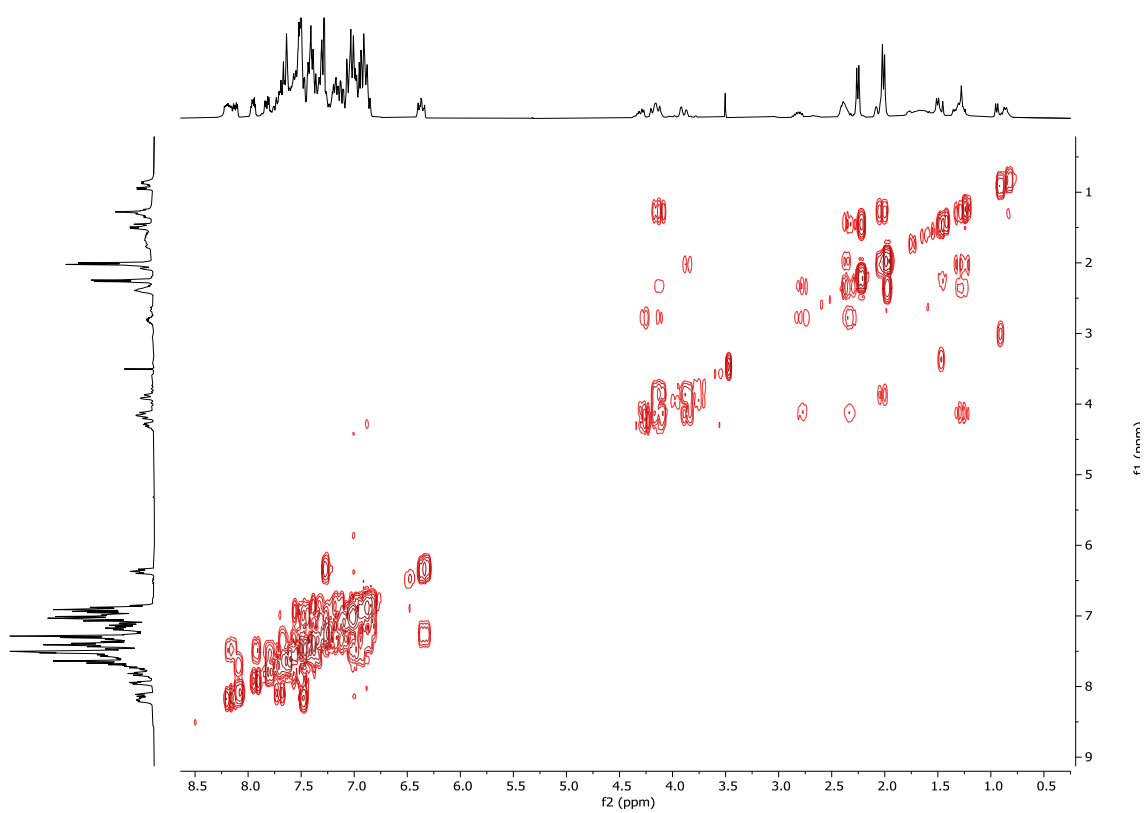
Figure B. 90 COSY spectrum of complex 23 in CDCl$_3$
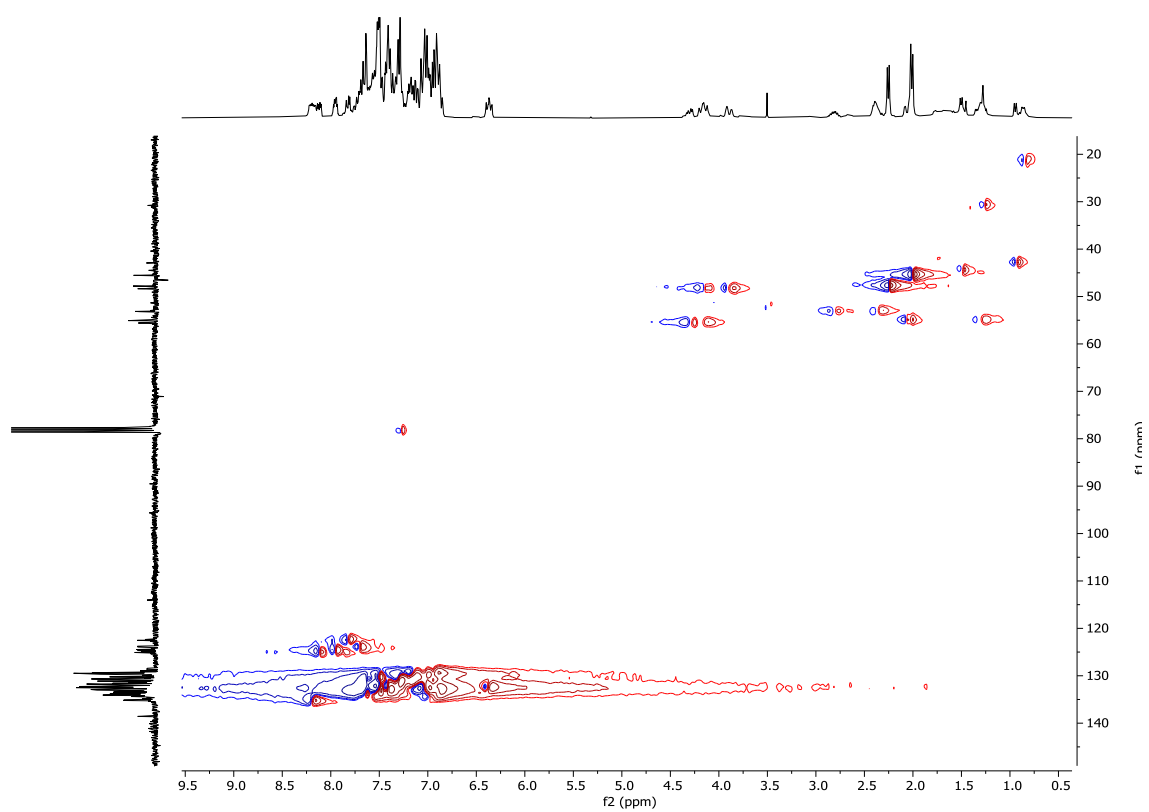
Figure B. 91 ^{1}H-^{13}C HSQC spectrum of complex 23 in CDCl$_3$

<u>Complex 24</u>
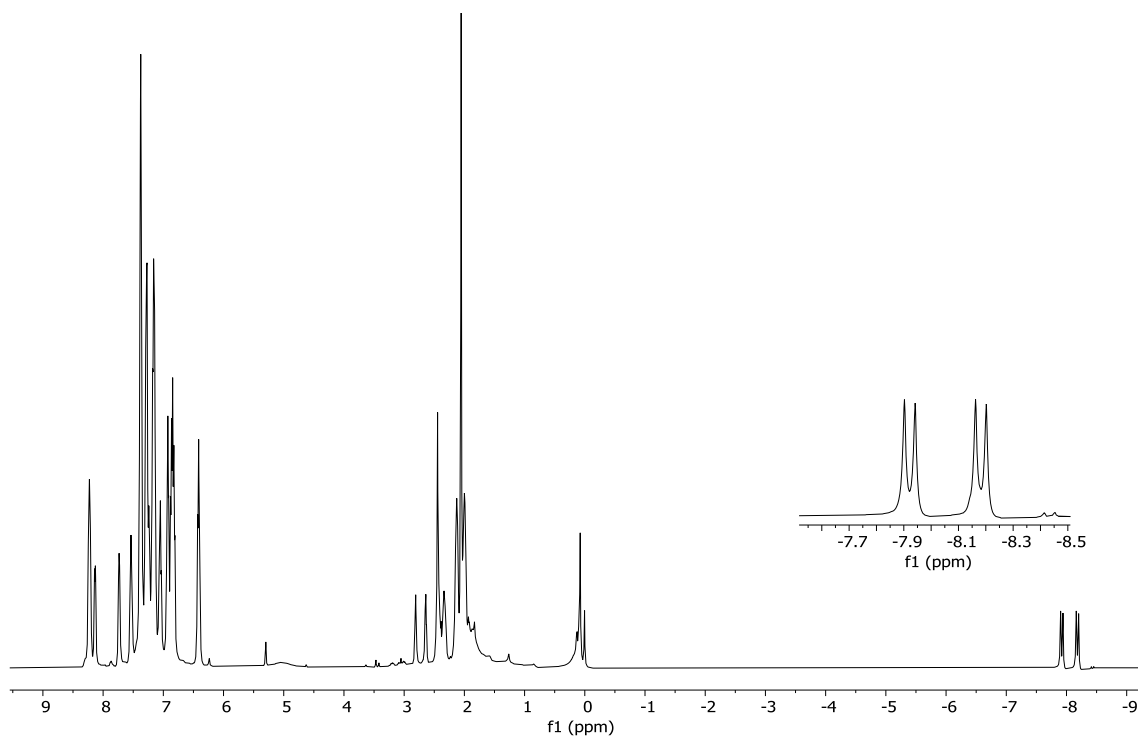
Figure B. 92 ^{1}H NMR of complex 24 in CDCl$_3$
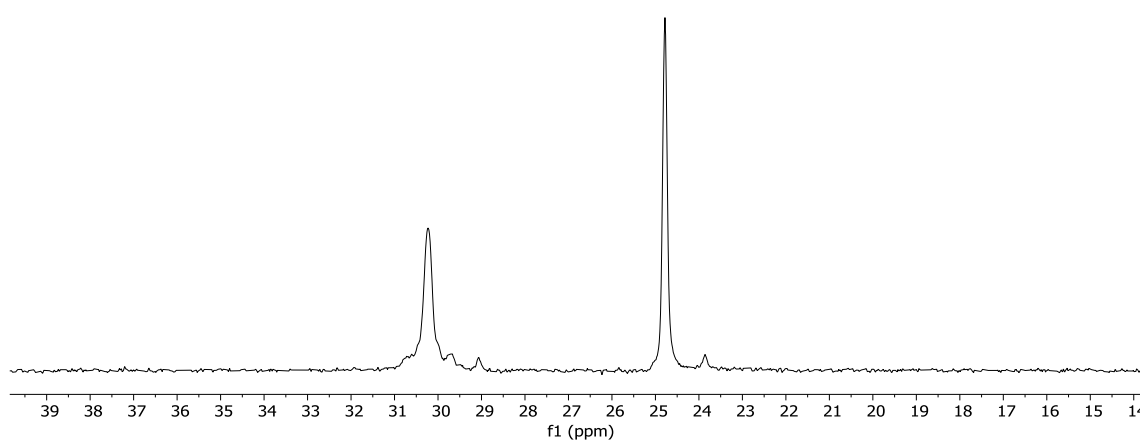
Figure B. 93 ^{31}P{^{1}H} NMR of complex 24 in CDCl$_3$
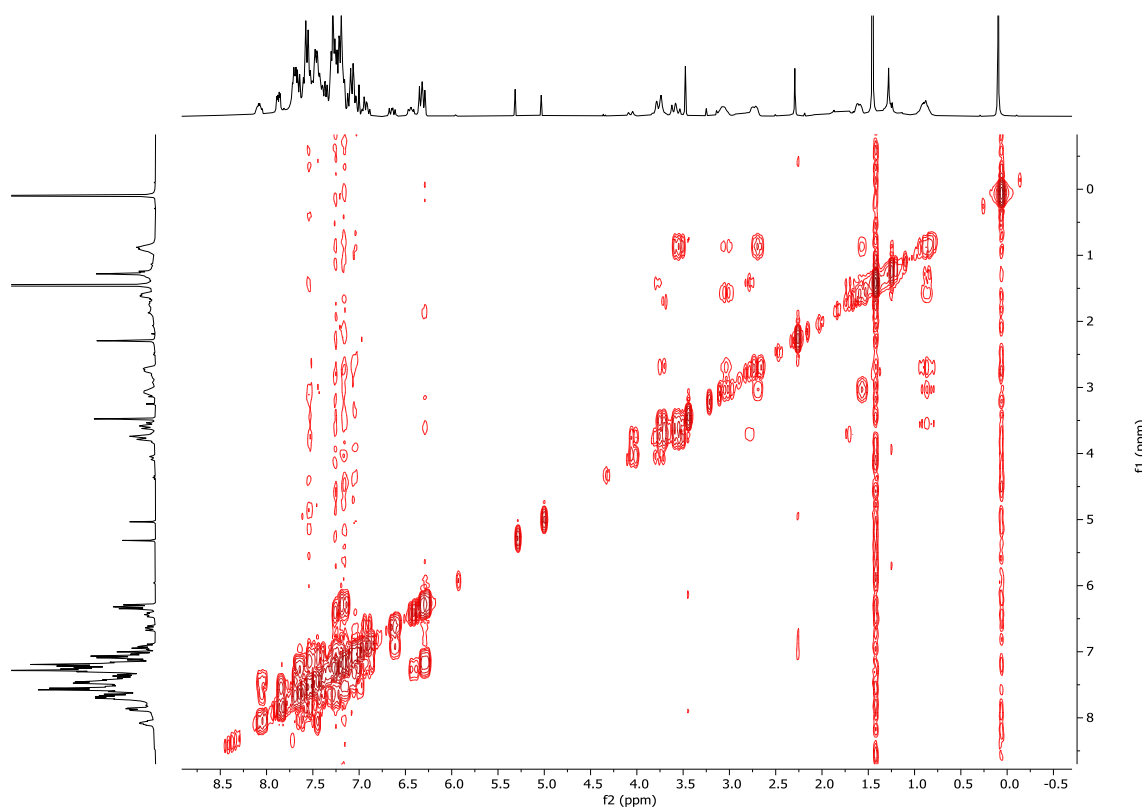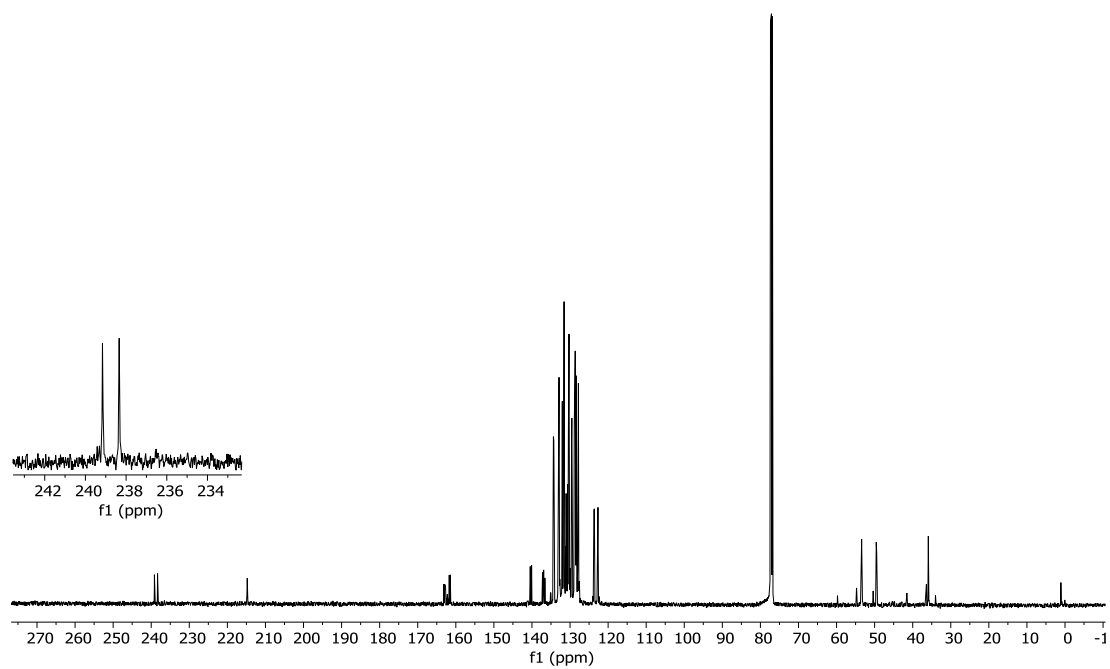
Figure B. 94 ^{13}C{^{1}H} NMR of complex 24 in CDCl$_3$
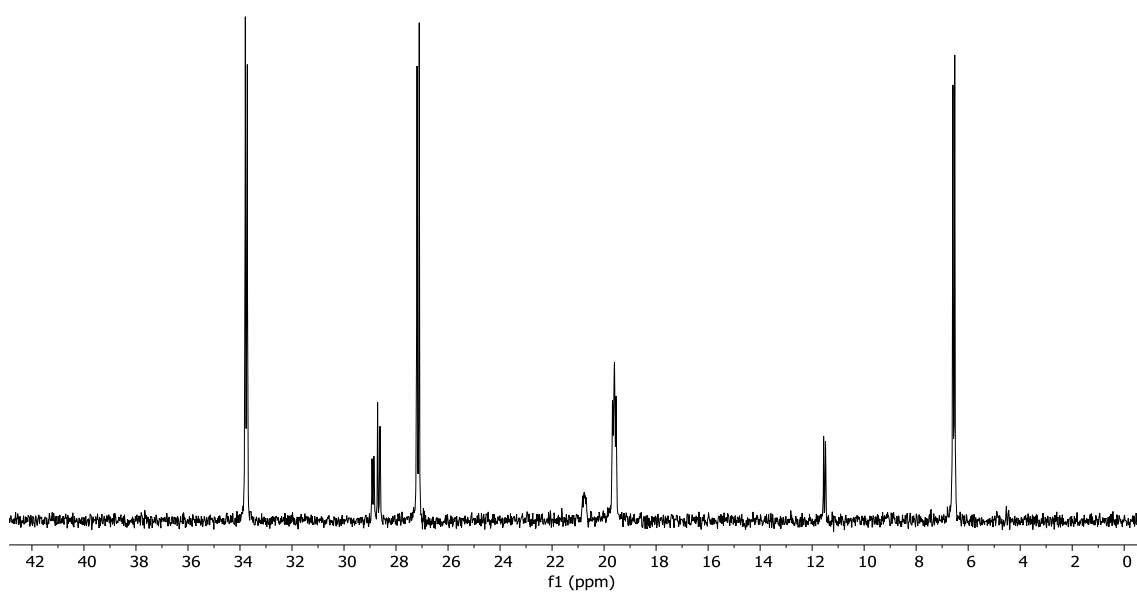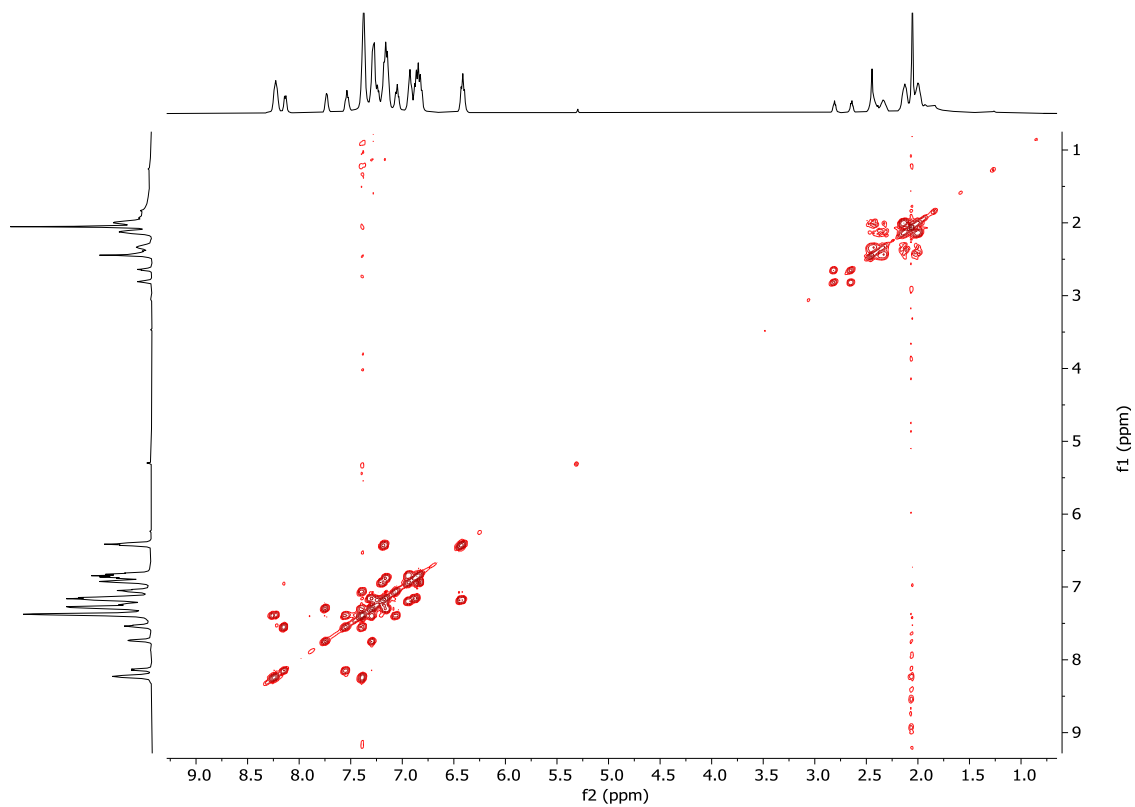

Figure B. 95 COSY spectrum of complex 24 in CDCl$_3$
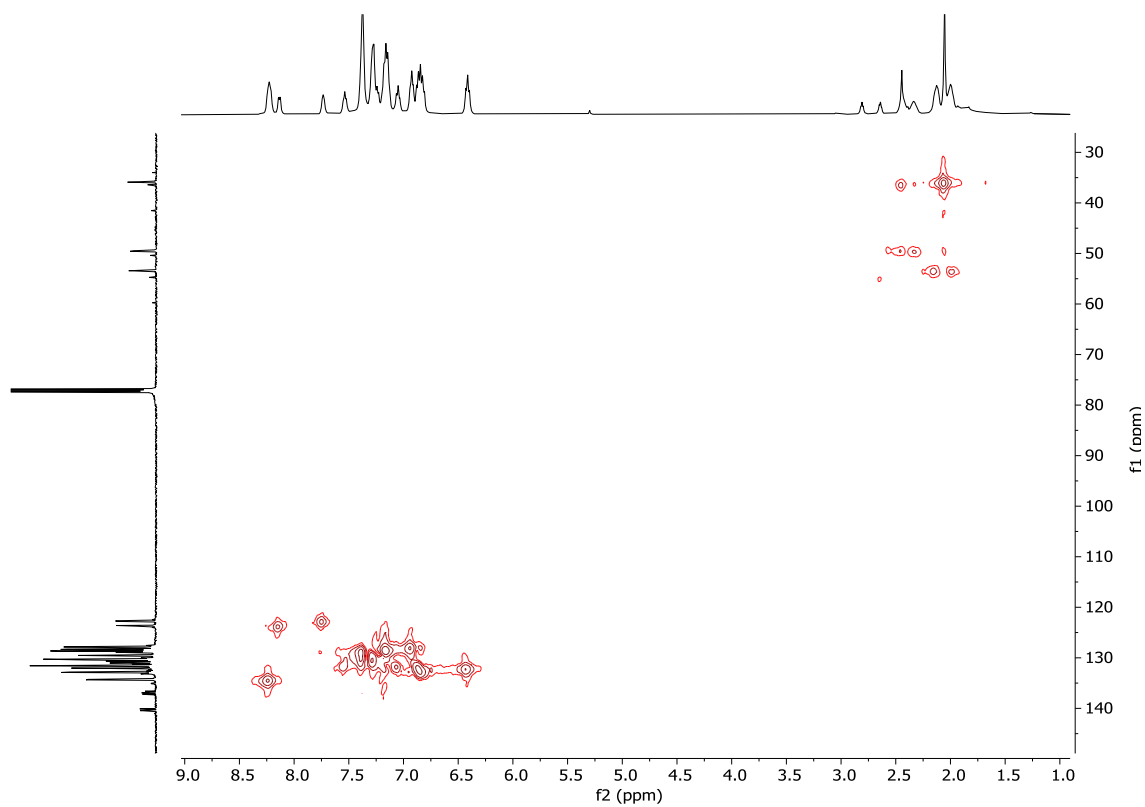
Figure B. 96 ^{1}H-^{13}C HSQC spectrum of complex 24 in CDCl$_3$

Complex 25
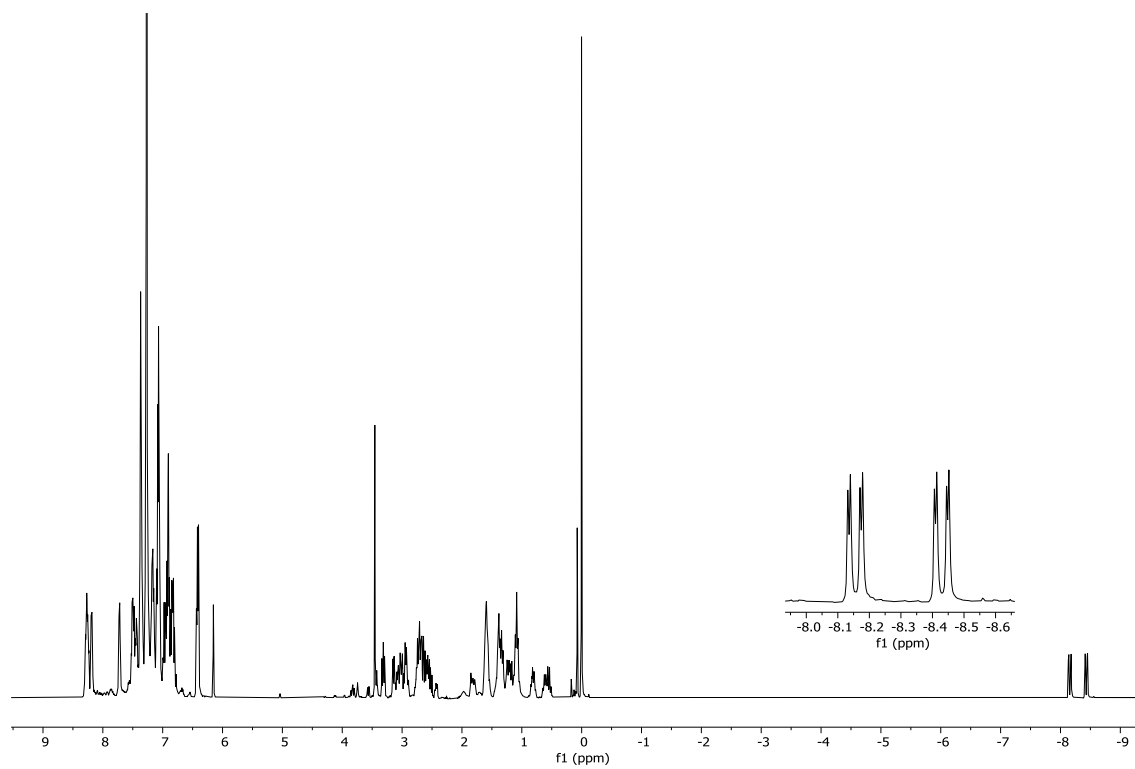
Figure B. 97 ^{1}H NMR of complex 25 in CDCl$_3$
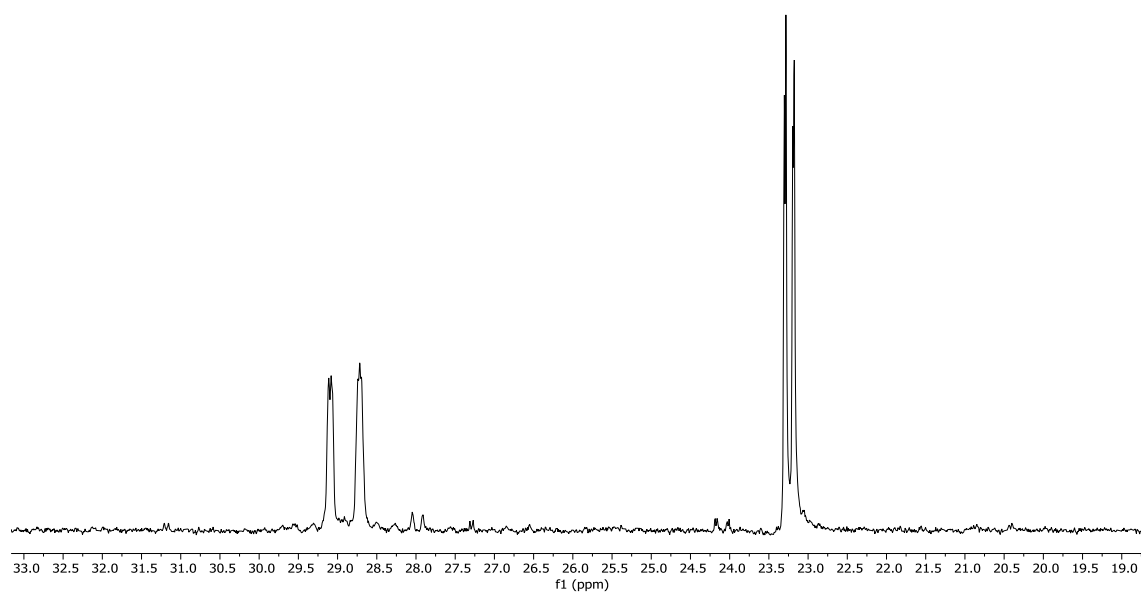
Figure B. 98 ^{31}P{^{1}H} NMR of complex 25 in CDCl$_3$
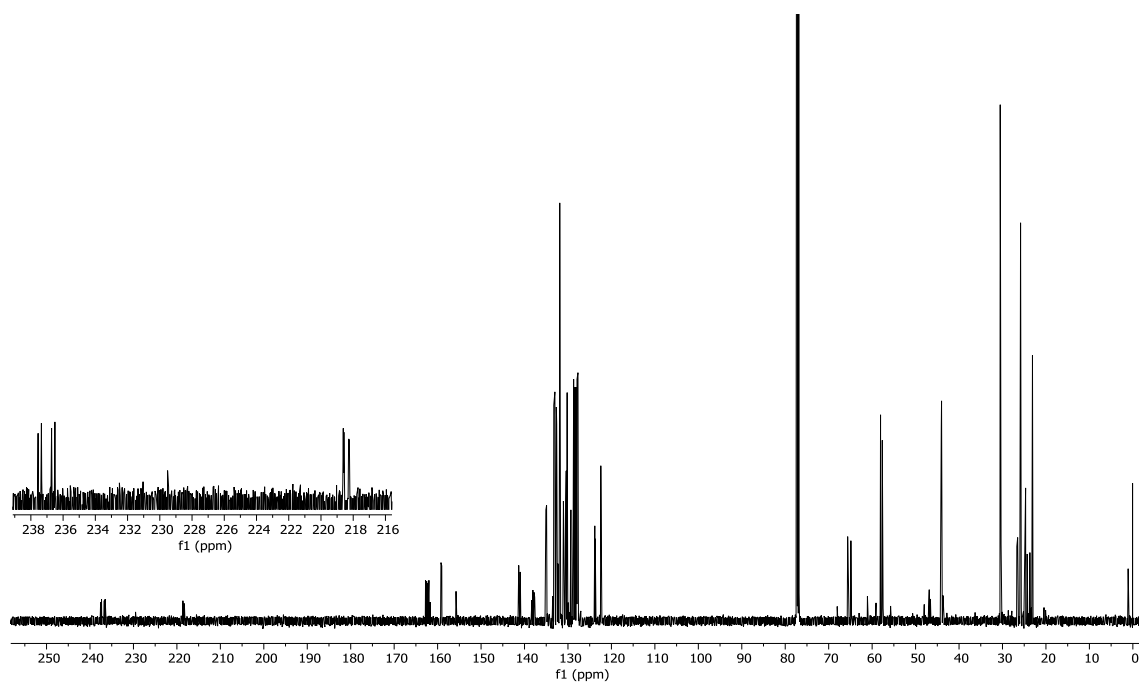
Figure B. 99 ^{13}C{^{1}H} NMR of complex 25 in CDCl$_3$
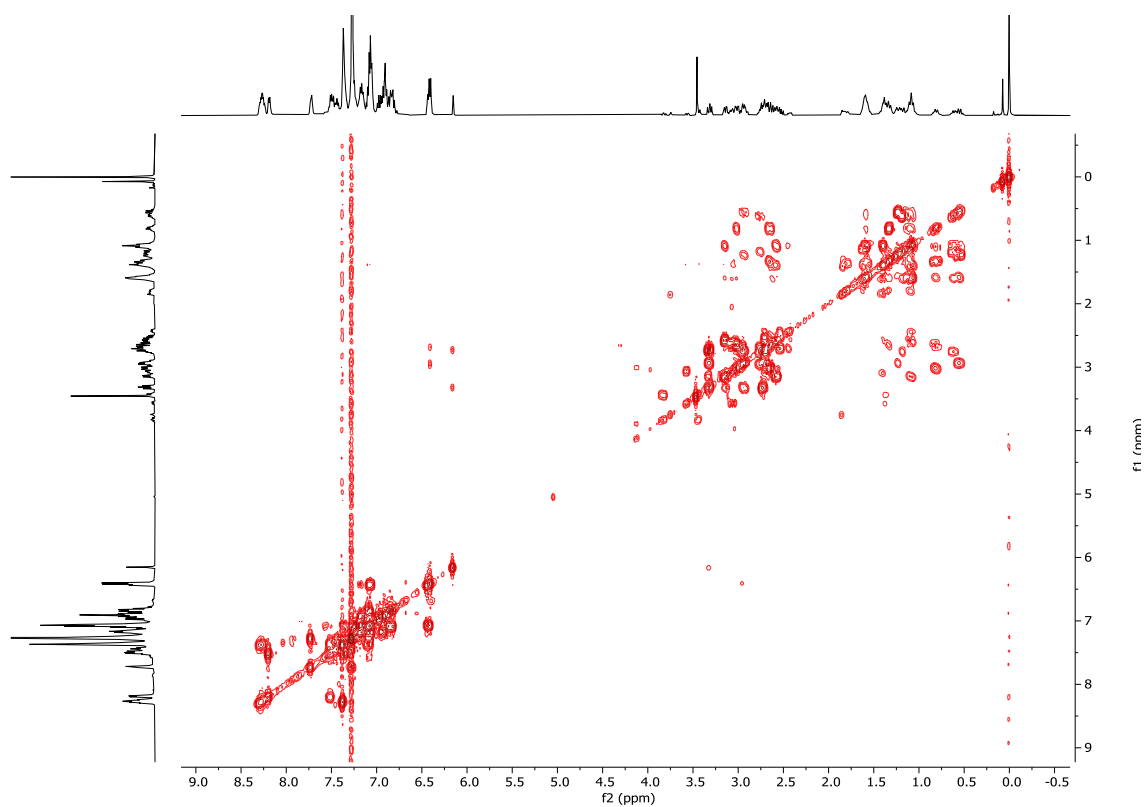
Figure B. 100 COSY spectrum of complex 25 in CDCl₃
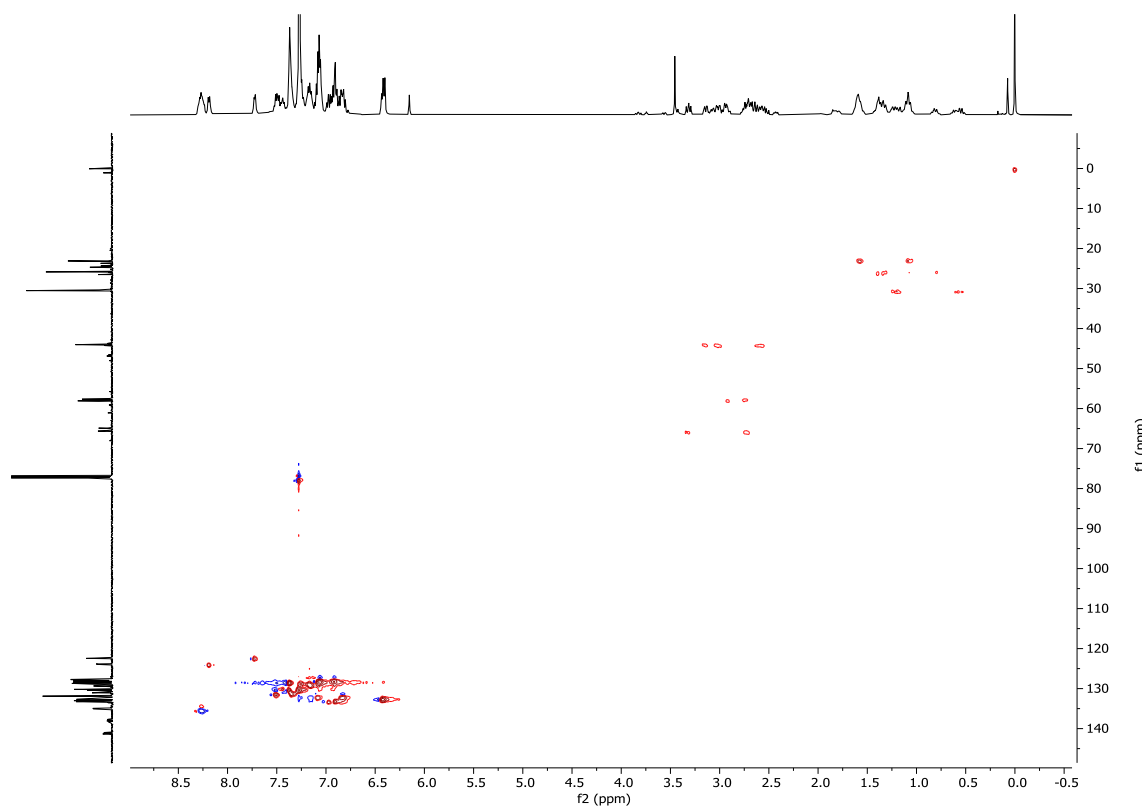
Figure B. 101 ¹H-¹³C HSQC spectrum of complex 25 in CDCl₃

Chapter 5

<u>L</u>$_1$
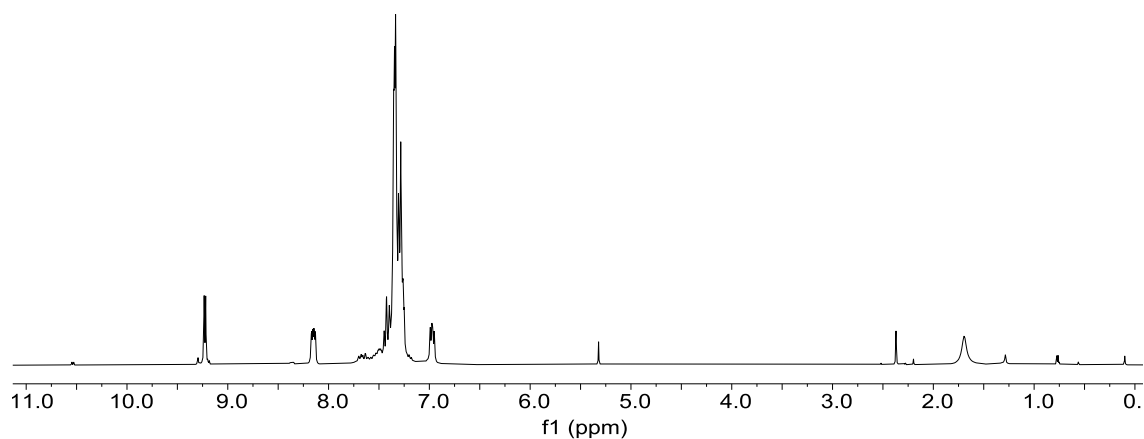
Figure B. 102 ^{1}H NMR of L$_1$ in CDCl$_3$
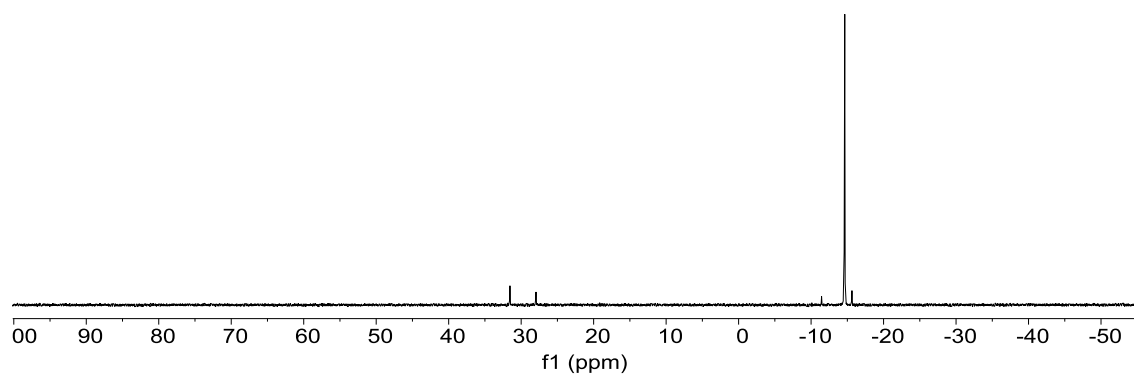
Figure B. 103 ^{31}P{^{1}H} NMR of L$_1$ in CDCl$_3$
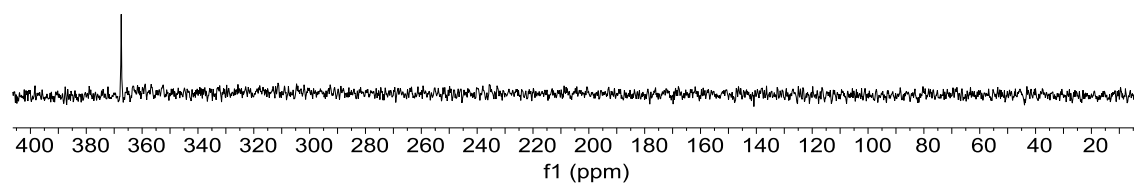
Figure B. 104 ^{15}N NMR of L$_1$ in CDCl$_3$

Complex 27
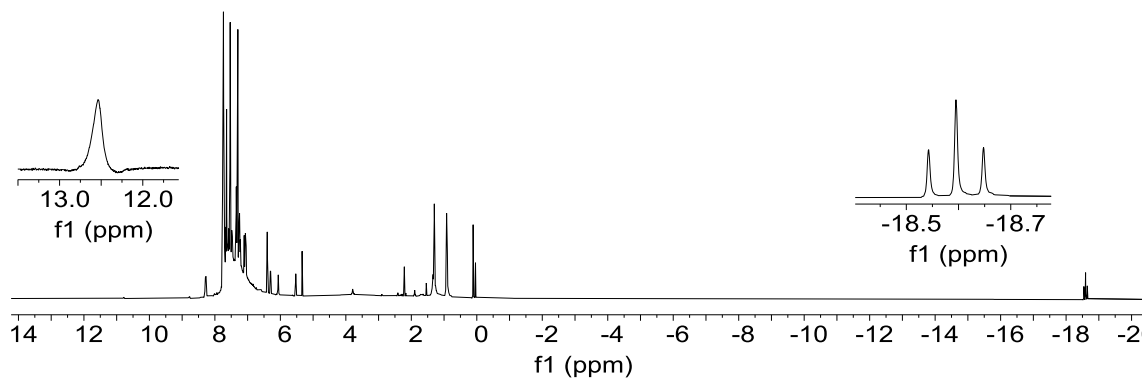
Figure B. 105 ^{1}H NMR of complex 27 in CDCl$_3$ at 297 K.
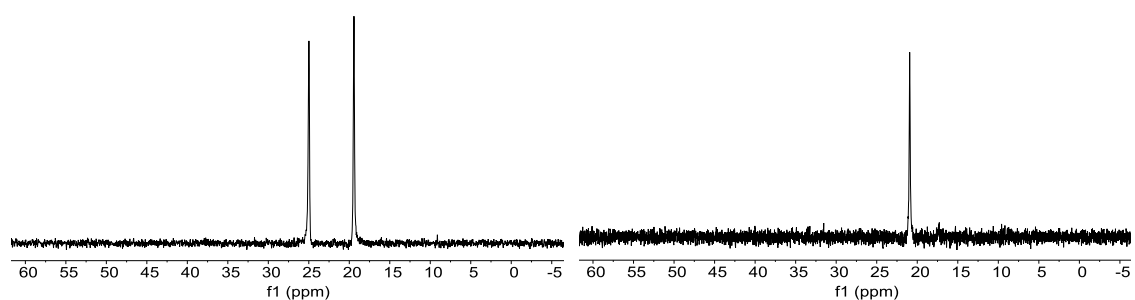
Figure B. 106 ^{31}P{^{1}H} NMR spectra of complex 27; in CD$_2$Cl$_2$ at 213 K (left) and in CDCl$_3$ at 297 K (right).
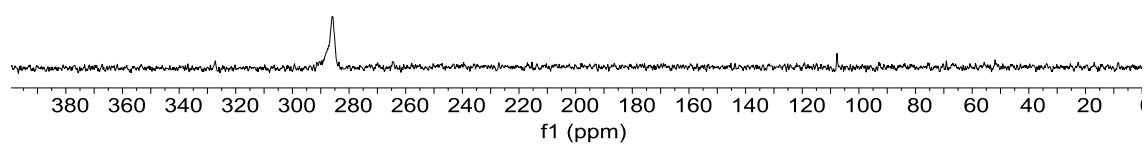
Figure B. 107 ^{15}N NMR of complex 27 in CDCl$_3$ at 297 K

Complex 28
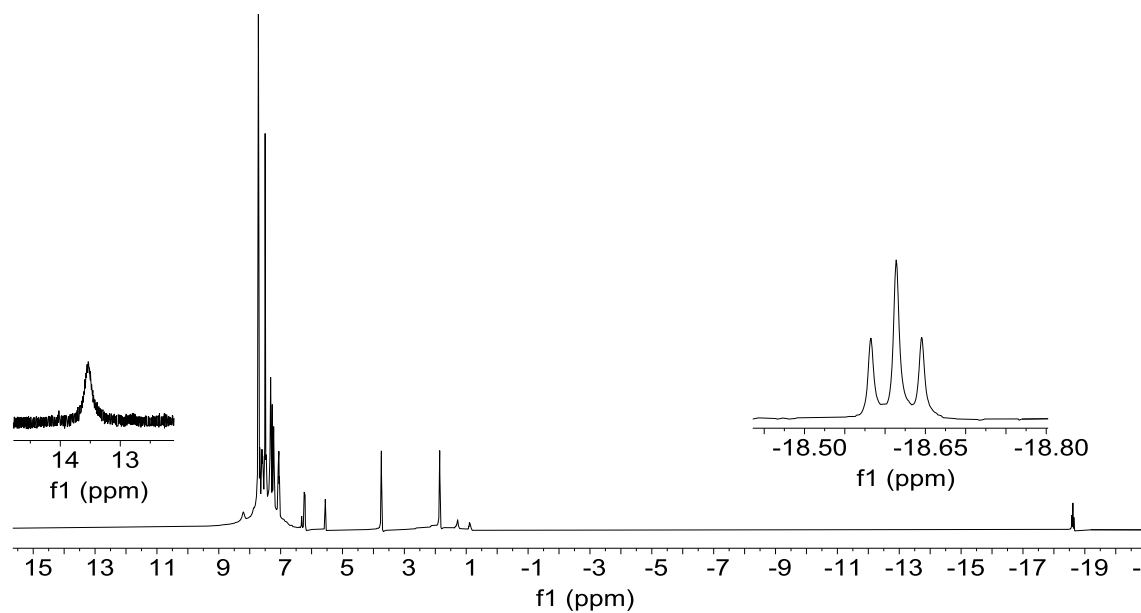
Figure B. 108 ^{1}H NMR of complex 28 in CD$_2$Cl$_2$ at 297K
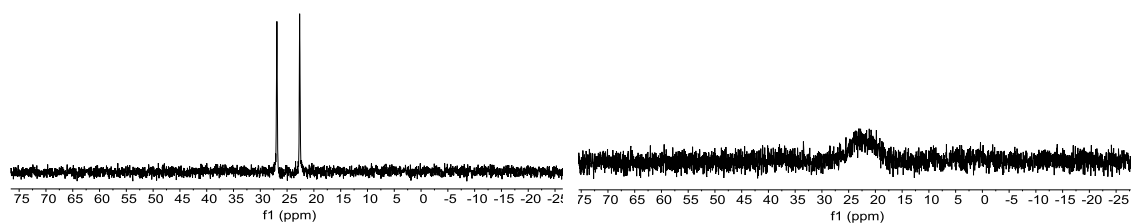
Figure B. 109 ^{31}P{^{1}H} NMR spectra of complex 28 in CD$_2$Cl$_2$ at 213 K (left) and at 297 K (right).

Complex 29
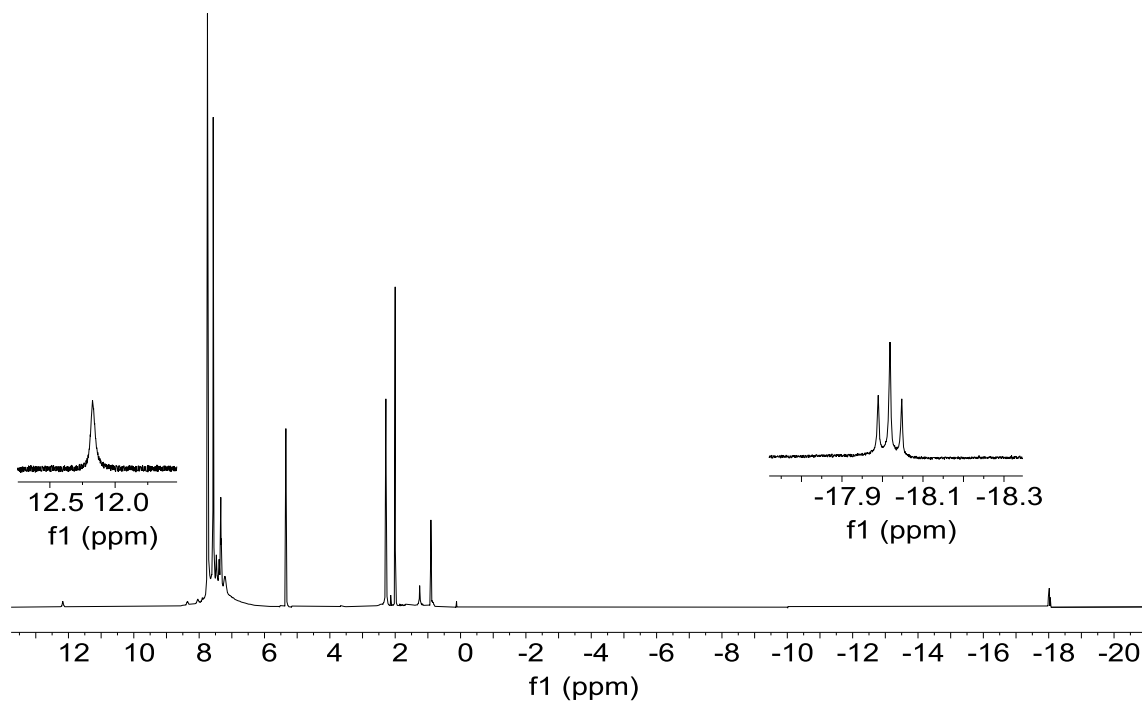
Figure B. 110 ^{1}H NMR of complex 29 in CD$_2$Cl$_2$ at 253 K
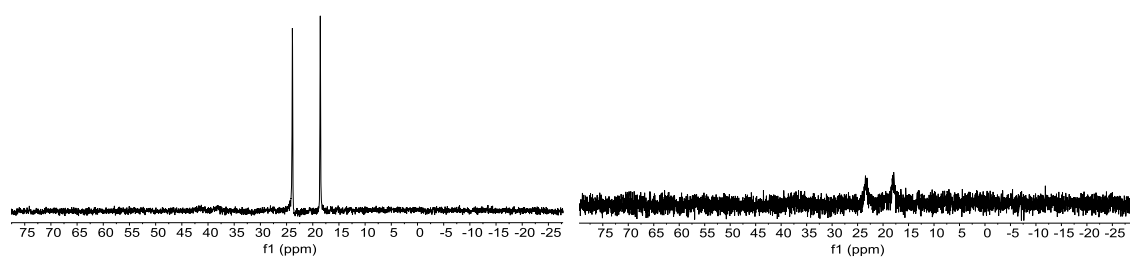
Figure B. 111 ^{31}P{^{1}H} NMR spectra of complex 29 in CD$_2$Cl$_2$ at 213 K (left) and at 297 K (right).

Complex 30
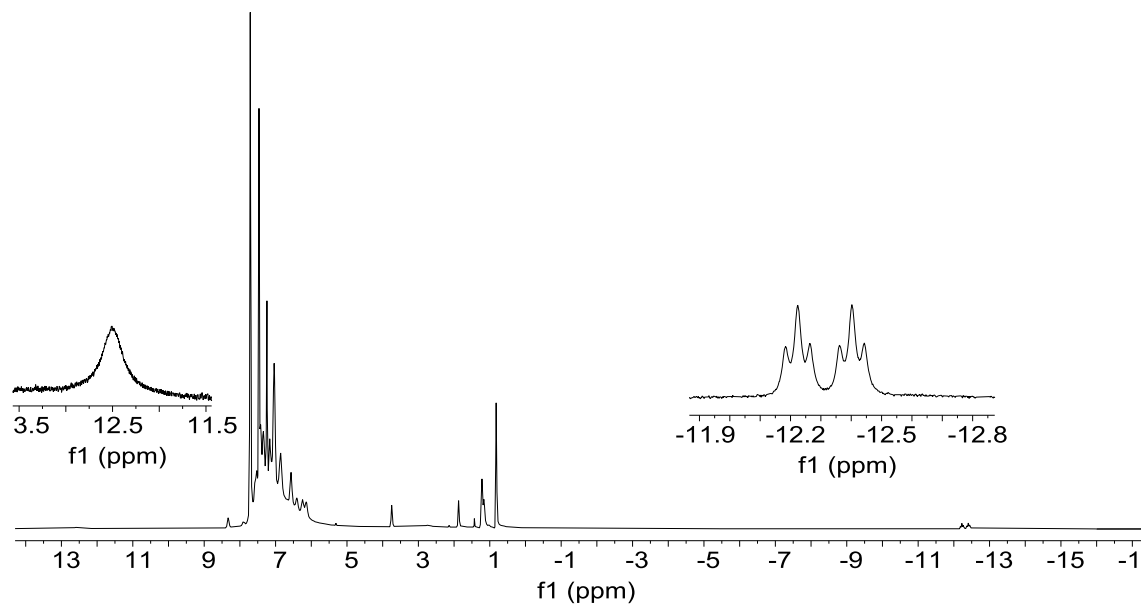
Figure B. 112 ^{1}H NMR of complex 30 in CDCl$_3$ at 297 K
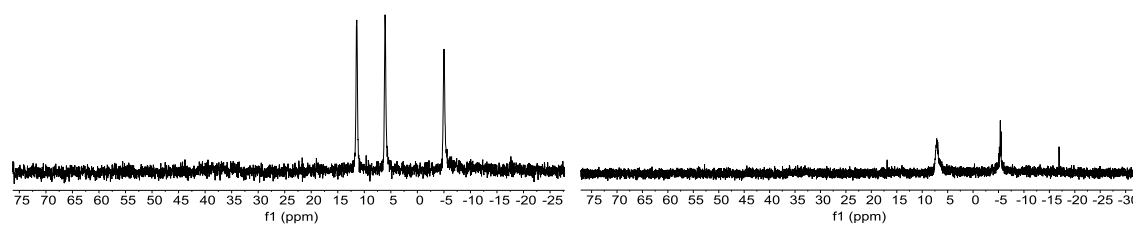
Figure B. 113 ^{31}P{^{1}H} NMR spectra of complex 30 in CD$_2$Cl$_2$ at 213 K (left) and at 297 K (right).

Complex 31
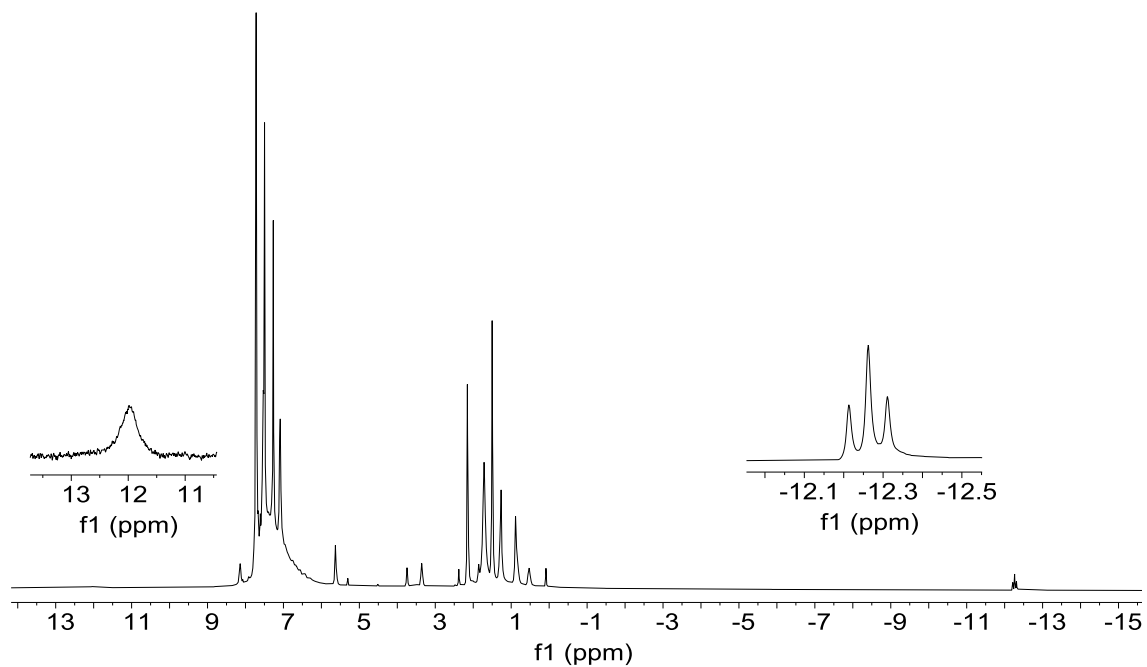
Figure B. 114 ^{1}H NMR of complex 31 in CDCl$_3$ at 297K
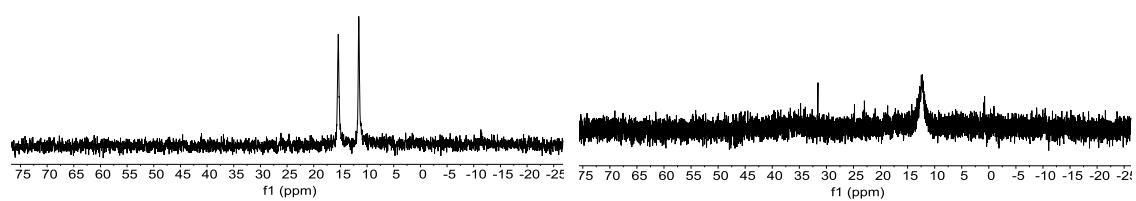
Figure B. 115 ^{31}P{^{1}H} NMR spectra of complex 31 in CDCl$_3$ at 213 K (left) and at 297 K (right).

Complex 32
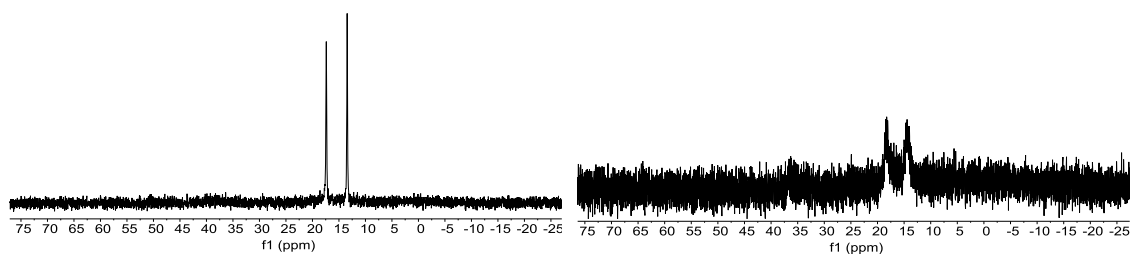
Figure B. 116 ^{31}P{^{1}H} **NMR spectra of complex 32 in CD$_2$Cl$_2$ at 210 K (left) and in CDCl$_3$ at 297 K (right).**

Complex 33
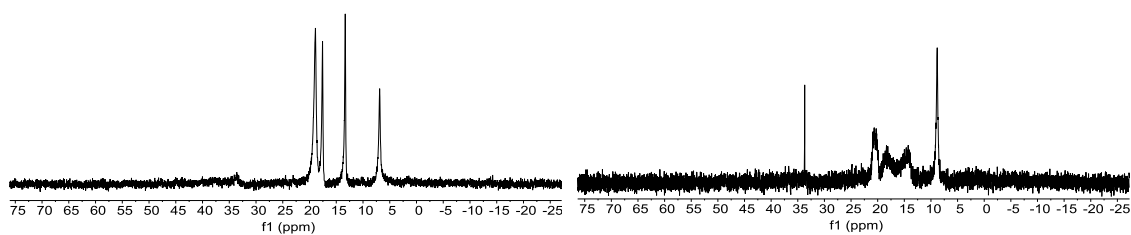
Figure B. 117 ^{31}P{^{1}H} **NMR spectra of complex 33 in CD$_2$Cl$_2$ at 212 K (left) and 297 K (right).**

<u>Complex 34</u>
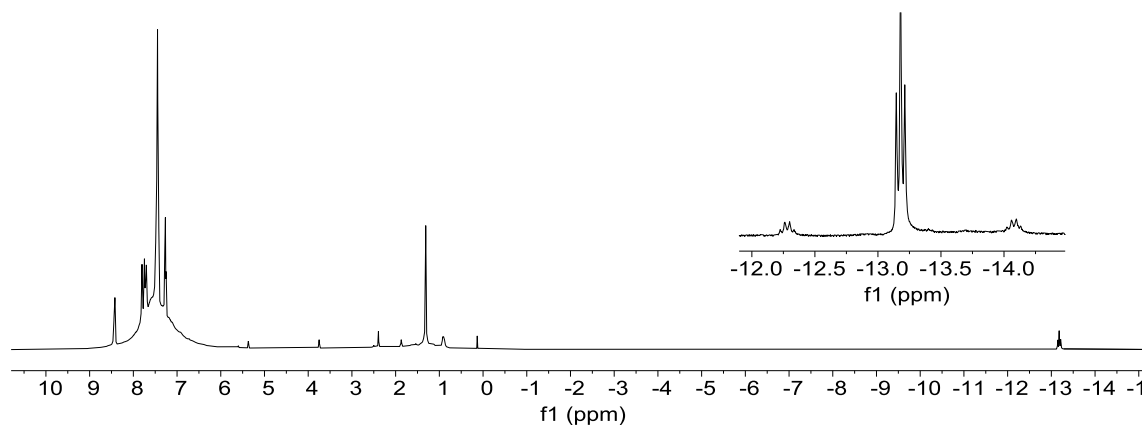
Figure B. 118 ^{1}H NMR of complex 34 in CDCl$_3$ at 297 K
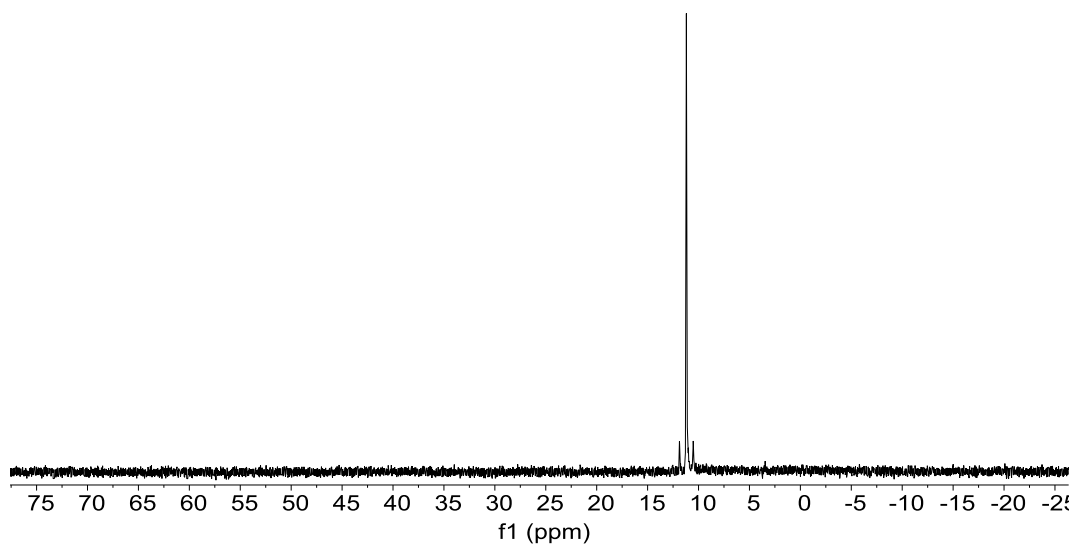
Figure B. 119 ^{31}P{^{1}H} NMR of complex 34 in CDCl$_3$ at 297 K
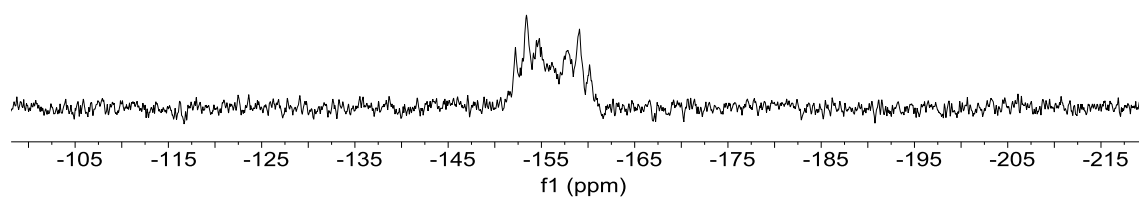
Figure B. 120 ^{119}Sn NMR of complex 34 in CDCl$_3$ at 297 K

Complex 35
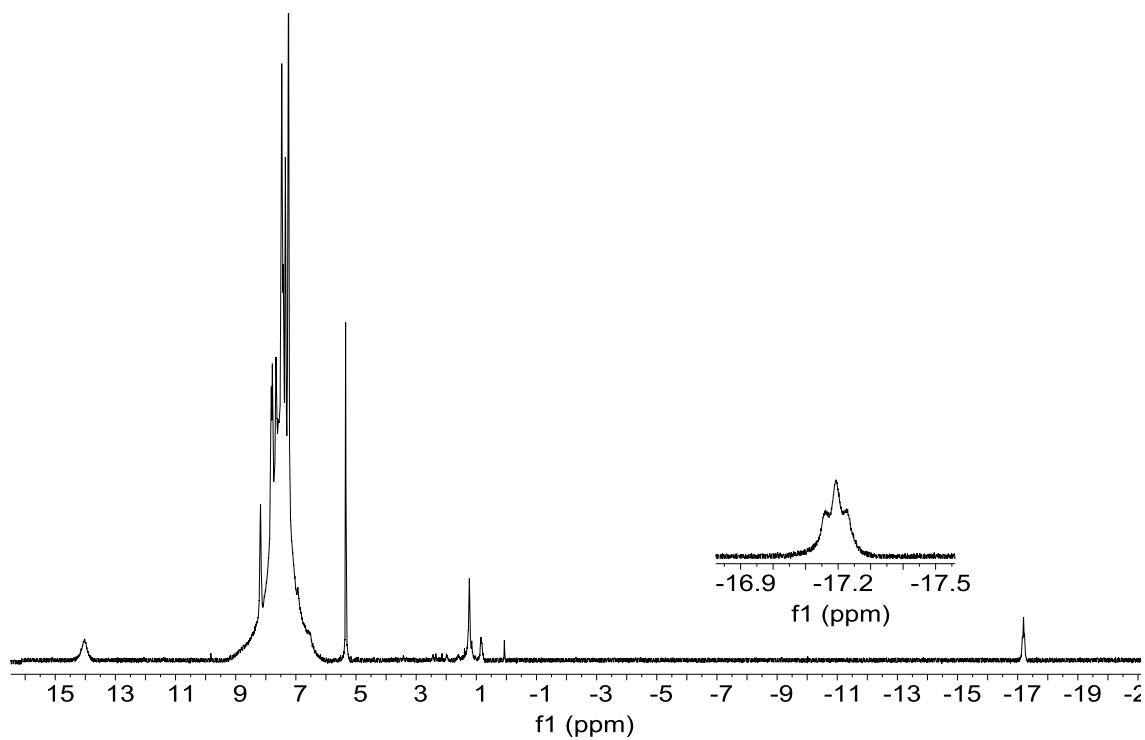
Figure B. 121 ^{1}H NMR of complex 35 in CD$_2$Cl$_2$ at 297K
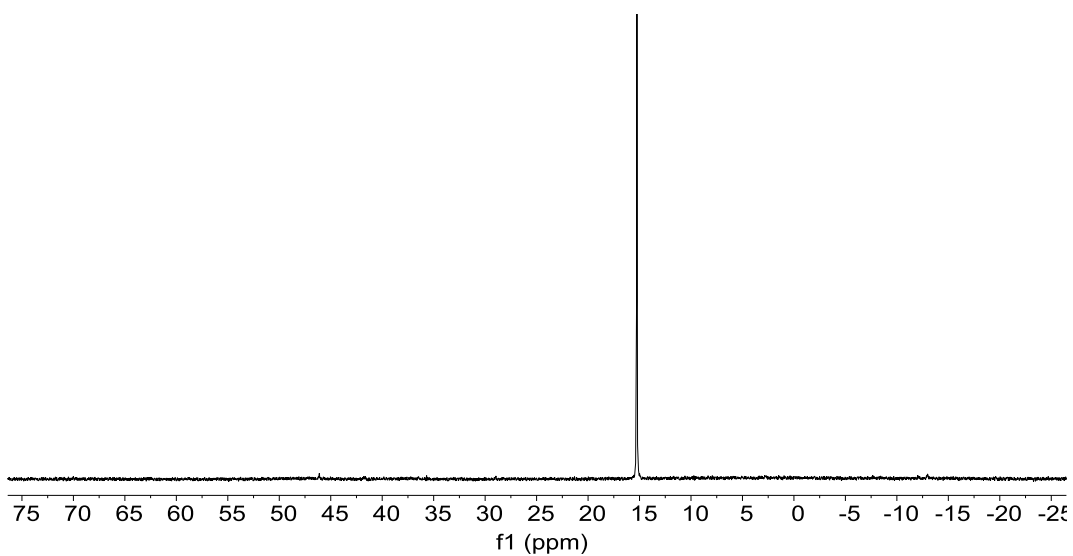
Figure B. 122 ^{31}P{^{1}H} NMR of complex 35 in CD$_2$Cl$_2$ at 297K
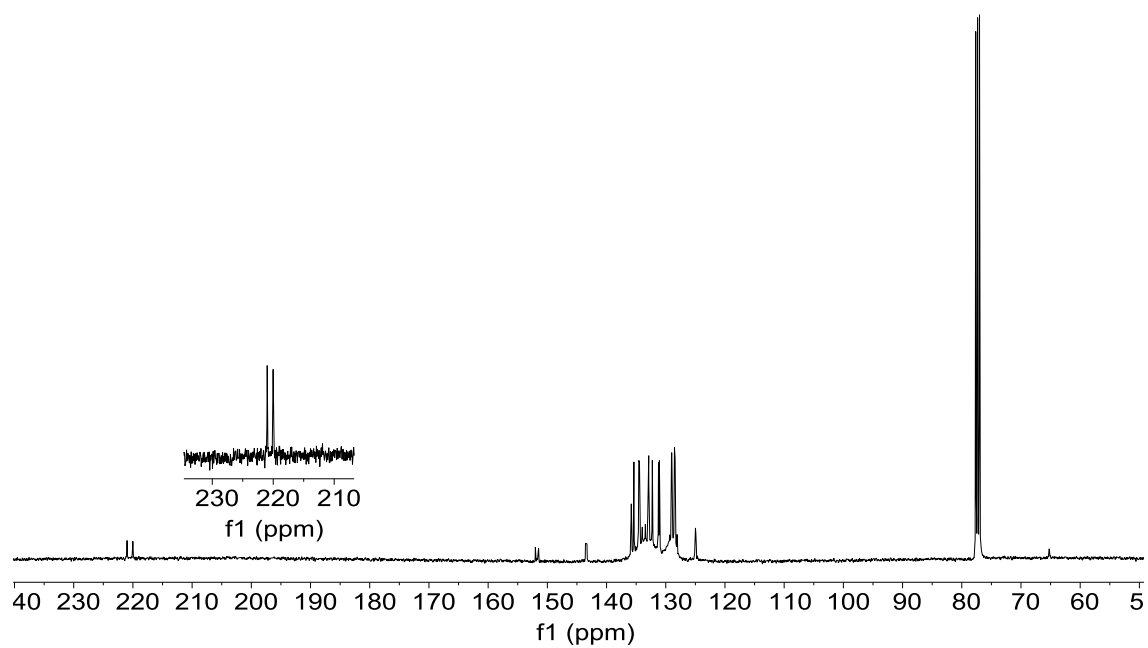
Figure B. 123 ^{13}C{^{1}H} NMR of complex 35 in CDCl$_3$ at 297 K
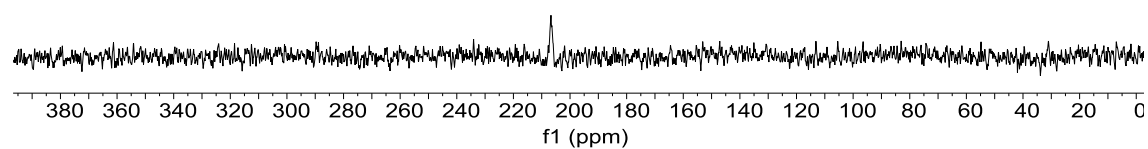
Figure B. 124 ^{15}N NMR of complex 36 in CDCl$_3$ at 297 K

Complex 36
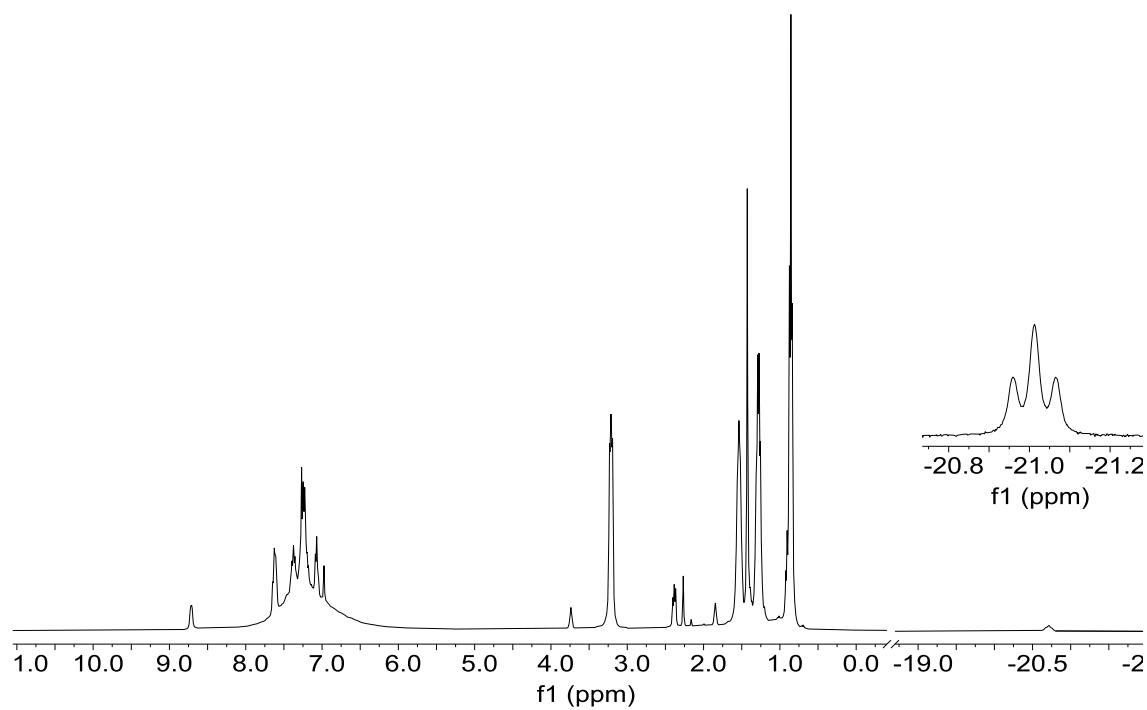
Figure B. 125 ^{1}H NMR of complex 36 in CDCl$_3$ at 297 K
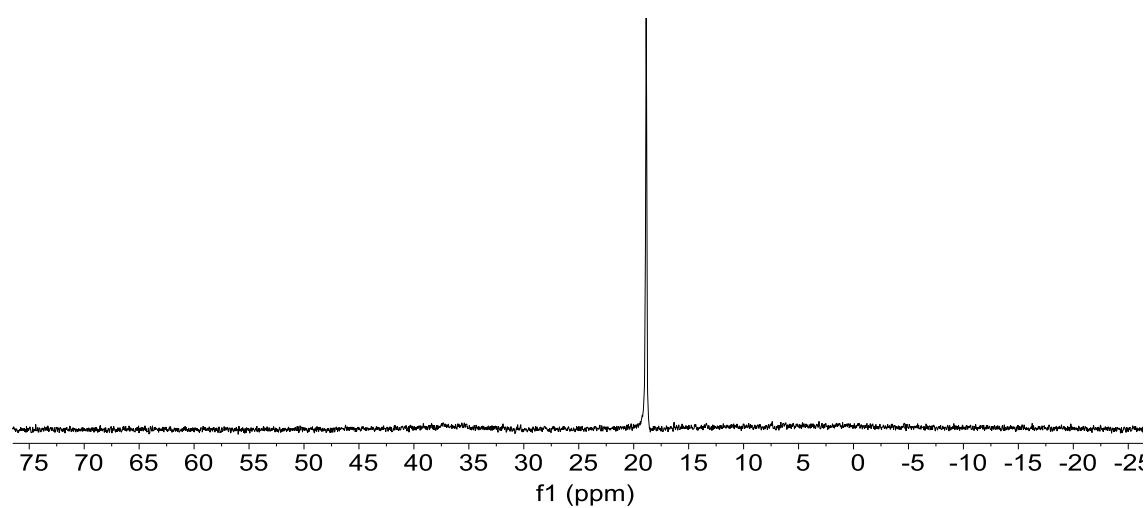
Figure B. 126 ^{31}P{^{1}H} NMR of complex 36 in CDCl$_3$ at 297 K
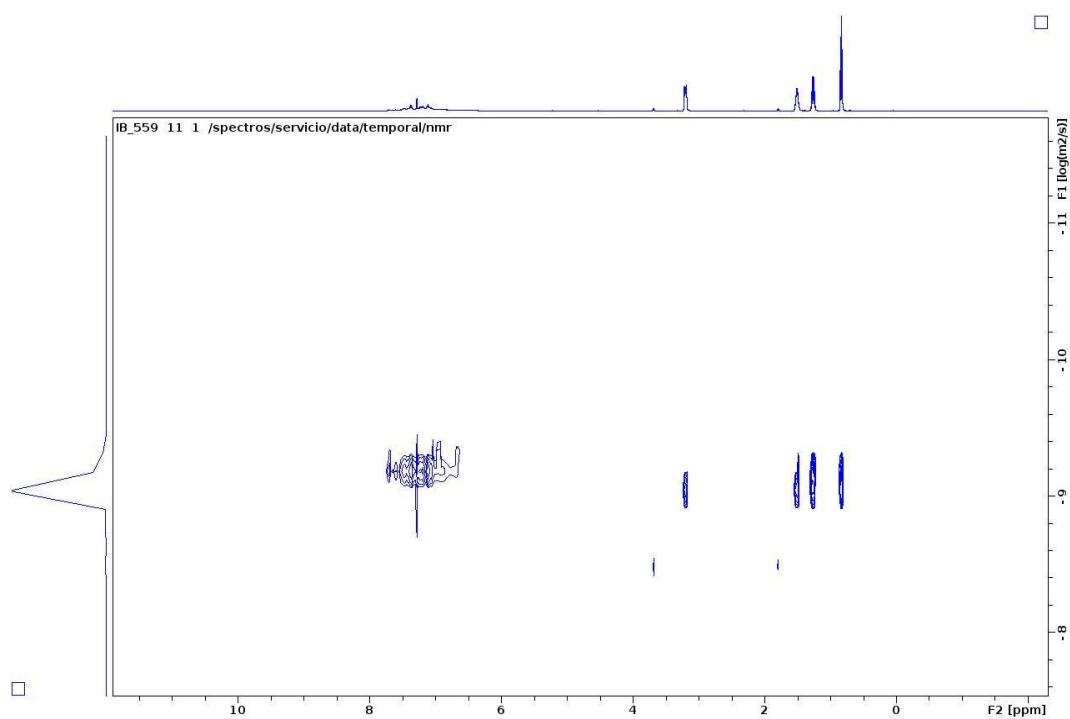
Figure B. 127 DOSY spectrum of complex 36 in CDCl$_3$ at 297 K

Complex 37
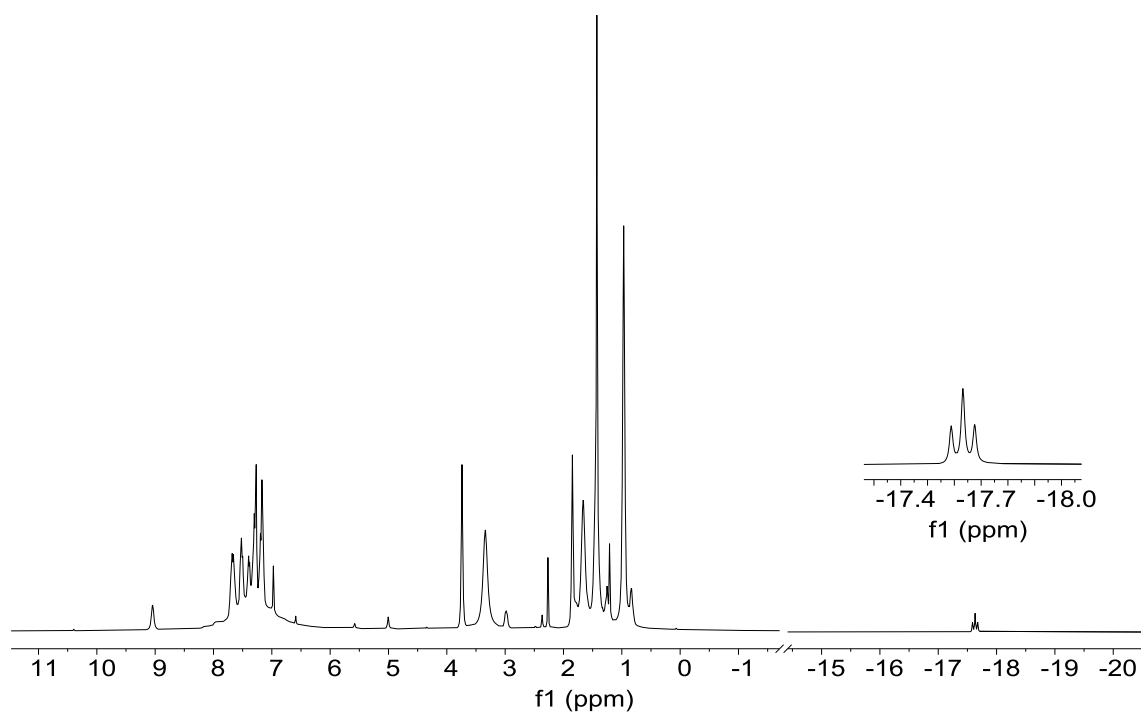
Figure B. 128 ^{1}H NMR of complex 37 in CDCl$_3$ at 297 K
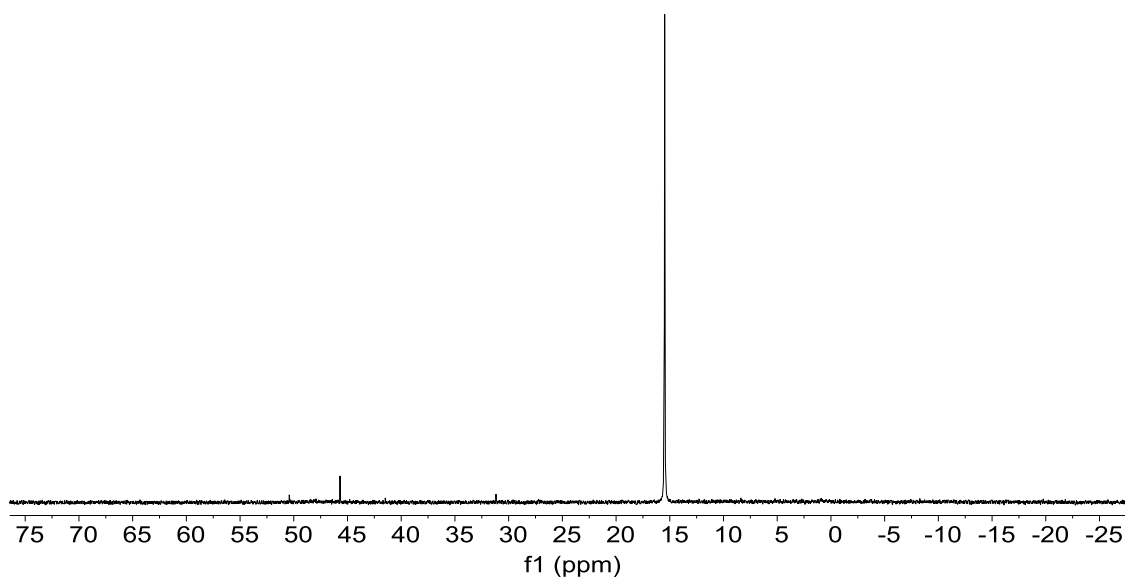
Figure B. 129 ^{31}P{^{1}H} NMR of complex 37 in CDCl$_3$ at 297 K
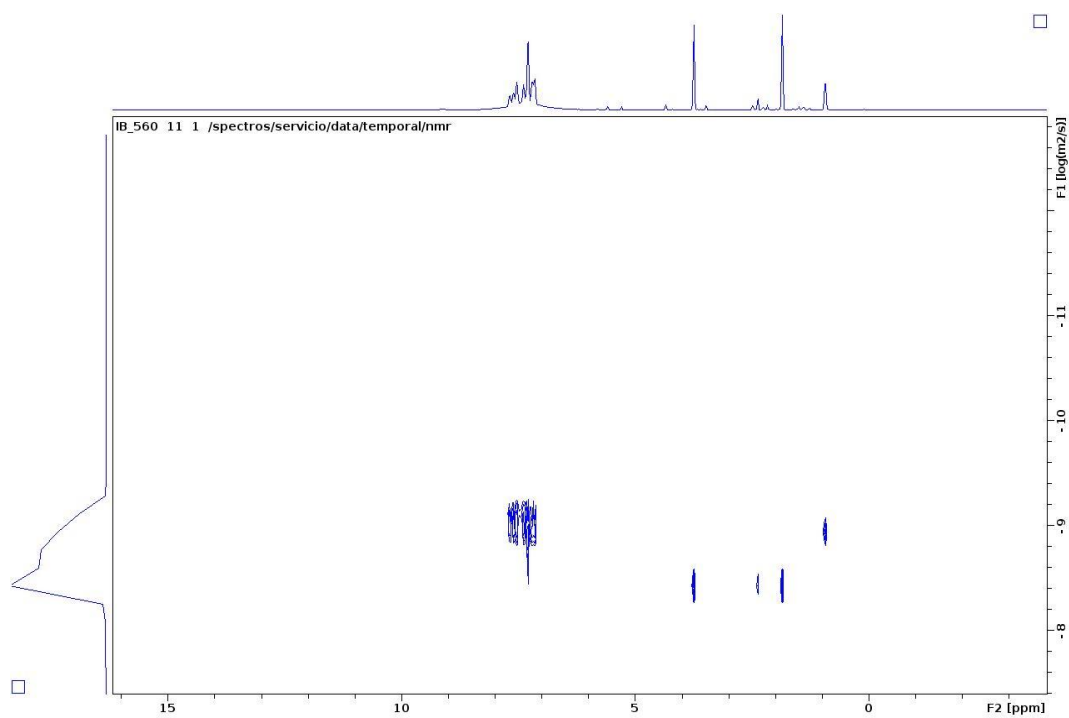
Figure B. 130 DOSY spectrum of complex 37 in CDCl$_3$ at 297 K

Complex 38
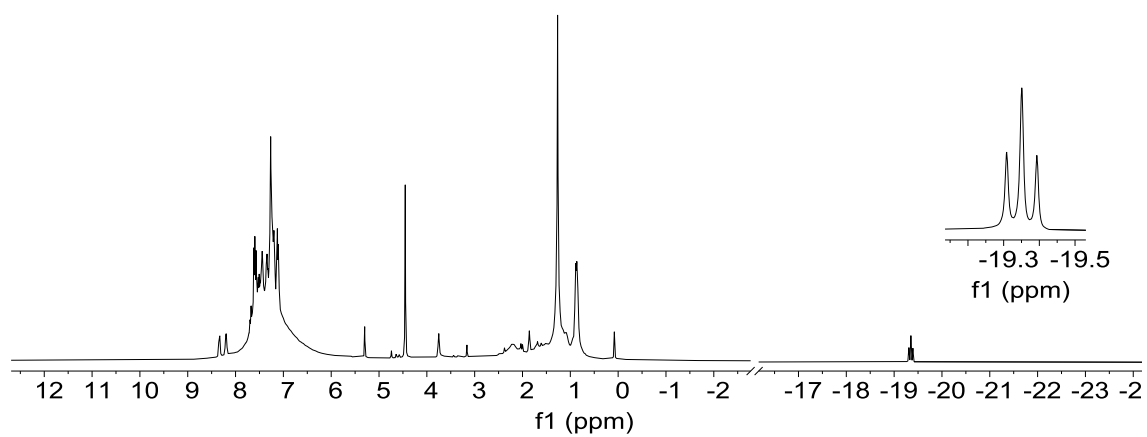
Figure B. 131 ^{1}H NMR of complex 38 in CDCl$_3$ at 297 K
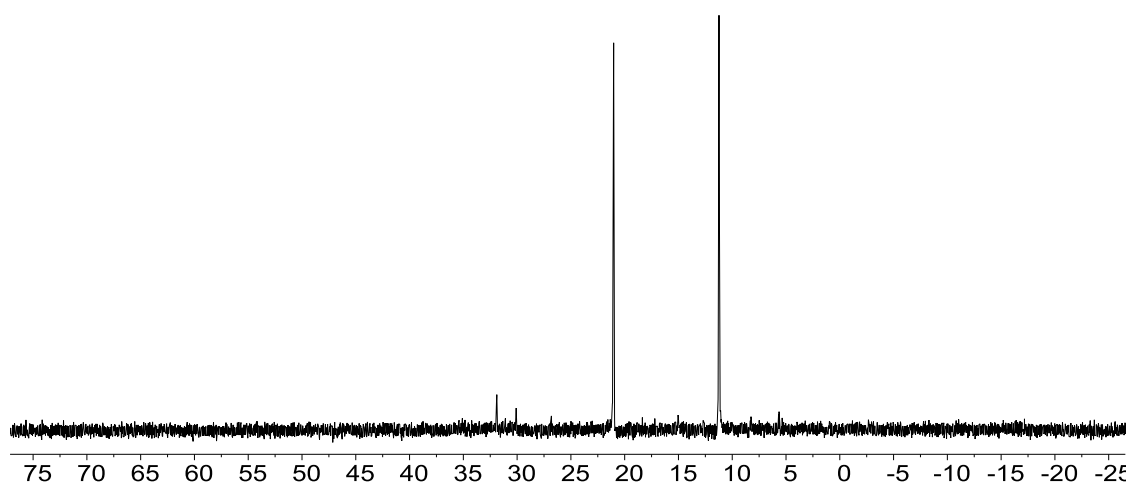
Figure B. 132 ^{31}P{^{1}H} NMR of complex 38 in CDCl$_3$ at 297 K
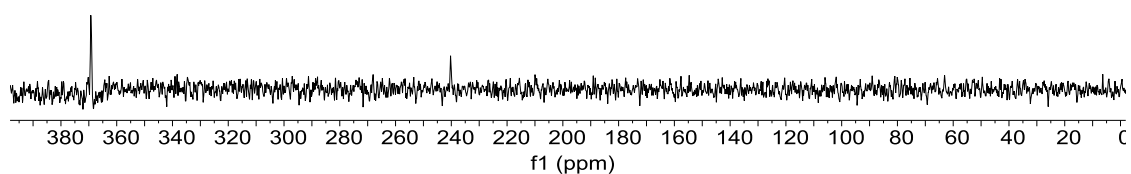
Figure B. 133 ^{15}N NMR of complex 38 in CDCl$_3$ at 297 K

Complex 39
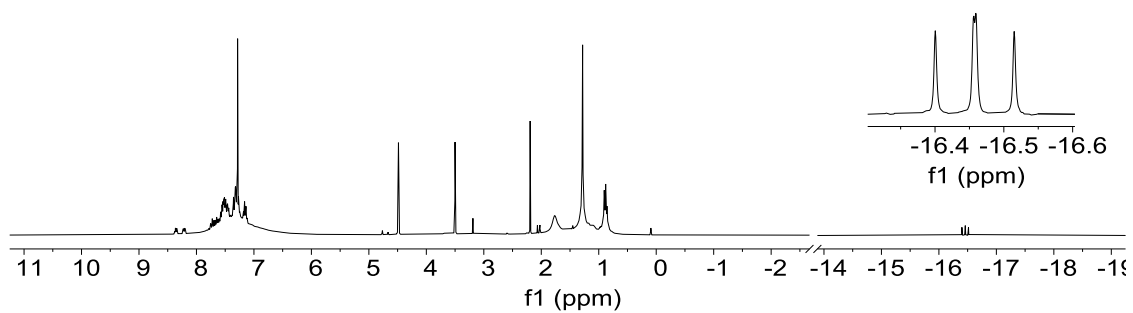
Figure B. 134 ^{1}H NMR of complex 39 in CDCl$_3$ at 297 K
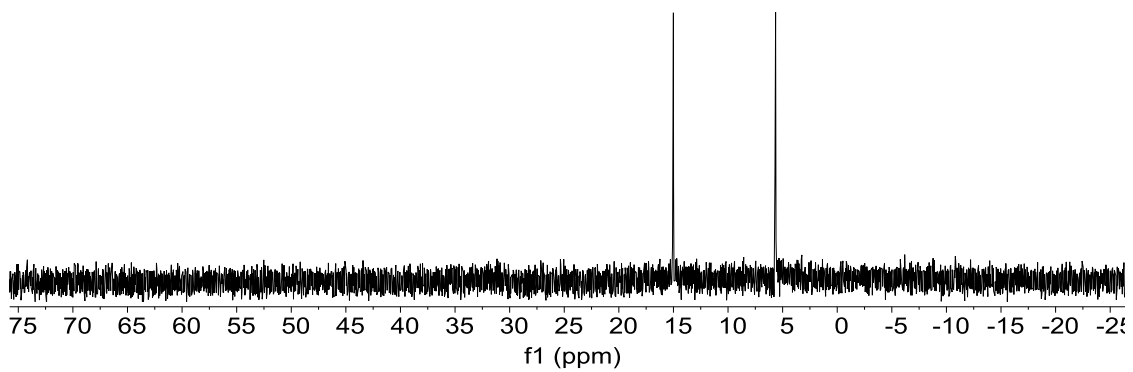
Figure B. 135 ^{31}P{^{1}H} NMR of complex 39 in CDCl$_3$ at 297 K

Complex 40
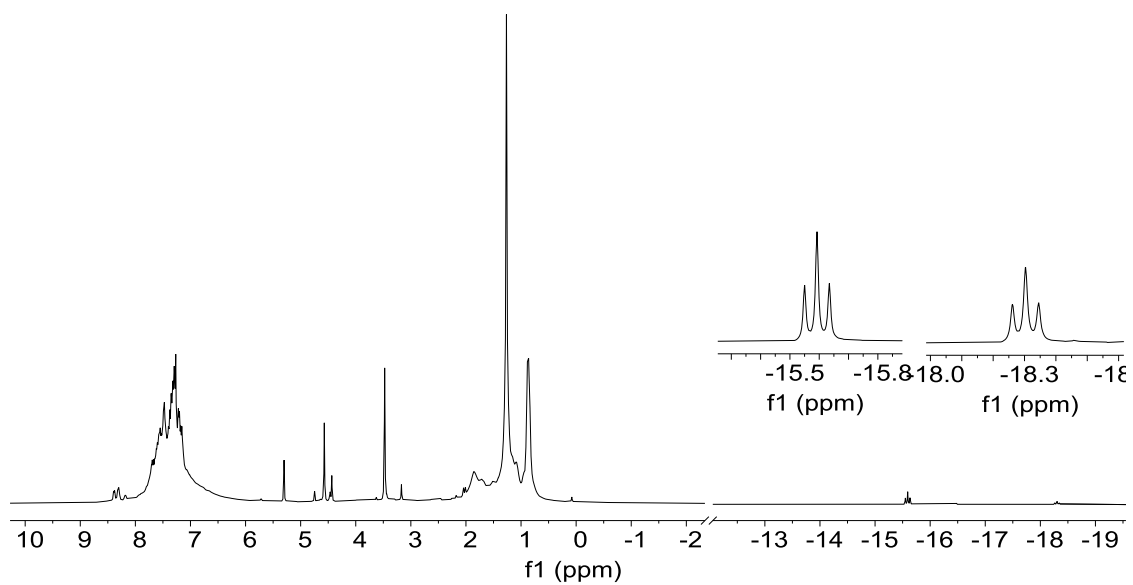
Figure B. 136 ^{1}H NMR of the mixture of kinetic and thermodynamic isomers of complex 40 in CDCl$_3$ at 297 K
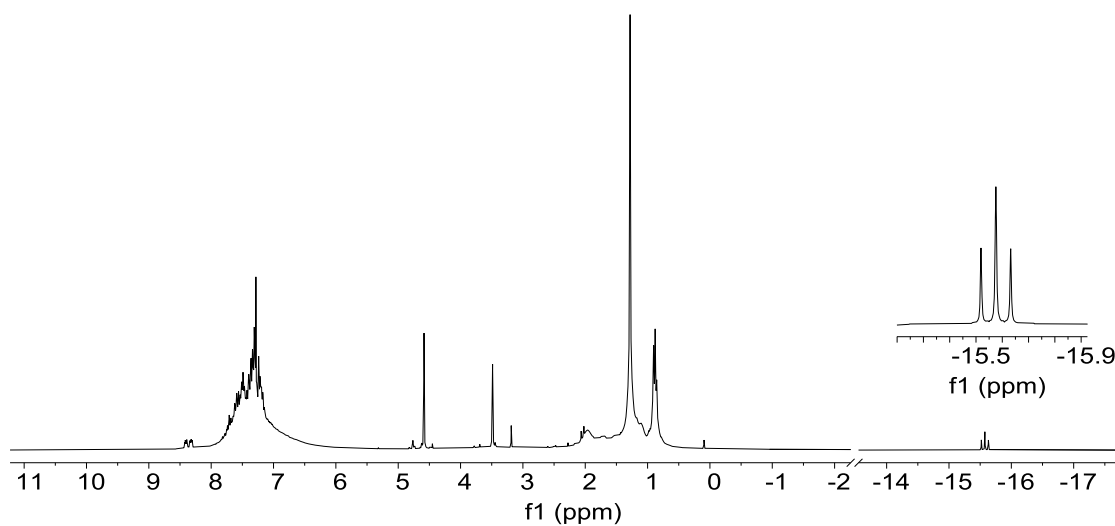
Figure B. 137 ^{1}H NMR of complex 40 in CDCl$_3$ at 297 K
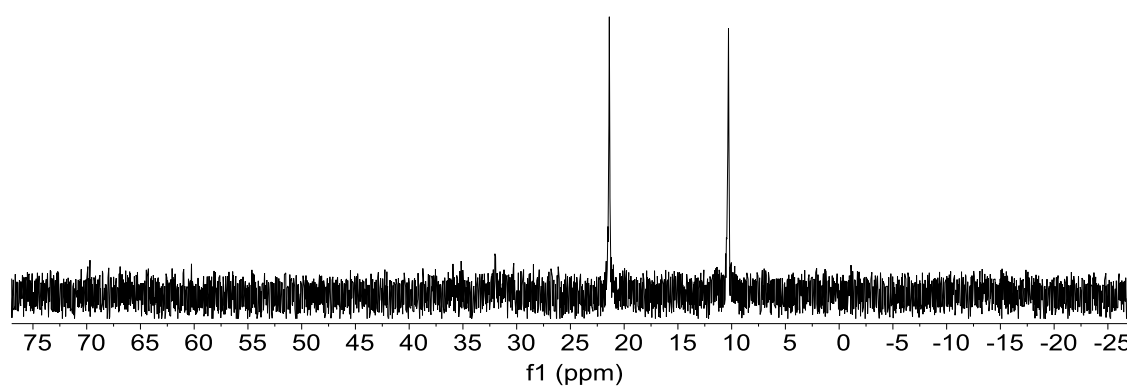
Figure B. 138 $^{31}P\{^1H\}$ **NMR of complex 40 in CDCl$_3$ at 297 K**

Complex 41
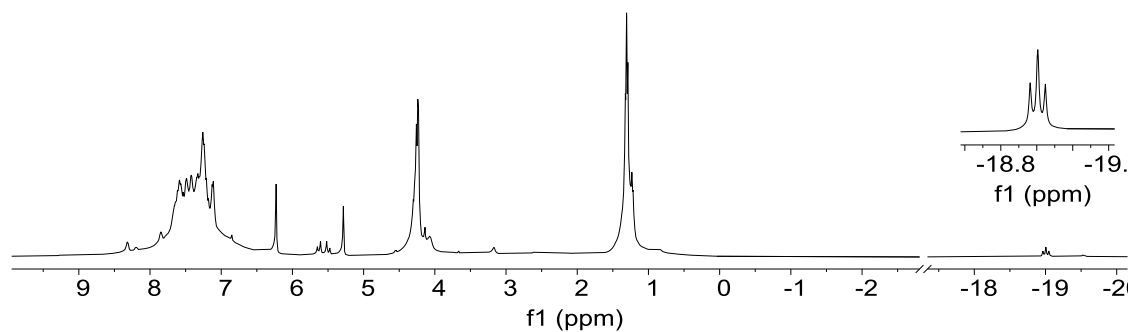
Figure B. 139 ^1H **NMR of complex 41 in CDCl$_3$ at 297 K**
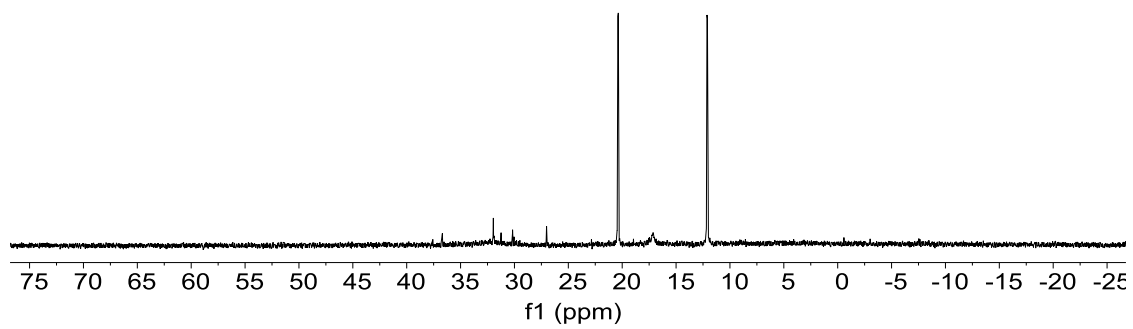
Figure B. 140 ^{31}P{^{1}H} **NMR of complex 41 in CD$_3$Cl**

Annex C

Crystallographic data

Chapter 2
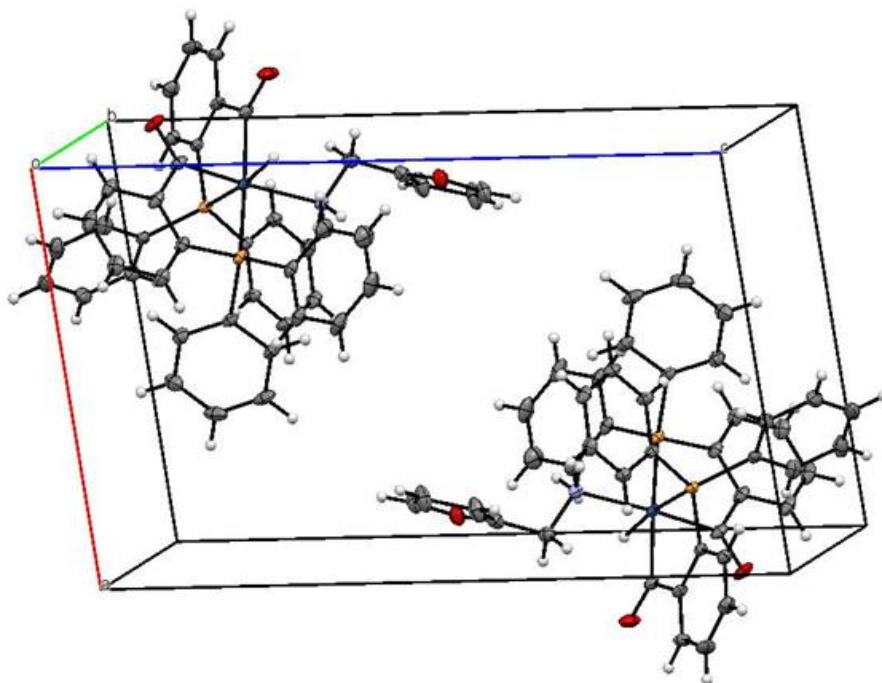
Figure C. 1 Unit cell of compound 4 showing the symmetry related enantiomers
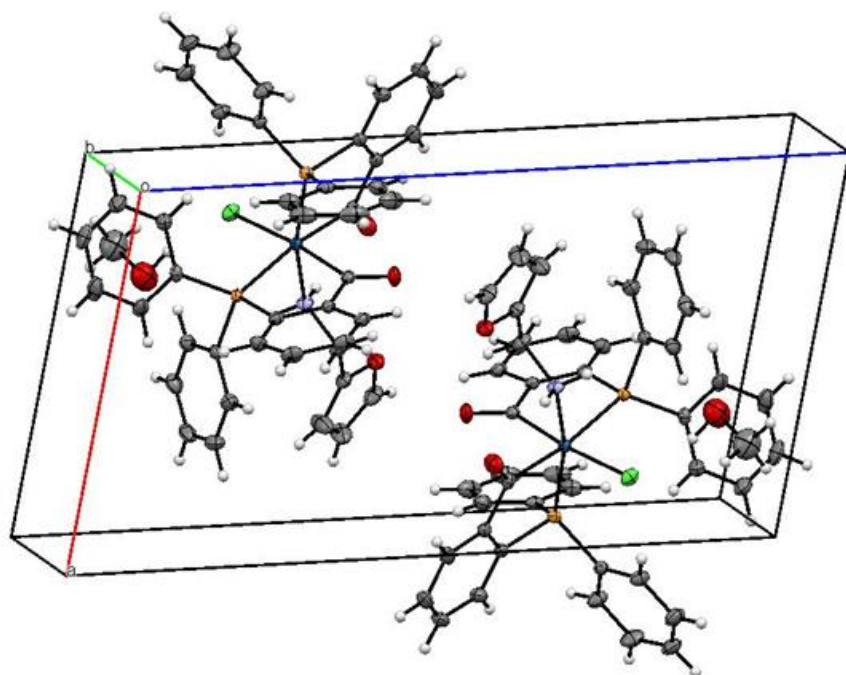
Figure C. 2 Unit cell of compound 5 showing the symmetry related enantiomers
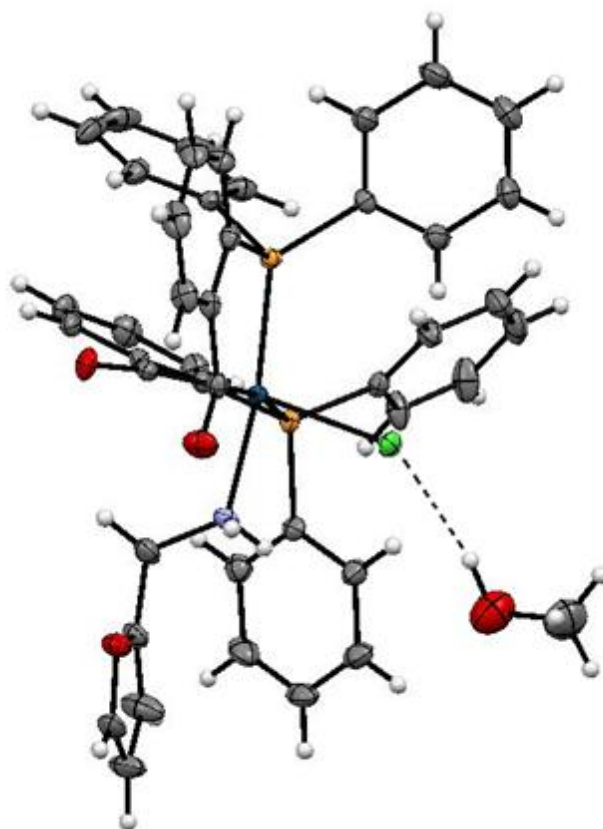
Figure C. 3 Hydrogen bond between a solvated methanol molecule and the coordinated chloride of 5
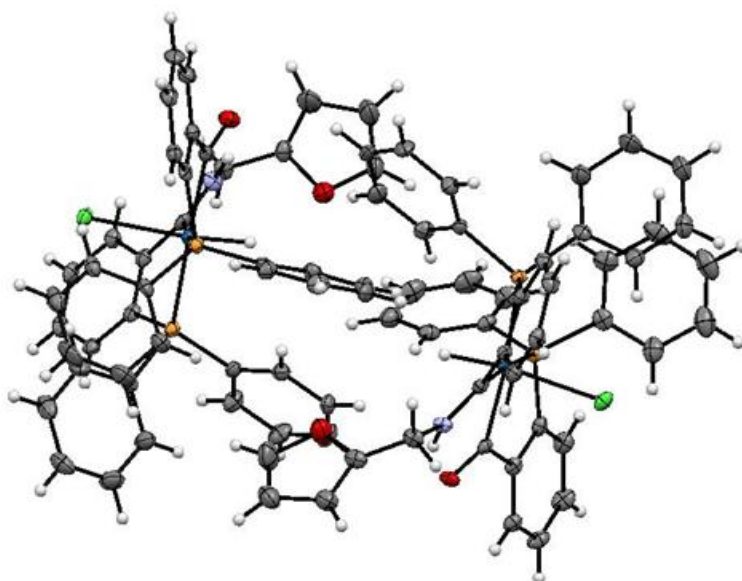
Figure C. 4 Symmetry independent units in the unit cell of compound 6

Table C. 1 Selected bond lengths (Å) and angles (°) for 4, 5 and 6. Standard deviation appears in parentheses.

	4	5	6
Ir1-P1	2.3263(9)	2.2849(5)	2.307(1) / 2.3106(9)
Ir1-P2	2.321(1)	2.3642(6)	2.3440(8) / 2.3446(9)
Ir1-C1	2.062(2)	2.066(2)	2.063(3) / 2.045(4)
Ir1-C20	2.012(3)	2.022(2)	2.066(4) / 2.043(3)
Ir1-N1	2.239(2)	2.150(1)	
Ir1-Cl1		2.5208(6)	2.492(1) / 2.509(1)
Ir1-H	1.52(2)		1.4708 / 1.4647
C20-N1			1.299(5) / 1.314(5)
P1-Ir-C1	84.09(6)	83.20(5)	82.84(9) / 82.2(1)
P2-Ir-C20	85.90(6)	83.80(5)	81.57(9) / 79.8(1)
P2-Ir-C1	168.92(6)	171.39(6)	172.47(9) / 171.9(1)
P1-Ir-C20	94.25(6)	85.85(5)	174.9(1) / 174.7(1)
C20-Ir1-N1	174.52(7)		
P1-Ir1-N1		169.93(5)	

Chapter 4

Table C. 2 Selected bond lengths (Å) and angles (º) on complex 10. Standard deviation appears in parentheses.

Bond lengths			
Ir1-P1	2.3000(7)	C1-O1	1.2499(3)
Ir1-P2	2.3361(8)	C20-N1	1.2994(3)
Ir1-C1	2.0486(7)	N1-H2	0.8033(3)
Ir1-C20	2.0625(7)	N1 - - O1	2.6528(8)
Ir1-H1	1.4844(4)	O1 - - H2	1.8799(6)
Ir1-Cl1	2.4919(7)		

Bond angles			
Cl1-Ir1-P1	89.54(3)	Cl1-Ir1-C20	89.9(1)
Cl1-Ir1-P2	94.66(3)	P1-Ir1-P2	102.57(3)
Cl1-Ir1-H1	177(1)	P1-Ir1-C20	175.9(1)
P1-Ir1-C1	82.9(1)	P2-Ir1-C1	173.0(1)
P1-Ir1-H1	91(1)	P2-Ir1-H1	88(1)
P2-Ir1-C20	81.5(1)	C1-Ir1-H1	88(1)
C1-Ir1-C20	93.1(2)	C20-N1-C21	132.5(3)
C20-Ir1-H1	89(1)	C28-C20-N1	119.7(3)
Cl1-Ir1-C1	89.8(1)	N1-H2 - - O1	161(4)

Table C. 3 Selected bond lengths (Å) and angles (º) on complex 15. Standard deviation appears in parentheses.

Bond lengths

Ir1-H1	1.4193(5)	Ir1-C20	2.0450(5)
Ir1-P1	2.2984(6)	Ir1-N2	2.2163(6)
Ir1-P2	2.3425(7)	C20-N1	1.2911(3)
Ir1-C1	2.0306(5)		

Bond angles

C1-Ir1-C20	92.6(2)	C20-Ir1-H1	90
C1-Ir1-N2	170.3(2)	N2-Ir1-P1	94.7(1)
C1-Ir1-P1	84.5(1)	N2-Ir1-P2	99.8(1)
C1-Ir1-P2	89.8(1)	N2-Ir1-H1	90(2)
C1-Ir1-H1	80(2)	P1-Ir1-P2	102(4)
C20-Ir1-N2	88.1(2)	P1-Ir1-H1	89(2)
C20-Ir1-P1	177.1(1)	P2-Ir1-H1	164(2)
C20-Ir1-P2	78.4(1)	Ir1-C20-N1	123.5(3)
C28-C20-N1	117.3(4)	Ir1-C20-C28	118.8(3)

Table C. 4 Selected bond lengths (Å) and angles (⁰) on complex 16. Standard deviation appears in parentheses.

Bond lengths

Ir1-H1	1.4955(3)	Ir1-C20	2.0390(6)
Ir1-P1	2.3241(7)	Ir1-N2	2.2846(7)
Ir1-P2	2.3425(5)	C20-N1	1.2966(3)
Ir1-C1	2.0258(6)	C1-O1	1.2198(4)

Bond angles

C1-Ir1-C20	91.2(3)	C20-Ir1-H1	94.9
C1-Ir1-N2	172.4(3)	N2-Ir1-P1	97.7(2)
C1-Ir1-P1	84.5(3)	N2-Ir1-P2	97.3(2)
C1-Ir1-P2	89.4(3)	N2-Ir1-H1	88.4
C1-Ir1-H1	84.6	P1-Ir1-P2	102(8)
C20-Ir1-N2	86.5(3)	P1-Ir1-H1	84.4
C20-Ir1-P1	175.7(2)	P2-Ir1-H1	170.7
C20-Ir1-P2	78.2(2)	Ir1-C20-N1	126.1
C21-C20-N1	115.9	Ir1-C20-C21	119.4

Table C. 5 Selected bond lengths (Å) and angles (º) on complex 20. Standard deviation appears in parentheses.

Bond lengths

Ir1-H1	1.59(6)	Ir1-C20	2.077(4)
Ir1-P1	2.3145(10)	Ir1-N2	2.249(4)
Ir1-P2	2.3268(10)	C20-N1	1.288(5)
Ir1-C1	2.014(4)	C1-O1	1.228(5)

Bond angles

C1-Ir1-C20	93.25(16)	C20-Ir1-H1	95(2)
C1-Ir1-N2	169.30(15)	N2-Ir1-P1	101.86(10)
C1-Ir1-P1	84.82(12)	N2-Ir1-P2	95.75(10)
C1-Ir1-P2	90.60(12)	N2-Ir1-H1	87(2)
C1-Ir1-H1	86(2)	P1-Ir1-P2	104.27(4)
C20-Ir1-N2	79.41(15)	P1-Ir1-H1	81(2)
C20-Ir1-P1	175.10(11)	P2-Ir1-H1	173(2)
C20-Ir1-P2	80.22(12)	Ir1-C20-N1	126.3(3)
C21-C20-N1	114.7(4)	Ir1-C20-C21	118.1(3)

Table C. 6 Selected bond lengths (Å) and angles (⁰) on complex 22. Standard deviation appears in parentheses.

Bond lengths

Ir1-H1	1.57(3)	Ir1-C20	2.038(3)
Ir1-P1	2.3029(8)	Ir1-N2	2.232(3)
Ir1-P2	2.3508(8)	C20-N1	1.296(4)
Ir1-C1	2.079(3)		

Bond angles

P1-Ir1-P2	104.99(3)	C20-Ir1-C1	94.7(1)
P1-Ir1-C20	177.2(1)	C20-Ir1-N2	88.5(1)
P1-Ir1-C1	83.22(9)	C20-Ir1-H1	89(1)
P1-Ir1-N2	93.46(8)	C1-Ir1-N2	88.5(1)
P1-Ir1-H1	89(1)	C1-Ir1-H1	89(1)
P2-Ir1-C20	76.81(9)	N2-Ir1-H1	176(1)
P2-Ir1-C1	169.10(9)	Ir1-P1-C8	121.8(1)
P2-Ir1-N2	97.43(8)	Ir1-P1-C7	103.3(1)
P2-Ir1-H1	86(1)	Ir1-P1-C14	114.6(1)
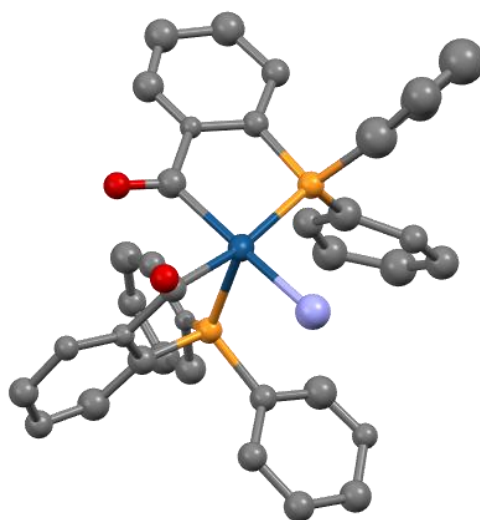
Figure C. 5

Annex D

Mass Spectrometry

Chapter 3

Complex 9
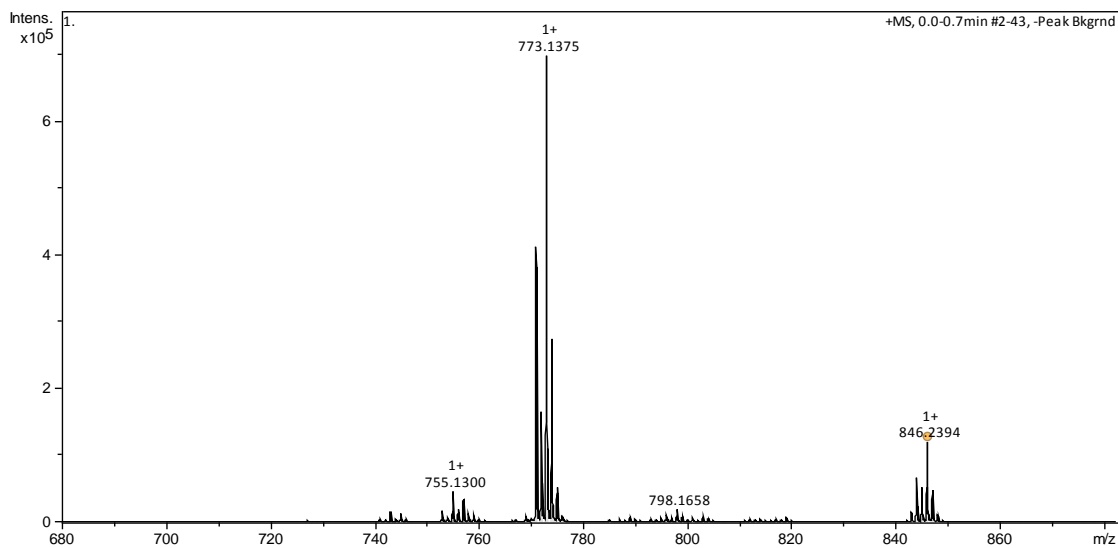
Figure D. 1 Mass spectrum of complex 9.
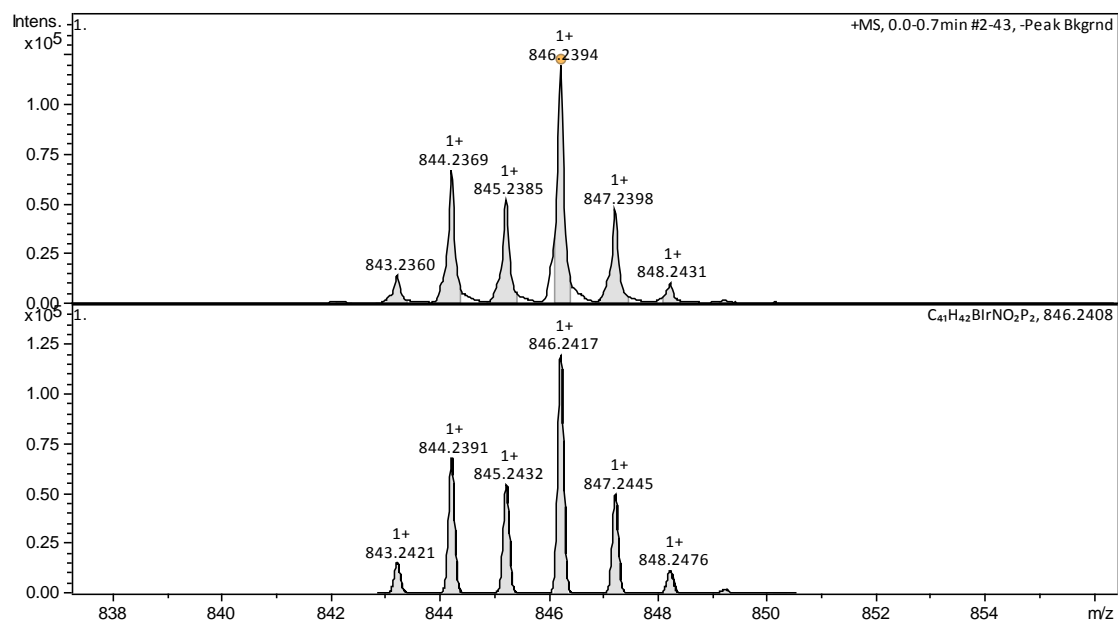
Figure D. 2 Comparison between experimental (above) and theoretical (below) mass spectrum of complex 9.

Chapter 4

Complex 15
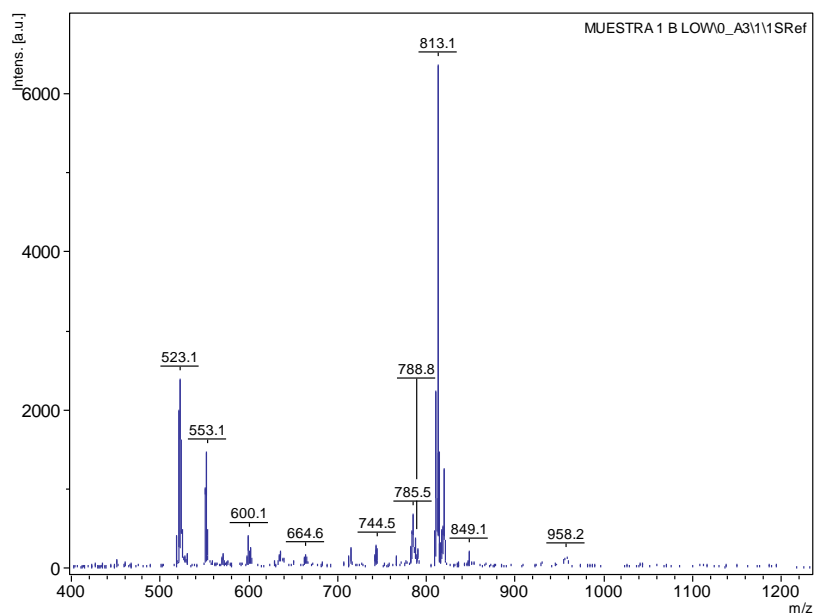
Figure D. 3 Mass spectrum of complex 15.
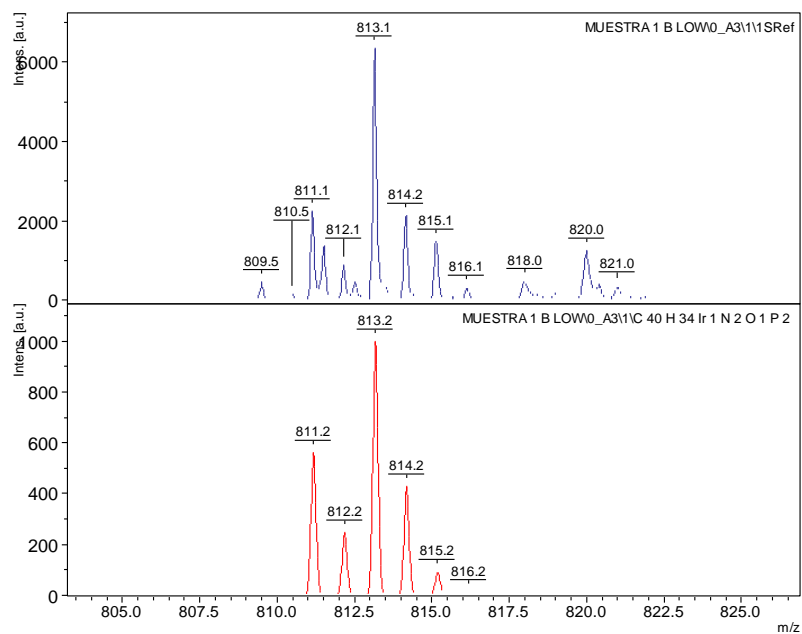
Figure D. 4 Comparison between experimental (above) and theoretical (below) mass spectrum of complex 15.

Complex 16
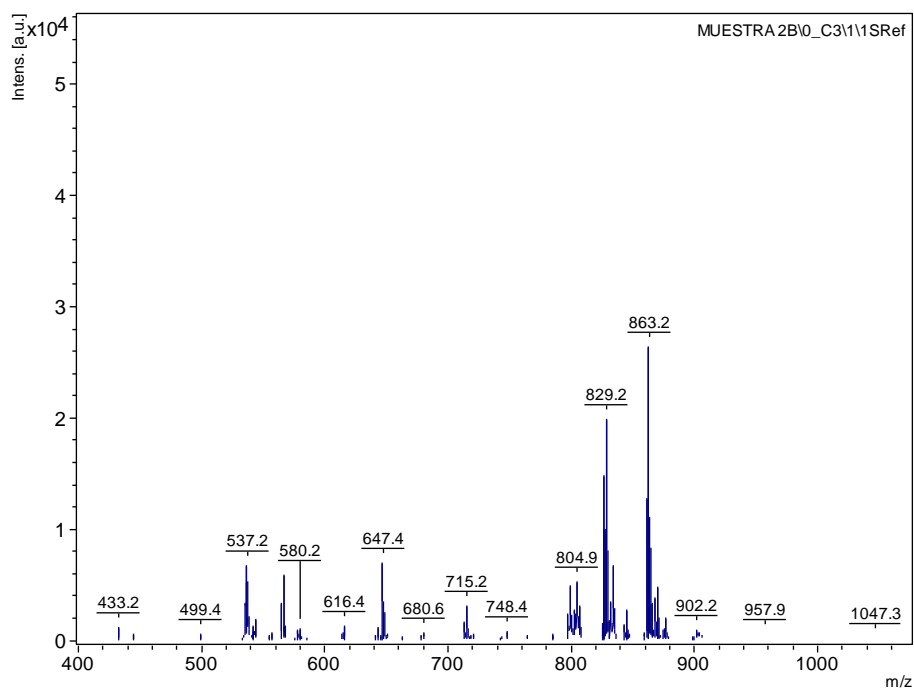
Figure D. 5 Mass spectrum of complex 16.
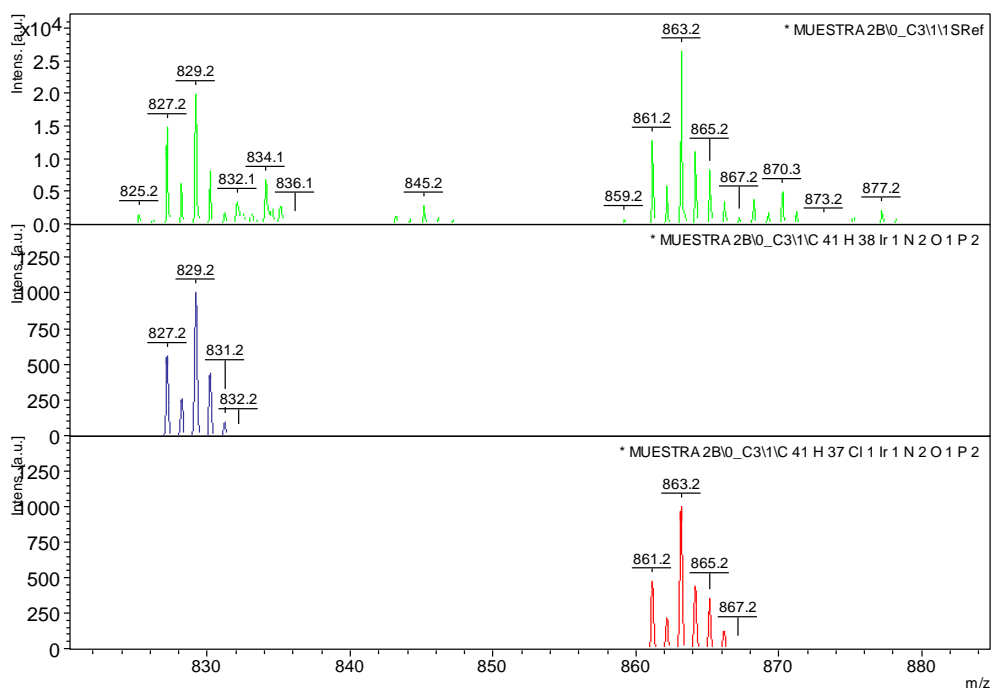
Figure D. 6 Comparison between experimental (above) and theoretical (below) mass spectrum of complex 16.

Complex 17
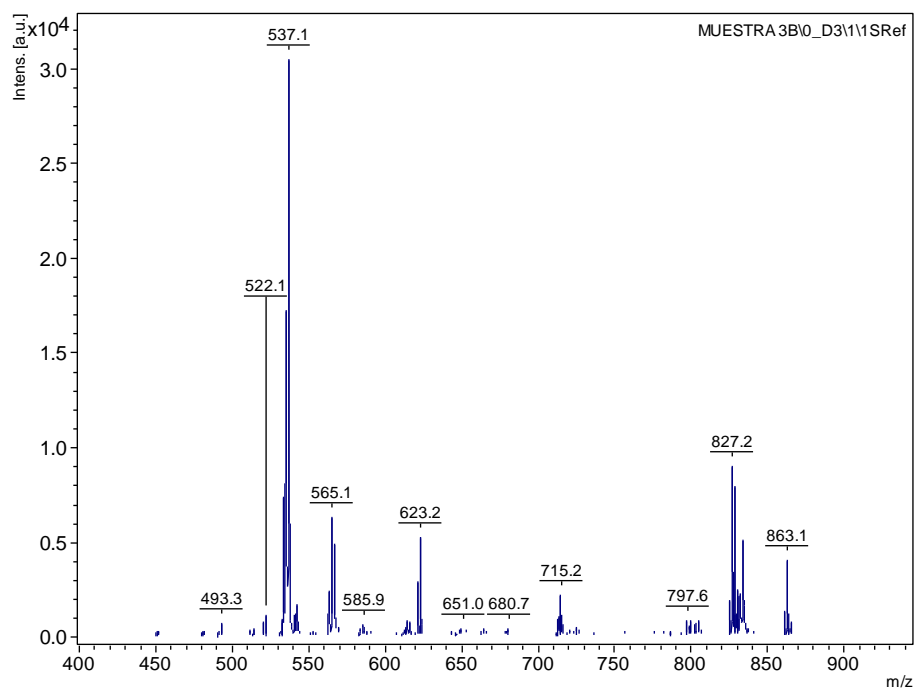
Figure D. 7 Mass spectrum of complex 17.
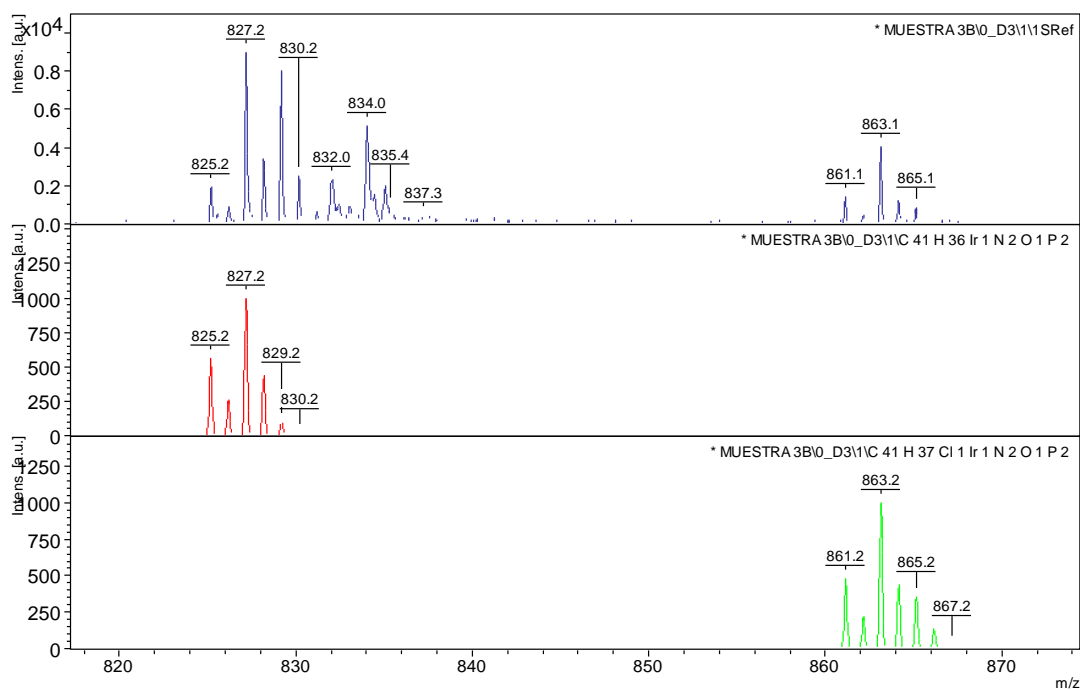
Figure D. 8 Comparison between experimental (above) and theoretical (below) mass spectrum of complex 17.

Complex 18
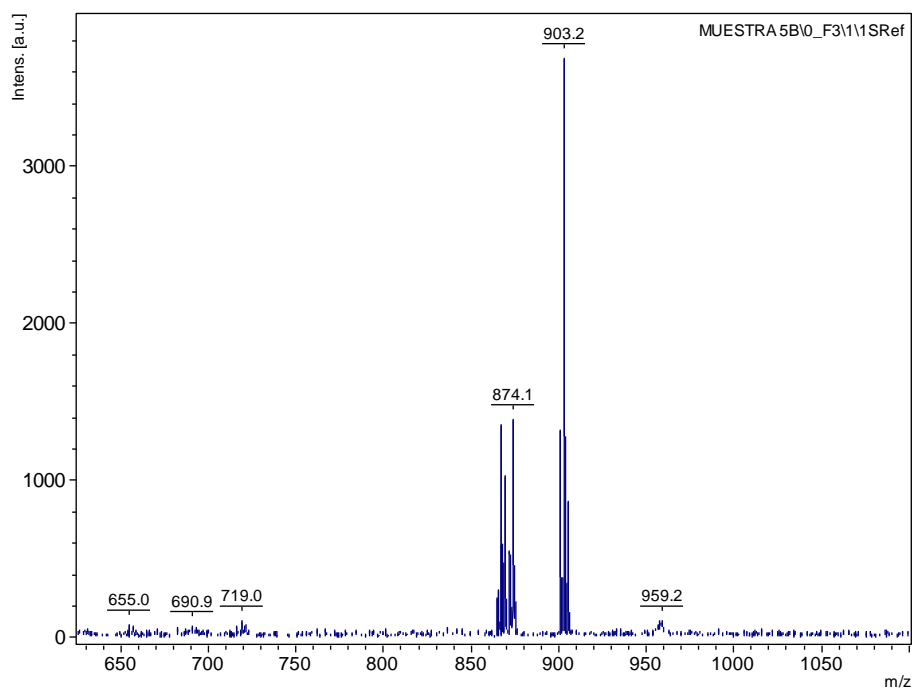
Figure D. 9 Mass spectrum of complex 18.
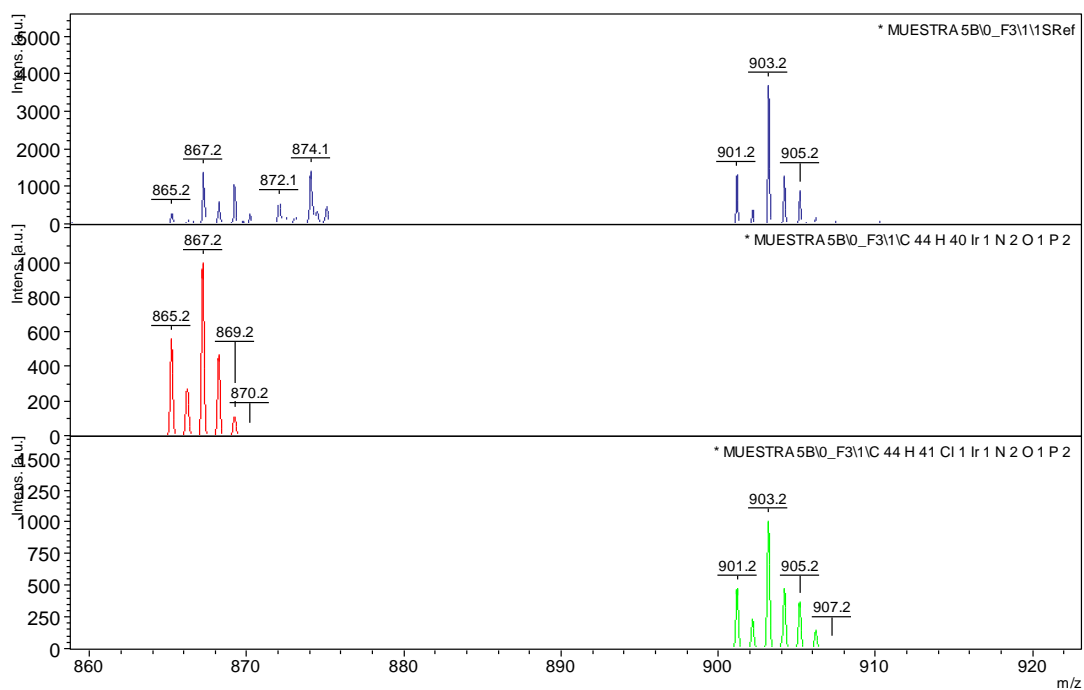
Figure D. 10 Comparison between experimental (above) and theoretical (below) mass spectrum of complex 18.

Complex 19
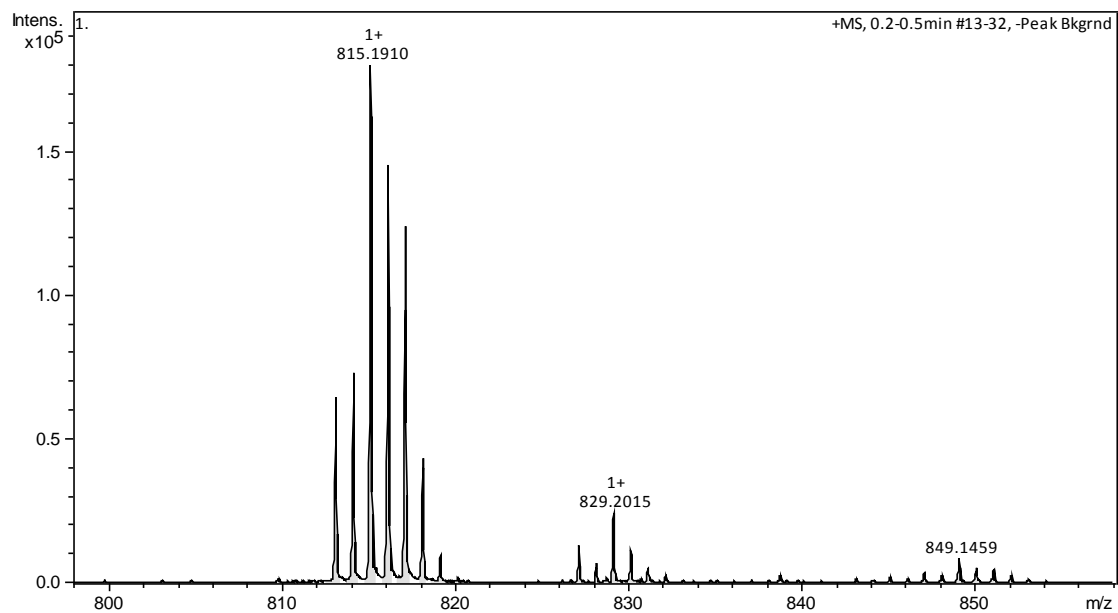
Figure D. 11 Mass spectrum of complex 19.
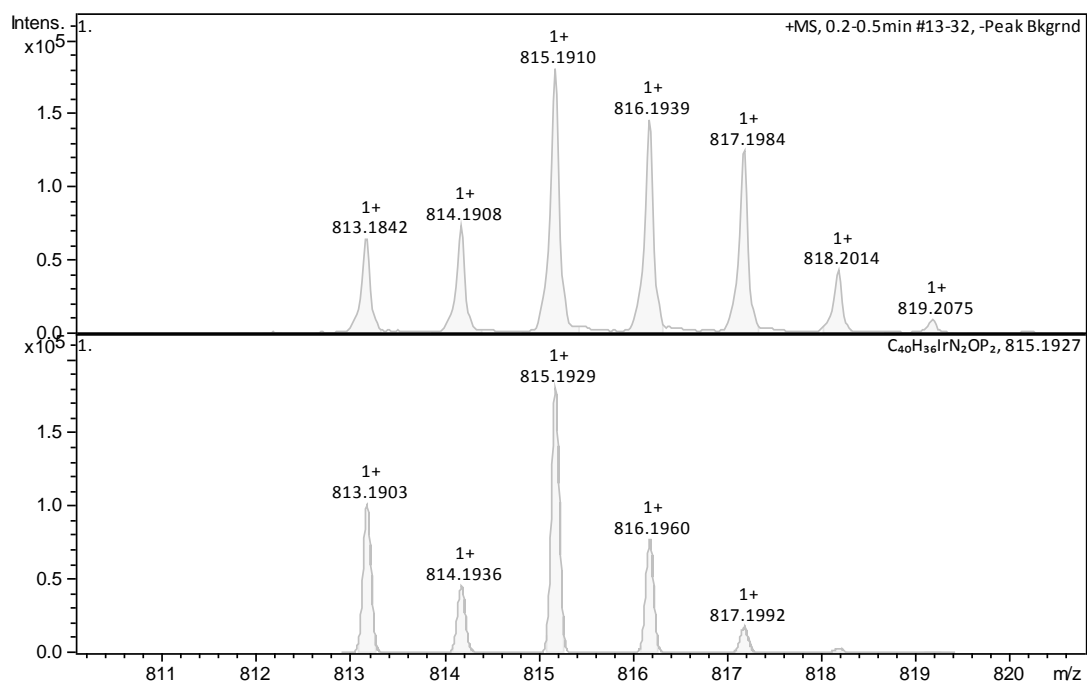
Figure D. 12 Comparison between experimental (above) and theoretical (below) mass spectrum of complex 19.

Complex 21
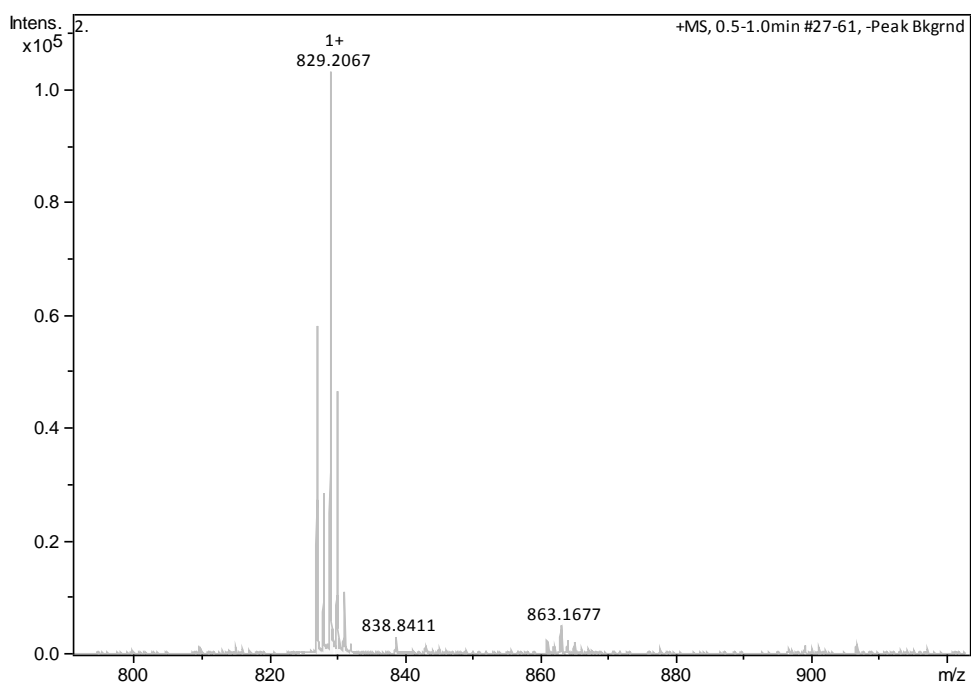
Figure D. 13 Mass spectrum of complex 21.
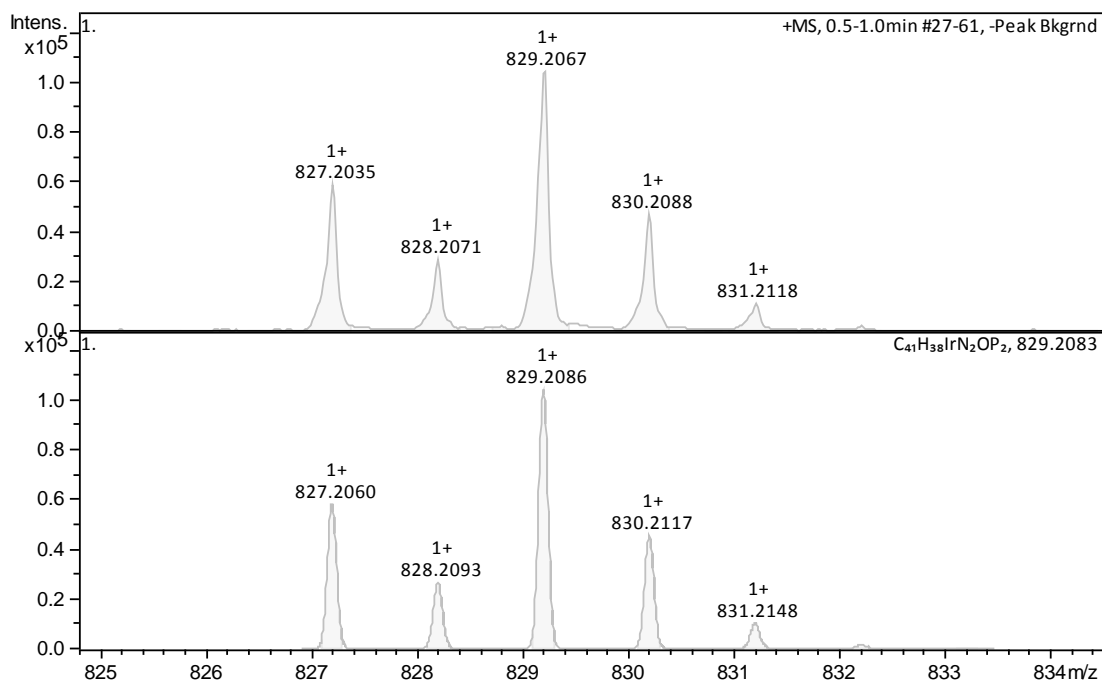
Figure D. 14 Comparison between experimental (above) and theoretical (below) mass spectrum of complex 21.

Chapter 5

<u>Complex 27</u>
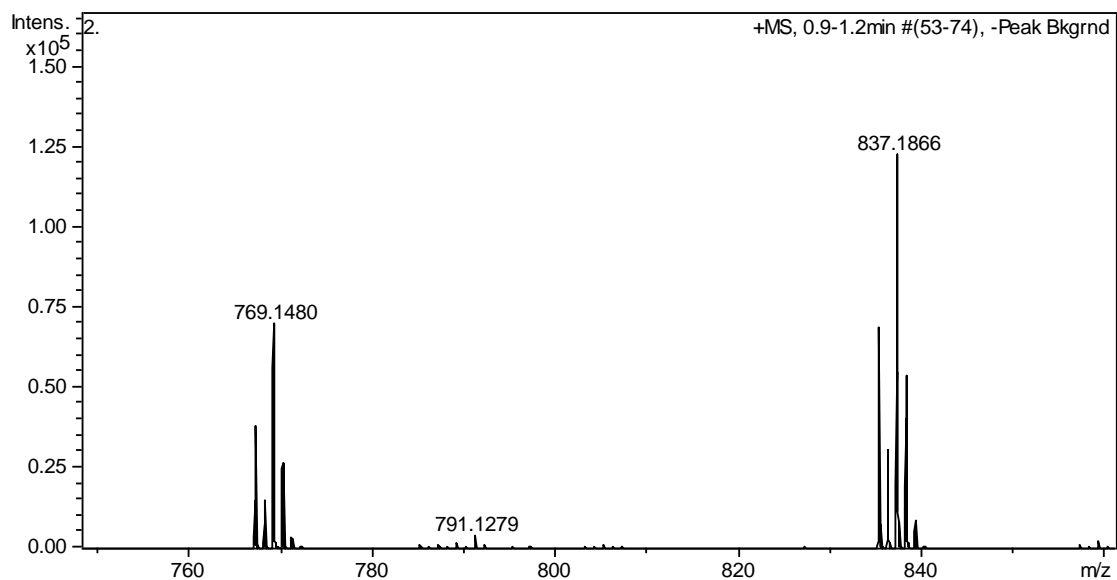
Figure D. 15 Mass spectrum of complex 27.
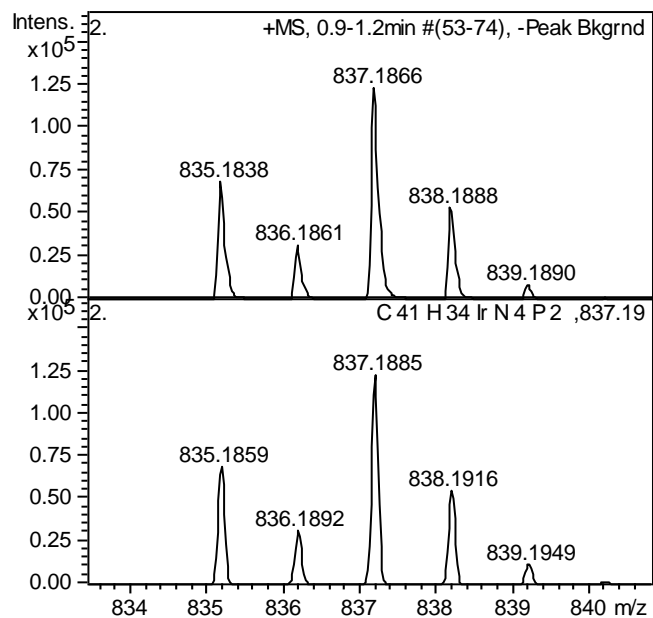
Figure D. 16 Comparison between experimental (above) and theoretical (below) mass spectrum of complex 27.

Complex 28
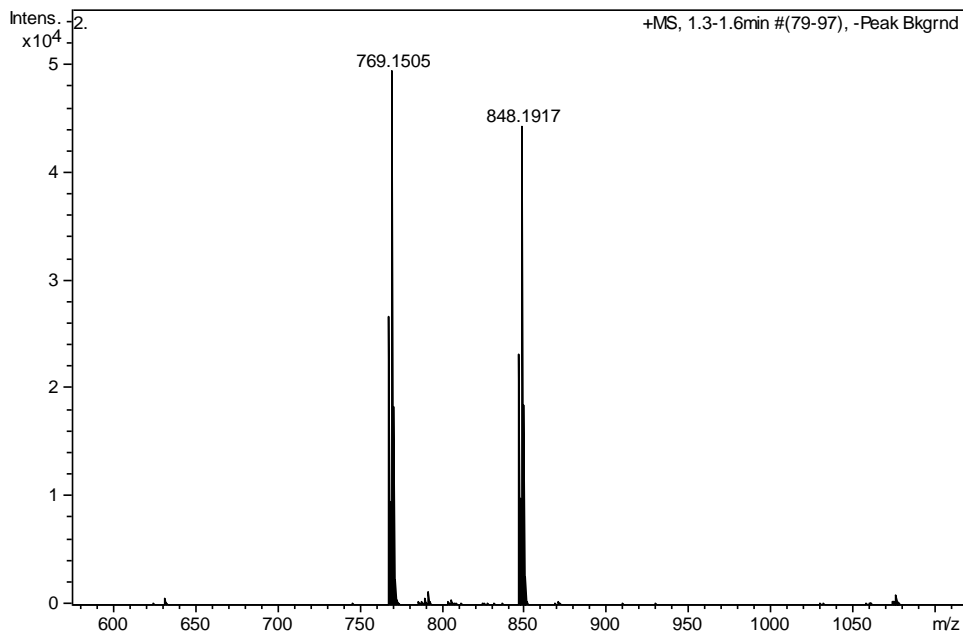
Figure D. 17 Mass spectrum of complex 28.
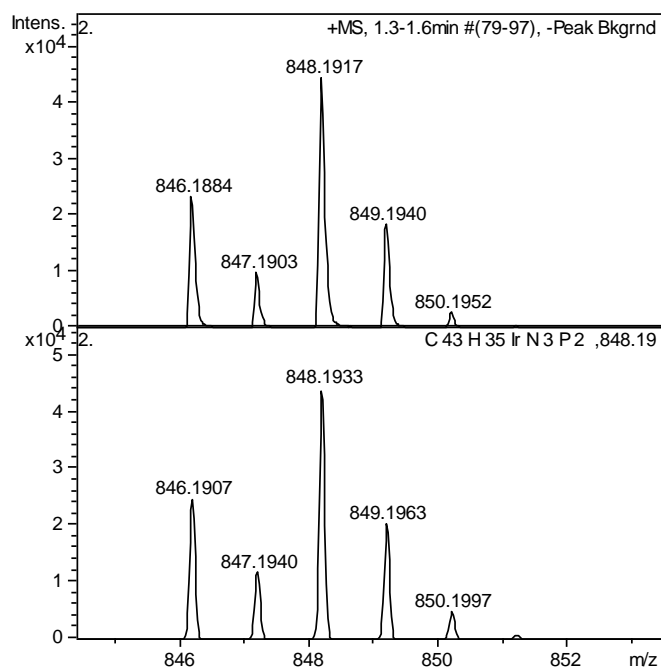
Figure D. 18 Comparison between experimental (above) and theoretical (below) mass spectrum of complex 28.

Complex 29
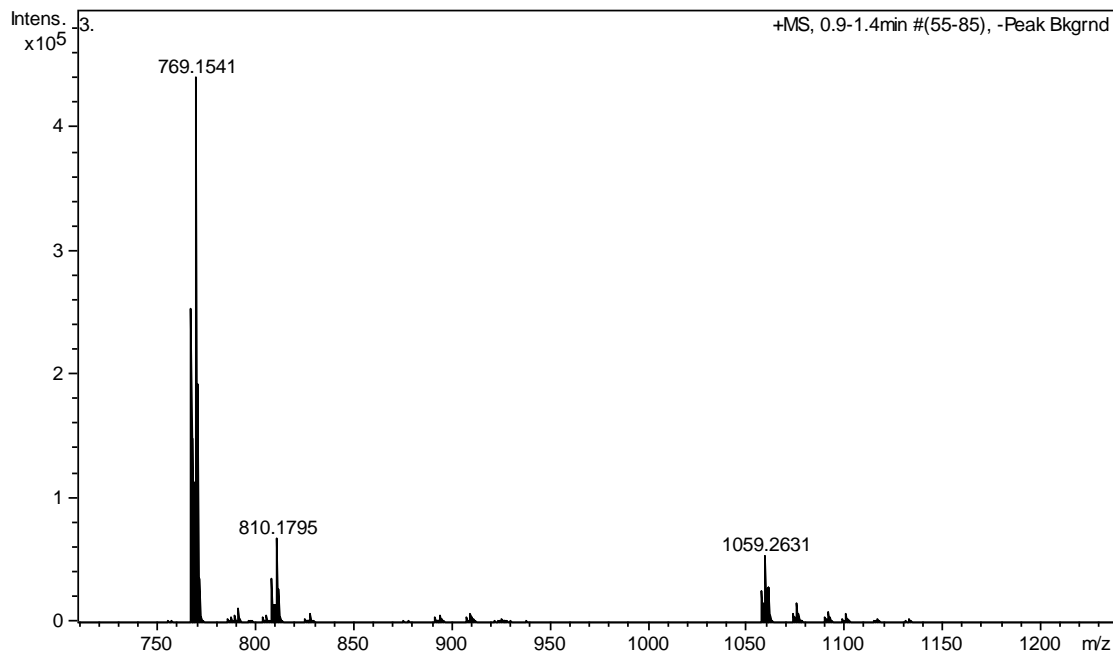
Figure D. 19 Mass spectrum of complex 29.
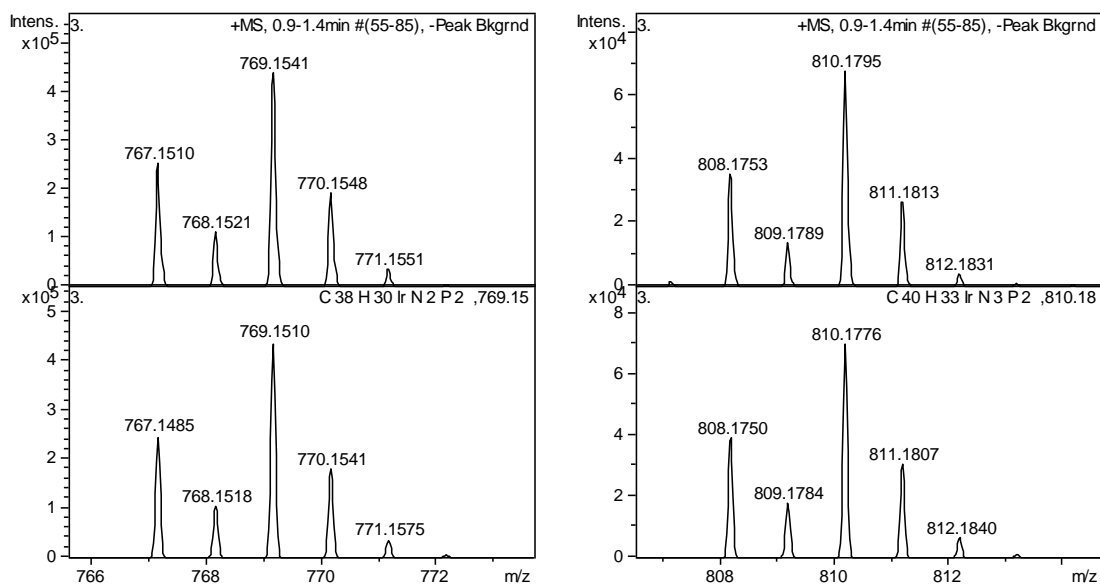
Figure D. 20 Comparison between experimental (above) and theoretical (below) mass spectrum of complex 29.

Complex 30
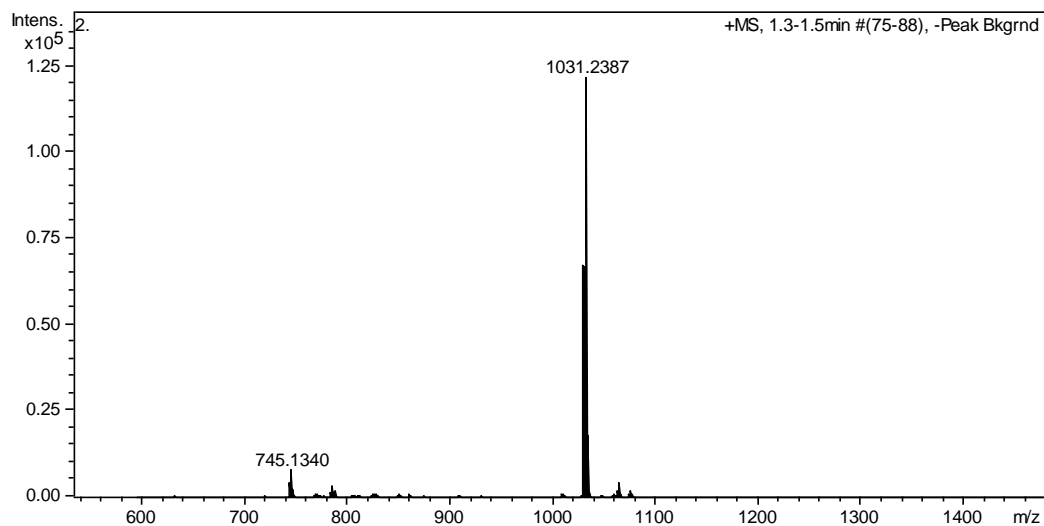
Figure D. 21 Mass spectrum of complex 30.
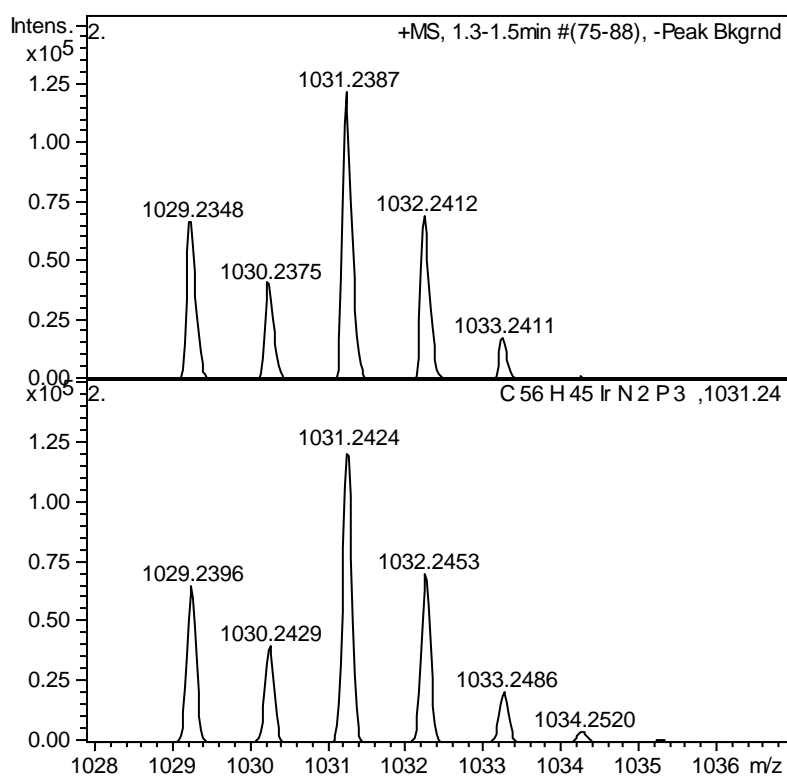
Figure D. 22 Comparison between experimental (above) and theoretical (below) mass spectrum of complex 30.

Complex 31
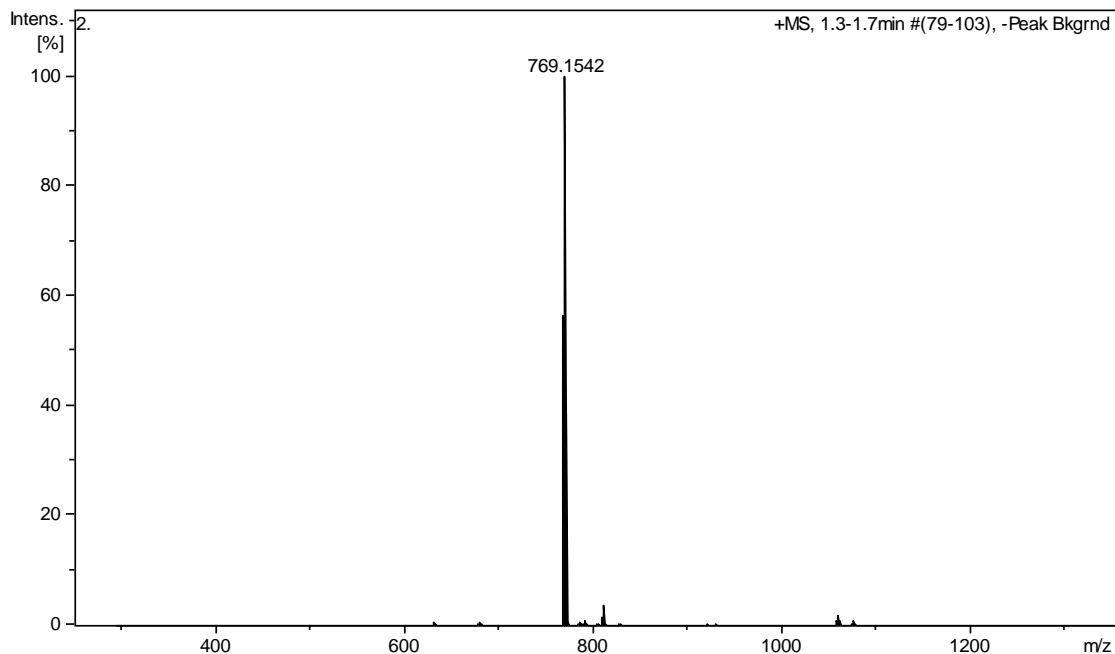
Figure D. 23 Mass spectrum of complex 31.
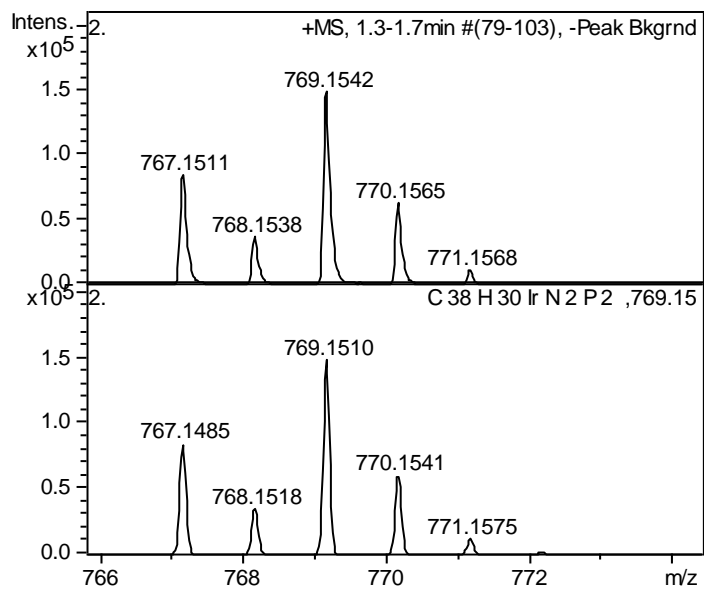
Figure D. 24 Comparison between experimental (above) and theoretical (below) mass spectrum of complex 31.

Complex 32
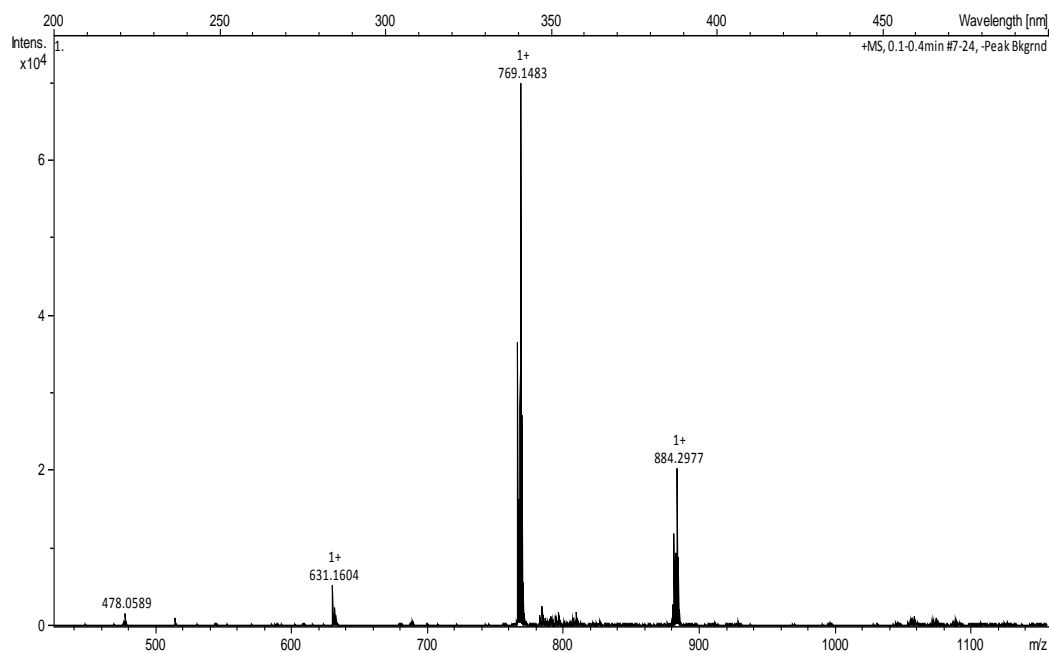
Figure D. 25 Mass spectrum of complex 32.
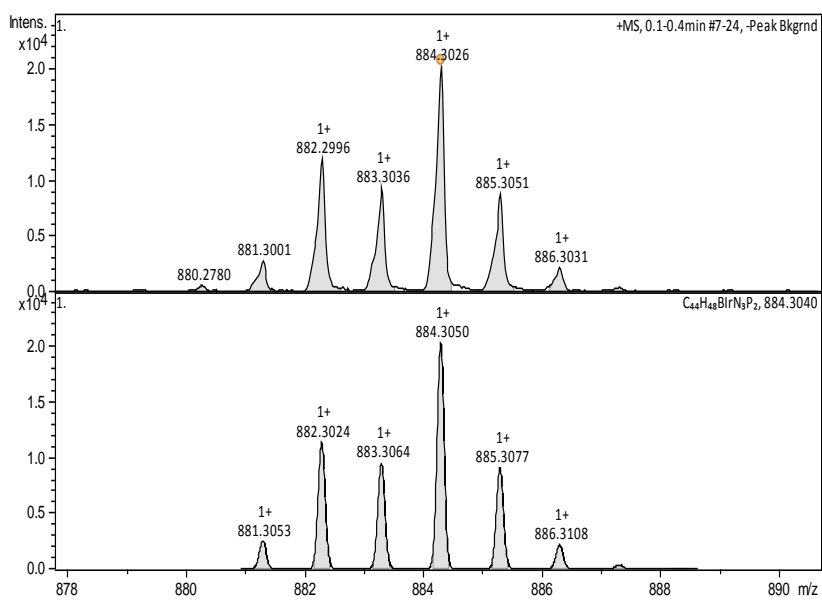
Figure D. 26 Comparison between experimental (above) and theoretical (below) mass spectrum of complex 32.

Complex 33
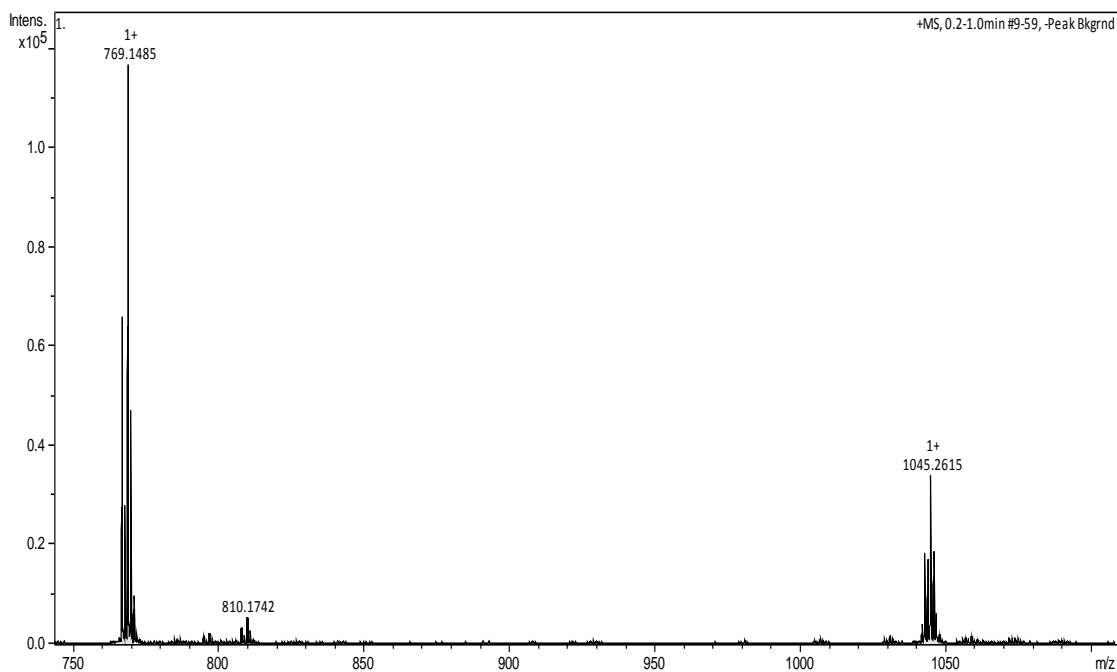
Figure D. 27 Mass spectrum of complex 33.
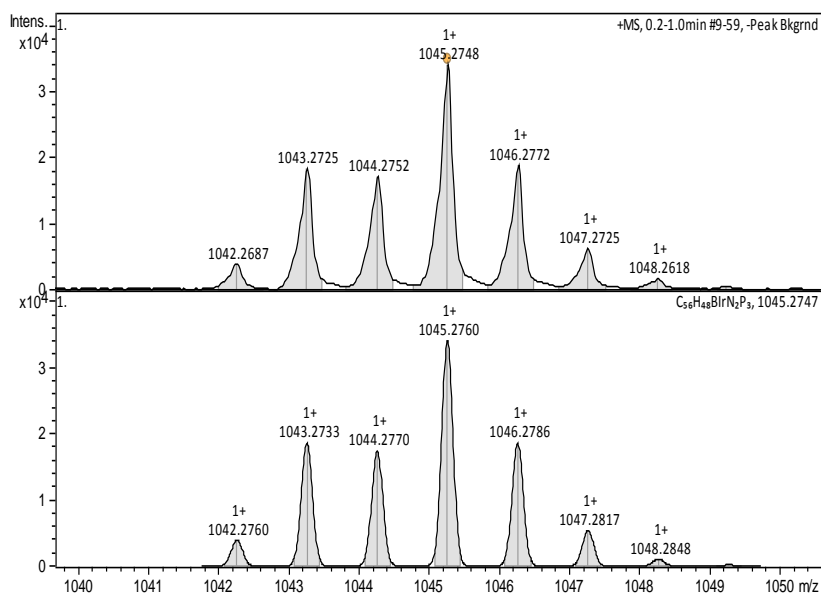
Figure D. 28 Comparison between experimental (above) and theoretical (below) mass spectrum of complex 33.

Complex 35
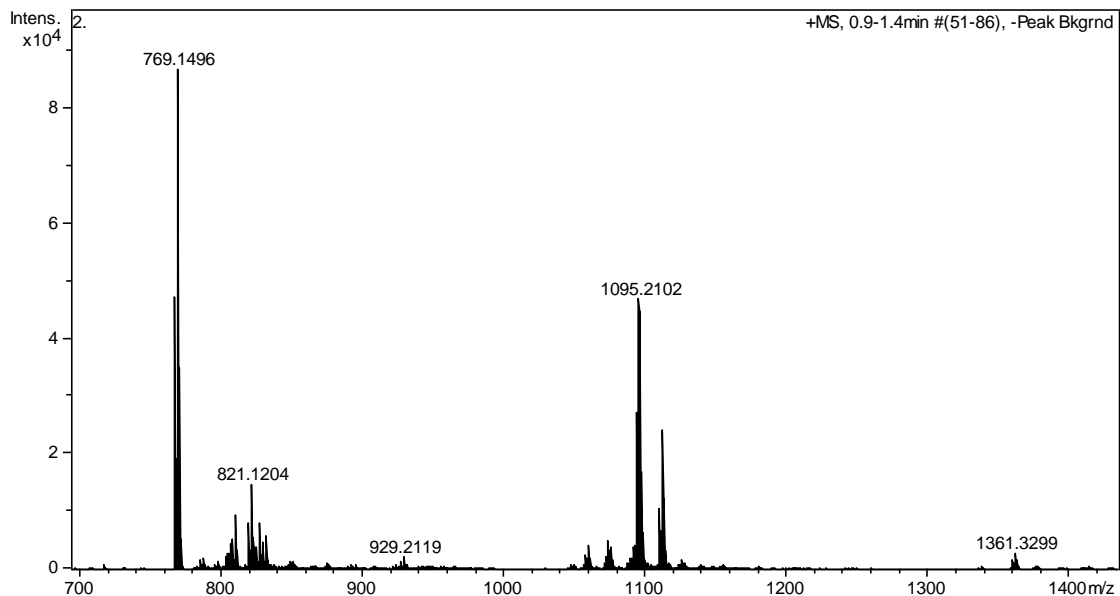
Figure D. 29 Mass spectrum of complex 35.
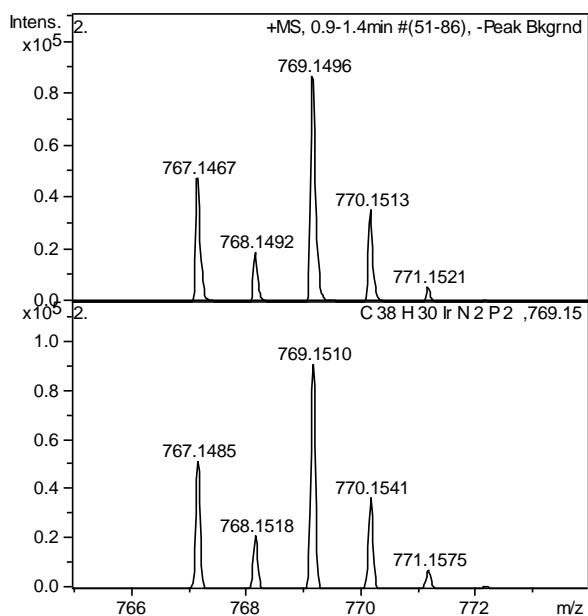
Figure D. 30 Comparison between experimental (above) and theoretical (below) mass spectrum of complex 35.

Complex 36
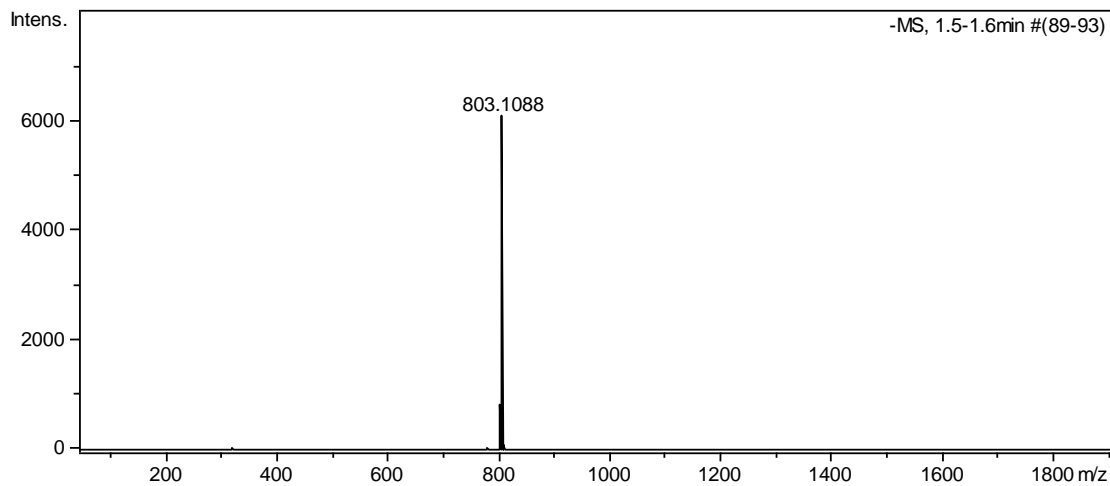
Figure D. 31 Mass spectrum of complex 36.
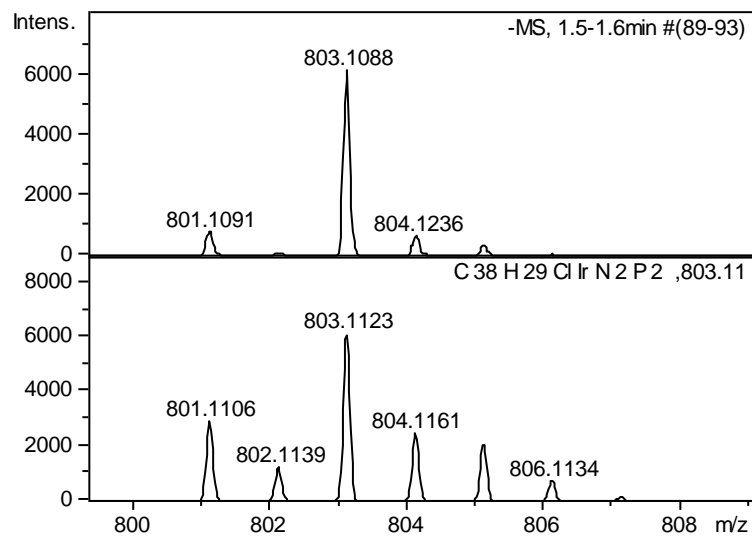
Figure D. 32 Comparison between experimental (above) and theoretical (below) mass spectrum of complex 36.

Complex 38
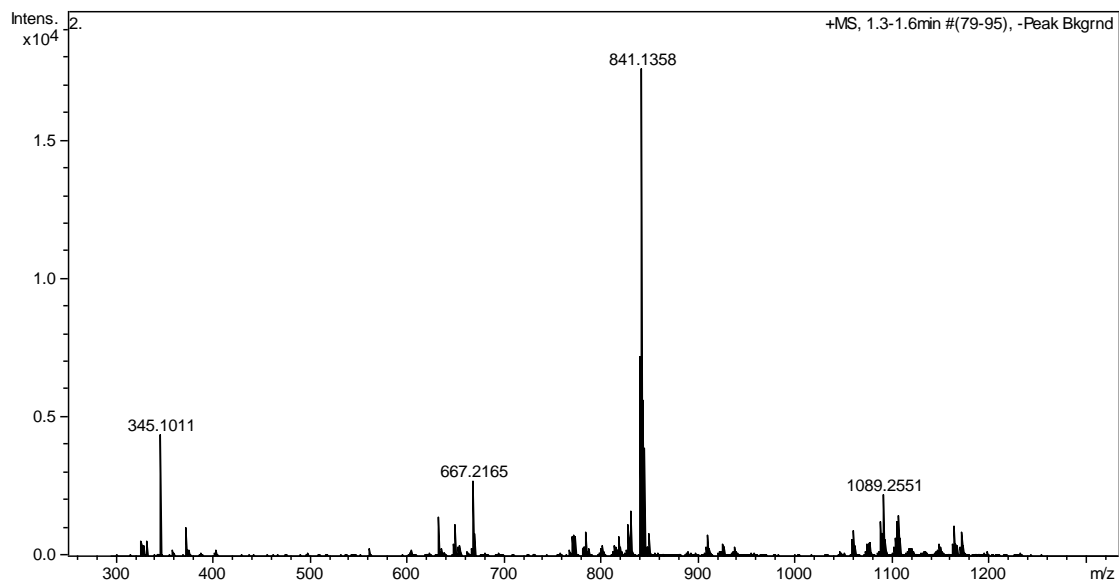
Figure D. 33 Mass spectrum of complex 38.
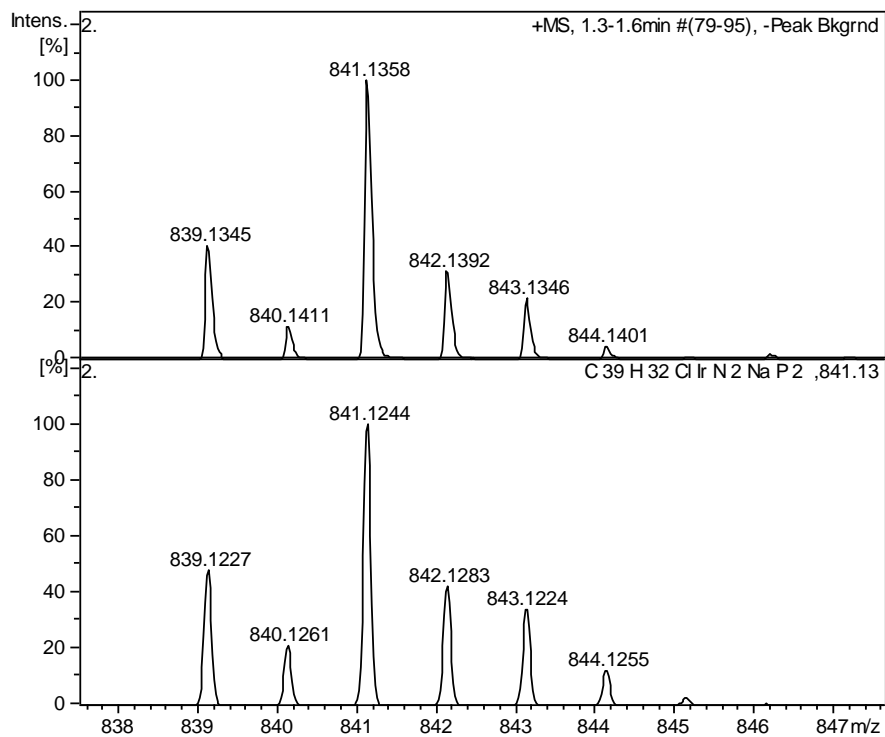
Figure D. 34 Comparison between experimental (above) and theoretical (below) mass spectrum of complex 38.

Complex 39
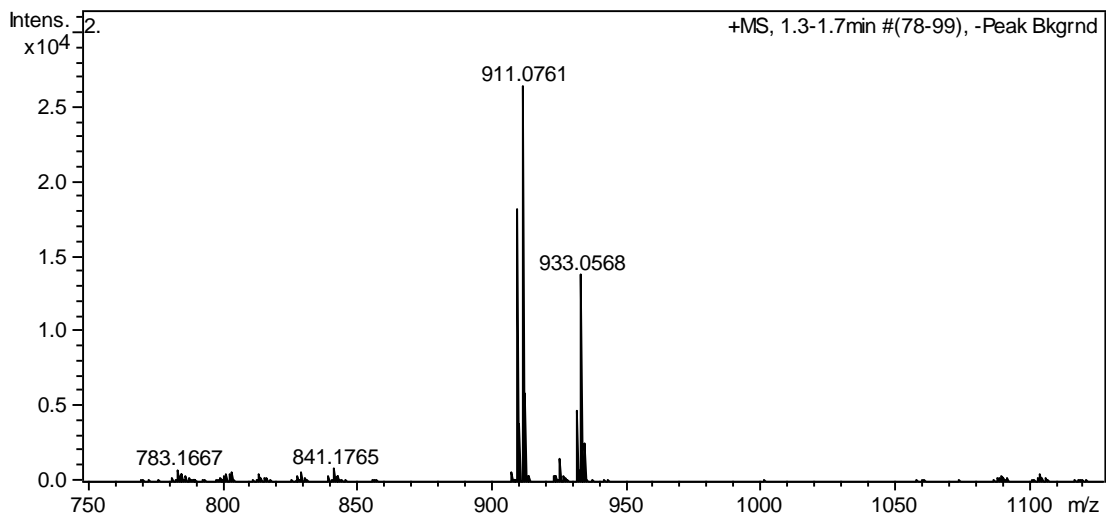
Figure D. 35 Mass spectrum of complex 39.
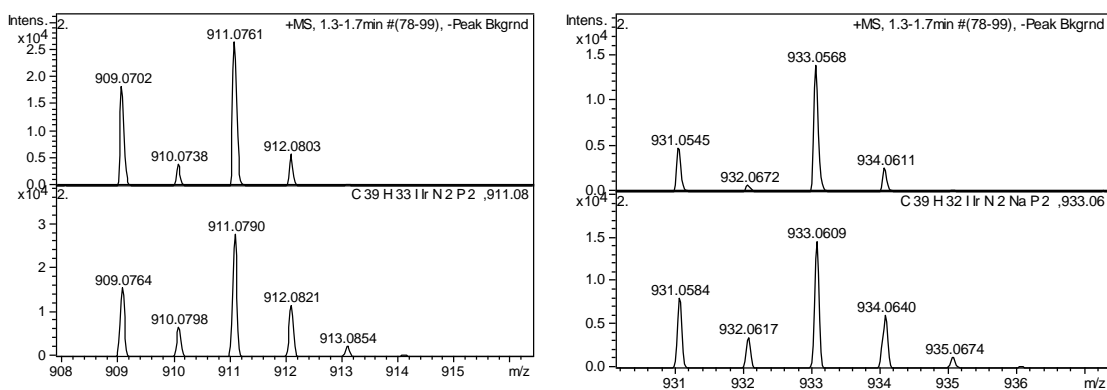
Figure D. 36 Comparison between experimental (above) and theoretical (below) mass spectrum of complex 39.

Complex 40
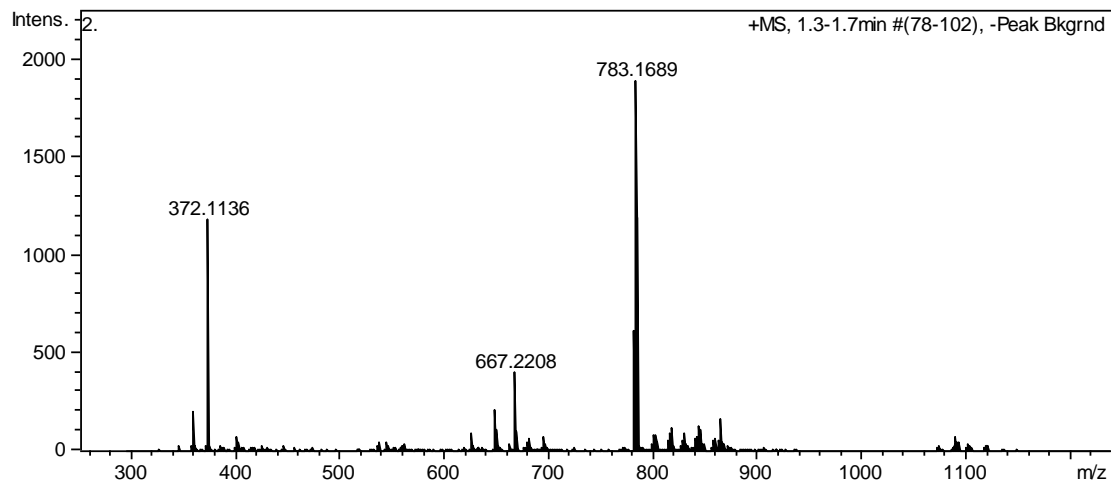
Figure D. 37 Mass spectrum of complex 40.
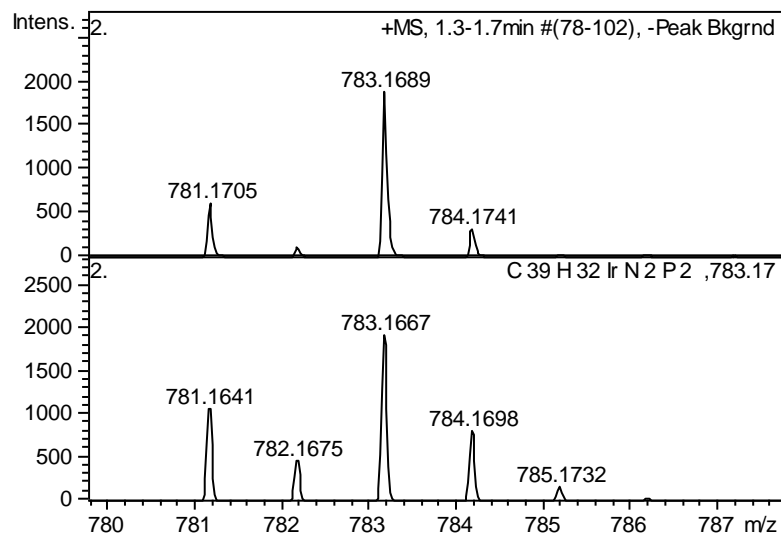
Figure D. 38 Comparison between experimental (above) and theoretical (below) mass spectrum of complex 40.

Complex 41
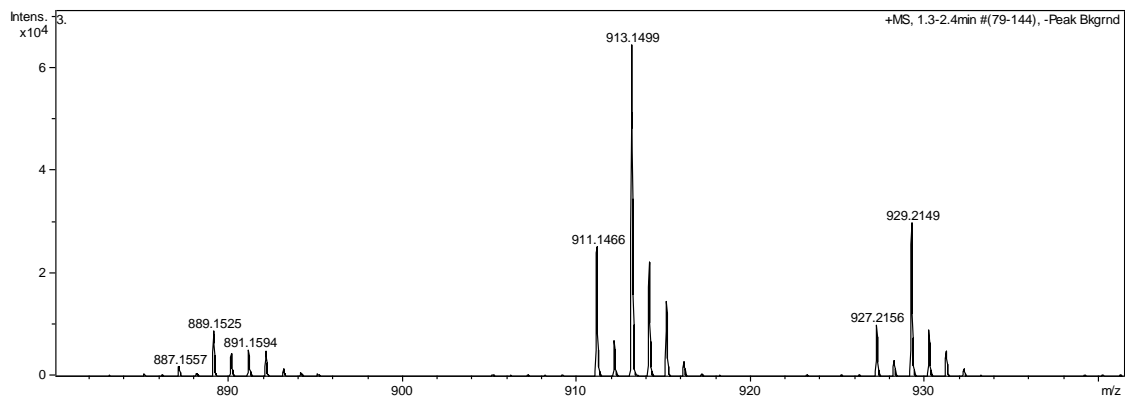
Figure D. 39 Mass spectrum of complex 41.
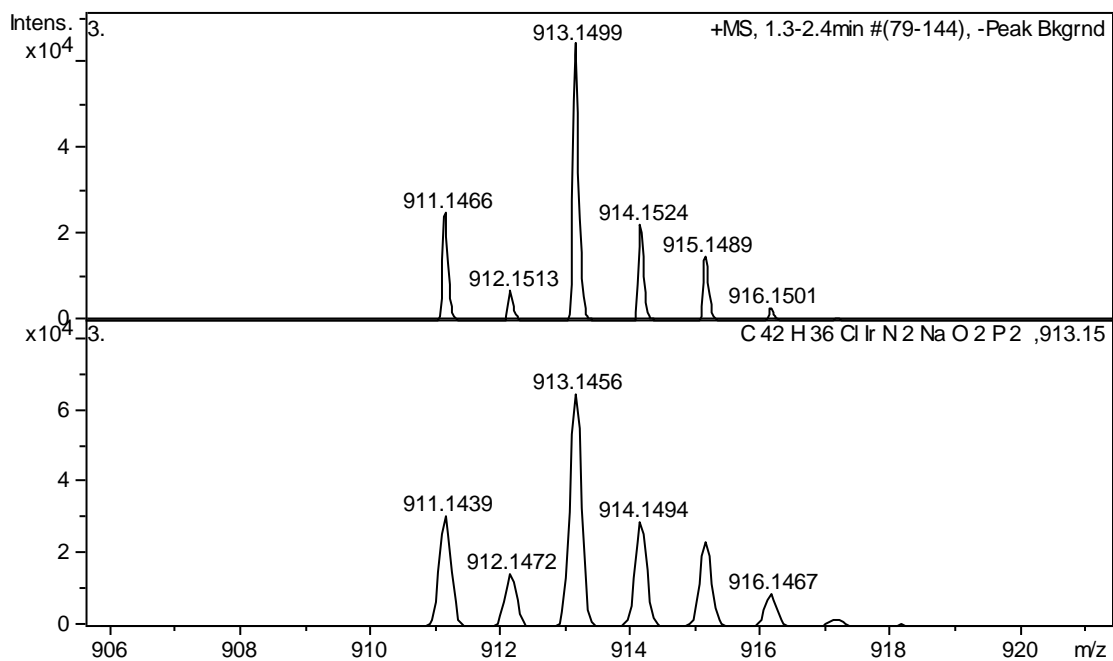
Figure D. 40 Comparison between experimental (above) and theoretical (below) mass spectrum of complex 41.

Annex E

Plots from catalysis

Chapter 3
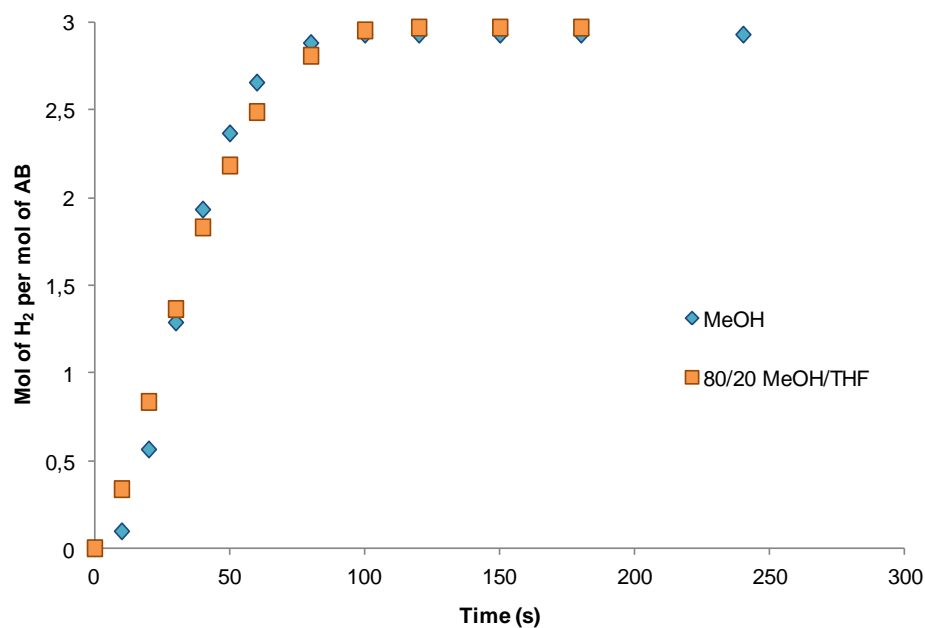
Figure E. 1 Hydrogen release from the methanolysis of AB with complex 1 as catalyst in different solvents: MeOH (◊, blue) and mixture of MeOH and THF (□, orange). T, 60 ⁰C.
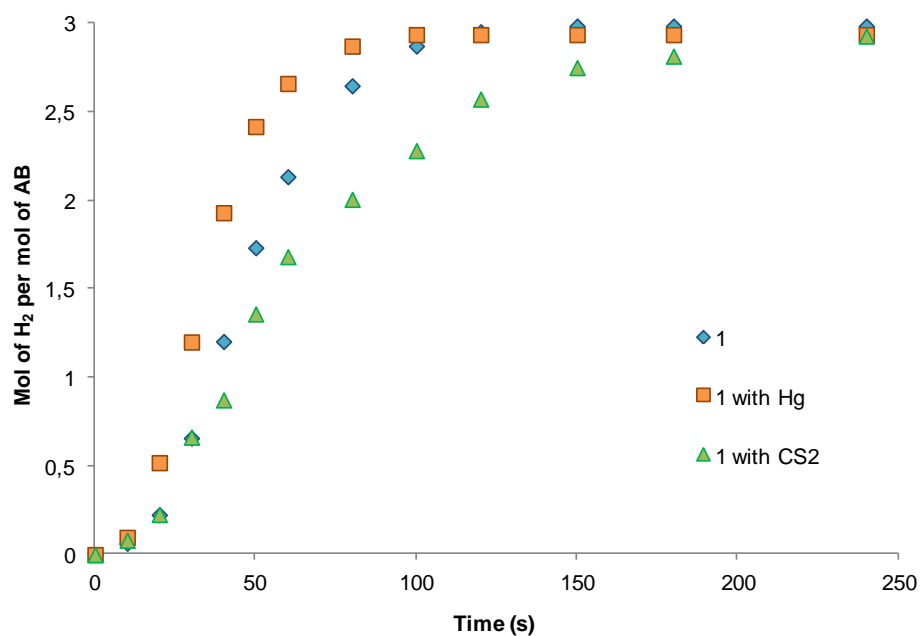
Figure E. 2 Hydrogen release from the methanolysis of AB with complex 1 as catalyst without Hg (◊, blue); with Hg (□, orange) and with CS_2 (Δ, green). T, 60 ⁰C.
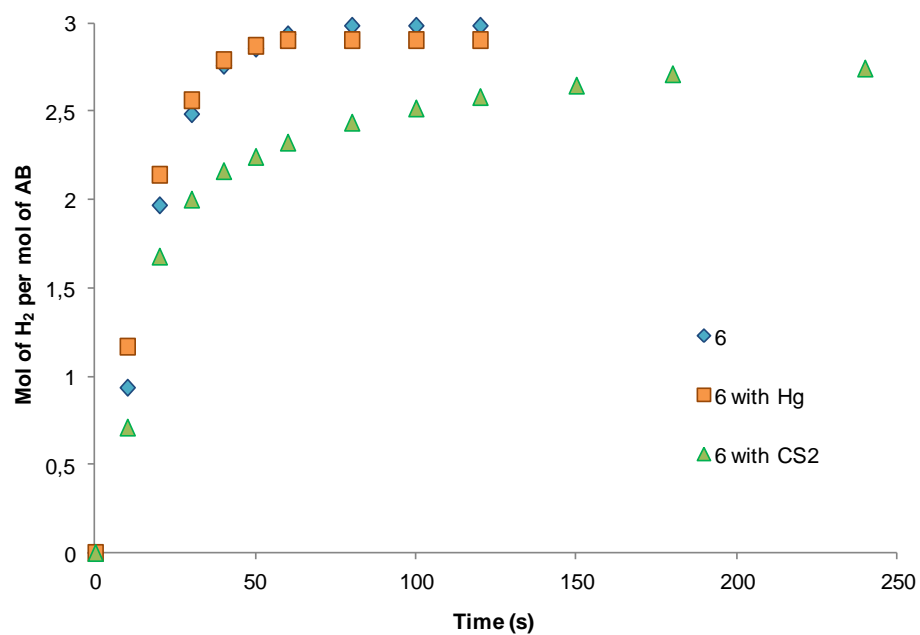
Figure E. 3 Hydrogen release from the methanolysis of AB with complex 7 as catalyst without Hg (◊, blue); with Hg (□, orange) and with CS$_2$ (Δ, green). T, 60 ºC.

Irida-β-dizetonak eta Iridapirazolak: Erreaktibitatea eta Aktibitate katalitikoa hidrogenoa amina-boranoen solbolisi erreakziotik askatzeko

Doktoretza ikaslea: ITXASO BUSTOS ROSAS

Zuzendariak: MARÍA ÁNGELES GARRALDA HUALDE

CLAUDIO MENDICUTE FIERRO

Euskal Herriko Unibertsitatea UPV-EHU

Donostia (Gipuzkoa), 2021

Aurkibidea

Laburduren, akronimoen eta sinboloen esanahia

AB	Amoniako-boranoa
ACN	Azetonitriloa
Bar$^F_4$	Sodio tetrakis[3,5-bis(trifluorometil)fenil]boratoa
COD	*Cis,cis*-1,5-ziklooktadienoa
COE	*Cis*-ziklooktenoa
DCM	Diklorometanoa
DMAB	Dimetilamina-boranoa
DMF	Dimetilformamida
EDA	Etildiazoazetatoa
EtOH	Etanola
^{i}PrOH	Isopropanola
IR	Espectroscopia Infragorria
m/z	Masa/karga erlazioa
MeOH	Metanola
Py	Piridina
Pyr	Pirazola
TBAB	Tert-butilamina-boranoa
TEAB	Trietilamina-boranoa
THF	Tetrahidrofuranoa
TOF	*Turnover frequency*

1. Kapitulua

Sarrera

1.1 Irida-β-dizetonak

Metala-β-dizetonak azilohidroxikarbeno motako konplexu organometalikoak dira. Koplexu hauek azilo eta hidroxikarbeno taldeen arteko hidrogeno lotura intramolekularraren bidez egonkortzen dira. Keto eta enol taldeen arteko hidrogeno lotura intramolekularra duten β-dizetona organikoen antzekoak dira (1.1 irudia).
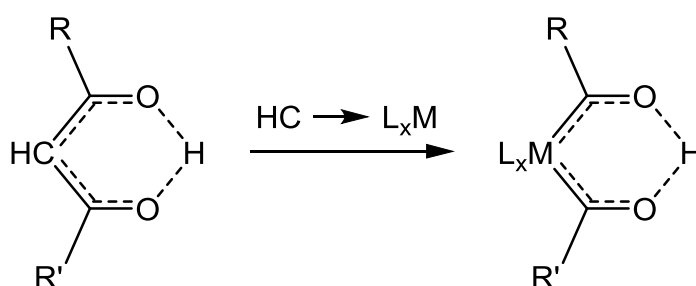
1.1 irudia. β-dizetona organikoak eta metala-β-dizetonak

Lukehart-ek 1981. urtean lehenengo aldiz aditzera eman zituen metalla-β-dizetona konplexuak. Konposatu hauek konplexu anioniko diazilometalatuak $[LxM(COR)]^-$ protonatzerakoan lortzen ziren, non M = Mo, W, Mn, Re, Fe eta Os baitziren.[1,2] Konplexu hauek koordinazio esfera elektronikoki asea zuten eta zinetikoki geldoak ziren.

Irida-β-dizetona motako konplexuak $[IrCl(COD)]_2$ dimero diolefinikotik eta o-(difenilfosfina)benzaldehido, $PPh_2(o\text{-}C_6H_4CHO)$, estekatzailetik sintetiza daitezke. Erreakzioa bentzenoan eginez gero konplexu hidruroazilo olefinikoa $[IrHCl(COD)(PPh_2(o\text{-}C_6H_4CO)]$ (**I**) lortzen da.[3] Prozesu horretan, hasierako dimeroko kloro zubiaren haustura gertatu da fosforoaren koordinazioarekin bat; aldehidoa, berriz, adizio oxidatzaile baten bitartez iridioari lotu da azilhidruro iridio(III) konplexu bat sortuz.

Bestalde, erreakzioa metanolean gertatzen denean Ir:P = 1:2 erlazioarekin, edo $[IrHCl(COD)(PPh_2(o\text{-}C_6H_4CO)]$ konplexua metanolean

disolbatzen eta PPh$_2$(o-C$_6$H$_4$CHO) beste baliokide bat gehitzen bada, bigarren aldehido baten adizio oxidatzailea gerta daiteke. Honen ondorioz dihidruro-diaziloiridio(V) bitartekari bat sortuko litzateke, zeinek iridiotik oxigenorako hidrogeno transferentzia baten ondoren hidruroirida-β-dizetona [IrHCl{(PPh$_2$(o-C$_6$H$_4$CO))$_2$H}] (**1**)[4] konplexua sortuko litzateke (1.1 eskema).
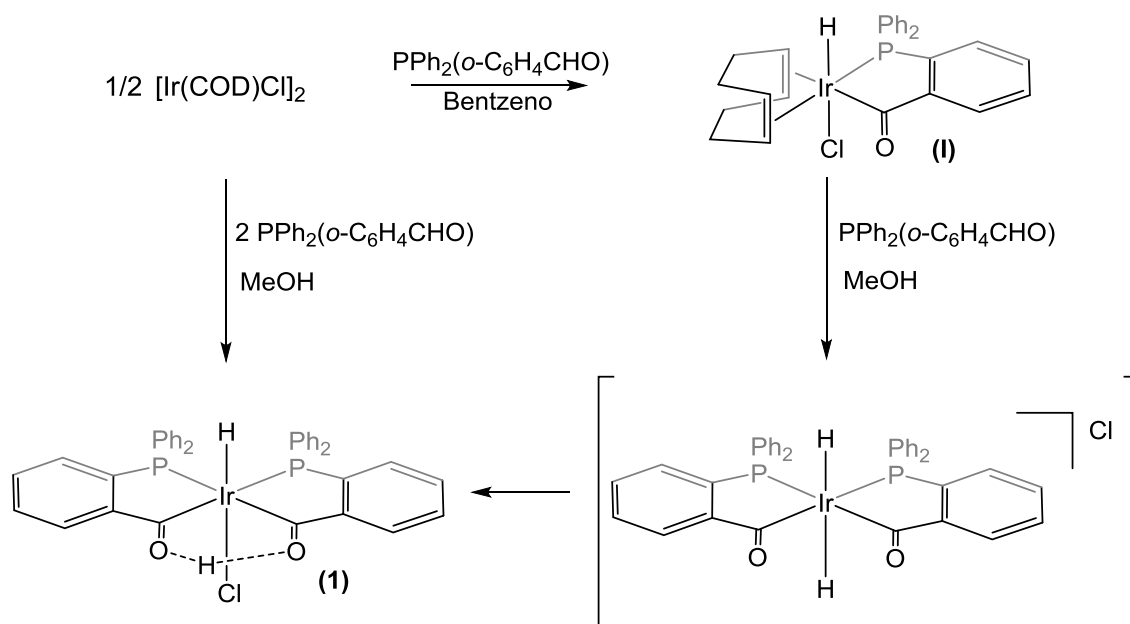
1.1 eskema. [IrHCl{(PPh$_2$(o-C$_6$H$_4$O))$_2$H}], 1 konplexuaren sintesia.

1.1.1 Klorohidruroirida-β-dizetona (1) konplexuaren erreaktibitatea.

Hidruroirida-β-dizetona [IrHCl{(PPh$_2$(o-C$_6$H$_4$CO))$_2$H}] egonkortasun handiko konplexua da, eta ez du erreakzionatzen σ-emaile estekatzaileekin, hala nola piridinarekin edo trifenilfosfinarekin.

Dena den, **1** konplexuak SnCl$_2$-arekin erreakziona dezake Ir-Cl loturan txertatuz. Prozesu honetan hasierako konplexuak daukan kloro atomoak eztainura migratzen du eta Ir-Sn lotura eratzen da hidruroiridatrikloroeztainato [IrH{(PPh$_2$(o-C$_6$H$_4$CO))$_2$H}(SnCl$_3$)] (**II**) konplexua sortuz.[4]

Gainera, 1 konplexuak halogeno abstraktoreekin erreakzionatzen du ere, hala nola AgClO$_4$, AgOTs eta AgOTf zilar gatzekin. Erreakzio horien ondorioz, kloro atomoa AgCl gatz moduan kanporatzen da, eta erabilitako zilar gatzaren anioia iridioari lotzen da, [IrHX{(PPh$_2$(*o*-C$_6$H$_4$CO))$_2$H}] (**III**) konplexu neutro berriak emanez, non X = ClO4$^-$, OTf$^-$.[4,5] Lortutako konplexu neutroek ligando labilak dituzte, eta horien ordez σ-emaile diren estekatzaileak erabil daitezke, hala nola piridina, trifenilfosfina eta karbono monoxidoa.[6] Aipatutako estekatzaileak erabiltzen direnean [IrHL{(PPh$_2$(*o*-C$_6$H$_4$CO))$_2$H}]X (**IV**) espezie kationikoak lortzen dira (1.2 eskema).
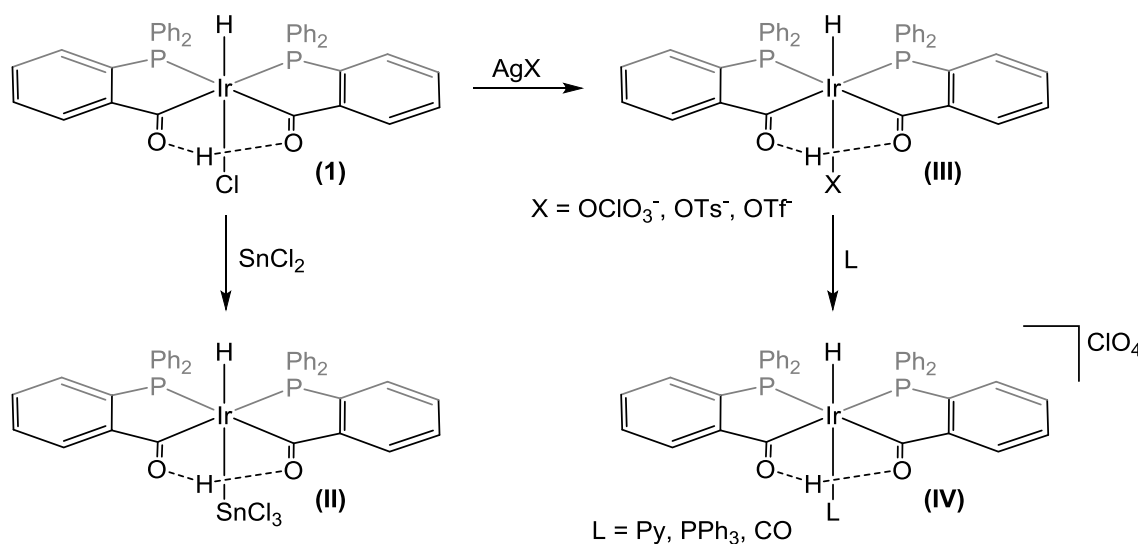
1.2 eskema. 1 konplexuaren erreaktibitatea, Ir-Cl loturaren haustura gertatzen delarik.

IV konplexuak (non L = CO den) desprotonazio/protonazio oreka du, zein tenperatura baxuetan protoi-formara lerratuta dagoen. **V** konplexua **IV** konplexuaren espezie desprotonatua da eta **IV** konplexua (L = CO) dimetilsulfoxidotan disolbatu eta trietilaminarekin erreakzionatu ondoren isola daiteke. Desprotonazio-erreakzioa gertatu ostean **V** konplexuaren estekatzaileak iridioaren inguruan berrantolatzen dira eta **VI** konplexua eratzen da. **VI** konplexuan hidruroak fosforo-atomo batekiko *trans* posizioa dauka. **V** eta **VI** konplexuak ingurune azidoan jartzen direnean hasierako **IV** konplexua

lortzen da (1.3 eskema). Emaitza hauen arabera, irida-β-dizetona konplexuetan behatutako PCCP koplanaritatea hidroxilo eta azilo taldeen arteko hidrogeno loturaren bidez egonkortuta dagoela baieztatu daiteke.[6]
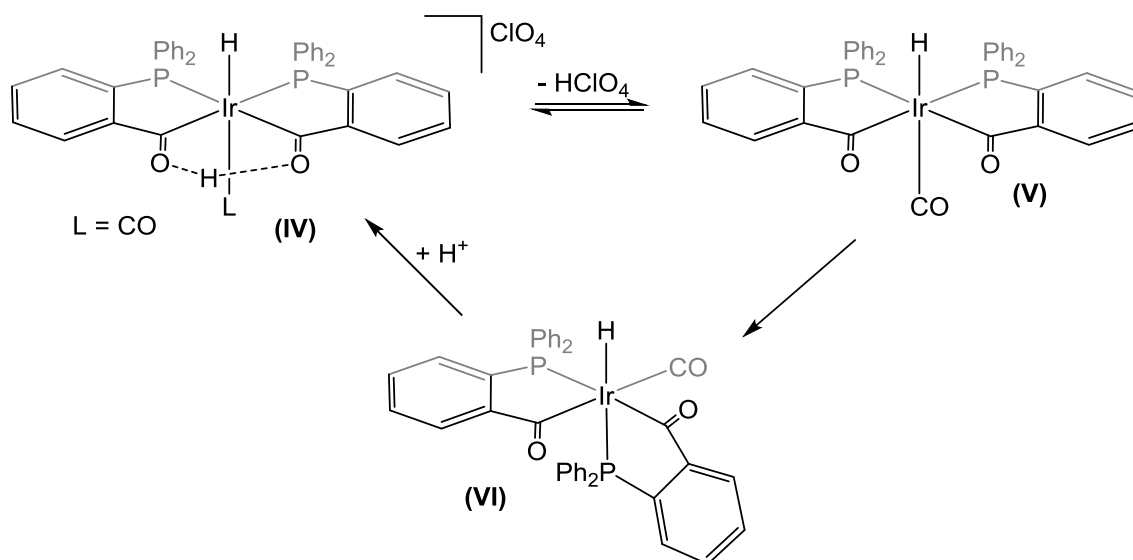
1.1 eskema. V konplexuaren protonazio / desprotonazio oreka eta isomerizazioa

Etileno-talde bat duen konplexu bat (**VII**) ere sintetiza daiteke **1** konplexutik eta etilenotik abiatuta AgBF$_4$-aren presentzian. Konplexu hori dimetilsulfoxidotan disolbatzen denean, disolbatzailearen molekula batek etilenoa ordezkatzen du **IX** konplexua eratuz. Ordezkapen honek hidruro batekiko *trans* posizioan dagoen etileno talde baten lekua koordinanteagoa den beste molekula batek erraz har dezakela baieztatzen du.[7] **VII** eta **IX** konplexuek trietilaminarekin erreakzionatu eta hidroxilo eta azilo taldeen arteko protoia galtzen dute **VIII** eta **X** konplexu neutroak osatuz (1.4 eskema), hidruroarekiko etilenoa eta dimetilsulfoxidoa *trans* posizioan dutenak hurrenez hurren.[6]
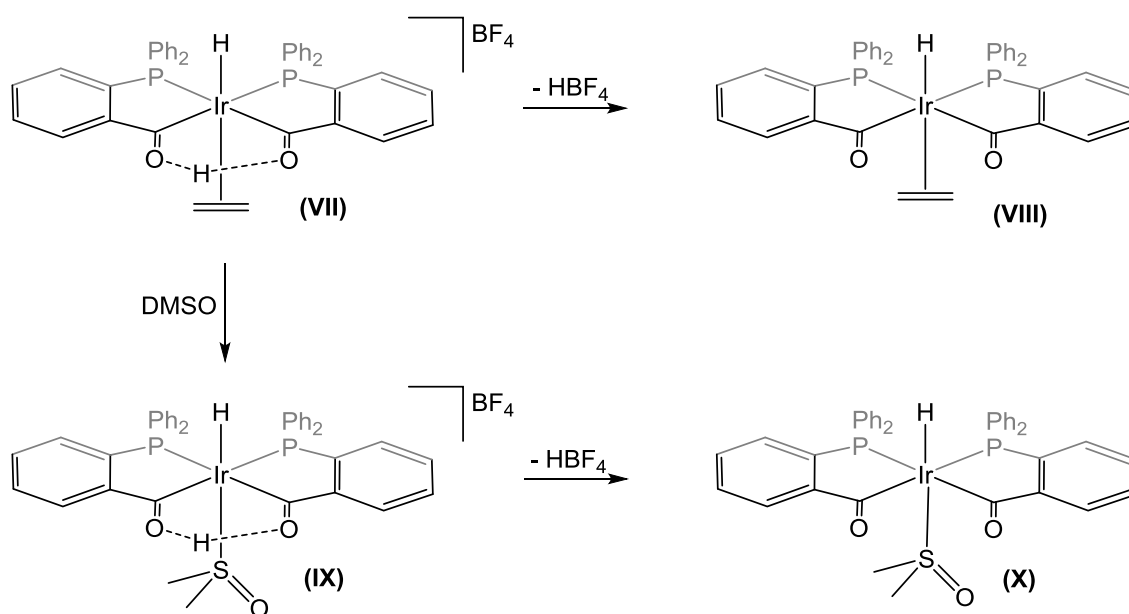
1.4 eskema. Hidruroirida-β-dizetona kationikoen desprotonazioa PCCP estruktura planarra mantenduz.

1, [IrHCl{(PPh$_2$(o-C$_6$H$_4$CO))$_2$H}], konplexuak anioi ez-koordinanteak dituzten haluro abstraktoreekin (AgBF$_4$, Et$_3$OBF$_4$ or Et$_3$OPF$_6$) Ir / abstraktore 2:1 erlazioan erreakzionatzen duenean kloruro estekatzailearen kopururaren erdia galdu eta **XI**, [{IrH[{PPh$_2$(o-C$_6$H$_4$CO)}$_2$H]}$_2$(μ-Cl)]X konposatua eratzen da (non X = BF$_4$ or PF$_6$ izan daitekeen).[5] **XI** konplexua kloro zubi batez lotuta dauden bi hidruroirida-β-dizetona talde dituen dimero kationikoa da (1.5 eskema).
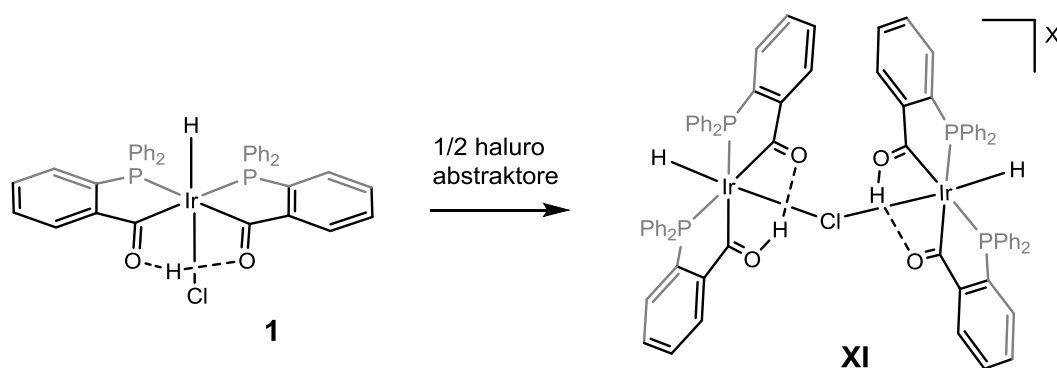
1.5 eskema. XI konplexuaren formazioa, hidruroirida-β-dizetona konplexu dinuklearra.

1 konplexuak metanol-disoluziotan baseekiko duen erreaktibitatea aztertu izan da. Erabilitako basea sodio hidroxidoa edo sodio bikarbonatoa denean, eta erreakzioa errefluxu-baldintzapetan egiten denean, dihidruroirida-β-dizetona **2** konplexua, $[IrH_2\{(PPh_2(o\text{-}C_6H_4CO))_2H\}]$, lortzen da.[8]
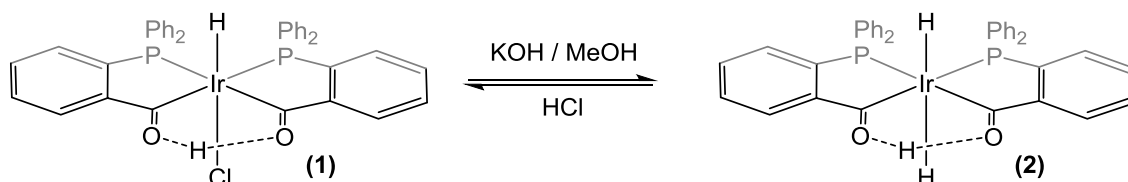
1.6 eskema. 2 konplexuaren formazioa.

Kloruro / hidruro ordezkapen erreakzio hau disolbatzailearen, metanolaren, bidez gertatzen dela proposatzen da. Disolbatzailea hidruro iturria izan baitaiteke metoxi taldearen koordinazio eta β-H transferentzia baten bidez.

1.1.1.1 Irida-β-dizetonen erreaktibitatea amina edo hidrazinarekiko

Hydridoirida-β-dizetonek aminekiko egin ditzaketen erreakzioei dagokionez kimika aberatsa dutela erakutsi dute. Konplexu hauek amina alifatiko eta aromatiko primario edo sekundarioekin eta amoniakoarekin erreakziona dezakete hainbat konplexu berriak sortuz. **1** konplexuak amina alifatiko primarioekin edo amoniakoarekin disolbatzaile lehorretan erreakziona dezake hidruroirida-β-zetoimina motako konplexuak (**XII**) lortuz, N-H--O hidrogeno lotura intramolekular batez egonkortuta daudenak. Hydridoirida-β-zetoimina konplexuek hidrolizatu eta hidruroamina konplexuak (**XIII**) sor ditzakete. Hidruroamina konplexuak **1** konplexuaren eta amoniakoaren edo amina alifatikoen arteko erreakzioaren bidez ere lor daitezke, erreakzioa tetrahidrofurano eta ur nahasketa batean eginez.[9,10]

Bestalde, amina sekundarioak ez dira gai kondentsazio-erreakzioa gauzatu eta hidruroirida-β-zetoimina konplexuak (**XII**) lortzeko. Amina sekundariak erabiliz hidruroamina konplexuak (**XIII**) soilik lor daitezke (1.7 eskema).
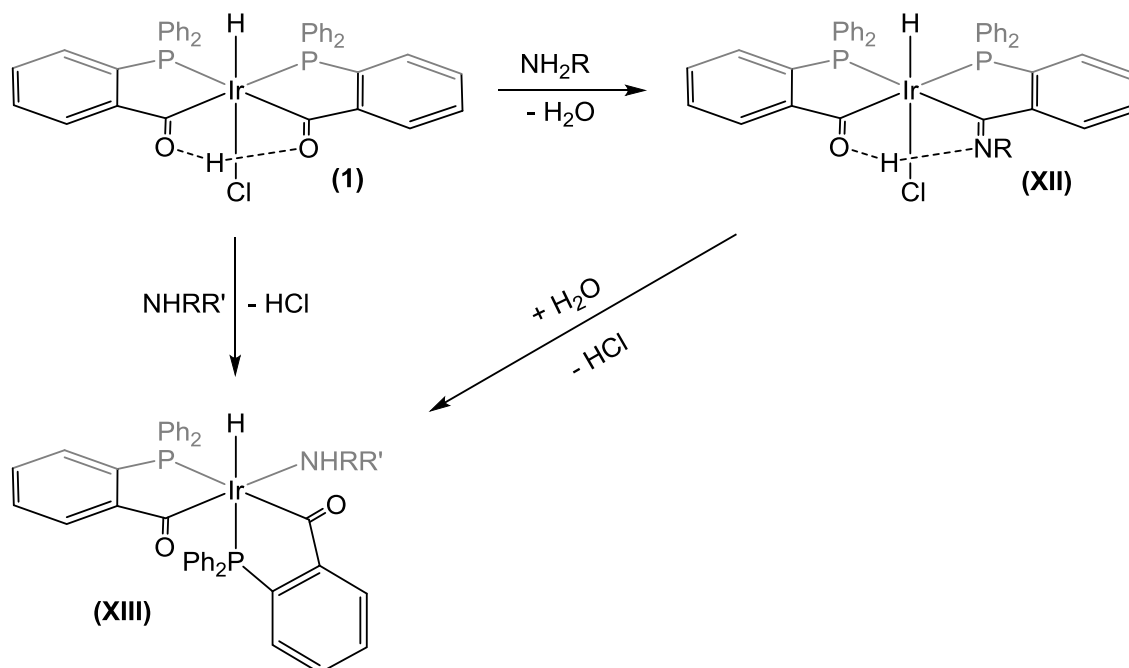
1.7 eskema. 1 Konplexuaren erreaktibitatea amoniako eta amina alifatikoekiko.

Gainera, irida-β-dizetona $IrH(OClO_3)\{(PPh_2(o\text{-}C_6H_4CO))_2H\}$-k (**III**) amina eta amoniakoarekiko duen erreaktibotasuna ere aztertua izan zen.[9] **III** konplexuak amina alifatikoekin edo amoniakoarekin erreakzionatzen duenean hidruroamina konplexua (**XIII**) sortzen da. Aitzitik, **III** konplexua eta anilina amina aromatikoaren arteko erreakzioaren ondorioz hidruroirida-β-dizetona konplexu kationiko berri bat sortzen da, **XIV** konplexua. Erreakzio honetan, anilinak (beste amina baino nukleozaletasun txikiagoa daukana) koordinatua dagoen perklorato estekatzailea ordezkatzen du (1.8 eskema).
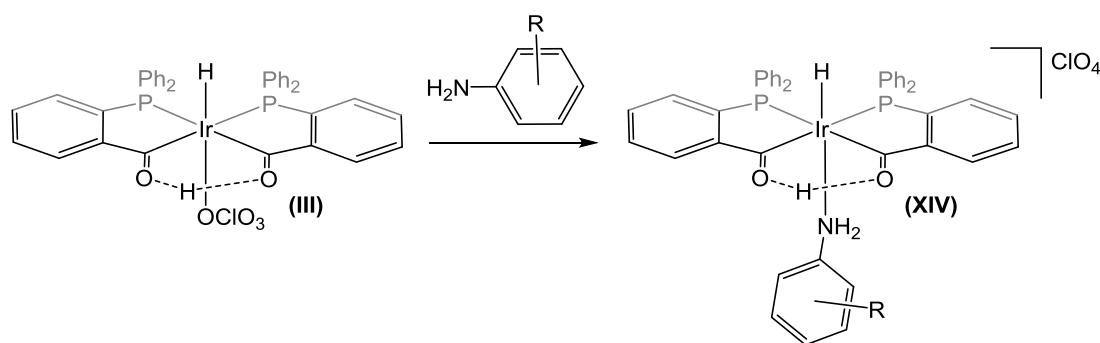
1.8 eskema. III konplexuaren erreaktibitatea amina aromatikoen aurrean.

2-aminopiridinek amina talde bat eta piridina talde bat dituzte, eta bi taldeek konposatu organometalikoekin erreakziona dezakete. Hain zuzen, **1** konplexua 2-aminopiridinekin erreakzionarazten denean, PCN estekatzaile bat duten klorodun konplexuak (**XV**) lortzen dira. PCN estekatzailea amina taldeak hidroxikarbeno taldean egindako kondentsazioaren ondorioz sortzen da. Erreakzio honek, piridina talde bat esekia duen aminokarbeno iragankorra eratzen du eta piridinaren koordinazioak iridiotik karbonorako hidrogeno transferentzia gertatzea eragiten du. **XV** konplexuak erreakzio produktu zinetikoak dira. Erreakzioa tenperatura handiagotan egiten bada, edo **XV** konplexuak metanoletan disolbatu eta berotzen badira, **XVI** konplexu termodinamikoki egonkorrak lortzen dira. Konplexu hauek bi fosforo-atomo bata bestearekiko *trans* posizioan dituzte (1.9 eskema).[10]
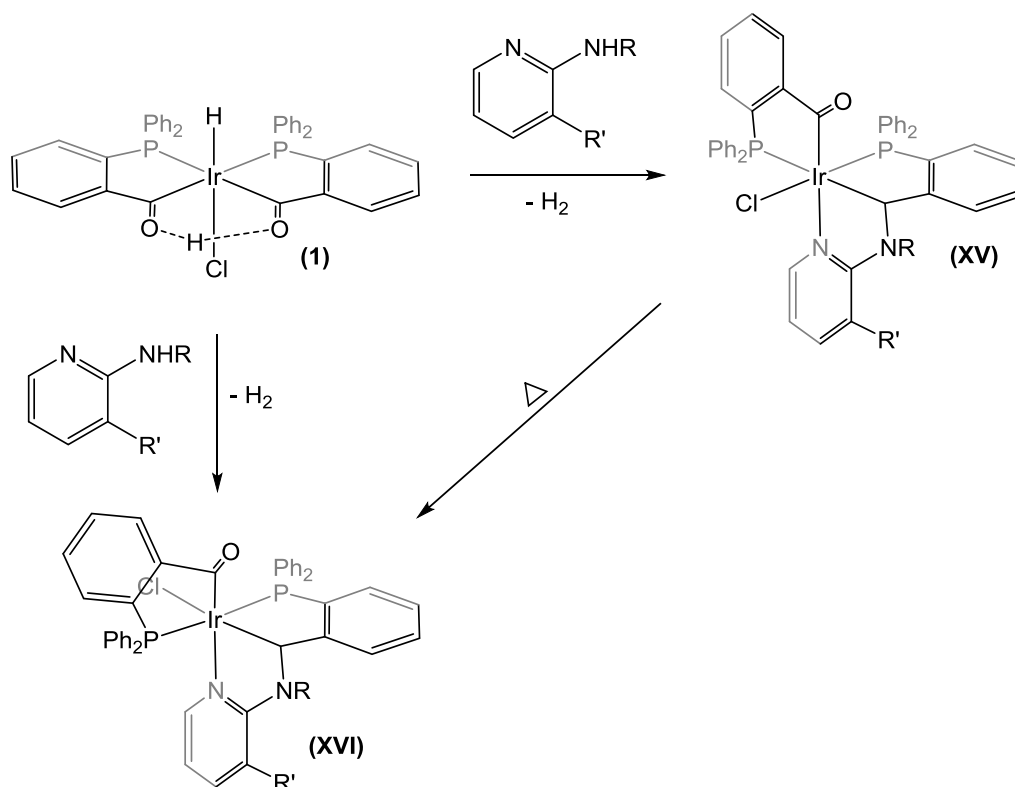
1.9 eskema.1 konplexuaren erreaktibitate 2-aminopiridinen aurrean.

Irida-β-dizetona den **1** konplexuak 2-aminoalkilpiridinekin erreakzionatzen duenean piridina taldea esekita duten hidruroirida-β-zetoimina konplexuak (**XVII**) lortzen dira. Konplexu hauek ingurune protikoan dehidroklorinazioa jasan ondoren PCN estekatzailedun konplexu (**XVIII**) bihurtzen dira. Bestalde, **2** konplexuak 2-aminoalkilpiridinekin erreakzionatzen duenean ingurune protikoan hidrogeno molekula bat askatzen du. Honen ondorioz, piridna bat esekita duten hidruroamina konplexu berriak (**XIX**) sortzen dira (1.10 eskema).[11]
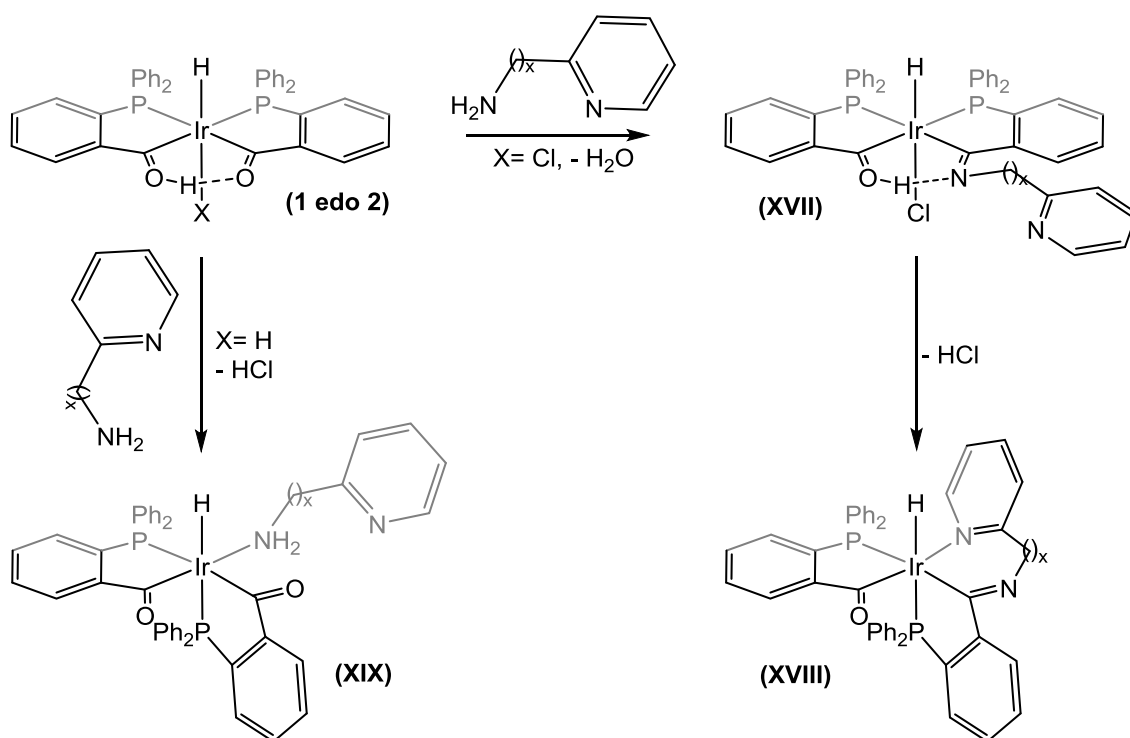
1.10 eskema. 1 eta 2 konplexuen erreaktibitatea 2-aminoalkilpiridineekiko

Azkenik, hidrazinak bi nitrogeno-atomo nukleozale ditu, eta horiek modu desberdinetan erreakziona dezakete irida-β-dizetona **1** konplexuarekin. **1** konplexua eta hidrazina tetrahidrofurotan nahasten direnean, hidruroirida-β-zetoimina den **XX** konplexua lortzen da, amina alifatikoekin eta amoniakoarekin gertatzen den bezala.[9,10] Kasu honetan, ordea, esekita dagoen bigarren amina taldearen kondentsazioa errefluxupean gerta daiteke, metalaziklo berri bat (**3** konplexua) sortuz (1.11 eskema).[12]
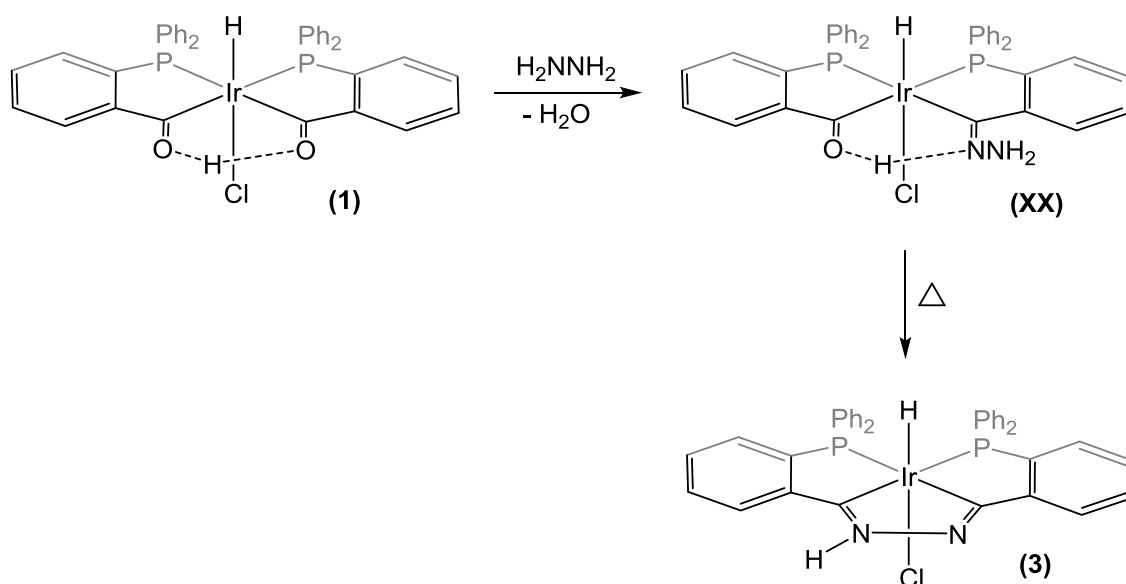
1.11 eskema. Hidruroiridapirazola den 3 konplexuaren formazioa.

3 konplexua, [IrHCl{Ph$_2$P(o-C$_6$H$_4$)CNNHC(o-C$_6$H$_4$)PPh$_2$}], eta bere dihidruro deribatua, [IrH$_2${Ph$_2$P(o-C$_6$H$_4$)CNNHC(o-C$_6$H$_4$)PPh$_2$}], lehenengo aldiz sintetizatutako metalapirazol motako konposatuak dira.[12] [Ir(F$_2$ppy)$_2$(CNAr)$_2$]PF$_6$ eta hidrazinaren arteko arreakzioaren ondorioz sortutako konposatua **3** konplexuaren antzekoa da,[13] izan ere konposatu berriak atomo-mota bera dituen zikloa badauka. Hala ere, azken hori hobeto deskribatzen da Chugaev - motako biskarbeno konposatu gisa eta ez iridapirazol moduan (1.12 eskema).
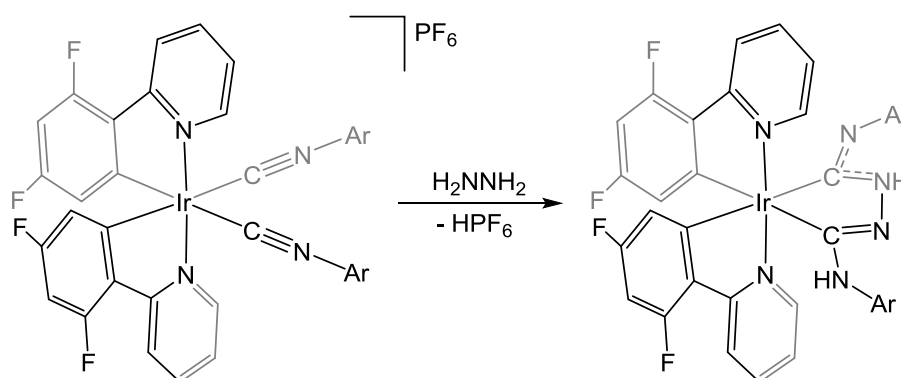
1.12 eskema. Chugaev – motako iridio biskarbeno konplexuen formazioa.

Chugaev-motako metalakarbeno konplexuak diaminakarbeno konplexu aziklikoak dira, zeinetan karbenoak amina taldeek egonkortzen dituzten.[14] Aipatutako iridapirazol konplexuek pirazol organikoen antzeko C=N lotura-luzera eta angeluak dituzte. Chugaev - motako biscarbeno konplexuek dituzten metalazikloetan, berriz, egitura-ezaugarri horiek desberdinak dira.

Antzeko iridapirazol konplexuak lortzeko hainbat saiakera egin ziren fenilhidrazinarekin, baina, zoritxarrez, zetoimina motako konplexua baino ez zen lortu; metalazikloa lortzeko beharrezkoa den bigarren kondentsazio-erreakzioa ez zen gertatu.[12]

1.2 Amoniako-boranoaren solbolisia H_2 askapenerako.

Hidrogenoa, energia horniduran erregai fosilak ordezkatzeko hautagai onenetarikoa da. Hori dela eta, hidruro kimikoetatik eskariaren arabera hidrogenoa askatzea ikerketa intentsiboko gaia bihurtu da azkenaldian.[15] Haren errekuntza-erreakzioa ez da erregai fosilena bezain kaltegarria ingurumenerako, azpiproduktu bakarra dagoelako, ura, eta energia-iturri ekologikoagoa delako.[16]

Hidrogenoa hainbat iturritatik katalitikoki ekoiz daiteke; adibidez, azido formikotik,[17] metanoletik[18] edota amoniako-boranotik (H_3N-BH_3, AB). Izan ere, izendatutako guztien artean AB-ak hidrogeno eduki handiena due, % 19.6 m/m,[19–21]. Honengatik substantzia erakargarria da hidrogenoa biltegiratzeko material solido gisa.

Amoniako eta amina-boranoek hidrogenoa katalitikoki aska dezakete dehidroakoplamendu-erreakzio baten bidez, 1.13 eskeman ageri den moduan.

$$H_3NBH_3 \xrightarrow{\text{kat.}} H_2NBH_2 + H_2$$
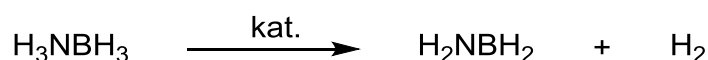
1.13 eskema. AB-aren dehidrogenazio katalitikoa.

Prozesu hau modu homogeneoan katalizatu daiteke, adibidez, iridio,[22,23] rutenio,[24,25] rodio,[26,27] burdin[28] eta kobalto[29] konplexuak erabiliz (1.2 irudia). Konplexu hauek AB atomo bakoitzeko 2 hidrogeno-baliokide aska ditzakete. AB-aren dehidroakoplamendu katalizatua nanopartikulak erabiliz ere lortu da, kasu honetan 2 hidrogeno-baliokide baino gehiago askatzea lortu zen.[30–32]
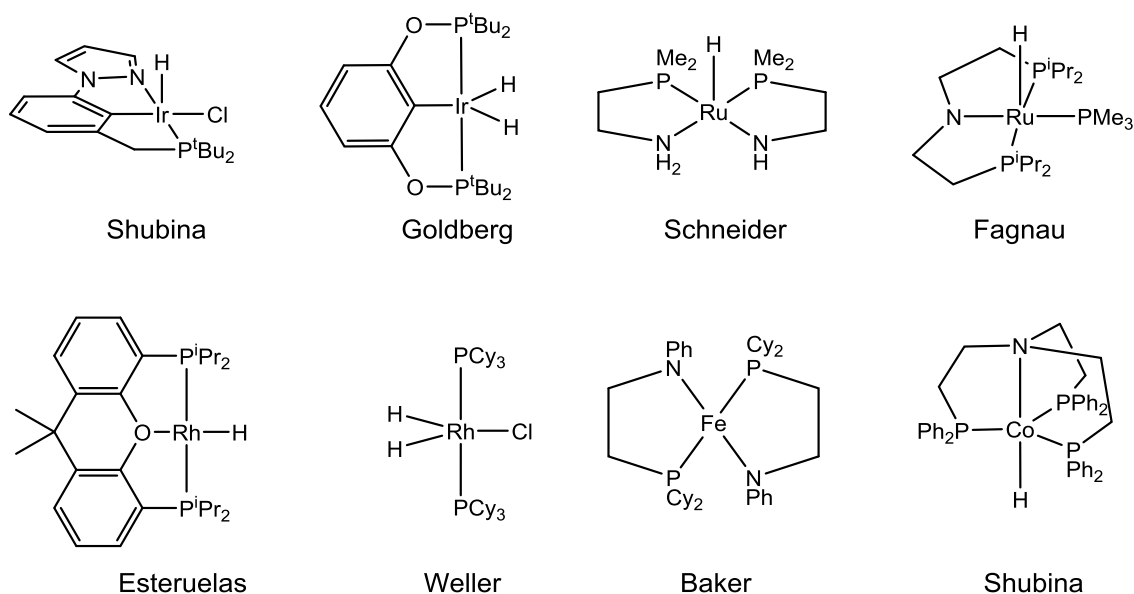
1.2 irudia. AB-aren dehidrogenazioa homogeneoki katalizatzen duten hainbat konplexu.

AB-atik hidrogenoa lortzeko beste metodo bat metalek lagundutako hidrolisia da (1.14 eskema). Prozesu horretan, AB-aren borano taldetik datorren hidruroak ura molekula batetik datorren protoiarekin erreakzionatu eta hidrogeno molekularra eratzen da. Erreakzio honekin hiru hidrogeno-baliokide aska daitezke.[20]

$$H_3NBH_3 \;+\; 2\,H_2O \xrightarrow{\text{kat.}} 3\,H_2 \;+\; BO_2^- \;+\; NH_4^+$$
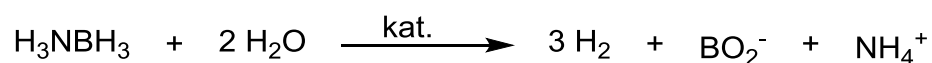
1.14 eskema. AB-aren hidrolisi katalitikoa.

Metal nobleek AB-aren hidrolisi erreakzioa era heterogeneoan kataliza dezakete, hidrogenoaren askapen azkarra lortuz.[34,35] Metal ez-nobleez osatutako nanopartikulak ere, gai dira aipatutako katalisia gauzatzeko, bai eta metal noble eta ez-noble konbinazioaz osaturiko nanopartikulak.[36–42]

Amoniako- eta amina-borano aduktuen hidrolisia homogeneoki katalizatzeko gai izan den lehenengo konplexua gure taldean aurkitu zen.[9,43] Aurrekatalizatzaileak aurretik deskribatutako hidruroirida-β-dizetona motako **1** eta **2** konplexuak dira.

Amoniako- eta amina-boranoen hidrolisi-erreakzioaren katalisia aztertu zen, eta ziklo katalitikoak agertzen zen jarduerarik gabeko espezie bat proposatu zen, [IrH(PPh$_2$(o-C$_6$H$_4$CO))$_2$(NHRR')].[9,43] Espezie honetan hidruroa mantentzen da, bi fosforo atomo *cis* posizioan eta amina talde bat *trans* posizioan dituelarik.

Aurrerago, trantsiziozko metalez osatutako beste katalizatzaile batzuek, hala nola: iridio PNP, karbeno edo hidroxi-bipiridina konplexuek,[44–46] azilhidruro-rodio deribatuek,[47,48] eta dikarbonilrutenaziklo edo rutenio-bipiridina-p-zimeno konplexuek,[49–51] AB-aren hidrolisi erreakziorako katalizatzaile homogeneo eraginkorrak zirela erakutsi zuten.

Amoniako- eta amina-borano aduktuetatik hiru hidrogeno-baliokide lortzeko beste metodo bat metanolisi katalizatua da (1.15 eskema). Prozedura horretan, hidruroak borano taldetik datoz eta protoiak metanol molekuletatik.

$$H_3NBH_3 \ + \ 4\ MeOH \ \xrightarrow{\text{kat.}} \ 3\ H_2 \ + \ [NH_4][B(OCH_3)_4]$$
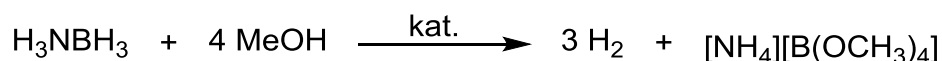
1.15 eskema. AB-aren metanolisi katalizatua.

Amoniako eta amina-borano aduktuen metanolisia ez da hidrolisia bezain sakon aztertu. Metanolisi erreakzio katalitiko heterogeneoek hidrolisi erreakzioek baino hidrogeno askapen motelagoa gauzaten dute. Gainera, hidrogenoaren pisu portzentaia kontuan hartuz ez da hidrolisi bezain desiragarria. Hala ere, metanol-disoluzioetan AB-a egonkorragoa da, eta 0 ºC-tik behera hidrogenoa askatzeko aukera ematen du.[52] Halaber, AB-a erraz birsortzeko metodo bat lortu da metanolisiaren produktutik abiatuta, $[NH_4][B(OCH_3)_4]$, tetrametoxiboratoatik eta giro tenperaturan.[53]

Hidrolisi erreakzioetan bezala, metal nobleen nanopartikulak ABaren metanolisirako katalizatzaile aktiboenen artean daude;[54–56] eta duela gutxi, homogeneizatutako metal nanopartikula batzuek AB-aren metanolisi hetereogeneoki katalizatuaren errendimendua hobetu dezaketela frogatu dute.[57]

Amoniako-boranoaren lehen metanolisi homogeneoa duela gutxi jakinarazi zen, honetan rutenio sandwich konplexu bat erabili zen, 6,6'-dihidroxi-2,2´-bipiridina estekatzailea zuena. Rutenio-konplexu horrek jarduera bikaina erakutsi zuen, hasierako $TOF_{\%10}$-arako 448 $mol_{H_2} \cdot mol_{Ir}^{-1} \cdot min^{-1}$-ko balioa eta $TOF_{\%50}$-arako 120 $mol_{H_2} \cdot mol_{Ir}^{-1} \cdot min^{-1}$-ko balioa 60 ºC-tan lortu ziren.[58]

1.3 Helburuak

Sarreran azaldutakoa kontuan hartuz, interesgarria iruditu zitzaigun irida-β-dizetona motako konplexuen erreaktibotasuna estekatzaile berrien aurrean eta lortzen diren konplexu berrien jarduera katalitikoa aztertzea.

Horretaz gain, irida-β-dizetona **1**, [IrHCl{(PPh$_2$(o-C$_6$H$_4$CO))$_2$H}], eta **7**, [(IrH{(PPh$_2$(o-C$_6$H$_4$CO))$_2$H})$_2$(μ-Cl)]BF$_4$, konplexuen jarduera katalitikoa AB-aren metanolisi homogeneo katalizatuan aztertzea egokia iruditu zitzaigun. Izan ere, erreakzio hau sakonki aztertua izan da prozesu heterogeneotarako baina ez homogeneotarako. Gainera, EMN *in situ* esperimentuak eta deuterazio-saiakerak egin ziren prozesu katalitikoa ulertzeko.

Azkenik, iridapirazol motako **3** konplexuan sakontzeko, konplexu hau lortzeko ibilbide sintetiko berri bat proposatu zen. Horren ondoren, **3** konplexuaren erreaktibotasuna aztertu zen zentro metalikoan eta iridapirazol eraztunean. Pirazol organikoen ohiko erreakzio batzuk egin ziren konplexuaren metalazikloa eta pirazol organikoaren antzekotasunak ikertzeko.

2. Kapitulua

Amoniako-boranoaren metanolisi homogeneoa, Hidruroirida-β-dizetonek katalizatua

2.1 Sarrera

Irida-β-dizetona konplexuak AB-aren hidrolisian hidrogenoa askatzeko katalizatzaile eraginkorrak direla frogatu da.[9,43] Hori kontuan hartuz, kapitulu honetan irida-β-dizetonek kalitalizaturiko AB-aren metanolisia aztertzen da. Metanolisi erreakzioan amoniako-borano aduktuaren hidruroak metanolaren protoiekin konbinatzen dira hidrogenoa sortu eta askatzeko, [NH$_4$][B(OMe)$_4$] sortuz (2.1. eskema).

$$H_3NBH_3 \ + \ 4\ MeOH \ \xrightarrow{\text{kat.}} \ 3\ H_2 \ + \ [NH_4][B(OCH_3)_4]$$
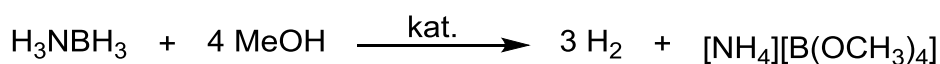
2.1. eskema. AB-aren metanolisi erreakzioa

2.2 (1), [IrHCl{PPh$_2$(*o*-C$_6$H$_4$CO))$_2$)H}] Klorohidruroirida-β-dizetonaren aktibitate katalitikoa

1 konplexua katalizatzaile eraginkorra da AB-ren metanolisi erreakzioaren bidez hidrogenoa askatzeko. Hasieran, 0.46 M-eko AB kontzentrazioa eta % 0.4-ko katalazitzailearen karga (1.86·10^{-3} M) erabilita, 2.7 hidrogeno baliokide lortzen dira 30 °C-tan 14 minutu igaro ondoren (2.1 irudia). Tenperatura horretan, hidrogenoa askatzen hasi aurretik 120 s-ko indukzio denbora ikus daiteke. Indukzio denbora hori **1** konplexuak metanoletan duen disolbagarritasun txikiaren ondorioa izan daiteke. Erreakzioa 60 °C-tan egiten denean, aldiz, indukzio denbora ia ikustezina da; izan ere, 10 s-takoa baino ez da eta 3 hidrogeno baliokide 2 minutu pasa baino lehen askatzen dira. TOF-aren balioak konbertsioa % 50-ekoa zenean kalkulatu ziren. Kontuan hartutako denborak indukzioaren ostekoak izan dira eta erabilitako tenperaturak 30 ºC eta 60 ºC-koak. Lortutako TOF balioak 104 mol$_{H_2}$·mol$_{Ir}^{-1}$·min^{-1}-koa eta 865 mol$_{H_2}$·mol$_{Ir}^{-1}$·min^{-1}-koa izan dira, hurrenez hurren.
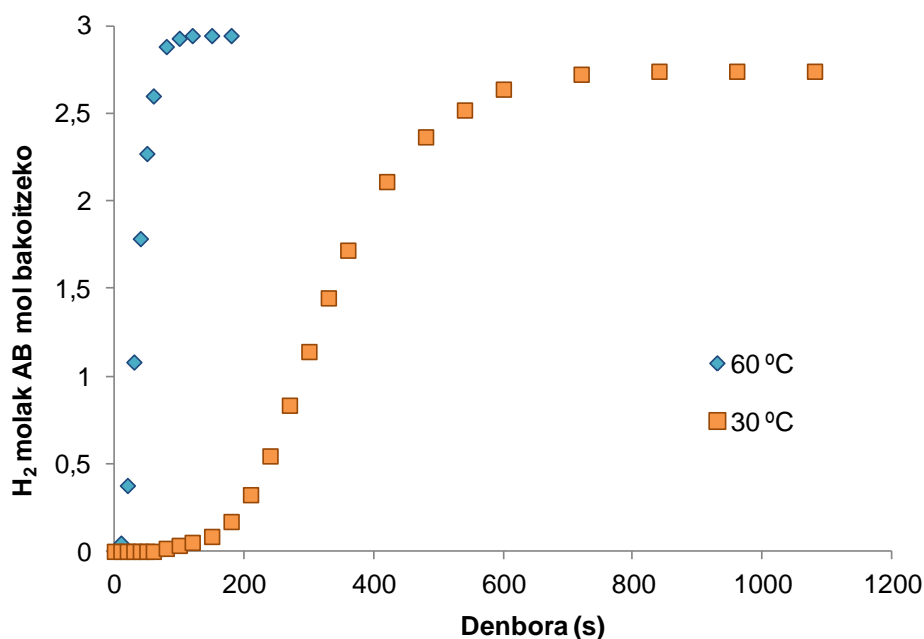
2.1. irudia. AB-aren metanolisitik askatutako hidrogenoa 1 konplexua katalizatzaile moduan erabilita, 30 ºC-tan (□, laranja) eta 60 ºC-tan (◊, urdina), metanoletan egin da.

Indukzio denbora saihestu nahian, AB-aren metanolisia **1** konplexua katalizatzaile gisa erabiliz 80/20 metanol/tetrahidrofurano nahastean egin zen; **1** konplexua tetrahidrofuranotan nahiko disolbagarria baita. E.1 irudian ikusten denez, 60 ºC-tan ez da indukziorik ageri MeOH/THF nahastean, eta hidrogenoaren bilakaera oso antzekoa da bi disolbatzaileetan (metanoletan eta metanol/tetrahidrofurano nahastean). Horrenbestez, prozesu katalitiko hauetarako metanola disolbatzaile bakar gisa erabiltzea erabaki zen.

Erreakzio katalitikoaren homogeneotasuna frogatzeko, hidrogeno askapena hasi eta 20 segundora Hg-a soberan gehitu zen. Emaitzak oso antzekoak izan ziren Hg-arekin eta Hg-rik gabe egindako saiakeretan (2.2 irudia); disoluzioa hori argia mantendu zen ilundu gabe eta horrek, katalisiaren homogeneotasuna erakutsi zuen.
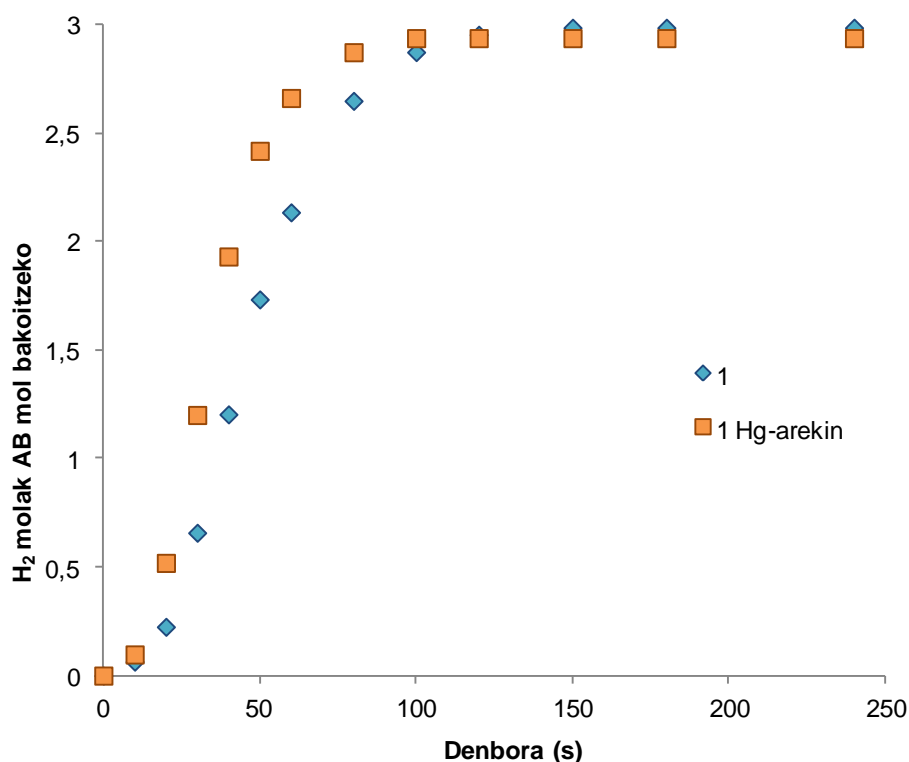
2.2 irudia. AB-aren metanolisitik askatutako hidrogenoa 1 konplexua katalizatzaile moduan erabilita, Hg-rik gabe (◊, urdina) eta Hg-arekin (□, laranja). 60 ºC-tan eta metanoletan egin da.

Erreakzio katalizatuetan nanopartikulen parte-hartzea probatzeko maiz erabiltzen den metodo bat CS_2-aren gehikuntza da; erreaktibo honek katalizatzailea desaktibatzen eta erreakzioa kolapsatzen baitu.[54] Katalisia hasi eta 20 segundora CS_2-a gehitu zitzaion disoluzioari, desazelerazio txiki bat eragin zuen (E.2 irudia). Kasu honetan, moteltze hori CS_2 molekula katalizatzailearen zentro metalikoara koordinatu daitekeelako gertatzen dela uste dugu.[59] Izan ere, CS_2-a AB substratuarekin lehian egon daiteke erreakzio homogeneoan.

Katalizatzailearen birziklagarritasuna aztertzeko **1** konplexuak katalizatutako ABren metanolisia sei aldiz segidan egin zen katalizatzaile kopurua berriztu gabe (2.3 irudia). Grafikak desintegrazio txiki bat erakusten badu ere, **1** konplexua gutxienez 4100 hidrogeno baliokide askatzeko katalizatzaile mol bakoitzeko gai da.
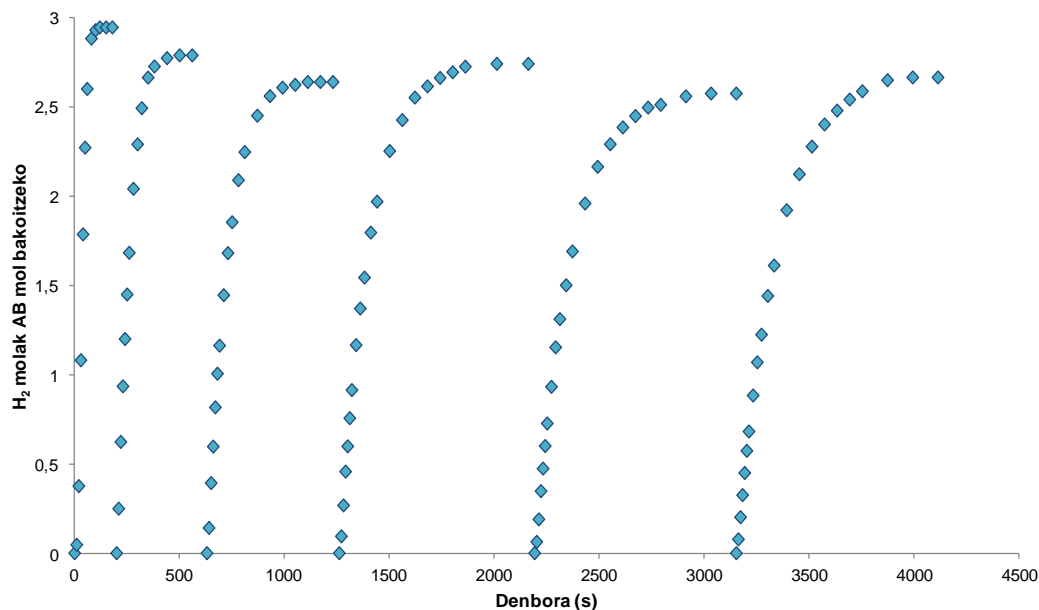
2.3 irudia. Sei AB-aren metanolisi erreakzio kontsekutibo hidrogenoa askatzen delarik. 1 konplexua katalizatzaile moduan erabili da, erreakzioa metanoletan eta 60 ºC-tan eman da. Erreakzio kontsekutiboetan AB 0.5 mL-ko metanol disoluzioak erabili dira.

Jarduera katalitikoak katalizatzailearen kontzentrazioarekiko duen mendekotasuna aztertu zen. Horretarako, AB-aren metanolisia AB 0.46 M-eko disoluzioekin eta katalizatzaile kontzentrazio desberdinekin –0.46·10^{-3} M (% 0.1) eta 1.86·10^{-3} M (% 0.4) arteko kontzentrazioekin– egin zen (2.4 irudia). **1** konplexuaren kontzentrazio baxuena erabiltzen denean (0.46·10^{-3} M) 3 hidrogeno baliokide askatzeko 360 s behar dira (6 min); 1.86·10^{-3} M-ko kontzentrazioa erabiltzen denean, aldiz, 150 s (2.5 min) baino ez dira behar 3 hidrogeno baliokide askatzeko.
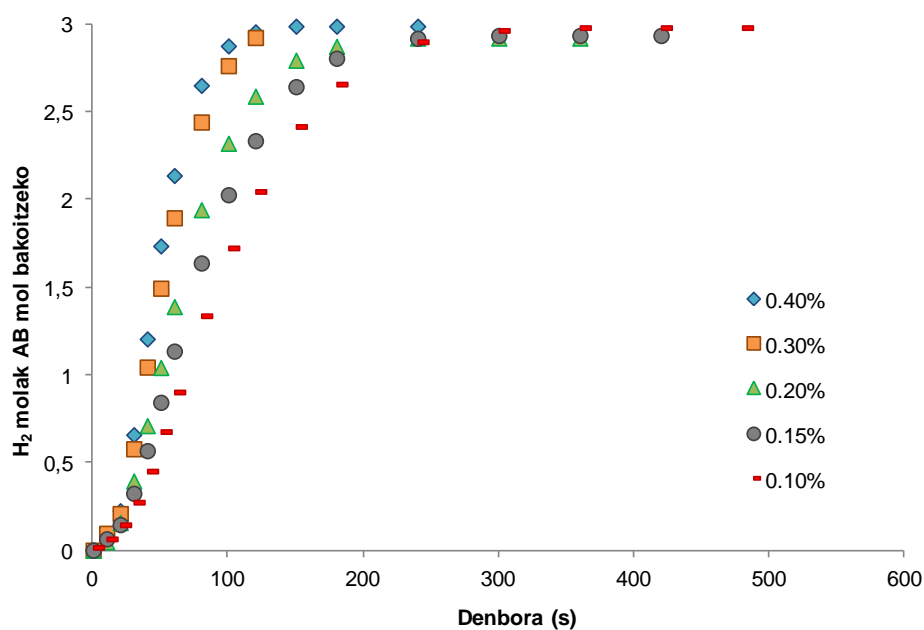
2.4 irudia. AB-aren metanolisitik askatutako hidrogenoa 1 konplexuaren karga desberdinekin:% 0.40 (◊, urdina), % 0.30 (□, laranja), % 0.20 (∆, berdea), % 0.15 (○, grisa) eta % 0.10 (-, gorria). Metanoletan eta 60ºC-tan egin da.

Erreakzio katalitiko horietan lortutako profil zinetikoa, substratuaren kontzentrazioari dagokionez, pseudo-lehen ordenako erreakzioen ereduarekin bat datorrela esan daiteke. Eredu hori abiadura-konstanteak (k_{ikus}) zehazteko aplikatu zen, ikus 2.5 irudia.
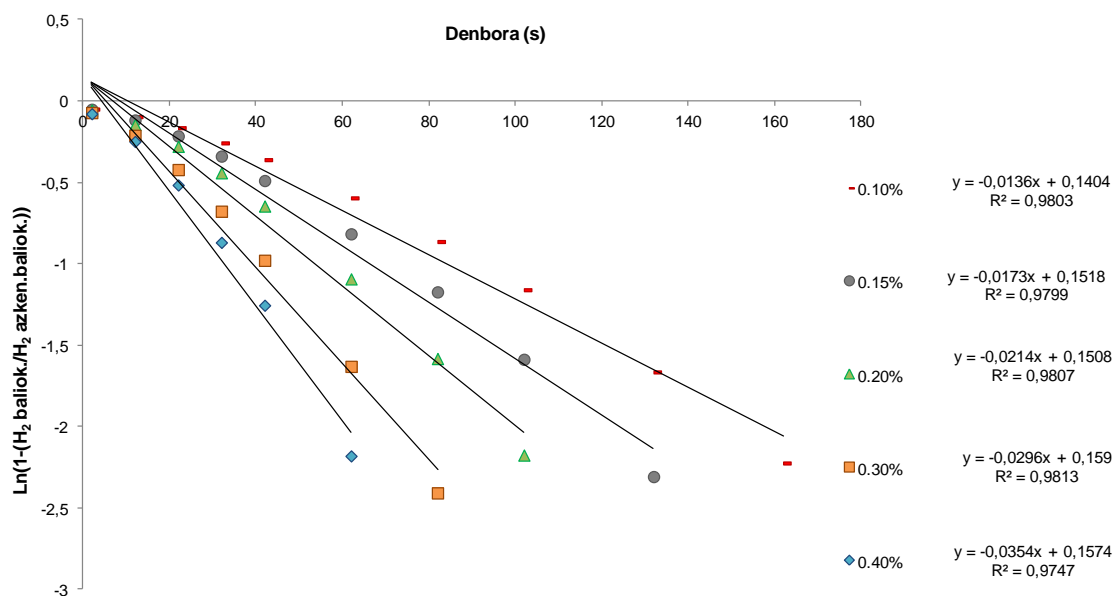
2.5 irudia. AB-aren metanolisitik askatutako hidrogeno kopuruaren lehen ordenako grafikak 1 konplexuaren [katalizatzaile]$_0$ desberdinak erabilita: % 40 ($\Diamond$, urdina), % 0.30 ($\Box$, laranja), % 0.20 ($\triangle$, berdea), % 0.15 ($\circ$, grisa) eta % 0.10 (-, gorria). Metanoletan eta 60ºC-tan eman da.

Aurreko irudian ikus daitekeenez, hidrogeno-askapenaren abiadura erabilitako katalizatzaile kontzentrazioaren araberakoa da. Hidrogenoaren askapen-abiadurak [katalizatzailea]$_0$-rekiko lehen ordenako mendekotasuna duela onartzen bada, abiadura legea honela adieraz daiteke:

$v_{esp} = k_{kat}$[katalizatzailea]$_0$[substratua], non $k_{ikus} = k_{kat}$[katalizatzailea]$_0$ den. 2.6 irudian, pseudo-lehen ordenako konstanteak marraztu dira, k_{ikus}-ak, *versus* hasierako katalizatzaile kontzentrazioak. Horrek metanolisi erreakzioa [katalizatzailea]$_0$-rekiko lehen mailako mendekotasuna duela berresten du, eta $k_{kat} = 16.0 \pm 0.6$ M^{-1}s^{-1}-en balioa zehazteko aukera ematen du. Datu esperimental zehatzetarako, ikus 2.1 taula.
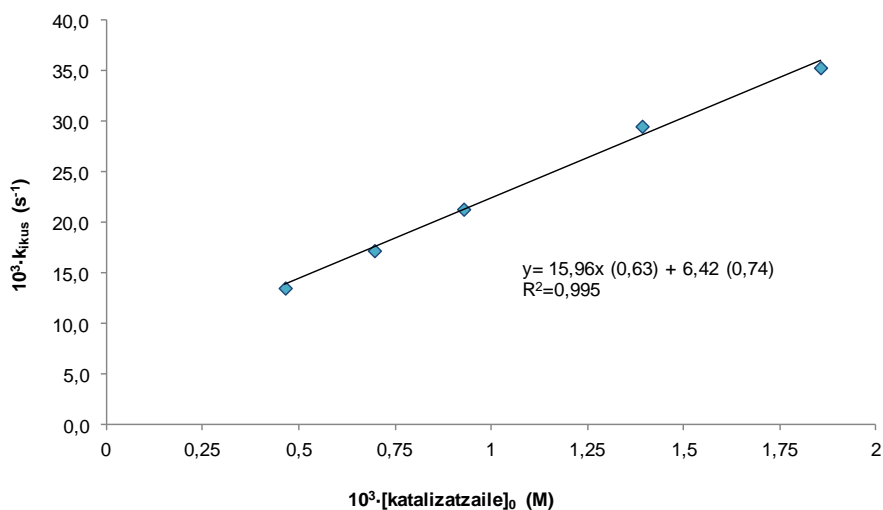
2.6 irudia. [katalizatzaile]$_0$-ren eragina AB-aren metanolisi erreakzioaren k_{ikus}-ean, **1** konplexua katalizatzaile gisa erabili da, metanoletan eta 60 °C-tan egin da. Desbiderapen estandarrak parantesi artean eman dira.

2.1 taula. Konbertsioaren %, beharrezko denbora, and konstanteen balioak AB-aren metanolisian **1** konplexuaren kontzentrazio ezberdinak erabilita, 60 °C-tan.

Katalizatzaile %	Konbertsioa %	Denbora (s)	$10^3 \cdot k_{ikus}$ (s^{-1})
0.10	99	360	13.6 ± 0.7
0.15	98	300	17.3 ± 0.9
0.20	97	240	21.4 ± 1.2
0.30	100	180	29.6 ± 1.8
0.40	100	150	35.4 ± 2.8

Bestalde, **1** konplexuak katalizatutako metanolisi erreakziorako beste amina-borano batzuk ere probatu ziren, hain zuzen ere, dimetilamina-boranoa

(DMAB), tert-butilamina-boranoa (TBAB) eta trietilamina-boranoa (TEAB). Proba guztiak metanoletan eta 60 ºC-tan egin ziren (2.7 irudia). Baldintza horietan, DMAB-aren kasuan 2.8 hidrogeno baliokide askatu ziren 100 s-tan eta aurretik ikusitako AB-ren antzeko profila ematen du. TBAB-a erabiltzen denean, berriz, 2.6 hidrogeno baliokide baino ez dira askatzen 180 s ondoren. Gutxiagotze hau TBAB-ak duen talde alkilikoak sortutako eragozpen esterikoen ondorio izan liteke, aurreko bi substratuek baino ordezkatzaile handiagoa baitu. TEAB-ak, aldiz, portaera desberdina erakutsi du eta litekeena da amina taldean protoirik ez edukitzearen ondorio izatea. **1** konplexuak katalizatutako amino-boranoen hidrolisian gertatzen zen bezala, TEAB-a erabilitzerakoan ez zen hidrogeno askapenik hantzeman.[43]
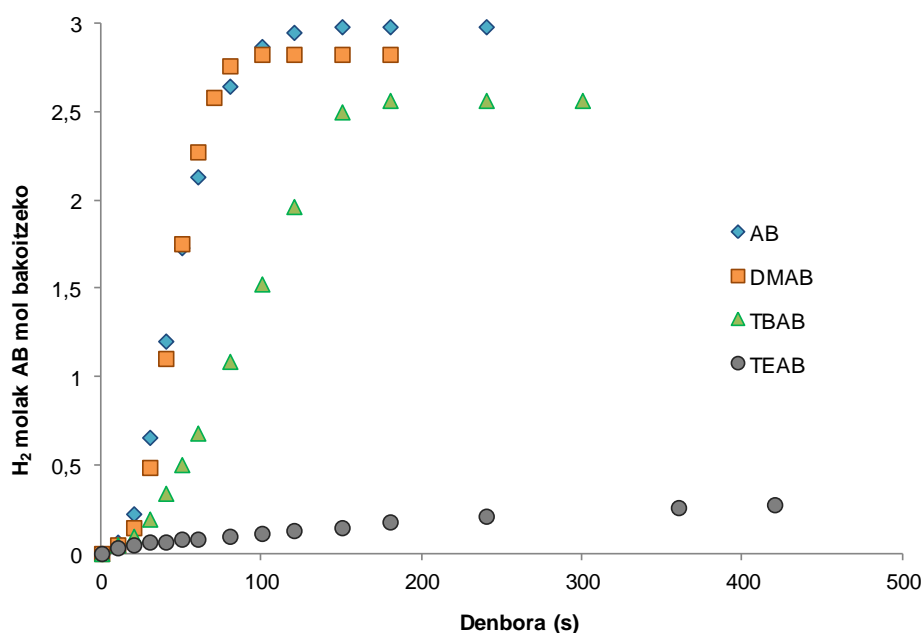
2.7 irudia. Hidrogeno askapena 1 konplexuak katalizatuta amina-borano desberdinen metanolisitik: AB (◊, urdina), DMAB (□, laranja), TBAB (∆, berdea), TEAB (○, gisa) Metanoletan, 60 ºC-tan eta 0.46 M-eko amina-borano disoluzioetan eman da.

Azkenik, katalizatzailea beste alkoholetan probatu zen erreakzioaren bidegarritasuna aztertzeko (2.8 irudia). Honetarako, **1** konplexuak katalizatutako AB-aren alkoholisia metanoletan, etanoletan eta isopropanoletan alderatu zen.

Alkoholisi erreakzioa etanolarekin edo isopropanolarekin egin zenean ez ziren metanolarekin bezain emaitza onak eskuratu. Halere, erreakzioa etanoletan egin zenean 10 minutu igaro ostean 3 hidrogeno baliokide askatu ziren eta isopropanoletan, berriz, 2.6 baliokide. Emaitza horiek AB-aren alkoholisia zenbait alkoholetan, eta ez soilik metanoletan, egin daitekela frogatzen dute.
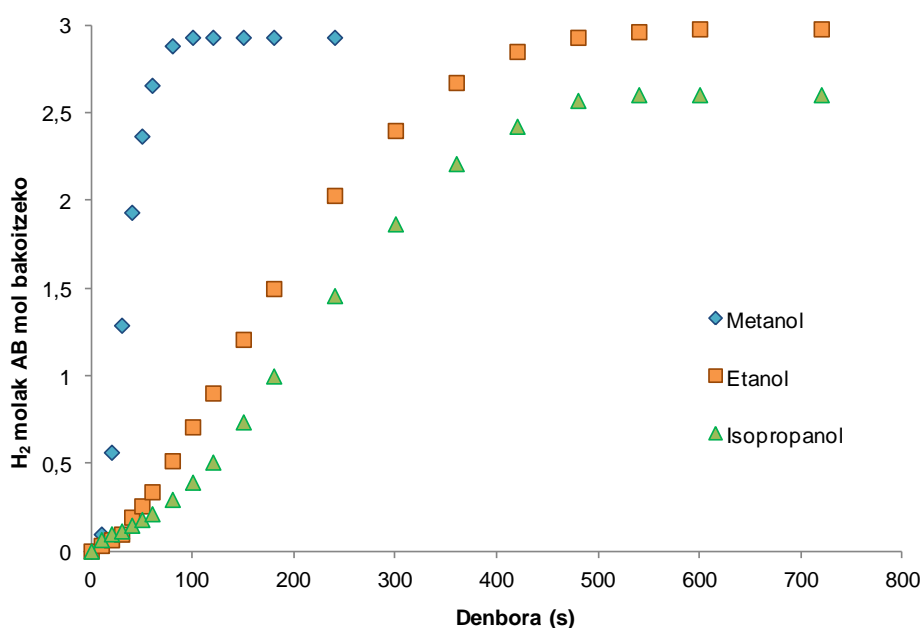
2.8 irudia. Hidrogeno-askapena AB-aren alkoholisitik 1 konplexua katalizatzaile gisa erabilita disolbatzaile desberdinetan: MeOH (◊, urdina), EtOH (□, laranja) eta ⁱPrOH (△, berdea). 60 ºC-tan egin da.

2.3 (7), [(IrH{(PPh$_2$(*o*-C$_6$H$_4$CO))$_2$H})$_2$(μ-Cl)]BF$_4$ dimero ionikoaren aktibitate katalitikoa.

2.1 azpikapituluan aipatu den bezala, hidrogeno askapenaren hasiera aurretik indukzio denbora agertzearen arrazoia **1** konplexuaren disolbagarritasun txikia metanoletan izan daiteke. Indukzio prozesua ekiditzeko metanoletan disolbagarriagoa den hidruroirida-β-dizetona dimero ionikoa hautatu zen [(IrH{(PPh$_2$(*o*-C$_6$H$_4$CO))$_2$H})$_2$(μ-Cl)]BF$_4$ **(7)** (2.9 irudia). **7** konplexuak bi hidruroirida-β-dizetona zati ditu, klorurozko zubi baten bidez lotuta daudenak, eta **1** konplexua baino disolbagarriagoa da metanolean.
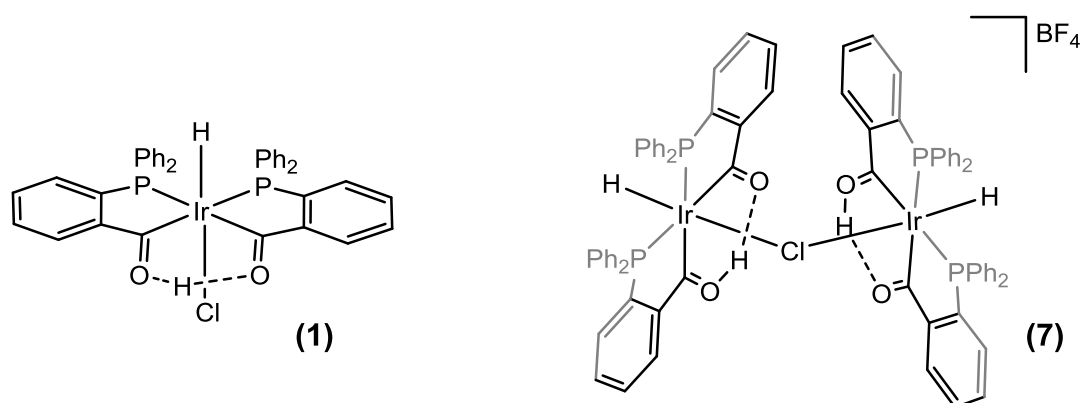
2.9 irudia. 1 eta 7 konplexuak

7 konplexua katalizatzaile moduan erabili zen AB-aren metanolisian hidrogenoren askapenarako. Metanoletan, 30 ºC-tan, AB-aren 0.46 M-eko hasierako kontzentrazioa eta **7** konplexuko % 0.2-ko karga (iridio % 0.4 karga dena) erabiltzen denean, 2.8 hidrogeno baliokide askatzen dira 6 minutu igaro ondoren. Baldintza horietan konbertsioa % 50-a zenean TOF-aren balioa 321 mol$_{H_2}$·mol$_{Ir}^{-1}$·min^{-1}-ekoa zela kalkulatu zen. Indukzio-denborari dagokionez 40 s-koa zela ikus zitekeen oraindik eta **1** konplexuarekin alderatuta laburragoa zen (2.10 irudia). Erreakzioa 60 °C-tan egiten denean, aurretik aipatutako baldintzetan, 3 hidrogeno baliokide askatzen dira 80 s pasa ondoren. Kasu honetarako konbertsioaren % 50-a zenean TOF-a kalkulatu zen eta 1991 mol$_{H_2}$·mol$_{Ir}^{-1}$·min^{-1}-eko balio bikaina lortu zen. Katalisia **7** konplexuarekin 60 ºC-tan egiten denean ez zen indukzio-denborarik ikusi (2.11 irudia).
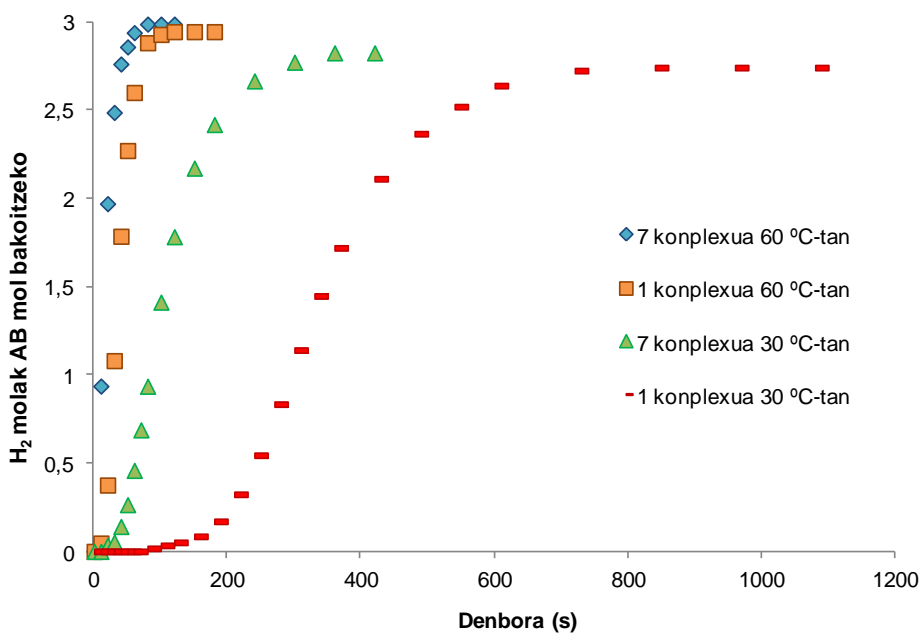
2.10 irudia. AB-aren metanolisitik askatutako hidrogenoa 1 eta 7 konplexuak katalizatzaile moduan erabilita tenperatura desberdinetan: 7, 60 ºC-tan (◊, urdina); 1, 60 ºC-tan (□, laranja); 7, 30 ºC-tan (Δ, berdea) eta 1, 30 ºC-tan (-, gorria). Metanoletan.
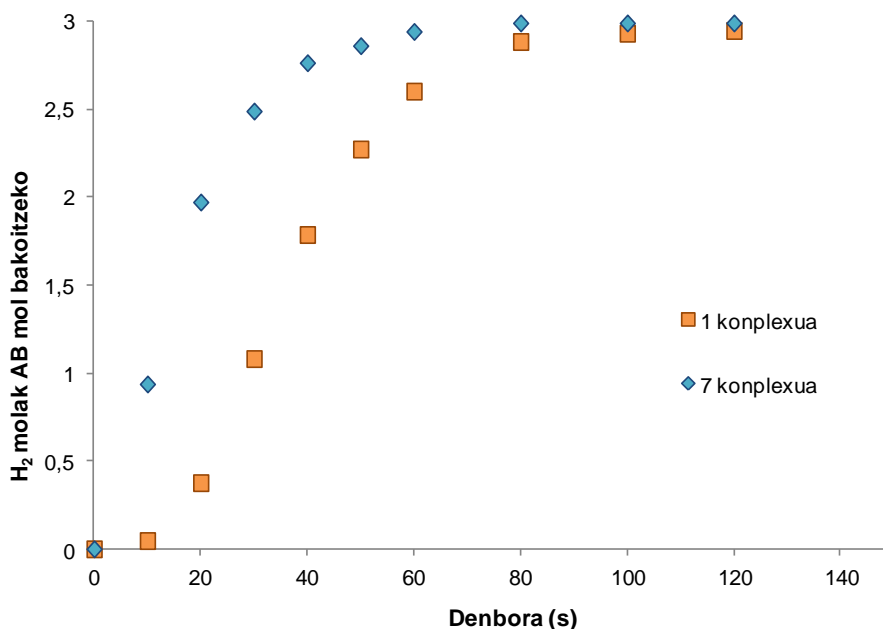
2.11 irudia. AB-aren metanolisitik askatutako hidrogenoa 7 (◊, urdina) eta 1 (□, laranja) konplexuak katalizatzaile gisa erabilita. Metanoletan eta 60 ºC-tan egin da.

Erreakzio katalitikoaren homogeneotasuna frogatzeko Hg-a soberan gehitu zen. 2.12 irudian ikus daitekeenez, Hg-arekin eta Hg-rik gabeko irudikapenak ia berdinak dira; gainera, disoluzioak hori argiak izaten jarraitu zuten, ilundu gabe, eta ez zen material disolbaezinik agertu.

CS_2 metodoa **7** konplexuarentzat ere aplikatu zen. Hg-arekin egin zen moduan CS_2-a erreakzioa hasi ostean 20 s-ra gehitu zen eta kasu honetan desazelerazio bat ikus daiteke (E.3 irudia). Aztertutako moteltzea CS_2-a zentro metalikoari koordinazioagatik gerta daiteke.
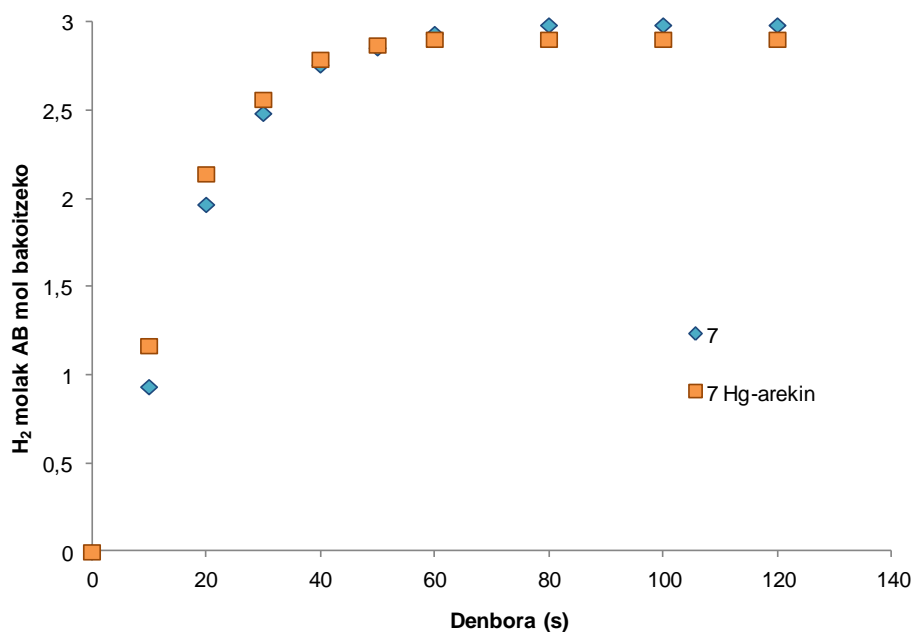
2.12 irudia. AB-aren metanolisitik askatutako hidrogenoa 7 konplexua katalizatzaile moduan erabilita, Hg-rik gabe (◊, urdina) eta Hg-arekin (□, laranja). 60 ºC-tan eta metanoletan egin dira.

7 konplexuaren aktibitatea ondoz-ondoko sei metanolisi katalitiko eginez (2.13 irudia) eta hasierako erreakzioari AB-a 0.5 mL metanoletan gehituz aztertu zen. **7** konplexuak, nahiz eta denbora aurrera egin, aktibo izaten jarraitzen du eta gutxienez konplexu mol bakoitzeko 8300 hidrogeno-baliokide askatzeko gai da, zehazki, 4150 baliokide Ir moleko. Horretaz gain, **7**

konplexuak 1600 s baino ez ditu behar AB-aren ondoz-ondoko sei metanolisi katalitiko egiteko; **1** konplexuak, berriz, ia 4.000 s behar ditu helburu bera lortzeko.
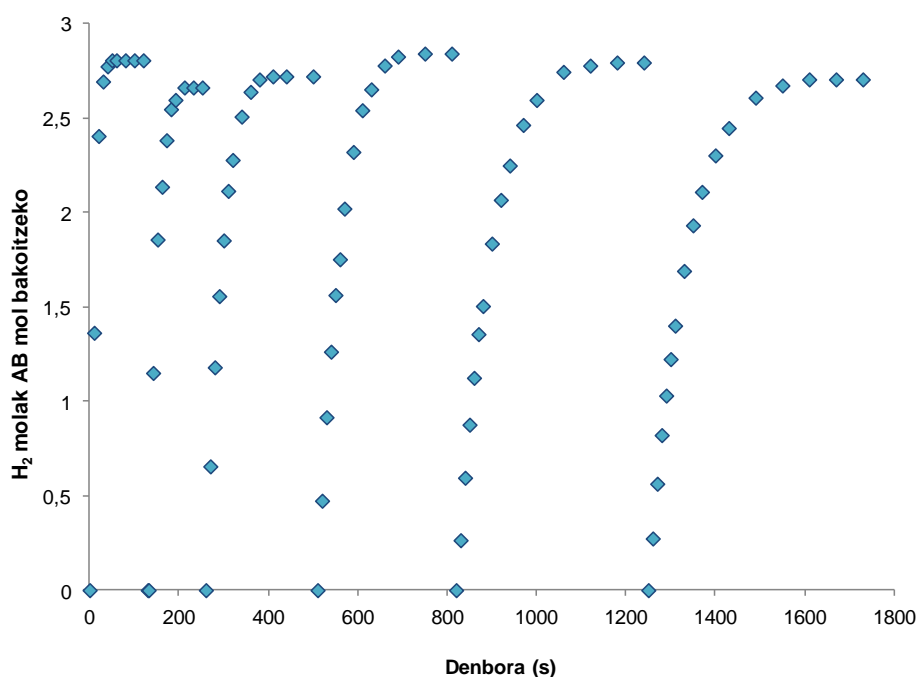
2.13 irudia. Hidrogenoa askatzen den sei AB-aren ondoz-ondoko metanolisi erreakzio. 7 konplexua katalizatzaile moduan erabili da, erreakzioa metanoletan eta 60 ºC-tan egin da. Erreakzio kontsekutiboetan AB 0.5 mL-ko metanol disoluzioak erabili dira.

7 konplexuaren azterketa zinetikoa egiteko, AB-aren metanolisia $[Ir]_0$ $0,46 \cdot 10^{-3}$ M (% 0.1-eko karga) eta $1,86 \cdot 10^{-3}$ M (% 0.4-eko karga) bitarteko kontzentrazioetan egin zen (ikus 2.14 irudia). Oraingoan dimero bat erabili denez –eta lortzen diren emaitzak **1** konplexuko emaitzekin konparatu nahi direnez–, mol kopuruaren erdia baino ez da erabili behar, bi kasuetan iridio kopurua berdina izan dadin.

$[Ir]_0$ kontzentrazio baxuena erabiltzen denean, $0.46 \cdot 10^{-3}$ M, 2.9 hidrogeno baliokide askatzen dira 240 s-tan (4 min). Aldiz, kontzentrazio altuena erabiltzen denean ($1.86 \cdot 10^{-3}$ M), 80 s besterik ez dira behar 3 hidrogeno baliokide askatzeko.
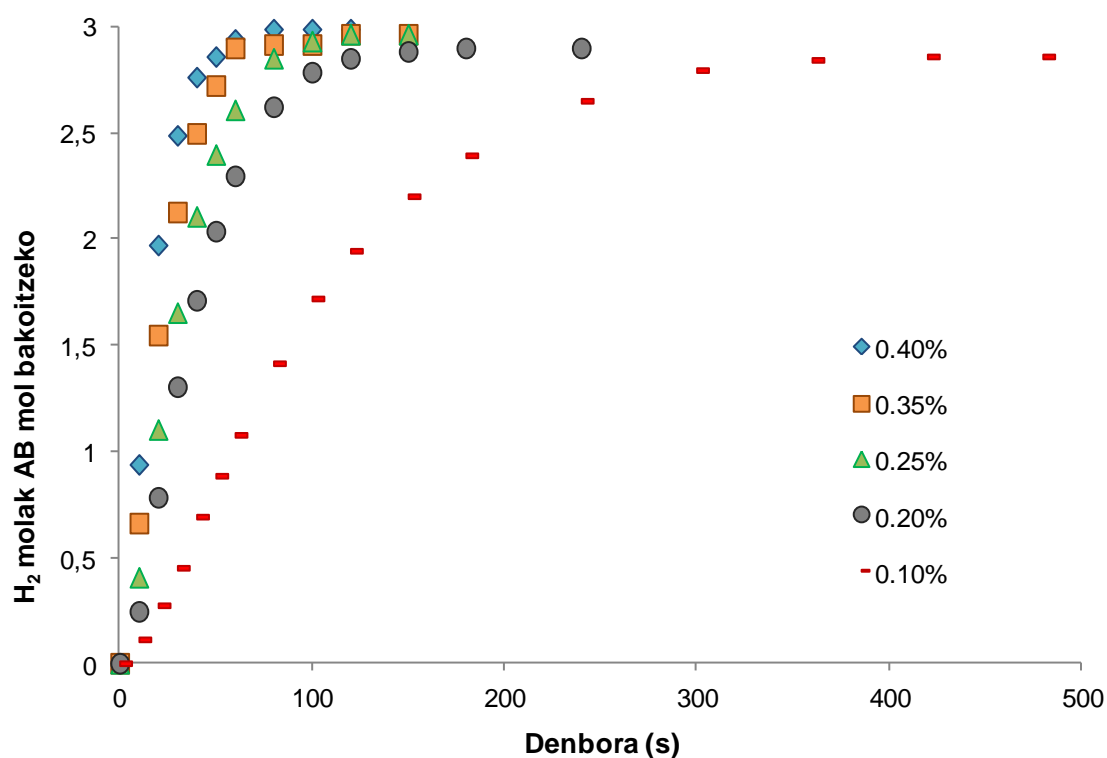
2.14 irudia. AB-aren metanolisitik askatutako hidrogenoa 7 konplexua eta zenbait [Ir]$_0$ karga erabiliz:% 0.40 (◊, urdina), % 0.30 (□, laranja), % 0.20 (△, berdea), % 0.15 (○, grisa) eta % 0.10 (-, gorria). Metanoletan eta 60ºC-tan egin da.

7 konplexuak, zenbait iridio kontzentrazioekin, katalizatutako AB-aren metanolisi guztiak [substratu]-arekiko pseudo-lehen ordenako profil zinetikoaren eredu direla esan daiteke. Aipatutako eredua abiadura konstanteak (*k$_{ikus}$*-ak) kalkulatzeko aplikatu da, horretarako denbora *versus* Ln(1-(H$_2$ baliok./H$_2$ azken.baliok.)) grafikatuz (2.15 irudia).
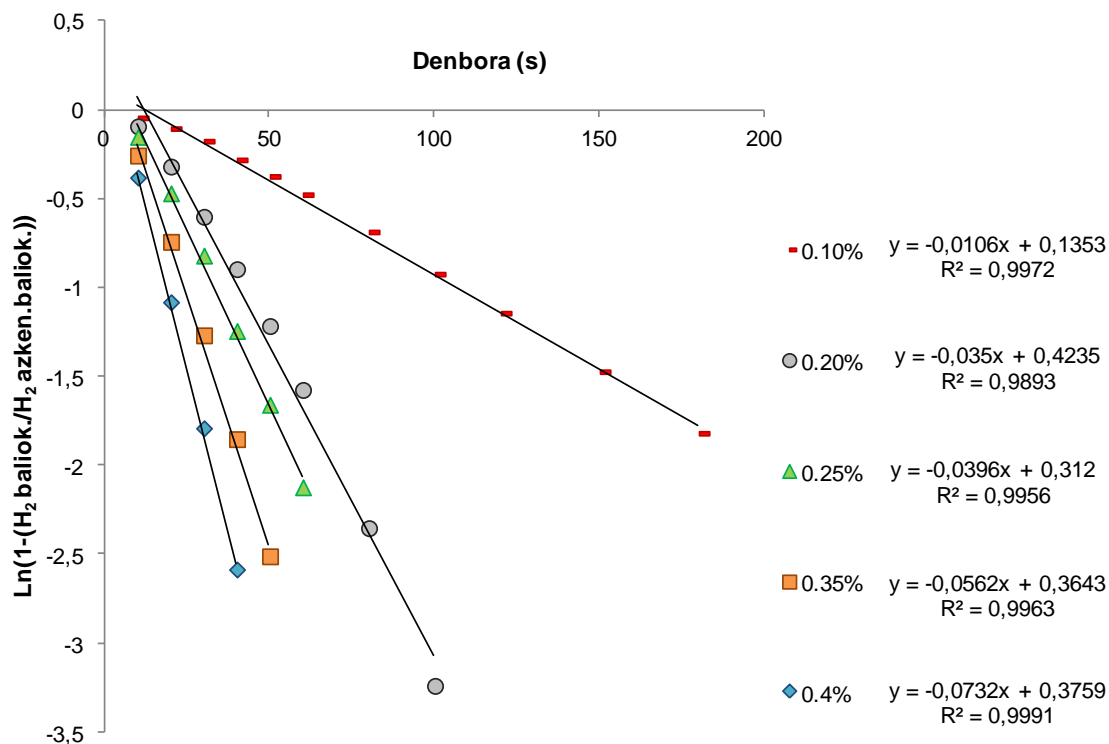
2.15 irudia. AB-aren metanolisiatik askatutako hidrogeno kopuruaren lehen ordenako grafikak 7 konplexua eta zenbait [Ir]$_0$ karga erabiliz:% 0.40 (◊, urdina), % 0.30 (□, laranja), % 0.20 (△, berdea), % 0.15 (○, grisa) eta % 0.10 (-, gorria). Metanoletan eta 60ºC-tan egin da.

1 konplexuarekin gertatzen den moduan, erreakzio-abiadura [katalizatzailea]$_0$-rekiko lehen ordenako mendekotasuna duela onartzen badugu, k_{kat}·[katalizatzailea]$_0$ = k_{ikus} legea aplika dezakegu. Hori kontuan hartuta, lortutako k_{ikus} balioak (balio zehatzetarako, ikus 2.2 taula) katalizatzaile kontzentrazioekiko irudikatu ziren (2.16 irudia). Irudikatutako grafikak gure hipotesia berretsi zuen, k_{kat} = 42.0 ± 0.6 M^{-1}s^{-1}-ko balioa lortu baitzen.
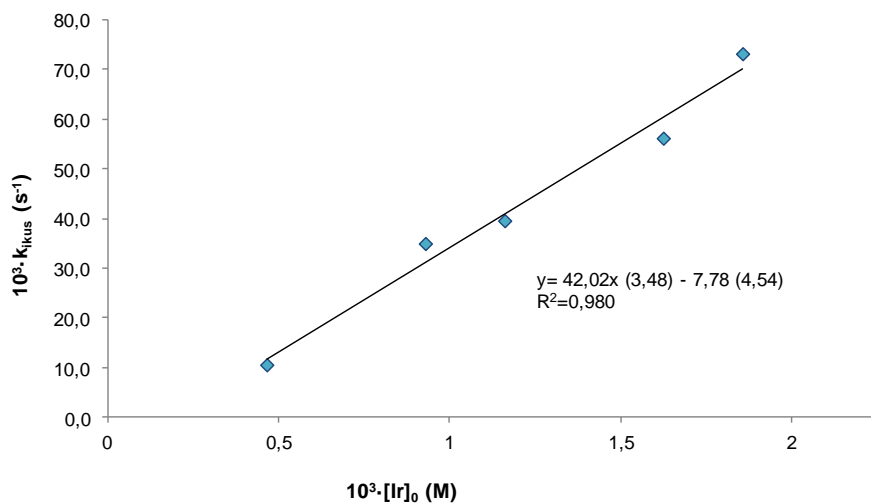
2.16 irudia. $[Ir]_0$-ren eragina AB-aren metanolisi erreakzioaren k_{ikus}-ean: 7 konplexua katalizatzaile gisa erabili da, metanoletan eta 60 ºC-tan egin da. Desbiderapen estandarrak parantesi artean jarri dira.

2.2 taula. Konbertsioaren %, beharrezko denbora, eta konstanteen balioak AB-aren metanolisian 7 konplexuatik $[Ir]_0$ ezberdinak erabilita, 60 ºC-tan.

Iridio %	Konbertsioa %	Denbora (s)	$10^3 \cdot k_{ikus}$ (s^{-1})
0.10	95	420	10.6 ± 0.2
0.20	97	180	35.0 ± 1.5
0.25	99	120	39.6 ± 1.3
0.35	99	120	56.2 ± 2.0
0.40	100	80	73.2 ± 1.6

AB-arekin batera, dimetilamina-boranoa (DMAB), *tert*-butilamina-boranoa (TBAB) eta trietilamina-boranoa (TEAB) erabili ziren metanolisi erreakzioaren bidez hidrogenoa askatzeko, **7** konplexuak katalizatuta. DMAB da AB-aren ondoren azkarrena, baina indukzio denbora erakusten du; DMAB-arekin, 2.9

hidrogeno baliokide askatzen dira 80 s igaro ondoren. Substratua TBAB-a denean 2.6 hidrogeno baliokide askatzen dira 240 s pasa (4 minutu). Azkenik, substratua TEAB-a denean, hidrogeno-askapena ez da gertatzen (2.17 irudia).
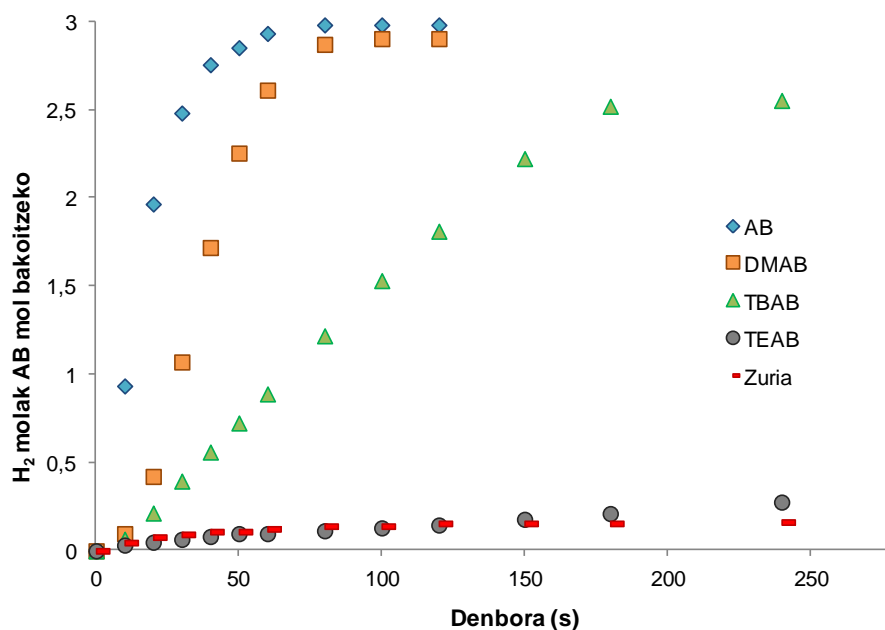
2.17 irudia. Hidrogeno-askapena 7 konplexuak katalizatutako zenbait amina-boranoen metanolisitik: AB (◊, urdina), DMAB (□, laranja), TBAB (△, berdea), TEAB (○, grisa) Metanoletan, 60 ºC-tan eta 0.46 M-eko amina-borano disoluzioetan egin da.

2.3 taula. Substratua, Konbertsio %, Beharrezko denbora, Indukzio denbora eta TOF-a % 50-an AB-aren metanolisian 7 konplexuak katalizatuta, metanoletan eta 60 ºC-tan.

Substratua	Konbertsioa %	Denbora (s)	Indukzio denbora (s)	$TOF_{\% 50}$ $(mol_{H_2} \cdot mol_{Ir}^{-1} \cdot min^{-1})$
AB	100	80	-	1991
DMAB	97	100	10	848
TBAB	85	240	15	271

2.3.1 Deuterazio saiakerak

AB-aren metanolisi erreakzio katalizatuei buruzko informazio gehiago lortzeko, deuterazio saiakerak azterketak egin dira. Metanolisia deuteratutako amoniako-boranoarekin (H_3NBD_3) egin zen eta lortutako aktibitatea AB arrunta erabili zenean lortutako aktibitatearekin alderatu zen. Bi probak **7** konplexua katalizatzaile gisa erabiliz, metanoletan eta 60 ºC-tan egin ziren. H_3NBD_3-rentzat neurtutako konstantea eta H_3NBH_3-rentzat neurtutakoa ia berdinak dira (2.18 irudia); eta 1 inguruko KIE ($k_{H_3NBH_3/H_3NBD_3}$) balorea lortu zen. Honek esan nahi du B-H lotura apurtzea ez dagoela urrats mugatzailearen barruan.
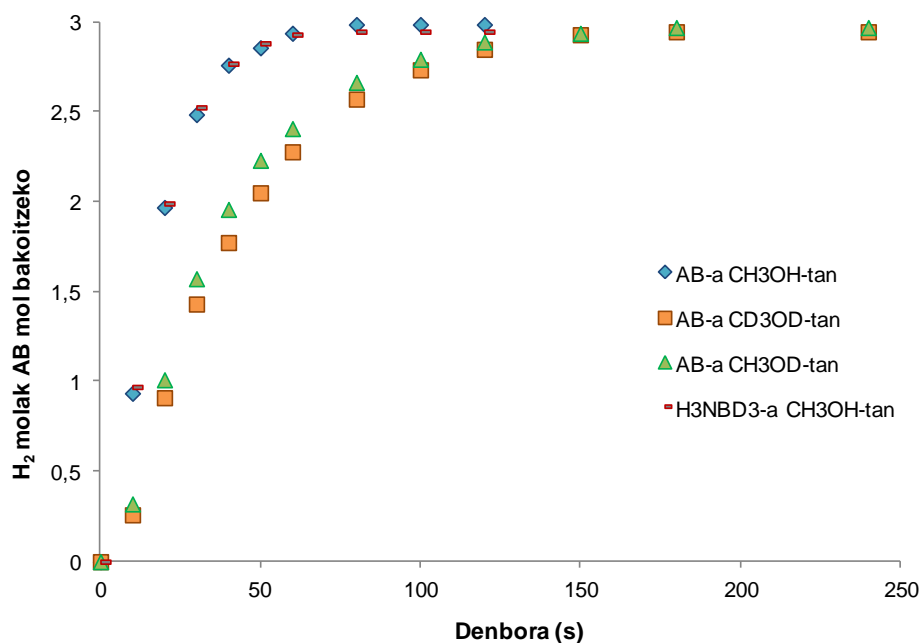
2.18 irudia. Hidrogeno-askapena 0.46 M H_3NBH_3 (◊, urdina) edo H_3NBD_3 (-, gorria) disoluzioetatik % 0.4 mol $[Ir]_0$ 7 konplexu katalizatzaileatik eta metanoletan. Hidrogeno-askapena 0.46 M H_3NBH_3 disoluzioetatik % 0.4 mol $[Ir]_0$ 7 konplexu katalizatzaileatik CD_3OD-tan (□, laranja) edo CH_3OD-tan (△, berdea), 60 ºC-tan.

Bestalde, **7** konplexuak katalizatutako AB-aren metanolisia disolbatzaile deuteratuetan egin zen: CD_3OD-tan eta CH_3OD-tan. Bi disolbatzaile deuteratuekin neurtutako hidrogeno-askapena CH_3OH-a erabiltzen denean baino motelagoa izan zen; k_{ikus} balioetarako ikusi 2.4 taula. Disolbatzaile

deuteratuetarako KIE baloreak kalkulau ziren eta 2.60 ± 0.08 (k_{CH_3OH/CD_3OD}) eta 2.44 ± 0.09 (k_{CH_3OH/CH_3OD})-koak izan ziren. Balio horiek kontuan hartuta, AB-ren metanolisi katalizatuaren urrats erabakigarrian metanolaren O-H loturaren apurtzea sartzen dela proposa daiteke.

2.4 taula. Konbertsio %, Beharrezko denbora eta Ikusitako konstanteak AB eta AB deuteratuaren metanolisian. 7 konplexuak katalizatuta, metanol eta metanol deuteratuetan eta 60 ºC-tan.

Disolbatzailea	Substratua	Konbertsioa %	Denbora (s)	$10^3 \cdot k_{ikus}$ (s^{-1})
CH_3OH	H_3NBH_3	100	80	73.2 ± 1.6
CH_3OH	H_3NBD_3	98	80	80.4 ± 2.1
CD_3OD	H_3NBH_3	98	180	28.2 ± 0.2
CH_3OD	H_3NBH_3	99	180	30.0 ± 0.5

2.4 Bitartekarien bilaketa *in situ* EMN multinuklearraren bidez

EMN multinuklearra tresna baliagarria da erreakzio katalitikoen nondik norakoak aztertzeko. Gainera, kasu honetan, erreakzioak CD_3OD-tan egiten direnean motelagoak dira eta hau probetxuzkoa izan zen informazio baliotsua lortzeko.

Egindako lehenengo esperimentuak *in situ* ^1H, ^{11}B eta $^{31}P\{^1H\}$ EMN-ak izan ziren **7** konplexuak katalizatutako AB-aren metanolisiari CD_3OD-tan. Erreakzioa azkarregia izan zen; izan ere, erreakzioan sortutako produktuak bakarrik ikusi ziren.

^{1}H EMN-an (2.19 irudia), borano taldearen hidruroen eta CD_3OD-aren protoien konbinazioatik sortutako hidrogenoa askatzearen ondoriozko HD-a 4.55 ppm-tan (t, $J_{D,H}$ = 42.6 Hz) ikus daiteke. 4.59 ppm-tan singlete bat ikus daiteke, H_2-ri dagokiona, disolbatzaile guztiz deuteratuta ez dagoelako. Ez dago AB-aren seinaleen arrastorik 1.45 ppm-an (q, $J_{B,H}$ = 90.4 Hz), eta horrek substratu guztia erreakzionatu duela adierazten du.
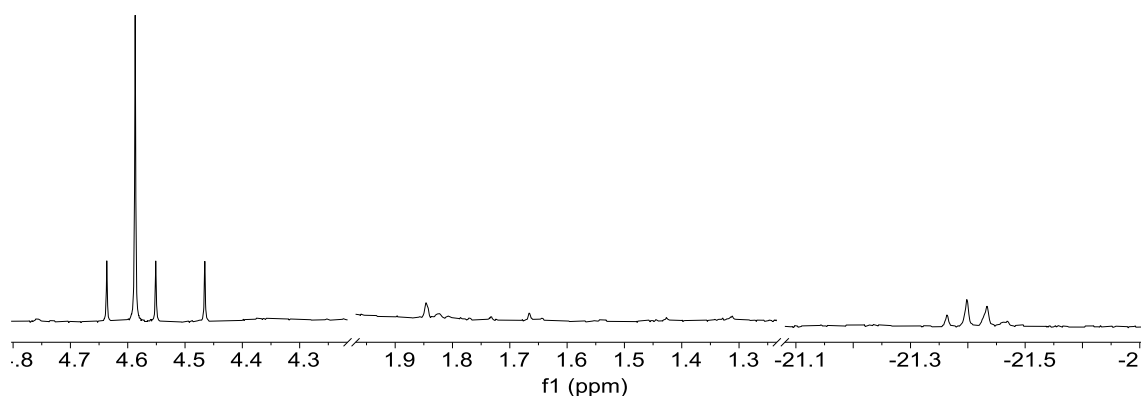
2.19 irudia. 7 konplexuak katalizatutako AB-aren metanolisiaren *in situ*-aren ^{1}H EMN espektroa. CD_3OD-tan eta 25 ºC-tan egin da.

Gainezarritako bi hirukote -21.40 ppm-tan (t, $J_{P,H}$ = 17.4 Hz) eta -21.43 ppm-tan (t, $J_{P,H}$ = 17.4 Hz) eremu altuan agertzen dira ^{1}H EMN-an. Seinale horiek, ^{31}P{^{1}H} EMN-an, 2.20 irudian, 19.3 ppm-tan ikusten den seinalearekin batera, bi iridio espezie berriei dagozkie. Espezie horiek hidruro bat edukiko lukete bi fosforo atomo baliokideekiko *cis* posizioan.
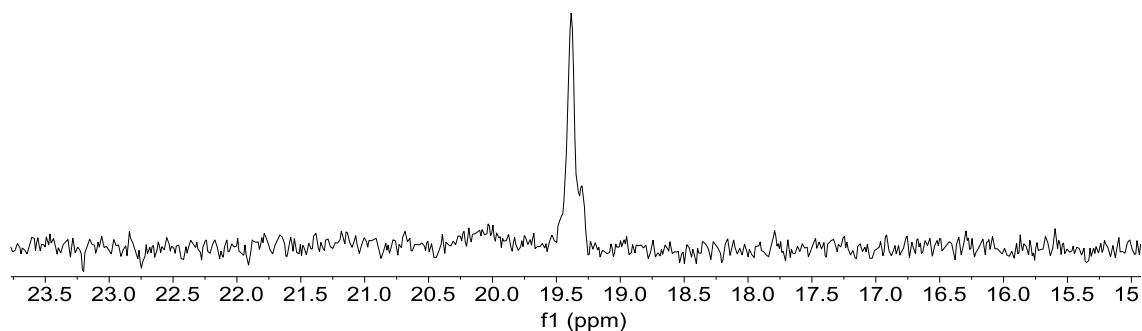
2.20 irudia. 7 konplexuak katalizatutako AB-aren metanolisiaren *in situ*-aren ^{31}P{^{1}H} EMN espektroa. CD$_3$OD-tan eta 25 ºC-tan egin da.

^{1}H EMN-ak bezala, ^{11}B EMN espektroak (2.21 irudia) ez du AB-ari dagokion seinalerik erakusten (23.5 ppm-ko quadruplet bat). Horren ordez, 9.3 ppm-tan singlete bat ikus daiteke. Singlete hori AB-aren metanolisian sortzen den produktuarena da, amonio tetrametoxiboratoarena (NH$_4$[B(OCH$_3$)$_4$]$^-$).[53] Honek ere esan nahi du AB guztiakk erreakzionatu duela. ^{11}B EMN delakoan agertzen den singlete txikia, -1.1 ppm-tan, **7** konplexuko kontraioiarena da, [BF$_4$]$^-$ anioiarena.
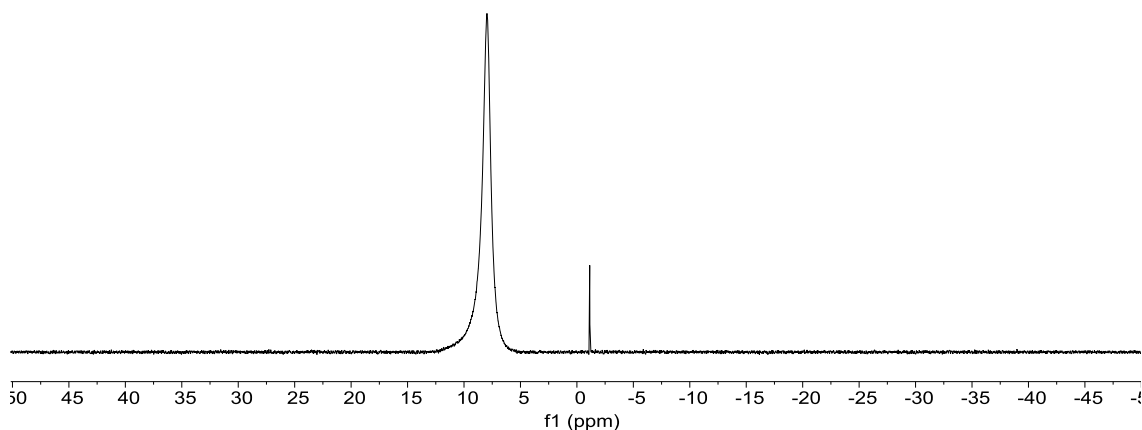
2.21 irudia. 7 konplexuak katalizatutako AB-aren metanolisiaren *in situ*-aren ^{11}B EMN espektroa. CD$_3$OD-tan eta 25 ºC-tan egin da.

Mekanismoaren inguruan informazio gehiago lortzeko, **1** konplexuak katalizatutako AB-aren metanolisiaren *in situ*-a EMN multinuklearraren bidez aztertu zen. **1** konplexuak katalizatutako erreakzioa **7** konplexuak katalizatutakoa baino motelagoa denez, **1** konplexua katalizatzaile gisa erabiltzen denean katalisian parte ahrtzen duten bitartekariak ikus daitezke.

Lehenengo [11]B EMN espektroak (2.22 irudia) AB substratuaren seinalea erakusten du -23.5 ppm-tan (q, $J_{H,B}$ = 93 Hz), AB borano guztia oraindik erreakzionatu ez duelako. Espektroan beste seinale handi bat ikus daiteke, singlete bat 9.3 ppm-tan, erreakzio-produktuari (tetrametoxiboratoari, $[B(OCH_3)_4]^-$) dagokiona. Intentsitate baxuagoko beste bi seinale ikus daitezke: hirukote bat -13.9 ppm-tan ($J_{H,B}$ = 100 Hz) eta bikote bat 5.9 ppm-tan ($J_{H,B}$ = 120 Hz). Seinale horiek amina-metoxiborano, $H_3NBH_2(OCH_3)$ eta amina-dimetoxiborano, $H_3NBH(OCH_3)_2$ aduktuei esleitu dakizkieke hurrenez hurren.[60]
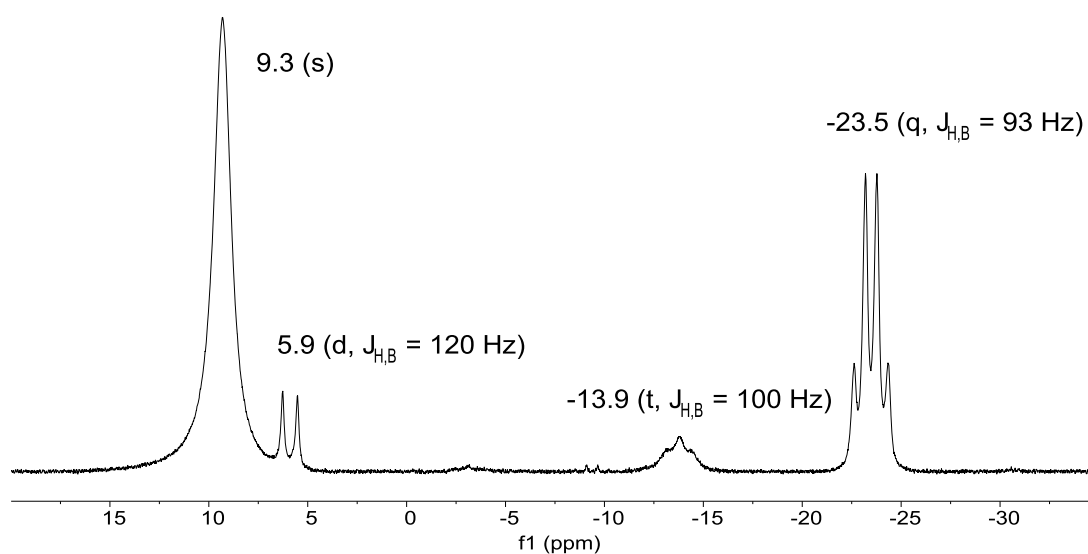
2.22 irudia. AB (0.65 mmol) / 1 konplexua (0.006 mmol) erlazioaren [11]B espektroa CD$_3$OD-tan AB-aren metanolisi katalizatua hasten den momentuan.

AB-aren desagerpena eta tetrametoxiborato produktuaren sorkuntza [11]B EMN-aren bidez jarrai daiteke katalisian zehar (2.23 irudia). Borano-aduktu bitartekarien seinaleak katalisia gertatzen ari denean ikus daitezke eta

substratuarekin batera desagertzen dira. Substratu gehiago gehitzen denean aipatutako bitartekariak berriz agertzen dira.
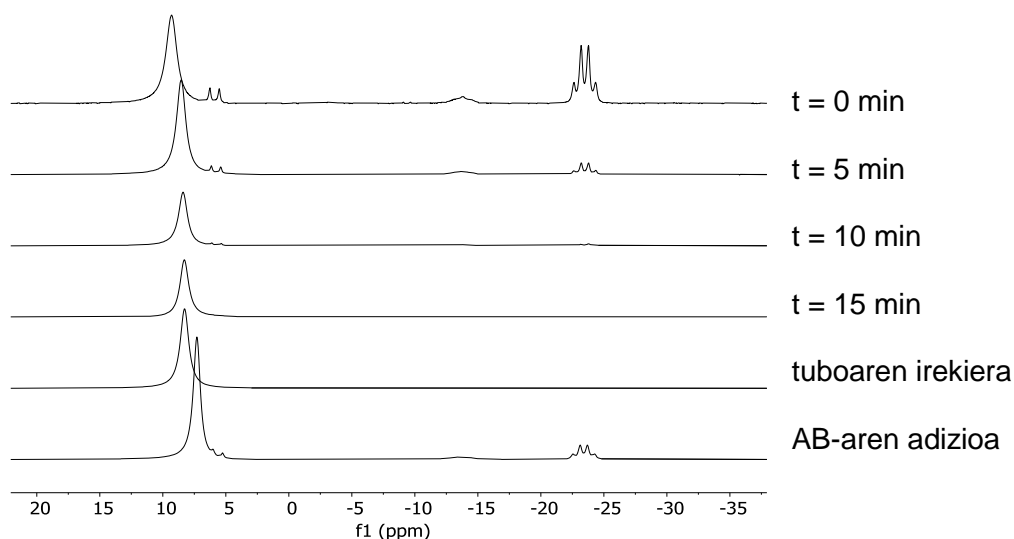
2.23 irudia. 1 konplexuak katalizatutako AB-aren metanolisiaren jarraipena ^{11}B EMN-aren bidez. CD$_3$OD-tan eta 25 ºC-tan egin da. Honetan borano aduktuen desagerpena, tetrametoxiboratoaren formazioa eta borano aduktuen agerpena AB-aren gehikuntzarekin ikusten da.

Substratuaren desagerpena ^{1}H EMN-aren bidez ere jarrai daiteke (2.24 irudia, ezkerraldea); 1.45 ppm-tan agertzen den laukoteak intentsitatea galtzen du AB-a desagertzen denean, eta intentsoago bihurtzen da substratua berriz gehituta. HD-ren agerpena 4.55 ppm-tan ikus daiteke, $J_{D,H}$ = 43 Hz akoplamendu-konstantea duen hirukote moduan.
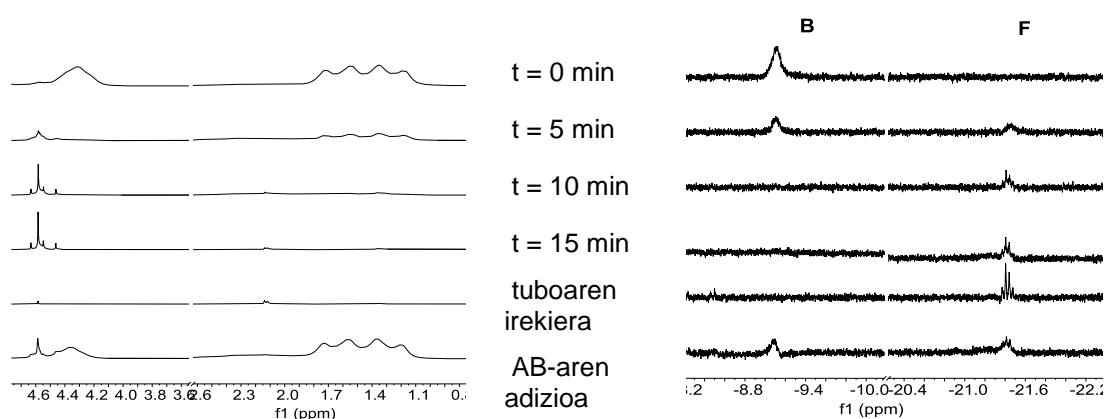
2.24 irudia. 1 konplexuak katalizatutako AB-aren metanolisiaren jarraipena ^{1}H EMN-aren bidez. CD$_3$OD-tan eta 25 ºC-tan egin da. Ezkerraldean AB-aren desagerpena eta H$_2$eta HD-aren askapena ikus daiteke. Eskuinaldean irido espezie berrien formazioa kus daiteke.

Hidruro bat duten iridio-espezie berrien osaketa ^{1}H EMN espektroan eremu altuan (2.24 irudia, eskuinaldean) eta ^{31}P{^{1}H} EMN espektroan (2.25 irudia) ikus daiteke. Katalisiaren lehen urratsetan iridio-espezie berri bat (B) identifika daiteke ^{1}H EMN espektroan, -9.15 ppm-tan, eta ^{31}P{^{1}H} EMN espektroan, 5.5 ppm-tan, agertzen diren seinale zabalengatik. Seinale horiek **1** konplexuaren bidez katalizatutako AB-aren hidrolisiaren antzekoak dira;[43] eta hidruro bat azilo talde batekiko *trans* posizioan eta bi fosforo atomoekiko *cis* posizioan daukan iridio-espezie batenak dira.

Katalisia aurrera egin ahala hasieran ikusitako **B** espeziea desagertu egiten da eta **7** konplexuak katalizatutako AB-aren metanolisian azken produktu gisa ikusi diren espezieak agertzen dira. AB gehiago gehitu ondoren hidrogeno askapena eta **B** espeziea berriro agertzen dira.
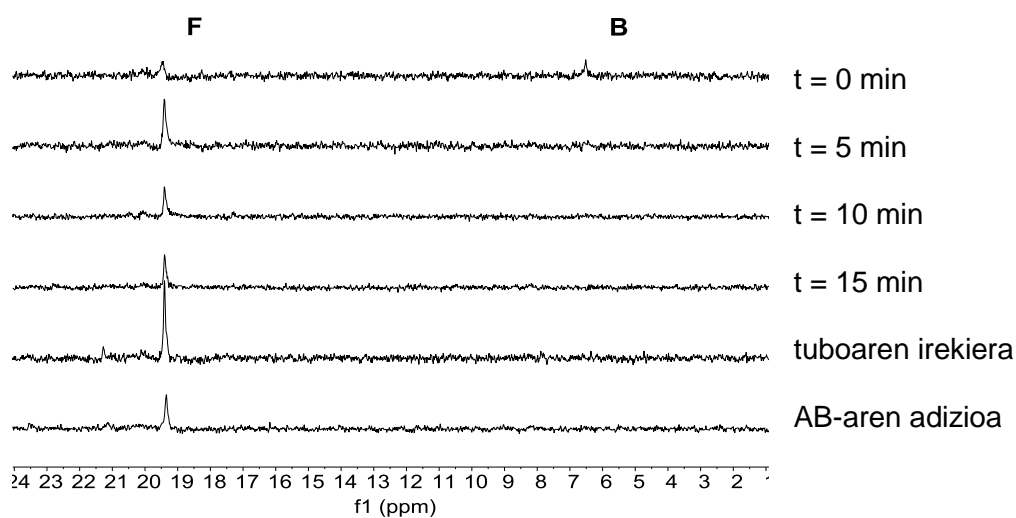
2.25 irudia. 1 konplexuak katalizatutako AB-aren metanolisiaren jarraipena ^{31}P{^{1}H} EMN-aren bidez. CD$_3$OD-tan eta 25 ⁰C-tan egin da. Honetan iridio espezie berrien formazioa ikus daiteke.

2.5 Erreaktibitate frogak. (9), [IrH(H$_3$BNH$_3$){(PPh$_2$(*o*-C$_6$H$_4$CO))(PPh$_2$(*o*-C$_6$H$_4$CO))H}]-ren sintesia

7 konplexuak metanoletan eta amina-boranoen aurrean duen portaera aztertu zen prozesu katalitikoa ulertzeko.

7 konplexua CDCl$_3$ eta CD$_3$OD 50/50 erlazioko nahasketa batean disolbatzen denean, bi zentro metalikoak lotzen dituen koro zubia hausten da. Honen ondorioz **1** konplexua eta **8** konplexu kartioniko berria lortzen dira (2.26 irudia).
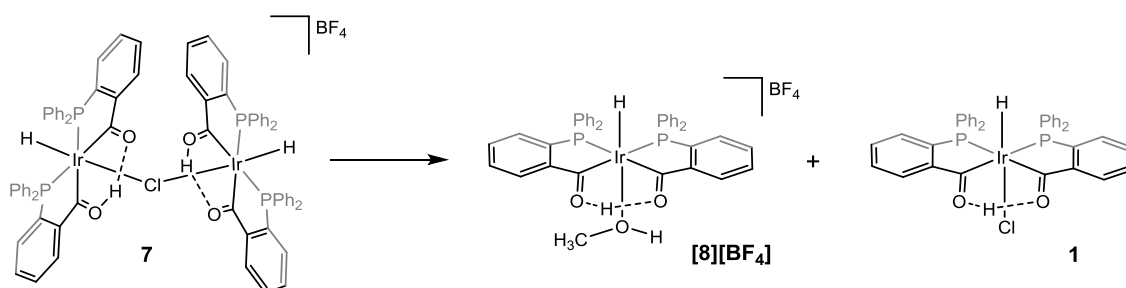
2.26 irudia. 7 konplexuaren kloro zubiaren apurtzea CDCl$_3$/CD$_3$OD disoluzio batean.

[1]H EMN eta ^{31}P EMN espektroetan (2.27 irudia) goiko irudian marraztutako hiru konplexuen nahasketa ikus daiteke. **8** konplexuan iridioak **1** konplexuaren koordinazio-ingurune bera du; baina, metanol molekula batek kloro atomoa ordezkatu du, [BF$_4$]$^-$ ioia kotraioi gisa duen konplexu kationikoa bihurtuz. **8** konplexua isolatzeko hainbat saiakera egin ziren baina hauek ez zuten arrakastarik izan. Hala ere, **8** konplexua EMN-ren bidez identifikatu zen: [1]H EMN-an -25.20 ppm-tan hirukote (J$_{P,H}$ = 14.3 Hz) eta ^{31}P EMN-an 29.4 ppm-tan ikusitako singleteaz. **8** konplexuaren datu espektroskopikoak eta metanol molekularen ordez azetona molekula duen ([IrH{PPh$_2$(*o*-C$_6$H$_4$CO))$_2$H}(azetona)]$^+$) konplexuarenak oso antzekoak dira.[61]
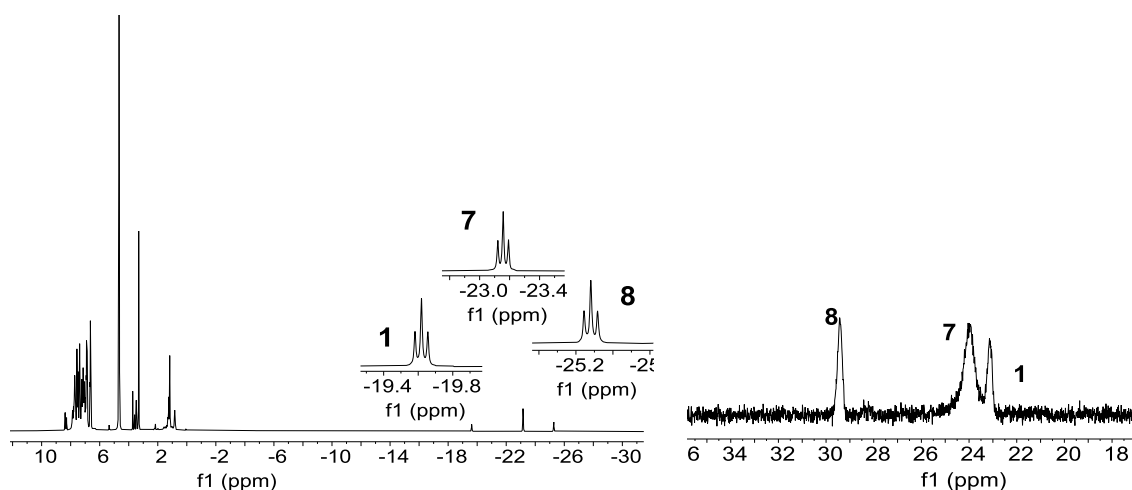
2.27 irudia. ^{1}H EMN (left) and ^{31}P EMN (right) spectra of a CDCl$_3$/CD$_3$OD solution of complex 7.

Bestalde, **7** konplexua CD$_3$OD-tan disolbatzen denean trimetilamina-borano aduktuaren presentzian espezie berri bat sortzen da. **7** dimeroa metanoletan disolbatu eta bi zatitan bereizi ondoren, amina-borano aduktua borano taldearen hidruro batetik iridiora koordinatzen da **9** konplexu ionikoa eratuz (2.28 irudia). Dimeroaren beste zatia **1** konplexua da, CD$_3$OD-tan duen disolbagarri baxuagatik hauspeatzen dena.
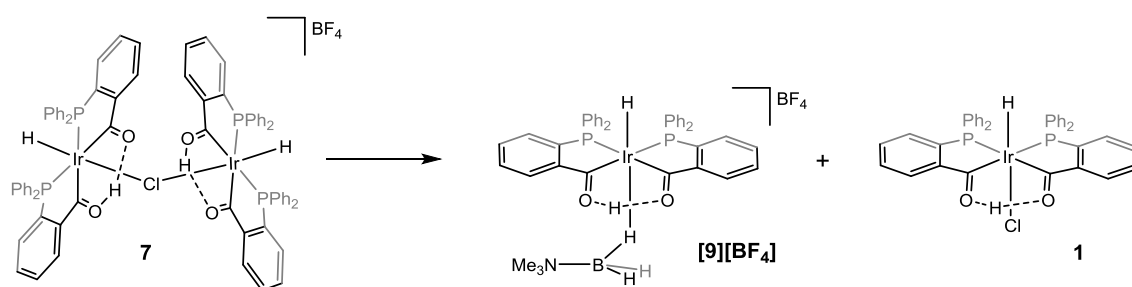
2.28 irudia. 7 konplexuaren *in situ* erreakzioa Me$_3$N-BH$_3$-rekin CD$_3$OD-tan.

EMN ^{1}H eta ^{31}P espektroetan (2.29 irudia) aipatutako hiru konplexuak identifika daitezke, non konplexu berria, **9** konplexua, produktu nagusia den.
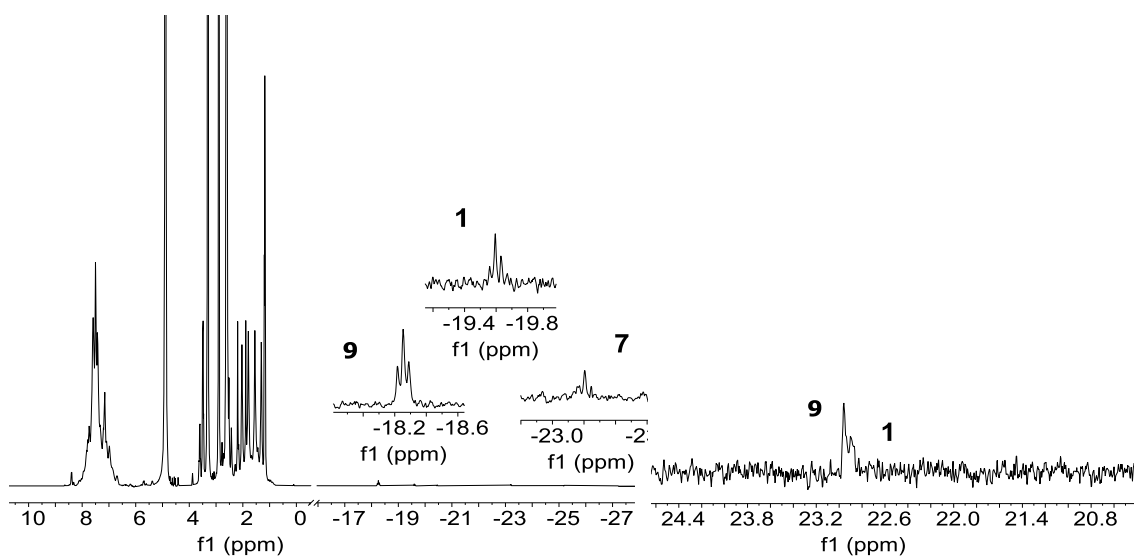
2.29 irudia. 7 konplexuaren eta Me₃N-BH₃-ren CD₃OD-tan egindako *in situ* erreakzioaren ¹H EMN (ezkerraldea) eta ³¹P EMN (eskuinaldea) espektroak.

9 konplexua [**9**][BAr$^F_4$] gisa isolatu zen, **1** konplexuaren eta Me₃N-BH₃-ren arteko erreakzioa Na[BAr$^F_4$] gatzaren aurrean diklorometanotan eginez (2.30 irudia). Konplexu honetan, borano taldea iridioari M-H-B η^1 moduan koordinatuta dago, hiru zentro bi elektroi loturaren bidez.[62] Konplexu berri hau hainbat tekniken bidez karakterizatu da.
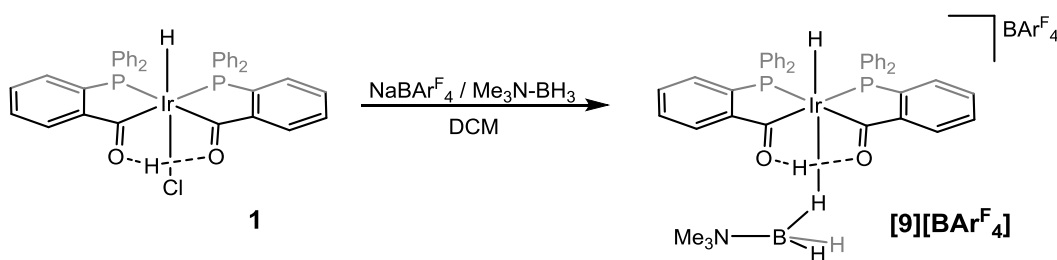
2.30 irudia. 1 konplexua eta Me₃N-BH₃-aren arteko erreakzioa NaBAr$^F_4$ gatzaren presentzian diklorometanotan.

IR espektroan (A. 4 irudia) borano taldearen hidruro terminalei dagozkien bandak 2504 eta 2444 cm^{-1}-ean ikus daitezke. ν(Ir-H) tentsioa 1793 cm^{-1}-ean ikus daiteke baina, seinalea hain zabala denez, Ir-H-B zubiaren seinalea azpian egon daiteke. Azkenik, ν(C=O) loturaren seinalea 1609 cm^{-1}-ean ikus daiteke.

9 konplexuarentzat, ESI-MS (*m/z*) masa espektroa egin zen eta 846.2 [M]$^+$-eko balioa lortu zen (D. 1 irudia eta D. 2 irudia); honek adierazten du borano aduktua zentro metalikoari lotuta dagoela.

EMN espektroskopia multinuklearra **9** konplexuarako egin zen. ^{31}P{^{1}H} EMN espektroan (B. 19 irudia) singlete bat 23.1 ppm-tan ikus daiteke; honek esan nahi du konposatuak bi fosforo baliokide dituela. Zoritxarrez, ^{11}B EMN espektroan, BAr$^F_4$ kontraioiaren seinalea baino ezin da ikusi (B. 20 irudia).

Bestalde, ^{1}H EMN espektroan (2.31 irudia) **9** konplexuari buruzko informazio baliotsua aurki daiteke. Konplexuaren hidruroaren seinalea eremu altuko eskualdean ikus daiteke, -18.39 ppm-tan, hirukote gisa, *cis* posizioan dauden bi fosforo baliokiderekin akoplatzearen ondorioz ($J_{P,H}$ = 14.6 Hz). Hidruroaren posizioa bat dator beste antzeko iridio konposatuentzat ikusitako datu espektroskopikoekin; izan ere konplexu horiek B-H talde bat hidruroarekiko *trans* posizioan zeukaten.[63] Eremu baxuko eskualdean, 22.61 ppm-tan, O -- H – O hidrogeno zubiari dagokion singlete bat ikus daiteke. Seinale honek hasierako materialaren PCCP egitura ez dela aldatu berretsi du. Giro tenperaturan borano taldearen seinalea -2.40 ppm-tan agertzen da eta seinale zabala da.
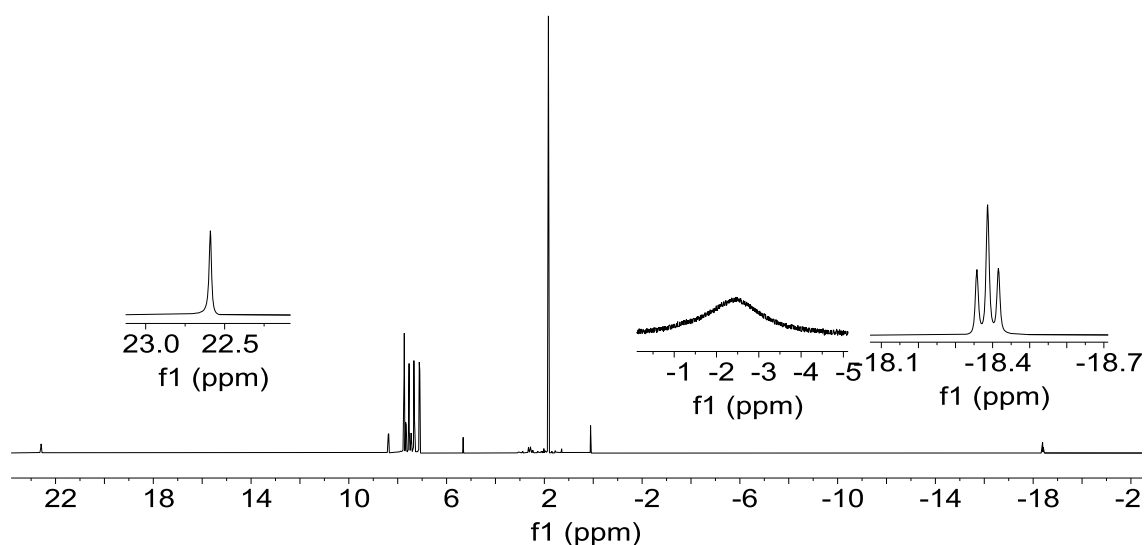
2.31 irudia. 9 konplexuaren ^{1}H EMN espektroa CDCl$_3$-tan eta 25 ºC-tan.

<mark>BH$_3$ taldea zentro metalikoari (hiru zentro bi elektroi moduan) lotuta duten</mark> antzeko beste konplexu batzuk bezala, **9** konplexuak portaera dinamikoa dauka giro-tenperaturan (2.32 irudia).
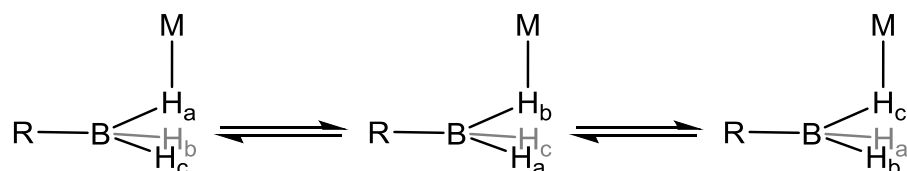
2.32 irudia. BH$_3$ taldea koordinatua dagoenean daukan portaera dinamikoa.

^{1}H EMN espektroak hainbat tenperaturatan egin ziren portaera dinamikoa frogatzeko. 3.33 irudian ikus daitekeenez, lehen aipatutako seinale zabala, -2.40 ppm-tan agerten dena (a), tenperatura jaitsi ahala desagertzen da, koaleszentziara iristen baita. 233 K-etara iristerakoan bi seinale berri ikus daitezke, bat -10.54 ppm-tan protoi bakar batena eta beste bat 1.50 ppm-tan bi protoiena. 213 K-etara iristerakoan konplexua ia portaera estatikoa lortzen duela esaten da. Hidruroaren eta protoi zetoenolikoaren seinaleak eta fosforoen seinalea ez dira aldatzen tenperatura-tarte osoan.

Datu hauek kontuan hartuz, esan daiteke irida-β-dizetona konplexuak zentro metalikoari borano aduktu bat koordinatua dutenak isola daitezkela.
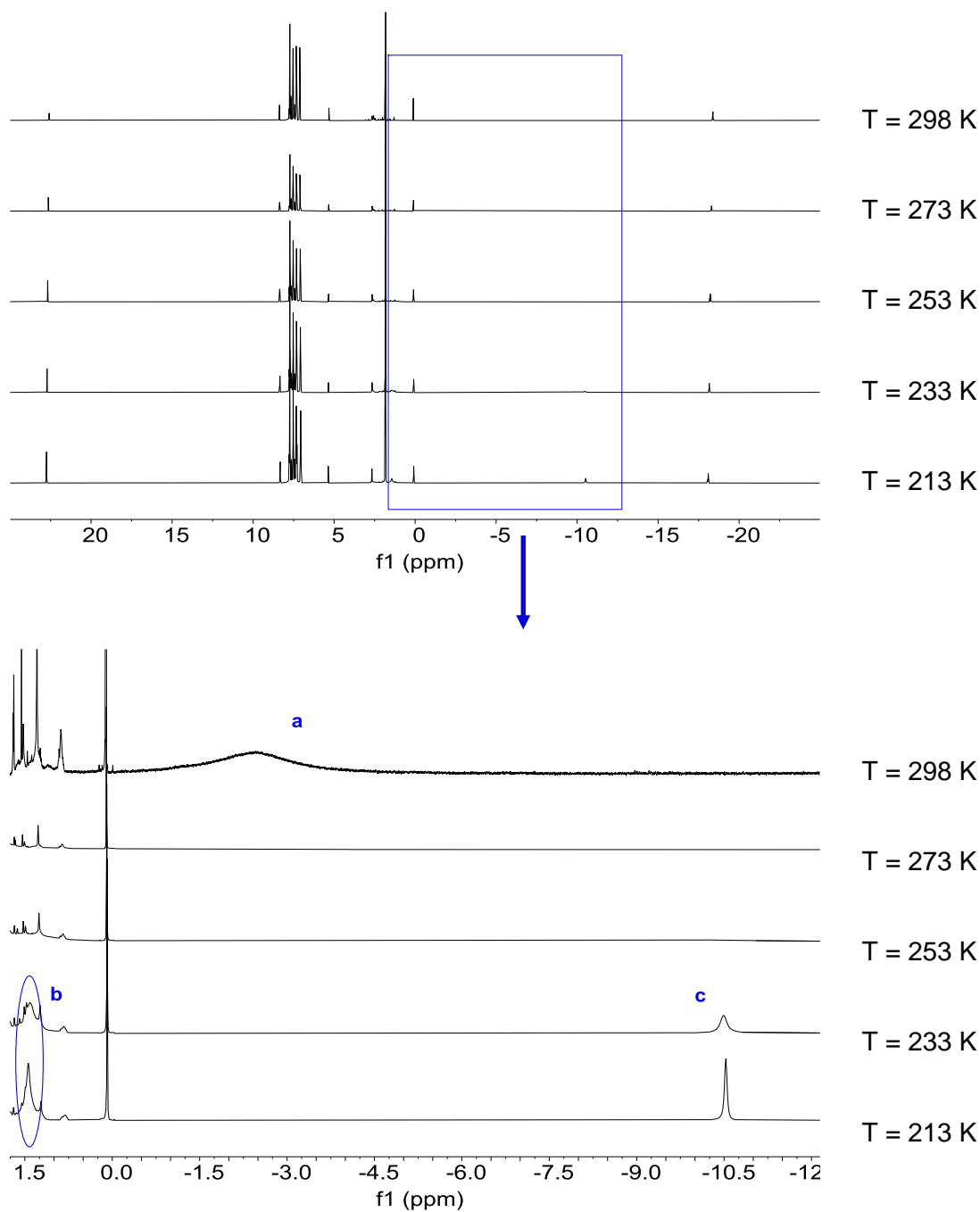
2.33 irudia. 9 konplexuaren ^{1}H EMN espektroak CDCl$_3$-tan hainbat tenperaturatan.

2.6 Proposatutako ziklo katalitiko sinplifikatua

Emaitza esperimentalak jaso ondoren, honako ziklo katalitiko sinplifikatua proposatzen da (2.34 irudia).
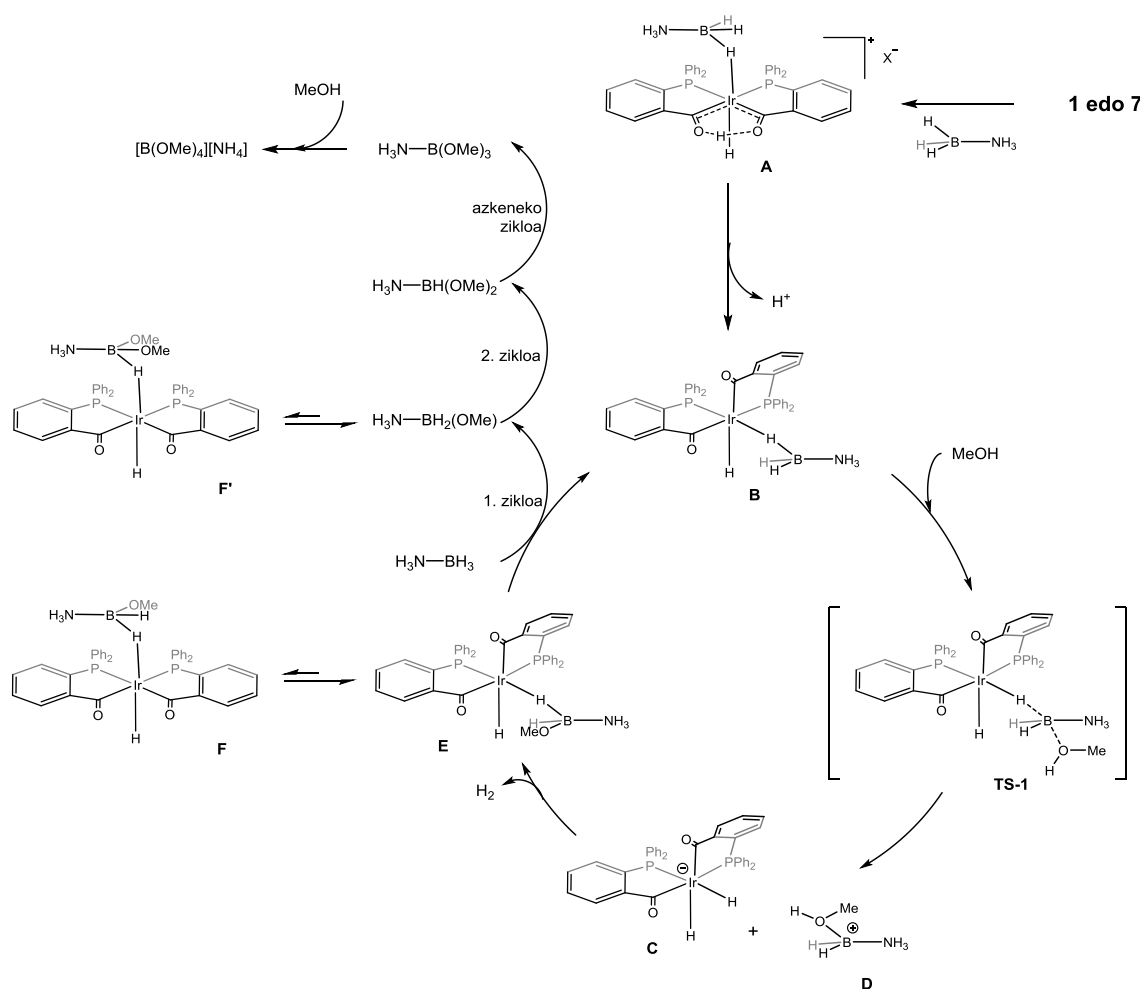
2.34 irudia. Hidruroirida-β-dizetonek katalizatutako AB-aren metanolisiarentzat proposatutako ziklo katalitiko sinplifikatua.

AB-aren metanolisia metalez katalizatutako prozesu homogeneo eta intermolekular gisa proposatzen dugu. Hidrogeno askapena ondoz ondoko urratsetan gertatzen da eta hiru hidrogeno molekula askatzen dira AB molekula bakoitzerako. Lehenengo urratsean hidrogeno molekula bat eta H_3N-$BH_2(OMe)$ sortzen dira; bigarren urratsean beste hidrogeno molekula bat eta H_3N-

BH(OMe)$_2$ sortzen dira; eta azkenik, hirugarren urratsean azkeneko hidrogeno molekula eta H$_3$N-B(OMe)$_3$ sortzen dira. Metanol molekula batek H$_3$N-B(OMe)$_3$ borano aduktuaren B-N lotura bereizten laguntzen du, eta ^{11}B EMN-an ikusitako [NH$_4$][B(OMe)$_4$] produktu ionikoa sortzen da. Aipatutako azken produktua, tetrametoxiboratoa, AB-aren hidrolisian sortutako produktuarekin[46,64,65] lotuta dago; kasu honetan hidroxilo taldea metoxi taldearekin ordezkatu da.

1 edo **7** konplexuek AB-zko metanol disoluzio batean disolbatzen direnean kloruro anioia askatzen dute. Ondoren, AB molekula batek kloruroak utzitako hutsunea betetzen du, irida-β-dizetona (**A**) konplexua sortuz. (**A**) konplexua **9** konplexuaren antzekoa da.

Irida-β-dizetona konplexuak metanol-disoluzioetan eta base baten aurrean disolbatzen direnean protoi zetoenolikoa gal dezakete; eta honen ondorioz, estekatzaileen kokapena metalaren inguruan alda daiteke.[4] Kasu honetan, **A**-ren desprotonazioa eta estekatzaileen berrantolaketa proposatzen da; **B** espeziea sortuz. Espezie berri honek azilo talde batekiko *trans* posizioan hidruro bat dauka, eta EMN bidez jarraitutako AB-aren metanolisiaren hasierako espektroetan ikusitako espeziea izango litzateke.

Hurrengo urratsean, **B** espezieak MeOH molekula baten eraso nukleozalea jasango luke boro-atomoan; TS-1 trantsizio egoeraren bidez. Honek dihidruroiridato(III) (**C**) espeziea eta metanolaren bidez egonkortutako boronio katioia (**D**) sortuko luke.

Boronio katioitik (**D**) dihidruroiridato(III) (**C**) espeziera O-tik Ir-rako hidrogeno transferentzia gerta daiteke. Honen ondorioz hidrogeno molekularra askatu eta **E** espeziea sortuko lirateke. **E** espeziea iridio(III) konplexu bat da H$_3$N$-$BH$_2$(OMe) borano aduktua koordinatua duena.

Jakina da dihidrurobis(azilodifenilfosfina)iridato(III) espezie iragankorrak hidroxilo talde batetik O-tik Ir-rako hidrogeno transferentzia egiteko gai direla;[4] prozesu honetan hidrogenoa askatu eta hidruro-deribatuak sortzen direlarik. Isomeroak diren **E** eta **F** espezieen artean oreka bat proposatzen dugu. Beraien

arteko desberdintasuna **E** espezieak hidruroa borano taldearekiko *cis* posizioan daukala eta **F** espezieak hidruroa borano taldearekiko *trans* posizioan daukala da. **F** espeziea EMN bidez jarraitutako AB-aren *in situ* metanolisian ikusitako bukaerako espeziea dela proposatzen dugu.

Borano aduktuen arteko lehiak $H_3N-BH_2(OMe)$ sortzen du; eta H_3N-BH_3 molekula berri baten koordinazioak **B** espeziea birsortu eta hidrogeno askapena berrabiarazten du. **E** espezietik abiatuta antzeko ziklo katalitikoa gerta daiteke; beste hidrogeno baliokide bat askatuko lukeena eta $H_3N-BH(OMe)_2$ eta **F'** espeziea sortuko lituzkeena. Iridioari $H_3N-BH(OMe)_2$-a koordinatzeak hirugarren hidrogeno-baliokidearen askapena eta $H_3N-B(OMe)_3$-aren formazioa sortuko luke. Azkenik, $H_3N-B(OMe)_3$ borano aduktua MeOH molekula batekin erreakzionatu ondoren tetrametoxiborato produktua sortuko luke.

3. Kapitulua

Iridapirazoletik eratorritako konplexuak,

sintesia eta aktibitate katalitikoa

3.1 Sarrera

Aurreko kapituluetan irida-β-diketonek aminekin duten erreaktibotasuna (konplexu berriak sor ditzakete, besteak beste, PCN estekatzaileak dituztenak) eta amoniako- eta amina-boranotik hidrogenoa askatzeko erakutsi duten jarduera katalitikoa azaldu dugu. Gure laborategiko aurreko lanak erakutsi zuenez, irida-β-diketona **1** konplexuak hidrazinarekin erreakzionatzean, aurretik ezezaguna zen metalaziklo berri bat sor dezake, iridapirazol-motakoa den **3** konplexua. Konplexu hau oso etekin txikian lortzen zen; eta, beraz, nahiz eta karakterizatu, erreaktibotasunari edo erabilerei buruzko azterketa ez zen egin.

Kapitulu honen helburua **3** konplexuaren sintesia hobetzea da, beste erreakzio-bide bat erabiliz.Hori lortutakoan, arestian aipatutako konplexuaren erreaktibotasuna aztertuko da. Alde batetik, iridioaren eta kloruro atomoen arteko loturaren erreaktibotasuna ikertuko da, iridapirazol konplexu berriak lortu nahian. Bestalde, iridapirazol eraztunaren portaera aztertuko da, pirazol organikoen portaerarekin konparatzeko.

Azkenik, iridapirazoletik eratorritako konplexu berrien jarduera katalitikoa AB-aren metanolisi homogeneorako aztertuko da.

3.2 Iridapirazol motako 3 konplexuaren sintesia

3.2.1 L$_1$-en sintesia

3 konplexua lortzeko etekin hobeago baten bila, *o*-(difenilfosfino)benzaldehidoaren iminazioa hidrazinarekin egitea proposatu zenzen. Etanoletan egindako errefluxu baten ondoren, 1,2-bis-2-((difenilfosfaneil)benziliden)hidrazina (**L$_1$**) estekatzailea lortu zen (3.1 irudia).
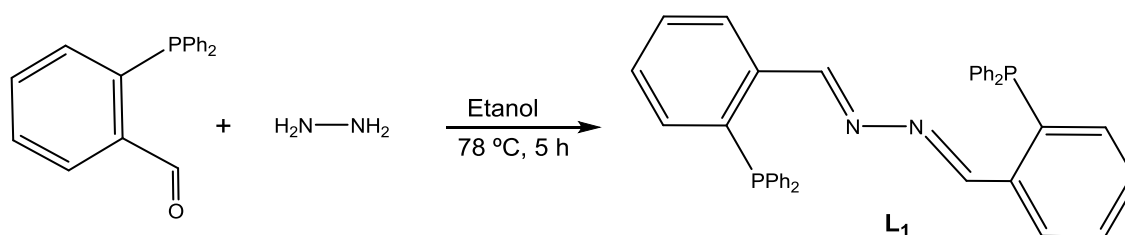
3.1 irudia. L$_1$ estekatzaile berriaren formazioa.

L$_1$-a EMN multinuklearraren, IR espektroskopiaren eta monokristalen X-izpien difrakzioaren bidez karakterizatu da.

^{1}H EMN-an, imino taldeen protoien seinalea 9.23 ppm-tan ikus daiteke, $J_{P,H}$ = 4.5 Hz-tako akoplamendu-konstantea duen bikote gisa (B.102 irudia). Hasierako materialaren aldehidoaren protoia 10.54 ppm-tan agertzen zen eta erreakzioa eta gero ez da seinalerik ikusten posizio horretan. Bestalde, protoi aromatikoek hasierako materialaren forma eta posizioari eusten diote. **L$_1$**-aren ^{31}P{^{1}H} EMN-an singlete bat ikus daiteke -14.6 ppm-tan (B. 103 irudia). ^{15}N EMN espektroa neurtu zen eta 367.4 ppm-tan singlete bat ikusi zen.

Era berean, IR espektroskopian imino-talde berriak detekta daitezke. C=N taldeari dagokion seinalea 1614 cm^{-1}etan agertzen delarik.

L₁-en monokristal horiak lortu ziren pentano lurruna **L₁**-en diklorometanozko disoluzio batera barreiatuz -20 ⁰C-tan, eta X-izpien difrakzioaren azterketa egin zen, ikus 3.1 taula.

3.1 taula. Aukeratutako L₁-en lotura-distantziak (Å) eta angeluak (⁰). Desbiazio estandarra parentesi artean agertzen da. Simetria eragiketa: (i) -x, -y, -z.

Lotura-distantziak			
N1-N1'(i)	1.406(3)	C1-C2	1.465(2)
N1-C1	1.276(2)		
Lotura-angeluak			
C1-N1-N1'(i)	111.88(18)	N1-C1-C2	120.37(16)

L₁-ek P2₁/c talde-espazial monoklinikoan kristalizatzen du, eta unitate asimetrikoa molekularen erdia izanda, simetria-eragiketa batek sortu du beste erdia.

N1-N1'-aren lotura-luzera bi nitrogeno atomoren arteko lotura simple baterako espero dena baino laburragoa da. Ezaugarri honek, C1 karbonoaren sp² hibridazioarekin batera, (N1-C1-C2), 120,37(16)⁰-koa dena, elektroien deslokalizazioa N1-N1' loturara zabaltzen dela berresten du.
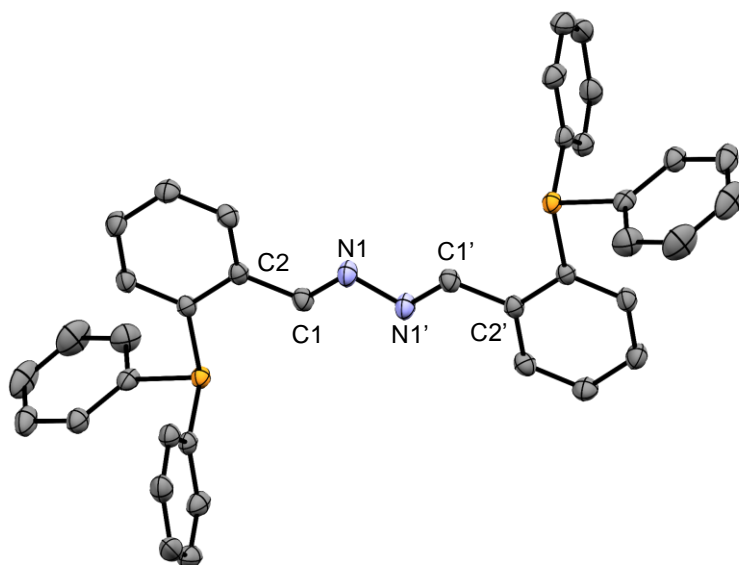
3.2 irudia. L₁-aren egitura molekularra.

L₁ beste modu batean ere sintetiza daiteke *o*-(difenilfosfino)benzaldehidoatik abiatuta hidrazinio sulfatoa ($N_2H_6SO_4$) eta ^{15}N hidrazinio sulfatoa-rekin arestian aipatutako baldintza beretan.

3.2.2 3 Konplexuaren formazioa L₁-etik abiatuta

L₁-ek [Ir(COD)Cl]₂ iridio dimeroarekin erreakzionatzen du kloroformotan, **3** konplexua sortuz. Guk proposatutako erreakzio-bidea honakoa da: ondoz ondoko bi adizio oxidatzaile iridio(V) den **A** bitartekariatik igaroz, hidrogeno-transferentzia baten ondoren iridio(III) den **3** konplexua lortzeko (3.3 irudia).
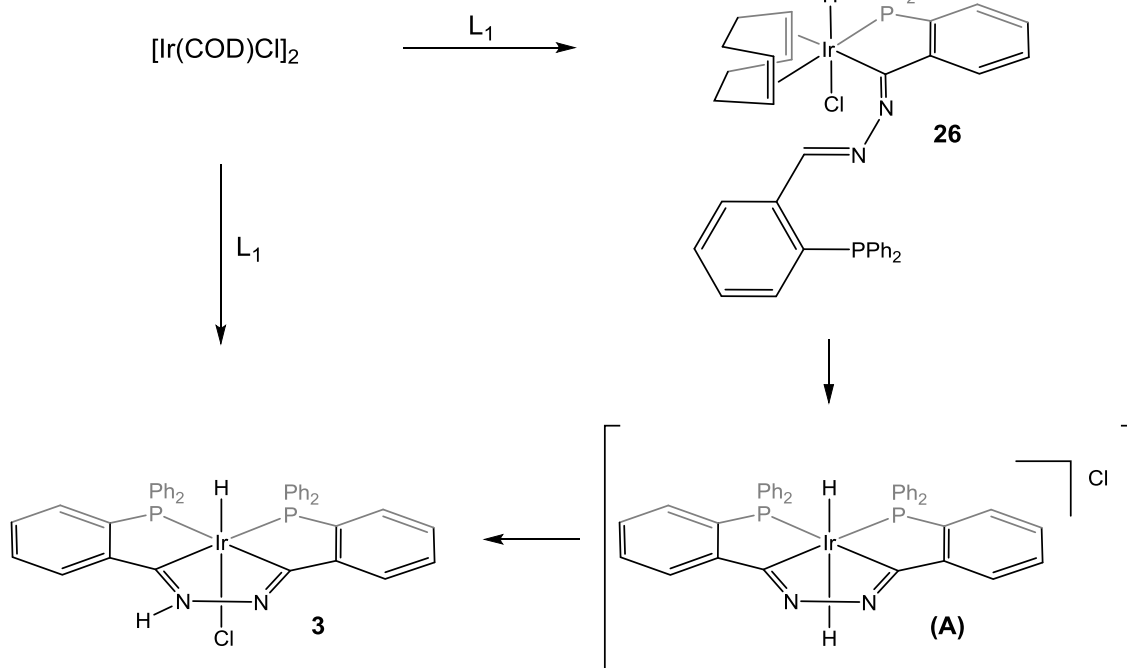
3.3 irudia. 3 konplexuaren formaziorako proposatutako erreakzio-bidea.

3 konplexuaren sorrera ^{1}H eta ^{31}P$\{^1$H$\}$ EMN-aren bidez jarraitu zen (3.4 irudia). Erreakzioaren lehenengo urratsetan, **L$_1$** oraindik erreakzionatu gabe badago ere, ^{1}H EMN espektroan bi seinale ikus daitezke eremua altuan, hidruroak agertzen diren tartean eta eremu baxuagoan, 1,5-ziklooktadieno askearen ondorioz. -19.69 ppm-tan ikusten den multipletea **3** konplexuari dagokio eta -16.19 ppm-tan agertzen de bikotea (J$_{P,H}$ = 10.4 Hz) **26** konplexuari dagokiola proposatzen dugu. **26** konplexua **L$_1$**-en imino talde batek eragindako adizio oxidatzailearen ondorioz sortutako iminoazil-iridio(III) bitartekaria da. ^{31}P$\{^1$H$\}$ EMN espektroan 31.4 ppm-tan singlete bat ikus daiteke. Ezaugarri espektroskopiko hauek aurretik aipatutako [IrHCl(COD)(PPh$_2$(*o*-C$_6$H$_4$CO))]-aren ezaugarrien antzekoak dira. Izan ere, [IrHCl(COD)(PPh$_2$(*o*-C$_6$H$_4$CO))]-a *o*-(difenilfosfino)benzaldehido eta [Ir(COD)Cl]$_2$ iridio dimeroaren arteko erreakzioan osatzen da adizio oxidatzaile baten ondorioz. Konplexu honen ^{1}H EMN espektroan bikote bat ikus daiteke -16.12 ppm-tan (J$_{P,H}$ = 15 Hz) eta ^{31}P$\{^1$H$\}$ EMN espektroan singlete bat 38.1 ppm-tan; eta bitartekaria da irida-β-

dizetonen sintesian.[3] **26** bitartekaria detektatu zen baina bere isolamendua ezinezkoa izan zen.

Esekita dagoen imina zatia, bigarren adizio oxidatzaile baten ondorioz, gehituz gero, iridio(V) den (**A**) dihidruro espeziea lor daiteke. Azkenik, iridiotik nitrogenorako protoi transferentzia eta kloruroaren koordinazioa gertatzean **3** konplexua lortzen da.

Bigarren bide bat, ordea, ezin da erabat baztertu, zeinetan hidrogeno kloruroa bigarren adizio oxidatzailea gertatu baino lehen aska daitekeen.
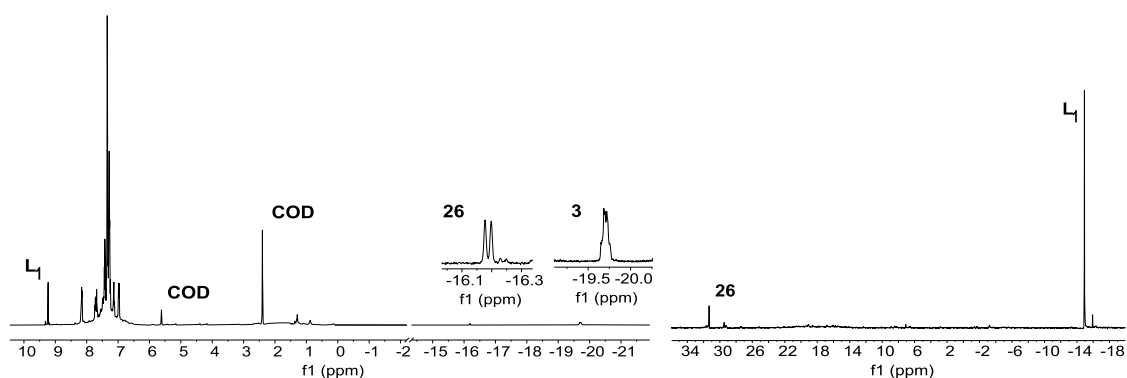
3.4 irudia 3 konplexuaren formazioaren *in situ* ¹H (ezkerraldea) eta ³¹P{¹H} (eskuinaldea) EMN espektroak CDCl₃-tan

3 konplexuko dimetilsulfoxido disoluziotik monokristal laranjak giro tenperaturan lortu ziren, eta X Izpien difrakzioaren azterketa egin zen. Emaitzak **3** konplexurako aurreko bide sintetikotik ateratako berberak izan ziren.[12] Honek **L₁** eta [Ir(COD)Cl]₂ iridio dimeroaren arteko erreakzioaren bidez konplexu bera etekin altuagoarekin lor daitekela frogatzen du.

3.3 3 Konplexuaren erreaktibitatea

3 konplexua metalaziklo bat duen konplexu organometalikoa da, kasu honetan metalazikloa iridapirazol ziklo bat da. **3** konplexuaren erreaktibotasuna erabat aztertzeko, bi ikuspegi hartu ziren kontuan: zentro metalikoaren erreaktibotasuna, kloro atomoak hartzen duen posizio labilagatik, eta iridapirazol eraztunaren erreaktibotasuna.

3.3.1 Erreaktibitatea iridio zentro metalikoan

3.3.1.1 Konplexu kationikoen formazioa

Kloro atomoa estekatzaile neutroekin ordezkatzeko nahian, **3** konplexua NaBAr$^F_4$ halogeno abstraktorearekin erreakzionatu zen estekatzaile neutroaren aurrean (3.5 irudia).
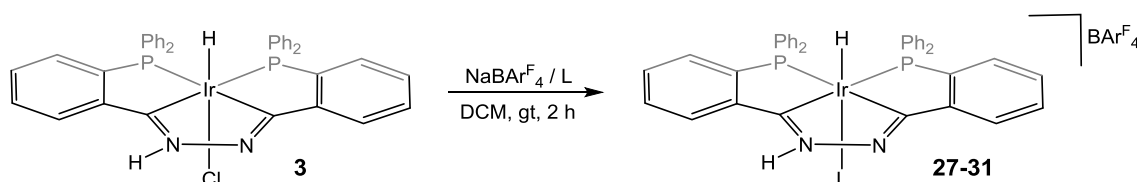
3.5 irudia. Hainbat konplexu kationikoen formazioa 3 konplexua NaBAr$^F_4$ eta L-rekin erreakzionatuz, non L: pirazol (27); piridina (28); azetonitrilo (29); trifenilfosfine (30) eta *cis*-ziklookteno (31) den.

Bost konplexu kationiko berri sintetizatu dira zenbait estekatzaile erabiliz, kloro atomoaren abstrakzioak utzitako leku hutsa betetzeko. Aukeratutako estekatzaileen artean, hiru nitrogeno emaile daude: pirazola (**27**), piridina (**28**) eta azetonitriloa (**29**); fosfina bat, trifenilfosfina (**30**); eta olefina bat, *cis*-ziklo-oktenoa (**31**). Konplexu guztiak EMN multinuklearrez, IR espektroskopiaz eta masen espektroskopiaz karakterizatu dira.
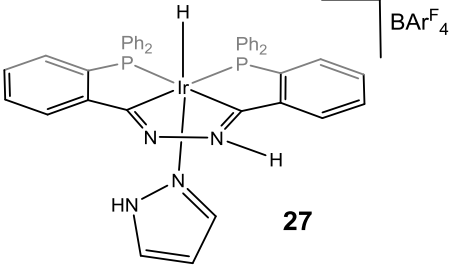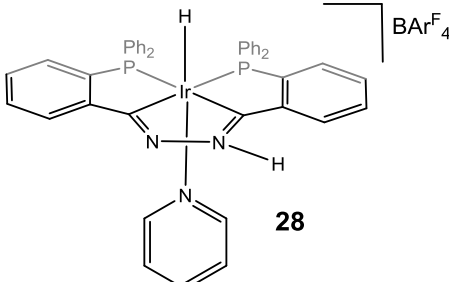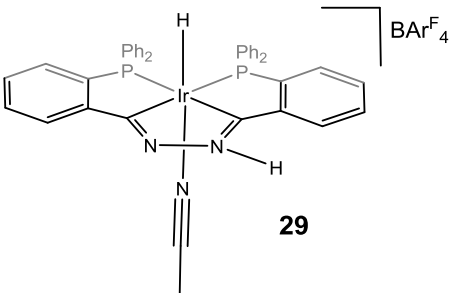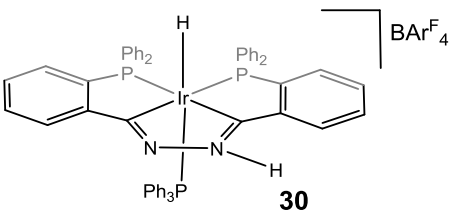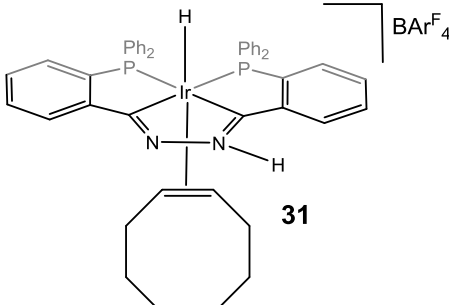
Erreakzio hauen arrakastaren oinarria sortu berri diren konplexuen disolbagarritasun handian dago, eta diklorometanotan hauspeatzen den NaCl gatzaren eraketan. Izan ere **3** konplexua ez da batere disolbagarria diklorometanotan.

Bost konplexuen EMN espektroak tenperatura baxuan (213 K) eta giro-tenperaturan (298 K) neurtu dira; iridapirazola osatzen duten bi nitrogeno atomoen arteko protoi trukaketarengatik konplexuek portaera fluxionala baitute. Izan ere, ezaguna da pirazolek NH prototropia eduki dezaketela. Tautomerismo honen ondorioz, fosforo-atomoak giro-tenperaturan baliokide bihurtzen dira. Portaera dinamiko hau tenperaturaren araberakoa ez ezik, ur-kantitatearen araberakoa ere bada; **3** konplexuaren antzeko den iridapirazol motako dihidruro konplexu batentzat frogatu zen bezala.[12] EMN espektroetan ikusitako seinale garrantzitsuenak 3.2 taulan ageri dira, espektro osoak ikusteko ikusi B. 105 irudia eta B. 106 irudia **(27)**; B. 108 irudia eta B. 109 irudia **(28)**; B. 110 irudia eta B. 111 irudia **(29)**; B. 112 irudia eta B. 113 irudia **(30)** eta B. 114 irudia eta B. 115 irudia **(31)**. Estekatzaileei dagozkien seinaleak zati esperimentalean jaso dira.

Nitrogeno emaile diren estekatzaileak erabiltzerakoan sortzen diren konplexuetan (**27**, **28** eta **29**) estekatzaileak hidruroarekiko *trans* posizioan daude. Konplexu hauetako hidruroen seinaleak -18 eta -18.6 ppm artean agertzen dira, hirukote gisa, *cis* posizioan dauden bi fosforo-atomorekin akoplatzearen ondorioz. Olefina bat koordinatua duen **31** konplexuaren seinalea, -12.26 ppm-tan agertzen da, hirukote gisa. Bestalde, **30** konplexuaren seinalea -12.31 ppm-tan ikus daiteke eta hiru fosforo-atomorekin egindako akoplamenduaren ondorioz hirukote bikoitz moduan agertzen da, jatorrizko konplexuko bi fosforo-atomorekin *cis* posizioan eta trifenilfosfinako hirugarren fosforo-atomoarekin *trans* posizioan daudenak.

3.2 taula. 27-31 konplexuean EMN datu garrantzitsuenak. Espektroak CD_2Cl_2 edo $CDCl_3$ disoluzioetan egin ziren, desfase kimikoa ppm-tan eta akoplamendu konstanteak Hz-etan neurtu dira.

Konplexu	^1H EMN (298 K)	$^{31}P\{^1H\}$ EMN (213 K)
27	δ Ir-H = -18.60 (t) $^2J_{P,H}$= 15.8 δ N-H = 12.54 (br)	δ Ir-P = 19.4 (s) δ Ir-P = 25.0 (s)
28	δ Ir-H = -18.57 (t) $^2J_{P,H}$= 15.9 δ N-H = 13.45 (br)	δ Ir-P = 22.7 (s) δ Ir-P = 26.9 (s)
29	δ Ir-H = -18.02 (t) $^2J_{P,H}$= 14.6 δ N-H = 12.18 (br)	δ Ir-P = 18.8 (s) δ Ir-P = 23.7 (s)
30	δ Ir-H = -12.31 (dt) $^2J_{P,H}$= 19.6 $^2J_{P,H}$= 89.3 δ N-H = 12.50 (br)	δ Ir-P = -5.0 (s) δ Ir-P = 6.1 (s) δ Ir-P = 11.4 (s)
31	δ Ir-H = -12.26 (t) $^2J_{P,H}$= 19.6 δ N-H = 11.96 (br)	δ Ir-P = 11.6 (s) δ Ir-P = 15.5 (s)

Konplexu guzti hauen $^{31}P\{^1H\}$ EMN espektroek tenperatura baxuan (213 K) seinale garbiak aurkezten dituzte, konplexuek portaera estatikoa dutelako. Seinaleak zabalduz doaz tenperatura handitu ahala. **27** konplexuaren kasuan, seinale bakarra ikus daiteke giro-tenperaturan konplexua tenperatura horretan koaleszentziatik gorago dagoelako.

27 konplexua ^{15}N EMN espektroa egiteko hautatu zen, eta 285.6 ppm-tan singletea ikusi daiteke; lortutako balioa eta pirazol organikoaren balioa oso antzekoak dira. [78]

Konplexu hauetarako IR espektroak neurtu ziren. Konplexu guztietan ν(Ir-H) tentsioaren seinalea oso ahula da; izan ere, kasu batzuetan bakarrik ikus daiteke eta seinale zabala da: 2192 **(27)**; 2191 **(28)**; 2190 **(29)** eta 2113 **(30)** cm^{-1}. ν(C=N)-ren tentsio seinale sendoagoa 1610 **(27)**; 1608 **(28)**; 1631 **(29)**; 1610 **(30)** eta 1610 **(31)** cm^{-1}-etan ikus daiteke.

Konplexu hauetako masa-espektroak egin ziren, eta hauek izan ziren lortutako balioak: ESI-MS (*m/z*): 837.2 [M]$^+$ **(27)**; 848.2 [M]$^+$ **(28)**; 810.2 [M]$^+$ **(29)**; 1031.2 [M]$^+$ **(30)** eta 769.2 [M-COE]$^+$ **(31)** (D. 15 iruditik D. 24 irudira) Lortutako balioak ioi molekular nagusiaren balioarekin eta distribuzio isotopikoarekin bat datoz.

Kloruro-ordezkapen erreakzioen arrakastaren ondoren, NaBAr$^F_4$ haluro abstraktorea eta arestian aipatutako estekatzaile neutroak erabiliz, baldintza berdinak erabili ziren borano taldea duten bi estekatzaileekin konplexu berriak sintetizatzeko, trietilamina-boranoa eta trifenilfosfina-boranoa (3.6 irudia).
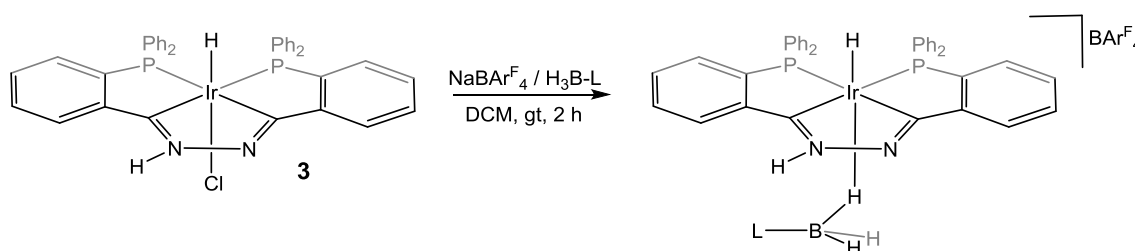
3.6 irudia. Hainbat konplexu kationikoen formazioa 3 konplexua NaBAr$^F_4$ eta L-rekin erreakzionatuz, non L: NEt$_3$ (32) eta PPh$_3$ (33) den.

32 eta **33** konplexuetan zentro metalikoak borano taldea M-H-B η^1 moduan lotzen du, hiru nukleo bi elektroi lotura baten bidez.[62] Bi konplexu hauek hainbat teknikekin karakterizatu dira.

Konplexu hauetako masa espektroak egin ziren, eta lortutako balioak ESI-MS (m/z): 884.3 [M]$^+$ (D. 25 irudia eta D. 26 irudia) izan ziren **32** konplexurako eta 1045.3 [M]$^+$ (D. 27 irudia eta D. 28 irudia) **33** konplexurako.

32 eta **33** konplexuek BH$_3$ modu berean koordinatutako beste konplexu batzuen portaera fluxional bereizgarria erakusten dute. Gainera, konplexu hauek iridapirazol eraztunean NH protoiaren trukea ere erakusten dute. Bi portaera hauek EMN espektroskopiaren bidez ikus daitezke.

Aztertutako lehen konplexua **32** konplexua izan zen, zeinetan zentro metalikoa trietilamina-borane estekatzaileari lotuta dagoen.

^{1}H EMN-ak (3.7 irudia) BH$_3$ taldearen portaera dinamikoari buruzko informazioa ematen du. Eremu altuko eskualdean hidruro bat ikus daiteke, -18.29 ppm-tan, J$_{P,H}$ = 16.1 Hz-eko akoplamendu-konstantea duen hirukote moduan, *cis* posizioan dauden bi fosforo-atomoren eraginez. **32** konplexuaren hidruroaren posizioa eta antzekoa den irida-β-dizetona motako **9** konplexuaren hidruroaren kokapena ia berdinak dira. Giro tenperaturan BH$_3$ taldeari dagokion seinalea -3.00 ppm-tan ikus daiteke. Seinale hau oso zabala da borano taldearen hiru B-H loturen arteko trukea etengabe gertatzen delako. Iridapirazol

eraztunaren NH-ari dagokion seinalea 12.11 ppm-tan agertzen da eta seinale zabala da.
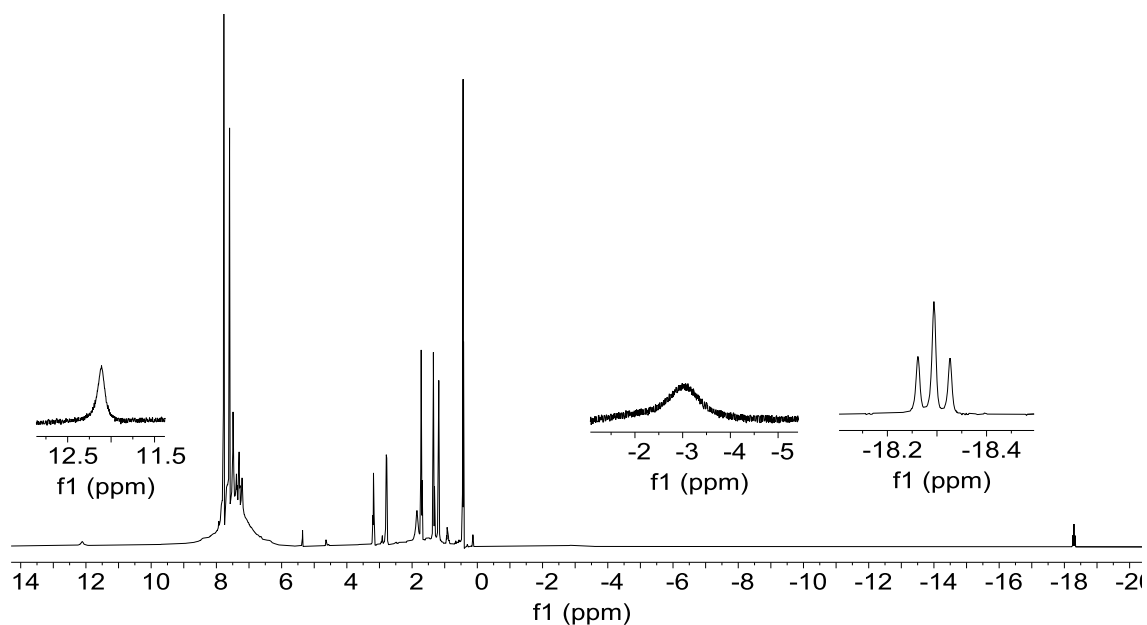
Figure 3.1 ^{1}H EMN of complex 32 in CDCl$_3$.

^{1}H EMN espektroak hainbat tenperaturatan neurtu ziren BH$_3$ taldeak eduki dezakeen B-H loturaren trukea frogatu nahian. BH$_3$ taldeari esleitutako seinale zabala, -3.00 ppm-tan agertzen dena, tenperatura jaisterakoan desagertzen da. EMN espektroa 233 K-etan neurtzen denean seinale bat -12.24 ppm-tan agertzen da, H bati dagokiona (3.8 irudia).Behaketa honek protoi terminal eta B-H zubiaren arteko trukea edo estekatzailearen disoziazioa gertatzen dela adierazten du. Tenperatura baxuetan 1.60 ppm inguruan BH$_3$ taldearen beste bi protoiei dagokien seinalea ikustea espero zitekeen; baina, zoritxarrez, ezin izan genuen identifikatu. Litekeena seinale hori trietil taldearen seinaleen azpian egotea da. **32** konplexuaren hidruroaren eta iridapirazol eraztunaren NH protoiaren seinaleek ez dute aldaketarik jasan tenperatura-tarte osoan.

Bestalde, $^{31}P\{^{1}H\}$ EMN espektroak iridapirazol eraztunaren NH protoiaren tautomerismoa erakusten du. Tenperatura baxuetan, bi seinale garbi ikus daitezke. Seinale horiek zabaldu eta koaleszentziara hurbiltzen dira tenperatura igotzen den heinean (B. 116 irudia).
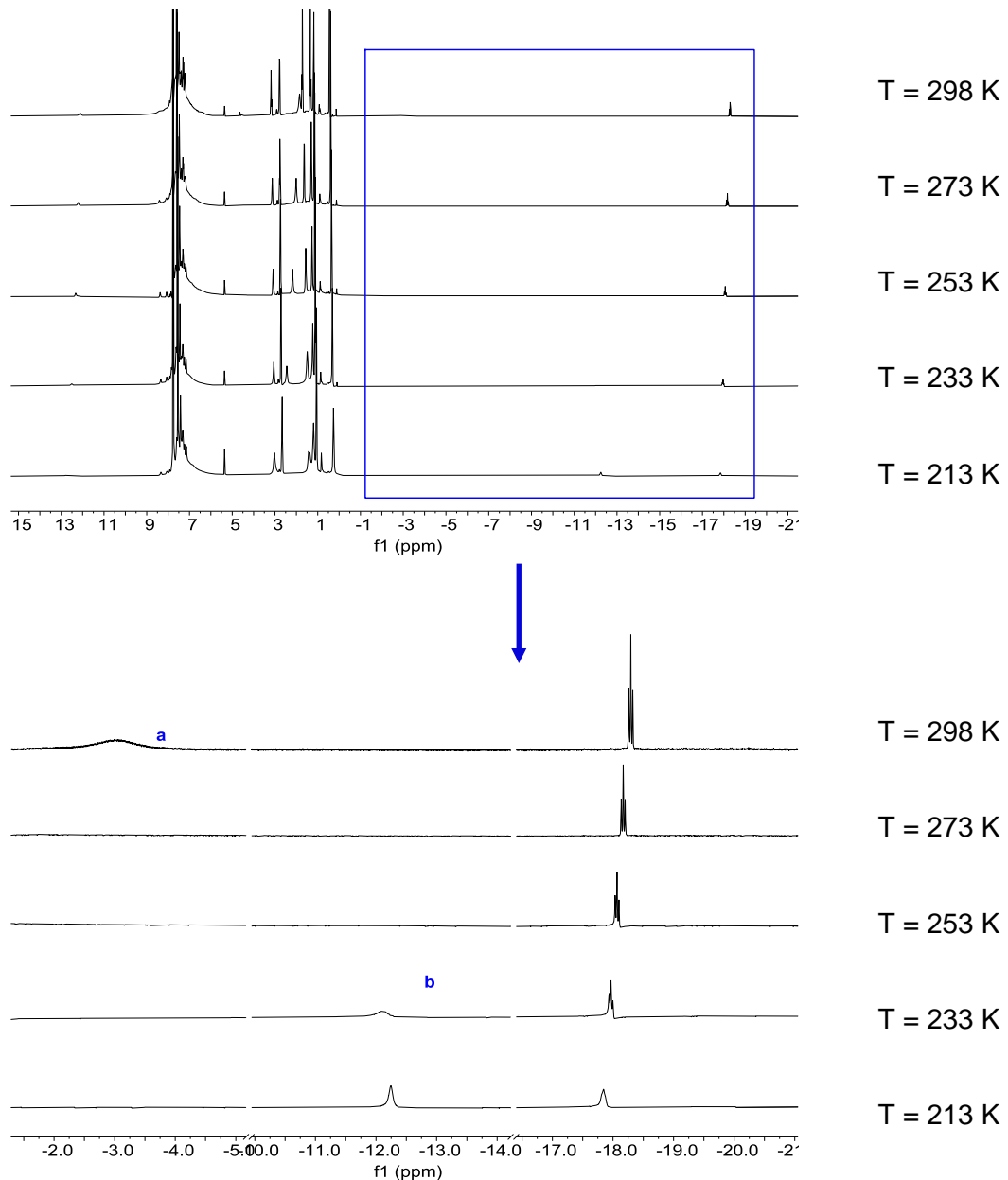
3.8 irudia. 32 konplexuaren ^{1}H EMN espektroa hainbat tenperaturatan eta CDCl$_3$-tan.

Erabilitako boranoa trifenilfosfina-boranoa denean, **33** konplexua lortzen da eta giro tenperaturan antzeko ^{1}H EMN espektroa ikus daiteke (3.9 irudia). Hirukote bikoitz bat ikus daiteke eremu altuko eskualdean, -18.02 ppm-tan eta hidruroaren seinalea da. Hidruroa *cis* posizioan dituen bi fosforo-atomorekin akoplatzen da, $J_{P,H}$ = 10.3 Hz-tako akoplamendu-konstantearekin, eta *trans* posizioan dagoen H_3B-PPh_3 estekatzailearekin (J = 16,3 Hz). BH_3 taldea -2.64 ppm-tan detekta daiteke, seinale zabal gisa. Azkenik, iridapirazol zikloak duen NH taldearen seinalea 11.92 ppm-tan ikus daiteke eta seinale zabala da.
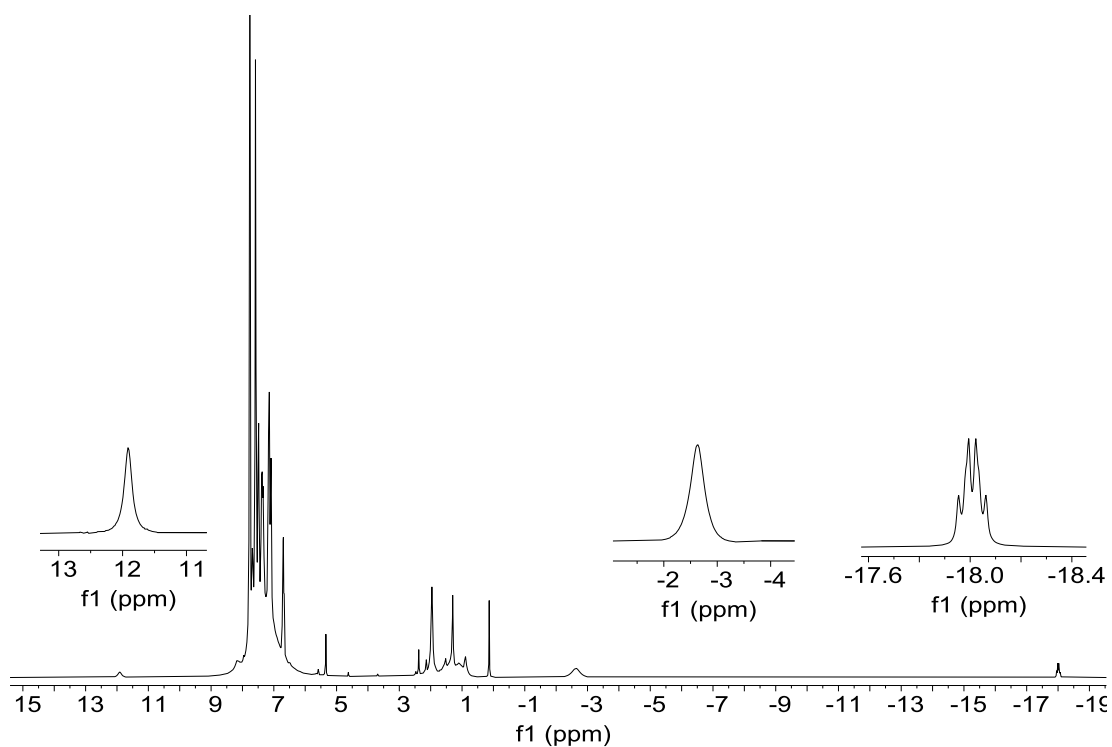
3.9 irudia. 33 konplexuaren ^{1}H EMN espektroa CD_2Cl_2-tan.

Giro tenperaturan neurtu den ^{31}P{^{1}H} EMN espektroak seinale oso zabalak ditu, eta hau zenbait prozesu fluxional agertzearen ondorio izan daiteke. Tenperatura 212 K-raino jaisten denean, lau seinale garbi ikus daitezke (ikus B. 117 irudia). 13.3 eta 17.6 ppm-tan agertzen diren singleteak iridapirazol eraztunari lotutako fosforo-atomoei eslei dakizkieke, eta -6.9 ppm-tan ikusten

den singletea BH_3 taldeari lotutako fosfinari. Laugarren seinalea, 18.9 ppm-tan agertzen dena, H_3B-PPh_3 librearen ondorio izan daiteke. Emaitza hauek direla eta, **33** konplexuan BH_3 protoi-trukean estekatzailearen disoziazioa inplikatuta dagoela proposatzen dugu.

3.3.1.2 Konplexu neutro baten formazioa

Konposatu neutro bat lortzeko nahian, hainbat saio egin ziren haluro eta hidruro iturriekin, baina zoritxarrez ez zen arrakastarik lortu. Bestalde, **3** konplexua gehiegizko $SnCl_2$-rekin erreakzionaraztean irida-β-dizetonekin egiterakoan lortutako antzeko emaitzak lortu ziren.[4] Erreakzio honetan, zentro metalikoari lotutako kloro atomoa eztainu atomora migratzen da eta trikloroeztainato konplexu bat sortzen da (3.10 irudia).
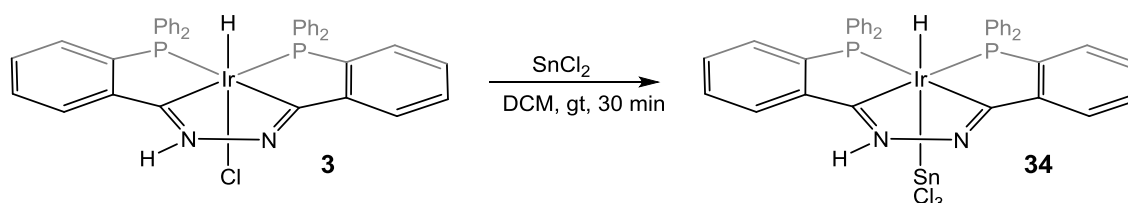
1.10 irudia. 3 konplexuaren erreakzioa eztainu dikloruroarekin 34 konplexua osatuz.

ν(Ir-H) tentsioa 2090 cm^{-1}-etan agertzen da IR espektroan, seinale zabal gisa, eta ν(Ir-H) tentsioa 1730 cm^{-1}-etan ikus daiteke.

Nukleo anitzeko EMN espektroak egin ziren **34** konplexurako. ^{1}H EMN espektroan seinale garrantzitsuena hidruroaren seinalea da. Hidruroarekiko *cis* posizioan dauden bi fosforo-atomoen eraginez, -12.85 ppm-tan hirukote bat ikus daiteke, $J_{P,H}$ = 16.9 Hz-tako akoplamendu-konstantearekin. Eztainu sateliteak $J_{119\ Sn,H}$ = 831.7 Hz eta $J_{117\ Sn,H}$ = 865.9 Hz-eko balioekin ikus

daitezke, eta honek hidruroa *trans* posizioan eztainu atomoarekiko dagoela frogatzen du (B. 118 irudia).

$^{31}P\{^{1}H\}$ EMN espektroak 10.2 ppm-tan singlete zorrotza erakusten du. Honek eta ^{1}H EMN espektroan NH-aren seinalerik ez ikusteak, giro tenperaturan **34** konplexua koaleszentzia-tenperaturaren oso gainetik dagoela esan nahi du. $^{31}P\{^{1}H\}$ EMN-an eztainuzko sateliteak ere ikus daitezke, eta $J_{119\ Sn,P}$ = 233.0 Hz eta $J_{117\ Sn,P}$ = 226.5 Hz-tako akoplamendu-konstanteak neurtu dira. Akoplamendu-konstante horien balioek eztainu atomoa fosforo atomoekiko *cis* posizioan dagoela adierazten dute (B. 119 irudia).

^{119}Sn EMN espektroa ere neurtu zen. Espektroan hirukote bikoitza agertzen da -146.5 ppm-tan ($J_{H,119\ Sn}$ = 1044.4 Hz eta $J_{P,119\ Sn}$ = 228,8 Hz) eta honek eztainu atomoarekiko hidruro bat *trans* posizioan eta bi fosforo *cis* daudela adierazten du (B. 120 irudia).

3.3.2 Erreaktibitatea iridapirazol eraztunean

3.3.2.1   Azido-base erreakzioak

Gure iridapirazol konplexua pirazol organikoek egin ditzaketen erreakzioak egiteko gai den ikusteko hainbat saiakera egin ziren. Aukeratutako lehenengo erreakzioak azidoekiko eta baseekiko erreakzioak izan ziren, pirazol eraztun protonatu eta desprotonatuak lortu nahian. Horretarako, aukeratutako azidoa azido tetrafluoroborikoa (HBF_4) izan zen, eta aukeratutako basea tetrabutilamonio hidroxidoa ($N(n\text{-}Bu)_4)(OH)$ (3.11 irudia).
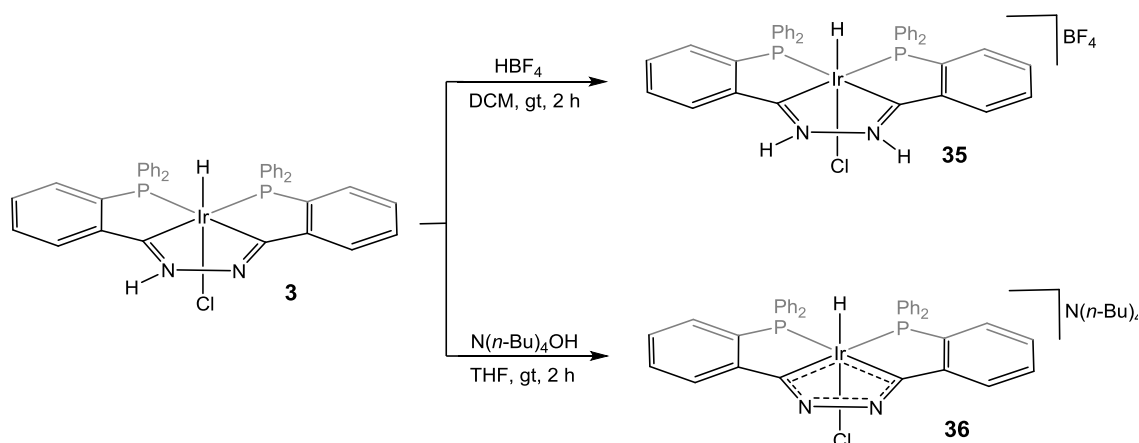
Figure 3.2 Reaction of complex 3 towards acid and bases.

3 konplexua aurretik aipatutako azido tetrafluoroborikoarekin erreakzionatu ondoren, **35** konplexu protonatua lortu zen. Konplexu honek iridapirazol eraztuneko bi nitrogeno atomoak protonatuta ditu, eta, beraz, hasierako materialean dagoen NH protoiaren fluxionaltasuna galdu du.

35 konplexua EMN multinuklearraren bitartez karakterizatu da. ^{1}H EMN espektroan bi seinale bereizgarri daude, bat hidruroarena eremu altuan eta bestea iridapirazol eraztuneko bi protoiena. Hidruroa hirukote baten moduan agertzen da -17.47 ppm-tan $J_{P,H}$ = 16.6 Hz-ko akoplamendu-konstante batekin, *cis* posizioan baliokideak diren bi fosforo-atomoren eraginez. NH bi protoiei dagokien seinalea 14.49 ppm-tan ageri da, singlete moduan.

^{31}P{^{1}H} EMN espektroak singlete bat erakusten du giro-tenperaturan 15.25 ppm-tan. Hau, portaera estatiko batekin bat dator, iridapirazol eraztuna protonatu delako eta **35** konplexua konplexu simetriko bihurtu delako. ^{13}C{^{1}H} espektroan, doblete bat ikusi daiteke 220.5 ppm-tan iminoaziliridio moteko konplexuak espero diren tartean,[4] akoplamendu-konstante handi batekin ($J_{P,C}$ = 97.6 Hz). Honek C=N taldeak fosforo-atomoekiko *trans* kokatuta daudela berresten du. ^{15}N EMN espektroa egin zen eta 206.7 ppm-tan singlete bat ikus daiteke. Balio hori pirazol organiko protonatuetan lortutakoaren antzekoa da.[67]

35 konplexuaren monokristal laranjak lortu ziren eter dietiliko lurruna **35**-ren kloroformozko disoluzio batera barreiatuz -20 ºC-tan, eta X Izpien difrakzioaren azterketa egin zen. Aukeratutako lotura-distantzien eta angeluen datuetarako ikus 3.3 taula.

3.3 taula. Aukeratutako 35-en lotura-distantziak (Å) eta angeluak (º). Desbiazio estandarra parentesi artean agertzen da.

Lotura-distantzia			
Ir1-P1	2.3321(11)	Ir1-Cl1	2.4835(11)
Ir1-P2	2.3333(11)	C1-N1	1.316(6)
Ir1-C1	1.973(4)	C2-N2	1.317(6)
Ir1-C2	1.983(4)	N1-N2	1.388(5)
Lotura-angelua			
P1-Ir1-C2	83.67(14)	Ir1-C2-N2	115.0(3)
P2-Ir1-C1	83.11(13)	C1-N1-N2	115.9(4)
C1-Ir1-C2	79.18(18)	C2-N2-N1	115.0(4)
Ir1-C1-N1	114.9(3)	C1-Ir1-Cl1	89.48(12)

35 konplexuan, iridio atomoaren koordinazio-ingurunea pixka bat distortsionatutako oktaedro bat da. Konplexuak hidruro bat eta kloro atomo bat ditu posizio axialetan, eta PCCP estekatzaile tetradentatu bat, posizio ekuatorial guztiak betetzen dituena.

35 konplexurako behatutako N–N distantzia (1.388(5) Å) **3** konplexuko distantzia esperimentala baino pixka bat motzagoa da (1.409(4) Å). Horrek esan nahiko du iridaziklo baten aromatizitatea handitu egin daitekeela haren protonazioarekin. Hori bat dator pirazol organikoaren kasuarekin, non N-N

distantzia ere murriztu egiten baita protonazioan, 1.351(10) Åtik[68] 1.343(6) Å[69]era aldatzen baita.

Iridapirazol eraztuneko C1–Ir1–C2 angelua (79,18(18)°) pirazol organikoek duten C-C-C angelua baino askoz txikiagoa da (106,5(5))[69]. Hori dela eta, iridapirazol eraztuneko gainerako angeluak handiagoak dira, eta 115º inguruko balioa dute guztiek. Pirazol organikoaren kasuan, beste angeluek C-C-C angeluaren oso antzeko balioak dituzte, 107º-tik 110º-ra bitartekoak.
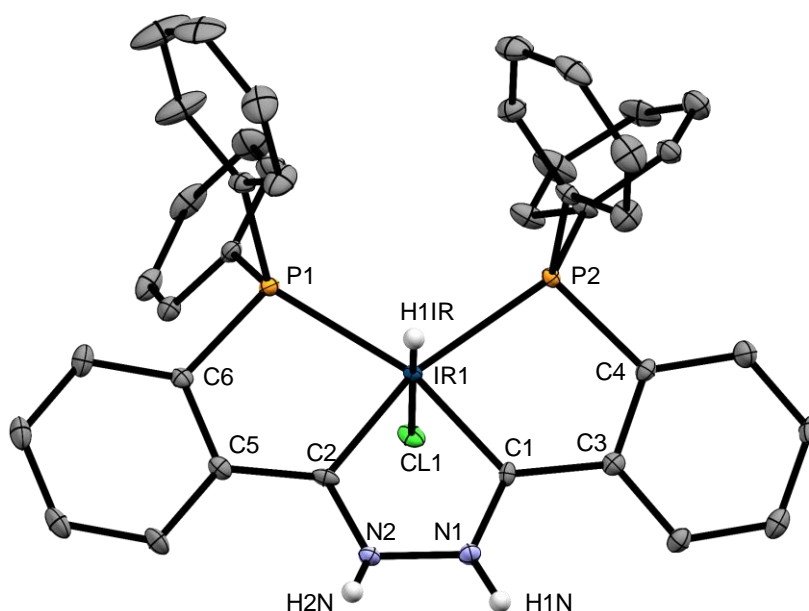
Figure 3.3 Molecular structure of complex 35 (elipsoideak % 50-ko probabilitarearekin).

Bestalde, **3** konplexuak tetrabutilamonio hidroxido basearekin erreakzionatzen duenean, iridapirazol eraztuneko protoia desagertu eta konplexu anioniko bat sortzen da, **36** konplexua.

[1]H EMN espektroan, hidruroa -21.01 ppm-tan ikus daiteke, $J_{P,H}$ = 15,9 Hz-tako akoplamendu konstantea duen hirukote gisa, *cis* posizioan dauden bi fosforo-atomoen eraginez. Espero zitekeen bezala, NH protoiaren seinalea ezin da ikusi **36** konplexuan. [31]P{[1]H} EMN espektroan, 18.9 ppm-tan singlete zorrotza ikusten da, aurreko fluxionaltasuna galdu dela adierazten duena.

Masa espektroa **36** konplexurako neurtu zen, baina kasu honetan ioi modu negatiboa hautatu zen. ESI-MS (m/z)-tik espero zen balioa lortu zen: 803.1 [M]⁻ (D. 31 irudia) eta (D. 32 irudia).

Oso ezaguna da pirazolatoen koordinazioa zentro metalikoei. Izan ere, hainbat metalaziklo sortzeko gai dira, hala nola 11. taldeko kobre(I) eta zilar(I) konplexu dimerikoak[70] eta urrezko konplexu trinuklearrak.[71] Pirazolatoak 4. taldeko metalei ere koordina daitezke η^2 moduan, η^2 pirazolato zirkonio eta hafnium konplexuetan bezala.[72] Gure iridapirazolatoak (**36**) trantsizio-metaleekiko antzeko portaera izan dezakeela frogatzeko, ZrCl$_4$ zirkonioaren gatzarekin erreakzionatu zen (3.13 irudia).
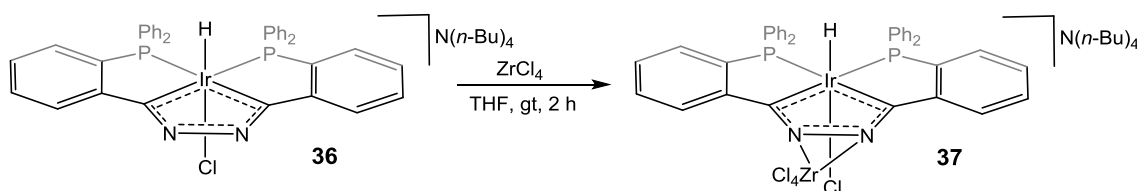
3.13 irudia. 37 konplexuaren formazioa.

37 konplexua EMN multinuklearraren bidez karakterizatu da. ¹H EMN espektroan, hidruroari dagokion seinalea ikus daiteke -17.63 ppm-tan, $J_{P,H}$ = 17.5 Hz-tako akoplamendu-konstantearekin. ³¹P{¹H} EMN espektroan, 15.5 ppm-tan singlete zorrotz bat ikus daiteke. Datu espektroskopiko hauen arabera, **37** konplexuak **36** konplexuak zuen simetriari eusten dio.

37 konplexua monomero bat dela frogatzeko, **36** konplexurako (B. 127 irudia) eta **37** konplexurako (B. 130 irudia) DOSY espektroak neurtu ziren. DOSY espektroetatik **36** eta **37** konplexuetarako difusio-koefizienteak lortzen dira, eta horiei Stokes-Einstein ekuazioa (1) aplikatzen zaie, konplexu bakoitzaren erradio hidrodinamikoa kalkulatzeko. Lortutako balioak r_s = 6,35 Å **36** konplexurako, eta r_s = 7,24 Å **37** konplexurako izan ziren. Balio hauek kontuan hartuz, **37** konplexuan zirkonioa pirazolato eraztunari lotuta dagoela eta monomero bat dela esan daiteke.

$$D = \frac{k \cdot T}{6\pi \cdot \eta \cdot r_s} \qquad \textbf{(1)}$$

3.3.2.2   Alkilazio-erreakzioak

Pirazol organikoen ohiko erreakzio mota bat alkilazio-erreakzioak dira. Azpikapitulu honen helburua gure iridapirazolak alkilazio-erreakzio batzuk egin ditzakeen ikustea da, hala nola metilazio erreakzioa. Horretarako, **3** konplexua sodio hidruro basearekin eta metilo ioduroarekin erreakzionarazi zen (3.14 irudia), indazoleen metilaziorako aurretik adierazitako baldintzetan.[73]
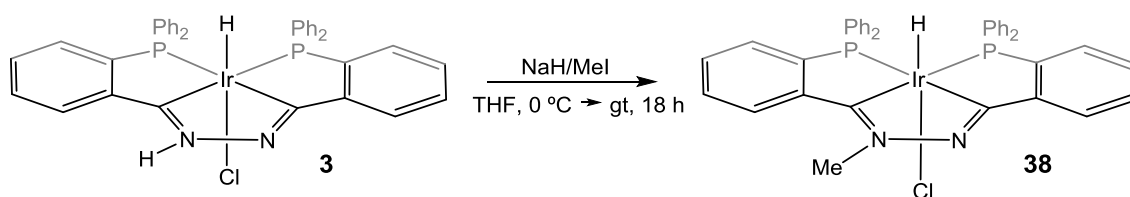
3.14 irudia. 38 konplexua, konplexu metilatuaren formazioa.

Nukleo anitzeko EMN espektroak neurtu ziren **38** konplexurako. ^{1}H EMN espektroan ez dago NH taldeari dagokion seinalerik, eta 4.45 ppm-tan singlete bat ikus daiteke, iridapirazol taldeari lotuta dagoen metiloari dagokiona. Beste seinale garrantzitsu bat -19.35 ppm-tan agertzen den hidruroaren seinalea da, $J_{P,H}$ = 16,9 Hz-tako akoplamendu-konstantearekin agertzen dena hirukote moduan. ^{31}P{^{1}H} EMN espektroan bi seinale ikus daitezke: singlete bat, 22.9 ppm-tan, eta bikote bat, 11.2 ppm-tan, $J_{P,P}$ = 5,6 Hz-tako akoplamendu-konstante batekin.

^{15}N EMN espektro bat ere egin zen **38** konplexurako eta bi singlete ikus daitezke, bat 240.3 ppm-tan, eta bestea, berriz, 369.0 ppm-tan. Eremu altuagoko seinalea, 240.3 ppm-takoa, metil taldea duen nitrogenoari dagokio. Azken hau pirazol organikoekin alderatutakoaren arabera ondorioztatu da.[66]

38 konplexua ESI-Mass espektroskopiaz karakterizatu zen ere. ESI-MS espektroan (m/z): 841.1 [M+Na]$^{+}$-ko balioa neurtu zen. (D. 33 irudia eta D. 34 irudia).

38 konplexua disolbatzaile protiko batean disolbatuz gero, metanola esaterako, gatz alkalino baten aurrean, kloro atomoa beste anioi batez ordezka daiteke. Prozesu hau arrakastatsua izanzen sodio ioduro eta potasio tiozianato gatzen kasuan (3.15 irudia).
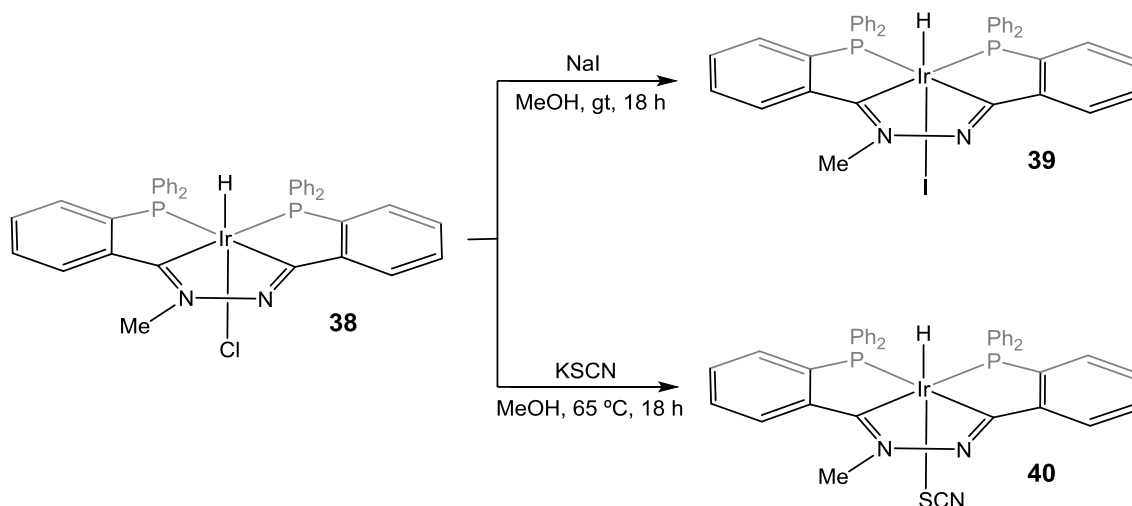
3.15 irudia. 39 eta 40 konplexuen formazioa.

39 konplexuak iodo atomo bat du hidruroarekiko *trans* posizioan. Kloruro/iodiduro metatesia ^{1}H EMN espektroan ikus daiteke (B. 134 irudia) hidruroaren seinalearen aldaketaren ondorioz. Hidruroa, orain, -16.46 ppm-tan agertzen da, $J_{P,H}$ = 16.7 Hz eta $J_{P,H}$ = 17.7 akoplamendu-konstanteak dituzten bikote bikoitz gisa, bi fosforo-atomoak ez-baliokideak direlako. Metil taldeko hiru protoiei dagokien seinalea 4.48 ppm-tan agertzen da singlete gisa, **38** konplexuan agertzen zen ia toki berean. ^{31}P{^{1}H} EMN espektroak desberdintasun handiagoak ikus daitezke. 15.0 eta 5.7 ppm-tan bi bikote zorrotz ikus daitezke, $J_{P,P}$ = 6.2 Hz-tako akoplamendu-konstantearekin (B.135 irudia).

Bestalde, potasio tiozianatoa erabiltzen denean bi isomero sintetiza daitezke, κ-S eta κ-N isomeroak. Erreakzioa giro tenperaturan egiten denean bi isomeroen nahasketa lortzen da. Hori ^{1}H EMN-aren bidez egiaztatu zen, bi

seinale desberdin ikus baitaitezke hidruroarentzat: bat nitrogeno-emaile taldea *trans* posizioan edukiz gero esperotako tartean eta beste bat sufre-emaile taldea edukiz gero esperotako tartean (B. 136 irudia). Konplexu bakar bat lortzeko nahian, erreakzioa errefluxu baldintzetan egin zen eta isomero termodinamikoa isolatu ahal izan zen, κ-S den **40** konplexua.

40 konplexua ^{1}H (B. 137 irudia) eta ^{31}P{^{1}H} (B. 138 irudia) EMN-aren bidez karakterizatu zen. ^{1}H EMN espektroan hidruroaren seinalea -15.58 ppm-tan ikus daiteke, $J_{P,H}$ = 16.9 Hz-tako akoplamendu-konstante bat duen hirukote gisa. Metil taldeari dagokion seinalea 4.59 ppm-tan ageri da, singlete baten moduan. ^{31}P{^{1}H} EMN espektroan bi singlete ikus daitezke, 10.3 eta 21.4 ppm-tan.

Bi konplexu horietarako masa-espektroskopia egin zen, eta lortutako balioak honako hauek izan ziren: ESi-MS (m/z): 901.1 [M+H]$^+$ eta 933.1 [M+Na]$^+$ **39** konplexurako (D. 35 irudia eta D. 36 irudia) eta 783.2 [M-SCN]$^+$ **40** konplexurako (D. 37 irudia eta 38 irudia).

39 konplexuaren monokristal laranjak lortu ziren **39**-ren kloroformozko disoluzio batetik -20 ºC-tan, eta X Izpien difrakzioaren azterketa egin ahal izan zen. Aukeratutako lotura-distantzien eta angeluen datuetarako ikus 3.4 taula.

39 konplexuan, iridio atomoaren koordinazio-ingurunea apur bat distortsionatutako oktaedroa da. Konplexuak hidruro bat eta iodo atomo bat ditu posizio axialetan, eta PCCP estekatzaile tetradentatu batek, posizio ekuatorial guztiak betetzen ditu (3.16 irudia).

39 konplexurako behatutako N–N distantzia (1.413(6) Å) **3** konplexurako aurkitutakoaren oso antzekoa da (1.409(4) Å). Metilazioak ez du iridapirazol eraztuneko sistema elektronikoan eragiten. Iridapirazol eraztuneko C1–Ir1–C2 angeluak 77.25(19)°-ko balioa du eta **3** eta **35** konplexuetarako aurkitutako balioa baino txikiagoa da Honen ondorioz, gainerako iridazikloaren angeluak beste konplexuetan iusitakoa baino handiagoak dira.

3.4 taula. Aukeratutako 39-en lotura-distantziak (Å) eta angeluak (º). Desbiazio estandarra parentesi artean agertzen da.

Lotura-distantzia

Ir1-P1	2.3150(12)	Ir1-I1	2.7574(4)
Ir1-P2	2.3109(11)	C1-N1	1.321(6)
Ir1-C1	1.997(5)	C2-N2	1.305(6)
Ir1-C2	2.003(4)	N1-N2	1.413(6)
N1-C1B	1.474(6)		

Lotura-angelua

P1-Ir1-C1	83.98(13)	Ir1-C2-N2	119.4(3)
P2-Ir1-C2	84.15(14)	C1-N1-N2	118.6(4)
C1-Ir1-C2	77.25(19)	C2-N2-N1	110.3(4)
Ir1-C1-N1	114.3(3)	C1-Ir1-I1	90.77(14)
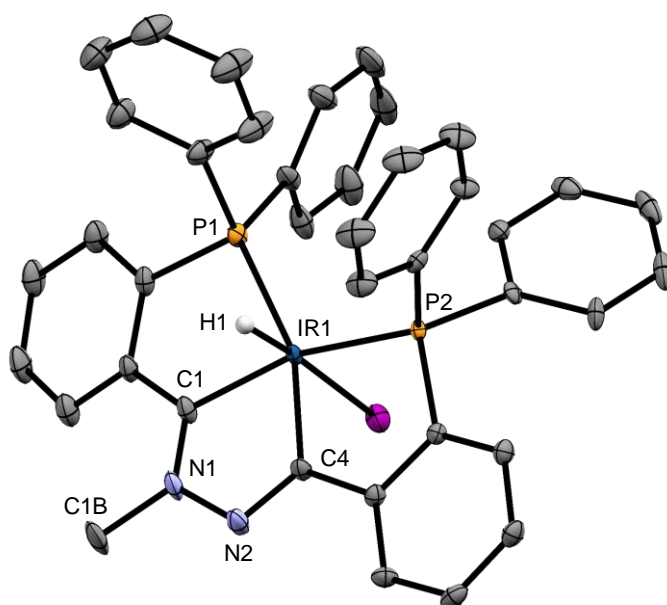
3.16 irudia. 38 konplexuaren egitura molekularra (elipsoideak % 50-ko probabilitarearekin)

Pirazolak selektiboki nitrogenoan alkilatzeko metodo bat etildiazoazetato (EDA) bezalako diazo konpposatuak erabiltzea da.[74] **3** konplexuan hau gerta daitekela frogatzeko EDA-arekin erreakzionarazi zen. Horretarako bi erreaktiboak diklorometanotan nahasi eta 48 orduz irabiatu ziren giro tenperaturan. Erreakzioaren ondorioz **41** konplexua sortu zen (3.17 irudia).
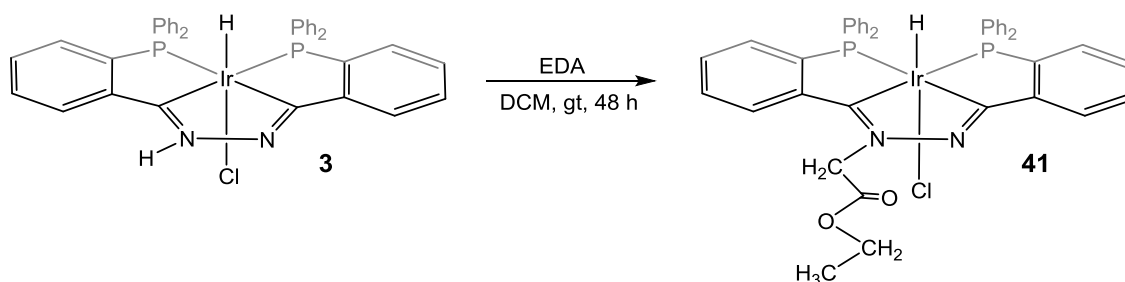
3.17 irudia. 41 konplexuaren formazioa.

41 konplexua nukleo anitzeko EMN eta ESI masa espektroskopiaren bidez karakterizatu zen. ^{1}H EMN espektroan hidruroarenseinalea -19.01 ppm-tan ikusten da, $J_{P,H}$ = 16.8 Hz-eko akoplamendu-konstantearekin, eta hirukote bat da. Behatutako hidruroaren seinalea metilatuta dagoen **38** konplexuaren seinalearen oso antzekoa da. 5.50 eta 5.63 ppm-tan bi bikote ikus daitezke, $J_{H,H}$ = 17.6 Hz-tako akoplamendu-konstantearekin; seinale hauek iridapirazol eraztunari lotuta dagoen CH_2 taldearen protoienak dira (B. 139 irudia).

^{31}P{^{1}H} EMN espektroan, bi bikote zorrotz ikus daitezke, 12.1 eta 20.4 ppm-tan, $J_{P,P}$ = 6,7 Hz-tako akoplamendu-konstantearekin (B. 140 irudia). Balio hauek eta **38** konplexurako lortutako baioak oso antzekoak dira.

ESI masa espektroskopia esperimentua **41** konplexurako ere egin zen. ESI-MS (m/z)-an honako balioa lortu zen: 913,15 [M+Na]$^+$ (D. 39 irudia eta D. 40 irudia).

3.4 Iridapirazoletik eratorritako konplexuen aktibitate katalitikoa amoniako-boranoaren metanolisian

2. kapituluan **1** eta **7** konplexuak AB-aren metanolisi homogeneorako katalizatzaile eraginkorrak direla frogatu da. Atal honetan, iridapirazoletik eratorritako konplexuak erreakzio homogeneo katalizatu horretarako probatuko dira. Iridapirazol konplexu horiek ez dira gai iridioaren inguruan berrantolaketa egiteko. Izan ere, PCCP estekatzaile sendoak planoaren lau posizioak betetzen baititu. Interesgarria izan daiteke konplexuen egituraren ezaugarri honek AB-aren metanolisiaren aktibitatean nola eragiten duen aztertzea.

27 – **31** konplexuak aurretik aipatutako erreakzio katalitikoan katalizatzaile gisa erabili ziren lehenengoak izan ziren. Konplexu horiek guztiek egitura berdina dute, desberdintasun bakarra hidruroarekiko *trans* posizioan dagoen estekatzailea da. Estekatzaile motak katalisian nola eragin dezakeen ikusteko konparatu ziren (3.18 irudia).
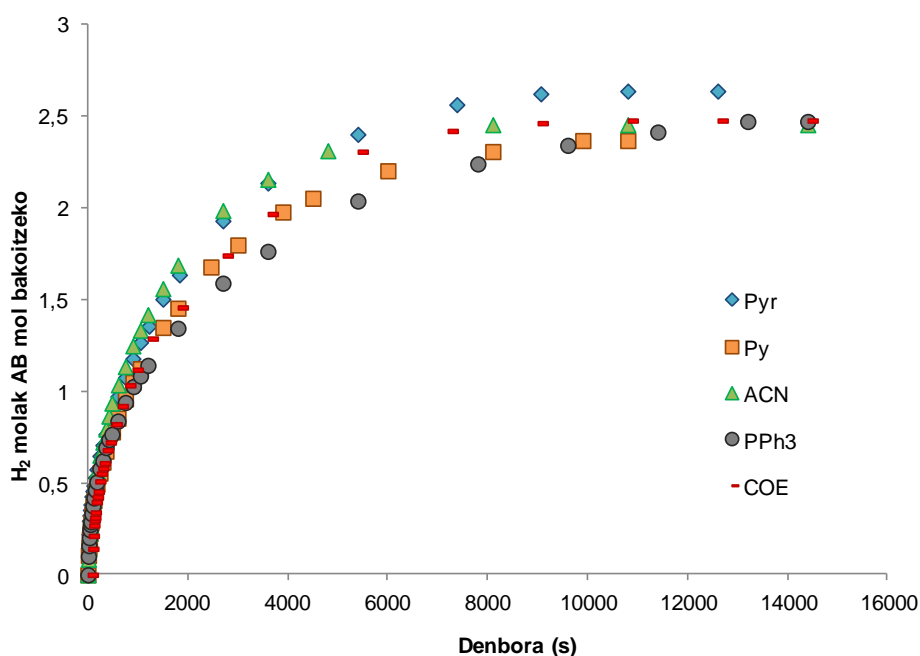
3.18 irudia. AB-aren metanolisitik askatutako hidrogenoa 27 – 31 konplexuak katalizatzaile moduan erabilita, metanoletan eta 35 ºC-tan egin da.

Aztertutako konplexu guztiek antzeko jarduera erakutsi zuten AB-aren metanolisian hidrogenoa katalitikoki askatzeko. Bost konplexuek 2.4 eta 2.6 hidrogeno-baliokide artean askatu zituzten 8100 eta 13200 segundo bitarteko denboretan.

3.18 irudian ageri diren profil zinetikoak [substratua]-rekiko pseudo-lehen-ordenako mendekotasuna dutela esan daiteke. Hori aplikatu zen abiadura konstanteak zehazteko, k_{ikus}, horretarako denbora *versus* Ln(1-(H_2 baliok./H_2 azken.baliok.) aurkeztu zen3.19 irudian.
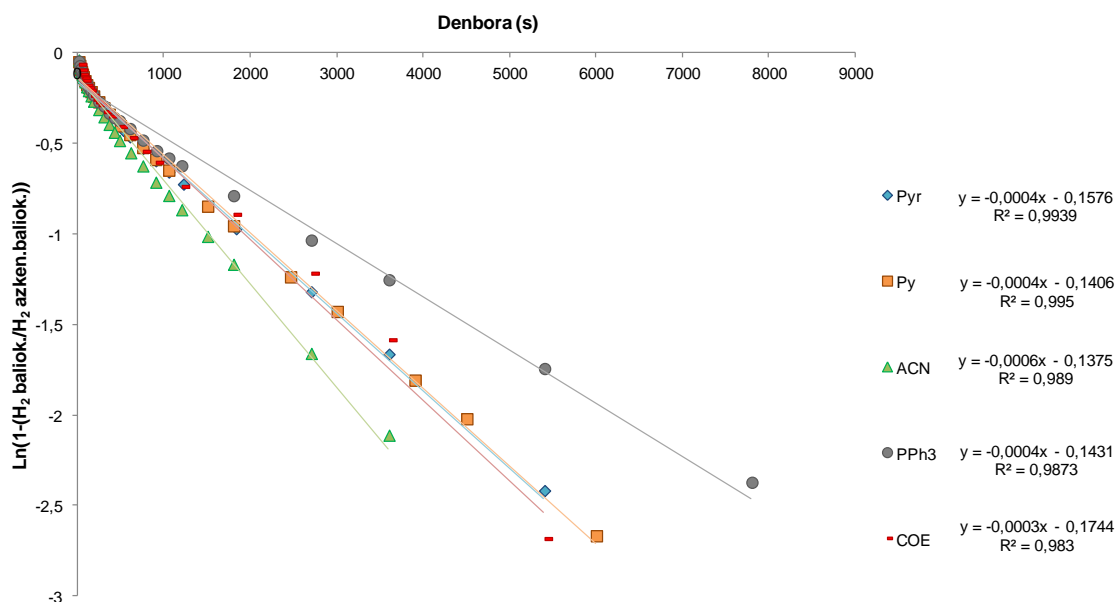
3.19 irudia. AB-aren metanolisiatik askatutako hidrogeno kopuruaren lehen ordenako grafikak 27-31 katalizatzaile moduan erabilita, metanoletan eta 35 ⁰C-tan egin da.

27 – **31** konplexuek katalizatutako AB-aren metanolisirako lortutako k_{ikus} balioak 3.5 taulan jaso dira, bai eta lortutako konbertsioa eta prozesurako behar den denbora ere. Konplexu hauek katalizatzaile gisa erabiliz lortutako erreakzio-abiadurak aurreko kapituluetan irida-β-dizetonatik eratorritako konplexuetarako aurkitutakoak baino askoz txikiagoak dira.

3.5 taula. Konbertsioaren %, beharrezko denbora, and konstanteen balioak AB-aren metanolisian 27 – 31 konpexuak katalizatzail gisa erabiliz, metanoletan eta 35 ºC-ta egin da.

Estekatzailea	% Konbertsioa	Denbora (s)	$10^3 \cdot k_{ikus}$ (s^{-1})
Pyrazola	88	10800	0.427 ± 0.007
Pyridina	79	9900	0.428 ± 0.006
Azetonitriloa	82	8100	0.570 ± 0.012
Trifenilfosfina	82	13200	0.294 ± 0.008
Cis-ziklooktenoa	82	10800	0.444 ± 0.011

32 konplexua, hemen aztertutako konplexuen oso antzekoa da, trietilamina-borano estekatzailea baitu hidruroarekiko *trans* posizioan koordinatua, eta erreakzio katalitiko honetarako ere probatu zen. **32** konplexuarentzat 0.427 ± 0,004 s^{-1} k_{ikus}-ko balioa kalkulatu zen eta % 81-eko konbertsioa lortu zuen 12600 s ondoren. **32** konplexuaren balioak **27 - 31** konplexuen 3.5 taulan ageri diren balioen tartearen barruan daude.

Datu hauek guztiak kontuan hartuta, konplexu hauek dituzten estekatzaileek eraginik ez dutela katalisiaren abiaduran esan daiteke. Ondorioz, kanpo-esferako mekanismo bat proposa daiteke.

AB-aren metanolisi katalitikoan iridapirazol motako konplexuen portaerari buruzko informazio gehiago biltzeko helburuarekin, iridapirazol eraztunean desberdintasun txikiak dituzten konplexuak aztertu ziren. Horretarako, **35 – 38** eta **41** konplexuak aukeratu ziren (3.20 irudia).
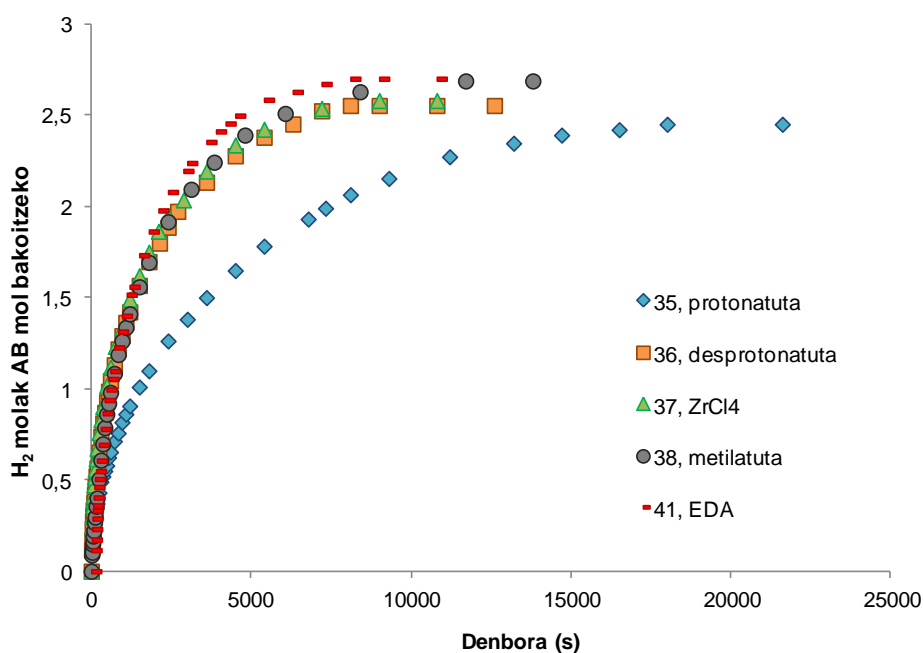
3.20 irudia. AB-aren metanolisitik askatutako hidrogenoa 35-38 eta 41 konplexuak katalizatzaile moduan erabilita, metanoletan eta 35 ⁰C-tan egin da.

Hautatutako konplexu guztiek antzeko jarduera katalitikoa erakutsi zuten **35** konplexua izan ezik. **35** konplexua protonatuta dagoen konplexu bakarra da eta ereakzio-abiadura baxuena azaltzen duena da. Profil zinetiko guztiek [substratu]-rekiko pseudo-lehen-ordenako mendekotasuna dutela onar daitezkeenez, ikuspegi hori abiadura konstanteak, k_{ikus}, zehazteko erabili zen (3.21 irudia).
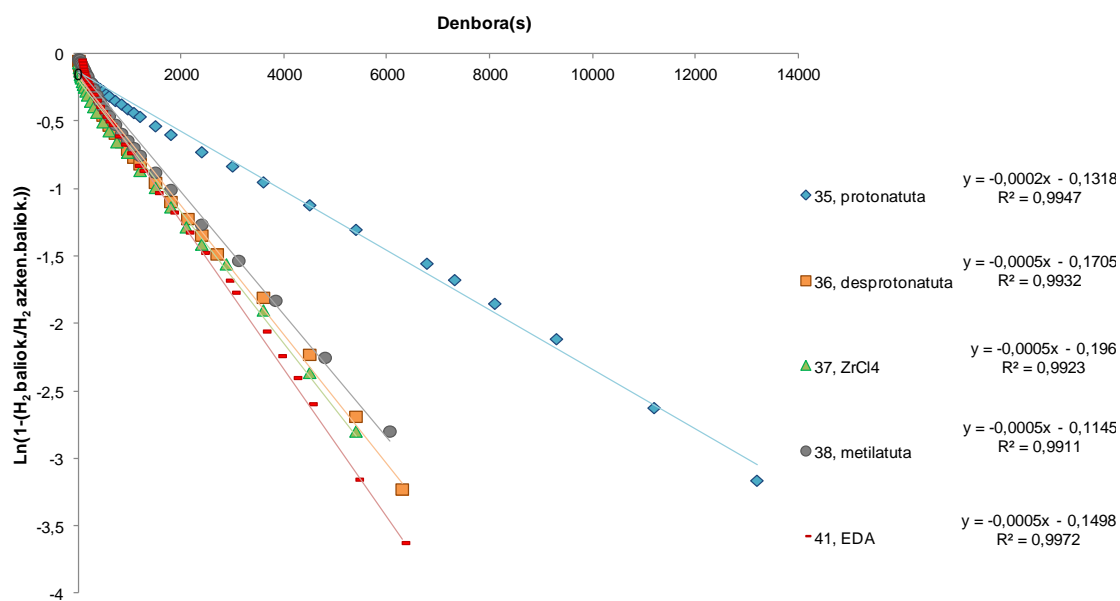
3.21 irudia. AB-aren metanolisiatik askatutako hidrogeno kopuruaren lehen ordenako grafikak 35-38 eta 41 konplexuak katalizatzaile moduan erabilita, metanoletan eta 35 ºC-tan egin da.

Konplexu horietarako lortutako k_{ikus} balioak 3.6 taulan jaso dira, bai eta lortutako konbertsioa eta katalisirako behar den denbora ere.

3.6 taula. Konbertsioaren %, beharrezko denbora, and konstanteen balioak AB-aren metanolisian 35-38 eta 41 konpexuak katalizatzail gisa erabiliz, metanoletan eta 35 ºC-ta egin da.

Konplexua	% Konbertsioa	Denbora (s)	$10^3 \cdot k_{ikus}$ (s^{-1})
35	82	16500	0.228 ± 0.003
36	85	8100	0.478 ± 0.007
37	86	9000	0.489 ± 0.009
38	90	11700	0.455 ± 0.008
41	90	8100	0.548 ± 0.005

Datu guztiak kontuan hartuta, ez da litekeena boranoaren eta iridioaren arteko koordinazioa katalisian zehar gertatzea; konplexu mota horien berri eman bada ere. Iridapirazol eraztuna aldatzeak eragina dauka katalisiaren abiaduran; horregatik esan liteke gutxienez elektroi bikote librea duen nitrogeno bat beharrezkoa dela katalisian abiadura handiagoak lortzeko. Litekeena da iridapirazol eraztunaren eta substratuaren arteko interakzioa prozesu katalitikoaren tartean egotea.

4. Kapitulua

Ondorioak

1. **1** eta **7** konplexuak, [IrHCl{(PPh$_2$(o-C$_2$H$_4$CO))$_2$H}] eta [(IrH{(PPh$_2$(o-C$_6$H$_4$CO))$_2$H})$_2$(μ-Cl)][BF$_4$] hurrenez hurren, AB-aren metanolisi homogeneoan hidrogeno askapenerako katalizatzaile gisa eraginkorrak direla frogatu da. Mekanismo sinplifikatu bat proposatu da zeinetan erreakzio katalizatua pauso paraleloetan eta bata bestearen atzetik gertatzen den. Gainera, hidrurodiazilo [IrH(H$_3$NBH$_{3-x}$(OCH$_3$)$_x$)(PPh$_2$(o-C$_6$H$_4$CO))$_2$] espeziea prozesu katalitikoan parte har dezakela proposatu da. Espezie honek borano-aduktu desberdinak koordinatuta eduki ditzake, denak irido atomoari borano taldetik koordinatuta daudenak. Borano-aduktuaren koordinazioa gertatu ondoren, metanol molekula batek eraso nukleozalea boro atomoan gauzatu lezake O-tik Ir-rako hidrogeno transferentzia eta hidrogeno askapena gertatuz. Deuterazio saiakerek O-H loturaren apurtzea AB-ren metanolisi katalizatuaren urrats erabakigarrian sartzen dela adierazi dute.

2. **1** konplexuaren eta trimetilamina-boranoaren arteko erreakzioaren ondorioz, borano taldea koordinatuta duen irida-β-dizetona motako [IrH(Me$_3$NBH$_3$){(PPh$_2$(o-C$_6$H$_4$CO))$_2$H}]$^+$, **9** konplexu berria sortu da. Konplexu honek portaera fluxionala erakusten du eta AB-aren metanolisi katalitikoan parte har dezakeen espeziearen antzeko konplexua da.

3. Iridapirazol motako **3** konplexua etekin handiagoarekin lortzeko bide sintetiko berri bat aurkeztu da. Horretarako **L$_1$** estekatzailea sintetizatu da PPh$_2$(o-C$_6$H$_4$CHO)-ren eta hidrazinaren arteko erreakzioaren bidez. [Ir(COD)Cl]$_2$ iridio dimeroaren eta **L$_1$**-en arteko erreakzioak modu erraz eta azkar batean **3** konplexua sortzen du.

4. **3** konplexuaren erreaktibitatea bi modu desberdinetan aztertu da: zentro metalikoaren erreaktibitatea eta pirazol eraztunaren erreaktibitate. Zentro metalikoaren erreaktibitatea aztertzeatik konplexu kationiko eta neutro berriak lortu dira kloro atomoaren ordez nitrogeno emaileak diren estekatzaileak, olefinak, trifenilfosfina, boranoak eta triklorostanatoa jarriz. Bestalde, konplexu kationiko bat lortu zen iridapirazol eraztunaren

protonazioaren bidez. Honekin batera, konplexu anioniko bat lortu zen desprotonazio erreakzioaren bidez eta konplexu neutro batzuk ere lortu ziren alkilazio-erreakzioen bidez.

5. Lortutako iridapirazol motako konplexu berriak katalizatzaile gisa probatu dira hidrogenoa askatzeko AB-aren metanolisi katalitikotik. Konplexu horien aktibitatea **1** eta **7** konplexuek erakusten dutena baino txikiagoa da; hau erabilitako konplexuek koordinazio-esfera berrantolatzeko gaitasunik ez dutelako gerta daiteke. Hala ere, aipatzekoa da **35** konplexuak katalisi horretarako erreakzio abiadura baxuena erakutsi zuela. Honek adierazten du elektroi bikote libre bat duen nitrogeno atomo bat beharrezkoa dela erreakzio abiadura altuagoak lortzeko.

5. Kapitulua

Alde esperimentala

5.1 Teknika instrumentalak

<u>Lan baldintza orokorrak</u>

Manipulazio guztiak, besterik ez bada adierazten, nitrogeno atmosfera azpian egin ziren, Schlenk teknika estandarrak erabiliz. Disolbatzaileak aldez aurretik nitrogeno azpian destilatu ziren, izozte- eta urtze-zikloetan desgasifikatu eta bahe molekularrekin hornitutako Schlenk-etan biltegiratu ziren.

<u>Amoniako- eta amina-borano solbolisia</u>

Hidrolisia

Amonioako-boranoaren hidrolisian THF/H_2O = 60/40 proportzio duten bolumen-nahasteak (bolumen osoa 3 mL izanik) eta % 0.5 mol-eko aurrekatalizatzaile kargak erabili ziren. Alde batetik, 1,38 mmol-eko amina-boranozko disoluzioa prestatu zen 1,2 mL uretan eta disoluzio hori 40 mL-ko matraze biribil batean jarri zen (matrazeak gas-hartune bat eta albo batean zigilatutako beso bat zuen). Matraze hori tubo baten bidez konektatu zen urez beteriko gasezko bureta batera. Bestetik, aldez aurretik lehortutako THF-tan aurrekatalizatzailearen disoluzioa (1.8 mL THF eta 0.007 mmol) prestatu zen. Azkenik, THF-tan prestatuko disoluzioa xiringa batekin agitazio magnetikoan zegoen amina-boranozko matrazera pasa zen katalisiari hasiera emateko. Une horretan, H_2 gasaren askapena hasi eta buretan desplazatutako uraren bolumena neurtzen hasi zen. Hidroilisiak sortutako bolumen-aldaketak presio atmosferikoan neurtu ziren, 20 eta 40 ºC artean.

Metanolisia

Hasteko, aukeratutako amina-borano aduktuaren 1,16 mmol-eko disoluzioa prestatu zen 2 mL metanoletan eta disoluzio hori 40 mL-ko matraze biribil batean jarri zen (matrazeak gas-hartune bat eta albo batean septu batez zigilatutako beso bat zuen). Matrazea tubo baten bidez konektatu zen urez beteriko gasezko bureta batera. Disoluzioa tenperatura jakin batean berotutako

ur bainuan murgildu zen nahi zen tenperatura lortzeko. Jarraitzeko, % 0,4 moleko karga duen aurrekatalizatzailearen disoluzioa ($4.64 \cdot 10^{-3}$ mmol 0.5 mL metanoletan) septuaren bidez xiringatu eta hidrogeno askapena berehala hasi zen. Azkenik, askatutako hidrogenoa buretan desplazatutako uraren bolumena neurtuz jarraitu zen. Metanolisi guztiak presio atmosferikoan (1 atm) eta airean egin ziren.

Bestalde, homogeneitate probak egiteko aurrekatalizatzaile/merkurio 1/70 mol proportzioa erabili zen. Horretarako katalisia aldez aurretik azaldutakoaren arabera prestatu eta merkurioa septuaren bidez xiringatu zen katalisiaren hasieran edo erdialdean.

Analisi elementala

Sintetizaturiko konplexuen karbono, nitrogeno, sufre eta hidrogeno masa ehunekoak analisi elementalaren bidez zehaztu ziren. Neurketak LECO Truspec Micro CHNS analizadorean egin ziren.

Konduktibitatea

Konduktibitatea giro tenperaturan neurtu zen Metrohm-Herisau 712 konduktometro elektriko batekin. Konduktometroak Metrohm 00450920 konduktibitate zelula dauka. Neurketak $2.5 \cdot 10^{-4}$ M-ko disoluzioetan egin ziren.

Espektroskopia infragorria

Infragorri espektroak Nicolet FTIR 510 espektrometro batean egin ziren, 4000-500 cm^{-1} bitarteko uhin luzeeren artean. Neurketak KBr pastilletan egin ziren.

Erresonantzia magnetiko nuklear espektroskopia (EMN)

^{1}H, ^{11}B, ^{11}B$\{^{1}$H$\}$, ^{13}C$\{^{1}$H$\}$, ^{15}N, ^{31}P, ^{31}P$\{^{1}$H$\}$ eta ^{119}Sn EMN espektroak Bruker AVD 500, 400 edo 300 MHz espektrometroetan neurtu ziren giro tenperaturan. ^{1}H eta ^{13}C$\{^{1}$H$\}$ EMN espektroak disolbatzaileen hondar seinaleekiko edo TMS barne patroiarekiko erreferentziatu ziren. ^{11}B eta ^{11}B$\{^{1}$H$\}$

EMN espektroak $BF_3 \cdot OEt_2$ kanpo patroiarekiko, $^{31}P\{^{1}H\}$ eta ^{31}P EMN espektroak H_3PO_4 (85%) kanpo patroiarekiko eta, azkenik, ^{119}Sn espektroak $SnMe_4$ kanpo patroiarekiko erreferentziatu ziren.

Elektroesprai ionizazio masa espektrometria (ESI-MS)

ESI-MS-ak Bruker MicrOTOF-Q ekipoan neurtu ziren. Lortutako balioak ioi molekular nagusiaren balioarekin eta distribuzio isotopikoarekin bat datozen aztertu zen.

X-Izpien difrakzioa

Lortutako monokristalak beirazko zuntz batean ipini eta Bruker D8 Venture ekipoarekin neurtu ziren. Ekipoa Photon detektorea eta MoKα erradiazioa (λ=0.71073 Å) duen grafitozko monokromadoreaz hornituta zegoen. SHELXS-97 eta SHELXS-2013 programak erabili ziren zuzeneko metodoen bidez estrukturak ebazteko.

5.2 Hasierako materialen sintesia

[Ir(COD)Cl]$_2$-aren sintesia

[Ir(COD)Cl]$_2$ konposatua Cushing-ek eta lankideek adierazitakoaren arabera sintetizatu zen. Honetarako IrCl$_3$·xH$_2$O eta 1,5-ziklooktadienoa ur eta isopropanol nahaste batean errefluxuan jarri ziren.[75]

PPh$_2$(*o*-C$_6$H$_4$CHO)-aren sintesia

O-(difenilfosfina)benzaldehidoa Liese-k eta lankideek adierazitaroaren arabera sintetizatu zen.[76]

(1), [IrHCl{(PPh$_2$(*o*-C$_6$H$_4$CO))$_2$H}]-ren sintesia

1 konplexua [Ir(COD)Cl]$_2$ eta PPh$_2$(*o*-C$_6$H$_4$CHO)-aren arteko erreakzioaren bidez lortzen da, erreakzioa metanoletan eta giro tenperturan ematen delarik.[4]

(2), [IrH$_2${(PPh$_2$(*o*-C$_6$H$_4$CO))$_2$H}]-ren sintesia

2 konplexua [IrHCl{(PPh$_2$(*o*-C$_6$H$_4$CO))$_2$H}], **(1)**, KOHrekin metanoletan errefluxuan ipiniz lortu zen.[4]

(7), [(IrH{(PPh$_2$(*o*-C$_6$H$_4$CO))$_2$H})$_2$(μ-Cl)]BF$_4$-ren sintesia

7 konplexua [IrHCl{(PPh$_2$(*o*-C$_6$H$_4$CO))$_2$H}] eta Et$_3$OBF$_4$-ren artean diklorometanotan eta giro tenperaturan gertatzen den erreakzioaren ondorioz lortu zen.[5]

(L$_1$), PPh$_2$(*o*-C$_6$H$_4$)CHNNCH(*o*-C$_6$H$_4$)PPh$_2$-ren sintesia

L$_1$ estekatzailea PPh$_2$(*o*-C$_6$H$_4$CHO) (2 mmol, 580.6 mg) eta hidrazina monohidratoaren (1 mmol, 48.5 μL) arteko erreakzioaren bidez lortu zen. Erreakzioa etanoletan gertatu zen. Suspentsioa berotu eta errefluxuan mantendu zen 5 orduz. Lortutako hauspeakina zentrifugatu, bi aldiz 5 mL metanolarekin garbitu eta hutsunepean lehortu zen. Solidoa

diklorometano/hexano nahasketa bat erabiliz berkristaldu zen. Lortutako etekina %84.

IR (KBr, cm^{-1}): 1614 (m), ν(C=N)

C$_{38}$H$_{30}$N$_2$P$_2$-ren analisi elementala:

Kalkulatua: C 79.15, H 5.24, N 4.86.

Neurtua: C 79.61, H 5.25, N 4.95.

^{1}H EMN (CDCl$_3$): δ 6.8-8.2 (28 H, Aromatikoak); 9.23 (d, $J_{P,H}$=4.5 Hz, ^2J_P, 2H, *H*-C=N) ppm.

^{31}P{^{1}H} EMN (CDCl$_3$): δ -14.6 (s) ppm.

^{15}N EMN (CDCl$_3$): δ 367.4 (s) ppm

5.3 Konplexuen sintesi eta karakterizazioa

(9), [IrH(H$_3$BNMe$_3$){(PPh$_2$(o-C$_6$H$_4$CO))(PPh$_2$(o-C$_6$H$_4$CO))H}] [BAr$^F_4$]-ren sintesia

(1), [IrHCl{PPh$_2$(o-C$_6$H$_4$CO))$_2$)H}]-zko diklorometano disoluzioa duen Schlenk batera trimetilamina-boranoa (0.037 mmol, 2.7 mg) gehitu zen. Ondoren, sodio tetrakis[3,5-bis(trifluorometil)fenil]borato gatza (0.037mmol, 32.8 mg) gehitu zen aurretik aipatutako nahastera eta 30 minutuz irabiatu zen giro tenperaturan. Erreakzioan sortutako NaCl gatza urarekin erauzi zen. Fase organikoa magnesio sulfatoarekin lehortu eta iragazi zen. Azkenik, disolbatzailea presio baxuan lurrundu eta solido hori argia jaso zen. Lortutako etekina %72.

IR (KBr, cm^{-1}): 2504 (w), ν(B-H$_t$); 2444 (w), ν(B-H$_t$); 1731 (br), ν(Ir-H); 1509 (m), ν(C=O)

IrC$_{74}$H$_{57}$P$_2$O$_2$NB$_2$F$_{24}$·(CH$_2$Cl$_2$)$_{0.6}$-ren analisi elementala:

Teorikoa: C 50.66, H 3.31, N 0.79.

Esperimentala: C 50.59, H 3.22, N 0.58.

^{1}H EMN (CDCl$_3$): δ -18.38 (t, ^{2}J$_{P,H}$= 14.6 Hz, 1H, H-Ir); -2.50 (br, 3H, H-B); 1.80 (s, 9H, H_3C); 7-8.5 (28H, Aromatikoak); 22.58 (br, 1H, O--H--O) ppm.

^{1}H EMN (CDCl$_3$) (-60 ºC): δ -18.09 (t, ^{2}J$_{P,H}$= 14.6 Hz, 1H, H-Ir); -10.50 (s, 1H, H-B); 1.42 (br, 2H, H-B); 1.80 (s, 9H, H_3C); 7-8.5 (28H, Aromatikoak); 22.75 (br, 1H, O--H--O) ppm.

^{31}P{^{1}H} EMN (CDCl$_3$): δ 23.1 (s) ppm.

ESI-MS (MeOH): C$_{41}$H$_{42}$BIrNO$_2$P$_2$-ren teorikoa: 846.24; esperimentala: 846.24 [M]$^+$.

Konduktibitatea (Λ$_M$): 130 ohm^{-1}·cm^2·mol^{-1}.

<u>**(27)**, [IrH(C$_3$H$_4$N$_2$){PPh$_2$(*o*-C$_6$H$_4$)CNNHC(*o*-C$_6$H$_4$)PPh$_2$}] [BAr$^F_4$]-ren sintesia</u>

Pirazola (0.037 mmol, 2.5 mg) **3** konplexuaren (0.037mmol, 30 mg) diklorometano suspentsioa duen Schlenk batera gehitu zen. Ondoren, sodio tetrakis[3,5-bis(trifluorometil)fenil]borato gatza (0.037mmol, 32.8 mg) gehitu eta berehala suspentsioa disoluzio bilakatu zen; disoluzioa 2 orduz irabiatu zen giro tenperaturan. Erreakzioan sortutako NaCl gatza urarekin erauzi zen. Fase organikoa magnesio sulfatoarekin lehortu eta iragazi zen. Azkenik, disolbatzailea presio baxuan lurrundu eta solido laranja jaso zen. Lortutako etekina %72.

IR (KBr, cm^{-1}): 2192 (br), v(Ir-H); 1610 (m), v(C=N)

IrC$_{73}$H$_{46}$BF$_{24}$N$_4$P$_2$-ren analisi elementala:

Teorikoa: C 51.57, H 2.73, N 3.30.

Esperimentala: C 51.31, H 2.80, N 3.29.

^{1}H EMN (CDCl$_3$, 298 K): δ -18.30 (t, ^{2}J$_{P,H}$= 16 Hz, 1H, *H*-Ir); 5.53 (t, ^{3}J$_{H,H}$= 2.5 Hz, 1H, *H*C (pyr)); 6.06 (m, 1H, *H*C (pyr)); 6.30 (d, ^{3}J$_{H,H}$= 2.5 Hz, 1H, *H*C (pyr)); 7-8.4 (40H, Aromatikoak); 12.54 (br, 1H, *H*-N) ppm.

^{31}P{^{1}H} EMN (CDCl$_3$, 213 K): δ 19.4 (s); 25.0 (s) ppm.

^{15}N EMN (CDCl$_3$, 298 K): δ 285.6 (s) ppm.

ESI-MS (MeOH): IrC$_{41}$H$_{34}$N$_4$P$_2$-ren teorikoa: 837.2; esperimentala: 837.2 [M]$^+$.

Konduktibitatea (Λ$_M$): 70 ohm^{-1}·cm^2·mol^{-1}.

<u>**(28)**, [IrH(C$_5$H$_5$N){PPh$_2$(*o*-C$_6$H$_4$)CNNHC(*o*-C$_6$H$_4$)PPh$_2$}] [BAr$^F_4$]-ren sintesia</u>

Piridina (0.037 mmol, 3 µL) **3** konplexuaren (0.037mmol, 30 mg) diklorometano suspentsioa duen Schlenk batera gehitu zen. Ondoren, sodio tetrakis[3,5-bis(trifluorometil)fenil]borato gatza (0.037mmol, 32.8 mg) gehitu eta

berehala suspentsioa disoluzio bilakatu zen; disoluzioa 2 orduz irabiatu zen giro tenperaturan. Erreakzioan sortutako NaCl gatza urarekin erauzi zen. Fase organikoa magnesio sulfatoarekin lehortu eta iragazi zen. Azkenik, disolbatzailea presio baxuan lurrundu eta solido laranja jaso zen. Lortutako etekina %68.

IR (KBr, cm^{-1}): 2191 (br), ν(Ir-H); 1608 (m), ν(C=N)

IrC$_{75}$H$_{48}$BF$_{24}$N$_3$P$_2$·(CH$_2$Cl$_2$)-ren analisi elementala:

Teorikoa: C 52.14, H 2.82, N 2.42.

Esperimentala: C 51.96, H 2.82, N 2.05.

^{1}H EMN (CDCl$_3$, 298 K): δ -18.57 (t, $^2J_{P,H}$= 15.9 Hz, 1H, *H*-Ir); 6.9-8.3 (46H, Aromatikoak); 13.45 (br, 1H, *H*-N) ppm.

^{31}P{^{1}H} EMN (CDCl$_3$, 213 K): δ 22.7 (s); 26.9 (s) ppm.

ESI-MS (MeOH): IrC$_{43}$H$_{36}$N$_3$P$_2$-ren teorikoa: 848.2; esperimentala: 848.2 [M]$^+$.

Konduktibitatea (Λ$_M$): 80 ohm^{-1}·cm^2·mol^{-1}.

(29), [IrH(C$_2$H$_3$N){PPh$_2$(*o*-C$_6$H$_4$)CNNHC(*o*-C$_6$H$_4$)PPh$_2$}] [BAr$^F_4$]-ren

Azetonitriloa (1.9 mmol, 100 µL) **3** konplexuaren (0.037mmol, 30 mg) diklorometano suspentsioa duen Schlenk batera gehitu zen. Ondoren, sodio tetrakis[3,5-bis(trifluorometil)fenil]borato gatza (0.037mmol, 32.8 mg) gehitu eta berehala suspentsioa disoluzio bilakatu zen; disoluzioa 2 orduz irabiatu zen giro tenperaturan. Erreakzioan sortutako NaCl gatza urarekin erauzi zen. Fase organikoa magnesio sulfatoarekin lehortu eta iragazi zen. Azkenik, disolbatzailea presio baxuan lurrundu eta solido laranja jaso zen. Lortutako etekina %64

IR (KBr, cm^{-1}): 2190 (br), ν(Ir-H); 1631 (m), ν(C=N)

IrC$_{72}$H$_{45}$BF$_{24}$IrN$_3$P$_2$-ren analisi elementala:

Teorikoa: C 51.69, H 2.71, N 2.51.

Esperimentala: C 51.39, H 2.67, N 2.36.

^{1}H EMN (CDCl$_3$): δ -18.02 (t, $^2J_{P,H}$= 14.6 Hz, 1H, *H*-Ir); 2.29 (s, 3H, *H*$_3$C); 7.1-8.4 (40H, Aromatikoak); 12.18 (br, 1H, *H*-N) ppm.

^{31}P{^{1}H} EMN (CDCl$_3$): δ 18.8 (s); 23.7 (s) ppm.

ESI-MS (MeOH): IrC$_{40}$H$_{33}$N$_3$P$_2$-ren teorikoa: 810.2; esperimentala: 810.2 [M]$^+$.

Konduktibitatea (Λ$_M$): 80 ohm^{-1}·cm^2·mol^{-1}.

(30), [IrH(PPh$_3$){PPh$_2$(*o*-C$_6$H$_4$)CNNHC(*o*-C$_6$H$_4$)PPh$_2$}] [BAr$^F_4$]-ren sintesia

Trifenilfosfina (0.037 mmol, 9.7 mg) **3** konplexuaren (0.037mmol, 30 mg) diklorometano suspentsioa duen Schlenk batera gehitu zen. Ondoren, sodio tetrakis[3,5-bis(trifluorometil)fenil]borato gatza (0.037mmol, 32.8 mg) gehitu eta berehala suspentsioa disoluzio bilakatu zen; disoluzioa 2 orduz irabiatu zen giro tenperaturan. Erreakzioan sortutako NaCl gatza urarekin erauzi zen. Fase organikoa magnesio sulfatoarekin lehortu eta iragazi zen. Azkenik, disolbatzailea presio baxuan lurrundu eta solido laranja jaso zen. Lortutako etekina %70.

IR (KBr, cm^{-1}): 2113 (br), v(Ir-H); 1610 (m), v(C=N)

IrC$_{88}$H$_{57}$BF$_{24}$IrN$_2$P$_3$-ren analisi elementala:

Teorikoa: C 55.80, H 3.03, N 1.48.

Esperimentala: C 56.10, H 3.17, N 1.59.

^{1}H EMN (CDCl$_3$): δ -12.31 (dt, $^2J_{P,H}$= 19.6 Hz, $^2J_{P,H}$= 89.3 Hz, 1H, *H*-Ir); 6.4-8.6 (55H, Aromatikoak); 12.50 (br, 1H, *H*-N) ppm.

^{31}**P{^{1}H} EMN (CDCl$_3$):** δ -5.0 (s); 6.1 (s); 11.4 (s) ppm.

ESI-MS (MeOH): IrC$_{56}$H$_{45}$N$_2$P$_3$-ren teorikoa: 1031.2; esperimentala: 1031.2 [M]$^+$.

Konduktibitatea (Λ$_M$): 80 ohm^{-1}·cm^2·mol^{-1}.

(31), [IrH(C$_8$H$_{12}$){PPh$_2$(_o_-C$_6$H$_4$)CNNHC(_o_-C$_6$H$_4$)PPh$_2$}] [BAr$^F_4$]-ren sintesia

Cis,cis-1,5-cyclooctadiene (0.037 mmol, 4.5 μL) **3** konplexuaren (0.037mmol, 30 mg) diklorometano suspentsioa duen Schlenk batera gehitu zen. Ondoren, sodio tetrakis[3,5-bis(trifluorometil)fenil]borato gatza (0.037mmol, 32.8 mg) gehitu eta berehala suspentsioa disoluzio bilakatu zen; disoluzioa 2 orduz irabiatu zen giro tenperaturan. Erreakzioan sortutako NaCl gatza urarekin erauzi zen. Fase organikoa magnesio sulfatoarekin lehortu eta iragazi zen. Azkenik, disolbatzailea presio baxuan lurrundu eta solido laranja jaso zen. Lortutako etekina %65.

IR (KBr, cm^{-1}): 1610 (m), ν(C=N)

IrC$_{78}$H$_{56}$BF$_{24}$IrN$_2$P$_2$-ren analisi elementala:

Teorikoa: C 53.77, H 3.24, N 1.61.

Esperimentala: C 53.51, H 3.12, N 1.48.

^{1}**H EMN (CDCl$_3$):** δ -12.26 (t, $^2J_{P,H}$= 19.6 Hz, 1H, _H_-Ir); 6.5-8.4 (40H, Aromatikoak); 11.96 (br, 1H, _H_-N) ppm.

^{31}**P{^{1}H} EMN (CDCl$_3$):** δ 11.6 (s); 15.5 (s) ppm.

ESI-MS (MeOH): IrC$_{38}$H$_{30}$N$_2$P$_2$-ren teorikoa: 769.2; esperimentala: 769.2 [M-COE]$^+$.

Konduktibitatea (Λ$_M$): 80 ohm^{-1}·cm^2·mol^{-1}.

(32), [IrH(C$_6$H$_{18}$NB){PPh$_2$(*o*-C$_6$H$_4$)CNNHC(*o*-C$_6$H$_4$)PPh$_2$}] [BAr$^F_4$]-ren sintesia

Trimethylamineborane (0.037 mmol, 5.5 µL) **3** konplexuaren (0.037mmol, 30 mg) diklorometano suspentsioa duen Schlenk batera gehitu zen. Ondoren, sodio tetrakis[3,5-bis(trifluorometil)fenil]borato gatza (0.037mmol, 32.8 mg) gehitu eta berehala suspentsioa disoluzio bilakatu zen; disoluzioa 2 orduz irabiatu zen giro tenperaturan. Erreakzioan sortutako NaCl gatza urarekin erauzi zen. Fase organikoa magnesio sulfatoarekin lehortu eta iragazi zen. Azkenik, disolbatzailea presio baxuan lurrundu eta solido laranja jaso zen. Lortutako etekina %64.

IR (KBr, cm^{-1}): 2090 (br), v(Ir-H); 1730 (m), v(C=N)

IrC$_{76}$H$_{60}$BF$_{24}$IrN$_3$P$_2$-ren analisi elementala:

Teorikoa: C 52.25, H 3.46, N 2.41.

Esperimentala: C 51.96, H 3.22, N 2.04.

^{1}H EMN (CDCl$_3$, 298K): δ -18.29 (t, ^{2}J$_{P,H}$ = 16.1 Hz, 1H, *H*-Ir); -3.00 (br, 3H, *H*-B); 1.11 (t, ^{4}J$_{P,H}$= 7.3 Hz, 3H, *H$_3$*C); 2.72 (q, ^{4}J$_{P,H}$= 7.3 Hz, 2H, *H$_2$*C); 6.8-8.4 (40H, Aromatikoak); 12.11 (br, 1H, *H*-N) ppm.

^{1}H EMN (CDCl$_3$, 213K): δ -17.84 (t, ^{2}J$_{P,H}$ = 16.1 Hz, 1H, *H*-Ir); -12.24 (s, 1H, *H*-B); 1.11 (t, ^{4}J$_{P,H}$= 7.3 Hz, 3H, *H$_3$*C); 2.72 (q, ^{4}J$_{P,H}$= 7.3 Hz, 2H, *H$_2$*C); 7-8.5 (40H, Aromatikoak); 12.11 (br, 1H, *H*-N) ppm.

^{31}P{^{1}H} EMN (CDCl$_3$): δ 13.6 (s); 17.6 (s) ppm.

ESI-MS (MeOH): IrC$_{44}$H$_{48}$BN$_3$P$_2$-ren teorikoa: 884.3; esperimentala: 884.3 [M]$^+$.

Konduktibitatea (Λ$_M$): 80 ohm^{-1}·cm^2·mol^{-1}.

(33), [IrH(H$_3$BPPh$_3$){PPh$_2$(*o*-C$_6$H$_4$)CNNHC(*o*-C$_6$H$_4$)PPh$_2$}] [BAr$^F_4$]-ren sintesia

Trifenilfosphinaborano (0.037 mmol, 10.2 mg) **3** konplexuaren (0.037mmol, 30 mg) diklorometano suspentsioa duen Schlenk batera gehitu zen. Ondoren, sodio tetrakis[3,5-bis(trifluorometil)fenil]borato gatza (0.037mmol, 32.8 mg) gehitu eta berehala suspentsioa disoluzio bilakatu zen; disoluzioa 2 orduz irabiatu zen giro tenperaturan. Erreakzioan sortutako NaCl gatza urarekin erauzi zen. Fase organikoa magnesio sulfatoarekin lehortu eta iragazi zen. Azkenik, disolbatzailea presio baxuan lurrundu eta solido laranja jaso zen. Lortutako etekina %68.

^{1}H EMN (CDCl$_3$, 298K): δ -18.02 (dt, ^{2}J$_{P,H}$= 10.3 Hz, ^{4}J$_{P,H}$= 16.3 Hz, 1H, *H*-Ir); -2.64 (br, 3H, *H*-B); 6.4-8.4 (40H, Aromatikoak); -11.92 (br, 1H, *H*-N) ppm.

^{31}P{^{1}H} EMN (CDCl$_3$, 213K): δ -6.9 (s); 13.3 (s); 17.6 (s) ppm.

ESI-MS (MeOH): IrC$_{56}$H$_{48}$BN$_2$P$_3$-ren teorikoa: 1045.3; esperimentala: 1045.3 [M]$^+$.

Konduktibitatea (Λ$_M$): 80 ohm^{-1}·cm^2·mol^{-1}.

(34), [IrH(SnCl$_3$){PPh$_2$(*o*-C$_6$H$_4$)CNNHC(*o*-C$_6$H$_4$)PPh$_2$}]-ren sintesia

SnCl$_2$ (0.074mmol, 14.0 mg) **3** konplexuaren (0.037mmol, 30 mg) diklorometano suspentsioa duen Schlenk batera gehitu eta 30 minutuz irabiatu zen. Ondoren, erreakzionatu gabeko SnCl$_2$-a iragaziz kendu zen. Azkenik, disolbatzailea presio baxuan lurrundu eta solido laranja argi bat jaso zen. Lortutako etekina %58.

IR (KBr, cm^{-1}): 2090 (br), v(Ir-H); 1730 (m), v(C=N)

IrC$_{38}$H$_{30}$N$_2$P$_2$SnCl$_3$·(CHCl$_3$)$_{0.5}$-ren analisi elementala:

Teorikoa: C 43.89, H 2.92, N 2.66.

Esperimentala: C 43.96, H 2.55, N 2.50.

^{1}H EMN (CDCl$_3$): δ -12.85 (t, eztainu sateliteekin, $^2J_{P,H}$= 16.9 Hz, $^2J_{119_{Sn,H}}$= 831.7 Hz, $^2J_{117_{Sn,H}}$= 865.9 Hz, 1H, *H*-Ir); 6.8-8.5 (28H, Aromatikoak) ppm.

^{31}P{^{1}H} EMN (CDCl$_3$): δ 10.2 (s, eztainu sateliteekin, $^2J_{119_{Sn,P}}$= 233.0 Hz, $^2J_{117_{Sn,P}}$= 226.5 Hz) ppm.

^{119}Sn EMN (CDCl$_3$): δ -146.5 (dt, $^2J_{H,119_{Sn}}$= 1044.4 Hz, $^2J_{P,119_{Sn}}$= 228.8 Hz) ppm.

Konduktibitatea (Λ$_M$): 20 ohm^{-1}·cm^2·mol^{-1}.

(35), [IrHCl{PPh$_2$(*o*-C$_6$H$_4$)CNHNHC(*o*-C$_6$H$_4$)PPh$_2$}] [BF$_4$]-ren sintesia

HBF$_4$·O(CH$_2$CH$_3$)$_2$ (0.037 mmol, 5 µL) **3** konplexuaren (0.037mmol, 30 mg) diklorometano suspentsioa duen Schlenk batera gehitu eta berehala suspentsioa disoluzio bilakatu zen; 2 orduz irabiatu zen giro tenperaturan. Ondoren, disolbatzailea presio baxuan lurrundu eta solido laranja bat jaso zen. Lortutako etekina %85.

IR (KBr, cm^{-1}): 2182 (br), ν(Ir-H); 1614 (m), ν(C=N)

IrC$_{38}$H$_{31}$N$_2$P$_2$ClBF$_4$-ren analisi elementala:

Teorikoa: C 51.16, H 3.50, N 3.14.

Esperimentala: C 50.60, H 3.12, N 3.51.

^{1}H EMN (CDCl$_3$): δ -17.47 (t, $^2J_{P,H}$= 16.6 Hz, 1H, *H*-Ir); 6.4-8.4 (40H, Aromatikoak); 14.49 (br, 2H, *H*-N) ppm.

^{31}P{^{1}H} EMN (CDCl$_3$): δ 15.25 (s) ppm.

^{13}C{^{1}H} EMN (CDCl$_3$): δ 220.5 (d, $^2J_{P,C}$= 97.6 Hz) ppm.

^{15}N EMN (CDCl$_3$): δ 206.7 (s), 120-150 (Aromatikoak) ppm.

ESI-MS (MeOH): Teorikoa for IrC$_{38}$H$_{30}$N$_2$P$_2$: 769.2; esperimentala: 769.2 [M-H-Cl]$^+$.

Konduktibitatea (Λ$_M$): 60 ohm^{-1}·cm^2·mol^{-1}.

(36), [IrHCl{PPh$_2$(*o*-C$_6$H$_4$)CNNC(*o*-C$_6$H$_4$)PPh$_2$}] [N(n-Bu)$_4$]-ren sintesia

Tetrabutilamonio hidroxidoa, %40 pisuan uretan dena (0.037 mmol, 24.2 µL) **3** konplexuaren (0.037mmol, 30 mg) tetrahidrofurano suspentsioa duen Schlenk batera gehitu eta berehala suspentsioa disoluzio bilakatu zen; 2 orduz irabiatu zen giro tenperaturan. Ondoren, disolbatzailea presio baxuan lurrundu eta solido laranja ilun bat jaso zen. Solidoa bitan garbitu zen eter dietilikoarekin. Lortutako etekina %78.

IR (KBr, cm^{-1}): 2161 (br), ν(Ir-H); 1620 (m), ν(C=N)

IrC$_{54}$H$_{65}$N$_3$P$_2$Cl-ren analisi elementala:

Teorikoa: C 62.02, H 6.27, N 4.02.

Esperimentala: C 61.78, H 6.13, N 3.99.

^{1}H EMN (CDCl$_3$): δ -21.01 (t, ^{2}J$_{P,H}$= 15.9 Hz, 1H, *H*-Ir); δ 3.34–3.16 (m, 2H, *H$_2$*C), 1.69–1.48 (m, 2H, *H$_2$*C), 1.33 (h, ^{3}J$_{H,H}$ = 7.2 Hz, 1H,), 0.90 (t, J = 7.3 Hz, 3H, *H$_3$*C); 6.6-8.6 (28H, Aromatikoak) ppm.

^{31}P{^{1}H} EMN (CDCl$_3$): δ 18.9 (s) ppm.

ESI-MS (MeOH): IrC$_{38}$H$_{29}$N$_2$P$_2$Cl-ren teorikoa: 803.1; esperimentala: 803.1 [M]$^-$.

Konduktibitatea (Λ$_M$): 120 ohm^{-1}·cm^2·mol^{-1}.

(37), [IrHCl{PPh$_2$(*o*-C$_6$H$_4$)CNNC(*o*-C$_6$H$_4$)PPh$_2$}(ZrCl$_4$)] [N(n-Bu)$_4$]-ren sintesia

ZrCl$_4$ (0.037 mmol, 8.6 mg) **36** konplexuaren (0.037mmol, 30 mg) tetrahidrofurano disoluzioa duen Schlenk batera gehitu eta 2 orduz irabiatu zen giro tenperaturan. Ondoren, disolbatzailea presio baxuan lurrundu eta solido laranja argi bat jaso zen. Solidoa bitan garbitu zen eter dietilikoarekin. Lortutako etekina %74.

^{1}H EMN (CDCl$_3$): δ -17.63 (t, ^{2}J$_{P,H}$= 17.5 Hz, 1H, *H*-Ir); 6.5-9.2 (28H, Aromatikoak) ppm.

^{31}P{^{1}H} EMN (CDCl$_3$): δ 15.5 (s) ppm.

Konduktibitatea (Λ$_M$): 130 ohm^{-1}·cm^2·mol^{-1}.

(38), [IrHCl{PPh$_2$(*o*-C$_6$H$_4$)CN(CH$_3$)NC(*o*-C$_6$H$_4$)PPh$_2$}]-ren sintesia

NaH (0.25 mmol, 8.9 mg) **3** konplexuaren (0.037mmol, 30 mg) tetrahidrofurano suspentsioa duen Schlenk batera gehitu zen hau 0 ºC-tan zegoelarik. 10 minutuz irabiatzen utzi eta MeI (0.037 mmol, 2.3 µL) gehitu zen nahasketa 0 ºC mantenduz. 18 orduz irabiatu zen giro tenperaturan. Ondoren, disolbatzailea presio baxuan lurrundu eta geratutako solidoa diklorometanotan birdisolbatu eta iragazi zen. Sortutako gatzak urarekin erauzi ziren. Fase organikoa magnesio sulfatoarekin lehortu eta iragazi zen. Azkenik, disolbatzailea presio baxuan lurrundu eta solido laranja jaso zen. Lortutako etekina %62.

IR (KBr, cm^{-1}): 2165 (br), v(Ir-H); 1636 (m), v(C=N)

IrC$_{39}$H$_{32}$N$_2$P$_2$Cl-ren analisi elementala:

Teorikoa: C 57.24, H 3.94, N 3.42.

Esperimentala: C 57.10, H 4.13, N 3.26.

^{1}H EMN (CDCl$_3$): δ -19.35 (t, $^2J_{P,H}$= 16.9 Hz, 1H, *H*-Ir); 4.45 (s, 3H, *H*$_3$C); 6.4-8.4 (28H, Aromatikoak) ppm.

^{31}P{^{1}H} EMN (CDCl$_3$): δ 11.2 (d, $^2J_{P,H}$= 5.6 Hz); 22.9 (br) ppm.

^{15}N EMN (CDCl$_3$): δ 243.0 (s); 369.0 (s) ppm.

ESI-MS (MeOH): IrC$_{39}$H$_{32}$N$_2$P$_2$ClNa-ren teorikoa: 841.1; esperimentala: 841.1 [M+Na]$^+$.

Konduktibitatea (Λ$_M$): 10 ohm^{-1}·cm^2·mol^{-1}.

(39), [IrHI{PPh$_2$(*o*-C$_6$H$_4$)CN(CH$_3$)NC(*o*-C$_6$H$_4$)PPh$_2$}]-ren sintesia

NaI (0.185 mmol, 27.7 mg) **38** konplexuaren (0.037mmol, 30 mg) metanol disoluzioa duen Schlenk batera gehitu eta 18 orduz irabiatu zen giro tenperaturan. Horren ostean, disolbatzailea presio baxuan lurrundu eta geratutako solidoa diklorometanotan birdisolbatu eta iragazi zen. Sortutako gatzak urarekin erauzi ziren. Fase organikoa magnesio sulfatoarekin lehortu eta iragazi zen. Azkenik, disolbatzailea presio baxuan lurrundu eta solido laranja jaso zen. Lortutako etekina %72.

IR (KBr, cm^{-1}): 2016 (br), ν(Ir-H); 1620 (m), ν(C=N)

IrC$_{39}$H$_{32}$N$_2$P$_2$I-ren analisi elementala:

Teorikoa: C 51.49, H 3.55, N 3.08.

Esperimentala: C 51.18, H 3.23, N 2.92.

^{1}H EMN (CDCl$_3$): δ -16.46 (dd, $^2J_{P,H}$= 16.7 Hz, $^2J_{P,H}$= 17.7 Hz 1H, *H*-Ir); 4.48 (s, 3H, *H*$_3$C); 6.8-8.4 (28H, Aromatikoak) ppm.

^{31}P{^{1}H} EMN (CDCl$_3$): δ 5.7 (d, $^2J_{P,H}$= 6.2 Hz); 15.0 (d, $^2J_{P,H}$= 5.6 Hz) ppm.

ESI-MS (MeOH): $IrC_{39}H_{33}N_2P_2I$-ren teorikoa: 901.1; esperimentala: 901.1 $[M+H]^+$ eta $IrC_{39}H_{32}N_2P_2INa$-ren teorikoa: 933.1; esperimentala:933.1 $[M+Na]^+$.

Konduktibitatea (Λ_M): 20 $ohm^{-1}\cdot cm^2\cdot mol^{-1}$.

(40), [IrH(SCN){PPh$_2$(o-C$_6$H$_4$)CN(CH$_3$)NC(o-C$_6$H$_4$)PPh$_2$}]-ren sintesia

KSCN (0.185 mmol, 18.0 mg) **38** konplexuaren (0.037mmol, 30 mg) metanol disoluzioa duen Schlenk batera gehitu eta 18 orduz errefluxupean mantendu zen. Ondoren, disolbatzailea presio baxuan lurrundu eta geratutako solidoa diklorometanotan birdisolbatu eta iragazi zen. Sortutako gatzak urarekin erauzi ziren. Fase organikoa magnesio sulfatoarekin lehortu eta iragazi zen. Azkenik, disolbatzailea presio baxuan lurrundu eta solido laranja jaso zen. Lortutako etekina %58.

IR (KBr, cm^{-1}): 2100 (s), v(SC=N); 1718 (m), v(C=N)

$IrC_{40}H_{32}N_3P_2S$-ren analisi elementala:

Teorikoa: C 57.13, H 3.84, N 5.00.

Esperimentala: C 56.94, H 3.72, N 5.13.

^{1}H EMN (CDCl$_3$): δ -15.58 (t, $^2J_{P,H}$= 16.9 Hz, 1H, *H*-Ir); 4.59 (s, 3H, *H$_3$*C); 6.8-8.5 (28H, Aromatikoak) ppm.

^{31}P{^{1}H} EMN (CDCl$_3$): δ 10.3 (s); 21.4 (s) ppm.

ESI-MS (MeOH): $IrC_{39}H_{32}N_2P_2$-ren teorikoa: 783.2; esperimentala: 783.2 [M-SCN]$^+$.

Konduktibitatea (Λ_M): 10 $ohm^{-1}\cdot cm^2\cdot mol^{-1}$.

(41), [IrHCl{PPh$_2$(*o*-C$_6$H$_4$)CN(C$_4$H$_7$O$_2$)NC(*o*-C$_6$H$_4$)PPh$_2$}]-ren sintesia

Etil diazoazetato (0.037 mmol, 4.5 μL) **3** konplexuaren (0.037mmol, 30 mg) diklorometano suspentsioa duen Schlenk batera gehitu eta 48 orduz irabiatu zen giro tenperaturan. Ondoren, disoluzioa iragazi eta disolbatzailea presio baxuan lurrundu eta solido laranja bat jaso zen. Lortutako etekina %68.

IrC$_{42}$H$_{36}$O$_2$N$_2$P$_2$Cl-ren analisia:

Teorikoa: C 56.66, H 4.08, N 3.15.

Esperimentala: C 57.08, H 4.23, N 2.87.

^{1}H EMN (CDCl$_3$): δ -19.01 (t, $^2J_{P,H}$= 16.8 Hz, 1H, *H*-Ir); 1.31 (m, 3H, *H$_3$*C); 4.24 (m, 2H, *H$_2$*C-O); 5.50 (d, $^2J_{H,H}$= 17.6 Hz, 1H, *H*-CN); 5.63 (d, $^2J_{H,H}$= 17.6 Hz, 1H, *H*-CHN); 6.8-8.4 (H, Aromatikoak) ppm.

^{31}P{^{1}H} EMN (CDCl$_3$): δ 12.1 (d, $^2J_{P,P}$= 6.7 Hz); 20.4 (d, $^2J_{P,P}$= 6.7 Hz) ppm.

ESI-MS (MeOH): IrC$_{42}$H$_{36}$N$_2$P$_2$ClNa-ren teorikoa: 913.2; esperimentala: 913.2 [M+Na]$^+$.

Konduktibitatea (Λ$_M$): 10 ohm^{-1}·cm^2·mol^{-1}.

Erreferentziak

(1) Lukehart, C. M. Metalla-β-Diketones and Their Derivatives. *Acc. Chem. Res.* **1981**, *14* (4), 109–116. https://doi.org/10.1021/ar00064a003.

(2) Lukehart, C. M. Metalla-Derivatives of β-Diketones. *Adv. Organomet. Chem.* **1986**, *25*, 45–71. https://doi.org/10.1016/S0065-3055(08)60572-9.

(3) Rauchfuss, T. B. Transition Metal Activation of Aldehydes: Platinum Metal Derivatives of *o*-Diphenylphosphinobenzaldehyde. *J. Am. Chem. Soc.* **1979**, *101* (4), 1045–1047. https://doi.org/10.1021/ja00498a049.

(4) Garralda, M. A.; Hernández, R.; Ibarlucea, L.; Pinilla, E.; Torres, M. R. Synthesis and Characterization of Hydridoirida-β-Diketones Formed by the Reaction of [{Ir(Cod)Cl}$_2$] (Cod = 1,5-Cyclooctadiene) with o-(Diphenylphosphino)Benzaldehyde. *Organometallics* **2003**, No. 22, 3600–3603. https://doi.org/10.1021/om0301278.

(5) Acha, F.; Garralda, M. A.; Hernández, R.; Ibarlucea, L.; Pinilla, E.; Torres, M. R.; Zarandona, M. Synthesis and Reactivity of New Mono- and Dinuclear Hydridoirida-β-Diketones - The Formation and Characterization of a Dinuclear Tris-μ-Acyliridium(III) Complex. *Eur. J. Inorg. Chem.* **2006**, *2* (19), 3893–3900. https://doi.org/10.1002/ejic.200600458.

(6) Acha, F.; Garralda, A.; Ibarlucea, L.; Pinilla, E.; Torres, M. R. Novel Hydridoirida-β-Diketones Containing Small Molecules , CO, or Ethylene : Their Behavior in Coordinating Solvents Such as Dimethylsulfoxide or Acetonitrile. *Inorg. Chem.* **2005**, *44* (24), 9084–9091. https://doi.org/10.1021/ic051219n.

(7)   Sola, E.; Navarro, J.; López, J. A.; Lahoz, F. J.; Oro, L. A.; Werner, H. Labile Hydrido Complexes of Iridium(III): Synthesis, Dynamic Behaviour in Solution, and Reactivity Towar Alkenes. *Organometallics* **1999**, *18* (17), 3534–3546.

(8)   Acha, F.; Ciganda, R.; Garralda, M. A.; Hernández, R.; Ibarlucea, L.; Pinilla, E.; Torres, M. R. Reactivity of Hydridoirida-β-Diketones with Bases : The Selective Formation of New Di-μ-Acyl-μ-Hydridodiiridium(III) or Dihydridoirida- β-Diketone Complexes and Heterometallic Ir(III)– Rh(I) Derivatives.   *Dalton   Trans.   **2008**,   4602–4611. https://doi.org/10.1039/b803488e.

(9)   Garralda, M. A.; Mendicute-fierro, C.; Rodríguez-Diéguez, A.; Seco, J. M.; Ubide, C.; Zumeta, I. Efficient Hydridoirida-β-Diketone-Catalyzed Hydrolysis of Ammonia- or Amine-Boranes for Hydrogen Generation in Air.   *Dalton   Trans.   **2013**,   *42*,   11652–11660. https://doi.org/10.1039/c3dt51261d.

(10)   Ciganda, R.; Garralda, M. A.; Ibarlucea, L.; Mendicute-fierro, C.; Torralba, M. C.; Torres, M. R. Reactions of Hydridoirida-β-Diketones with Amines or with 2-Aminopyridines: Formation of Hydridoirida-β-Ketoimines, PCN Terdentate Ligands, and Acyl Decarbonylation. *Inorg. Chem.* **2012**, *51*, 1760–1768. https://doi.org/10.1021/ic202065d.

(11)   Zumeta, I.; Mendicute-fierro, C.; Rodríguez-diéguez, A.; Seco, J. M.; Garralda, M. A. Acyliridium (III) Complexes with PCN Terdentate Ligands Including Imino- or Iminium-Acyl Moieties or Formation of Hydrido from Hydroxyl.   *Eur.   J.   Inorg.   Chem.*   **2016**,   1790–1797. https://doi.org/10.1002/ejic.201600056.

(12)   Zumeta, I.; Mendicute-Fierro, C.; Bustos, I.; Huertos, M. A.; Rodríguez-Diéguez, A.; Seco, J. M.; San Sebastian, E.; Garralda, M. A. Irida-β-Ketoimines Derived from Hydrazines to Afford Metallapyrazoles or N-N Bond Cleavage: A Missing Metallacycle Disclosed by a Theoretical and

Experimental Study. *Inorg. Chem.* **2016**, *55* (20), 10284–10293. https://doi.org/10.1021/acs.inorgchem.6b01550.

(13) Na, H.; Maity, A.; Morshed, R.; Teets, T. S. Bis-Cyclometalated Iridium Complexes with Chelating Dicarbene Ancillary Ligands. *Organometallics* **2017**, *36* (15), 2965–2972. https://doi.org/10.1021/acs.organomet.7b00428.

(14) Cazin, C. S. J. *N-Heterocyclic Carbenes in Transition Metal Catalysis and Organocatalysis*; Springer Science & Business Media, 2010.

(15) Crabtree, G. W.; Dresselhaus, M. S.; Buchanan, M. V. The Hydrogen Economy. *Phys. Today* **2004**, *57* (12), 39–44. https://doi.org/10.1063/1.1878333.

(16) Service, R. F. The Hydrogen Backlash. *Science* **2004**, *305* (5686), 958–961. https://doi.org/10.1126/science.305.5686.958.

(17) Grasemann, M.; Laurenczy, G. Formic Acid as a Hydrogen Source - Recent Developments and Future Trends. *Energy Environ. Sci.* **2012**, *5* (8), 8171–8181. https://doi.org/10.1039/c2ee21928j.

(18) Nielsen, M.; Alberico, E.; Baumann, W.; Drexler, H. J.; Junge, H.; Gladiali, S.; Beller, M. Low-Temperature Aqueous-Phase Methanol Dehydrogenation to Hydrogen and Carbon Dioxide. *Nature* **2013**, *495* (7439), 85–89. https://doi.org/10.1038/nature11891.

(19) Stephens, F. H.; Pons, V.; Tom Baker, R. Ammonia–Borane: The Hydrogen Source Par Excellence? *Dalton Trans.* **2007**, *2* (25), 2613–2626. https://doi.org/10.1039/b703053c.

(20) Staubitz, A.; Robertson, A. P. M.; Manners, I. Ammonia-Borane and Related Compounds as Dihydrogen Sources. *Chem. Rev.* **2010**, *110* (7), 4079–4124. https://doi.org/10.1021/cr100088b.

(21) Bhunya, S.; Malakar, T.; Ganguly, G.; Paul, A. Combining Protons and

Hydrides by Homogeneous Catalysis for Controlling the Release of Hydrogen from Ammonia-Borane: Present Status and Challenges. *ACS Catal.* **2016**, *6* (11), 7907–7934. https://doi.org/10.1021/acscatal.6b01704.

(22) Denney, M. C.; Pons, V.; Hebden, T. J.; Heinekey, D. M.; Goldberg, K. I. Efficient Catalysis of Ammonia Borane Dehydrogenation. *J. Am. Chem. Soc.* **2006**, *128*, 12048–12049. https://doi.org/10.1021/ja062419g.

(23) Luconi, L.; Osipova, E. S.; Giambastiani, G.; Peruzzini, M.; Rossin, A.; Belkova, N. V; Filippov, O. A.; Titova, E. M.; Pavlov, A. A.; Shubina, E. S. Amine Boranes Dehydrogenation Mediated by an Unsymmetrical Iridium Pincer Hydride: (PCN) vs (PCP) Improved Catalytic Performance. *Organometallics* **2018**, *37*, 3142–3153. https://doi.org/10.1021/acs.organomet.8b00488.

(24) Blaquiere, N.; Diallo-garcia, S.; Gorelsky, S. I.; Black, D. A.; Fagnou, K. Ruthenium-Catalyzed Dehydrogenation of Ammonia Boranes. *J. Am. Chem. Soc.* **2008**, No. 130, 14034–14035.

(25) Marziale, A. N.; Friedrich, A.; Klopsch, I.; Drees, M.; Celinski, V. R.; Schmedt auf der Günne, J.; Schneider, S. The Mechanism of Borane − Amine Dehydrocoupling with Bifunctional Ruthenium Catalysts. *J. Am. Chem. Soc.* **2013**, *135*, 13342–13355. https://doi.org/10.1021/ja311092c.

(26) Sewell, L. J.; Huertos, M. A.; Dickinson, M. E.; Weller, A. S. Dehydrocoupling of Dimethylamine Borane Catalyzed by $Rh(PCy_3)_2H_2Cl$. *Inorg. Chem.* **2013**, *52*, 4509–4516. https://doi.org/10.1021/ic302804d.

(27) Esteruelas, M. A.; Nolis, P.; Oliván, M.; Oñate, E.; Vallribera, A.; Vélez, A. Ammonia Borane Dehydrogenation Promoted by a Pincer-Square- Planar Rhodium(I) Monohydride: A Stepwise Hydrogen Transfer from the Substrate to the Catalyst. *Inorg. Chem.* **2016**, *55,* 7176–7181. https://doi.org/10.1021/acs.inorgchem.6b01216.

(28) Baker, R. T.; Gordon, J. C.; Hamilton, C. W.; Henson, N. J.; Lin, P.;

Maguire, S.; Murugesu, M.; Scott, B. L.; Smythe, N. C. Iron Complex-Catalyzed Ammonia−Borane Dehydrogenation. A Potential Route toward B−N-Containing Polymer Motifs Using Earth-Abundant Metal Catalysts. *J. Am. Chem. Soc.* **2012**, *134,* 5598–5609. https://doi.org/10.1021/ja210542r.

(29) Todisco, S.; Luconi, L.; Giambastiani, G.; Rossin, A.; Peruzzini, M.; Golub, I. E.; Filippov, O. A.; Belkova, N. V; Shubina, E. S. Ammonia Borane Dehydrogenation Catalyzed by ($κ^4$-EP$_3$)Co(H) [EP$_3$ = E(CH$_2$CH$_2$PPh$_2$)$_3$; E = N, P] and H$_2$ Evolution from Their Interaction with NH Acids. *Inorg. Chem.* **2017**, *56,* 4296–4307. https://doi.org/10.1021/acs.inorgchem.6b02673.

(30) Kim, S.; Kim, T.; Kim, T.; Lee, G.; Park, J. T.; Nam, S. W.; Kang, S. O. Tetraglyme-Mediated Synthesis of Pd Nanoparticles for Dehydrogenation of Ammonia Borane. *Chem. Commun.* **2012**, *48,* 2021–2023. https://doi.org/10.1039/c2cc15931g.

(31) Park, J. H.; Kim, S. K.; Kim, H. S.; Cho, Y. J.; Park, J.; Lee, K. E.; Yoon, C. W.; Nam, S. W.; Kang, S. O. Convenient Metal Embedment into Mesoporous Silica Channels for High Catalytic Performance in AB Dehydrogenation. *Chem. Commun.* **2013**, *49* (92), 10832–10834. https://doi.org/10.1039/c3cc46758a.

(32) Chen, G.; Desinan, S.; Rosei, R.; Rosei, F.; Ma, D. Synthesis of Ni − Ru Alloy Nanoparticles and Their High Catalytic Activity in Dehydrogenation of Ammonia Borane. *Chem. A Eur. J.* **2012**, *18,* 7925–7930. https://doi.org/10.1002/chem.201200292.

(33) Chandra, M.; Xu, Q. A High-Performance Hydrogen Generation System : Transition Metal-Catalyzed Dissociation and Hydrolysis of Ammonia – Borane. *J. Power Sources* **2006**, *156,* 190–194. https://doi.org/10.1016/j.jpowsour.2005.05.043.

(34) Fetz, M.; Gerber, R.; Blacque, O.; Frech, C. M. Hydrolysis of Ammonia

Borane Catalyzed by Aminophosphine-Stabilized Precursors of Rhodium Nanoparticles : Ligand Effects and Solvent-Controlled Product Formation. *Chem. A Eur. J.* **2011**, *17*, 4732–4736. https://doi.org/10.1002/chem.201003543.

(35)   Clark, T. J.; Whittell, G. R.; Manners, I. Highly Efficient Colloidal Cobalt- and Rhodium-Catalyzed Hydrolysis of $H_3N \cdot BH_3$ in Air. *Inorg. Chem.* **2007**, *46* (18), 7522–7527. https://doi.org/10.1021/ic700806b.

(36)   Yan, J.; Zhang, X.; Han, S.; Shioyama, H.; Xu, Q. Iron-Nanoparticle-Catalyzed Hydrolytic Dehydrogenation of Ammonia Borane for Chemical Hydrogen Storage. *Angew. Chemie Int. Ed.* **2008**, *47*, 2287–2289. https://doi.org/10.1002/anie.200704943.

(37)   Peng, C.; Kang, L.; Cao, S.; Chen, Y.; Lin, Z.; Fu, W. Nanostructured Ni_2P as a Robust Catalyst for the Hydrolytic Dehydrogenation of Ammonia – Borane. *Angew. Chemie Int. Ed.* **2015**, *54*, 15725–15729. https://doi.org/10.1002/anie.201508113.

(38)   Fu, Z.-C.; Xu, Y.; Chan, S. L.-F.; Wang, W.-W.; Li, F.; Liang, F.; Chen, Y.; Lin, Z.-S.; Fu, W.-F.; Che, C. Highly Efficient Hydrolysis of Ammonia Borane by Anion ($^-$OH, F$^-$,Cl$^-$)-Tuned Interactions between Reactant Molecules and CoP Nanoparticles. *Chem. Commun.* **2017**, *53*, 705–708. https://doi.org/10.1039/c6cc08120g.

(39)   Metin, Ö.; Mazumder, V.; Özkar, S.; Sun, S. Monodisperse Nickel Nanoparticles and Their Catalysis in Hydrolytic Dehydrogenation of Ammonia Borane. *J. Am. Chem. Soc.* **2010**, *132*, 1468–1469. https://doi.org/10.1021/cm9013046.(14).

(40)   Zacho, S. L.; Mielby, J.; Kegnæs, S. Hydrolytic Dehydrogenation of Ammonia Borane over ZIF-67 Derived Co Nanoparticle Catalysts. *Catal. Sci. Technol.* **2018**, No. 8, 4741. https://doi.org/10.1039/c8cy01500g.

(41)   Baguc, I. B.; Ertas, I. E.; Yurderi, M.; Bulut, A.; Zahmakiran, M.; Kaya, M.

Nanocrystalline Metal Organic Framework (MIL-101) Stabilized Copper Nanoparticles : Highly Efficient Nanocatalyst for the Hydrolytic Dehydrogenation of Methylamine Borane. *Inorganica Chim. Acta* **2018**, *483*, 431–439. https://doi.org/10.1016/j.ica.2018.08.056.

(42) Fu, F.; Wang, C.; Wang, Q.; Martinez-Villacorta, A. M.; Escobar, A.; Chong, H.; Wang, X.; Moya, S.; Salmon, L.; Fouquet, E.; Ruiz, J.; Astruc, D. Highly Selective and Sharp Volcano-Type Synergistic Ni_2Pt@ZIF-8-Catalyzed Hydrogen Evolution from Ammonia Borane Hydrolysis. *J. Am. Chem. Soc.* **2018**, *140* (1), 10034–10042. https://doi.org/10.1021/jacs.8b06511.

(43) Ciganda, R.; Garralda, M. A.; Ibarlucea, L.; Pinilla, E.; Torres, M. R. A Hydridoirida-β-Diketone as an Efficient and Robust Homogeneous Catalyst for the Hydrolysis of Ammonia–Borane or Amine-Borane Adducts in Air to Produce Hydrogen. *Dalton Trans.* **2010**, *39*, 7226–7229. https://doi.org/10.1039/c0dt00091d.

(44) Graham, T. W.; Tsang, C.; Chen, X.; Guo, R.; Jia, W.; Lu, S.; Sui-seng, C.; Ewart, C. B.; Lough, A.; Amoroso, D.; Abdur-Rashid, K. Catalytic Solvolysis of Ammonia Borane. *Angew. Chemie Int. Ed.* **2010**, *49*, 8708–8711. https://doi.org/10.1002/anie.201003074.

(45) Nelson, D. J.; Truscott, B. J.; Egbert, J. D.; Nolan, S. P. Exploring the Limits of Catalytic Ammonia−Borane Dehydrogenation Using a Bis(N‑Heterocyclic Carbene) Iridium(III) Complex. *Organometallics* **2013**, *32*, 3769–3772. https://doi.org/10.1021/om400402r.

(46) Wang, W.; Tang, H.; Lu, W.; Li, Y.; Bao, M.; Himeda, Y. Mechanistic Insights into the Catalytic Hydrolysis of Ammonia Borane with Proton-Responsive Iridium Complexes : An Experimental and Theoretical Study. *ChemCatChem* **2017**, *9*, 3191–3196. https://doi.org/10.1002/cctc.201700325.

(47) San Nacianceno, V.; Ibarlucea, L.; Mendicute-fierro, C.; Rodríguez-

Diéguez, A.; Seco, J. M.; Zumeta, I.; Ubide, C.; Garralda, M. A. Hydrido{(Acylphosphine)(Diphenylphosphinous Acid)}rhodium(III) Complexes. Catalysts for the Homogeneous Hydrolysis of Ammonia- or Amine-Boranes under Air. *Organometallics* **2014**, *33*, 6044–6052. https://doi.org/10.1021/om500666w.

(48) San Nacianceno, V.; Azpeitia, S.; Ibarlucea, L.; Mendicute-fierro, C.; Rodríguez-diéguez, A.; Seco, J. M.; San Sebastian, E.; Garralda, M. A. Stereoselective Formation and Catalytic Activity of Hydrido(Acylphosphane)(Chlorido)(Pyrazole)Rhodium(III) Complexes. Experimental and DFT Studies. *Dalton Trans.* **2015**, *44*, 13141–13155. https://doi.org/10.1039/c5dt01705j.

(49) Boulho, C.; Djukic, J. The Dehydrogenation of Ammonia–Borane Catalysed by Dicarbonylruthenacyclic(II) Complexes. *Dalton Trans.* **2010**, *39*, 8893–8905. https://doi.org/10.1039/c0dt00241k.

(50) Muñoz-Olasagasti, M.; Telleria, A.; Pérez-Miqueo, J.; Garralda, M. A.; Freixa, Z. A Readily Accessible Ruthenium Catalyst for the Solvolytic Dehydrogenation of Amine–Borane Adducts. *Dalton Trans.* **2014**, *43*, 11404–11409. https://doi.org/10.1039/c4dt01216j.

(51) Telleria, A.; Vicent, C.; San Nacianceno, V.; Garralda, M. A.; Freixa, Z. Experimental Evidence Supporting Related Mechanisms for Ru(II)-Catalyzed Dehydrocoupling and Hydrolysis of Amine-Boranes. *ACS Catal.* **2017**, *7*, 8394–8405. https://doi.org/10.1021/acscatal.7b02958.

(52) Zhan, W.-W.; Zhu, Q.-L.; Xu, Q. Dehydrogenation of Ammonia Borane by Metal Nanoparticle Catalysts. *ACS Catal.* **2016**, *6* (10), 6892–6905. https://doi.org/10.1021/acscatal.6b02209.

(53) Ramachandran, P. V.; Gagare, P. D. Preparation of Ammonia Borane in High Yield and Purity, Methanolysis, and Regeneration. *Inorg. Chem.* **2007**, *46* (19), 7810–7817. https://doi.org/10.1021/ic700772a.

(54) Özhava, D.; Özkar, S. Rhodium(0) Nanoparticles Supported on Hydroxyapatite Nanospheres and Further Stabilized by Dihydrogen Phosphate Ion: A Highly Active Catalyst in Hydrogen Generation from the Methanolysis of Ammonia Borane. *Int. J. Hydrogen Energy* **2015**, *40*, 10491–10501. https://doi.org/10.1016/j.ijhydene.2015.06.144.

(55) Özkar, S. Transition Metal Nanoparticle Catalysts in Releasing Hydrogen from the Methanolysis of Ammonia Borane. *Int. J. Hydrogen Energy* **2020**, *45* (14), 7881–7891. https://doi.org/10.1016/j.ijhydene.2019.04.125.

(56) Lara, P.; Philippot, K.; Suárez, A. Phosphane-Decorated Platinum Nanoparticles as Efficient Catalysts for H_2 Generation from Ammonia Borane and Methanol. *ChemCatChem* **2019**, *11* (2), 766–771. https://doi.org/10.1002/cctc.201801702.

(57) Sun, J.-K.; Zhan, W.-W.; Akita, T.; Xu, Q. Toward Homogenization of Heterogeneous Metal Nanoparticle Catalysts with Enhanced Catalytic Performance: Soluble Porous Organic Cage as a Stabilizer and Homogenizer. *J. Am. Chem. Soc.* **2015**, *137* (22), 7063–7066.

(58) San Nacianceno, V.; García, M. Á.; Matxain, J. M.; Freixa, Z. Proton-Responsive Ruthenium(II) Catalysts for the Solvolysis of Ammonia-Borane. *Organometallics* **2020**, *39* (8), 1238–1248.

(59) Yagupsky, M. P.; Wilkinson, G. Cationic π-Carbon Disulphide Complexes of Rhodium and Iridium; Thio-Carbonyl Complexes of Iridium. *J. Chem. Soc. A Inorg. Phys. Theor.* **1967**, 2813–2817.

(60) Kemmitt, T.; Gainsford, G. J. Regeneration of Sodium Borohydride from Sodium Metaborate , and Isolation of Intermediate Compounds. *Int. J. Hydrogen Energy* **2009**, *34* (14), 5726–5731. https://doi.org/10.1016/j.ijhydene.2009.05.108.

(61) Ciganda, R.; Garralda, M. A.; Ibarlucea, L.; Mendicute, C.; Pinilla, E.; Torres, M. R. Dehydrogenation of Hydridoirida-β-Diketones in Methanol :

The Selective Formation of Mono- and Dinuclear Acyl Complexes. *Eur. J. Inorg. Chem.* **2010**, 3167–3173. https://doi.org/10.1002/ejic.201000250.

(62) Shimoi, M.; Nagai, S.; Ichikawa, M.; Kawano, Y.; Katoh, K.; Uruichi, M.; Ogino, H. Coordination Compounds of Monoborane-Lewis Base Adducts: Syntheses and Structures of $[M(CO)_5(\eta^1\text{-}BH_3 \cdot L)]$ (M = Cr, Mo, W; L = NMe_3, PMe_3, PPh_3). *J. Am. Chem. Soc.* **1999**, *121* (50), 11704–11712. https://doi.org/10.1021/ja990828p.

(63) Hebden, T. J.; Denney, M. C.; Pons, V.; Piccoli, P. M. B.; Koetzle, T. F.; Schultz, A. J.; Kaminsky, W.; Goldberg, K. I.; Heinekey, D. M. σ -Borane Complexes of Iridium : Synthesis and Structural Characterization. *J. Am. Chem. Soc.* **2008**, *130*, 10812–10820. https://doi.org/10.1021/ja801898m.

(64) Wang, Q.; Fu, F.; Yang, S.; Martinez Moro, M.; Ramirez, M. D. L. A.; Moya, S.; Salmon, L.; Ruiz, J.; Astruc, D. Dramatic Synergy in CoPt Nanocatalysts Stabilized by "Click" Dendrimers for Evolution of Hydrogen from Hydrolysis of Ammonia Borane. *ACS Catal.* **2019**, *9*, 1110–1119. https://doi.org/10.1021/acscatal.8b04498.

(65) Na, C.; Ma, H. Isokinetic Temperature and Size-Controlled Activation of Ruthenium-Catalyzed Ammonia Borane Hydrolysis. *ACS Catal.* **2015**, *5*, 1726–1735. https://doi.org/10.1021/cs5019524.

(66) Bocian, W.; Jaźwiński, J.; Sadlej, A. ^{1}H, ^{13}C and ^{15}N NMR Studies on Adducts Formation of Rhodium(II) Tetraacylates with Some Azoles in $CDCl_3$ Solution. *Magn. Reson. Chem.* **2008**, *46* (2), 156–165. https://doi.org/10.1002/mrc.2149.

(67) Claramunt, R. M.; López, C.; García, M. Á.; Denisov, G. S.; Alkorta, I.; Elguero, J. Protonation and Phase Effects on the NMR Chemical Shifts of Imidazoles and Pyrazoles: Experimental Results and GIAO Calculations. *New J. Chem.* **2003**, *27* (4), 734–742. https://doi.org/10.1039/b210251j.

(68) Nygaard, L.; Christen, D.; Nielsen, J. T.; Pedersen, E. J.; Snerling, O.;

Vestergaard, E.; Sørensen, G. O. Microwave Spectra of Isotopic Pyrazoles and Molecular Structure of Pyrazole. *J. Mol. Struct.* **1974**, *22* (3), 401–413. https://doi.org/10.1016/0022-2860(74)85010-6.

(69) Węcławik, M.; Szklarz, P.; Medycki, W.; Janicki, R.; Piecha-Bisiorek, A.; Zieliński, P.; Jakubas, R. Unprecedented Transformation of $[I^-\cdot I_3^-]$ to $[I_4^{2-}]$ Polyiodides in the Solid State: Structures, Phase Transitions and Characterization of Dipyrazolium Iodide Triiodide. *Dalton Trans.* **2015**, *44* (42), 18447–18458. https://doi.org/10.1039/c5dt02265g.

(70) Titov, A. A.; Filippov, O. A.; Smol'yakov, A. F.; Baranova, K. F.; Titova, E. M.; Averin, A. A.; Shubina, E. S. Dinuclear Cu^I and Ag^I Pyrazolates Supported with Tertiary Phosphines: Synthesis, Structures, and Photophysical Properties. *Eur. J. Inorg. Chem.* **2019**, *2019* (6), 821–827. https://doi.org/10.1002/ejic.201801318.

(71) Kishimura, A.; Yamashita, T.; Aida, T. Phosphorescent Organogels via "Metallophilic" Interactions for Reversible RGB-Color Switching. *J. Am. Chem. Soc.* **2005**, *127* (1), 179–183. https://doi.org/10.1021/ja0441007.

(72) Sebe, E.; Guzei, I. A.; Heeg, M. J.; Liable-Sands, L. M.; Rheingold, A. L.; Winter, C. H. Synthesis, Structure, and Properties of Zirconium and Hafnium Complexes Containing η^2-Pyrazolato Ligands. *Eur. J. Inorg. Chem.* **2005**, No. 19, 3955–3961. https://doi.org/10.1002/ejic.200500378.

(73) Palit, S.; Bera, S.; Singh, M.; Mondal, D. Synthesis of Novel Indazole-Derived Ionic Liquids. *Synthesis* **2015**, *47* (21), 3371–3384. https://doi.org/10.1055/s-0034-1381135.

(74) Solovyev, I. V.; Zhukovsky, D. D.; Dar'in, D. V.; Krasavin, M. Y. N-Alkylation of Nitrogen Heterocycles with α-Diazocarbonyl Compounds. *Chem. Heterocycl. Compd.* **2020**, *56* (7), 809–813. https://doi.org/10.1007/s10593-020-02736-y.

(75) Herde, J. L.; Lambert, J. C.; Senoff, C. V.; Cushing, M. A. Cyclooctene

and 1,5-Cyclooctadiene Complexes of Iridium(I). *Inorg. Synth.* **1974**, *15*, 18–20.

(76) Laue, S.; Greiner, L.; Wöltinger, J.; Liese, A. Continuous Application of Chemzymes in a Membrane Reactor: Asymmetric Transfer Hydrogenation of Acetophenone. *Adv. Synth. Catal.* **2001**, *343* (6–7), 711–720. https://doi.org/10.1002/1615-4169(200108)343:6/7<711::aid-adsc711>3.3.co;2-t.